symmetry

Symmetry in Applied Mathematics

Edited by

Lorentz Jäntschi and Sorana D. Bolboacă

Printed Edition of the Special Issue Published in *Symmetry*

www.mdpi.com/journal/symmetry

MDPI

Symmetry in Applied Mathematics

Symmetry in Applied Mathematics

Editors

Lorentz Jäntschi
Sorana D. Bolboacă

MDPI • Basel • Beijing • Wuhan • Barcelona • Belgrade • Manchester • Tokyo • Cluj • Tianjin

Editors

Lorentz Jäntschi
Department of Physics and
Chemistry, Technical University
of Cluj-Napoca
Romania

Sorana D. Bolboacă
Department of Medical
Informatics and Biostatistics,
"Iuliu Haţieganu" University of
Medicine and Pharmacy
Romania

Editorial Office
MDPI
St. Alban-Anlage 66
4052 Basel, Switzerland

This is a reprint of articles from the Special Issue published online in the open access journal *Symmetry* (ISSN 2073-8994) (available at: https://www.mdpi.com/journal/symmetry/special_issues/Symmetry_Applied_Mathematics).

For citation purposes, cite each article independently as indicated on the article page online and as indicated below:

LastName, A.A.; LastName, B.B.; LastName, C.C. Article Title. *Journal Name* **Year**, *Volume Number*, Page Range.

ISBN 978-3-03943-791-7 (Hbk)
ISBN 978-3-03943-792-4 (PDF)

Contents

About the Editors

Lorentz Jäntschi was born in Făgăraș, Romania, in 1973. In 1991 he moved to Cluj-Napoca, Cluj, where he completed his studies. In 1995 he was awarded a B.Sc. and M.Sc. in Informatics, in 1997 a B.Sc. and M.Sc. in Physics and Chemistry, in 2000 a Ph.D. in Chemistry under the supervision of Prof. Mircea V. Diudea, in 2002 an M.Sc. in Agriculture, in 2010 a Ph.D. in Horticulture under the supervision of Prof. Radu E. Sestraș, and, finally, in 2013 a postdoctorate in Horticulture. That same year (2013), he became a Full Profesor of chemistry at the Technical University of Cluj-Napoca and an associate at Babes-Bolyai University, where he advises Ph.D. studies in chemistry. Both positions are to date. During the time he had research and education activities deployed under auspices of different institutions: the G. Barițiu (1995–1999) and Bălcescu (1999–2001) National Colleges, the Iuliu Hațieganu University of Medicine and Pharmacy (2007–2012), Oradea University (2013–2015), and the Institute of Agricultural Sciences and Veterinary Medicine at University of Cluj-Napoca (2011–2016). He serves as an editor for the journals Notulae Scientia Biologicae, Notulae Horti Agro Botanici Cluj-Napoca, Open Agriculture and Symmetry. He was Editor-in-Chief of the Leonardo Journal of Sciences and the Leonardo Electronic Journal of Practices and Technologies (2002–2018) and guest editor (2019–2020) for Mathematics.

Sorana D. Bolboacă is a professor of medical informatics and biostatistics at the ”Iuliu Hațieganu” University of Medicine and Pharmacy Cluj-Napoca, Romania. She earned her Ph.D. in Medicine (2006) from the Iuliu Haţieganu University of Medicine and Pharmacy (thesis title: “Evidence-Based Medicine: Logistics and Implementation”) and a Ph.D. in Horticulture (2010) from the University of Agriculture Sciences and Veterinary Medicine Cluj-Napoca (thesis title: “Statistical Models for Analysis of Genetic Variability”). Her research interests are multidisciplinary, e.g., applied & computational statistics, molecular modeling, genetic analysis, statistical modeling in medicine, integrated health informatics system and application of new technologies in medicine, medical diagnostics research, medical imaging analysis, assisted decision systems, research ethics, social media and health information, and evidence-based medicine. She is an active member of the scientific community with more than 200 papers and 19 monographs as well as editorial and reviewing activities (https://publons.com/researcher/249582/sorana-d-bolboaca/).

Preface to ”Symmetry in Applied Mathematics”

The Symmetry in Applied Mathematics special issue of Symmetry Journal reprinted here is collecting fourteen papers dealing with various subjects under the auspices of using symmetry for solving problems. The special issue called for articles from a broad interdisciplinary area, since 'applied mathematics' is a specific form of mathematics that involves creating and use of mathematical models to map out the mathematical core of a practical problem. There is probably no scientific field in which applied mathematics has not made its necessary presence. On the other hand, symmetry is about identification and use invariants to any of various transformations for any paired dataset and characterizations associated with. Inside applied mathematics, symmetry may work as a powerful tool for problems reduction and solving. Applications include probability theory (all probabilistic reasoning is ultimately based on judgments of symmetry), fractals (geometry), supersymmetry (physics), nanostructures (chemistry), taxonomy (biology), bilateral symmetry (medicine), and the list can go on. The call for papers was closed on November 15, 2019. The papers reports from mathematical theoretical results (Khovanov Homology of Three-Strand Braid Links https://www.mdpi.com/2073-8994/10/12/720, Volume Preserving Maps Between p-Balls https://www.mdpi.com/2073-8994/11/11/1404, Generation of Julia and Mandelbrot Sets via Fixed Points https://www.mdpi.com/2073-8994/12/1/86) applications in physics or chenistry (A Continuous Coordinate System for the Plane by Triangular Symmetry https://www.mdpi.com/2073-8994/11/2/191, One-Dimensional Optimal System for 2D Rotating Ideal Gas https://www.mdpi.com/2073-8994/11/9/1115, Minimal Energy Configurations of Finite Molecular Arrays https://www.mdpi.com/2073-8994/11/2/158), designing of the algorithms and their efficiency (Noether-Like Operators and First Integrals for Generalized Systems of Lane-Emden Equations https://www.mdpi.com/2073-8994/11/2/162, Algorithm for Neutrosophic Soft Sets in Stochastic Multi-Criteria Group Decision Making Based on Prospect Theory https://www.mdpi.com/2073-8994/11/9/1085, On a Reduced Cost Higher Order Traub-Steffensen-Like Method for Nonlinear Systems https://www.mdpi.com/2073-8994/11/7/891, On a Class of Optimal Fourth Order Multiple Root Solvers without Using Derivatives https://www.mdpi.com/2073-8994/11/12/1452), to specific uses (Facility Location Problem Approach for Distributed Drones https://www.mdpi.com/2073-8994/11/1/118, Parametric Jensen-Shannon Statistical Complexity and Its Applications on Full-Scale Compartment Fire Data https://www.mdpi.com/2073-8994/12/1/22) and to probability and statistics (The Asymmetric Alpha-Power Skew-t Distribution https://www.mdpi.com/2073-8994/12/1/82, A Test Detecting the Outliers for Continuous Distributions Based on the Cumulative Distribution Function of the Data Being Tested https://www.mdpi.com/2073-8994/11/6/835).

Lorentz Jäntschi, Sorana D. Bolboacă
Editors

symmetry

MDPI

Article

Khovanov Homology of Three-Strand Braid Links

Young Chel Kwun [1], Abdul Rauf Nizami [2], Mobeen Munir [3,*], Zaffar Iqbal [4], Dishya Arshad [3] and Shin Min Kang [5,6,*]

[1] Department of Mathematics, Dong-A University, Busan 49315, Korea; yckwun@dau.ac.kr
[2] Faculty of Information Technology, University of Central Punjab, Lahore 54000, Pakistan; arnizami@ucp.edu.pk
[3] Department of Mathematics, Division of Science and Technology, University of Education, Lahore 54000, Pakistan; dishyaarshad@gmail.com
[4] Department of Mathematics, University of Gujrat, Gujrat 50700, Pakistan; zaffar.iqbal@uog.edu.pk
[5] Department of Mathematics and RINS, Gyeongsang National University, Jinju 52828, Korea
[6] Center for General Education, China Medical University, Taichung 40402, Taiwan
[*] Correspondence: mmunir@ue.edu.pk (M.M.); smkang@gnu.ac.kr (S.M.K.)

Received: 7 November 2018; Accepted: 15 November 2018; Published: 5 December 2018

Abstract: Khovanov homology is a categorication of the Jones polynomial. It consists of graded chain complexes which, up to chain homotopy, are link invariants, and whose graded Euler characteristic is equal to the Jones polynomial of the link. In this article we give some Khovanov homology groups of 3-strand braid links $\Delta^{2k+1} = x_1^{2k+2}x_2x_1^2x_2^2x_1^2\cdots x_2^2x_1^2x_1^2$, $\Delta^{2k+1}x_2$, and $\Delta^{2k+1}x_1$, where Δ is the Garside element $x_1x_2x_1$, and which are three out of all six classes of the general braid $x_1x_2x_1x_2\cdots$ with n factors.

Keywords: Khovanov homology; braid link; Jones polynomial

MSC: 57M27; 55N20

1. Introduction

Khovanov homology was introduced by Mikhail Khovanov in 2000 in Reference [1] as a categorification of the Jones polynomial, which was introduced by Jones in [2]. His construction, using geometrical and topological objects instead of polynomials, was so interesting that it offered a completely new approach to tackle problems in low-dimensional topology.

Khovanov homology plays a vital role in developing several important results in the field of knot theory. Soon after the discovery of Khovanov homology, Bar-Natan proved in Reference [3] that Khovanov's invariant is stronger than the Jones polynomial. He also proved that the graded Euler characteristic of the chain complex of a link L is the un-normalized Jones polynomial of that link. In 2005, Bar-Natan extended the Khovanov homology of links to tangles, cobordisms, and two-knots [4]. In [5] Bar-Natan gave a fast way of computing the Khovanov homology. In 2013, Ozsvath, Rasmussen, and Szabo introduced the odd Khovanov homology by using exterior algebra instead of symmetric algebra [6]. Gorsky, Oblomkov, and Rasmussen gave some results on stable Khovanov homology of torus links in Reference [7]. Putyra introduced a triply graded Khovanov homology and used it to prove that odd Khovanov homology is multiplicative with respect to disjoint unions and connected sums of links Reference [8]. Manion gave rational Khovanov homology of three-strand pretzel links in 2011 [9]. Nizami, Mobeen, and Ammara gave Khovanov homology of some families of braid links in Reference [10]. Nizami, Mobeen, Sohail, and Usman gave Khovanov homology and graded Euler characteristic of 2-strand braid links in [11].

In Reference [12], Marko used a long exact sequence to prove that the Khovanov homology groups of the torus link $T(n;m)$ stabilize as $m \to \infty$. A generalization of this result to the context of tangles came in the form of Reference [13], where Lev Rozansky showed that the Khovanov chain complexes for torus braids also stabilize (up to chain homotopy) in a suitable sense to categorify the Jones–Wenzl projectors. At roughly the same time, Benjamin Cooper and Slava Krushkal gave an alternative construction for the categorified projectors in Reference [14]. These results, along with connections between Khovanov homology, HOMFLYPT homology, Khovanov–Rozansky homology, and the representation theory of rational Cherednik algebra (see [15]) have led to conjectures about the structure of stable Khovanov homology groups in limit $Kh(T(n;1))$ (see [15], and results along these lines in Reference [16]). More recently, in Reference [17], Robert Lipshitz and Sucharit Sarkar introduced the Khovanov homotopy type of a link L. This is a link invariant taking the form of a spectrum whose reduced cohomology is the Khovanov homology of L.

Although computing the Khovanov homology of links is common in the literature, no general formulae have been given for all families of knots and links. In this paper, we give Khovanov homology of the three-strand braid links Δ^{2k+1}, $\Delta^{2k+1}x_2$, and $\Delta^{2k+1}x_1$, where Δ is the Garside element $x_1x_2x_1$. Particularly, we focus on the top homology groups.

2. Braid Links

Definition 1. *A* knot *is a simple, closed curve in the three-space. More precisely, it is the image of an injective, smooth function from the unit circle to $\mathbb{R}^3$ with a nonvanishing derivative [18]. You can see some knots in Figure 1*:

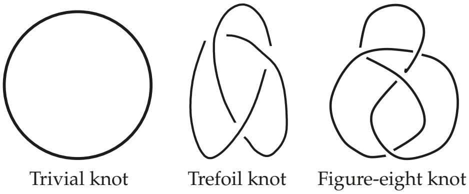

Figure 1. Knots.

Definition 2. *An m-component* link *is a collection of m nonintersecting knots [18]. A trivial two-component link and the Hopf link are given in Figure 2:*

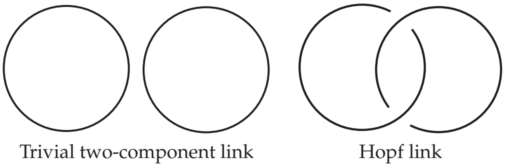

Figure 2. Links.

Definition 3. *Two links L_1 and L_2 are said to be* isotopic *or* equivalent *if there is a smooth map F: $[0,1] \times S^1 \to \mathbb{R}^3$, which confirms that F_t is a link for all $t \in [0,1]$ and that that $F_0 = L_1$ and $F_1 = L_2$. Map F is called* isotopy*. By the isotopy class of a link L, denoted $[L]$, we mean the collection of all links that are isotopic to L.*

Since it is hard to work with links in $\mathbb{R}^3$, people usually prefer working with their projections on a plane. These projections should be generic, which means that all multiple points are double points with a clear information of over- and undercrossing, as you can see in Figure 3. Such a projection of a link is called the *diagram* of the link.

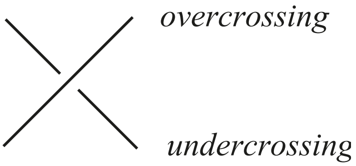

Figure 3. Crossing.

Theorem 1. (**Reidemeister**, [19]). *Let D_1 and D_2 be two diagrams of links L_1 and L_2. Then, links L_1 and L_2 are isotopic if and only if D_1 is transformed into D_2 by planar isotopies and by a finite sequence of three local moves represented in Figure 4:*

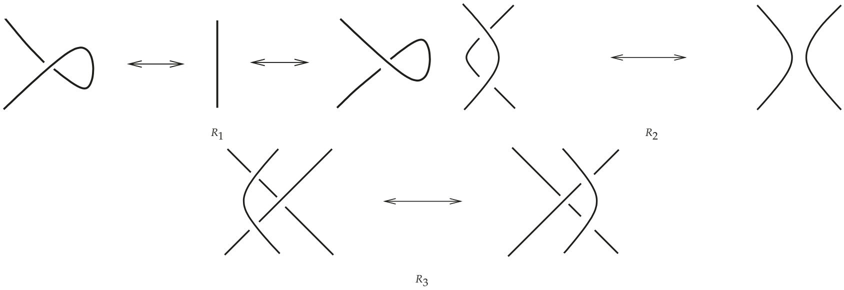

Figure 4. Reidemeister moves.

Definition 4. *A* link invariant *is a function that remains constant on all elements in an isotopy class of a link.*

Remark 1. *A function to qualify as a link invariant should be invariant under the Reidemeister moves.*

Definition 5. *An n-strand braid is a collection of n nonintersecting, smooth curves joining n points on a plane to n points on another parallel plane in an arbitrary order such that any plane parallel to the given planes intersects exactly n number of curves [20]. The smooth curves are called the strands of the braid. You can see a 2-strand braid in Figure 5:*

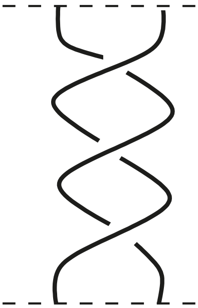

Figure 5. 2-strand braid.

Definition 6. *The* product *of two n-strand braids α and β, denoted by $\alpha\beta$, is defined by putting β below α and then gluing their common endpoints.*

Definition 7. *A braid is said to be* elementary *if it consists of just one crossing. The* i*th elementary braid, denoted by* x_i*, is given in Figure 6:*

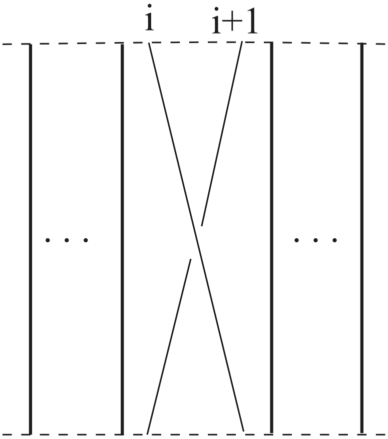

Figure 6. Elementary braid x_i.

Remark 2. *Each braid is a product of elementary braids.*

Definition 8. *The* closure *of a braid* β*, denoted by* $\widehat{\beta}$*, is defined by connecting its lower endpoints to its corresponding upper endpoints with smooth curves, as you can see in Figure 7.*

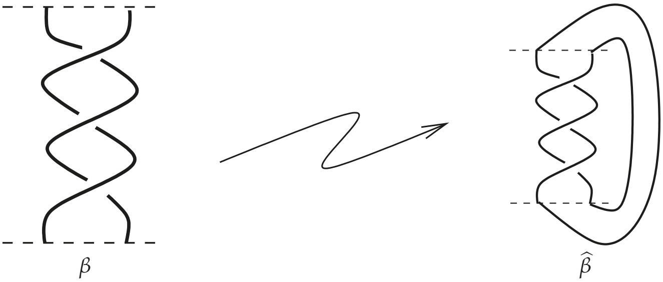

Figure 7. Braid closure.

Remark 3.

1 *All braids are oriented from top to bottom.*

2 *From now onward, by braid* β *we mean its closure* $\widehat{\beta}$*, which is actually a link.*

An important result by Alexander, connecting links and braids, is:

Theorem 2. (**Alexander** [21]). *Each link is a closure of some braid.*

Definition 9. *The* 0*- and* 1*-smoothings of crossing* *are defined, respectively, by* *and* .

Definition 10. *A collection of disjoint circles obtained by smoothing out all the crossings of a link L is called the Kauffman* state *of the link [22].*

3. Homology

Definition 11. *Let $V = \bigoplus_n V_n$, be a graded vector space with homogeneous components $\{V_n\}$ of degree n. The graded dimension of V is the power series $q \dim V: = \sum_n q^n \dim V_n$.*

Definition 12. *The* degree *of the tensor product of graded vector space $V_1 \otimes V_2$ is the sum of the degrees of the homogeneous components of graded vector spaces V_1 and V_2.*

Remark 4. *In our case, the graded vector space V has the basis $< v_+, v_- >$ with degree $p(v_\pm) = \pm 1$ and the q-dimension $q + q^{-1}$.*

Definition 13. *The degree shift $.\{l\}$ operation on a graded vector space $V = \bigoplus V_n$ is defined by*

$$\Big(V.\{l\}\Big)_n = V_{n-l}.$$

Construction of Chain Groups: Let L be a link with n crossings, and let all crossings be labeled from 1 to n. Arrange all its 2^n Kauffman states into columns $1, 2, \ldots, n$ so that the rth column contains all states having r number of 1-smoothings in it. To every stat α in the rth column we assign graded vector space $V_\alpha(L) := V^{\otimes m}\{r\}$, where m is the number of circles in α. The rth *chain group*, denoted by $[[L]]^r := \bigoplus_{\alpha : r = |\alpha|} V_\alpha(L)$, is the direct sum of all vector spaces corresponding to all states in the rth column.

Definition 14. *The chain complex $\overline{C}$ of graded vector spaces $\overline{C^r}$ is defined as:*

$$\ldots \to \overline{C}^{r+1} \xrightarrow{d^{r+1}} \overline{C}^{r} \xrightarrow{d^{r}} \overline{C}^{r-1} \xrightarrow{d^{r-1}} \ldots$$

such that $d^r \circ d^{r+1} = 0$ for each r.

In a system of converting the chain group into a complex, we use the maps between graded vector spaces to satisfy $d \circ d$. For this purpose we can label the edges of the cube $\{0,1\}^\chi$ by the sequence $\xi \epsilon \{0, 1, \star\}^\chi$, where ξ contains only one $\star$ at a time. Here, $\star$ indicates that we change a 1-smoothing to a 0-smoothing. The maps on the edges is denoted by d_ξ, the height of edges $|\xi|$. The direct sum of differentials in the cube along the column is

$$d^r := \sum_{|\xi| = r} (-1)^\xi d_\xi.$$

Now, we discuss the reason behind the sign of $(-1)^\xi$. As we want from the differentials to satisfy $d \circ d = 0$, the maps d_ξ have to anticommute on each of the vertex of the cube. A way to do this is by multiplying edges d_ξ by $(-1)^\xi := (-1)^{\sum_{i<j} \xi_i}$, where j is the location of $\star$ in ξ.

For better understanding, please see the n-cube of trefoil knot x_1^{-3} in Figure 8.

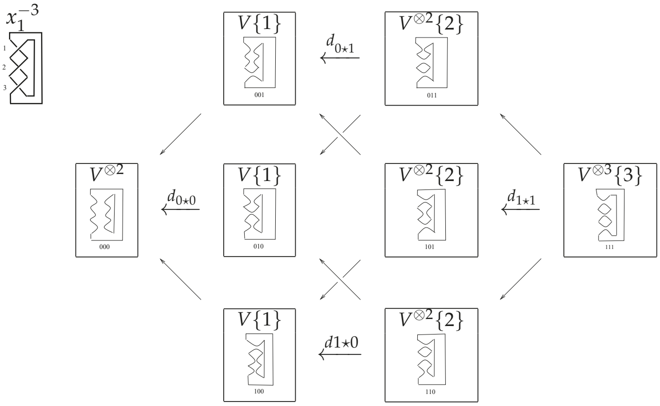

Figure 8. n-cube of x_1^{-3}.

It is useful to note that the ordered basis of V is $\langle v_+, v_- \rangle$ and the ordered basis of $V \otimes V$ is $\langle v_+ \otimes v_+, v_- \otimes v_+, v_+ \otimes v_-, v_- \otimes v_- \rangle$.

Definition 15. *Linear map $m : V \otimes V \to V$ that merges two circles into a single circle is defined as $m(v_+ \otimes v_+) = v_+, m(v_+ \otimes v_-) = v_-, m(v_- \otimes v_+) = v_-$ and $m(v_- \otimes v_-) = 0$.*

Map $\Delta : V \to V \otimes V$ that divides a circle into two circles is defined as $\Delta(v_+) = v_+ \otimes v_- + v_- \otimes v_+$ and $\Delta(v_-) = v_- \otimes v_-$; see Figure 9.

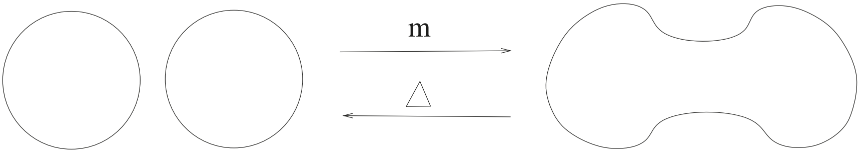

Figure 9. m and Δ maps.

Definition 16. *The homology group associated with the chain complex of a link L is defined as $\mathcal{H}^r(L) = \frac{\ker d^r}{\operatorname{im} d^{r+1}}$.*

Definition 17. *The kernel of the map $d^r : V^{\otimes r-1} \to V^{\otimes r}$, denoted by $\ker d^r$, is the set of all elements of $V^{\otimes r-1}$ that go to the zero element of $V^{\otimes r}$. The elements of the kernel are called cycles, while the elements of $\operatorname{im} d^{r+1}$ are called boundaries.*

Remark 5. *Note that the image of the chain complex of d^{r+1} is a subset of kernel d^r as, in general, $d^r \circ d^{r+1} = 0$.*

Definition 18. *The graded Poincaré polynomial $\mathrm{Kh}(L)$ in variables q and t of the complex is defined as*

$$\mathrm{Kh}(L) := \sum_r t^r qdim \mathcal{H}^r(L).$$

Theorem 3. (**Khovanov** [1]). *The graded dimension of homology groups $\mathcal{H}^r(L)$ are link invariants. The graded Poincaré polynomial* $\mathrm{Kh}(L)$ *is also a link invariant and* $\mathrm{Kh}(L)\big|_{t=-1} = \hat{J}(L)$.

3.1. Homology of x_1^{-3}

Now, we give the Khovanov homology of link $x_1^{-3} =$ 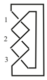 :

1. **The n-cube:** The 3-cube of x_1^{-3} is given in Figure 10:

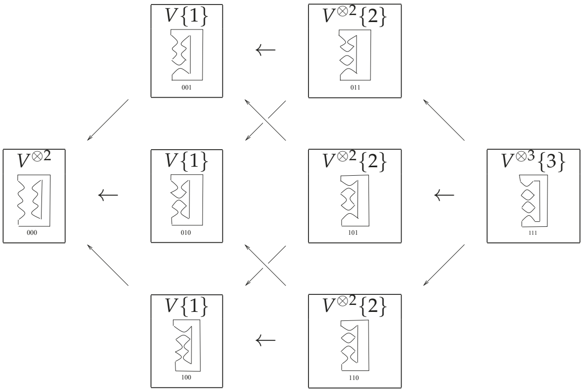

Figure 10. The 3-cube of x_1^{-3}.

2. **Chain complex:** The chain complex of $\widehat{x_1^3}$ is

$$0 \xrightarrow{d^4} V^{\otimes 3} \xrightarrow{d^3} \oplus_3 V^{\otimes 2} \xrightarrow{d^2} \oplus_3 V \xrightarrow{d^1} V^{\otimes 2} \xrightarrow{d^0} 0.$$

3. **Ordered basis of the chain complex:** The following are the vector spaces of the chain complex along with their ordered bases:

$V \otimes V \otimes V = \big\langle v_+ \otimes v_+ \otimes v_+, v_- \otimes v_+ \otimes v_+, v_+ \otimes v_- \otimes v_+, v_+ \otimes v_+ \otimes v_-, v_- \otimes v_- \otimes v_+, v_- \otimes v_+ \otimes v_-, v_+ \otimes v_- \otimes v_-, v_- \otimes v_- \otimes v_-\big\rangle$
$(V \otimes V) \oplus (V \otimes V) \oplus (V \otimes V) = \big\langle (v_+ \otimes v_+, 0, 0), (0, v_+ \otimes v_+, 0), (0, 0, v_+ \otimes v_+), (v_- \otimes v_+, 0, 0), (0, v_- \otimes v_+, 0), (0, 0, v_- \otimes v_+), (v_+ \otimes v_-, 0, 0), (0, v_+ \otimes v_-, 0), (0, 0, v_+ \otimes v_-), (v_- \otimes v_-, 0, 0)(0, v_- \otimes v_-, 0), (0, 0, v_- \otimes v_-)\big\rangle$
$V \oplus V \oplus V = \big\langle (v_+, 0, 0), (0, v_+, 0), (0, 0, v_+), (v_-, 0, 0), (0, v_-, 0), (0, 0, v_-)\big\rangle$
$V \otimes V = \big\langle v_+ \otimes v_+, v_- \otimes v_+, v_+ \otimes v_-, v_- \otimes v_-\big\rangle$

4. **Differential maps in matrix form:** Differential map $d^3\Big(V_1 \otimes V_2 \otimes V_3\Big) = \Big(m(v_1 \otimes v_2) \otimes v_3, v_1 \otimes m(v_2 \otimes v_3), v_2 \otimes m(v_1 \otimes v_3)\Big)$ in terms of a matrix is:

$$d^3 = \begin{pmatrix} 1 & 0 & 0 & 0 & 0 & 0 & 0 & 0 \\ 1 & 0 & 0 & 0 & 0 & 0 & 0 & 0 \\ 1 & 0 & 0 & 0 & 0 & 0 & 0 & 0 \\ 0 & 1 & 1 & 0 & 0 & 0 & 0 & 0 \\ 0 & 1 & 0 & 0 & 0 & 0 & 0 & 0 \\ 0 & 0 & 1 & 0 & 0 & 0 & 0 & 0 \\ 0 & 0 & 0 & 1 & 0 & 0 & 0 & 0 \\ 0 & 0 & 1 & 1 & 0 & 0 & 0 & 0 \\ 0 & 1 & 0 & 1 & 0 & 0 & 0 & 0 \\ 0 & 0 & 0 & 0 & 0 & 1 & 1 & 0 \\ 0 & 0 & 0 & 0 & 1 & 1 & 0 & 0 \\ 0 & 0 & 0 & 0 & 1 & 0 & 1 & 0 \end{pmatrix},$$

and map $d^2\Big(V_1 \otimes V_2, V_3 \otimes V_4, V_5 \otimes V_6\Big) = \Big(m(v_3 \otimes v_4) - m(v_1 \otimes v_2), m(v_5 \otimes v_6) - m(v_1 \otimes v_2), m(v_5 \otimes v_6) - m(v_3 \otimes v_4)\Big)$ is $d^2 = \begin{pmatrix} A & 0 & 0 & 0 \\ 0 & A & A & 0 \end{pmatrix}$, where $A = \begin{pmatrix} -1 & 1 & 0 \\ -1 & 0 & 1 \\ 0 & -1 & 1 \end{pmatrix}$. Also, $d^1\Big(V_1, V_2, V_3\Big) = \Delta(v_1) - \Delta(v_2) + \Delta(v_3)$ is $d^1 = \begin{pmatrix} 0 & 0 & 0 & 0 & 0 & 0 \\ 1 & -1 & 1 & 0 & 0 & 0 \\ 1 & -1 & 1 & 0 & 0 & 0 \\ 0 & 0 & 0 & 1 & -1 & 1 \end{pmatrix}$.

5. **Khovanov Homology:** On solving $d^3x = 0$ or

$$\begin{pmatrix} 1 & 0 & 0 & 0 & 0 & 0 & 0 & 0 \\ 1 & 0 & 0 & 0 & 0 & 0 & 0 & 0 \\ 1 & 0 & 0 & 0 & 0 & 0 & 0 & 0 \\ 0 & 1 & 1 & 0 & 0 & 0 & 0 & 0 \\ 0 & 1 & 0 & 0 & 0 & 0 & 0 & 0 \\ 0 & 0 & 1 & 0 & 0 & 0 & 0 & 0 \\ 0 & 0 & 0 & 1 & 0 & 0 & 0 & 0 \\ 0 & 0 & 1 & 1 & 0 & 0 & 0 & 0 \\ 0 & 1 & 0 & 1 & 0 & 0 & 0 & 0 \\ 0 & 0 & 0 & 0 & 0 & 1 & 1 & 0 \\ 0 & 0 & 0 & 0 & 1 & 1 & 0 & 0 \\ 0 & 0 & 0 & 0 & 1 & 0 & 1 & 0 \end{pmatrix} \begin{pmatrix} x_1 \\ x_2 \\ x_3 \\ x_4 \\ x_5 \\ x_6 \\ x_7 \\ x_8 \end{pmatrix} = 0,$$

we receive $x_1 = x_2 = x_3 = x_4 = 0$, $x_2 + x_3 = 0$, $x_3 + x_4 = 0$, $x_2 + x_4 = 0$, $x_6 + x_7 = 0$, $x_5 + x_6 = 0$, and $x_5 + x_7 = 0$. So the kernel of $d^3 = \left\langle \begin{bmatrix} 0 \\ 0 \\ 0 \\ 0 \\ 0 \\ 0 \\ 0 \\ 1 \end{bmatrix} \right\rangle$. Similarly, the image of d^3 is

$$\left\langle \begin{bmatrix} 1 \\ 1 \\ 1 \\ 0 \\ 0 \\ 0 \\ 0 \\ 0 \\ 0 \\ 0 \\ 0 \\ 0 \end{bmatrix}, \begin{bmatrix} 0 \\ 0 \\ 0 \\ 1 \\ 1 \\ 0 \\ 0 \\ 0 \\ 1 \\ 0 \\ 0 \\ 0 \end{bmatrix}, \begin{bmatrix} 0 \\ 0 \\ 0 \\ 1 \\ 0 \\ 1 \\ 0 \\ 1 \\ 0 \\ 0 \\ 0 \\ 0 \end{bmatrix}, \begin{bmatrix} 0 \\ 0 \\ 0 \\ 0 \\ 0 \\ 0 \\ 1 \\ 1 \\ 1 \\ 0 \\ 0 \\ 0 \end{bmatrix}, \begin{bmatrix} 0 \\ 0 \\ 0 \\ 0 \\ 0 \\ 0 \\ 0 \\ 0 \\ 0 \\ 0 \\ 1 \\ 1 \end{bmatrix}, \begin{bmatrix} 0 \\ 0 \\ 0 \\ 0 \\ 0 \\ 0 \\ 0 \\ 0 \\ 0 \\ 1 \\ 1 \\ 0 \end{bmatrix}, \begin{bmatrix} 0 \\ 0 \\ 0 \\ 0 \\ 0 \\ 0 \\ 0 \\ 0 \\ 0 \\ 1 \\ 0 \\ 1 \end{bmatrix} \right\rangle.$$

Thus,

$$\mathcal{H}^3(\widehat{x_1^3}) \quad = \quad \frac{\ker d^3}{\operatorname{im} d^4} = \frac{\mathbb{Z}_{(v_-\otimes v_-\otimes v_-)}}{0} = \mathbb{Z}_{(v_-\otimes v_-\otimes v_-)}.$$

To compute the homology of the next level, we first cancel out the terms that appear in both $\ker d^2$ and $\operatorname{im} d^3$, and then use a special trick: Note that the last three summands of $\ker d^2$ make up all of $\mathbb{Z}^3_{(v_-\otimes v_-)}$, where the last three summands of $\operatorname{im} d^3$ span the subspace of $\mathbb{Z}^3_{(v_-\otimes v_-)}$ generated by vectors $(0,1,1)$, $(1,1,0)$ and $(1,0,1)$. Now, form a matrix whose columns are these vectors. Since the eigenvalues of this matrix are $-1, 1$, and 2, we can write:

$$\frac{\mathbb{Z}^3}{\langle (0,1,1),(1,1,0),(1,0,1)\rangle} = \frac{\mathbb{Z}}{2\mathbb{Z}} \oplus \frac{\mathbb{Z}}{\mathbb{Z}_1} \oplus \frac{\mathbb{Z}}{\mathbb{Z}_{-1}} = \mathbb{Z}_2.$$

Reducing the remaining matrices of kernel of d^2 and image of d^3 into reduced row echelon form, quotient $\frac{\ker d^2}{\operatorname{im} d^3}$ becomes isomorphic to $\mathbb{Z}$. Hence,

$$\mathcal{H}^2(\widehat{x_1^3}) \quad = \quad \frac{\ker d^2}{\operatorname{im} d^3} = \mathbb{Z} \oplus \mathbb{Z}_2.$$

The range of d^2 is $\mathbb{Z}_{(v_+,v_+,0)} \oplus \mathbb{Z}_{(v_+,0,-v_+)} \oplus \mathbb{Z}_{(0,v_+,v_+)} \oplus \mathbb{Z}_{(v_-,v_-,0)} \oplus \mathbb{Z}_{(v_-,0,-v_-)} \oplus \mathbb{Z}_{(0,v_-,v_-)}$ and the kernel of d^1 is $\mathbb{Z}_{(v_+,v_+,0)} \oplus \mathbb{Z}_{(0,v_+,v_+)} \oplus \mathbb{Z}_{(v_+,0,-v_+)} \oplus \mathbb{Z}_{(v_-,v_-,0)} \oplus \mathbb{Z}_{(0,v_-,v_-)} \oplus \mathbb{Z}_{(v_-,0,-v_-)}$. Since $\ker d^1 = \operatorname{im} d^2$,

$$\mathcal{H}^1(\widehat{x_1^3}) = 0.$$

It is clear from the chain complex that the kernel of d^0 is the full space $V \otimes V$.

$$\mathcal{H}^0(\widehat{x_1^3}) = \frac{\mathbb{Z}_{(v_+\otimes v_+)} \oplus \mathbb{Z}_{(v_-\otimes v_+)} \oplus \mathbb{Z}_{(v_+\otimes v_-)} \oplus \mathbb{Z}_{(v_-\otimes v_-)}}{\mathbb{Z}_{(v_-\otimes v_+ + v_+\otimes v_-)} \oplus \mathbb{Z}_{(v_-\otimes v_-)}} = \mathbb{Z}_{(v_+\otimes v_+)} \oplus \mathbb{Z}.$$

3.2. Homology of Δ^{2k+1}

We now compute the homology of braid link Δ^{2k+1}, where $\Delta = x_1x_2x_1$. The canonical form of this braid is $\Delta^{2k+1} = x_1^{2k+2}x_2x_1^2x_2^2x_1^2\cdots x_2^2x_1^2x_1^2$, having $2k+2$ factors; you can see Δ^3 in Figure 11.

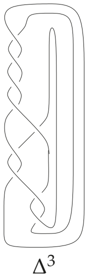

Figure 11. Δ^3.

The co-chain complex of the link Δ^{2k+1} is $0 \xrightarrow{d^{-1}} V^{\otimes 3} \xrightarrow{d^0} \bigoplus_{6k+3} V^{\otimes 2} \xrightarrow{d^1} \bigoplus_{\binom{2k+1}{1}\binom{4k+2}{1}} V^{\otimes 1} \bigoplus_{\binom{2k+1}{1}+\binom{4k+2}{2}} V^{\otimes 3} \xrightarrow{d^3} \bigoplus_{\binom{2k+1}{1}\binom{4k+2}{2}+\binom{2k+1}{2}\binom{4k+2}{1}} V^{\otimes 1} \bigoplus_{\binom{2k+1}{1}+\binom{4k+2}{2}} V^{\otimes 3} \xrightarrow{d^4} \cdots \xrightarrow{d^{6k+1}} \bigoplus_{\binom{4k+2}{1}} V^{\otimes 2k+1} \bigoplus_{\binom{2k+1}{1}} V^{\otimes 2k+3} \xrightarrow{d^{6k+2}} V^{\otimes 2k+2} \xrightarrow{d^{6k+3}} 0.$

We now represent the differential maps in terms of matrices. The matrix representing differential d^0 has order $24k + 12 \times 8$ and is

$$d^0 = \begin{pmatrix} A & 0 & 0 & 0 & 0 & 0 & 0 & 0 \\ 0 & A & B & 0 & 0 & 0 & 0 & 0 \\ 0 & 0 & C & A & 0 & 0 & 0 & 0 \\ 0 & 0 & 0 & 0 & C & A & B & 0 \end{pmatrix}.$$

Here, each matrix A, B, and C has a $(6k+3) \times 1$ order:

$$\begin{aligned} A &= \begin{pmatrix} 1 & 1 & 1 & 1 & 1 & 1 & 1 & \cdots & 1 \end{pmatrix}^t \\ B &= \begin{pmatrix} 0 & 1 & 0 & 0 & 1 & 0 & 0 & \cdots & 1 & 0 \end{pmatrix}^t \\ C &= \begin{pmatrix} 1 & 0 & 1 & 1 & 0 & 1 & 1 & \cdots & 0 & 1 \end{pmatrix}^t \end{aligned}$$

Since $\ker d^0 = \mathbb{Z}_{v_-\otimes v_-\otimes v_-} \oplus \mathbb{Z}_{v_+\otimes v_-\otimes v_- - v_-\otimes v_+\otimes v_- + v_+\otimes v_-\otimes v_-}$ and $\operatorname{im} d^{-1} = 0$, the homology at this level is

$$\mathcal{H}^0(\Delta^{2k+1}) = \mathbb{Z}_{v_-\otimes v_-\otimes v_-} \oplus \mathbb{Z}_{v_+\otimes v_-\otimes v_- - v_-\otimes v_+\otimes v_- + v_+\otimes v_-\otimes v_-}.$$

Now, we go for differential map d^1. The matrix that represents it has an order of $20(6k^2+3) \times 4(6k+3)$ and is

$$d^1 = \begin{pmatrix} R_1 & 0 & 0 & 0 \\ 0 & R_1 & R_1 & 0 \\ 0 & 0 & 0 & 0 \\ 0 & 0 & 0 & 0 \\ 0 & 0 & 0 & 0 \\ R_2 & 0 & 0 & 0 \\ R_2 & 0 & 0 & 0 \\ 0 & R_2 & 0 & 0 \\ 0 & 0 & R_2 & 0 \\ 0 & 0 & 0 & R_2 \\ 0 & R_3 & R_4 & 0 \\ \vdots & \vdots & \ddots & \vdots \\ 0 & 0 & R_{n-1} & R_n \end{pmatrix}.$$

The order of each of the matrix R_i is $(12k+6) \times (6k+3)$:

$$R_1 = \begin{pmatrix} 1 & -1 & 0 & 0 & 0 & \dots & 0 & 0 \\ 1 & 0 & 0 & 0 & -1 & 0 & \dots & 0 \\ 1 & 0 & 0 & 0 & 0 & 0 & \dots & -1 \\ 0 & 1 & -1 & 0 & 0 & 0 & \dots & 0 \\ 0 & 1 & 0 & -1 & 0 & 0 & \dots & 0 \\ 0 & 1 & 0 & 0 & 0 & -1 & \dots & 0 \\ 0 & 1 & 0 & 0 & 0 & 0 & \dots & -1 \\ \vdots & \vdots & \vdots & \vdots & \vdots & \vdots & \vdots & \vdots \\ 0 & 0 & 0 & 0 & 0 & \dots & 1 & -1 \end{pmatrix},$$

$$R_2 = \begin{pmatrix} 1 & 0 & -1 & 0 & 0 & \dots & 0 & 0 \\ 1 & 0 & \dots & -1 & 0 & 0 & 0 & 0 \\ 1 & 0 & \dots & 0 & 0 & -1 & 0 & 0 \\ 1 & 0 & \dots & 0 & 0 & 0 & -1 & 0 \\ 1 & 0 & \dots & 0 & 0 & 0 & 0 & -1 \\ 0 & 1 & 0 & 0 & -1 & 0 & \dots & 0 \\ 0 & 1 & \dots & 0 & 0 & -1 & 0 & 0 \\ \vdots & \vdots & \vdots & \vdots & \vdots & \vdots & \vdots & \vdots \\ 0 & 0 & 0 & 0 & \dots & 1 & 0 & -1 \end{pmatrix},$$

$$R_3 = \begin{pmatrix} 1 & 0 & -1 & 0 & 0 & \dots & 0 & 0 \\ 1 & 0 & \dots & -1 & 0 & 0 & 0 & 0 \\ 1 & 0 & \dots & 0 & 0 & -1 & 0 & 0 \\ 1 & 0 & \dots & 0 & 0 & 0 & -1 & 0 \\ 1 & 0 & \dots & 0 & 0 & 0 & 0 & -1 \\ 0 & 0 & 1 & -1 & 0 & 0 & \dots & 0 \\ 0 & 0 & 1 & 0 & 0 & -1 & \dots & 0 \\ 0 & 0 & 1 & 0 & \dots & -1 & 0 & 0 \\ 0 & 0 & 1 & 0 & \dots & 0 & 0 & -1 \\ \vdots & \vdots & \vdots & \vdots & \vdots & \vdots & \vdots & \vdots \\ 0 & 0 & 0 & 0 & \dots & 1 & 0 & -1 \end{pmatrix},$$

$$R_4 = \begin{pmatrix} 0 & 0 & 0 & 0 & 0 & \dots & 0 & 0 \\ \vdots & \vdots & \vdots & \vdots & \vdots & \vdots & \vdots & \vdots \\ 0 & 1 & 0 & 0 & -1 & 0 & \dots & 0 \\ 0 & 1 & \dots & 0 & 0 & -1 & 0 & 0 \\ \vdots & \vdots & \vdots & \vdots & \vdots & \vdots & \vdots & \vdots \\ 0 & 0 & 0 & 0 & 1 & 0 & \dots & -1 \end{pmatrix},$$

and, at the end, all rows of matrix R_n are zero except for the last row, which is

$$\begin{pmatrix} 0 & \dots & 0 & 0 & 1 & 0 & \dots & -1 \end{pmatrix}.$$

Here, $\ker d^1 = \mathbb{Z}_{(v_+\otimes v_+ + v_+\otimes v_+ + v_+\otimes v_+ + v_+\otimes v_+ + v_+\otimes v_+ + v_+\otimes v_+ + v_+\otimes v_+ + v_+\otimes v_+)}$
$\oplus\, \mathbb{Z}_{(v_+\otimes v_- + v_+\otimes v_- + v_+\otimes v_- + v_+\otimes v_- + v_+\otimes v_- + v_+\otimes v_- + v_+\otimes v_- + v_+\otimes v_-)}$
$\oplus\, \mathbb{Z}_{(v_-\otimes v_+ + v_-\otimes v_+ - v_+\otimes v_- - v_+\otimes v_- - v_+\otimes v_-)}$
$\oplus\, \mathbb{Z}_{(v_+\otimes v_- + v_+\otimes v_- + v_+\otimes v_- + v_-\otimes v_+ + v_-\otimes v_+ + v_-\otimes v_+ + v_-\otimes v_+ + v_-\otimes v_+)}$
$\oplus\, \mathbb{Z}_{(v_-\otimes v_- + v_-\otimes v_-)} \oplus \mathbb{Z}_{(v_-\otimes v_- + v_-\otimes v_- + v_-\otimes v_- + v_-\otimes v_- + v_-\otimes v_-)}$
and
$\operatorname{im} d^0 = \mathbb{Z}_{(v_+\otimes v_+)} \oplus \mathbb{Z}_{(v_+\otimes v_-)} \oplus \mathbb{Z}_{(v_-\otimes v_+)} \oplus \mathbb{Z}_{(v_-\otimes v_-)} \oplus \mathbb{Z}_{(v_+\otimes v_+)} \oplus \mathbb{Z}_{(v_+\otimes v_-)} \oplus \mathbb{Z}_{(v_-\otimes v_+)}$.
Since the number of $\mathbb{Z}$ spaces appear in the kernel of d^1, it is exactly the same as the image of d^0, $\mathcal{H}^1(\Delta^{2k+1}) = 0$.
The image of d^1 is obvious. We just need the kernel of d^2. The matrix that represents d^2 has an order of $(2^{6k+3} + 2^{2k+2})(6k+5) \times 20(6k^2+3)$ and is

$$\begin{pmatrix} S_1 & S_2 & S_3 & S_4 & S_5 & S_6 & S_7 & S_8 & S_9 & \dots & S_{20} \\ S_{21} & S_{21} & S_{22} & S_{23} & S_{24} & S_{25} & S_{26} & S_{27} & S_{28} & \dots & S_{40} \\ \vdots & \vdots & \vdots & \vdots & \vdots & \vdots & \vdots & \vdots & \vdots & \vdots & \vdots \\ S_{n-19} & S_{n-18} & S_{n-17} & S_{n-16} & S_{n-15} & S_{n-14} & S_{n-13} & S_{n-12} & S_{n-11} & \dots & S_n \end{pmatrix}.$$

Here, the order of each S_i is $(4k^2+3) \times (6k^2+3)$, and is:

$$S_1 = \begin{pmatrix} 0 & -1 & 0 & 0 & 0 & 0 & \dots & 0 \\ 1 & 0 & 0 & 0 & 0 & 0 & \dots & 1 \\ 1 & 0 & 0 & 0 & 0 & 0 & \dots & 1 \\ 0 & 0 & 0 & 0 & 0 & 0 & \dots & 0 \\ 0 & 0 & -1 & 0 & 0 & 0 & \dots & 0 \\ 1 & 0 & 0 & 0 & 0 & 0 & \dots & 0 \\ 1 & 0 & 0 & 0 & 0 & 0 & \dots & 0 \\ \vdots & \vdots & \vdots & \vdots & \vdots & \vdots & \vdots & \vdots \\ 0 & 0 & 0 & 0 & 0 & 0 & \dots & 0 \end{pmatrix}, S_2 = \begin{pmatrix} 0 & 0 & 0 & 0 & 0 & 0 & \dots & 0 \\ 0 & 0 & 0 & 0 & 0 & 0 & \dots & 0 \\ 0 & 0 & 0 & 0 & 0 & 0 & \dots & 0 \\ 0 & 0 & 0 & 0 & 0 & 0 & \dots & 0 \\ 0 & 0 & 0 & 0 & 0 & 0 & \dots & 0 \\ 1 & 0 & 0 & 0 & 0 & 0 & \dots & 0 \\ \vdots & \vdots & \vdots & \vdots & \vdots & \vdots & \vdots & \vdots \\ 1 & 0 & 0 & 0 & 0 & 0 & \dots & 0 \end{pmatrix},$$

$$S_3 = \begin{pmatrix} 0 & 0 & 0 & 0 & 0 & 0 & \dots & 0 \\ 0 & -1 & 0 & 0 & 0 & 0 & \dots & 0 \\ 0 & 0 & 0 & 0 & 0 & 0 & \dots & 0 \\ 1 & 0 & 0 & 0 & 0 & 0 & \dots & 1 \\ 0 & 0 & -1 & 0 & 0 & 0 & \dots & 0 \\ 0 & 0 & 0 & 0 & 0 & 0 & \dots & 0 \\ \vdots & \vdots & \vdots & \vdots & \vdots & \vdots & \vdots & \vdots \\ 0 & 0 & 0 & 0 & 0 & 0 & \dots & 0 \end{pmatrix}, S_4 = \begin{pmatrix} 0 & 0 & 0 & 0 & 0 & 0 & \dots & 0 \\ 0 & 0 & 0 & 0 & 0 & 0 & \dots & 0 \\ -1 & 0 & 0 & 0 & 0 & 0 & \dots & 0 \\ 0 & 0 & 0 & 0 & 0 & 0 & \dots & 0 \\ 0 & 0 & 0 & 0 & 0 & 0 & \dots & 0 \\ 0 & 0 & 0 & 0 & 0 & 0 & \dots & 0 \\ 0 & -1 & 0 & 0 & 0 & 0 & \dots & 0 \\ \vdots & \vdots & \vdots & \vdots & \vdots & \vdots & \vdots & \vdots \\ 0 & 0 & 0 & 0 & 0 & 0 & \dots & 0 \end{pmatrix},$$

$$\vdots$$

$$S_{n-2}=\begin{pmatrix} 0 & 0 & 0 & 0 & 0 & 0 & \dots & 0\\ 0 & 0 & 0 & 0 & 0 & 0 & \dots & 0\\ 0 & 0 & -1 & 0 & 0 & 0 & \dots & 0\\ 0 & 0 & 0 & 0 & 0 & 0 & \dots & 0\\ 0 & 0 & 0 & 0 & 0 & 0 & \dots & 0\\ 0 & 0 & 0 & 0 & 0 & 0 & \dots & 0\\ \vdots & \vdots & \vdots & \vdots & \vdots & \vdots & \vdots & \vdots\\ 0 & 0 & 0 & 0 & 0 & 0 & \dots & 0 \end{pmatrix},$$

$$S_{n-1}=\begin{pmatrix} 0 & 0 & 0 & 0 & 0 & 0 & \dots & 0\\ 0 & 0 & 0 & 0 & 0 & 0 & \dots & 0\\ 0 & 0 & 0 & 0 & 0 & 0 & \dots & 0\\ -1 & 0 & 0 & 0 & 0 & 0 & \dots & -1\\ 0 & 0 & 0 & 0 & 0 & 0 & \dots & 0\\ 0 & 0 & 0 & 0 & 0 & 0 & \dots & 0\\ \vdots & \vdots & \vdots & \vdots & \vdots & \vdots & \vdots & \vdots\\ 0 & -1 & 0 & 0 & 0 & 0 & \dots & 0 \end{pmatrix},$$

$$S_{n}=\begin{pmatrix} 0 & 0 & 0 & 0 & 0 & 0 & \dots & 0\\ 0 & 0 & 0 & 0 & 0 & 0 & \dots & 0\\ 0 & 0 & 0 & 0 & 0 & 0 & \dots & 0\\ 0 & 0 & 0 & 0 & 0 & 0 & \dots & 0\\ 0 & 0 & 0 & 0 & 0 & 0 & \dots & 0\\ 0 & 0 & 0 & 0 & 0 & 0 & \dots & 0\\ \vdots & \vdots & \vdots & \vdots & \vdots & \vdots & \vdots & \vdots\\ -1 & 0 & 0 & 0 & 0 & 0 & \dots & 0 \end{pmatrix}.$$

Thus, $\mathcal{H}^2(\Delta^{2k+1})=\mathbb{Z}\oplus\mathbb{Z}$. Differential d^{6k+2} of order $(2^{2k+2})\times(2k+1)(2^{2k+2}+2^{2k+3})$ is

$$d^{6k+2}=\begin{pmatrix} Y_1 & Y_2 & Y_3 & Y_4 & Y_5 & \dots & Y_{6k+3}\end{pmatrix},$$

where Y_i are matrices, each having an order of $2^{2k+2}\times 2^{2k+2}$:

$$Y_1=\begin{pmatrix} 0 & -1 & 0 & 0 & 1 & 0 & \cdots & 0\\ 0 & 0 & 0 & 0 & 0 & 0 & \cdots & 0\\ \vdots & \vdots & \vdots & \vdots & \vdots & \vdots & \vdots & \vdots\\ 0 & 0 & 1 & -1 & 0 & -1 & \cdots & 0\\ 1 & 0 & 1 & -1 & 0 & -1 & \cdots & 0\\ 1 & 0 & 0 & 0 & 0 & 0 & \cdots & -1\\ 0 & 0 & 0 & 0 & 0 & 0 & \cdots & -1\\ \vdots & \vdots & \vdots & \vdots & \vdots & \vdots & \vdots & \vdots\\ 0 & 0 & 0 & 0 & 0 & 0 & \cdots & 0 \end{pmatrix},$$

$$Y_2=\begin{pmatrix} 0 & 0 & \cdots & 0 & 0 & 0 & 0 & 0 & 0\\ -1 & 0 & \cdots & 0 & 0 & 0 & 0 & 0 & 0\\ \vdots & \vdots & \vdots & \vdots & \vdots & \vdots & \vdots & \vdots & \vdots\\ 0 & 1 & \cdots & 1 & 0 & -1 & 0 & 0 & 1\\ 0 & 1 & \cdots & 1 & 0 & 0 & 1 & -1 & 0\\ 0 & 0 & \cdots & 0 & 1 & 0 & 1 & -1 & 0 \end{pmatrix},$$

$$Y_3 = \begin{pmatrix} 0 & 0 & 0 & 0 & 0 & 0 & 0 & 0 & \cdots \\ 0 & 0 & 0 & 0 & 0 & 0 & 0 & 0 & \cdots \\ 0 & 0 & -1 & 0 & 0 & 0 & 0 & 0 & \cdots \\ 0 & 0 & 0 & 0 & 0 & -1 & 0 & 0 & \cdots \\ \vdots & \vdots & \vdots & \vdots & \vdots & \vdots & \vdots & \vdots & \vdots \\ -1 & 1 & 0 & 0 & 0 & 0 & 0 & 0 & \cdots \\ -1 & 1 & 0 & 1 & 0 & 0 & 1 & -1 & \cdots \end{pmatrix},$$

$$Y_4 = \begin{pmatrix} 0 & 0 & 0 & 0 & 0 & 0 & 0 & \cdots \\ 0 & 0 & 0 & 0 & 0 & 0 & 0 & \cdots \\ \vdots & \vdots & \vdots & \vdots & \vdots & \vdots & \vdots & \vdots \\ 0 & 1 & 0 & 0 & -1 & 0 & 0 & \cdots \\ 0 & 0 & 0 & 0 & 0 & 0 & 0 & \cdots \\ -1 & 0 & -1 & 1 & 0 & 0 & 0 & \cdots \\ -1 & 0 & -1 & 1 & 0 & 0 & 0 & \cdots \\ \vdots & \vdots & \vdots & \vdots & \vdots & \vdots & \vdots & \vdots \\ 0 & 0 & 0 & 0 & 0 & 0 & 1 & \cdots \end{pmatrix},$$

$$\vdots$$

$$Y_i = \begin{pmatrix} 0 & 0 & 0 & 0 & 0 & 0 & 0 & 0 & \cdots \\ 0 & 0 & 0 & 0 & 0 & 0 & 0 & 0 & \cdots \\ \vdots & \vdots & \vdots & \vdots & \vdots & \vdots & \vdots & \vdots & \vdots \\ 0 & -1 & 0 & 0 & 0 & 0 & 0 & 0 & \cdots \\ 0 & 0 & 0 & 0 & 0 & 0 & 0 & 0 & \cdots \\ 0 & 0 & 0 & 0 & -1 & 1 & -1 & 0 & \cdots \\ 0 & 0 & 1 & -1 & 0 & 0 & 0 & -1 & \cdots \\ -1 & 0 & 0 & 0 & 0 & 0 & 0 & 0 & \cdots \\ \vdots & \vdots & \vdots & \vdots & \vdots & \vdots & \vdots & \vdots & \vdots \\ 0 & 0 & 0 & 0 & 0 & 0 & 0 & 0 & \cdots \end{pmatrix},$$

$$\vdots$$

$$Y_{6k+3} = \begin{pmatrix} 0 & 0 & 0 & 0 & 0 & 0 & 0 & \cdots & 0 \\ 0 & 0 & 0 & 0 & 0 & 0 & 0 & \cdots & 0 \\ 0 & 0 & 0 & 0 & 0 & 0 & 0 & \cdots & 0 \\ 0 & 0 & 0 & 0 & 0 & 0 & 0 & \cdots & 0 \\ \vdots & \vdots & \vdots & \vdots & \vdots & \vdots & \vdots & \vdots & \vdots \\ 0 & -1 & 1 & -1 & 0 & 0 & 0 & \cdots & 0 \end{pmatrix}.$$

Here $\ker d^{6k+3}$ is the full space $V^{\otimes 2k+1}$ and the $\operatorname{im} d^{6k+2}$ is

$$\begin{aligned}
&\mathbb{Z}_{(v_+\otimes v_+\otimes v_+\otimes v_+)} \oplus \mathbb{Z}_{(v_+\otimes v_-\otimes v_+\otimes v_+ + v_-\otimes v_+\otimes v_+\otimes v_+)} \\
&\oplus \mathbb{Z}_{(v_+\otimes v_+\otimes v_-\otimes v_+ + v_+\otimes v_-\otimes v_+\otimes v_+)} \mathbb{Z}_{(v_+\otimes v_-\otimes v_+\otimes v_+)} \\
&\oplus \mathbb{Z}_{(v_+\otimes v_-\otimes v_+\otimes v- + v_-\otimes v_+\otimes v_+\otimes v_-)} \oplus \mathbb{Z}_{(v_+\otimes v_+\otimes v_-\otimes v- + v_+\otimes v_-\otimes v_+\otimes v_-)} \\
&\oplus \mathbb{Z}_{(v_+\otimes v_+\otimes v_+\otimes v-)} \oplus \mathbb{Z}_{(v_+\otimes v_-\otimes v_-\otimes v+ + v_-\otimes v_+\otimes v_-\otimes v_+)} \\
&\oplus \mathbb{Z}_{(v_+\otimes v_-\otimes v_+\otimes v- + v_-\otimes v_+\otimes v_+\otimes v_-)} \oplus \mathbb{Z}_{(v_+\otimes v_-\otimes v_-\otimes v+)} \oplus \mathbb{Z}_{(v_-\otimes v_-\otimes v_+\otimes v+)} \\
&\oplus \mathbb{Z}_{(v_+\otimes v_+\otimes v_-\otimes v+)} \oplus \mathbb{Z}_{(v_-\otimes v_+\otimes v_-\otimes v+ + v_-\otimes v_-\otimes v_+\otimes v_+)} \\
&\oplus \mathbb{Z}_{(v_+\otimes v_-\otimes v_-\otimes v- + v_-\otimes v_+\otimes v_-\otimes v_-)} \oplus \mathbb{Z}_{(v_+\otimes v_-\otimes v_-\otimes v-)} \oplus \mathbb{Z}_{(v_-\otimes v_-\otimes v_+\otimes v-)} \\
&\oplus \mathbb{Z}_{(v_-\otimes v_-\otimes v_-\otimes v+)} \oplus \mathbb{Z}_{(v_+\otimes v_-\otimes v_+\otimes v-)} \oplus \mathbb{Z}_{(v_-\otimes v_-\otimes v_-\otimes v-)}
\end{aligned}$$

$$\oplus \mathbb{Z}_{(v_+\otimes v_+\otimes v_-\otimes v-)} \oplus \mathbb{Z}_{(v_-\otimes v_+\otimes v_+\otimes v-)}$$
$$\oplus \mathbb{Z}_{(v_-\otimes v_+\otimes v_-\otimes v+)} \oplus \mathbb{Z}_{(v_-\otimes v_+\otimes v_-\otimes v-)}.$$

Thus, $\mathcal{H}^{6k+3}(\Delta^3) = 0$, and we finally obtain the result:

Theorem 4. *The Khovanov homology of the link* Δ^{2k+1} *is*

$$\mathcal{H}^i(\Delta^{2k+1}) = \begin{cases} 0 & 6k \leq i \leq 3 \\ \mathbb{Z} \oplus \mathbb{Z} & i = 2 \\ 0 & i = 1 \\ \mathbb{Z} \oplus \mathbb{Z} & i = 0 \end{cases}$$

The following result gives some homology groups of $\Delta^{2k+1}x_2 = x_1^{2k+3}\ x_2x_1^2x_2^2x_1^2 \cdots x_2^2x_1^2x_1^2$.

Theorem 5.

$$\mathcal{H}^i(\Delta^{2k+1}x_2) = \begin{cases} \mathbb{Z} \oplus \mathbb{Z} & i = 0 \\ 0 & i = 1 \\ 0 & i = 6k+4 \end{cases}$$

Proof. The cochain complex of link $\Delta^{2k+1}x_2$ is

$$0 \xrightarrow{d^{-1}} V^{\otimes 3} \xrightarrow{d^0} \oplus_{6k+4} V^{\otimes 2} \xrightarrow{d^1} \oplus_{\binom{2k+2}{1}\binom{4k+2}{1}} V^{\otimes 1} \oplus_{\binom{2k+2}{2}+\binom{4k+2}{2}} V^{\otimes 3}$$
$$\xrightarrow{d^2} \oplus_{\binom{2k+2}{1}\binom{4k+2}{2}+\binom{2k+2}{2}\binom{4k+2}{1}} V^{\otimes 2} \oplus_{\binom{2k+2}{1}+\binom{4k+2}{1}} V^{\otimes 4} \xrightarrow{d^3}$$
$$\cdots \xrightarrow{d^{6k+2}} \oplus_{\binom{2k+2}{1}} V^{\otimes 2k} \oplus_{\binom{4k+2}{1}} V^{\otimes 2k+2} \xrightarrow{d^{6k+3}} V^{\otimes 2k+1} \xrightarrow{d^{6k+4}} 0$$

Differential d^0 having an order of $24k + 16 \times 8$ is

$$d^0 = \begin{pmatrix} A & 0 & 0 & 0 & 0 & 0 & 0 & 0 \\ 0 & A & B & 0 & 0 & 0 & 0 & 0 \\ 0 & 0 & C & A & 0 & 0 & 0 & 0 \\ 0 & 0 & 0 & 0 & C & A & B & 0 \end{pmatrix},$$

where A, B, and C, each having an order of $(6k+4) \times 1$, are:

$$\begin{aligned} A &= \begin{pmatrix} 1 & 1 & 1 & 1 & 1 & 1 & 1 & \cdots & 1 \end{pmatrix}^t \\ B &= \begin{pmatrix} 0 & 1 & 0 & 0 & 1 & 0 & 0 & \cdots & 0 & 1 \end{pmatrix}^t \\ C &= \begin{pmatrix} 1 & 0 & 1 & 1 & 0 & 1 & 1 & \cdots & 1 & 0 \end{pmatrix}^t \end{aligned}$$

Since $\operatorname{im} d^{-1} = 0$ and $\ker d^0 = \mathbb{Z}_{(v_+\otimes v_-\otimes v_- - v_-\otimes v_+\otimes v_- + v_-\otimes v_-\otimes v_+)} \oplus \mathbb{Z}_{(v_-\otimes v_-\otimes v_-)}$, $\mathcal{H}^0(\Delta^{2k+1}x_2) = \mathbb{Z}_{(v_+\otimes v_-\otimes v_- - v_-\otimes v_+\otimes v_- + v_-\otimes v_-\otimes v_+)} \oplus \mathbb{Z}_{(v_-\otimes v_-\otimes v_-)}$.

Now, differential d^1 of an order of $18(6k^2+6) \times 4(6k+4)$ is

$$d^1 = \begin{pmatrix} M_1 & -M_1 & 0 & 0 \\ M_1 & 0 & -M_1 & 0 \\ M_1 & 0 & 0 & -M_1 \\ M_2 & -M_2 & 0 & 0 \\ M_2 & 0 & -M_2 & 0 \\ M_3 & -M_3 & 0 & 0 \\ M_3 & 0 & -M_3 & 0 \\ 0 & M_4 & -M_4 & 0 \\ 0 & M_4 & 0 & -M_4 \\ \vdots & \vdots & \ddots & \vdots \\ 0 & 0 & M_{n-1} & M_n \end{pmatrix},$$

where the order of each M_i is $(16k+2) \times (6k+4)$ and is

$$M_1 = \begin{pmatrix} -1 & 0 & 0 & 0 & 1 & 0 & \dots & 0 \\ 0 & -1 & -1 & 0 & 0 & 1 & \dots & 0 \\ 0 & 0 & 0 & 0 & 0 & 0 & \dots & 0 \\ 0 & 0 & 0 & 0 & 0 & 0 & \dots & 0 \\ -1 & 0 & 0 & 0 & 0 & 0 & \dots & 0 \\ -1 & 0 & 0 & 0 & 0 & 0 & \dots & 0 \\ 0 & -1 & 0 & 0 & 0 & 0 & \dots & 1 \\ \vdots & \vdots & \vdots & \vdots & \vdots & \vdots & \vdots & \vdots \\ 0 & 0 & 0 & -1 & 0 & \dots & 0 & 0 \end{pmatrix},$$

$$M_2 = \begin{pmatrix} 0 & \dots & -1 & 0 & \dots & 0 & 0 \\ 0 & \dots & 0 & 0 & 0 & 0 & 0 \\ 0 & \dots & 0 & -1 & 0 & 0 & 0 \\ 0 & \dots & 0 & 0 & -1 & 0 & 0 \\ 0 & \dots & 0 & 0 & -1 & 0 & 0 \\ 0 & \dots & -1 & 0 & \dots & 0 & 0 \\ 0 & \dots & 0 & -1 & -1 & 0 & 0 \\ \vdots & \vdots & \vdots & \vdots & \vdots & \vdots & \vdots \\ 0 & \dots & 0 & -1 & 0 & 0 & 0 \end{pmatrix},$$

$$M_3 = \begin{pmatrix} 0 & \dots & -1 & 0 & 0 & 0 & 0 & 0 & 0 \\ 0 & \dots & 0 & -1 & -1 & 0 & 0 & 0 & 0 \\ 0 & \dots & 0 & 0 & 0 & 0 & 0 & 0 & 0 \\ 0 & \dots & -1 & 0 & 0 & 1 & 0 & 0 & 0 \\ 0 & \dots & -1 & 0 & 0 & 1 & 0 & 0 & 0 \\ 0 & \dots & 0 & 0 & 0 & 0 & 0 & 0 & -1 \\ 0 & \dots & 0 & 0 & 0 & 0 & 0 & 0 & -1 \\ \vdots & \vdots & \vdots & \vdots & \vdots & \vdots & \vdots & \vdots & 0 \\ 0 & \dots & 0 & 0 & 0 & 0 & 0 & 0 & 0 \end{pmatrix},$$

$$M_4 = \begin{pmatrix} -1 & 0 & 0 & 0 & \dots & \dots & \dots & 1 & 0 \\ 0 & -1 & -1 & 0 & \dots & \dots & \dots & 0 & 1 \\ 0 & 0 & 0 & 0 & \dots & \dots & \dots & 0 & 0 \\ 0 & 0 & 0 & 0 & \dots & \dots & \dots & 0 & 0 \\ \vdots & \vdots & \vdots & \vdots & \vdots & \vdots & \vdots & \vdots & 0 \\ 0 & -1 & 0 & 0 & \dots & \dots & \dots & 0 & 0 \\ 0 & 0 & -1 & 0 & \dots & \dots & \dots & 0 & 0 \\ 0 & 0 & 0 & -1 & 0 & 0 & \dots & 0 & 0 \end{pmatrix},$$

and $M_n = \begin{pmatrix} 0 & \dots & -1 & 0 & -1 & 0 & \dots & -1 \end{pmatrix}$.

In this case, the kernel of d^1 and image of d^0 contain the same number of $\mathbb{Z}$ spaces. So, $\mathcal{H}^1(\Delta^{2k+1}x_2) = 0$.

Finally, the differential of d^{6k+4} of an order of $2^{2k+1} \times (2k+3)(2^{2k})(2^{2k+1})$ is

$$d^{6k+4} = \begin{pmatrix} Y_1 & Y_2 & Y_3 & Y_4 & \dots & Y_i \end{pmatrix},$$

where each Y_i has an order of $2^{2k+1} \times 6k+4$ and is

$$Y_1 = \begin{pmatrix} -1 & 1 & -1 & 0 & 0 & 1 & 0 & 0 & -1 & 1 \\ 0 & 0 & 0 & 0 & 0 & 0 & 0 & 0 & 0 & 0 \\ \vdots & \vdots & \vdots & 1 & -1 & \vdots & -1 & 1 & \vdots & \vdots \\ \vdots & \vdots & \vdots & 1 & -1 & \vdots & -1 & 1 & \vdots & \vdots \\ \vdots & \vdots & \vdots & \vdots & \vdots & \vdots & \vdots & \vdots & \vdots & \vdots \\ 0 & 0 & 0 & 0 & 0 & 0 & 0 & 0 & 0 & 0 \end{pmatrix},$$

$$Y_2 = \begin{pmatrix} 0 & 0 & 0 & 0 & 0 & 0 & 0 & 0 & 0 & 0 \\ 1 & 1 & -1 & 0 & 0 & 1 & 0 & 0 & -1 & 1 \\ \vdots & \vdots & \vdots & \vdots & \vdots & \vdots & \vdots & \vdots & \vdots & \vdots \\ \vdots & \vdots & \vdots & 1 & -1 & \vdots & -1 & 1 & \vdots & \vdots \\ \vdots & \vdots & \vdots & 1 & -1 & \vdots & -1 & 1 & \vdots & \vdots \\ \vdots & \vdots & \vdots & \vdots & \vdots & \vdots & \vdots & \vdots & \vdots & \vdots \\ 0 & 0 & 0 & 0 & 0 & 0 & 0 & 0 & 0 & 0 \end{pmatrix},$$

$$Y_3 = \begin{pmatrix} 0 & 0 & 0 & 0 & 0 & 0 & 0 & 0 & 0 & 0 \\ \vdots & \vdots & \vdots & \vdots & \vdots & \vdots & \vdots & \vdots & \vdots & \vdots \\ -1 & 1 & -1 & 0 & 0 & 1 & 0 & 0 & -1 & 1 \\ \vdots & \vdots & \vdots & \vdots & \vdots & \vdots & \vdots & \vdots & \vdots & \vdots \\ \vdots & \vdots & \vdots & 1 & -1 & 0 & -1 & 1 & \vdots & \vdots \\ 0 & 0 & 0 & 0 & 0 & 0 & 0 & 0 & 0 & 0 \end{pmatrix},$$

$$Y_4 = \begin{pmatrix} 0 & 0 & 0 & 0 & 0 & 0 & 0 & 0 & 0 & 0 \\ \vdots & \vdots & \vdots & \vdots & \vdots & \vdots & \vdots & \vdots & \vdots & \vdots \\ -1 & 1 & -1 & 0 & 0 & 1 & 0 & 0 & -1 & 1 \\ \vdots & \vdots & \vdots & \vdots & \vdots & \vdots & \vdots & \vdots & \vdots & \vdots \\ 0 & 0 & 0 & 1 & -1 & 0 & -1 & 1 & 0 & 0 \end{pmatrix},$$

$$\vdots$$

$$and \;\; Y_i = \begin{pmatrix} 0 & 0 & 0 & 0 & 0 & 0 & 0 & \cdots & 0 \\ 0 & 0 & 0 & 0 & 0 & 0 & 0 & \cdots & 0 \\ 0 & 0 & 0 & 0 & 0 & 0 & 0 & \cdots & 0 \\ 0 & 0 & 0 & 0 & 0 & 0 & 0 & \cdots & 0 \\ \vdots & \vdots & \vdots & \vdots & \vdots & \vdots & \vdots & \vdots & \vdots \\ -1 & 1 & -1 & 0 & 0 & 1 & 0 & \cdots & 0 \end{pmatrix}.$$

□

It is evident that $\ker d^{6k+4}$ is full space $V^{\otimes 2k+1}$. Moreover, $\operatorname{im} d^{6k+3}$ is also $V^{\otimes 2k+1}$. We also get the Khovanov homology of braid link $\Delta^{2k+1}x_1$:

Theorem 6.

$$\mathcal{H}^i(\Delta^{2k+1}x_1) = \begin{cases} \mathbb{Z} \oplus \mathbb{Z} & i = 0 \\ 0 & i = 1 \\ 0 & i = 6k+1 \end{cases}$$

Proof. The proof is similar to the proof of Theorem 5: Obtain all states, organized them in columns, assign a graded vector space to each state, form chain groups as a direct sum of all vector spaces along a column, and form the chain complex. Then, write the differential maps in terms of matrices using the ordered bases of the chain groups, and compute their kernels and images. Finally, find the Khovanov homology groups using the relation $\mathcal{H}^r(L) = \frac{\ker d^r}{\operatorname{im} d^{r+1}}$. □

4. Conclusions

Although computing the Khovanov homology of links is common in the literature, no general formulae have been given for all families of knots and links. In this paper, we considered a general three-strand braid $x_1x_2x_1x_2\cdots$, which, depending on the powers of Garside element $\Delta = x_1x_2x_1$, is divided into six subclasses, and gave the Khovanov homology of Δ^{2k+1}, $\Delta^{2k+1}x_2$, and $\Delta^{2k+1}x_1$ (To learn more about these classes, see Reference [23–26].) The results particularly cover the 0th, 1st, and top homology groups of these classes, and all homology groups, in general, of link Δ^{2k+1}. We hope the results will help classifying links, and in studying the important properties of these links.

Author Contributions: Formal analysis, Y.C.K.; writing—original draft, A.R.N., Z.I., D.A., and S.M.K.; writing—review and editing, M.M.

Funding: This work was supported by the Dong-A University research fund.

Acknowledgments: We are very thankful to the reviewers for their valuable suggestions to improve the quality of this paper.

Conflicts of Interest: The authors declare that they have no conflicts of interest.

References

1. Khovanov, M. A Categorification of the Jones Polynomial. *Duke Math. J.* **2000**, *101*, 359–426. [CrossRef]
2. Jones, V.F.R. A Polynomial Invariant for Knots via Von Neumann Algebras. *Bull. Am. Math. Soc.* **1985**, *12*, 103–111. [CrossRef]

3. Bar-Natan, D. On Khovanov's categorification of the Jones polynomial. *Algeb. Geom. Topol.* **2002**, *2*, 337–370. [CrossRef]
4. Bar-Natan, D. Khovanov Homology for Tangles and Cobordisms. *Geom. Topol.* **2005**, *9*, 1443–1499. [CrossRef]
5. Bar-Natan, D. Fast Khovanov Homology Computations. *J. Knot Theory Ramif.* **2007**, *16*, 243–255. [CrossRef]
6. Ozsváth, P.; Rasmussen, J.; Szabó, Z. Odd Khovanov Homology. *Algebr. Geom. Topol.* **2013**, *13*, 1465–1488. [CrossRef]
7. Gorsky, E.; Oblomkov, A.; Rasmussen, J. On Stable Khovanov Homology of Torus Knots. *Exp. Math.* **2013**, *22*, 265–281. [CrossRef]
8. Putyra, K.K. On Triply Graded Khovanov Homology. *arXiv* **2015**, arXiv:1501.05293v1.
9. Manion, A. The Rational Khovanov Homology of 3-Strand Pretzel Links. *arXiv* **2011**, arXiv:1110.2239.
10. Nizami, A.R.; Munir, M.; Usman, A. Khovanov Homology of Braid Links. *Rev. UMA* **2016**, *57*, 95–118.
11. Nizami, A.R.; Munir, M.; Sohail, T.; Usman, A. On the Khovanov Homology of 2- and 3-Strand Braid Links. *Adv. Pure Math.* **2016**, *6*, 481–491. [CrossRef]
12. Stosic, M. Properties of Khovanov Homology for Positive Braid Knots. *arXiv* **2006**, arXiv:math/0511529.
13. Rozansky, L. An Infinite Torus Braid Yields a Categorified Jones-Wenzl Projector. *Fundam. Math.* **2014**, *225*, 305–326. [CrossRef]
14. Cooper, B.; Krushkal, V. Categorification of the Jones-Wenzl projectors. *Quantum Topol.* **2012**, *3*, 139–180. [CrossRef] [PubMed]
15. Gorsky, E.; Oblomkov, A.; Rasmussen, J.; Shende, V. Torus Knots and the Rational DAHA. *Duke Math. J.* **2014**, *163*, 2709–2794. [CrossRef]
16. Hogancamp, M. Categorified Young Symmetrizers and Stable Homology of Torus Links. *Geom. Topol.* **2018**, *22*, 2943–3002. [CrossRef]
17. Lipshitz, R.; Sarkar, S. A Khovanov Stable Homotopy Type. *J. Am. Math. Soc.* **2014**, *27*, 983–1042. [CrossRef]
18. Manturov, V. *Knot Theory*; Chapman and Hall/CRC: Boca Raton, FL, USA, 2004.
19. Reidemeister, K. Elementary Begründung der Knotentheorie. *Abh. Math. Sem. Univ. Hambg.* **1927**, *5*, 24–32. [CrossRef]
20. Artin, E. Theory of Braids. *Ann. Math.* **1947**, *48*, 101–126. [CrossRef]
21. Alexander, J. Topological invariants of knots and links. *Trans. Am. Math. Soc.* **1928**, *20*, 275–306. [CrossRef]
22. Kauffman, L.H. State Models and the Jones Polynomial. *Topology* **1987**, *26*, 395–407. [CrossRef]
23. Berceanu, B.; Nizami, A.R. A recurrence relation for the Jones polynomial. *J. Korean Math. Soc.* **2014**, *51*, 443–462. [CrossRef]
24. Khovanov, M. Patterns in Knot Cohomology I. *Exp. Math.* **2003**, *12*, 365–374. [CrossRef]
25. Lawson, T.; Lipshitz, R.; Sarkar, S. The Cube and the Burnside Category. *arXiv* **2015**, arXiv:1505.00512.
26. Reidemeister, K. *Knot Theory*; Chelsea Publ. and Co.: New York, NY, USA, 1948.

symmetry

Article

Volume Preserving Maps Between p-Balls

Adrian Holhoş * and Daniela Roşca

Department of Mathematics, Technical University of Cluj-Napoca, str. Memorandumului 28,
RO-400114 Cluj-Napoca, Romania; daniela.rosca@math.utcluj.ro
* Correspondence: Adrian.Holhos@math.utcluj.ro

Received: 19 October 2019; Accepted: 12 November 2019; Published: 14 November 2019

Abstract: We construct a volume preserving map $\mathcal{U}_p$ from the p-ball $\mathcal{B}_p(r) = \left\{\mathbf{x} \in \mathbb{R}^3,\ \|\mathbf{x}\|_p \leq r\right\}$ to the regular octahedron $\mathcal{B}_1(r')$, for arbitrary $p > 0$. Then we calculate the inverse $\mathcal{U}_p^{-1}$ and we also deduce explicit expressions for $\mathcal{U}_\infty$ and $\mathcal{U}_\infty^{-1}$. This allows us to construct volume preserving maps between arbitrary balls $\mathcal{B}_p(r)$ and $\mathcal{B}_{p'}(\tilde{r})$, and also to map uniform and refinable grids between them. Finally we list some possible applications of our maps.

Keywords: equal volume projection; hierarchical grid

1. Introduction

The p-norms in $\mathbb{R}^3$ have applications in many branches of mathematics, physics and computer science. For $p \geq 1$, the p-norm of the vector $\mathbf{x} = (x, y, z) \in \mathbb{R}^3$ (also called L_p-norm) is defined as

$$\|\mathbf{x}\|_p = \left(|x|^p + |y|^p + |z|^p\right)^{1/p}. \tag{1}$$

For $p = 2$, we arrive at the Euclidean norm, and when $p \to \infty$ the norm is called the infinity norm or the maximum norm and is given by

$$\|\mathbf{x}\|_\infty = \max(|x|, |y|, |z|).$$

When $p \in (0, 1)$, Formula (1) does not define a norm, because the triangle inequality is not satisfied.

2. Preliminaries

For $p > 0$, let $\mathcal{B}_p(r)$ be the 3D p-ball of radius $r > 0$ centered at the origin, defined by

$$\mathcal{B}_p(r) = \left\{\mathbf{x} \in \mathbb{R}^3, \|\mathbf{x}\|_p \leq r\right\}.$$

For finite p the parametric equations of $\mathcal{B}_p(r)$ are

$$\begin{aligned}
x &= \rho\, |\cos\theta|^{2/p}\, |\sin\varphi|^{2/p}\, \operatorname{sgn}(\cos\theta)\, \operatorname{sgn}(\sin\varphi),\\
y &= \rho\, |\sin\theta|^{2/p}\, |\sin\varphi|^{2/p}\, \operatorname{sgn}(\sin\theta)\, \operatorname{sgn}(\sin\varphi),\\
z &= \rho\, |\cos\varphi|^{2/p}\, \operatorname{sgn}(\cos\varphi),
\end{aligned}$$

with $\rho \in [0, r]$, $\theta \in [0, 2\pi)$, $\varphi \in [0, \pi]$.

For $p = 1$ the ball $\mathcal{B}_1(r)$ is the regular octahedron with the vertices on the axes, at distance r from the origin. For $p = \infty$, the set $\mathcal{B}_\infty(r)$ is the cube with edge of length $2r$ and for $p = 2$ the region $\mathcal{B}_2(r)$ represents the Euclidean ball. For $p > 2$ the balls are called *superellipsoids* and they are used in computer graphics (see [1,2], where the author uses the name *superquadrics* to refer to both superellipsoids and supertoroids). Some examples of balls $\mathcal{B}_p(r)$, for different values of p are given in Figure 1.

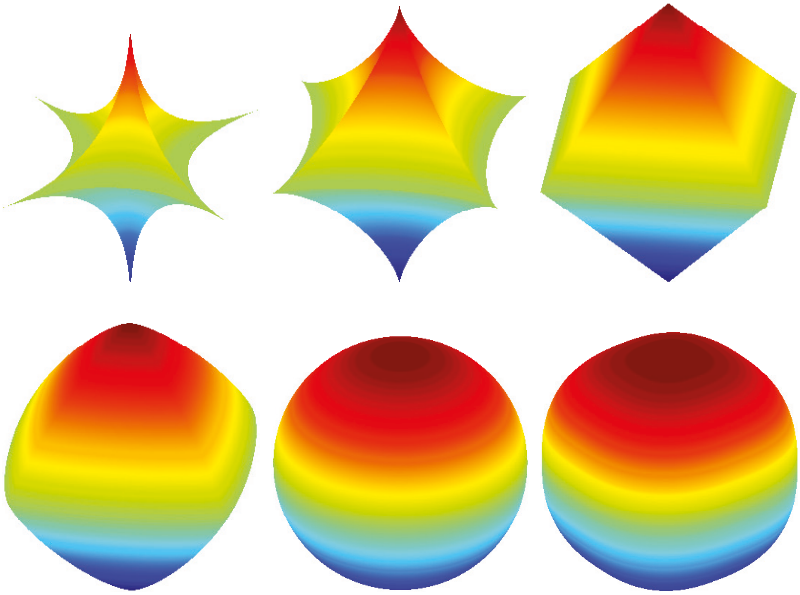

Figure 1. Some balls $\mathcal{B}_p(r)$ for $p = 0.5$, $p = 0.75$, $p = 1$ (**first line**) and $p = 1.2$, $p = 2$ and $p = 2.5$ (**second line**), respectively.

The volume of the 3D p-ball is

$$\begin{aligned}\mathrm{Vol}(\mathcal{B}_p(r)) &= 8\int_0^r \int_0^{(r^p-x^p)^{1/p}} \int_0^{(r^p-x^p-y^p)^{1/p}} \mathrm{d}z\,\mathrm{d}y\,\mathrm{d}x \\ &= 8r^3 \frac{\Gamma^3(1/p+1)}{\Gamma(3/p+1)}.\end{aligned}$$

We notice that the radius r' of the regular octahedron $\mathcal{B}_1(r')$ with the same volume as the p-ball $\mathcal{B}_p(r)$ must be

$$r' = rc_p, \quad \text{with } c_p = \sqrt[3]{6}\frac{\Gamma(1/p+1)}{\sqrt[3]{\Gamma(3/p+1)}}.$$

We will construct a map $\mathcal{U}_p : \mathcal{B}_p(r) \to \mathcal{B}_1(r')$ which preserves the volume, i.e., $\mathcal{U}_p$ satisfies

$$\mathrm{Vol}(D) = \mathrm{Vol}(\mathcal{U}_p(D)), \qquad \text{for all domains } D \subseteq \mathcal{B}_p(r). \tag{2}$$

Consider the bijections $F_{1,p}, F_{2,p} : [0,1] \to [0,1]$, which are particular cases of the regularized incomplete Beta function (also known in statistics as cumulative beta distribution functions)

$$F_{1,p}(t) = \frac{1}{\int_0^1 [u(1-u)]^{\frac{1}{p}-1}\,\mathrm{d}u} \int_0^t u^{\frac{1}{p}-1}(1-u)^{\frac{1}{p}-1}\,\mathrm{d}u, \quad \text{for } t \in [0,1],$$
$$F_{2,p}(t) = \frac{1}{\int_0^1 u^{\frac{2}{p}-1}(1-u)^{\frac{1}{p}-1}\,\mathrm{d}u} \int_0^t u^{\frac{2}{p}-1}(1-u)^{\frac{1}{p}-1}\,\mathrm{d}u, \quad \text{for } t \in [0,1].$$

In the standard notation we have $F_{1,p}(t) = I_t(1/p, 1/p)$ and $F_{2,p}(t) = I_t(2/p, 1/p)$, where I_t is the so-called regularized incomplete beta function defined as $I_t(\alpha, \beta) = B(t; \alpha, \beta)/B(1; \alpha, \beta)$, with

$$B(t; \alpha, \beta) = \int_0^t u^{\alpha-1}(1-u)^{\beta-1} du, \quad \text{for } \alpha, \beta > 0.$$

One has $F_{1,p}(0) = F_{2,p}(0) = 0$ and $F_{1,p}(1) = F_{2,p}(1) = 1$, further $F_{1,p}, F_{2,p}$ are increasing functions. Let $G_{1,p}, G_{2,p} : [0,1] \to [0,1]$ be the inverses (in Mathematica one can use the command `InverseBetaRegularized` for the inverses $G_{1,p}$ and $G_{2,p}$) of the functions $F_{1,p}$ and $F_{2,p}$, respectively.

For $a \in (0, \pi/2)$, let

$$\mathcal{B}_{p,a}(r) = \left\{ (x,y,z) \in \mathcal{B}_p(r),\ x,y,z \geq 0,\ x \tan a \geq y \right\}.$$

Lemma 1. *For $a \in (0, \pi/2)$ we have*

$$\mathrm{Vol}(\mathcal{B}_{p,a}(r)) = \frac{1}{8} F_{1,p}\left(\frac{\tan^p a}{1+\tan^p a}\right) \mathrm{Vol}(\mathcal{B}_p(r)).$$

Proof. The volume of $\mathcal{B}_{p,a}(r)$ can be computed using the double integral

$$\mathrm{Vol}(\mathcal{B}_{p,a}(r)) = \iint_D (r^p - x^p - y^p)^{1/p}\, \mathrm{d}x\, \mathrm{d}y,$$

where $D = \left\{ (x,y) \in \mathbb{R}^2,\ x^p + y^p \leq r^p,\ 0 \leq y \leq x \tan a \right\}$. With the change of variables $x = (\rho \cos t)^{2/p}$ and $y = (\rho \sin t)^{2/p}$ the Jacobian is

$$J = \left(\frac{2}{p}\right)^2 \rho^{\frac{4}{p}-1} (\cos t)^{\frac{2}{p}-1} (\sin t)^{\frac{2}{p}-1}$$

and the new domain of integration is

$$\Delta = \left\{ (\rho, t) \in \mathbb{R}^2,\ 0 \leq \rho \leq r^{p/2},\ 0 \leq t \leq \arctan(\tan^{p/2} a) \right\}.$$

The volume of $\mathcal{B}_{p,a}(r)$ is

$$\mathrm{Vol}(\mathcal{B}_{p,a}(r)) = \frac{4}{p^2} \int_0^{r^{p/2}} (r^p - \rho^2)^{\frac{1}{p}} \rho^{\frac{4}{p}-1}\, \mathrm{d}\rho \int_0^{\arctan(\tan^{\frac{p}{2}} a)} (\cos t)^{\frac{2}{p}-1} (\sin t)^{\frac{2}{p}-1}\, \mathrm{d}t.$$

With the change of variables $u = \rho^2/r^p$ and $v = \sin^2 t$ in the two independent integrals we get

$$\begin{aligned} \mathrm{Vol}(\mathcal{B}_{p,a}(r)) &= \frac{r^3}{p^2} \int_0^1 (1-u)^{\frac{1}{p}} u^{\frac{2}{p}-1}\, \mathrm{d}u \int_0^{\frac{\tan^p a}{1+\tan^p a}} v^{\frac{1}{p}-1} (1-v)^{\frac{1}{p}-1}\, \mathrm{d}v \\ &= \frac{r^3}{p^2} B(1/p+1, 2/p) B(1/p, 1/p) F_{1,p}\left(\frac{\tan^p a}{1+\tan^p a}\right) \\ &= r^3 \frac{\Gamma^3(1/p+1)}{\Gamma(3/p+1)} F_{1,p}\left(\frac{\tan^p a}{1+\tan^p a}\right). \end{aligned}$$

□

3. Construction of the Volume Preserving Map $\mathcal{U}_p : \mathcal{B}_p(r) \to \mathcal{B}_1(r')$ and Its Inverse

Of course, there is no unique map $\mathcal{U}_p$ with the volume preserving property. In this section, we will construct a map $\mathcal{U}_p : \mathcal{B}_p(r) \to \mathcal{B}_1(r')$ satisfying the following conditions:

(a) $\mathcal{U}_p$ has the volume preserving property (2);

(b) $\mathcal{U}_p$ is continuous on $\mathcal{B}_p(r)$ and has continuous partial derivatives at every point of $\mathcal{B}_p(r)$, except the points of the coordinate planes;

(c) $\mathcal{U}_p$ has the symmetry property

$$\mathcal{U}_p(x,y,z) = (\operatorname{sgn}(x)\overline{X}, \operatorname{sgn}(y)\overline{Y}, \operatorname{sgn}(z)\overline{Z}), \quad \text{where } (\overline{X},\overline{Y},\overline{Z}) = \mathcal{U}_p(|x|,|y|,|z|);$$

(d) $\mathcal{U}_p$ maps every $\mathcal{B}_{p,a}(\widetilde{r})$ onto some $\mathcal{B}_{1,b}(c_p\widetilde{r})$.

Theorem 2. *The map $\mathcal{U}_p = (X,Y,Z)$ with the properties (a)–(d) is defined by*

$$\begin{aligned}
X &= \operatorname{sgn}(x)c_p\left(|x|^p+|y|^p+|z|^p\right)^{\frac{1}{p}}\left[1-F_{1,p}\left(\frac{|y|^p}{|x|^p+|y|^p}\right)\right]\sqrt{F_{2,p}\left(\frac{|x|^p+|y|^p}{|x|^p+|y|^p+|z|^p}\right)},\\
Y &= \operatorname{sgn}(y)c_p\left(|x|^p+|y|^p+|z|^p\right)^{\frac{1}{p}}\ F_{1,p}\left(\frac{|y|^p}{|x|^p+|y|^p}\right)\sqrt{F_{2,p}\left(\frac{|x|^p+|y|^p}{|x|^p+|y|^p+|z|^p}\right)},\\
Z &= \operatorname{sgn}(z)c_p\left(|x|^p+|y|^p+|z|^p\right)^{\frac{1}{p}}\left[1-\sqrt{F_{2,p}\left(\frac{|x|^p+|y|^p}{|x|^p+|y|^p+|z|^p}\right)}\right],
\end{aligned}$$

when $|x|^p+|y|^p>0$, and $(X,Y,Z)=(0,0,c_pz)$ when $|x|^p+|y|^p=0$.

Proof. Let $(x,y,z)\in\mathcal{B}_p(r)$. Then $(X,Y,Z)=\mathcal{U}_p(x,y,z)\in\mathcal{B}_1(r')$. Consider first the case $x,y,z>0$. From condition (d) for the limit case $a=\frac{\pi}{2}$ and using (a) and (c) we deduce that $\operatorname{Vol}(\mathcal{B}_p(r))=\operatorname{Vol}(\mathcal{B}_1(c_pr))$. This relation gives us

$$X+Y+Z=c_p(x^p+y^p+z^p)^{1/p}. \tag{3}$$

From conditions (a) and (d) there is some $b>0$ such that

$$\operatorname{Vol}(\mathcal{B}_{p,a}(\widetilde{r}))=\operatorname{Vol}(\mathcal{B}_{1,b}(c_p\widetilde{r})).$$

From Lemma 1 we have

$$F_{1,p}\left(\frac{\tan^p a}{1+\tan^p a}\right)\operatorname{Vol}(\mathcal{B}_p(\widetilde{r}))=F_{1,1}\left(\frac{\tan b}{1+\tan b}\right)\operatorname{Vol}(\mathcal{B}_1(c_p\widetilde{r})).$$

Since $\mathcal{B}_p(\widetilde{r})$ and $\mathcal{B}_1(c_p\widetilde{r})$ have the same volume and $F_{1,1}(t)=t$ we obtain

$$F_{1,p}\left(\frac{\tan^p a}{1+\tan^p a}\right)=\frac{\tan b}{1+\tan b}.$$

Further, since $\tan a=y/x$ and $\tan b=Y/X$, this equality can be written as

$$F_{1,p}\left(\frac{y^p}{x^p+y^p}\right)=\frac{Y}{X+Y}. \tag{4}$$

From conditions (a) and (b) the Jacobian of $\mathcal{U}_p$ must be 1, i.e.

$$\begin{vmatrix} \frac{\partial X}{\partial x} & \frac{\partial X}{\partial y} & \frac{\partial X}{\partial z}\\ \frac{\partial Y}{\partial x} & \frac{\partial Y}{\partial y} & \frac{\partial Y}{\partial z}\\ \frac{\partial Z}{\partial x} & \frac{\partial Z}{\partial y} & \frac{\partial Z}{\partial z}\end{vmatrix}=1. \tag{5}$$

Further, taking into account Formulas (3) and (4) we have

$$Z = c_p(x^p + y^p + z^p)^{1/p} - X - Y,$$
$$Y = XF_{1,p}\left(\frac{y^p}{x^p + y^p}\right)\left(1 - F_{1,p}\left(\frac{y^p}{x^p + y^p}\right)\right)^{-1},$$

then we calculate the partial derivatives of Y and Z with respect to x, y and z and introduce them in (5). After some calculations, we find that X must be solution of the following first order partial differential equation

$$\frac{\partial X}{\partial x}xz^{p-1} + \frac{\partial X}{\partial y}yz^{p-1} - \frac{\partial X}{\partial z}(x^p + y^p) = \frac{(x^p + y^p)^{\frac{2}{p}}\left[1 - F_{1,p}\left(\frac{y^p}{x^p+y^p}\right)\right]^2 B\left(\frac{1}{p}, \frac{1}{p}\right)}{c_p pX(x^p + y^p + z^p)^{\frac{1}{p}-1}}.$$

With $U = X^2$ the equation is rewritten

$$\frac{\partial U}{\partial x}xz^{p-1} + \frac{\partial U}{\partial y}yz^{p-1} - \frac{\partial U}{\partial z}(x^p + y^p) = 2\frac{(x^p + y^p)^{\frac{2}{p}}\left[1 - F_{1,p}\left(\frac{y^p}{x^p+y^p}\right)\right]^2 B\left(\frac{1}{p}, \frac{1}{p}\right)}{c_p p(x^p + y^p + z^p)^{\frac{1}{p}-1}}.$$

We have to solve the symmetric system

$$\frac{\mathrm{d}x}{xz^{p-1}} = \frac{\mathrm{d}y}{yz^{p-1}} = \frac{\mathrm{d}z}{-(x^p + y^p)} = \frac{c_p p(x^p + y^p + z^p)^{\frac{1}{p}-1}\,\mathrm{d}u}{2(x^p + y^p)^{\frac{2}{p}}\left[1 - F_{1,p}\left(\frac{y^p}{x^p+y^p}\right)\right]^2 B\left(\frac{1}{p}, \frac{1}{p}\right)}.$$

The first equality gives us $y = xC_1$, for some constant C_1. Replacing this in the equality

$$\frac{\mathrm{d}x}{xz^{p-1}} = \frac{\mathrm{d}z}{-(x^p + y^p)}$$

we get $x^p + y^p + z^p = C_2$, for some constant C_2. Replacing these two relations in the equality

$$\frac{\mathrm{d}x}{xz^{p-1}} = \frac{c_p p(x^p + y^p + z^p)^{\frac{1}{p}-1}\,\mathrm{d}u}{2(x^p + y^p)^{\frac{2}{p}}\left[1 - F_{1,p}\left(\frac{y^p}{x^p+y^p}\right)\right]^2 B\left(\frac{1}{p}, \frac{1}{p}\right)},$$

integrating and using that the plane $x = 0$ is mapped onto $U = 0$ (this follows from the conditions (b) and (c) of the map), we obtain

$$U = \frac{2C_2^{\frac{2}{p}} B(1/p, 1/p)B(2/p, 1/p)}{p^2 c_p}\left[1 - F_{1,p}\left(\frac{C_1^p}{1 + C_1^p}\right)\right]^2 F_{2,p}\left(\frac{x^p(1 + C_1^p)}{C_2}\right),$$

which is equivalent to

$$X = c_p(x^p + y^p + z^p)^{1/p}\left[1 - F_{1,p}\left(\frac{y^p}{x^p + y^p}\right)\right]\sqrt{F_{2,p}\left(\frac{x^p + y^p}{x^p + y^p + z^p}\right)}. \tag{6}$$

Then,

$$Y = c_p(x^p + y^p + z^p)^{1/p}\, F_{1,p}\left(\frac{y^p}{x^p + y^p}\right)\sqrt{F_{2,p}\left(\frac{x^p + y^p}{x^p + y^p + z^p}\right)}, \tag{7}$$

$$Z = c_p(x^p + y^p + z^p)^{1/p}\left[1 - \sqrt{F_{2,p}\left(\frac{x^p + y^p}{x^p + y^p + z^p}\right)}\right]. \tag{8}$$

In the case when $z = 0$ and also in the case when $x = 0$ or $y = 0$ but $x + y > 0$ we use Formulas (6)–(8) to define the map $\mathcal{U}_p$. In the case when $x = y = 0$, we define $\mathcal{U}_p(0,0,z) = (0,0,c_p z)$, for all $z \geq 0$, using the continuity property of the map $\mathcal{U}_p$.

Finally, for the points (x, y, z) in the other seven octants, the map $\mathcal{U}_p$ will be defined as

$$\mathcal{U}_p(x,y,z) = (\mathrm{sgn}(x)\overline{X}, \mathrm{sgn}(y)\overline{Y}, \mathrm{sgn}(z)\overline{Z}), \quad \text{where } (\overline{X}, \overline{Y}, \overline{Z}) = \mathcal{U}_p(|x|, |y|, |z|).$$

□

Remark. *Not all the partial derivatives of the map $\mathcal{U}_p$ which occur in Theorem 2 exist at the points of the coordinates planes. For example, $\frac{\partial Y}{\partial x}$ does not exist at the points $(0, y, z)$, because the partial derivative of $F_{1,p}\left(\frac{|y|^p}{|x|^p+|y|^p}\right)$ with respect to x does not exist at the points $(0, y, z)$.*

The expression of the inverse map of $\mathcal{U}_p$ is given in the next theorem.

Theorem 3. *The map $\mathcal{U}_p^{-1} : \mathcal{B}_1(r') \to \mathcal{B}_p(r)$ is defined by*

$$x = \frac{X+Y+Z}{c_p} G_{1,p}^{\frac{1}{p}}\left(\frac{Y}{X+Y}\right) G_{2,p}^{\frac{1}{p}}\left(\left(\frac{X+Y}{X+Y+Z}\right)^2\right), \tag{9}$$

$$y = \frac{X+Y+Z}{c_p}\left(1 - G_{1,p}\left(\frac{Y}{X+Y}\right)\right)^{\frac{1}{p}} G_{2,p}^{\frac{1}{p}}\left(\left(\frac{X+Y}{X+Y+Z}\right)^2\right), \tag{10}$$

$$z = \frac{X+Y+Z}{c_p}\left(1 - G_{2,p}\left(\left(\frac{X+Y}{X+Y+Z}\right)^2\right)\right)^{\frac{1}{p}}, \tag{11}$$

for every $(X, Y, Z) \in \mathcal{B}_1(r')$ and $X \geq 0$, $Y \geq 0$, $Z \geq 0$, $X + Y > 0$. If $X = Y = 0$, we have $\mathcal{U}_p^{-1}(0,0,Z) = (0, 0, Z/c_p)$.

In the other seven octants, we define the inverse of the map $\mathcal{U}_p$ using the symmetry property (c) of $\mathcal{U}_p$.

Proof. Condition (4) is equivalent to

$$\frac{y^p}{x^p + y^p} = G_{1,p}\left(\frac{Y}{X+Y}\right).$$

Replacing (3) in (7) we obtain

$$\frac{X+Y}{X+Y+Z} = \sqrt{F_{2,p}\left(\frac{x^p + y^p}{x^p + y^p + z^p}\right)},$$

which is equivalent to

$$\frac{x^p + y^p}{x^p + y^p + z^p} = G_{2,p}\left(\left(\frac{X+Y}{X+Y+Z}\right)^2\right).$$

After some computations we can express x, y, z in terms of X, Y, Z to obtain (9)–(11). □

4. Particular Cases

4.1. The Cases $p = 1$ and $p = 2$

For $p = 1$ one has $c_1 = 1$, $F_{1,p}(t) = t$ and $F_{2,p}(t) = t^2$, therefore $\mathcal{U}_1$ is the identity.

For $p = 2$ one has $c_2 = \pi^{\frac{1}{3}}$, $F_{1,p}(t) = \frac{1}{\pi}\left(\arcsin(2t-1) + \frac{\pi}{2}\right) = \frac{2}{\pi}\arcsin\sqrt{t}$, $F_{2,p}(t) = 1 - \sqrt{1-t}$ and for $x, y, z > 0$, the map $\mathcal{U}_2$ is

$$
\begin{aligned}
X &= 2\pi^{-2/3}\sqrt{x^2+y^2+z^2 - z\sqrt{x^2+y^2+z^2}}\arccos\frac{y}{\sqrt{x^2+y^2}},\\
Y &= 2\pi^{-2/3}\sqrt{x^2+y^2+z^2 - z\sqrt{x^2+y^2+z^2}}\arcsin\frac{y}{\sqrt{x^2+y^2}},\\
Z &= \pi^{1/3}\sqrt{x^2+y^2+z^2}\left(1 - \sqrt{1 - \frac{z}{\sqrt{x^2+y^2+z^2}}}\right).
\end{aligned}
$$

If we use the spherical coordinates defined by $x = \rho\cos\theta\sin\varphi$, $y = \rho\sin\theta\sin\varphi$ and $z = \rho\cos\varphi$ we obtain relations (9), (10), (11) from [3], where we also gave the inverse, which has an explicit expression.

4.2. The Case $p = \infty$

In this case we will obtain a new map, different from the one constructed in [4].

We restrict again to the case $x, y, z > 0$ because of the symmetry property of the map.

First, a simple calculation shows that $c_\infty = 6^{1/3}$ and

$$\lim_{p\to\infty}(x^p + y^p + z^p)^{1/p} = \max(x, y, z).$$

In order to calculate the limits in (6)–(8) when $p \to \infty$ we use the following result.

Lemma 4. *For $\alpha, \beta > 0$ we have*

$$\lim_{p\to\infty}\frac{p}{B\left(\frac{\alpha}{p}, \frac{\beta}{p}\right)} = \frac{\alpha\beta}{\alpha+\beta}. \tag{12}$$

Proof. We use the equality $\Gamma(x) = \Gamma(x+1)/x$, which holds for $x > 0$. One has

$$\frac{p}{B\left(\frac{\alpha}{p}, \frac{\beta}{p}\right)} = \frac{p\,\Gamma\left(\frac{\alpha+\beta}{p}\right)}{\Gamma\left(\frac{\alpha}{p}\right)\cdot\Gamma\left(\frac{\beta}{p}\right)} = \frac{p\cdot\frac{\alpha}{p}\cdot\frac{\beta}{p}\cdot\Gamma\left(1+\frac{\alpha+\beta}{p}\right)}{\Gamma\left(1+\frac{\alpha}{p}\right)\cdot\Gamma\left(1+\frac{\beta}{p}\right)\cdot\frac{\alpha+\beta}{p}},$$

and now it is easy to see that the limit when $p \to \infty$ is the one in (12). □

Proposition 5. *For $x, y, z > 0$ we have*

$$\lim_{p\to\infty} F_{1,p}\left(\frac{y^p}{x^p+y^p}\right) = \begin{cases} \frac{y}{2x}, & x > y, \\ 1 - \frac{x}{2y}, & y \geq x. \end{cases}$$

Proof. We use the idea in [5].

Suppose $x > y$.

$$F_{1,p}\left(\frac{y^p}{x^p+y^p}\right) = \frac{1}{B\left(\frac{1}{p}, \frac{1}{p}\right)}\int_0^{y^p/(x^p+y^p)}(u(1-u))^{\frac{1}{p}-1}\,du.$$

With the change of variable $u = t^p$ we have

$$F_{1,p}\left(\frac{y^p}{x^p+y^p}\right) = \frac{p}{B\left(\frac{1}{p},\frac{1}{p}\right)} \int_0^{y/(x^p+y^p)^{1/p}} (1-t^p)^{\frac{1}{p}-1}\,\mathrm{d}t.$$

From $0 < t < y/(x^p+y^p)$ we further deduce that $x^p/(x^p+y^p) < 1 - t^p < 1$, and therefore

$$\left(\frac{x^p}{x^p+y^p}\right)^{\frac{1}{p}-1} > (1-t^p)^{\frac{1}{p}-1} > 1.$$

After integration we obtain

$$\frac{y}{(x^p+y^p)^{\frac{1}{p}}}\left(\frac{x^p}{x^p+y^p}\right)^{\frac{1}{p}-1} \geq \int_0^{y/(x^p+y^p)^{1/p}} (1-t^p)^{\frac{1}{p}-1}\,\mathrm{d}t \geq \frac{y}{(x^p+y^p)^{\frac{1}{p}}},$$

and further,

$$\frac{p}{B\left(\frac{1}{p},\frac{1}{p}\right)}\frac{y}{(x^p+y^p)^{\frac{1}{p}}}\left(\frac{x^p}{x^p+y^p}\right)^{\frac{1}{p}-1} \geq F_{1,p}\left(\frac{y^p}{x^p+y^p}\right) \geq \frac{p}{B\left(\frac{1}{p},\frac{1}{p}\right)}\frac{y}{(x^p+y^p)^{\frac{1}{p}}}.$$

After applying Lemma 4 for $\alpha = \beta = 1$ and replacing the limits

$$\lim_{p\to\infty}(x^p+y^p)^{\frac{1}{p}} = \max(x,y) = x \text{ and } \lim_{p\to\infty}\frac{x^p}{x^p+y^p} = 1,$$

□

We finally obtain

$$\lim_{p\to\infty} F_{1,p}\left(\frac{y^p}{x^p+y^p}\right) = \frac{y}{2x}. \tag{13}$$

For the case $y \geq x$ we use the formula $F_{1,p}(1-t) = 1 - F_{1,p}(t)$ for $t = x^p/(x^p+y^p)$ and Formula (13), interchanging x and y.

Proposition 6. *For $x,y,z > 0$ we have*

$$\lim_{p\to\infty} F_{2,p}\left(\frac{x^p+y^p}{x^p+y^p+z^p}\right) = \begin{cases} \frac{1}{3z^2}\max(x,y)^2, & \text{if } z = \max(x,y,z), \\ 1 - \frac{2}{3}\frac{z}{\max(x,y)}, & \text{otherwise.} \end{cases}$$

Proof. *Case 1.* Suppose $\max(x,y,z) = z$.

With the change of variable $t = u^{2/p}$ we obtain

$$F_{2,p}\left(\frac{x^p+y^p}{x^p+y^p+z^p}\right) = \frac{p}{2B\left(\frac{2}{p},\frac{1}{p}\right)} \int_0^{\left(\frac{x^p+y^p}{x^p+y^p+z^p}\right)^{2/p}} \left(1-t^{\frac{p}{2}}\right)^{\frac{1}{p}-1}\,\mathrm{d}t.$$

Applying Lemma 4 for $\alpha = 2$, $\beta = 1$ we have

$$\lim_{p\to\infty}\frac{p}{2B\left(\frac{2}{p},\frac{1}{p}\right)} = \frac{1}{3}.$$

Further, from the condition that t belongs to the interval of integration we can write

$$\frac{z^p}{x^p+y^p+z^p} < 1-t^{\frac{p}{2}} < 1,$$

and therefore

$$\left(\frac{z^p}{x^p+y^p+z^p}\right)^{\frac{1}{p}-1} > \left(1-t^{\frac{p}{2}}\right)^{\frac{1}{p}-1} > 1.$$

After integration we obtain

$$\left(\frac{x^p+y^p}{x^p+y^p+z^p}\right)^{\frac{2}{p}} \left(\frac{z^p}{x^p+y^p+z^p}\right)^{\frac{1}{p}-1} \geq \int_0^{\left(\frac{x^p+y^p}{x^p+y^p+z^p}\right)^{\frac{2}{p}}} \left(1-t^{\frac{p}{2}}\right)^{\frac{1}{p}-1} \mathrm{d}t \geq \left(\frac{x^p+y^p}{x^p+y^p+z^p}\right)^{\frac{2}{p}}.$$

A simple calculation shows that

$$\lim_{p\to\infty}\left(\frac{x^p+y^p}{x^p+y^p+z^p}\right)^{2/p} = \frac{(\max(x,y))^2}{z^2} \quad \text{and} \quad \lim_{p\to\infty}\frac{z^p}{x^p+y^p+z^p} = 1,$$

which imply that

$$\lim_{p\to\infty}\int_0^{\left(\frac{x^p+y^p}{x^p+y^p+z^p}\right)^{\frac{2}{p}}} \left(1-t^{\frac{p}{2}}\right)^{\frac{1}{p}-1} \mathrm{d}t = \frac{(\max(x,y))^2}{z^2}.$$

Case 2. Suppose $\max(x,y,z) = x$ or y.

Using the equality

$$I_x(\alpha,\beta) = 1 - I_{1-x}(\beta,\alpha), \quad \alpha,\beta > 0, \quad x \in [0,1],$$

we have

$$F_{2,p}\left(\frac{x^p+y^p}{x^p+y^p+z^p}\right) = 1 - \frac{1}{B\left(\frac{2}{p},\frac{1}{p}\right)}\int_0^{\frac{z^p}{x^p+y^p+z^p}} u^{\frac{1}{p}-1}(1-u)^{\frac{2}{p}-1}\,\mathrm{d}u.$$

With the change of variable $u = t^p$ we get

$$F_{2,p}\left(\frac{x^p+y^p}{x^p+y^p+z^p}\right) = 1 - \frac{p}{B\left(\frac{2}{p},\frac{1}{p}\right)}\int_0^{\left(\frac{z^p}{x^p+y^p+z^p}\right)^{1/p}} (1-t^p)^{\frac{2}{p}-1}\,\mathrm{d}t.$$

Similarly

$$\frac{z}{(x^p+y^p+z^p)^{1/p}}\left(\frac{x^p+y^p}{x^p+y^p+z^p}\right)^{\frac{2}{p}-1} \geq \int_0^{\left(\frac{z^p}{x^p+y^p+z^p}\right)^{1/p}} (1-t^p)^{\frac{2}{p}-1}\,\mathrm{d}t \geq \frac{z}{(x^p+y^p+z^p)^{1/p}}.$$

Using

$$\lim_{p\to\infty}\frac{z}{(x^p+y^p+z^p)^{1/p}} = \frac{z}{\max(x,y)} \quad \text{and} \quad \lim_{p\to\infty}\frac{x^p+y^p}{x^p+y^p+z^p} = 1,$$

the proof is complete. □

In conclusion, for $x, y, z > 0$, the map $\mathcal{U}_\infty$ has the values $(X, Y, Z) = \mathcal{U}_\infty(x, y, z)$ given by:

$$\begin{aligned}
&6^{1/3}\left(\frac{x}{2\sqrt{3}}, \frac{2y-x}{2\sqrt{3}}, z - \frac{y}{\sqrt{3}}\right), \ x \le y \le z,\\
&6^{1/3}\left(\frac{x}{2}\sqrt{1-\frac{2z}{3y}}, \left(y-\frac{x}{2}\right)\sqrt{1-\frac{2z}{3y}}, y\left(1-\sqrt{1-\frac{2z}{3y}}\right)\right), \ x \le z \le y,\\
&6^{1/3}\left(\frac{2x-y}{2\sqrt{3}}, \frac{y}{2\sqrt{3}}, z - \frac{x}{\sqrt{3}}\right), \ y \le x \le z,\\
&6^{1/3}\left(\left(x-\frac{y}{2}\right)\sqrt{1-\frac{2z}{3x}}, \frac{y}{2}\sqrt{1-\frac{2z}{3x}}, x\left(1-\sqrt{1-\frac{2z}{3x}}\right)\right), \ y \le z \le x,\\
&6^{1/3}\left(\frac{x}{2}\sqrt{1-\frac{2z}{3y}}, \left(y-\frac{x}{2}\right)\sqrt{1-\frac{2z}{3y}}, y\left(1-\sqrt{1-\frac{2z}{3y}}\right)\right), \ z \le x \le y,\\
&6^{1/3}\left(\left(x-\frac{y}{2}\right)\sqrt{1-\frac{2z}{3x}}, \frac{y}{2}\sqrt{1-\frac{2z}{3x}}, x\left(1-\sqrt{1-\frac{2z}{3x}}\right)\right), \ z \le y \le x,
\end{aligned}$$

and can be reduced to

$$\begin{aligned}
&6^{1/3}\left(\frac{x}{2\sqrt{3}}, \frac{2y-x}{2\sqrt{3}}, z - \frac{y}{\sqrt{3}}\right), \ x \le y \le z,\\
&6^{1/3}\left(\frac{x}{2}\sqrt{1-\frac{2z}{3y}}, \left(y-\frac{x}{2}\right)\sqrt{1-\frac{2z}{3y}}, y\left(1-\sqrt{1-\frac{2z}{3y}}\right)\right), \ x \le y, \ z \le y,\\
&6^{1/3}\left(\frac{2x-y}{2\sqrt{3}}, \frac{y}{2\sqrt{3}}, z - \frac{x}{\sqrt{3}}\right), \ y \le x \le z,\\
&6^{1/3}\left(\left(x-\frac{y}{2}\right)\sqrt{1-\frac{2z}{3x}}, \frac{y}{2}\sqrt{1-\frac{2z}{3x}}, x\left(1-\sqrt{1-\frac{2z}{3x}}\right)\right), \ y \le x, \ z \le x.
\end{aligned}$$

The above formulas can also be used in the case when $x = 0$ or $y = 0$ or $z = 0$, with the mention that the denominators cannot be zero, except the case when $x = y = z = 0$, when we take $\mathcal{U}_\infty(0, 0, 0) = (0, 0, 0)$.

After some calculations we get that, for $X, Y, Z > 0$ the inverse $\mathcal{U}_\infty^{-1}(X, Y, Z)$ is given by

$$\begin{aligned}
&6^{-1/3}\left(2\sqrt{3}X, \sqrt{3}(X+Y), X+Y+Z\right), \text{on } D_1,\\
&6^{-1/3}\left(\frac{2X(X+Y+Z)}{X+Y}, X+Y+Z, \frac{3Z(2X+2Y+Z)}{2(X+Y+Z)}\right), \text{ on } D_2,\\
&6^{-1/3}\left(\sqrt{3}(X+Y), 2\sqrt{3}Y, X+Y+Z\right), \text{ on } D_3,\\
&6^{-1/3}\left(X+Y+Z, \frac{2Y(X+Y+Z)}{X+Y}, \frac{3Z(2X+2Y+Z)}{2(X+Y+Z)}\right), \text{ on } D_4,
\end{aligned}$$

where D_i, $i = 1, 2, 3, 4$ are the set of points (X, Y, Z) satisfying the following conditions, respectively:

$$\begin{aligned}
&X \le Y, \quad \sqrt{3}(X+Y) \le X+Y+Z,\\
&X \le Y, \quad \frac{3Z(2X+2Y+Z)}{2(X+Y+Z)} \le X+Y+Z,\\
&Y \le X, \quad (X+Y)\sqrt{3} \le X+Y+Z,\\
&Y \le X, \quad \frac{3Z(2X+2Y+Z)}{2(X+Y+Z)} \le X+Y+Z.
\end{aligned}$$

Condition

$$\frac{3Z(2X+2Y+Z)}{2(X+Y+Z)} \leq X+Y+Z$$

can be written as $3((X+Y+Z)^2-(X+Y)^2) \leq 2(X+Y+Z)^2$, and is equivalent to $X+Y+Z \leq \sqrt{3}(X+Y)$, since $X,Y,Z>0$.

Therefore,

$$\begin{aligned}
D_1 &= \{X \leq Y, \quad \sqrt{3}(X+Y) \leq X+Y+Z\}, \\
D_2 &= \{X \leq Y, \quad X+Y+Z \leq \sqrt{3}(X+Y)\}, \\
D_3 &= \{Y \leq X, \quad (X+Y)\sqrt{3} \leq X+Y+Z\}, \\
D_4 &= \{Y \leq X, \quad X+Y+Z \leq \sqrt{3}(X+Y)\}.
\end{aligned}$$

Finally, the expressions of $(x,y,z)=\mathcal{U}_\infty^{-1}(X,Y,Z)$ can be reduced to

$$\begin{aligned}
x &= 6^{-1/3}\min\left(\sqrt{3}, 1+\frac{Z}{X+Y}\right)(X+\min(X,Y)), \\
y &= 6^{-1/3}\min\left(\sqrt{3}, 1+\frac{Z}{X+Y}\right)(Y+\min(X,Y)), \\
z &= 6^{-1/3}\min\left(X+Y+Z, 3Z\left(1-\frac{Z}{2(X+Y+Z)}\right)\right).
\end{aligned}$$

These formulas can also be used in the case when $Z=0$ and in the case when $X=0$ or $Y=0$, but $X+Y>0$. In the case when $X=Y=0$ we take $\mathcal{U}_\infty^{-1}(0,0,Z)=(0,0,6^{-1/3}Z)$.

If we take arbitrary numbers $p,\widetilde{p}>0$, the application

$$\mathcal{U}_{\widetilde{p}}^{-1}\circ\mathcal{U}_p : \mathcal{B}_p(r) \to \mathcal{B}_{\widetilde{p}}(\widetilde{r}), \quad \text{with } \widetilde{r}=c_p c_{\widetilde{p}}^{-1} r,$$

is a volume preserving map, therefore we have defined a volume preserving map between arbitrary p-balls.

5. Possible Applications

A uniform grid of a 3D domain D is a grid in which all the cells have the same volume. This is required in statistical applications, in computer graphics in the theory of deformable bodies (see, for example, Ref. [6] and the references therein) and in construction of wavelet bases of the space $L^2(D)$. A refinement process is needed for multiresolution analysis or for multigrid methods, when a grid is not fine enough to solve a problem accurately. A refinement of a 3D grid is called uniform when each cell is divided into a given number of smaller cells having the same volume. To be efficient in practice, a refinement procedure should also be a simple one. One efficient way to construct a uniform and refinable (UR) grid on a domain D is to map on D an existing UR grid by a volume preserving map. In our case, we can construct (UR) grids on a ball $\mathcal{B}_{p'}$ by transporting from a ball $\mathcal{B}_p$ an already constructed (UR) grid. The simplest example of such a ball with (UR) grids is the cube $\mathcal{B}_\infty$, but we have also constructed such (UR) grids on the regular octahedron $\mathcal{B}_1$ (see [3,4]) and on the 3D Euclidean ball $\mathcal{B}_2$ (see [3,7]).

The technique used in [3] can be easily adapted to the p-ball $\mathcal{B}_p$ in order to construct multiresolution analysis of $L^2(\mathcal{B}_p)$ and orthonormal wavelet bases on the p-ball $\mathcal{B}_p$.

The centers of the cells in our (UR) grids in $\mathcal{B}_p$ can be taken as points in interpolation formulas, as Monte Carlo interpolation or adaptive interpolation formulas.

Another application of volume preserving maps is in the theory of partial differential equations on Lipschitz domains (see [8]).

Author Contributions: Writing—original draft preparation, A.H.; Writing—review and editing, A.H., D.R.; Visualization, D.R.

Funding: This research received no external funding.

Conflicts of Interest: The authors declare no conflict of interest.

References

1. Barr, A.H. Superquadrics and Angle-Preserving Transformations. *IEEE-CGA* **1981**, *1*, 11–23. [CrossRef]
2. Barr, A.H. Rigid Physically Based Superquadrics. In *Graphics Gems III*; Kirk, D., Ed.; Academic Press: San Diego, CA, USA, 1992; pp. 137–159.
3. Holhoş, A.; Roşca, D. Orhonormal Wavelet Bases on the 3D Ball via Volume Preserving Map from the Regular Octahedron. Available online: https://arxiv.org/abs/1910.08067 (accessed on 10 October 2019).
4. Holhoş, A.; Roşca, D. Uniform refinable 3D grids of regular convex polyhedrons and balls. *Acta Math. Hung.* **2018**, *156*, 182–193. [CrossRef]
5. Holhoş, A. Two Area Preserving Maps from the Square to the *p*-Ball. *Math. Modell. Anal.* **2017**, *22*, 157–166. [CrossRef]
6. Savoye, Y. *Cage-Based Performance Capture*; Springer: Basel, Switzerland, 2014.
7. Roşca, D.; Morawiec, A.; De Graef, M. A new method of constructing a grid in the space of 3D rotations and its applications to texture analysis. *Model. Simul. Mater. Sci. Eng.* **2014**, *22*, 075013. [CrossRef]
8. Griepentrog, J.; Höpner, W.; Kaiser, H.C.; Rehberg, J. A bi-Lipschitz continuous, volume preserving map from the unit ball onto a cube. *Note Mat.* **2008**, *28*, 177–193.

symmetry

MDPI

Article

Generation of Julia and Mandelbrot Sets via Fixed Points

Mujahid Abbas [1,2], Hira Iqbal [3] and Manuel De la Sen [4,*]

[1] Department of Mathematics, Government College University, Lahore 54000, Pakistan; abbas.mujahid@gmail.com

[2] Department of Medical Research, China Medical University No. 91, Hsueh-Shih Road, Taichung 400, Taiwan

[3] Department of Sciences and Humanities, National University of Computer and Emerging Sciences, Lahore Campus, Lahore 54000, Pakistan; hira.iqbal@nu.edu.pk

[4] Institute of Research and Development of Processes, University of the Basque Country, Campus of Leioa (Bizkaia), P.O. Box 644, Bilbao, Barrio Sarriena, 48940 Leioa, Spain

* Correspondence: manuel.delasen@ehu.eus

Received: 27 November 2019; Accepted: 26 December 2019; Published: 2 January 2020

Abstract: The aim of this paper is to present an application of a fixed point iterative process in generation of fractals namely Julia and Mandelbrot sets for the complex polynomials of the form $T(x) = x^n + mx + r$ where $m, r \in \mathbb{C}$ and $n \geq 2$. Fractals represent the phenomena of expanding or unfolding symmetries which exhibit similar patterns displayed at every scale. We prove some escape time results for the generation of Julia and Mandelbrot sets using a Picard Ishikawa type iterative process. A visualization of the Julia and Mandelbrot sets for certain complex polynomials is presented and their graphical behaviour is examined. We also discuss the effects of parameters on the color variation and shape of fractals.

Keywords: iteration; fixed points; fractals

MSC: Primary: 47H10; Secondary:47J25

1. Introduction

Fixed point theory provides a suitable framework to investigate various nonlinear phenomena arising in the applied sciences including complex graphics, geometry, biology and physics [? ? ? ?]. Complex graphical shapes such as fractals, were discovered as fixed points of certain set maps [?]. Informally, fractals can be treated as self similar mathematical structures which have similarity and symmetry such that considerably small parts of the shape are geometrically akin to the whole shape. Fractals are also known as expanding symmetries or unfolding symmetries. Although, fractals do not have a formal definition, however they are identified through their irregular structure that cannot be found in Euclidean geometry. Julia [?] who is considered as one of the pioneers of fractal geometry, studied iterated complex polynomials and introduced Julia set as a classical example of fractals. Let $\mathbb{C}$ be the complex space, $T : \mathbb{C} \to \mathbb{C}$ be a complex polynomial of degree $n \geq 2$ with complex coefficients and $T^i(x)$ be the i^{th} iterate of x. The behaviour of the iterates $T^i(x)$ for large i determine the Julia set (see [? ? ? ?]).

Definition 1 ([?]). *The set of points in $\mathbb{C}$ whose orbits do not converge to a point at infinity is known as filled Julia set, K_T, that is,*

$$K_T = \left\{ x \in \mathbb{C} : \{|T^i(x)|\}_{i=0}^{\infty} \quad \text{is bounded} \right\}.$$

Julia set of T denoted by J_T is the boundary of filled Julia set, that is, $J_T = \partial K_T$.

Therefore, we may say that $x \in J_T$ if for every neighborhood of x there exist points w and v such that $T^i(w) \to \infty$ and $T^i(v) \nrightarrow \infty$. The complement of a Julia set is a Fatou set.

Let $p \in \mathbb{C}$ be a fixed point of T and $|(T^i)'p| = \rho$, where prime denotes the complex differentiation. A point p is called a periodic point if $p = T^i p$ for some integer $i \geq 0$. Let $\{p, Tp, ..., T^i p, ...\}$ be an orbit of p. The point p is called an attracting point if $0 \leq \rho < 1$ and a repelling point if $\rho > 1$ [**? ?**]. The following result gives a significant connection between repelling points of a polynomial and the Julia set.

Theorem 1 ([**?**])**.** *If T is a complex polynomial, then J_T is the closure of the repelling periodic points of T.*

Let p be an attracting fixed point of T. Then, the set $A(p)$ is called the basin of attraction of p if

$$A(p) = \left\{ x \in \mathbb{C} : T^i x \to p \;\text{ as }\; i \to \infty \right\}.$$

The basin of attraction of infinity, $A(\infty)$, is defined in the same way. The following lemma is pivotal in determining Julia sets.

Lemma 1. *[**?**] Let p be an attracting fixed point of T. Then, $J_T = \partial A(p)$.*

Thus, the Julia set is the boundary of the basin of attraction of each attracting fixed point of T, including ∞. The existence of the fixed point p for any complex polynomial is guaranteed by Brouwer fixed point theorem [**?**]. However, the existence of an attracting fixed point depends on the choice of the parameters. Consider the polynomial $Q_r(x) = x^2 + r$. Then it has two fixed points excluding infinity. In this case, a fixed point p is attracting if $|2p| < 1$ i.e., $|1 - \sqrt{\frac{1}{4} - r}| < 1$. Fix $v_r = \sqrt{\frac{1}{4} - r}$, then the set of parameters r such that Q_r has an attracting fixed point is given by $S = \{r \in \mathbb{C} : |1 - v_r| < 1\}$. Julia sets, J_{Q_r}, on the real axis i.e., $r = 0$ are reflection symmetric while those with complex parameter values, $r \in \mathbb{C}$ demonstrate rotational symmetry.

Mandelbrot [**?**] extended the idea of Julia sets and presented the notion of fractals. He investigated the graphical behaviour of connected Julia sets and plotted them for complex function, $Q_r(x) = x^2 + r$, where $x \in \mathbb{C}$ is a complex variable and $r \in \mathbb{C}$ is an input parameter. He noted that various geometrical properties involving dimension, symmetry and similarity play consequential role in the study of fractal geometry.

Definition 2 ([**?**])**.** *Let T be any complex polynomial of degree $n \geq 2$. A Mandelbrot set M is the set consisting of all parameters r for which the Julia set, J_{Q_r}, is connected, that is,*

$$M = \left\{ r \in \mathbb{C} : J_{Q_r} \quad \textit{is connected} \right\},$$

or an equivalent definition is

$$M = \{ r \in \mathbb{C} : \{|Q_r^n(0)|\} \nrightarrow \infty \quad \textit{as} \quad n \to \infty \}.$$

Mandelbrot [**? ?**] noted that records of heart beat, irregular coastal structures, variations of traffic flow and many naturally existing textures are examples of fractals.

In order to generate and analyze fractals, various techniques are used such as iterated function systems, random fractals, escape time criterion etc. The escape time algorithm is the stopping criterion that is based on the number of iterations necessary to determine if the orbit sequence tends to infinity or not. This algorithm provides a suitable mechanism used to demonstrate some attributes of dynamic system under iterative process. Generally, the escape criterion for Julia and Mandelbrot sets is given by:

Theorem 2 ([**?**])**.** *For $Q_r(x) = x^2 + r$, $x, r \in \mathbb{C}$, if there exists $i \geq 0$ such that*

$$|Q_r^i(x)| > \max\{|r|, 2\},$$

then $Q_r^i(x) \to \infty$ as $i \to \infty$.

The term $\max\{|r|, 2\}$ is also known as escape radius threshold. The escape radius varies in each iteration. The escape radius has a key role in visualizing the fractals.

Historically, Julia and Mandelbrot sets are investigated for the polynomials Q_r but the study has been extended to quadratic, cubic, and n^{th} degree complex polynomials. Lakhtakia et al. [**?**] explored the Julia sets for general complex function of the form $T(x) = x^n + r$ where $n \in \mathbb{N}$. The superior Julia and superior Mandelbrot sets for such complex polynomials in the context of noises arising in the objects were analyzed by Negi et al. [**? ?**]. Rochon [**?**] considered a more generalized form of Mandelbrot sets in bi-complex planes, see also [**? ?**].

Many authors have utilized various iterative processes to generate fractals. Julia and Mandelbrot sets have usually been studied for quadratic, cubic and higher degree polynomials in Picard orbit [**?**]. Let $T : \mathbb{C} \to \mathbb{C}$ and $x_0 \in \mathbb{C}$. The Picard orbit [**?**] is a sequence $\{x_i\}$ which is given by

$$x_{i+1} = T(x_i),$$

where $i \geq 0$.

Since the convergence of Picard process is slow, various faster converging iterative processes have been introduced to generate Julia and Mandelbrot sets. Rani and Kumar [**? ?**] used one-step Mann iterative process to generate superior Julia and Mandelbrot sets for n^{th} degree complex polynomials of the form $T(x) = x^n + r$. The Mann orbit, for any $x_0 \in \mathbb{C}$, is a sequence $\{x_i\}$ which is given by

$$x_{i+1} = (1 - \alpha)(x_i) + \alpha T(x_i),$$

where $i = 0, 1, ...$ and $\alpha \in (0, 1]$.

In 2010, a two-step Ishikawa iteration was used by Rana and Kumar [**?**] and Chauhan et al. [**?**] to study relative superior Julia and relative superior Mandelbrot sets, respectively. The dynamics of the nth order complex polynomial for non integer values were investigated in [**?**]. The authors also obtained new Julia and Mandelbrot sets via Ishikawa orbit. The Ishikawa orbit, for any $x_0 \in \mathbb{C}$, is a sequence $\{x_i\}$ which is given by

$$\begin{cases} x_{i+1} & = (1 - \alpha)x_i + \alpha T y_i, \\ y_i & = (1 - \beta)x_i + \beta T x_i, \end{cases}$$

where $i = 0, 1, ...$ and $\alpha, \beta \in (0, 1]$.

Ashish and Rani [**?**] investigated the three-step Noor iteration process for Julia and Mandelbrot sets. The Noor orbit, for any $x_0 \in \mathbb{C}$, is a sequence $\{x_i\}$ which is given by

$$\begin{cases} x_{i+1} = (1 - \alpha)T x_i + \alpha T y_i, \\ y_i = (1 - \beta)T x_i + \alpha T u_i, \\ u_i = (1 - \gamma)T x_i + \gamma T x_i, \end{cases}$$

where $i = 0, 1, ...$ and $\alpha, \beta, \gamma \in (0, 1]$.

The modified Ishikawa process, S-iteration, was employed by Kang et al. [**? ?**] to study relative superior Mandelbrot sets, tricorn and multicorns. The S-orbit, for any $x_0 \in \mathbb{C}$, is a sequence $\{x_i\}$ given by

$$\begin{cases} x_{i+1} = (1-\alpha)x_i + \alpha T y_i, \\ y_i = (1-\beta)x_i + \alpha T x_i, \end{cases}$$

where $i = 0, 1, ...$ and $\alpha, \beta \in (0, 1]$.

Kumari et al. [**?**] used a four-step iterative process which is faster than of Picard, Mann and S-iteration processes and obtained some generalizations of Julia and Mandelbrot sets for quadratic, cubic and higher degree polynomials.

It is noteworthy that for each iterative process the behaviour and dynamics of the Julia and Mandelbrot sets differ. For some thought-provoking and fascinating comparisons, the reader may refer to [**? ? ? ? ?**] and references therein.

Complex polynomials of the form $T(x) = x^n + mx + r$, where $m, r \in \mathbb{C}$ occur in various engineering problems including digital signal processing. These complex polynomials are used to determine the pole-zero plots for signals and the study of the structure and solutions of linear time invariant (LTI) state-space models, for details see [**?**]. Thus the study of behaviour of these polynomials and their Julia and Mandelbrot sets has gained immense interest among researchers. Kang et al. [**?**] introduced Julia and Mandelbrot sets in implicit Jungck Mann and Jungck Ishikawa orbits. Later, several researchers [**? ? ? ? ?**] employed this implicit iterative process to generate graphs of such complex polynomials. In order to achieve this, they split the polynomial T into two functions $T_1(x) = x^n + r$ and $T_2(x) = mx$. However, the Jungck iterative process and its variants are used to determine the common fixed points of two mappings. Therefore, the question arises whether we can obtain an escape criterion and generate fractals for polynomials of the form T using explicit iterative processes.

The purpose of this paper is to answer this question. In this paper, we discuss the graphical behaviour of the complex polynomial of the form $T(x) = x^n + mx + r$ where $m, r \in \mathbb{C}$ and $n \geq 2$ using Picard Ishikawa type fixed point iteration process for the generation of fractals. Note that the Julia and Mandelbrot sets generated have distinctive shapes for the proposed iterative process as compared to already present iterative processes in the literature. Further, we show the effect of change of parameters on color variation and graph of the sets.

The Picard Ishikawa type iteration process was introduced by Piri et al. [**?**]. They claimed that this iterative process converges faster than Mann and Ishikawa iteration processes. Let D be a subset of a Banach space and $f : D \to D$ then the three step iteration process is given by

$$\begin{cases} x_1 = x \in D, \\ x_{i+1} = (1-\alpha_i)y_i + \alpha_i f y_i, \\ y_i = f z_i, \\ z_i = f((1-\beta_i)x_i + \beta_i f x_i), & i \geq 0, \end{cases} \tag{1}$$

where $\alpha_i, \beta_i \in (0, 1]$.

2. Main Results

In this section, we use a Picard Ishikawa type iterative process and some prove escape criterions to determine the escape radius for this process. Throughout this paper we assume that for any complex polynomial the parameters are chosen in a way that at the least one attracting fixed point exists.

Let $\mathbb{C}$ be a complex space and $T_{\mathbb{C}} : \mathbb{C} \to \mathbb{C}$ be a complex polynomial with complex coefficients. The Picard Ishikawa type orbit around any $x_0 \in \mathbb{C}$, is a sequence $\{x_i\}$ given by

$$\begin{cases} x_{i+1} = (1-\alpha)y_i + \alpha T_{\mathbb{C}} y_i, \\ y_i = T_{\mathbb{C}} z_i, \\ z_i = T_{\mathbb{C}} t_i, \\ t_i = (1-\beta)x_i + \beta T_{\mathbb{C}} x_i, \end{cases} \tag{2}$$

where $i = 0, 1, 2, ...$ and $\alpha, \beta \in (0, 1]$.

We need the following escape criterions for the quadratics, cubic and higher degree polynomials.

2.1. Escape Criterion for Quadratic Complex Polynomials in a Picard Ishikawa Type Orbit

For the quadratic polynomial $T_{\mathbb{C}}(x) = x^2 + mx + r$ where $m, r \in \mathbb{C}$, we have the following result.

Theorem 3. *Suppose that* $|x| \geq |r| > \max\left\{\frac{2(1+|m|)}{\alpha}, \frac{2(1+|m|)}{\beta}\right\}$, $\alpha, \beta \in (0, 1]$. *Define* $\{x_i\}_{i\in\mathbb{N}}$ *as in* (**??**) *where* $x_0 = x$, $y_0 = y$, $z_0 = z$ *and* $t_0 = t$. *Then,* $|x_i| \to \infty$ *as* $i \to \infty$.

Proof. As, $T_{\mathbb{C}}(x) = x^2 + mx + r$. From (**??**), we have

$$\begin{aligned} |t| =& |(1-\beta)x + \beta T_{\mathbb{C}} x| \\ =& |(1-\beta)x + \beta(x^2 + mx + r)| \\ \geq& |(1-\beta)x + \beta(x^2 + mx)| - \beta|r|. \end{aligned}$$

The assumption $|x| \geq |r|$ yields

$$\begin{aligned} |t| \geq& |(1-\beta)x + \beta(x^2 + mx)| - \beta|x| \\ \geq& \beta|x^2| - (1 - \beta + \beta|m|)|x| - \beta|x| \\ =& \beta|x^2| - (1 + \beta|m|)|x| \\ =& |x|\Big(\beta|x| - (1 + \beta|m|)\Big). \end{aligned}$$

Since $\beta \leq 1$, we obtain $-(1 + \beta|m|) > -(1 + |m|)$ which implies that

$$|t| \geq |x|\Big(\beta|x| - (1 + |m|)\Big).$$

Thus, we have

$$|t| \geq |x|(1 + |m|)\left(\frac{\beta|x|}{1 + |m|} - 1\right).$$

Therefore,

$$\begin{aligned} |t| \geq& \frac{|t|}{(1 + |m|)} \\ \geq& |x|\left(\frac{\beta|x|}{1 + |m|} - 1\right). \end{aligned} \tag{3}$$

From our assumption; $|x| > \max\left\{\frac{2(1+|m|)}{\alpha}, \frac{2(1+|m|)}{\beta}\right\}$, we get

$$\left(\frac{\beta|x|}{1 + |m|} - 1\right) > 1. \tag{4}$$

Now, (**??**) gives that

$$|t| > |x|. \tag{5}$$

As $z = z_0$, (**??**) gives

$$\begin{aligned}|z| =&|T_{\mathbb{C}}(t)|\\ =&|t^2 + mt + r| \geq |t^2 + mt| - |r|.\end{aligned}$$

Since $\beta \leq 1$, it follows from (**??**) and assumption $|x| \geq |r|$ that

$$\begin{aligned}|z| \geq&|t^2 + mt| - |x|\\ \geq&\beta|t^2| - |m||t| - |t|\\ =&|t|\Big(\beta|t| - (1 + |m|)\Big),\end{aligned}$$

which further implies that

$$|z| \geq \frac{|z|}{(1 + |m|)} \geq |t|\Big(\frac{\beta|t|}{(1 + |m|)} - 1\Big). \tag{6}$$

Using (**??**) and (**??**) we have

$$\begin{aligned}|t| >&|x|\\ \implies \frac{\beta|t|}{1 + |m|} >&\frac{\beta|x|}{1 + |m|}\\ \implies \Big(\frac{\beta|t|}{1 + |m|} - 1\Big) >&\Big(\frac{\beta|x|}{1 + |m|} - 1\Big) > 1.\end{aligned} \tag{7}$$

Consequently, (**??**)–(**??**) yield

$$|z| > |x|. \tag{8}$$

Moreover, let $y = y_0$, $|y| = |T_{\mathbb{C}}(z)| = |z^2 + mz + r|$. Then, by an assumption $|x| \geq |r|$, (**??**) and the fact that $\beta \leq 1$ we obtain

$$\begin{aligned}|y| \geq&|z^2 + mz| - |r|\\ \geq&\beta|z|^2 - |m||z| - |z|\\ \geq&|z|\Big(\beta|z| - (1 + |m|)\Big).\end{aligned}$$

This implies

$$|y| \geq |z|\Big(\frac{\beta|z|}{1 + |m|} - 1\Big).$$

From (**??**) and (**??**) we obtain

$$|y| \geq |x|\Big(\frac{\beta|x|}{1 + |m|} - 1\Big) > |x|. \tag{9}$$

Finally, we have

$$\begin{aligned}|x_1| =&|(1 - \alpha)y + \alpha T_{\mathbb{C}}(y)|\\ =&|(1 - \alpha)y + \alpha(y^2 + my + r)|.\end{aligned}$$

Furthermore, from $|x| \geq |r|$ and (**??**) we get that

$$\begin{aligned}|x_1| =&|(1-\alpha)y + \alpha(y^2 + my + r)|\\ \geq&\alpha|y^2| - (1-\alpha+\alpha|m|)|y| - \alpha|r|\\ \geq&\alpha|y^2| - (1-\alpha+\alpha|m|)|y| - \alpha|y|\\ =&\alpha|y^2| - (1+\alpha|m|)|y|\\ =&|y|\bigg(\alpha|y| - (1+\alpha|m|)\bigg).\end{aligned}$$

As $\alpha \leq 1$, we obtain

$$\begin{aligned}|x_1| \geq&|y|\bigg(\alpha|y| - (1+\alpha|m|)\bigg)\\ \geq&|y|\bigg(\alpha|y| - (1+|m|)\bigg)\\ \geq&|y|(1+|m|)\bigg(\frac{\alpha|y|}{(1+|m|)} - 1\bigg).\end{aligned}$$

By (**??**), we have

$$|x_1| \geq |x|\bigg(\frac{\alpha|x|}{1+|m|} - 1\bigg).$$

From our given assumption, we have $|x| > \frac{2(1+|m|)}{\alpha}$ and hence $\bigg(\frac{\alpha|x|}{1+|m|} - 1\bigg) > 1$. Thus, there exists a real number $\rho > 0$ such that

$$\bigg(\frac{\alpha|x|}{1+|m|} - 1\bigg) > 1 + \rho.$$

It follows that

$$|x_1| > (1+\rho)|x|.$$

In particular, $|x_1| > |x|$. Continuing in the same manner yields

$$|x_i| > (1+\rho)^i|x|.$$

Therefore, the orbit of x tends to infinity. □

The following corollary is the refinement of the Theorem **??**.

Corollary 1. *Suppose that* $|x_i| > \max\left\{|r|, \frac{2(1+|m|)}{\alpha}, \frac{2(1+|m|)}{\beta}\right\}$ *where* $\alpha, \beta \in (0,1]$ *then* $|x_i| \to \infty$ *as* $i \to \infty$.

2.2. Escape Criterion for Cubic Complex Polynomials in a Picard Ishikawa Type Orbit

For the cubic polynomial $T_{\mathbb{C}}(x) = x^3 + mx + r$ where $m, r \in \mathbb{C}$, we have the following result.

Theorem 4. *Suppose* $|x| \geq |r| > \max\left\{\left(\frac{2(1+|m|)}{\alpha}\right)^{\frac{1}{2}}, \left(\frac{2(1+|m|)}{\beta}\right)^{\frac{1}{2}}\right\}$, $\alpha, \beta \in (0,1]$. *Define a sequence* $\{x_i\}_{i\in\mathbb{N}}$ *as in* (**??**) *where* $x_0 = x$, $y_0 = y$, $z_0 = z$ *and* $t_0 = t$. *Then,* $|x_i| \to \infty$ *as* $i \to \infty$.

Proof. As $T_{\mathbb{C}}(x) = x^3 + mx + r$, from (**??**) we have

$$\begin{aligned}|t| =&|(1-\beta)x + \beta T_{\mathbb{C}}(x)|\\ =&|(1-\beta)x + \beta(x^3 + mx + r)|\\ \geq&|(1-\beta)x + \beta(x^3 + mx)| - \beta|r|.\end{aligned}$$

The assumption $|x| \geq |r|$ yields that

$$\begin{aligned}|t| \geq&|(1-\beta)x + \beta(x^3 + mx)| - \beta|x|\\ \geq&\beta|x^3| - (1 - \beta + \beta|m|)|x| - \beta|x|\\ =&\beta|x^3| - (1 + \beta|m|)|x|\\ =&|x|\bigg(\beta|x^2| - (1 + \beta|m|)\bigg).\end{aligned}$$

As $\beta \leq 1$,

$$|t| \geq |x|\bigg(\beta|x^2| - (1 + |m|)\bigg).$$

Therefore,

$$\begin{aligned}|t| \geq&\frac{|t|}{(1+|m|)}\\ \geq&|x|\bigg(\frac{\beta|x^2|}{1+|m|} - 1\bigg).\end{aligned} \tag{10}$$

The assumption, $|x| > \max\left\{\left(\frac{2(1+|m|)}{\alpha}\right)^{\frac{1}{2}}, \left(\frac{2(1+|m|)}{\beta}\right)^{\frac{1}{2}}\right\}$ implies that

$$\bigg(\frac{\beta|x^2|}{1+|m|} - 1\bigg) > 1. \tag{11}$$

It follows from (**??**) that

$$|t| > |x|. \tag{12}$$

As $z = z_0$, by (**??**) we have

$$\begin{aligned}|z| =&|T_{\mathbb{C}}(t)|\\ \geq&|t^3 + mt| - |r|.\end{aligned}$$

As $\beta \leq 1$, from (**??**) and assumption $|x| \geq |r|$ we obtain

$$\begin{aligned}|z| \geq&|t^3 + mt| - |x|\\ =&|t|\bigg(\beta|t^2| - (1 + |m|)\bigg)\end{aligned}$$

which further implies that

$$|z| \geq |t|\bigg(\frac{\beta|t^2|}{(1+|m|)} - 1\bigg). \tag{13}$$

Now by (**??**) and (**??**), we have

$$\bigg(\frac{\beta|t|^2}{1+|m|} - 1\bigg) \geq \bigg(\frac{\beta|x|^2}{1+|m|} - 1\bigg) > 1. \tag{14}$$

Consequently, (**??**), (**??**) and (**??**) imply that

$$|z| > |x|. \tag{15}$$

Also, $y = y_0$, $|y| = |T_{\mathbb{C}}(z)| = |z^3 + mz + r|$. Then, the given assumption $|x| \geq |r|$, (**??**) and the fact that $\beta \leq 1$ yield

$$\begin{aligned}|y| \geq & |z^3 + mz| - |r| \\ \geq & |z|\Big(\beta|z^2| - (1 + |m|)\Big).\end{aligned}$$

Thus

$$|y| \geq |z|\left(\frac{\beta|z^2|}{1 + |m|} - 1\right).$$

From (**??**) and (**??**), we obtain

$$|y| \geq |x|\left(\frac{\beta|x^2|}{1 + |m|} - 1\right) > |x|. \tag{16}$$

Lastly, we have

$$\begin{aligned}|x_1| =& |(1 - \alpha)y + \alpha T_{\mathbb{C}} y| \\ =& |(1 - \alpha)y + \alpha(y^3 + my + r)|.\end{aligned}$$

From $|x| \geq |r|$, (**??**) and $\alpha \leq 1$, we have

$$\begin{aligned}|x_1| =& |(1 - \alpha)y + \alpha(y^3 + my + r)| \\ \geq & \alpha|y^3| - (1 - \alpha + \alpha|m|)|y| - \alpha|y| \\ =& \alpha|y^2| - (1 + \alpha|m|)|y| \\ \geq & |y|\Big(\alpha|y^2| - (1 + |m|)\Big) \\ \geq & |y|(1 + |m|)\left(\frac{\alpha|y^2|}{(1 + |m|)} - 1\right).\end{aligned}$$

From (**??**), we have

$$|x_1| \geq |x|\left(\frac{\alpha|x^2|}{1 + |m|} - 1\right).$$

By our assumption we have $|x| > \left(\frac{2(1+|m|)}{\alpha}\right)^{\frac{1}{2}}$ and hence $\left(\frac{\alpha|x^2|}{1+|m|} - 1\right) > 1$. Thus, there exists a real number $\rho > 0$ such that

$$\left(\frac{\alpha|x^2|}{1 + |m|} - 1\right) > 1 + \rho.$$

It follows that

$$|x_1| > (1 + \rho)|x|.$$

Continuing in the same manner, we obtain

$$|x_i| > (1 + \rho)^i |x|.$$

Therefore, the orbit of x tends to infinity. □

The following corollary is the refinement of the Theorem **??**.

Corollary 2. *Suppose that* $|x_i| > \max\left\{|r|, \left(\frac{2(1+|m|)}{\alpha}\right)^{\frac{1}{2}}, \left(\frac{2(1+|m|)}{\beta}\right)^{\frac{1}{2}}\right\}$ *where* $\alpha, \beta \in (0,1]$ *then* $|x_i| \to \infty$ *as* $i \to \infty$.

2.3. Escape Criterion for General Complex Polynomials in a Picard Ishikawa Type Orbit

For the general complex polynomial $T_{\mathbb{C}}(x) = x^n + mx + r$ where $m, r \in \mathbb{C}$, we have the following result.

Theorem 5. *Suppose* $|x| \geq |r| > \max\left\{\left(\frac{2(1+|m|)}{\alpha}\right)^{\frac{1}{n-1}}, \left(\frac{2(1+|m|)}{\beta}\right)^{\frac{1}{n-1}}\right\}$, *with* $n \geq 2$ *and* $\alpha, \beta \in (0,1]$. *Define a sequence* $\{x_i\}_{i\in\mathbb{N}}$ *as in* (**??**) *where* $x_0 = x$, $y_0 = y$, $z_0 = z$ *and* $t_0 = t$. *Then,* $|x_i| \to \infty$ *as* $i \to \infty$.

Proof. Let $T_{\mathbb{C}}(x) = x^n + mx + r$. Note that (**??**), assumptions $|x| \geq |r|$ and $\beta \leq 1$ give

$$\begin{aligned} |t| =& |(1-\beta)x + \beta T_{\mathbb{C}}(x)| \\ \geq& |(1-\beta)x + \beta(x^n + mx)| - \beta|r| \\ \geq& \beta|x^n| - (1 - \beta + \beta|m|)|x| - \beta|x| \\ =& |x|\bigg(\beta|x^{n-1}| - (1 + \beta|m|)\bigg) \\ \geq& |x|\bigg(\beta|x^{n-1}| - (1 + |m|)\bigg). \end{aligned}$$

Therefore,

$$|t| \geq |x|\bigg(\frac{\beta|x^{n-1}|}{1+|m|} - 1\bigg). \tag{17}$$

By our assumption, we have $|x| > \left(\frac{2(1+|m|)}{\beta}\right)^{\frac{1}{n-1}}$ and hence

$$\bigg(\frac{\beta|x^{n-1}|}{1+|m|} - 1\bigg) > 1. \tag{18}$$

It follows from (**??**) that

$$|t| > |x|. \tag{19}$$

Since $z = z_0$, so from (**??**) we obtain

$$|z| \geq |t^n + mt| - |r|.$$

As $\beta \leq 1$, from (**??**) and assumption $|x| \geq |r|$, we have

$$|z| \geq |t|\bigg(\frac{\beta|t^{n-1}|}{(1+|m|)} - 1\bigg). \tag{20}$$

Now by (**??**) and (**??**), we have

$$\bigg(\frac{\beta|t|^{n-1}}{1+|m|} - 1\bigg) > 1.$$

Hence,

$$|z| > |x|. \tag{21}$$

As $y = y_0$, $|y| = |T_{\mathbb{C}}(z)| = |z^n + mz + r|$, so using the similar arguments as before we obtain

$$|y| \geq |x|\left(\frac{\beta|x^{n-1}|}{1+|m|} - 1\right) > |x|. \tag{22}$$

Also, from $|x| \geq |r|$, (**??**), and $\alpha \leq 1$ we have

$$\begin{aligned}|x_1| =& |(1-\alpha)y + \alpha(y^n + my + r)| \\ \geq& \alpha|y^n| - (1 - \alpha + \alpha|m|)|y| - |r| \\ =& \alpha|y^2| - (1 + \alpha|m|)|y| \\ =& |y|\Big(\alpha|y^2| - (1 + \alpha|m|)\Big) \\ \geq& |x|\left(\frac{\alpha|x^2|}{1+|m|} - 1\right).\end{aligned}$$

Furthermore, from our assumption we have $|x| > \left(\frac{2(1+|m|)}{\alpha}\right)^{\frac{1}{n-1}}$ and thus $\left(\frac{\alpha|x^{n-1}|}{1+|m|} - 1\right) > 1$. Thus, there exists a real number $\rho > 0$ such that

$$\left(\frac{\alpha|x^{n-1}|}{1+|m|} - 1\right) > 1 + \rho.$$

Finally, we obtain

$$|x_1| > (1+\rho)|x|.$$

Now, continuing this process

$$|x_i| > (1+\rho)^i|x|.$$

Therefore, the orbit of x tends to infinity. □

The following corollary is the refinement of the Theorem **??**.

Corollary 3. *Suppose that* $|x_i| > \max\left\{|r|, \left(\frac{2(1+|m|)}{\alpha}\right)^{\frac{1}{n-1}}, \left(\frac{2(1+|m|)}{\beta}\right)^{\frac{1}{n-1}}\right\}$ *where* $n \geq 2$ *and* $\alpha, \beta \in (0, 1]$ *then* $|x_i| \to \infty$ *as* $i \to \infty$.

Theorem 6. *Suppose that* $\{x_i\}_{i\in\mathbb{N}\cup\{0\}}$ *is a sequence in the Picard Ishikawa type orbit for the complex polynomial* $T_{\mathbb{C}}(x) = x^n + mx + r$ *where* $m, r \in \mathbb{C}$ *with* $n \geq 2$ *such that* $|x_i| \to \infty$ *as* $i \to \infty$, *then* $|x| \geq |r| > \left(\frac{2(1+|m|)}{\alpha}\right)^{\frac{1}{n-1}}$ *and* $|x| \geq |r| > \left(\frac{2(1+|m|)}{\beta}\right)^{\frac{1}{n-1}}$, $\alpha, \beta \in (0, 1]$.

Proof. Let $\{x_i\}_{i\in\mathbb{N}}$ be a sequence in Picard Ishikawa type orbit. First, we prove that $|x| \geq |r|$. According to hypothesis, $|x_i| \to \infty$ as $i \to \infty$, the sequence $\{|x_i|\}$ must be unbounded. Hence, $|x_i| \geq |r|$ for all $i \in \mathbb{N} \cup \{0\}$ and therefore $|x| \geq |r|$. Let $T_{\mathbb{C}}(x) = x^n + mx + r$, $m, r \in \mathbb{C}$ where $t_0 = t$, $x_0 = x$, $y_0 = y$ and $z_0 = z$, then $|x| \geq |r|$ implies that

$$\begin{aligned}|t| =& |(1-\beta)x + \beta T_{\mathbb{C}}x| \\ =& |(1-\beta)x + \beta(x^n + mx + r)| \\ \geq& |\beta x^n| + ((1-\beta) + m\beta)x| - \beta|r| \\ \geq& \beta|x^n| - ((1-\beta) + |m|\beta)|x| - \beta|x| \\ \geq& \beta|x^n| - (1 + |m|\beta)|x|.\end{aligned}$$

Thus,

$$\begin{aligned}|t| \geq &|x|(\beta|x^{n-1}| - (1+|m|))\\ &= |x|(1+|m|)\left(\frac{\beta|x^{n-1}|}{1+|m|} - 1\right)\end{aligned}$$

implies

$$|t| \geq |x|\left(\frac{\beta|x^{n-1}|}{1+|m|} - 1\right). \tag{23}$$

Here, we have two possibilities; either $\left(\frac{\beta|x^{n-1}|}{1+|m|} - 1\right) \leq 1$ or $\left(\frac{\beta|x^{n-1}|}{1+|m|} - 1\right) > 1$. If $\left(\frac{\beta|x^{n-1}|}{1+|m|} - 1\right) \leq 1$ we have

$$\frac{\beta|x^{n-1}|}{1+|m|} \leq 2$$

which implies that

$$|x^{n-1}| \leq \frac{2(1+|m|)}{\beta}$$

and hence

$$|x| \leq \left(\frac{2(1+|m|)}{\beta}\right)^{\frac{1}{n-1}},$$

a contradiction. Indeed, $\{|x_i|\}$ is not bounded where $i \in \mathbb{N} \cup \{0\}$. Therefore, we must have $\left(\frac{\beta|x^{n-1}|}{1+|m|} - 1\right) > 1$. Thus, $|x| > \left(\frac{2(1+|m|)}{\beta}\right)^{\frac{1}{n-1}}$. Now, inequality (**??**) implies that

$$|t| \geq |x|\left(\frac{\beta|x^{n-1}|}{1+|m|} - 1\right) > |x|.$$

Furthermore, $\beta \leq 1$ and $|x| \geq |r|$ give

$$\begin{aligned}|z| =&|T_{\mathbb{C}}(t)|\\ \geq&|t^n + mt| - |r| \geq \beta|t^n| - |m||t| - |x|\\ =&|t|(\beta|t^{n-1}| - |(1+|m|)).\end{aligned}$$

As $\left(\frac{\beta|x^{n-1}|}{(1+|m|)} - 1\right) > 1$, so we have

$$|t| > |x|\left(\frac{\beta|x^{n-1}|}{1+|m|} - 1\right) > |x|.$$

As a consequence we obtain

$$|z| \geq|x|\left(\frac{\beta|x^{n-1}|}{1+|m|} - 1\right)(1+|m|).$$

Thus,

$$|z| \geq |x|\left(\frac{\beta|x^{n-1}|}{1+|m|} - 1\right) > |x|. \tag{24}$$

Similarly, $|y| = |T_{\mathbb{C}}(z)| = |z^n + mz + r|$, $|x| > |r|$ and $\beta \leq 1$ imply that

$$|y| \geq |x|\left(\frac{\beta|x^{n-1}|}{1+|m|} - 1\right).$$

Consequently,

$$|y| \geq |x|\left(\frac{\beta|x^{n-1}|}{1+|m|} - 1\right) > |x|. \tag{25}$$

Finally, we have

$$\begin{aligned}
|x_1| =& |(1-\alpha)y + \alpha T_{\mathbb{C}}(y)| \\
=& |(1-\alpha)y + \alpha(y^n + my + r)| \\
\geq& \alpha|y^n| - (1-\alpha+\alpha|m|)|y| - \alpha|r| \\
\geq& \alpha|y^n| - (1-\alpha+\alpha|m|)|y| - \alpha|y| \\
\geq& \alpha|y^n| - (1+\alpha|m|)|y| \\
\geq& \alpha|y^n| - (1+|m|)|y| \\
=& |y|(\alpha|y^{n-1}| - (1+|m|)) \\
\geq& |x|(\alpha|x^{n-1}| - (1+|m|)).
\end{aligned}$$

Hence

$$|x_1| \geq |x|\left(\frac{\alpha|x^{n-1}|}{1+|m|} - 1\right).$$

Using arguments similar to those as before, we only have one possibility that $\left(\frac{\alpha|x^{n-1}|}{1+|m|} - 1\right) > 1$. Therefore, $|x| > \left(\frac{2(1+|m|)}{\alpha}\right)^{\frac{1}{n-1}}$. This completes the proof. □

3. Visualization of Fractals

In this section, we present some Julia and Mandelbrot sets for quadratic and higher order polynomials. We found several captivating new fractals having various geometric shapes. However, we have chosen some figures. The color variation occurs due to the change of input parameters. We have also investigated the effect of change of parameters α and β on the shape and the variation of colors. The number of iterations was fixed at 10.

3.1. Generation of Julia sets

Following Algorithm 1 is the pseudocode for the generation of Julia sets. Note that $T'(z)$ represents the iteration process.

```
Algorithm 1: Generation of Julia Set
    Input  : complex polynomial–$T : \mathbb{C} \to \mathbb{C}$, parameters–$r, m \in \mathbb{C}$, Area–$A \subset \mathbb{C}$, number of
             iterations–$N$, colormap with $M$ colors–$colormap[0...M-1]$
    Output: $\Re$ is the area for Julia set
$R$ = Threshold radius
for $c \in A$
 do
    $k = 0$
    while $k \leq N$ do
        $z = T'(z)$
        if $|z| > R$ then
            break
        end
        $k = k + 1$
    end
    $m = \lfloor (M-1)\frac{k}{N} \rfloor$
    color $c$ with $colormap[m]$
end
```

Now, we present quadratic, cubic and septic Julia sets in Picard Ishikawa type orbit for the complex polynomial, $T_{\mathbb{C}}(x) = x^n + mx + r$.

1. For Figure **??**, we consider the polynomial $T(x) = x^2 + (-0.5 + 0.7i)x + (-0.01 + 0.18i)$ and $A = [-2.5, 2.5] \times [-2.1, 2.1]$. It is easy to see that T has one attracting fixed point, $p = -0.1427 + 0.1019i$. Observe that for $\alpha = 0.2$, $\beta = 0.097$ and $\alpha = 0.11$,$\beta = 0.18$ we obtain different images due to color variation caused by parameters. It is interesting to note that for $\alpha = 1$, $\beta = 1$ and $\alpha = 10^{-10}$, $\beta = 10^{-10}$ we have similar shapes but there is clear variation of colors.
2. For Figure **??**, we consider the polynomial $T(x) = x^3 + (-0.275 + 0.5i)x + (-0.559 + 0.35i)$ and $A = [-1.5, 1.5] \times [-1.8, 1.8]$. The polynomial T has attracting fixed point $p \sim -0.6434 + 0.2687i$ in A. Note that the cubic Julia sets for $\alpha = 0.08$ and $\beta = 0.09$ have more color variation as compared to the Julia sets for $\alpha = 0.1$, and $\beta = 0.2$. Again, for $\alpha = 1$, $\beta = 1$ and $\alpha = 10^{-10}$, $\beta = 10^{-10}$ the shapes are same but there is variability in colors.
3. For Figure **??**, we input $T(x) = x^7 + (0.23 + 1.2i)x + (0.5 + 0.7i)$ and $A = [-1.3, 1.3]^2$. The attracting fixed point of the polynomial is $p \sim -0.2391 + 0.5835i$. We can see that for $\alpha = 0.01$ and $\beta = 0.08$ the shape is spread and stretched while the shape is dense and neatly packed for $\alpha = 0.1$ and $\beta = 0.05$. Note the variation of colors in figures (C) and (D) as well.

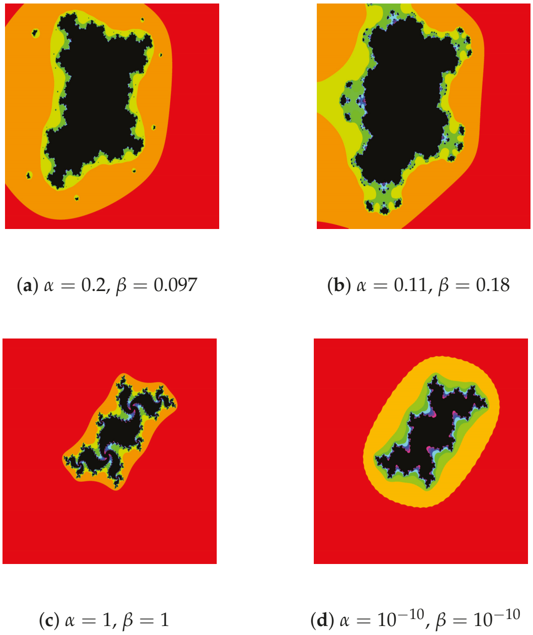

(**a**) $\alpha = 0.2$, $\beta = 0.097$

(**b**) $\alpha = 0.11$, $\beta = 0.18$

(**c**) $\alpha = 1$, $\beta = 1$

(**d**) $\alpha = 10^{-10}$, $\beta = 10^{-10}$

Figure 1. Quadratic Julia sets.

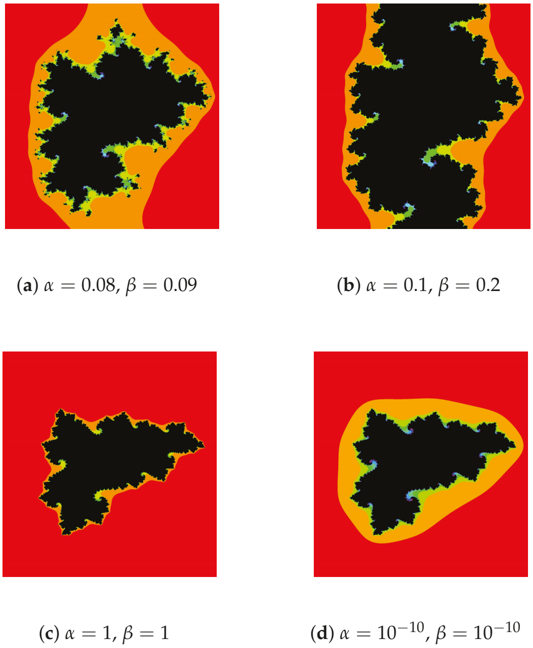

(**a**) $\alpha = 0.08$, $\beta = 0.09$

(**b**) $\alpha = 0.1$, $\beta = 0.2$

(**c**) $\alpha = 1$, $\beta = 1$

(**d**) $\alpha = 10^{-10}$, $\beta = 10^{-10}$

Figure 2. Cubic Julia sets.

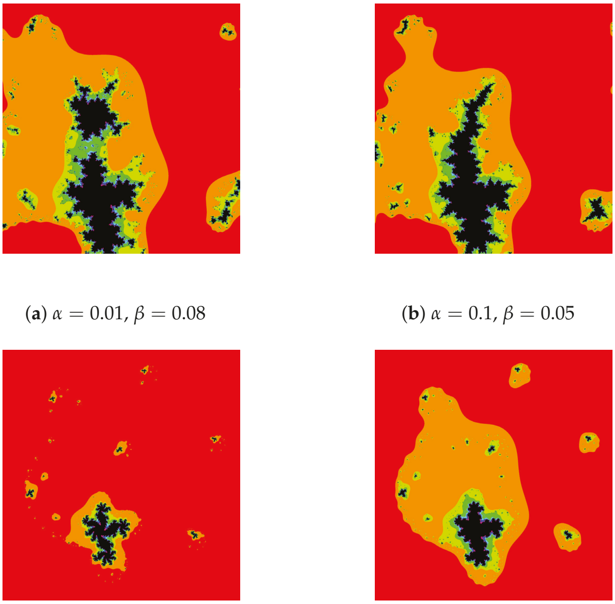

(**a**) $\alpha = 0.01, \beta = 0.08$

(**b**) $\alpha = 0.1, \beta = 0.05$

(**c**) $\alpha = 1, \beta = 1$

(**d**) $\alpha = 0.009, \beta = 0.009$

Figure 3. Septic Julia sets.

3.2. Generation of Mandelbrot Sets

Following Algorithm 2 is the pseudocode for the generation of Mandelbrot sets. Note that $T'(z)$ represents the iteration process.

Algorithm 2: Generation of Mandelbrot set.

```
Input  : complex polynomial–$T : \mathbb{C} \to \mathbb{C}$, parameters–$r, m \in \mathbb{C}$, Area–$A \subset \mathbb{C}$, number of
         iterations–$N$, colormap with $M$ colors–$colormap[0...M-1]$
Output: $\Re$ is the area for Mandelbrot set

for $c \in A$
 do
    $R$ = Threshold radius
    $k = 0$
    $x_0$ = critical point of $T$
    while $k \leq N$ do
        $z = T'(z)$
        if $|z| > R$ then
            break
        end
        $k = k + 1$
    end
    $m = \lfloor (M-1)\frac{k}{N} \rfloor$
    color $c$ with $colormap[m]$
end
```

For Figure **??** we input $A = [-2, 2] \times [-1.2, 2.5]$ and observe that for $\alpha = 0.1$ and $\beta = 0.3$, the shape is stretched and the bulb is wider and for $\alpha = 0.75$ and $\beta = 0.7$ the shape is compact with defined bulb. Notice the variation of colors for Mandelbrot sets for $\alpha = 1$, $\beta = 1$ and $\alpha = 0.009$, $\beta = 0.009$. Also, observe that Mandelbot sets generated are symmetric about origin.

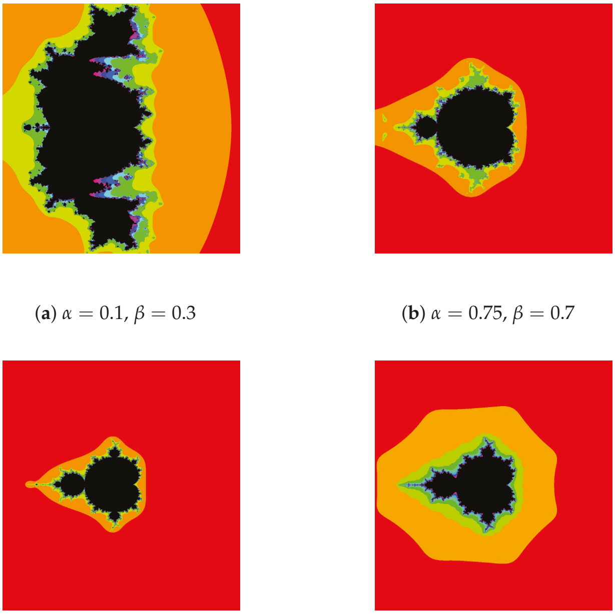

(**a**) $\alpha = 0.1$, $\beta = 0.3$

(**b**) $\alpha = 0.75$, $\beta = 0.7$

(**c**) $\alpha = 1$, $\beta = 1$

(**d**) $\alpha = 0.009$, $\beta = 0.009$

Figure 4. Mandelbrot sets.

4. Conclusions

In this paper, a Picard Ishikawa type orbit was used to study the behaviour of complex poylnomials. We obtained escape criterions for complex quadratic, cubic and higher degree polynomials. Some alluring Julia and Mandelbrot sets have been generated. We also observed that the variation of parameters has shown eminent changes in the Julia and Mandelbrot sets. Our results are different from comparable existing results as we obtain escape criterion and fractals for polynomials of the form $T(x) = x^n + mx + r$ where $m, r \in \mathbb{C}$ without using the Jungck iterative process. It is also worth mentioning that the behaviour of the polynomial and shape of the fractal generated under the iterative process (**??**) is different and unique as compared to the iterative process studied before in the literature [**? ? ? ?**].

Author Contributions: Conceptualization, M.A. and H.I.; methodology, M.A. and H.I.; validation, M.A. and M.D.l.S., formal analysis H.I.; investigation, H.I. and M.A.; writing—original draft preparation, H I.; writing—review and editing, H.I.; visualization, M.D.l.S.; supervision, M.A. and M.D.l.S.; project administration, M.D.l.S.; funding acquisition, M.D.l.S. All authors have read and agreed to the published version of the manuscript.

Funding: This research was funded by Basque Government through grant number IT 1207-19.

Acknowledgments: All the authors are grateful to the referees for their critical remarks and valuable suggestions which helped to improve the presentation of the paper.

Conflicts of Interest: The authors declare no conflict of interest.

References

1. Barnsley, M. *Fractals Everywhere*, 2nd ed.; Academic Press: San Diego, CA, USA, 1993.
2. Hundertmark-Zauôkovù, A. On the convergence of fixed point iterations for the moving geometry in a fluid-structure interaction problem. *J. Differ. Equ.* **2019**, *267*, 7002–7046. [CrossRef]
3. Rahmani, M.; Koutsopoulos, H.N.; Jenelius, E. Travel time estimation from sparse floating car data with consistent path inference: A fixed point approach. *Transp. Res. Part C Emerg. Technol.* **2017**, *85*, 628–643. [CrossRef]
4. Strogatz, S.H. *Nonlinear Dynamics and Chaos With Applications to Physics, Biology, Chemistry, and Engineering*, 2nd ed.; CRC Press: Boca Raton, FL, USA, 2018.
5. Julia, G. Memoire sur l'iteration des functions rationnelles. *J. Math. Pures Appl.* **1918**, *8*, 737–747.
6. Devaney, R.L. *A First Course in Chaotic Dynamical Systems: Theory and Experiment*, 2nd ed.; Addison-Wesley: Boston, MA, USA, 1992.
7. Falconer, K. *Fractal Geometry: Mathematical Foundations and Applications*, 2nd ed.; John Wiley & Sons: Chichester, UK, 2004.
8. Frame, M.; Robertson, J. A generalized Mandelbrot set and the role of critical points. *Comput. Graph.* **1992**, *16*, 35–40. [CrossRef]
9. Brouwer, L.E.J. Über Abbildungen von Mannigfaltigkeiten. *Math. Ann.* **1912**, *71*, 97–115. [CrossRef]
10. Mandelbrot, B.B. *The Fractal Geometry of Nature*; W.H. Freeman: New York, NY, USA, 1983; Volume 2.
11. Debnath, L. A brief historical introduction to fractals and fractal geometry. *Int. J. Math. Educ. Sci. Technol.* **2006**, *37*, 29–50. [CrossRef]
12. Lakhtakia, A.; Varadan, W.; Messier, R.; Varadan, V.K. On the symmetries of the Julia sets for the process $z^p + c$. *J. Phys. A Math. Gen.* **1987**, *20*, 3533–3535. [CrossRef]
13. Negi, A.; Rani, M. Midgets of superior Mandelbrot set. *Chaos Solitons Fract.* **2008**, *36*, 237–245. [CrossRef]
14. Negi, A.; Rani, M. A new approach to dynamic noise on superior Mandelbrot set. *Chaos Solitons Fract.* **2008**, *36*, 1089–1096. [CrossRef]
15. Rochon, D. A generalized Mandelbrot set for bicomplex numbers. *Fractals* **2000**, *8*, 355–368. [CrossRef]
16. Wang, X.; Sun, Y. The general quaternionic M-J sets on the mapping $z \leftarrow z^\alpha + c(\alpha \in \mathbb{N})$. *Comput. Math. Appl.* **2007**, *53*, 1718–1732. [CrossRef]
17. Rani, M. Theoretical Framework for Fractal Models under Two-Step Feedback Process. Ph.D. Thesis, Kumaun University, Nainital, India, 2016.
18. Rani, M.; Kumar, V. Superior Julia set. *Res. Math. Educ.* **2004**, *8*, 261–277.
19. Rani, M.; Kumar, V. Superior Mandelbrot set. *Res. Math. Educ.* **2004**, *8*, 279–291.
20. Rani, M.; Chauhan, Y.S.; Negi, A. Non linear dynamics of Ishikawa iteration. *Int. J. Comput. Appl.* **2010**, *7*, 43–49. [CrossRef]
21. Chauhan, Y.S.; Rana, R.; Negi, A. New Julia sets of Ishikawa iterates. *Int. J. Comput. Appl.* **2010**, *7*, 34–42. [CrossRef]
22. Chauhan, Y.S.; Rana, R.; Negi, A. Complex dynamics of Ishikawa iterates for non integer values. *Int. J. Comput. Appl.* **2010**, *9*, 9–16. [CrossRef]
23. Ashish; Rani, M.; Chugh, R. Julia sets and Mandelbrot sets in Noor orbit. *Appl. Math. Comput.* **2014**, *228*, 615–631.
24. Kang, S.M.; Rafiq, A.; Latif, A.; Shahid, A.A.; Ali, F. Fractals through modified iteration scheme. *Filomat* **2016**, *30*, 3033–3046. [CrossRef]
25. Kang, S.M.; Rafiq, A.; Latif, A.; Shahid, A.A.; Kwun, Y.C. Tricorns and multicorns of S-iteration scheme. *J. Funct. Spaces* **2015**, *2015*, 417167.
26. Kumari, M.; Ashish, R.C. New Julia and Mandelbrot sets for a new faster iterative process. *Int. J. Pure Appl. Math.* **2016**, *107*, 161–177. [CrossRef]
27. Kang, S.M.; Nazeer, W.; Tanveer, M.; Shahid, A.A. New fixed point results for fractal generation in Jungck Noor orbit with s-convexity. *J. Funct. Spaces* **2015**, *2015*, 963016. [CrossRef]
28. Kang, S.M.; Rafiq, A.; Tanveer, M.; Ali, F.; Kwun, Y.C. Julia and Mandelbrot sets in modified Jungck three-step orbit. *Wulfenia J.* **2015**, *22*, 167–185.
29. Kwun, Y.C.; Tanveer, M.; Nazeer, W.; Abbas, M.; Kang, S.M. Fractal generation in modified Jungck-S orbit. *IEEE Access* **2019**, *7*, 35060–35071. [CrossRef]

30. Proakis, J.G.; Manolakis, D.G. *Digital Signal Processing: Principles, Algorithms and Applications*, 4th ed.; Pearson: Bengaluru, India, 2007.
31. Mishra, M.K.; Ojha, D.B.; Sharma, D. Fixed point results in tricorn and multicorns of Ishikawa iteration and s-convexity. *IJEST* **2011**, *2*, 157–160.
32. Cho, S.Y.; Shahid, A.A.; Nazeer, W.; Kang, S.M. Fixed point results for fractal generation in noor orbit and s-convexity. *SpringerPlus* **2016**, *5*, 1843. [CrossRef] [PubMed]
33. Nazeer, W.; Kang, S.M.; Tanveer, M.; Shahid, A.A. Fixed point results in the generation of Julia and Mandelbrot sets. *J. Inequal. Appl.* **2015**, *2015*, 298. [CrossRef]
34. Piri, H.; Daraby, B.; Rahrovi, S.; Ghasemi, M. Approximating fixed points of generalized α-nonexpansive mappings Banach spaces by new faster iteration process. *Numer. Algorithms* **2018**, *81*, 1129–1148. [CrossRef]

symmetry

Article

A Continuous Coordinate System for the Plane by Triangular Symmetry

Benedek Nagy * and Khaled Abuhmaidan

Department of Mathematics, Faculty of Arts and Sciences, Eastern Mediterranean University, via Mersin 10, Turkey, Famagusta 99450, North Cyprus; kabuhumaidan@yahoo.com

* Correspondence: nbenedek.inf@gmail.com

Received: 20 December 2018; Accepted: 31 January 2019; Published: 9 February 2019

Abstract: The concept of the grid is broadly used in digital geometry and other fields of computer science. It consists of discrete points with integer coordinates. Coordinate systems are essential for making grids easy to use. Up to now, for the triangular grid, only discrete coordinate systems have been investigated. These have limited capabilities for some image-processing applications, including transformations like rotations or interpolation. In this paper, we introduce the continuous triangular coordinate system as an extension of the discrete triangular and hexagonal coordinate systems. The new system addresses each point of the plane with a coordinate triplet. Conversion between the Cartesian coordinate system and the new system is described. The sum of three coordinate values lies in the closed interval $[-1, 1]$, which gives many other vital properties of this coordinate system.

Keywords: barycentric coordinate system; coordinate system; hexagonal grid; triangular grid; tri-hexagonal grid; transformations

1. Introduction

The concept of the grid is essential and heavily used in digital geometry and in digital image processing. A grid is comprised of discrete points addressed with integer vectors. There are three regular tessellations of the plane, which define the square, hexagonal, and triangular grids (named after the form of the pixels used as tiles) [1]. Most of the applications use the square grid because its orthogonal coordinate system, known as the Cartesian coordinate system (CCS), which fits very well to it. This addresses each square pixel of the grid by a pair of independent integers. The dual of the square grid (the grid formed by the nodes, which are the crossing points of the gridlines) is again a square grid. Therefore, essentially, the same CCS is used as well. Working with real images, we may need to perform operations that do not map the grid to itself, e.g., zooming or rotations. The Cartesian coordinate system allows real numbers to be used in such cases. Moreover, the digitization operation can easily be defined by a rounding operation.

The hexagonal grid, tiling the plane by the same size regular hexagons (hexagonal pixels), has been used for decades in image processing applications [2], in cartography [3,4], in biological simulations [5], and in other fields, since the digital geometry of the hexagonal grid provides better results than the square grid in various cases. In addition, it is used in various table and computer games based on its compactness. It is the simplest 2D grid, since the only usual neighborhood using the nearest neighbors is simpler and less confusing than the two types of neighbors in the square grid [6]. The neighborhood of a pixel contains six other hexagons (see Figure 1a). In contrast to the square grid, the dual of the hexagonal grid is not the hexagonal, but the triangular grid (see Figure 1a,b). Adequate and elegant coordinate systems for these kinds of grids are required for their use in both theory and applications, e.g., in image processing or engineering applications. In Reference [7], a three-coordinate-valued system of zero-sum triplets is used to describe the hexagonal grid capturing the triangular symmetry of the grid. In Figure 1a, the first coordinate value is ascending right-upwardly, the second values are ascending into the right-downward direction, and the third one is ascending into the left-upward direction [7,8]. We should mention that this system could be seen as the extension of the oblique coordinate system using two independent integer values [9] by concerning the third value to obtain zero-sum for every triplet. The digital distance based on the neighborhood relation is computed in Reference [9]. Since the vectors describing the grid are not orthogonal, some geometric descriptions based on Cartesian coordinates are not very clear. However, to simplify the expressions of the constrained three-dimensional coordinate system is recommended. We should also mention that 0-sum triplets allowing real numbers were used in Reference [8] to describe rotations (that may not map the hexagonal grid to itself). In this way, a useful digitization operator is found. Her's system was mentioned and used in References [10,11] for various imaging-related disciplines.

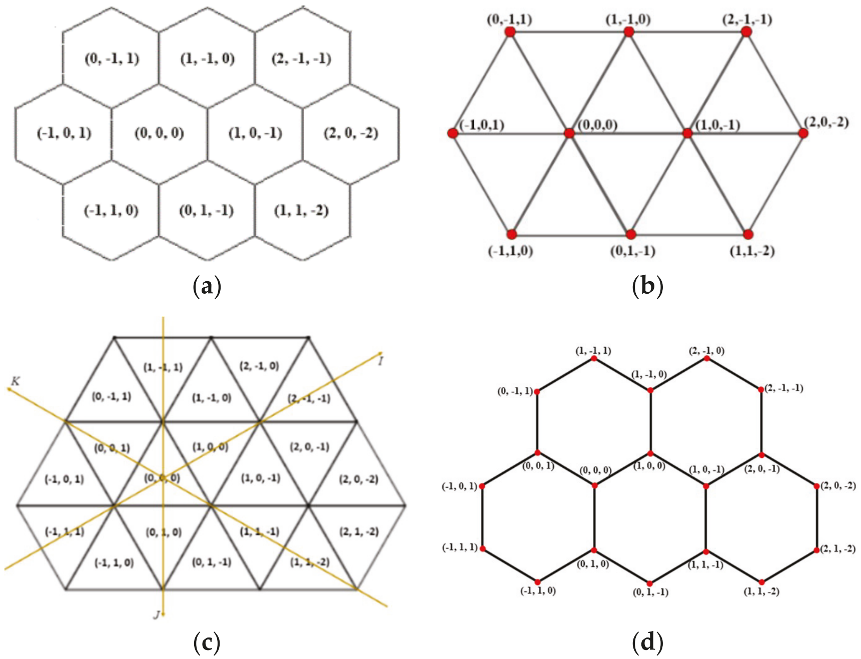

(**a**) (**b**)

(**c**) (**d**)

Figure 1. The coordinate system for the hexagonal grid (**a**) and its dual (**b**). The coordinate system for the triangular grid (**c**) and its dual (**d**).

The triangular grid is the third regular grid. It is generated by tiling the plane regularly with equilateral triangles. Although it is the most complex among the three regular tessellations (it has the largest number and types of neighbors), it has various advantages in applications, e.g., by the flexibility of the used neighborhood. The triangular grid is built by triangles in two different orientations. Moreover, it is not a point lattice since some of the grid vectors, i.e., the vectors connecting the midpoints of triangles with different orientations, do not translate the grid into itself [12]. However, the triangular grid gives a valid alternative for applications in image processing. In some cases, it gives better results than the usual square grid due to its better symmetric properties and larger, natural neighborhood structure. Each pixel has 12 neighbors sharing at least a corner. They are categorized into three types of neighbor relations [13,14]. The triangular grid has similar symmetry to the hexagonal grid. Therefore, in Reference [15], a coordinate system with zero-sum and one-sum triplets are used to describe this grid (the three values are not independent, since this is also a 2D grid, see Figure 1c,d). The angle between any two of the three coordinate axes is 120° as for the hexagonal grid. In this description, two pixels are neighbors if their coordinate values differ by at most one. Moreover, at the closest neighbors, only one coordinate differs [15,16]. Observe that exactly the same coordinate triplets are used on the left and on the right-hand side in Figure 1c,d, respectively, which shows the duality of the triangular and hexagonal grids. In Reference [17], a combinatorial coordinate system was shown that addresses the pixels, the corners, and the edges between them. That coordinate system gives an efficient tool to work with digital cell complexes on the triangular grid. Various image processing algorithms have been defined and implemented for the triangular grid recently such as discrete tomography [18,19], thinning [20], and mathematical morphology [21]. We should also mention that triangulation is a frequently used technique in imaging and computer graphics. However, the obtained grid is usually not the regular triangular grid. Lastly, we should note that several non-regular grids have various applications in 2D and in higher dimensions.

The coordination is vital because it is a leading tool in making a simple, easily usable, and effectively programmable system with integer numbers (coordinates). The isometric transformations are described in Reference [12]. However, up to now, there was no such extension of this coordinate system that is able to address the entire plane. For various applications, including, e.g., arbitrary angled rotations, an extension of the coordinate system is needed. We note here that Her's zero-sum triplets could match only up to half of the grid points in the triangular grid (Figure 1c,d), and, therefore, the coordinate system addressing the whole plain cannot be used for the triangular grid.

In this paper, we introduce a continuous coordinate system for the plain based on the symmetry of the triangular grid, where every point of the 2D plane has its unique coordinate triplet. We use three coordinate values to describe the triangular grid as in Reference [15] but also to address the points of the plane "between" and "around" the nodes of the dual grid. Our new coordinate system is shown to be an extension of the hexagonal and of the triangular coordinate systems. Moreover, our system builds upon the coordinate system for the so-called, tri-hexagonal grid, also called the three-plane triangular grid in Reference [16].

For further applications, we also provide a mapping between our continuous coordinate system for the triangular grid and the Cartesian coordinate system of the 2D plane.

The rest of this paper is as follows. The next, preliminary section, describes some important discrete coordinate systems and the barycentric coordinate system. The continuous coordinate system for the triangular grid is then introduced in Section 3. Conversions to and from Cartesian coordinates are also presented. Some important properties of the new coordinate system are presented in Section 4. Lastly, conclusions close the paper.

2. Preliminaries

In this paper, as usual, Z^3 denotes the cubic grid, whose points are addressed by integer triplets, according to the three coordinates x, y, z.

In order to create a continuous coordinate system for the triangular grid that enables us to uniquely address any point of the triangular grid, we combine discrete triangular coordinate systems from Reference [22] (see also Figure 1 for some examples) with the barycentric coordinate system (BCS), discovered by Möbius (see References [1,23]).

In Figure 2, a coordinate system for the tri-hexagonal grid (the three-plane triangular grid of regions [16]) and its dual is given. This grid resembles a mix of the triangular and hexagonal grids since it is a combination of the one-plane and two-plane grids [7,22]. The new coordinate system will be an extension of the discrete triangular and hexagonal coordinate systems.

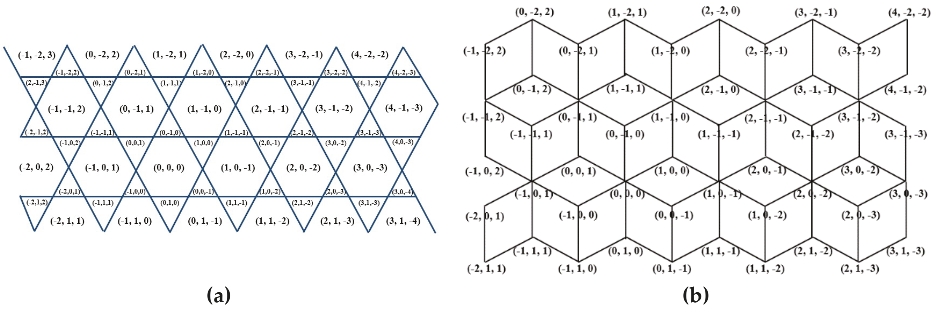

Figure 2. Representation of the tri-hexagonal coordinate system (**a**) and its dual (**b**). The same coordinate system is used to address the pixels (**a**) and the nodes of the dual grid (**b**).

Next, a brief description is given for the discrete triangular coordinate system and BCS.

2.1. Discrete Triangular Coordinate System

The discrete Hexagonal Coordinate System uses 0-sum triplets (Figure 1a,b). The discrete Triangular Coordinate System [22] is a symmetric coordinate system that addresses each pixel by an integer triplet. The three coordinate axes have angles of 120° as in the hexagonal grid. The sum of the triplets is equal to 0 or 1, which refers to the two types of orientations of triangles (△, ▽). The triangles with zero-sum are the "even" triangles (△), and the triangles with one-sum triplets are the "odd" triangles (▽) (see Figure 1).

For finding an appropriate extension to this system that is able to address all points of the 2D plane, we start by addressing the midpoints of triangles with integer triplets of +1 and -1 sum. Therefore, we call them "positive △" and "negative ▽" triangles, respectively. According to Figure 3, the coordinate system of Figure 2b is used to address midpoints of triangles of the triangular grid. Observe that each triplet assigned to a midpoint (see the blue triplets in Figure 3) builds up from the coordinate values shared by two of the corners of the given pixel (see the three red triplets around each blue triplet). There is already an important difference between our proposed and Her's zero-sum coordinate system, which includes the use of zero-sum triplets to address these midpoints as well (actually, three fractional values for each midpoint), which was a very good and efficient choice to extend the coordinate system of the hexagonal grid. However, it does not meet our requirements. Therefore, we have fixed these coordinate values in another way. We should also mention that Her's system inside the regular triangles can be seen as an application of the barycentric coordinate system (see next subsection) based on the values assigned to the corners of the triangle.

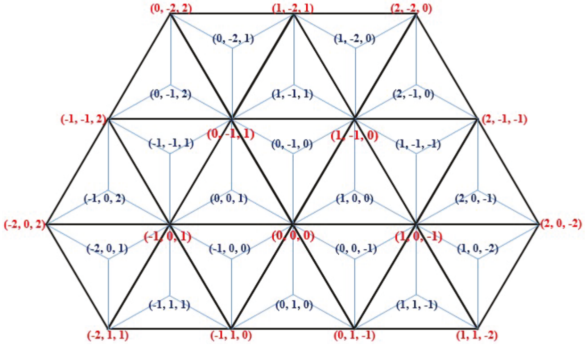

Figure 3. The coordinate system for the tri-hexagonal grid is used for the triangular grid (and for its dual at the same time).

2.2. The Barycentric Coordinate System (BCS)

One of the main motivations of the barycentric technique is to use a coordinate system only for a finite (bordered) segment of the plane, which is also more "balanced" inside this region than the values of the Cartesian frame.

The barycentric technique uses coordinate triplets to address any points inside (and on the border) of a given triangle. We put three one-sum weights, (w, v, u), to the corners known as a, b, and c of the triangle and the mass center p inside the triangle is assigned to the triplet of weights. It is also known that, if the area of the triangle abc is one unit, then the areas of bcp, acp, and abp are exactly w, v, and u, respectively. The coordinates of p can be computed from the coordinates of the corners of the triangle by weighted average, i.e., $p = wa + vb + uc$ (where p, a, b, and c are the vectors representing the positions of these points).

This formula can easily be transformed to the following formula using the fact that $w = 1 - v - u$:

$$p = a + v\,(b - a) + u\,(c - a) \tag{1}$$

Actually, since the three barycentric coordinate values (w, v, and u) of point p are not independent (sum of 1), we may use only two of them, v and u, to address point p similarly as in an oblique coordinate system. One may understand Equation (1) as stating that the starting point is a, and we can go to the direction of b and the direction of c by some distance, which is indicated by v and u, respectively. However, in our approach, the starting point a is the midpoint of the regular triangle and, according to the values of v and u, the coordinate triplet for point p is calculated (see Figure 4 and Example 1).

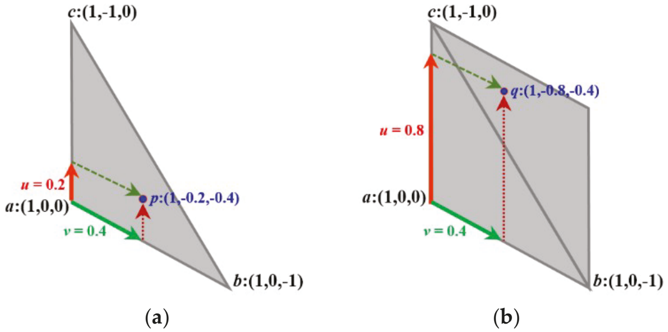

Figure 4. A composition of the barycentric technique and discrete coordinate system to address points p and q in the triangular plane by coordinate triplets in (**a**) and (**b**), respectively.

In the classical barycentric technique, the point is considered to be inside a triangle, as long as the sum of (u and v) is between 0 and 1: $0 < u + v < 1$. If the sum is equal to 1, then the point will be on the edge (cb), while it will be out of the triangle if the sum is less than 0 or greater than 1 (see Figure 4a). Now, we relax the condition of the barycentric technique and allow the sum of u and v to be any real number between 0 and 2 besides the conditions $0 \leq u \leq 1$ and $0 \leq v \leq 1$ hold (see Figure 4b). In this way, we may also address some points outside of the triangle. In Figure 4 and Example 1, a composition of the barycentric technique and the discrete coordinate system (assigned to the corners of an isosceles triangle in the regular triangle) is given to address other points of the plane.

Example 1. *Consider the triangle defined by corners (1, 0, 0), (1, 0, −1), and (1, −1, 0), which represent the three vertices a, b, and c, respectively. Let u = 0.2 and v = 0.4, where 0 < u + v < 1. Then, based on Equation (1), the coordinate triplet of point p is (1, −0.2, −0.4). If u = 0.8 and v = 0.4 (0 < u + v < 2), then the coordinate triplet of point q is (1, −0.8, −0.4) (see Figure 4).*

3. Continuous Coordinate System for Reflecting the Triangular Symmetry

In order to create a continuous triangular coordinate system that works efficiently, we combine the discrete coordinate system for the triangle grid with BCS. In the discrete triangular coordinate system, integer coordinate triplets with various sums were used. In BCS, coordinate triplets with fractional values address the points inside a triangle. We develop a new system, which uses triplets on the entire plane. We start by dividing each equilateral triangle of the triangular grid into three isosceles obtuse-angled triangles, which will possess areas A, B, and C, as shown in Figure 5. In this case, the midpoint m between areas will be the start point (the red point), which is represented by the letter a in Equation (1). This point will be used to calculate the coordinates of the points in the three areas A, B, and C.

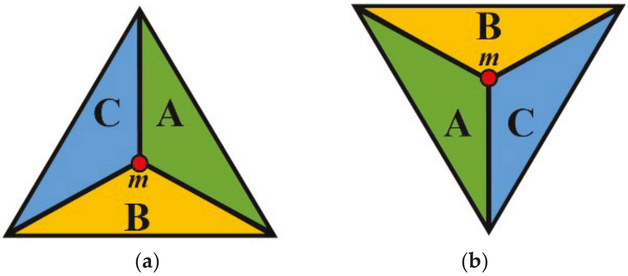

Figure 5. Dividing positive (**a**) and negative (**b**) triangles to three areas A, B, and C. The letters assigned to the isosceles triangles are based on the orientation of the sides.

As we have already mentioned above, we use coordinate triplets with sum +1 and -1 for these midpoints, depending on the orientation of the original triangle. The sum of 1 represents the midpoint of the positive triangles △ and the sum of -1 represents the midpoint of negative triangles ▽. Therefore, using the barycentric Equation (1) based on these midpoints, we obtain a unique triplet for each point in each area of the plane, which we will describe below.

Based on the barycentric Equation (1), we know that the values u and v are limited by $0 \leq u + v \leq 1$ (inside or on the border of the given triangle), which gives the ability to address the points inside areas A, B, and C of each type of triangle (△, ▽), separately. However, let us consider the case in which the sum of u and v satisfies $0 \leq u + v \leq 2$, such that the conditions $0 \leq u \leq 1$ and $0 \leq v \leq 1$ hold. Then, consequently, each midpoint can be used to address not only the points in the area located in this original triangle but also the points in the neighboring area denoted with the same letters. To illustrate this, the green area in Figure 6a can be completely addressed by using either midpoint $a^{(+)}$ or $a^{(-)}$ as the starting point in Equation (1).

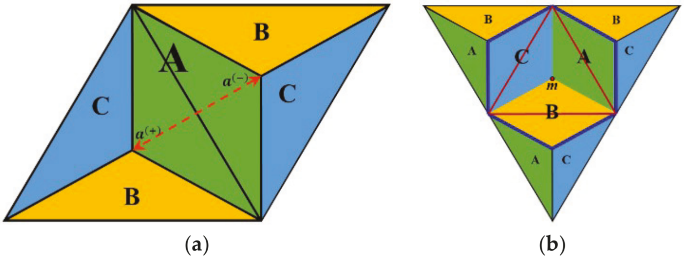

Figure 6. (**a**) By using either $a^{(+)}$ or $a^{(-)}$, the whole green area A could be addressed. (**b**) The hexagon surrounded by the thick dark blue line shows the entire area that can be addressed by using a positive midpoint m.

Proposition 1. *To address the points inside a rhombus A, B, or C, the coordinate triplet of a point does not depend on the choice of whether the midpoint of the positive or the negative triangle is used for addressing.*

Proof. Assume point (p) in area A of the negative triangle. Let $a^{(+)} = (a_1, a_2, a_3)$, $a^{(-)} = (a_1, a_2 - 1, a_3 - 1)$, $p = (p_1, p_2, p_3)$, $b = (b_1, b_2, b_3)$, and $c = (c_1, c_2, c_3)$ where $a^{(+)}$ is the midpoint of the positive triangle and $a^{(-)}$ is the midpoint of the negative one (see Figure 7).

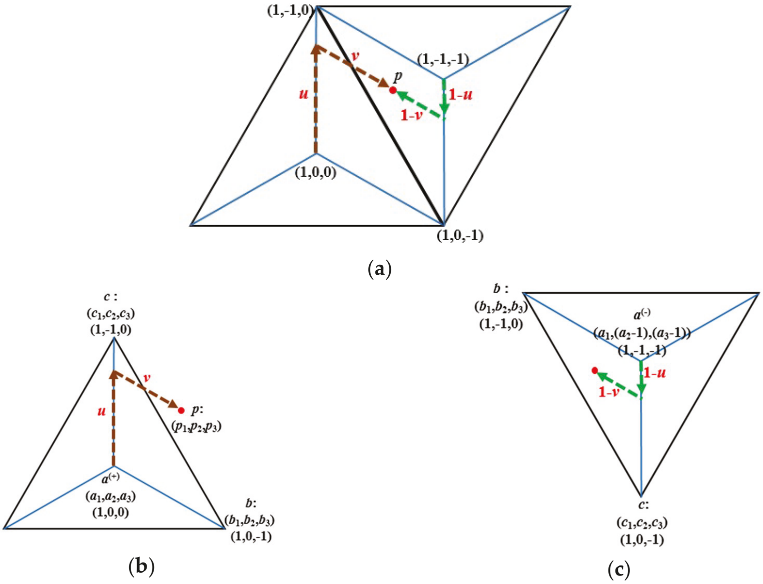

(**a**)

(**b**)

(**c**)

Figure 7. Proving how point p can be calculated by either the positive or negative midpoint ($a^{(+)}$ or $a^{(-)}$). (**a**) Shows the position of point p with respect to both a positive and a negative triangle, while (**b**) and (**c**) represent the calculation of the coordinates of point p based on the positive and negative triangles, respectively.

As we mentioned earlier, each triplet assigned to a midpoint builds up from the coordinate values shared by two of the corners of the given pixel (see Section 2.1). Thus, we have some equalities.

In the positive triangle, we have:

$$a_1 = b_1 = c_1,\ b_2 = a_2,\ c_3 = a_3 \text{ and } c_2 = a_2 - 1,$$

In the negative triangle, we have:

$$a_1 = b_1 = c_1,\ b_2 = a_2,\ c_3 = a_3 \text{ and } b_2 = a_2 - 1.$$

Now, to compute the first coordinate value, a_1, from the positive triangle, we have the following.

$$p_{1(+)} = a_1 + v\,(b_1 - a_1) + u\,(c_1 - a_1) \text{ since } a_1 = b_1 = c_1 \text{ then } p_{1(+)} = a_1.$$

From the negative side, we have the following.

$$p_{1(-)} = a_1 + (1 - v)\,(b_1 - a_1) + (1 \text{ - } u)\,(c_1 - a_1) \text{ then also } p_{1(-)} = a_1.$$

For the second coordinate value, a_2, from the positive triangle, we have the following.

$$p_{2(+)} = a_2 + v\ (b_2 - a_2) + u\ (c_2 - a_2),$$

since $b_2 = a_2$, then:

$$p_{2(+)} = a_2 + u\ (c_2 - a_2).$$

Using $c_2 = a_2 - 1$, we get $p_{2(+)} = a_2 - u$.

From the negative side, we have the following.

$$p_{2(-)} = (a_2 - 1) + (1 - v)\ (b_2 - (a_2 - 1)) + (1 - u)\ (c_2 - (a_2 - 1)),$$

since $b_2 = (a_2 - 1)$, it is:

$$p_{2(-)} = (a_2 - 1) + (1 - u)\ (c_2 - (a_2 - 1)),$$

since $c_2 = a_2$, then we have $p_{2(-)} = a_2 - u$.

Lastly, for the third coordinate value, a_3, from the positive triangle, we have:

$$p_{3(+)} = a_3 + v\ (b_3 - \mathrm{a}_3) + u\ (c_3 - a_3).$$

Since $c_3 = a_3$,

$$p_{3(+)} = a_3 + v\ (b_3 - a_3).$$

Furthermore, $b_3 = a_3 – 1$, which yields to $p_{3(+)} = a_3 - v$.

From the negative side, we have the following.

$$p_{3(-)} = (a_3 - 1) + (1 - v)\ (b_3 - (a_3 - 1)) + (1 - u)\ (c_3 - (a_3 - 1)).$$

Since $c_3 = a_3 - 1$ and $b_3 = a_3$, it can be written as:

$$p_{3(-)} = (a_3 - 1) + (1 - v)\ (b_3 - (a_3 - 1)) = a_3 - v.$$

Having the point inside other regions, the proof goes in a similar manner. □

As we have already mentioned, a popular way to understand BCS for a point (inside a triangle) goes by the ratio of the areas defined by the triangles determined by the point and two of the triangle corners. In fact, our system uses a similar technique to address the points inside a triangle since it is stated in the next corollary based on the previous proposition.

Corollary 1. *Let p be any point inside or on the border of an obtuse-angled triangle determined by a midpoint* $a = (a_1, a_2, a_3)$, *and corners* $b = (b_1, b_2, b_3)$, $c = (c_1, c_2, \mathrm{c}_3)$. *Let the barycentric coordinates of p be* (w, v, u), *with* $w + v + u = 1$, *i.e., by assigning these weights to a and b and c, respectively, the weighted midpoint is at p. Then, the coordinates of* $p = (p_1, p_2, p_3)$ *are exactly* $p_i = w\ a_i + v\ b_i + u\ c_i$ *for* $i = 1, 2, 3$.

Notice that the three points *a, b,* and *c* above must have a fixed coordinate value (depending on the type of the triangle). The weighted average of this coordinate value will be the same for any point inside or on the border of this obtuse-angled triangle.

As we have seen a given triplet of corners, including a midpoint can be used to address points not only on the inside but also on the border of the triangle determined by them. The type of these regions is important in this issue. In Figure 6b, the thick, dark blue line shows the entire area that the positive midpoint can address. The key issue is to use triplets of the discrete coordinate system and to use only two barycentric fractional values inside, by using the directions of the sides of the appropriate rhombus in which the point is located. The sides of a rhombus are actually parallel to two of the coordinate axes.

Hereafter, for simplicity, we will use only the positive midpoints for further calculations, while ignoring the negative ones. The triangular plane can be seen in Figure 8a.

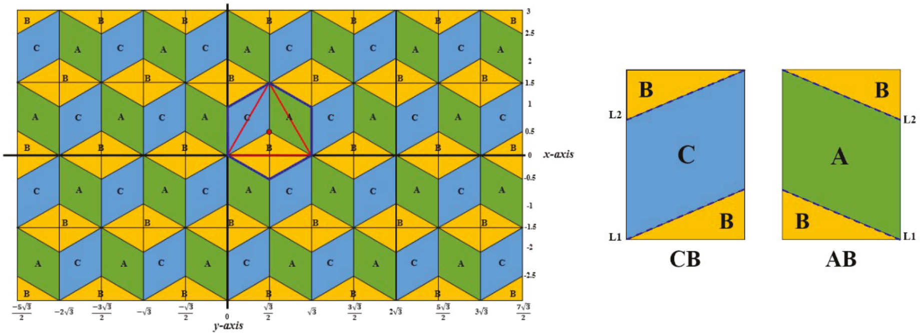

(**a**) (**b**)

Figure 8. (**a**) Re-structuring the triangular plane to fit the Cartesian plane. (**b**) The two distinguished rectangles of the plane.

In the next two subsections, we will illustrate the conversion between the continuous coordinate system to/from the Cartesian coordinate system. Namely, we can convert the coordinate triplet of a certain point in our new coordinate system to its corresponding Cartesian coordinates and vice versa.

3.1. Converting Triplets to Cartesian Coordinates

Assume that we use (i, j, k) as a coordinate triplet of a point, where I, J, and K are the axes of the triangular plane (see Figure 1), and suppose (x, y) is used to indicate the same point in the Cartesian plane where X and Y are the axes.

For the conversion, we fix the side-length of the triangle of the triangular grid to $\sqrt{3}$. Consequently, its height is 1.5 (see the dashed blue lines in Figure 9). Then, the following matrix equation computes the corresponding coordinate values x and y for the given triplet (i, j, k):

$$\begin{pmatrix} \frac{\sqrt{3}}{2} & 0 & -\frac{\sqrt{3}}{2} \\ \frac{1}{2} & -1 & \frac{1}{2} \end{pmatrix} \cdot \begin{pmatrix} i \\ j \\ k \end{pmatrix} = \frac{1}{2} \cdot \begin{pmatrix} \sqrt{3}(i-k) \\ i-2j+k \end{pmatrix} = \begin{pmatrix} x \\ y \end{pmatrix} \tag{2}$$

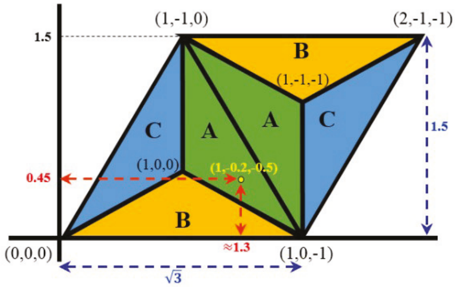

Figure 9. The dashed red lines indicate the Cartesian coordinates of the point.

Example 2. *Let (1, −0.2, −0.5) be a point in the triangular plane. Then, based on (2):*

$$\begin{pmatrix} \frac{\sqrt{3}}{2} & 0 & -\frac{\sqrt{3}}{2} \\ \frac{1}{2} & -1 & \frac{1}{2} \end{pmatrix} \cdot \begin{pmatrix} 1 \\ -0.2 \\ -0.5 \end{pmatrix} \approx \begin{pmatrix} 1.3 \\ 0.45 \end{pmatrix}$$

Thus, (x, y) ≈ (1.3, 0.45), as shown in Figure 9.

3.2. Converting Cartesian Coordinates to Equivalent Triplets

One of the simplest ways to do such a conversion is to determine the midpoint and the two corner points, which defines the triangle in which the given point locates (inside or on the border). Then, by computing the barycentric coordinates (weights) of the point with respect to these triangle corners, by Corollary 1, the continuous coordinate triplet is computed. In this subsection, we present a slightly different method with little more details to convert Cartesian coordinates to continuous triangular coordinates.

As we already mentioned earlier, the midpoints of positive triangles are used to address all points in the triangular plane. Therefore, every positive midpoint will address areas A, B, and C in neighbor (negative) triangles, as already seen in Figure 6b. Consequently, the triangular plane will be re-structured, which can be seen in Figure 8a. However, two kinds of rectangles can be clearly distinguished in this plane, called CB and AB (see Figure 8b).

We may start by specifying the area (i.e., rhombus) A, B, or C that a Cartesian point (x, y) belongs to. Then, we can use appropriate formulae that are assigned to each type of area, which is a process we will describe later in this section (see Table 1). Hence, the following three steps are used to specify the area.

Step 1 Which quarter of the Cartesian plane is involved? Note that the 1st and 3rd quarters have the same structure, while the 2nd and 4th quarters have another one.
Step 2 Which rectangle is involved (AB or CB)?
Step 3 Which area is involved (A, B, or C)?

Table 1. The coordinate triplets formulae, based on area type, where $\langle \ldots \rangle$ is a rounding operation *.

Coordinate Triplet	Area A	Area B	Area C
i	$\langle \frac{x}{\sqrt{3}} \rangle + \langle \frac{y}{3} \rangle$	$\frac{x\sqrt{3}}{3} + y + j$	$\frac{2x}{\sqrt{3}} + k$
j	$\frac{i+k}{2} - y$	$\langle \frac{-2y}{3} \rangle$	$\frac{i+k}{2} - y$
k	$i - \frac{2x}{\sqrt{3}}$	$i - \frac{2x}{\sqrt{3}}$	$\langle \frac{y}{3} \rangle - \langle \frac{x}{\sqrt{3}} \rangle$

* rounding operation returns the nearest integer to the real number, such that numbers exactly the same distance from two integers are rounded to the larger absolute valued one, e.g., $\langle 1.5 \rangle = 2$, $\langle -1.5 \rangle = -2$ and $\langle -0.4 \rangle = 0$.

We show how these steps can be computed by pseudo codes. The first step is the easiest one since we can inquire whether the values of (x, y) are greater or equal to zero or not. Then, this task is completed and the involved quarter is specified (see Code 1).

Code 1.

```
IF (($x \geq 0$) AND ($y \geq 0$)) OR (($x < 0$) AND ($y < 0$))
THEN "1st or 3rd quarter"
ELSE "2nd or 4th quarter"
```

To complete the second step, note that the basic measurements of every rectangle are known, with a height and width equal to 1.5 and $\left(\sqrt{3}/2\right)$, respectively. Then, the CB rectangle is involved whenever the integer part of x and y, are both even or both odd. Otherwise, the AB rectangle is involved. See Code 2 to clarify this step.

Code 2.

```
IF ((int ($2x/\sqrt{3}$) mod 2 = 0) AND (int ($y/1.5$) mod 2) = 0) OR
(int ($2x/\sqrt{3}$) mod 2 = 1) AND (int ($y/1.5$) mod 2) = 1))
THEN "CB Rectangle is involved"
ELSE "AB Rectangle is involved"
```

where:

- int takes the integer part of the (decimal) number,
- mod is the modulus (or remainder, here after division by two).

Now, the involved rectangle is specified and the third step follows. Since we have two types of rectangles AB and CB, and they are symmetric, we will discuss only one of them known as type AB rectangles.

In rectangle AB, a point (x, y) will belong to either part A or part B. To decide which one is involved, we consider Line 1 (L1) and Line 2 (L2) in Figure 8b, where they divide the rectangle into parts A and B. If the point is between L1 and L2, then part A is involved. Otherwise, it is in part B. However, L1 and L2 are considered to be within the area A in cases when the point is on the lines. Equations (3) and (4) of a straight line are used for Line 1 and Line 2, respectively.

$$m{\cdot}x + r_1 - y = 0, \tag{3}$$

$$m{\cdot}x + r_2 - y = 0, \tag{4}$$

where:

- m is the slope of L1 and L2, which is a constant here, equal to $\left(-\sqrt{3}/3\right)$,
- r_1 and r_2 are the *y-axis* intercept with L1 and L2, respectively, where $r_2 = r_1 + 1$

This step is started by substituting the point (x, y) in Equations (3) and (4). Then, it is determined that part A is involved if the left side of Equation (3) is not greater than 0 and the left side of Equation (4) is not less than 0. Otherwise, part B is involved. Code 3 is used to clarify this step.

Code 3.

```
IF (($r_1 - x\sqrt{3}/3 - y$) $\leq$ 0) AND (($r_2 - x\sqrt{3}/3 - y$) $\geq$ 0)
THEN "Area A is involved"
ELSE "Area B is involved"
```

The *y-axis* intercept with Line 1, r_1, in area AB, is computed by computing any point (x, y) on Line 1. Therefore, the point at the bottom-right corner of rectangle AB is computed for this purpose (see the red point in Figure 10). Hence, Equation (5) is used to find the value of r_1. In Equation (5), we used the modulus (mod) as a function naturally extended to real numbers, i.e., it gives the remainder after the division by a real number (and that is between 0 and the divisor). Moreover, by adding 1 to r_1, we get the value of the *y-axis* intercept with Line 2, r_2 (see Code 3).

$$r_1 = y - \left(y \; mod \; \frac{3}{2}\right) + \frac{\sqrt{3}}{3}{\cdot}\left(x + \frac{\sqrt{3}}{2} - \left(x \; mod \; \frac{\sqrt{3}}{2}\right)\right) \tag{5}$$

Similar strategies are used when the CB rectangle is involved, taking care that the slopes of Line 1 and Line 2 will be equal to $\left(\sqrt{3}/3\right)$.

Lastly, when the involved area A, B, or C is specified, particular formulae are used that are specified in Table 1. Example 3 is used for a further explanation.

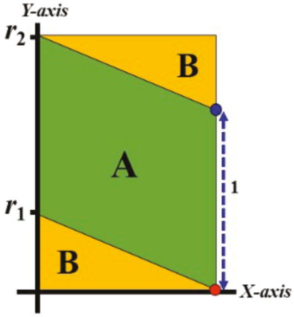

Figure 10. The red point is used to compute the value of r_1, which is the Y-axis intercept with Line 1.

Example 3. *Consider a point with Cartesian coordinates: (x, y) = (1.299, 0.45). In order to convert this Cartesian coordinate pair to its corresponding triangular triplet, the three steps below will be followed.*

Step 1 *The 1st or 3rd quarter is involved.*
Step 2 *It's odd and even. Therefore, rectangle AB is involved.*
Step 3 *Area A is matched.*

Thus, formulae of area A (see Table 1) should be applied in this order, so:

(1) $i = \langle 0.75\rangle + \langle 0.15\rangle = 1 + 0 = 1$
(2) $k = 1 - \frac{2x}{\sqrt{3}} \approx -0.500.$
(3) $j \approx -y + 0.5 \cdot 0.5 = -0.2$

The corresponding triplet is (i, j, k) ≈ (1, −0.2, −0.5), which is approximately the same as in Example 2, as it should be.

To show the conversion of points on other areas (e.g., Area B or Area C), the following examples are given:

Example 4. *(Point in Area B)*

(a) *Converting from Continuous Coordinate System to CCS.*

Let (i, j, k) = (0.683, 0, −0.183) be a point in the triangular plane. To convert to CCS, Equation (2) is used:

$$\begin{pmatrix} \frac{\sqrt{3}}{2} & 0 & -\frac{\sqrt{3}}{2} \\ \frac{1}{2} & -1 & \frac{1}{2} \end{pmatrix} \cdot \begin{pmatrix} 0.683 \\ 0 \\ -0.183 \end{pmatrix} \approx \begin{pmatrix} 0.75 \\ 0.25 \end{pmatrix}$$

(b) *Converting from CCS to a Continuous Coordinate System.*

Let (x, y) = (0.75, 0.25). The corresponding Continuous Coordinate System triplet can be calculated based on the three steps above as follows.

Step 1 *It belongs to the 1st quarter.*
Step 2 *It belongs to rectangle CB.*
Step 3 *Area B is matched.*

Thus, formulae of area B from Table 1 are applied in the following order:

(1) $j = \langle \frac{-2y}{3} \rangle = 0$

(2) $i = \frac{x\sqrt{3}}{3} + y + j \approx 0.433 + 0.25 + 0 = 0.683$

(3) $k = i - \frac{2x}{\sqrt{3}} \approx 0.683 - 0.866 = -0.183$

The corresponding triplet is (i, j, k) = (0.683, 0, −0.183), which is exactly the original value.

Example 5. *(Point in Area C)*

(a) *Converting from the Continuous Coordinate System to CCS.*

Let (i, j, k) = (0.346, −0.626, 0) be a point in the triangular plane. To convert to CCS, we use Equation (2) below.

$$\begin{pmatrix} \frac{\sqrt{3}}{2} & 0 & -\frac{\sqrt{3}}{2} \\ \frac{1}{2} & -1 & \frac{1}{2} \end{pmatrix} \cdot \begin{pmatrix} 0.346 \\ -0.626 \\ 0 \end{pmatrix} \approx \begin{pmatrix} 0.299 \\ 0.799 \end{pmatrix}$$

(b) *Converting from CCS to a Continuous Coordinate System*

Let (x, y) = (0.299, 0.799). The corresponding Continuous Coordinate System triplet can be calculated based on the three steps below.

Step 1 *It belongs to the first quarter.*
Step 2 *It belongs to rectangle CB.*
Step 3 *Area C is matched.*

Thus, formulae of area C from Table 1 are applied in the following order.

(1) $k = \langle \frac{y}{3} \rangle - \langle \frac{x}{\sqrt{3}} \rangle = 0 - 0 = 0$

(2) $i = \frac{2x}{\sqrt{3}} + k \approx 0.346 + 0 = 0.346$

(3) $j = \frac{i+k}{2} - y \approx 0.173 - 0.799 = -0.626$

The corresponding triplet is (i, j, k) = (0.346, −0.626, 0), which is exactly the original triplet.

Example 6. *(A mid-point)*

(a) *Converting from Continuous Coordinate System to CCS.*

Let (i, j, k) = (1, 0, 0) be a point in the triangular plane. To convert to CCS, Equation (2) is used below.

$$\begin{pmatrix} \frac{\sqrt{3}}{2} & 0 & -\frac{\sqrt{3}}{2} \\ \frac{1}{2} & -1 & \frac{1}{2} \end{pmatrix} \cdot \begin{pmatrix} 1 \\ 0 \\ 0 \end{pmatrix} = \begin{pmatrix} \frac{\sqrt{3}}{2} \\ \frac{1}{2} \end{pmatrix}$$

(b) *Converting from CCS to a Continuous Coordinate System.*

Let (x, y) = ($\sqrt{3}/2$, 0.5). The corresponding Continuous Coordinate System triplet can be calculated based on the three steps below.

Step 1 *It belongs to the first quarter.*
Step 2 *Based on Code 2, it belongs to rectangle CB (but, since it is a mid-point, then either rectangle AB or CB may be used).*
Step 3 *Area B is matched.*

Thus, formulae of area B from Table 1 are applied in the following order.

(1) $j = \langle \frac{-2y}{3} \rangle = 0$

(2) $i = \frac{x\sqrt{3}}{3} + y + j = 0.5 + 0.5 + 0 = 1$

(3) $k = i - \frac{2x}{\sqrt{3}} = 1 - 1 = 0$

The corresponding triplet is (i, j, k) = (1, 0, 0), which is exactly the original value.

4. Properties of the Continuous Triangular Coordinate System

In this section, we will focus on the most important properties of this continuous coordinate system.

4.1. On the Triplets of a General Point

In Figure 6a, consider the red straight line between $a^{(+)}$ and $a^{(-)}$, in the green area. Then, the sum of the coordinate values of the points on this line would change continuously from 1 until −1. Depending on the sum, we can classify the points as follows:

If a point with 3 CV's sum is:

- equal to 1, then it indicates the positive midpoint (i.e., $a^{(+)}$);
- equal to −1, then it indicates the negative midpoint (i.e., $a^{(-)}$);
- equal to 0, then it indicates the point on the triangle's edge;
- positive, then the point belongs to the positive triangle;
- negative, then the point belongs to the negative triangle.

Theorem 1. *The sum of the coordinate triplet of any point in the plane is in the range of the closed interval* $[-1, 1]$.

Proof. Consider an area A of a positive triangle with the corners $a = (a_1, a_2, a_3)$, $b = (b_1, b_2, b_3)$, and $c = (c_1, c_2, c_3)$, where b and c are vertices (corners of an equilateral triangle) of the grid, while a is the midpoint of a positive triangle and $p = (p_1, p_2, p_3)$ is a randomly chosen point belonging to this area (inside or on the border of A). Now based on the barycentric Equation (1), we have the following.

$$\sum_{i=1}^{3} p_i = \sum_{i=1}^{3} a_i + v \cdot (\sum_{i=1}^{3} (c_i - a_i)) + u \cdot (\sum_{i=1}^{3} (b_i - a_i))$$

It is clear that $\sum_{i=1}^{3} a_i = 1$, whereas

$$\begin{aligned}\textstyle\sum_{i=1}^{3}(c_i - a_i) &= (c_1 - a_1) + (c_2 - a_2) + (c_3 - a_3)\\ &= (c_1 + c_2 + c_3) - (a_1 + a_2 + a_3)\\ &= 0 - 1 = -1\end{aligned}$$

Similarly, $\sum_{i=1}^{3}(b_i - a_i) = -1$.

Then, by substitution, we have the following.

$$\sum_{i=1}^{3} p_i = 1 - u - v = 1 - (u + v). \tag{6}$$

Since $0 \le u + v \le 2$, the maximal and minimal value of the sum of any coordinate triplet is equal to 1 (when $u + v = 0$) and to −1 (when $u + v = 2$), respectively. □

Theorem 2. *The sum of the coordinates of a triplet is non-negative in a positive triangle and non-positive in a negative triangle.*

Proof. Consider a point p that belongs to a positive triangle. Clearly, the coordinates of p are based on u and v such that $0 \le u + v \le 1$. Now, by substituting $u + v$ in Formula (6) (at the proof of Theorem 1, the summation will always be non-negative (moreover, it is positive inside the triangle).

Similarly, let p belong to a negative triangle, then $1 < u + v \leq 2$. Thus, by substituting into Formula (6), the sum will always be a non-positive value. □

Every point in the triangular plane has at least one integer value in its triplet. Moreover, the place of the integer value indicates its area (A, B, or C).

Theorem 3. *The* first *coordinate value of every point in area* A *is the same as the* first *coordinate value of the midpoint. The* second *coordinate value of every point in area* B *equals the* second *coordinate value of the midpoint. Similarly, the third coordinate value of any point in area* C *equals the third coordinate value of the midpoint* (Figure 11).

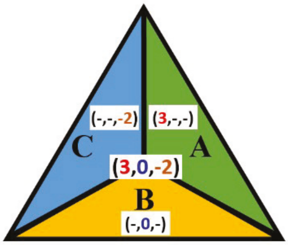

Figure 11. The corresponding constant coordinate value for each area.

Proof. Consider an area A of a positive triangle with the corners $a = (a_1, a_2, a_3)$, $b = (b_1, b_2, b_3)$, and $c = (c_1, c_2, c_3)$, where b and c are vertices (corners of an equilateral triangle) of the grid, while a is the midpoint and $p = (p_1, p_2, p_3)$ is a randomly chosen point belonging to this area (i.e., inside or on the border of the triangle abc). Since it is area A, we have $a_1 = b_1 = c_1$. Substituting this into Equation (1), $p_1 = a_1$ follows for any point p in this area. A similar proof can be considered for areas B and C. □

If a triplet contains two integer values, then the point is located on the line bordering the areas. For example, a triplet of the form $(1, 0, k)$ addresses a point on the line (side of the obtuse-angled triangle) between area A and B $(0 \leq k \leq -1)$. However, if three integers are a triplet, then this triplet addresses either a midpoint or a vertex (corner) of a triangle.

4.2. Relation to Discrete Coordinate Systems

In Reference [16], the hexagonal grid is called a one-plane triangular grid since it is a sub-plane of Z^3 and because of its symmetry. The triangular grid (nodes of the hexagonal grid) is called a two-plane triangular grid. Combining one-plane and two-plane grids produces the so-called three-plane triangular grid, which is known as the tri-hexagonal grid (Reference [24], Figure 2). In this subsection, their coordinate systems are compared to the new coordinate system.

Theorem 4. *The triplets containing only integers such that their sum equals* zero *represent exactly the hexagonal grid (one-plane triangular grid).*

Proof. See Figure 1b for the points of this grid. One may check that exactly those points are addressed with zero-sum integer triplets for which the Cartesian coordinate pair is described below.

$$\mathrm{H} = \left\{(x,\ y)\middle|x = \left(m\sqrt{3}\right)/2,\ y\ =\ 1.5n,\ \text{where } m, n \text{ are integers such that } m + n \text{ is even}\right\}.$$

□

Theorem 5. *The triplets containing only integers such that their sum is either* 0 *or* 1 *represent exactly the triangular grid (two-plane triangular grid).*

Proof. See Figure 1d for the points of this grid. The locations of the points with zero-sum coordinate triplets are already known by Theorem 4. Now, we give the locations of the points addressed with 1-sum (integer) triplets.

$$\mathrm{T} = \left\{(x,\ y)\middle|x = \left(m\sqrt{3}\right)/2,\ y = 1.5n - 1,\ \text{where } m, n \text{ are integers such that } m + n \text{ is even}\right\}.$$

One can easily see that the union of these two sets (H and T) of points gives back exactly the vertices of the hexagons of the figure, i.e., the coordinate system of the dual triangular grid. □

Theorem 6. *The triplets containing only integers such that their sum is either* 0 *or* ±1 *represent exactly the tri-hexagonal grid (that is the three-plane triangular grid).*

Proof. See Figure 3 for the points of this grid. According to Theorem 5, the locations of the zero-sum and one-sum integer coordinate triplets are already shown. We need to show the locations of the points addressed with (integer) triplets that have −1-sum. They are:

$$\mathrm{M} = \left\{(x,\ y)\middle|x = \left(m\sqrt{3}\right)/2,\ y\ =\ 1.5n + 1,\ \text{where } m, n \text{ are integers such that } m + n \text{ is even}\right\}.$$

Actually, the points of this grid, T ∪ H ∪ M, are exactly those that were the base of the method of creating the coordinate system. □

5. Conclusions

The presented continuous coordinate system is an extension of some previously known discrete coordinate systems, e.g., of the symmetric coordinate frame for the triangular grid. This extension is needed and helpful for various applications, where the grid points are not necessarily mapped to grid points, e.g., arbitrary angled rotations, zooming or interpolation of images. We should also mention translations of images [25] since the triangular grid is not a point lattice. Mathematical morphology operators are also based on local translations [21]. Thus, our coordinate system provides a new tool for the research direction as well. The proposed system addresses each point of the 2D (triangular) plane. Conversion to and from the Cartesian coordinate system is provided. These mappings are inverses of each other. Thus, the new coordinate system is ready to use in various applications including those operations that do not necessarily map the grid to itself.

Author Contributions: B.N. and K.A. both designed research and wrote the paper. Both authors have read and approved the final manuscript.

Funding: The research was completed under the research project BAPC-04-18-03 of the Eastern Mediterranean University.

Acknowledgments: Comments of the anonymous reviewers are gratefully acknowledged.

Conflicts of Interest: The authors declare no conflict of interest.

References

1. Coxeter, H.S.M. *Introduction to Geometry*, 2nd ed.; Wiley: New York, NY, USA, 1969.
2. Middleton, L.; Sivaswamy, J. *Hexagonal Image Processing—A Practical Approach*; Springer: London, UK, 2005.
3. Carr, D.B.; Olsen, A.R.; White, D. Hexagon mosaic maps for display of univariate and bivariate geographical data. *Cartogr. Geograph. Inform. Syst.* **1992**, *19*, 228–236. [CrossRef]
4. Sahr, K. Hexagonal discrete global grid systems for geospatial computing. *Arch. Photogramm. Cartogr. Remote Sens.* **2011**, *22*, 363–376.

5. Sakai, K.I. Studies on the competition in plants. VII. Effect on competition of a varying number of competing and non-competing individuals. *J. Genet.* **1957**, *55*, 227–234. [CrossRef]
6. Birch, C.P.; Oom, S.P.; Beecham, J.A. Rectangular and hexagonal grids used for observation, experiment and simulation in ecology. *Ecol. Model.* **2007**, *206*, 347–359. [CrossRef]
7. Her, I. A symmetrical coordinate frame on the hexagonal grid for computer graphics and vision. *J. Mech. ASME* **1993**, *115*, 447–449. [CrossRef]
8. Her, I. Geometric Transformations on the Hexagonal Grid. *IEEE Trans. Image Proc.* **1995**, *4*, 1213–1222. [CrossRef] [PubMed]
9. Luczak, E.; Rosenfeld, A. Distance on a hexagonal grid. *IEEE Trans. Comput.* **1976**, 532–533. [CrossRef]
10. Almansa, A. Sampling, Interpolation and Detection. Applications in Satellite Imaging. Ph.D. Thesis, École Normale Supérieure de Cachan-ENS Cachan, Cachan, France, 2002.
11. Pluta, K.; Romon, P.; Kenmochi, Y.; Passat, N. Honeycomb geometry: Rigid motions on the hexagonal grid. In Proceedings of the International Conference on Discrete Geometry for Computer Imagery, Vienna, Austria, 19 September 2017; LNCS; Springer: Cham, Switzerland, 2017; Volume 10502, pp. 33–45.
12. Nagy, B. Isometric transformations of the dual of the hexagonal lattice. In Proceedings of the 6th International Symposium on Image and Signal Processing and Analysis, Salzburg, Austria, 16–18 September 2009; pp. 432–437.
13. Deutsch, E.S. Thinning algorithms on rectangular, hexagonal and triangular arrays. *Commun. ACM* **1972**, *15*, 827–837. [CrossRef]
14. Bays, C. Cellular automata in the triangular tessellation. *Complex Syst.* **1994**, *8*, 127.
15. Nagy, B. Finding shortest path with neighbourhood sequences in triangular grids. In Proceedings of the 2nd International Symposium, in Image and Signal Processing and Analysis, Pula, Croatia, 19–21 June 2001; pp. 55–60.
16. Nagy, B. A symmetric coordinate frame for hexagonal networks. In Proceedings of the ACM Theoretical Computer Science-Information Society, Ljubljana, Slovenia, 11–15 October 2004; Volume 4, pp. 193–196.
17. Nagy, B. Cellular topology and topological coordinate systems on the hexagonal and on the triangular grids. *Ann. Math. Artif. Intel.* **2015**, *75*, 117–134. [CrossRef]
18. Nagy, B.; Lukic, T. Dense Projection Tomography on the Triangular Tiling. *Fundam. Inform.* **2016**, *145*, 125–141. [CrossRef]
19. Nagy, B.; Valentina, E. Memetic algorithms for reconstruction of binary images on triangular grids with 3 and 6 projections. *Appl. Soft Comput.* **2017**, *52*, 549–565. [CrossRef]
20. Kardos, P.; Palágyi, K. Topology preservation on the triangular grid. *Ann. Math. Artif. Intell.* **2015**, *75*, 53–68. [CrossRef]
21. Abdalla, M.; Nagy, B. Dilation and Erosion on the Triangular Tessellation: An Independent Approach. *IEEE Access* **2018**, *6*, 23108–23119. [CrossRef]
22. Nagy, B. Generalized triangular grids in digital geometry. *Acta Math. Acad. Paedagog. Nyházi* **2004**, *20*, 63–78.
23. Skala, V. Barycentric coordinates computation in homogeneous coordinates. *Comput. Graph.* **2008**, *32*, 120–127. [CrossRef]
24. Kovács, G.; Nagy, B.; Vizvári, B. Weighted Distances on the Trihexagonal Grid. In Proceedings of the International Conference on the Discrete Geometry for Computer Imagery, Vienna, Austria, 19 September 2017; LNCS; Springer: Cham, Switzerland, 2017; Volume 10502, pp. 82–93.
25. Abuhmaidan, K.; Nagy, B. Non-bijective translations on the triangular plane. In Proceedings of the 2018 IEEE 16th World Symposium on Applied Machine Intelligence and Informatics (SAMI), Kosice, Slovakia, 7–10 February 2018; pp. 183–188.

symmetry

MDPI

Article

One-Dimensional Optimal System for 2D Rotating Ideal Gas

Andronikos Paliathanasis

Institute of Systems Science, Durban University of Technology, P.O. Box 1334, Durban 4000, South Africa; anpaliat@phys.uoa.gr

Received: 9 July 2019; Accepted: 2 September 2019; Published: 3 September 2019

Abstract: We derive the one-dimensional optimal system for a system of three partial differential equations, which describe the two-dimensional rotating ideal gas with polytropic parameter $\gamma > 2$. The Lie symmetries and the one-dimensional optimal system are determined for the nonrotating and rotating systems. We compare the results, and we find that when there is no Coriolis force, the system admits eight Lie point symmetries, while the rotating system admits seven Lie point symmetries. Consequently, the two systems are not algebraic equivalent as in the case of $\gamma = 2$, which was found by previous studies. For the one-dimensional optimal system, we determine all the Lie invariants, while we demonstrate our results by reducing the system of partial differential equations into a system of first-order ordinary differential equations, which can be solved by quadratures.

Keywords: lie symmetries; invariants; shallow water; similarity solutions; optimal system

1. Introduction

A powerful mathematical treatment for the determination of exact solutions for nonlinear differential equations is the Lie symmetry analysis [1–3]. Specifically, Lie point symmetries help us in the simplification of differential equations by means of similarity transformations, which reduce the differential equation. The reduction process is based on the existence of functions that are invariant under a specific group of point transformations. When someone uses these invariants as new dependent and independent variables, the differential equation is reduced. The reduction process differs between ordinary differential equations (ODEs) and partial differential equations (PDEs). For ODEs, Lie point symmetries are applied to reduce the order of ODE by one; while on PDEs, Lie point symmetries are applied to reduce by one the number of independent variables, while the order of the PDEs remains the same. The solutions that are found with the application of those invariant functions are called similarity solutions. Some applications on the determination of similarity solutions for nonlinear differential equations can be found in [4–9] and the references therein.

A common characteristic in the reduction process is that the Lie point symmetries are not preserved during the reduction; hence, we can say that the symmetries can be lost. That is not an accurate statement, because symmetries are not "destroyed" or "created" under point transformations, but the "nature" of the symmetry changes. In addition, Lie symmetries can be used to construct new similarity solutions for a given differential equation by applying the adjoint representation of the Lie group [10].

It is possible that a given differential equation admits more than one similarity solution when the given differential equation admits a "large" number of Lie point symmetries. Hence, in order for someone to classify a differential equation according to the admitted similarity solutions, all the inequivalent Lie subalgebras of the admitted Lie symmetries should be determined.

The first group classification problem was carried out by Ovsiannikov [11], who demonstrated the construction of the one-dimensional optimal system for the Lie algebra. Since then, the classification of the one-dimensional optimal system has become a main tool for the study of nonlinear differential equations [12–15].

In this work, we focus on the classification of the one-dimensional optimal system for the two-dimensional rotating ideal gas system described by the following system of PDEs [16–18]:

$$h_t + (hu)_x + (hv)_y = 0, \tag{1}$$

$$u_t + uu_x + vu_y + h^{\gamma-2}h_x - fv = 0, \tag{2}$$

$$v_t + uv_x + vv_y + h^{\gamma-2}h_y + fu = 0. \tag{3}$$

where u and v are the velocity components in the x and y directions, respectively, h is the density of the ideal gas, f is the Coriolis parameter, and γ is the polytropic parameter of the fluid. Usually, γ is assumed to be $\gamma = 2$ where Equations (1)–(3) reduce to the shallow water system. However, in this work, we consider that $\gamma > 2$. In this work, polytropic index γ is defined as $\frac{C_p}{C_v} = \gamma - 1$.

Shallow water equations describe the flow of a fluid under a pressure surface. There are various physical phenomena that are described by the shallow water system with emphasis on atmospheric and oceanic phenomena [19–21]. Hence, the existence of the Coriolis force becomes critical in the description of the physical phenomena.

In the case of $\gamma = 2$, the complete symmetry analysis of the system (1)–(3) is presented in [22]. It was found that for $\gamma = 2$, the given system of PDEs is invariant under a nine-dimensional Lie algebra. The same Lie algebra, but in a different representation, is also admitted by the nonrotating system, i.e., $f = 0$. One of the main results of [22] is that the transformation that relates the two representations of the admitted Lie algebras for the rotating and nonrotating system transforms the rotating system (1)–(3) into the nonrotating one. For other applications of Lie symmetries on shallow water equations, we refer the reader to [23–28].

For the case of an ideal gas [17], i.e., parameter $\gamma > 1$ from our analysis, it follows that this property is lost. The nonrotating system and the rotating one are invariant under a different number of Lie symmetries and consequently under different Lie algebras. For each of the Lie algebras, we have the one-dimensional optimal system and all the Lie invariants. The results are presented in tables. We demonstrate the application of the Lie invariants by determining some similarity solutions for the system (1)–(3) for $\gamma > 2$. The paper is structured as follows.

In Section 2, we briefly discuss the theory of Lie symmetries for differential equations and the adjoint representation. The nonrotating system (1)–(3) is studied in Section 3. Specifically, we determine the Lie points symmetries, which form an eight-dimensional Lie algebra. The commutators and the adjoint representation are presented. We make use of these results, and we perform, a classification of the one-dimensional optimal system. We found that in total, there are twenty-three one-dimensional independent Lie symmetries and possible reductions, and the corresponding invariants are determined and presented in tables. In Section 4, we perform the same analysis for the rotating system. There, we find that the admitted Lie symmetries form a seven-dimensional Lie algebra, while there are twenty independent one-dimensional Lie algebras. We demonstrate the results by reducing the system of PDEs (1)–(3) into an integrable system of three first-order ODEs, the solution of which is given by quadratures. In Section 5, we discuss our results and draw our conclusions. Finally, in Appendix A, we present the tables, which include the results of our analysis.

2. Lie Symmetry Analysis

Let $H^A\left(x^i, \Phi^A, \Phi^A_i, ...\right) = 0$ be a system of partial differential equations (PDEs) where Φ^A denotes the dependent variables and x^i are the independent variables. At this point, it is important to mention that we make use of the Einstein summation convention. By definition, under the action of the infinitesimal one-parameter point transformation (1PPT):

$$\bar{x}^i = x^i\left(x^j, \Phi^B; \varepsilon\right), \;\; \bar{\Phi}^A = \Phi^A\left(x^j, \Phi^B; \varepsilon\right), \tag{4}$$

which connects two different points $P\left(x^j,\Phi^B\right)\rightarrow Q\left(\bar{x}^j,\bar{\Phi}^B,\varepsilon\right)$, the differential equation $H^A=0$ remains invariant if and only if $\bar{H}^A=H^A$, that is [2]:

$$\lim_{\varepsilon\to 0}\frac{\bar{H}^A\left(\bar{y}^i,\bar{u}^A,...;\varepsilon\right)-H^A\left(y^i,u^A,...\right)}{\varepsilon}=0. \tag{5}$$

The latter condition means that the $\Phi^A\left(P\right)$ and $\Phi^A\left(Q\right)$ are connected through the transformation.

The lhs of Expression (5) defines the Lie derivative of H^A along the vector field X of the one-parameter point transformation (4), in which X is defined as:

$$X=\frac{\partial\bar{x}^i}{\partial\varepsilon}\partial_i+\frac{\partial\bar{\Phi}}{\partial\varepsilon}\partial_A.$$

Thus, Condition (5) is equivalent to the following expression: [2]

$$\mathcal{L}_X\left(H^A\right)=0, \tag{6}$$

where $\mathcal{L}$ denotes the Lie derivative with respect to the vector field $X^{[n]}$, which is the n^{th}-extension of generator X of the transformation (4) in the jet space $\left\{x^i,\Phi^A,\Phi^A_{,i},\Phi^A_{,ij},...\right\}$ given by the expression [2]:

$$X^{[n]}=X+\eta^{[1]}\partial_{\Phi^A_i}+...+\eta^{[n]}\partial_{\Phi^A_{i_i i_j...i_n}}, \tag{7}$$

in which:

$$\eta^{[n]}=D_i\eta^{[n-1]}-u_{i_1i_2...i_{n-1}}D_i\left(\frac{\partial\bar{x}^j}{\partial\varepsilon}\right)\ ,\ i\succeq 1\ ,\ \eta^{[0]}=\left(\frac{\partial\bar{\Phi}^A}{\partial\varepsilon}\right). \tag{8}$$

Condition (6) provides a system of PDEs whose solution determines the components of the X, consequently the infinitesimal transformation. The vector fields X, which satisfy condition (6), are called Lie symmetries for the differential equation $H^A=0$. The Lie symmetries for a given differential equation form a Lie algebra.

Lie symmetries can be used in different ways [2] in order to study a differential equation. However, their direct application is on the determination of the so-called similarity solutions. The steps that we follow to determine a similarity solution are based on the determination and application of the Lie invariant functions.

Let X be a Lie symmetry for a given differential equation $H^A=0$, then the differential equation $X\left(F\right)=0$, where F is a function, provides the Lie invariants where by replacing in the differential equation $H^A=0$, we reduce the number of the independent variables (in the case of PDEs) or the order of the differential equation (in the case of ordinary differential equations (ODEs)).

Optimal System

Consider the n-dimensional Lie algebra G_n with elements $X_1,\ X_2,\ ...\ X_n$. Then, we shall say that the two vector fields [2]:

$$Z=\sum_{i=1}^n a_iX_i\ ,\ W=\sum_{i=1}^n b_iX_i\ ,\ \ a_i,\ b_i\text{ are constants.} \tag{9}$$

are equivalent iff there:

$$\mathbf{W}=lim^n_{j=i}Ad\left(\exp\left(\varepsilon_iX_i\right)\right)\mathbf{Z} \tag{10}$$

or:

$$W=cZ\ ,\ c=const. \tag{11}$$

where the operator [2]:

$$Ad\left(\exp\left(\varepsilon X_i\right)\right)X_j = X_j - \varepsilon\left[X_i, X_j\right] + \frac{1}{2}\varepsilon^2\left[X_i,\left[X_i, X_j\right]\right] + \ldots \tag{12}$$

is called the adjoint representation.

Therefore, in order to perform a complete classification for the similarity solutions of a given differential equation, we should determine all the one-dimensional independent symmetry vectors of the Lie algebra G_n.

We continue our analysis by calculating the Lie point symmetries for the system (1)–(3) for the case where the system is rotating $(f \neq 0)$ and nonrotating $(f = 0)$.

3. Symmetries and the Optimal System for Nonrotating Shallow Water

We start our analysis by applying the symmetry condition (6) for the Coriolis free system (1)–(3) with $f = 0$. We found that the system of PDEs admits eight Lie point symmetries, as are presented in the following [11]:

$$\begin{aligned}
X_1 &= \partial_t\ ,\ X_2 = \partial_x\ ,\ X_3 = \partial_y\ ,\\
X_4 &= t\partial_x + \partial_u\ ,\ X_5 = t\partial_y + \partial_v\ ,\\
X_6 &= y\partial_x - x\partial_y + v\partial_u - u\partial_v,\\
X_7 &= t\partial_t + x\partial_x + y\partial_y,\\
X_8 &= (\gamma - 1)\left(x\partial_x + y\partial_y + u\partial_u + v\partial_v\right) + 2h\partial_h.
\end{aligned}$$

The commutators of the Lie symmetries and the adjoint representation are presented in Table 1 and Table A1, respectively.

Table 1. Commutators of the admitted Lie point symmetries for the nonrotating 2D shallow water.

$[\,,\,]$	$\mathbf{X}_1$	$\mathbf{X}_2$	$\mathbf{X}_3$	$\mathbf{X}_4$	$\mathbf{X}_5$	$\mathbf{X}_6$	$\mathbf{X}_7$	$\mathbf{X}_8$
$\mathbf{X}_1$	0	0	0	X_2	X_3	0	$-(\gamma-1)X_1$	0
$\mathbf{X}_2$	0	0	0	0	0	$-X_3$	0	$(\gamma-1)X_2$
$\mathbf{X}_3$	0	0	0	0	0	X_2	0	$(\gamma-1)X_3$
$\mathbf{X}_4$	$-X_2$	0	0	0	0	$-X_5$	$(\gamma-1)X_4$	$(\gamma-1)X_4$
$\mathbf{X}_5$	$-X_3$	0	0	0	0	X_4	$(\gamma-1)X_5$	$(\gamma-1)X_5$
$\mathbf{X}_6$	0	X_3	$-X_2$	X_5	$-X_4$	0	0	0
$\mathbf{X}_7$	$(\gamma-1)X_1$	0	0	$-(\gamma-1)X_4$	$-(\gamma-1)X_5$	0	0	0
$\mathbf{X}_8$	0	$-(\gamma-1)X_2$	$-(\gamma-1)X_3$	$-(\gamma-1)X_4$	$-(\gamma-1)X_5$	0	0	0

We continue by determining the one-dimensional optimal system. Let us consider the generic symmetry vector:

$$Z^8 = a_1X_1 + a_2X_2 + a_3X_3 + a_4X_4 + a_5X_5 + a_6X_6 + a_7X_7 + a_8X_8$$

From Table A1, we see that by applying the following adjoint representations:

$$Z'^8 = Ad\left(\exp\left(\varepsilon_5X_5\right)\right)Ad\left(\exp\left(\varepsilon_4X_4\right)\right)Ad\left(\exp\left(\varepsilon_3X_3\right)\right)Ad\left(\exp\left(\varepsilon_2X_2\right)\right)Ad\left(\exp\left(\varepsilon_1X_1\right)\right)Z^8$$

parameters $\varepsilon_1,\ \varepsilon_2,\ \varepsilon_3,\ \varepsilon_4$, and ε_5 can be determined such that:

$$Z'^8 = a'_6X_6 + a'_7X_7 + a'_8X_8$$

Parameters a_6, a_7, and a_8 are the relative invariants of the full adjoint action. Indeed, in order to determine the relative invariants, we solve the following system of partial differential equations [1]:

$$\Delta\left(\phi\left(a_i\right)\right) = C_{ij}^k a^i \frac{\partial}{\partial a_j}$$

where C_{ij}^k are the structure constants of the admitted Lie algebra as presented in Table 1. Consequently, in order to derive all the possible one-dimensional Lie symmetries, we should study various cases were none of the invariants are zero, one of the invariants is zero, two of the invariants are zero, or all the invariants are zero.

Hence, for the first three cases, infer the following one-dimensional independent Lie algebras:

$$X_6\ ,\ X_7\ ,\ X_8\ ,\ \xi_{(67)} = X_6 + \alpha X_7\ ,\ \xi_{(68)} = X_6 + \alpha X_8$$

$$\xi_{(78)} = X_7 + \alpha X_8\ ,\ \xi_{(678)} = X_6 + \alpha X_7 + \beta X_8.$$

We apply the same procedure for the rest of the possible linear combinations of the symmetry vectors, and we find the one-dimensional-dependent Lie algebras:

$$X_1,\ X_2\ ,\ X_3\ ,\ X_4\ ,\ X_5\ ,\ \xi_{(12)} = X_1 + \alpha X_2\ ,\ \xi_{(13)} = X_1 + \alpha X_3\ ,\ \xi_{(23)} = X_2 + \alpha X_3\ ,\ \xi_{(14)} = X_1 + \alpha X_4\ ,$$

$$\xi_{(15)} = X_1 + \alpha X_5\ ,\ \xi_{(16)} = X_1 + \alpha X_6,\ \xi_{(34)} = X_3 + \alpha X_4\ ,\ \xi_{(25)} = X_2 + \alpha X_5\ \ \xi_{(45)} = X_4 + \alpha X_5\ ,$$

$$\xi_{(123)} = X_1 + \alpha X_2 + \beta X_3\ \xi_{(145)} = X_1 + \alpha X_4 + \beta X_5\ ,\ \xi_{(125)} = X_1 + \alpha X_2 + \beta X_5\ ,\ \xi_{(134)} = X_1 + \alpha X_3 + \beta X_4,$$

in which α and β are constants.

Therefore, by applying one of the above Lie symmetry vectors, we find all the possible reductions from a system of $1+2$ PDEs to a system of $1+1$ PDEs. The reduced system will not admit all the remaining Lie symmetries. The Lie symmetries that survive under a reduction process are given as described in the following example.

Let a PDE admit the Lie point symmetries Γ_1, Γ_2, which are such that $[\Gamma_1, \Gamma_2] = C_{12}^1 X_1$, with $C_{12}^1 \neq 0$. Reduction with the symmetry vector Γ_1 leads to a reduced differential equation, which admits Γ_2 as the Lie symmetry. On the other hand, reduction of the mother equation with respect to the Lie symmetry Γ_2 leads to a different reduced differential equation, which does not admit as a Lie point symmetry the vector field Γ_1. In case the two Lie symmetries form an Abelian Lie algebra, i.e., $C_{12}^1 = 0$, then under any reduction process, symmetries are preserved by any reduction.

We found that the optimal system admits twenty-three one-dimensional Lie symmetries and possible independent reductions. All the possible twenty-three Lie invariants are presented in Tables A2 and A3.

An application of the Lie invariants is presented below.

Application of ξ_{145}

Let us now demonstrate the results of Tables A2 and A3 by the Lie invariants of the symmetry vector ξ_{145} and construct the similarity solution for the system.

The application of ξ_{145} in the nonrotating system (1)–(3) reduces the PDEs in the following system:

$$(hu)_z + (hv)_w = 0 \tag{13}$$

$$\alpha + uu_z + vu_w + h^{\gamma-2}h_z = 0 \tag{14}$$

$$\beta + uv_z + vv_w + h^{\gamma-2}h_w = 0 \tag{15}$$

where $z = x - \frac{\alpha}{2}t^2$ and $w = y - \frac{\beta}{2}t^2$.

System (13)–(15) admits the Lie point symmetries:

$$\partial_z\ ,\ \partial_w\ ,\ z\partial_z + w\partial_w + \frac{2}{\gamma-1}h\partial_h + u\partial_u + v\partial_v \tag{16}$$

Reduction with the symmetry vector $\partial_z + c\partial_w$ provides the following system of first-order ODEs:

$$Fh_\sigma = (c\alpha-\beta)\,h^2, \tag{17}$$

$$Fv_\sigma = \frac{(\alpha-c\beta)\,ch^\gamma - \alpha h\,(v-cu)^2}{v-cu}, \tag{18}$$

$$Fh_\sigma = \frac{(\alpha-c\beta)\,cu^\gamma - \beta h\,(v-cu)^2}{v-cu}. \tag{19}$$

where $F = \left(1+c^2\right)h^\gamma - h\,(v-cu)^2$ and $\sigma = z + cw$.

By performing the change of variable $d\sigma = f d\tau$, function f can be removed from the above system. For $h\,(\tau) = 0$, the system (17)–(19) admits a solution $u = u_0,\ v = v_0$, which is a critical point. The latter special solutions are always unstable when $\alpha c > \beta$.

We proceed with our analysis by considering the rotating system.

4. Symmetries and Optimal System for Rotating Shallow Water

For the rotating system $(f \neq 0)$, the Lie symmetries are:

$$\begin{aligned}
Y_1 &= \partial_t\ ,\ Y_2 = \partial_x\ ,\ Y_3 = \partial_y\ ,\\
Y_4 &= y\partial_x - x\partial_y + v\partial_u - u\partial_v\ ,\\
Y_5 &= \sin(ft)\,\partial_x + \cos(ft)\,\partial_y + f\left(\cos(ft)\,\partial_u - \sin(ft)\,\partial_v\right)\\
Y_6 &= \cos(ft)\,\partial_x - \sin(ft)\,\partial_y - f\left(\sin(ft)\,\partial_u + \cos(ft)\,\partial_v\right)\\
Y_7 &= (\gamma-1)\left(x\partial_x + y\partial_y + u\partial_u + v\partial_v\right) + 2h\partial_h
\end{aligned}$$

The commutators and the adjoint representation are given in Table 2 and Table A4. The Lie symmetries for the rotating system form a smaller dimension Lie algebra than the non-rotating system. That is not the case when $\gamma = 2$, where the two Lie algebras have the same dimension and are equivalent under point transformation [22]. Therefore, for $\gamma > 2$, the Coriolis force cannot be eliminated by a point transformation as in the $\gamma = 2$ case.

Table 2. Commutators of the admitted Lie point symmetries for the rotating 2D shallow water.

$[\,,\,]$	$\mathbf{Y}_1$	$\mathbf{Y}_2$	$\mathbf{Y}_3$	$\mathbf{Y}_4$	$\mathbf{Y}_5$	$\mathbf{Y}_6$	$\mathbf{Y}_7$
$\mathbf{Y}_1$	0	0	0	0	fY_6	$-fY_5$	0
$\mathbf{Y}_2$	0	0	0	$-Y_3$	0	0	$(\gamma-1)\,Y_2$
$\mathbf{Y}_3$	0	0	0	Y_2	0	0	$(\gamma-1)\,Y_3$
$\mathbf{Y}_4$	0	Y_3	$-Y_2$	0	$-Y_6$	Y_5	0
$\mathbf{Y}_5$	$-fY_6$	0	0	Y_6	0	0	$(\gamma-1)\,Y_5$
$\mathbf{Y}_6$	fY_5	0	0	$-Y_5$	0	0	$(\gamma-1)\,Y_6$
$\mathbf{Y}_7$	0	$-(\gamma-1)\,Y_2$	$-(\gamma-1)\,Y_3$	0	$-(\gamma-1)\,Y_5$	$-(\gamma-1)\,Y_6$	0

As for the admitted Lie symmetries admitted by the given system of PDEs with or without the Coriolis terms for $\gamma > 2$, we remark that the rotating and the nonrotating systems have a common Lie subalgebra of one-parameter point transformations consisting of the symmetry vectors $Y_1,\ Y_2,\ Y_3,\ Y_4,$ and Y_7 or for the nonrotating system $X_1,\ X_2,\ X_3,\ X_6,$ and X_8.

We proceed with the determination of the one-dimensional optimal system and the invariant functions. Specifically, the relative invariants for the adjoint representation are calculated to be a_1 , a_7 and a_8. From Table 2 and Table A4, we can find the one-dimensional optimal system, which is:

$$Y_1,\ Y_2,\ Y_3,\ Y_4,\ Y_5,\ Y_6,\ Y_7,\ \chi_{12}=Y_1+\alpha Y_2,\ \chi_{13}=Y_1+\alpha Y_3,$$

$$\chi_{14}=Y_1+\alpha Y_4\ ,\ \chi_{15}=Y_1+\alpha Y_5,\ \ \chi_{16}=Y_1+\alpha Y_6,\ \chi_{17}=Y_1+\alpha Y_7,$$

$$\chi_{23}=Y_2+\alpha Y_3\ ,\ \ \chi_{45}=Y_4+\alpha Y_5,\ \chi_{46}=Y_4+\alpha Y_6,\ \chi_{56}=Y_5+\alpha Y_6$$

$$\chi_{47}=Y_4+\alpha Y_6\ ,\ \chi_{123}=Y_1+\alpha Y_2+\beta Y_3,\ \chi_{147}=Y_1+\alpha Y_4+\beta Y_7.$$

The Lie invariants, which correspond to all the above one-dimensional Lie algebras, are presented in Tables A5 and A6.

Let us demonstrate the application of the Lie invariants by the following, from which we can see that the Lie invariants reduce the nonlinear field equations into a system of integrable first-order ODEs, which can be solved with quadratures.

4.1. Application of χ_{12}

We consider the travel-wave similarity solution in the x-plane provided by the symmetry vector χ_{12} and the vector field Y_3. The resulting equations are described by the following system of first order ODEs:

$$v_z = f\frac{u}{\alpha-u} \tag{20}$$
$$\bar{F}u_z = f(\alpha-u)\,vh \tag{21}$$
$$\bar{F}h_z = fvh^2 \tag{22}$$

where $\bar{F}=h^{\gamma}-(a-u)^2h$ and $z=t-\alpha x$. Because we performed reduction with a subalgebra admitted by the nonrotating system, by setting $f=0$ in (20)–(22), we get the similarity solution for the nonrotating system, where in this case, it is found to be $h(z)=h_0,\ u(z)=u_0$ and $v(z)=v_0$.

We perform the substitution $dz=\frac{\bar{F}}{fv}d\tau$, and the latter system is simplified as follows:

$$\frac{v}{\bar{F}}v_\tau = \frac{u}{\alpha-u} \tag{23}$$
$$u_\tau = (\alpha-u)\,h \tag{24}$$
$$h_\tau = h^2 \tag{25}$$

from which we get the solution:

$$h(\tau)=(h_0-\tau)^{-1}\ ,\ u(\tau)=\alpha+u_0-\frac{u_0}{h_0}\tau \tag{26}$$

and:

$$v(t)^2=2\int\frac{\left(a+u_0-\frac{u_0}{h_0}\tau\right)}{\frac{u_0}{h_0}(h_0-\tau)}\left((h_0-\tau)^{-\gamma}+\left(\frac{u_0}{h_0}\right)^2\tau-\frac{(u_0)^2}{h_0}\right)d\tau. \tag{27}$$

4.2. Application of χ_{23}

Consider now the reduction with the symmetry vector fields χ_{23}. The resulting system of 1 + 1 differential equations admits five Lie point symmetries, and they are:

$$\partial_t,\ \partial_w\ ,\ (\sin(ft)+\alpha\cos(ft))\,\partial_w+f(\sin(ft)\,\partial_u+\cos(ft)\,\partial_v)$$
$$(\alpha\sin(ft)-\cos(ft))\,\partial_w-f(\cos(ft)\,\partial_u-\sin(ft)\,\partial_v)\ ,\ (\gamma-1)(\partial_w+u\partial_u+v\partial_v)+2h\partial_h.$$

where $w = y - \alpha x$. For simplicity of our calculations, let us assume $\gamma = 3$.

Reduction with the scaling symmetry provides the following system of first order ODEs:

$$
\begin{aligned}
H_t &= 2H\left(\alpha U - V\right), & (28)\\
U_t &= \alpha H^2 + u\left(\alpha U - V\right) + fV, & (29)\\
V_t &= -H^2 - v\left(\alpha U - V\right) - fU, & (30)
\end{aligned}
$$

where $h = wH$, $u = wU$, and $v = wU$. The latter system is integrable and can be solved with quadratures.

Reducing with respect to the symmetry vector $\left(\alpha \sin\left(ft\right) - \cos\left(ft\right)\right)\partial_w - f\left(\cos\left(ft\right)\partial_u - \sin\left(ft\right)\partial_v\right)$, we find the reduced system:

$$
\begin{aligned}
\frac{H_t}{H} &= -\frac{\alpha\cos\left(ft\right) + \sin\left(ft\right)}{\cos\left(ft\right) - \alpha\sin\left(ft\right)}, & (31)\\
U_t &= -\alpha f\frac{\sin\left(ft\right)V - \cos\left(ft\right)U}{\cos\left(ft\right) - \alpha\sin\left(ft\right)}, & (32)\\
V_t &= -f\frac{\sin\left(ft\right)V - \cos\left(ft\right)U}{\cos\left(ft\right) - \alpha\sin\left(ft\right)}, & (33)
\end{aligned}
$$

where now:

$$
\begin{aligned}
h &= H\left(t\right), & (34)\\
u &= \frac{\cos\left(ft\right)}{\cos\left(ft\right) - \alpha\sin\left(ft\right)}fw + U\left(t\right), & (35)\\
v &= -\frac{\sin\left(ft\right)}{\cos\left(ft\right) - \alpha\sin\left(ft\right)}fw + V\left(t\right). & (36)
\end{aligned}
$$

System (31)–(33) is integrable, and the solution is expressed in terms of quadratures.

5. Conclusions

In this work, we determined the one-dimensional optimal system for the two-dimensional ideal gas equations. The nonrotating system was found to be invariant under an eight-dimensional group of one-parameter point transformations. and there were twenty-three independent one-dimensional Lie algebras. One the other hand, when the Coriolis force was introduced, the dynamical admitted seven Lie point symmetries and twenty one-dimensional Lie algebras.

For all the independent Lie algebras, we determined all the invariant functions, which corresponded to all the independent similarity solutions.

In a future work, we plan to classify all the independent one-dimensional Lie algebras, which lead to analytic forms for the similarity solutions.

Funding: This research received no external funding.

Acknowledgments: The author wants to thank Kevin Duffy for gracious hospitality and P.G.L.Leach for a fruitful discussion on the subject.

Conflicts of Interest: The author declare no conflict of interest.

Appendix A

In this Appendix, we present the Tables A1–A6, which are referenced in the main article.

Table A1. Adjoint representation of the admitted Lie point symmetries for the nonrotating 2D shallow water.

$Ad\left(e^{(\varepsilon X_i)}\right) X_j$	$\mathbf{X}_1$	$\mathbf{X}_2$	$\mathbf{X}_3$	$\mathbf{X}_4$	$\mathbf{X}_5$	$\mathbf{X}_6$	$\mathbf{X}_7$	$\mathbf{X}_8$
$\mathbf{X}_1$	X_1	X_2	X_3	$X_4-\varepsilon X_2$	$X_5-\varepsilon X_3$	X_6	$X_7+\varepsilon(\gamma-1)X_1$	X_8
$\mathbf{X}_2$	X_1	X_2	X_3	X_4	X_5	$X_6+\varepsilon X_3$	X_7	$X_8-\varepsilon(\gamma-1)X_2$
$\mathbf{X}_3$	X_1	X_2	X_3	X_4	X_5	$X_6-\varepsilon X_2$	X_7	$X_8-\varepsilon(\gamma-1)X_3$
$\mathbf{X}_4$	$X_1+\varepsilon X_2$	X_2	X_3	X_4	X_5	$X_6+\varepsilon X_5$	$X_7-\varepsilon(\gamma-1)X_4$	$X_8-\varepsilon(\gamma-1)X_4$
$\mathbf{X}_5$	$X_1+\varepsilon X_3$	X_2	X_3	X_4	X_5	$X_6-\varepsilon X_4$	$X_7-\varepsilon(\gamma-1)X_5$	$X_8-\varepsilon(\gamma-1)X_5$
$\mathbf{X}_6$	X_1	$X_2\cos\varepsilon-X_3\sin\varepsilon$	$X_2\sin\varepsilon+X_3\cos\varepsilon$	$X_4\cos\varepsilon-X_5\sin\varepsilon$	$X_4\sin\varepsilon+X_5\cos\varepsilon$	X_6	X_7	X_8
$\mathbf{X}_7$	$e^{-(\gamma-1)\varepsilon}X_1$	X_2	X_3	$e^{-(\gamma-1)\varepsilon}X_4$	$e^{-(\gamma-1)\varepsilon}X_5$	X_6	X_7	X_8
$\mathbf{X}_8$	X_1	$e^{(\gamma-1)\varepsilon}X_3$	$e^{(\gamma-1)\varepsilon}X_4$	$e^{-(\gamma-1)\varepsilon}X_4$	$e^{-(\gamma-1)\varepsilon}X_5$	X_6	X_7	X_8

Table A2. Lie invariants for the optimal system of the nonrotating system.

Symmetry	**Invariants**
$\mathbf{X}_1$	$x,\ y,\ h\left(x,y\right),\ u\left(x,y\right),\ v\left(x,y\right)$
$\mathbf{X}_2$	$t,\ y,\ h\left(t,y\right),\ u\left(t,y\right),\ v\left(t,y\right)$
$\mathbf{X}_3$	$t,\ x,\ h\left(t,x\right),\ u\left(t,x\right),\ v\left(t,x\right)$
$\mathbf{X}_4$	$t,\ y,\ h\left(t,y\right),\ \frac{x}{t}+U\left(t,y\right),\ v\left(t,y\right)$
$\mathbf{X}_5$	$t,\ x,\ h\left(t,x\right),\ u\left(t,x\right),\ \frac{y}{t}+V\left(t,x\right)$
$\mathbf{X}_6$	$t,\ x^2+y^2,\ h\left(t,x^2+y^2\right),\ \frac{xU\left(t,x^2+y^2\right)+yV\left(t,x^2+y^2\right)}{\sqrt{x^2+y^2}},\ \frac{yU\left(t,x^2+y^2\right)-xV\left(t,x^2+y^2\right)}{\sqrt{x^2+y^2}}$
$\mathbf{X}_7$	$\frac{x}{t},\ \frac{y}{t},\ h\left(\frac{x}{t},\frac{y}{t}\right),\ u\left(\frac{x}{t},\frac{y}{t}\right),\ v\left(\frac{x}{t},\frac{y}{t}\right)$
$\mathbf{X}_8$	$H\left(x,y\right)t^{\frac{2}{1-\gamma}},\ U\left(x,y\right)t^{-1},\ V\left(x,y\right)t^{-1}$
$\xi_{(12)}$	$x-\alpha t,\ y,\ h\left(x-\alpha t,y\right),\ u\left(x-\alpha t,y\right),\ v\left(x-\alpha t,y\right)$
$\xi_{(13)}$	$x,\ y-\alpha t,\ h\left(x,y-\alpha t\right),\ u\left(x,y-\alpha t\right),\ v\left(x,y-\alpha t\right)$
$\xi_{(14)}$	$x-\frac{\alpha}{2}t^2,\ y,\ h\left(x-\frac{\alpha}{2}t^2,y\right),\ u\left(x-\frac{\alpha}{2}t^2,y\right),\ v\left(x-\frac{\alpha}{2}t^2,y\right)$
$\xi_{(15)}$	$x,\ y-\frac{\alpha}{2}t^2,\ h\left(x,y-\frac{\alpha}{2}t^2\right),\ u\left(x,y-\frac{\alpha}{2}t^2\right),\ v\left(x,y-\frac{\alpha}{2}t^2\right)$

Table A3. Lie invariants for the optimal system of the nonrotating system.

Symmetry	Invariants
$\xi_{(16)}$	$t,\ e^{-\alpha t}\left(x^2+y^2\right),\ u\left(t,e^{-\alpha t}x^2+y^2\right)\cos(\alpha t)+v\left(t,e^{-\alpha t}x^2+y^2\right)\sin(\alpha t)$ $\frac{y}{x},\ h\left(e^{-\alpha t}x^2+y^2,\frac{y}{x}\right),\ u\left(t,e^{-\alpha t}x^2+y^2\right)\sin(\alpha t)-v\left(t,e^{-\alpha t}x^2+y^2\right)\cos(\alpha t)$
$\xi_{(23)}$	$t,\ x-\alpha y,\ h\left(t,x-\alpha y\right),\ u\left(t,x-\alpha y\right),v\left(t,x-\alpha y\right)$
$\xi_{(34)}$	$t,\ y-\frac{x}{\alpha t},\ h\left(t,y-\frac{x}{\alpha t}\right),\ u\left(t,y-\frac{x}{\alpha t}\right),\ v\left(t,y-\frac{x}{\alpha t}\right)$
$\xi_{(25)}$	$t,\ y-\alpha tx,\ h\left(t,y-\alpha tx\right),\ u\left(t,y-\alpha tx\right),\ v\left(t,y-\alpha tx\right)$
$\xi_{(45)}$	$t,\ y-\alpha x,\ h\left(t,y-\alpha x\right),\ \alpha\frac{x}{t}+U\left(t,y-\alpha x\right),\ \alpha\frac{x}{t}+V\left(t,y-\alpha x\right)$
$\xi_{(123)}$	$t-\alpha x,\ t-\beta y,\ h\left(t-\alpha x,t-\beta y\right),\ u\left(t-\alpha x,t-\beta y\right),v\left(t-\alpha x,t-\beta y\right)$
$\xi_{(145)}$	$x-\frac{\alpha}{2}t^2,\ y-\frac{\beta}{2}t^2,\ h\left(x-\frac{\alpha}{2}t^2,y-\frac{\beta}{2}t^2\right),\ \alpha t+U\left(x-\frac{\alpha}{2}t^2,\ y-\frac{\beta}{2}t^2\right),\ \beta t+V\left(x-\frac{\alpha}{2}t^2,\ y-\frac{\beta}{2}t^2\right)$
$\xi_{(125)}$	$x-\alpha t,\ y-\frac{\beta}{2}t^2,\ h\left(x-\alpha t,y-\frac{\beta}{2}t^2\right),\ u\left(x-\alpha t,y-\frac{\beta}{2}t^2\right),\ \beta t+V\left(x-\alpha t,y-\frac{\beta}{2}t^2\right)$
$\xi_{(134)}$	$x-\frac{\beta}{2}t^2,\ y-\alpha t,\ h\left(x-\frac{\beta}{2}t^2,y-\alpha t\right),\ \beta t+U\left(x-\frac{\beta}{2}t^2,y-\alpha t\right),\ V\left(x-\frac{\beta}{2}t^2,y-\alpha t\right)$
$\xi_{(67)}$	$\frac{\ln t}{\alpha},w=\frac{t^{-\frac{\alpha+\sqrt{\alpha(\alpha-4)-4}}{2\alpha}}}{2\sqrt{\alpha(\alpha-4)-4}}\left(x-\left(\alpha+\sqrt{\alpha\left(\alpha-4\right)-4}\right)y\right),\ z=\frac{t^{-\frac{\alpha+\sqrt{\alpha(\alpha-4)-4}}{2\alpha}}}{2\sqrt{\alpha(\alpha-4)-4}}\left(x+\left(\alpha+\sqrt{\alpha\left(\alpha-4\right)-4}\right)y\right)$ $h\left(w,z\right),\ U\left(w,z\right)\sin\left(\frac{\ln t}{\alpha}\right)+V\left(w,z\right)\sin\left(\frac{\ln t}{\alpha}\right),\ U\left(w,z\right)\cos\left(\frac{\ln t}{\alpha}\right)-\ V\left(w,z\right)\sin\left(\frac{\ln t}{\alpha}\right)$
$\xi_{(68)}$	$t,\ x^2+y^2,\ x^{-\frac{2}{\gamma-1}}h\left(t,x^2+y^2\right),\ \frac{U\left(t,x^2+y^2\right)\cos\left(\frac{\ln x}{\alpha}\right)+V\left(t,x^2+y^2\right)\sin\left(\frac{\ln x}{\alpha}\right)}{x},\ \frac{U\left(t,x^2+y^2\right)\sin\left(\frac{\ln x}{\alpha}\right)-V\left(t,x^2+y^2\right)\cos\left(\frac{\ln x}{\alpha}\right)}{x}$
$\xi_{(78)}$	$w=xt^{-\frac{(\gamma-1)}{\alpha(\gamma-1)-2}},\ z=yt^{-\frac{(\gamma-1)}{\alpha(\gamma-1)-2}},\ t^{-\frac{2\alpha}{\alpha(\gamma-1)-2}}h\left(w,z\right),t^{-\frac{(\gamma-1)\alpha}{\alpha(\gamma-1)-2}}u\left(w,z\right),\ t^{-\frac{(\gamma-1)\alpha}{\alpha(\gamma-1)-2}}v\left(w,z\right)$
$\xi_{(678)}$	$t\ ,\ t^{-1-\beta}\left(x^2+y^2\right)\ ,t^{-\beta}\left(U\left(t,x^2+y^2\right)\sin(\alpha t)+V\left(t,x^2+y^2\right)\cos(\alpha t)\right)$ $t^{-\frac{2\beta}{\gamma-1}}H\left(t,x^2+y^2\right)\ ,\ t^{-\beta}\left(U\left(t,x^2+y^2\right)\cos(\alpha t)-V\left(t,x^2+y^2\right)\sin(\alpha t)\right)$

Table A4. Adjoint representation of the admitted Lie point symmetries for the rotating 2D shallow water.

$Ad\left(e^{(\varepsilon Y_i)}\right)Y_j$	$\mathbf{Y}_1$	$\mathbf{Y}_2$	$\mathbf{Y}_3$	$\mathbf{Y}_4$	$\mathbf{Y}_5$	$\mathbf{Y}_6$	$\mathbf{Y}_7$
$\mathbf{Y}_1$	Y_1	Y_2	Y_3	Y_4	$Y_5\cos(f\varepsilon)-Y_6\sin(f\varepsilon)$	$Y_5\sin(f\varepsilon)+Y_6\cos(f\varepsilon)$	Y_7
$\mathbf{Y}_2$	Y_1	Y_2	Y_3	$Y_4+\varepsilon Y_3$	Y_5	Y_6	$Y_7-\varepsilon(\gamma-1)Y_2$
$\mathbf{Y}_3$	Y_1	Y_2	Y_3	$Y_4-\varepsilon Y_2$	Y_5	Y_6	$Y_7-\varepsilon(\gamma-1)Y_3$
$\mathbf{Y}_4$	Y_1	$Y_2\cos\varepsilon-Y_3\sin\varepsilon$	$Y_2\sin\varepsilon+Y_3\cos\varepsilon$	Y_4	$Y_5\cos\varepsilon+Y_6\sin\varepsilon$	$Y_6\cos\varepsilon-Y_5\sin\varepsilon$	Y_7
$\mathbf{Y}_5$	$Y_1+f\varepsilon Y_6$	Y_2	Y_3	$Y_4-\varepsilon Y_6$	Y_5	Y_6	$Y_7-\varepsilon(\gamma-1)Y_5$
$\mathbf{Y}_6$	$Y_1-f\varepsilon Y_5$	Y_2	Y_3	$Y_4+\varepsilon Y_5$	Y_5	Y_6	$Y_7-\varepsilon(\gamma-1)Y_6$
$\mathbf{Y}_7$	Y_1	$e^{(\gamma-1)\varepsilon}Y_2$	$e^{(\gamma-1)\varepsilon}Y_3$	Y_4	$e^{(\gamma-1)\varepsilon}Y_5$	$e^{(\gamma-1)\varepsilon}Y_6$	Y_7

Table A5. Lie invariants for the optimal system of the rotating system.

Symmetry	Invariants
$\mathbf{Y}_1$	$x,\ y,\ h\left(x,y\right),\ u\left(x,y\right),\ v\left(x,y\right)$
$\mathbf{Y}_2$	$t,\ y,\ h\left(t,y\right),\ u\left(t,y\right),\ v\left(t,y\right)$
$\mathbf{Y}_3$	$t,\ x,\ h\left(t,x\right),\ u\left(t,x\right),\ v\left(t,x\right)$
$\mathbf{Y}_4$	$t,\ x^2+y^2,\ h\left(t,x^2+y^2\right),\ \frac{xU\left(t,x^2+y^2\right)+yV\left(t,x^2+y^2\right)}{\sqrt{x^2+y^2}},\ \frac{yU\left(t,x^2+y^2\right)-xV\left(t,x^2+y^2\right)}{\sqrt{x^2+y^2}}$
$\mathbf{Y}_5$	$t,\ x\cot\left(ft\right)-y\ ,\ h\left(t,x\cot\left(ft\right)-y\right),\ fx\cot\left(ft\right)+U\left(t,x\cot\left(ft\right)-y\right),\ -fx+V\left(t,x\cot\left(ft\right)-y\right)$
$\mathbf{Y}_6$	$t,\ x\tan\left(ft\right)+y,\ h\left(t,x\tan\left(ft\right)+y\right),\ -fx\tan\left(ft\right)+U\left(t,x\tan\left(ft\right)+y\right),\ -fx+V\left(t,x\tan\left(ft\right)+y\right)$
$\mathbf{Y}_7$	$\frac{x}{t},\ \frac{y}{t},\ h\left(\frac{x}{t},\frac{y}{t}\right),\ u\left(\frac{x}{t},\frac{y}{t}\right),\ v\left(\frac{x}{t},\frac{y}{t}\right)$
$\mathcal{X}_{(12)}$	$x-\alpha t,\ y,\ h\left(x-\alpha t,y\right),\ u\left(x-\alpha t,y\right),\ v\left(x-\alpha t,y\right)$
$\mathcal{X}_{(13)}$	$x,\ y-\alpha t,\ h\left(x,y-\alpha t\right),\ u\left(x,y-\alpha t\right),\ v\left(x,y-\alpha t\right)$
$\mathcal{X}_{(14)}$	$t,\ e^{-\alpha t}\left(x^2+y^2\right),\ u\left(t,e^{-\alpha t}x^2+y^2\right)\cos\left(\alpha t\right)+v\left(t,e^{-\alpha t}x^2+y^2\right)\sin\left(\alpha t\right)$ $\frac{y}{x},\ h\left(e^{-\alpha t}x^2+y^2,\frac{y}{x}\right),\ u\left(t,e^{-\alpha t}x^2+y^2\right)\sin\left(\alpha t\right)-v\left(t,e^{-\alpha t}x^2+y^2\right)\cos\left(\alpha t\right)$

Table A6. Lie invariants for the optimal system of the rotating system.

Symmetry	Invariants
$X_{(15)}$	$x+\frac{\alpha}{f}\cos(ft)\,,\ y-\frac{\alpha}{f}\sin(ft)\ ,\ h\left(x+\frac{\alpha}{f}\cos(ft)\,,y-\frac{\alpha}{f}\sin(ft)\right),$ $\alpha\sin(ft)+U\left(x+\frac{\alpha}{f}\cos(ft)\,,y-\frac{\alpha}{f}\sin(ft)\right),\ \alpha\cos(ft)+V\left(x+\frac{\alpha}{f}\cos(ft)\,,y-\frac{\alpha}{f}\sin(ft)\right)$
$X_{(16)}$	$x-\frac{\alpha}{f}\sin(ft)\,,\ y-\frac{\alpha}{f}\cos(ft)\ ,\ h\left(x-\frac{\alpha}{f}\sin(ft)\,,y-\frac{\alpha}{f}\cos(ft)\right),$ $\alpha\cos(ft)+U\left(x-\frac{\alpha}{f}\sin(ft)\,,y-\frac{\alpha}{f}\cos(ft)\right),\ -\alpha\sin(ft)+V\left(x-\frac{\alpha}{f}\sin(ft)\,,y-\frac{\alpha}{f}\cos(ft)\right)$
$X_{(17)}$	$xe^{-\alpha t},\ ye^{-\alpha t},\ e^{\frac{2\alpha}{\gamma-1}t}h\left(xe^{-\alpha t},ye^{-\alpha t}\right),\ e^{\alpha t}u\left(xe^{-\alpha t},ye^{-\alpha t}\right),\ e^{\alpha t}v\left(xe^{-\alpha t},ye^{-\alpha t}\right)$
$X_{(23)}$	$t,\ x-\alpha y,\ h(t,x-\alpha y)\,,\ u(t,x-\alpha y)\,,\ v(t,x-\alpha y)$
$X_{(45)}$	$t,\ w=\left(x^2+y^2-2x\ \cos(ft)+2y\sin(ft)\right),\ \frac{U(t,w)+f\sin(ft)}{V(t,w)+f\cos(ft)},\ \frac{U(t,w)^2+V(t,w)^2}{2}+f\left(U(t,w)\sin(ft)+V(t,w)\cos(ft)\right)$
$X_{(46)}$	$t,\ w=\left(x^2+y^2-2x\ \sin(ft)-2y\cos(ft)\right),\ \frac{U(t,w)-f\cos(ft)}{V(t,w)+f\sin(ft)},\ \frac{U(t,w)^2+V(t,w)^2}{2}+f\left(V(t,w)\sin(ft)-U(t,w)\cos(ft)\right)$
$X_{(56)}$	$t,\ z=y-\frac{x(\cos(ft)-\alpha\sin(ft))}{\sin(ft)+\alpha\cos(ft)},\ h(t,z)\,,\ f\frac{x(\cos(ft)-\alpha\sin(ft))}{\sin(ft)+\alpha\cos(ft)}+U(t,z)\,,\ -x+V(t,z)$
$X_{(47)}$	$t,\ x^2+y^2\ ,\ x^{-\frac{2}{\gamma-1}}h\left(t,x^2+y^2\right)\ ,\ \frac{U\left(t,x^2+y^2\right)\cos\left(\frac{\ln x}{\alpha}\right)+V\left(t,x^2+y^2\right)\sin\left(\frac{\ln x}{\alpha}\right)}{x}\ ,\ \frac{U\left(t,x^2+y^2\right)\sin\left(\frac{\ln x}{\alpha}\right)-V\left(t,x^2+y^2\right)\cos\left(\frac{\ln x}{\alpha}\right)}{x}$
$X_{(123)}$	$t-\alpha x,\ t-\beta y,\ h(t-\alpha x,t-\beta y)\,,\ u(t-\alpha x,t-\beta y)\,,v(t-\alpha x,t-\beta y)$
$X_{(147)}$	$z=e^{-t(\gamma-1)}\left(x\cos t-y\sin t\right)\ ,\ w=e^{-t(\gamma-1)}\left(y\cos t+x\sin t\right)\ ,$ $e^{-t(\gamma-1)}h(z,w)\,,\ e^{-t(\gamma-1)}\left(U(z,w)\cos t-V(z,w)\sin t\right)\ ,\ e^{-t(\gamma-1)}\left(U(z,w)\sin t+V(z,w)\cos t\right)$

References

1. Olver, P.J. *Applications of Lie Groups to Differential Equations*; Springer: New York, NY, USA, 1993.
2. Bluman, G.W.; Kumei, S. *Symmetries and Differential Equations*; Springer: New York, NY, USA, 1989.
3. Ibragimov, N.H. *CRC Handbook of Lie Group Analysis of Differential Equations, Volume I: Symmetries, Exact Solutions, and Conservation Laws*; CRS Press LLC: Boca Raton, FL, USA, 2000.
4. Webb, G.M. Lie symmetries of a coupled nonlinear Burgers-heat equation system. *J. Phys A Math. Gen.* **1990**, *23*, 3885. [CrossRef]
5. Tsamparlis, M.; Paliathanasis, A.; Karpathopoulos, L. Dynamics of ionization wave splitting and merging of atmospheric-pressure plasmas in branched dielectric tubes and channels. *J. Phys. A Math. Theor.* **2012**, *45*, 275201. [CrossRef]
6. Azad, H.; Mustafa, M.T. Group classification, optimal system and optimal reductions of a class of Klein Gordon equations. *Commun. Nonlinear Sci. Numer. Simul.* **2010**, *15*, 1132. [CrossRef]
7. Tsamparlis, M.; Paliathanasis, A. Symmetry analysis of the Klein–Gordon equation in Bianchi I spacetimes. *Int. J. Geom. Methods Mod. Phys.* **2005**, *12*, 155003.
8. Meleshko, S.V.; Shapeev, V.P. Nonisentropic solutions of simple wave type of the gas dynamics equations. *J. Nonlinear Math. Phys.* **2011**, *18*, 195. [CrossRef]
9. Halder, A.; Paliathanasis, A.; Leach, P.G.L. Noether's Theorem and Symmetry. *Symmetry* **2018**, *10*, 744. [CrossRef]
10. Jamal, S.; Leach, P.G.L.; Paliathanasis, A. Nonlocal Representation of the sl (2,R) Algebra for the Chazy equation. *Quaest. Math.* **2019**, *42*, 125. [CrossRef]
11. Ovsiannikov, L.V. *Group Analysis of Differential Equations*; Academic Press: New York, NY, USA, 1982.
12. Chou, K.S.; Qu, C.Z. Optimal systems and group classification of (1 + 2)-dimensional heat equation. *Acta Appl. Math.* **2004**, *83*, 257. [CrossRef]
13. Galas, F.; Richter, E.W. Exact similarity solutions of ideal MHD equations for plane motions. *Phys. D* **1991**, *50*, 297. [CrossRef]
14. Coggeshalla, S.V.; Meyer-ter-Vehn, J. Group-invariant solutions and optimal systems for multidimensional hydrodynamics. *J. Math. Phys.* **1992**, *33*, 3585. [CrossRef]
15. Hu, X.; Li, Y.; Chen, Y. A direct algorithm of one-dimensional optimal system for the group invariant solutions. *J. Math. Phys.* **2015**, *56*, 053504. [CrossRef]
16. Vallis, G.K. *Atmospheric and Oceanic Fluid Dynamics: Fundamentals and Large-Scale Circulation*; Cambridge University Press: Cambridge, UK, 2006.
17. Courant, R.; Friedrichs, K.O. *Supersonic Flow and Shock Waves*; Interscience Publishers: Geneva, Switzerland, 1948.
18. Kevorkian, J. *Partial Differential Equations: Analytical Solutions Techniques*; Chapman and Hall: New York, NY, USA, 1990.
19. Caleffi, V.; Valiani, A.; Zanni, A. Finite volume method for simulating extreme flood events in natural channels. *J. Hydraul. Res.* **2003**, *41*, 167. [CrossRef]
20. Akkermans, R.A.D.; Kamp, L.P.J.; Clercx, H.J.H.; van Heijst, G.J.F. Three-dimensional flow in electromagnetically driven shallow two-layer fluids. *Phys. Rev. E* **2010**, *82*, 026314. [CrossRef] [PubMed]
21. Kim, D.H.; Cho, Y.S.; Yi, Y.K. Propagation and run-up of nearshore tsunamis with HLLC approximate Riemann solver. *Ocean Eng.* **2007**, *34*, 1164. [CrossRef]
22. Chesnokov, A.A. Symmetries and exact solutions of the rotating shallow-water equations. *Eur. J. Appl. Math.* **2009**, *20*, 461. [CrossRef]
23. Xin, X.; Zhang, L.; Xia, Y.; Liu, H. Nonlocal symmetries and exact solutions of the (2 + 1)-dimensional generalized variable coefficient shallow water wave equation. *Appl. Math. Lett.* **2019**, *94*, 112. [CrossRef]
24. Szatmari, S.; Bihlo, A. Symmetry analysis of a system of modified shallow-water equations. *Comm. Nonlinear Sci. Num. Simul.* **2014**, *19*, 530. [CrossRef]
25. Chesnokov, A.A. Symmetries and exact solutions of the shallow water equations for a two-dimensional shear flow. *J. Appl. Mech. Tech. Phys.* **2008**, *49*, 737. [CrossRef]
26. Liu, J.-G.; Zeng, Z.-F.; He, Y.; Ai, G.-P. A Class of Exact Solution of $(3+1)$-Dimensional Generalized Shallow Water Equation System. *Int. J. Nonlinear Sci. Num. Simul.* **2014**, *19*, 37. [CrossRef]

27. Pandey, M. Lie Symmetries and Exact Solutions of Shallow Water Equations with Variable Bottom. *Int. J. Nonlinear Sci. Num. Simul.* **2015**, *16*, 93. [CrossRef]
28. Paliathanasis, A. Lie symmetries and similarity solutions for rotating shallow water. *Preprint arXiv* **2019**, arXiv:1906.00689.

symmetry

MDPI

Article

Minimal Energy Configurations of Finite Molecular Arrays

Pablo V. Negrón-Marrero * and Melissa López-Serrano

Department of Mathematics, University of Puerto Rico, Humacao, PR 00791-4300, USA; melissa.lopez3@upr.edu

* Correspondence: pablo.negron1@upr.edu

Received: 26 December 2018; Accepted: 28 January 2019; Published: 31 January 2019

Abstract: In this paper, we consider the problem of characterizing the minimum energy configurations of a finite system of particles interacting between them due to attractive or repulsive forces given by a certain intermolecular potential. We limit ourselves to the cases of three particles arranged in a triangular array and that of four particles in a tetrahedral array. The minimization is constrained to a fixed area in the case of the triangular array, and to a fixed volume in the tetrahedral case. For a general class of intermolecular potentials we give conditions for the homogeneous configuration (either an equilateral triangle or a regular tetrahedron) of the array to be stable that is, a minimizer of the potential energy of the system. To determine whether or not there exist other stable states, the system of first-order necessary conditions for a minimum is treated as a bifurcation problem with the area or volume variable as the bifurcation parameter. Because of the symmetries present in our problem, we can apply the techniques of equivariant bifurcation theory to show that there exist branches of non-homogeneous solutions bifurcating from the trivial branch of homogeneous solutions at precisely the values of the parameter of area or volume for which the homogeneous configuration changes stability. For the triangular array, we construct numerically the bifurcation diagrams for both a Lennard–Jones and Buckingham potentials. The numerics show that there exist non-homogeneous stable states, multiple stable states for intervals of values of the area parameter, and secondary bifurcations as well.

Keywords: molecular arrays; constrained optimization; equivariant bifurcation theory

1. Introduction

Consider a system of N molecules, modeled as identical spherical particles, enclosed in a bounded region $\mathcal{B}$ of $\mathbb{R}^3$. At any given instant (or in an equilibrium configuration), the total potential energy of the molecular array is given by:

$$E = \sum_{i<j} \phi(\|\vec{\mathbf{r}}_i - \vec{\mathbf{r}}_j\|), \tag{1}$$

where ϕ is the intermolecular potential energy with $\|\cdot\|$ the standard Euclidean or two-vector norm, and $\vec{\mathbf{r}}_1, \ldots, \vec{\mathbf{r}}_N \in \mathbb{R}^3$ are the positions of the particles. More general energy potentials have been considered of which (1) is a special case (cf. [1,2]), or those based on the eigenvalues of adjacency matrices like in [3]. The problem of minimizing (1) subject to certain type of global or local conditions have been studied extensively (see e.g., [4–6] and the references there in). In these models either the array is infinite, with some local repeating structure, or finite but with $N \to \infty$. In this paper, none of these conditions are required but we expect that our results can be extrapolated to such more general scenarios. Also, we do not commit to any particular intermolecular potential ϕ (but give examples for instance for Lennard–Jones type potentials) so that our results are applicable to any such smooth potential.

The particular problems that we consider in this paper are those of characterizing the minimum energy configurations of (1) in the case of three particles ($N = 3$) arranged in a triangle and that of four particles ($N = 4$) in a tetrahedral array. The minimization problem is subject to the constraint of fixed area for the triangular array and of fixed volume in the tetrahedral case. We are particularly interested on the dependence of the minimizing states on the parameter of area or volume in the constraint. Both problems have the particularity that they can be formulated in terms of the intermolecular distances only, that is, without specifying the coordinates corresponding to the positions of the particles, thus substantially reducing the number of unknowns in each problem.

The motivation to study these problems comes from the following phenomena observed both in laboratory experiments and molecular dynamics simulations (see e.g., [7,8]). As the density of a fluid is progressively lowered (keeping the temperature constant), there is a certain "critical" density such that if the density of the fluid is lower than this critical value, then bubbles or regions with very low density appear within the fluid. This phenomenon is usually called "cavitation" and it has been extensively studied as well in solids. (See for instance [9,10] for discussions and further references.) When using discrete models of materials like (1), distinguishing between regions of low vs. high density, or whether bubbles or holes have form within the array, is not obvious since one is dealing essentially with a set of points. (See for instance [11,12] for the use of Voronoi polyhedra to study such arrays.) Thus, to study this phenomenon within this discrete model, one is naturally led to study or characterize the stability of homogeneous energy minimizing configurations of such an array, as the density of the array changes. The problems considered in this paper are the simplest problems within such a model. Our main contribution is on the application of global bifurcation theory (as opposed to just local) to study the set of equilibrium configurations for (1) under the stated constraints. In particular, to give specific conditions in terms of the intermolecular potential ϕ for the existence of nontrivial states.

In Section 3 we consider the problem of three particles. By Heron's formula for the area of a triangle, any three numbers (representing the intermolecular distances) that yield a positive value for the area formula, represent a triangle. In this case, we show that the functional (1) subject to the constraint of fixed area A, has for any value of A, a critical point representing an equilateral triangle. Moreover, in Theorem 2 we give a necessary and sufficient condition (cf. (22)), in terms of the intermolecular potential, for this equilibrium point to be a (local) minimizer of the energy functional. This condition leads to a set of values $\mathcal{A}$ for the area parameter A for which the equilateral triangle is a stable configuration. We give examples of how this set looks for various intermolecular potentials including the classical Lennard–Jones [13] and Buckingham [14] potentials, and those that model hard and soft springs including the usual Hooke's law.

Next in Section 3.2 we turn to the question of whether there exists other (not equilateral) equilibrium configurations for those values of the area parameter A for which the equilateral triangle becomes unstable, that is, when it ceases to be a local minimizer. To answer this question, we treat the system of equations characterizing the equilibrium points (cf. (13)) as a bifurcation problem with the parameter A as a bifurcation parameter, and the set of equilateral equilibrium configurations as the trivial solution branch. We find that the necessary condition for bifurcation from the trivial branch for this system occurs exactly at the boundary points of the set $\mathcal{A}$ given by the stability condition (22). To check the sufficiency condition for bifurcation, one must consider the linearization of the system (13) about the trivial branch at a boundary point A_0 of $\mathcal{A}$. However, since the kernel of this linearization is two-dimensional we cannot immediately apply the usual or standard results from bifurcation theory (cf. [15–18]). Because of the symmetries present in this problem (cf (32)), we can apply bifurcation equivariant theory (cf. [16,19]) to construct a suitable reduced problem corresponding to isosceles triangular equilibrium configurations. The linearization of the reduced problem at the point where $A = A_0$ has now a one-dimensional kernel and provided that a certain transversality condition is satisfied (cf. (34)), we can show that there are three branches corresponding to isosceles triangles bifurcating from the trivial branch at the point where $A = A_0$. Since the stability of these bifurcating branches can only be determined numerically (because one must linearize about an unknown solution), in Section 5 we construct numerically the bifurcation diagrams, with their respective stability patterns, for instances of the Lennard–Jones and Buckingham potentials. These examples show that the primary bifurcations off the trivial branch are of trans-critical type, and that at least for the Lennard–Jones potential, there are secondary bifurcations corresponding to stable scalene triangles. Moreover, there are intervals of values of the area parameter, for which there exists multiple stable states of the system for each value of A in such an interval.

In Section 4 we consider an array of four molecules in a tetrahedron. The general treatment in this case is similar to the three particle case but with two main differences. First the characterization of when six numbers (representing the lengths of the sides of the tetrahedron) determine a tetrahedron, is given in terms of the Cayley-Menger determinant and the triangle inequalities of one of its faces (cf. [20]). The next complication arises from the fact that the tetrahedron has 24 symmetries as compared to only six for the triangle! To deal with this many possibilities, once again we make use of the basic techniques of equivariant theory to get suitable reduced problems to work with. As the Cayley–Menger determinant is proportional to the volume of the corresponding tetrahedron, the volume constraint in our problem is basically that of setting this determinant to a given value V for the volume. In this case we show in Section 4.1 that the functional (1) subject to the constraint of fixed volume V, has for any value of V a critical point representing a regular or equilateral tetrahedron. Moreover, in Theorem 4 we give necessary and sufficient conditions (cf. (43)), in terms of the intermolecular potential, for this equilibrium point to be a (local) minimizer of the energy functional. As for the triangular case, these conditions determine a set of values $\mathcal{V}$ for the volume parameter V for which the equilateral tetrahedron is a stable configuration.

In Section 4.2 we consider the question of the existence of non-equilateral equilibrium configurations. The equilibrium configurations in this case are given as solutions to a nonlinear system of seven equations in eight unknowns (cf. (40)). We treat this system as a bifurcation problem with the parameter V as a bifurcation parameter, and the set of equilateral tetrahedrons as the trivial solution branch. The necessary condition for bifurcation from the trivial branch for this system occurs exactly at the boundary points of the set $\mathcal{V}$ given by the stability conditions (43). At a boundary point V_0 of $\mathcal{V}$ there are two possibilities: the kernel of the linearization has dimension two or three. Using some of the machinery of equivariance theory as in [16], we can construct suitable reduced problems in each of these two cases, which enables us to establish the existence of non-equilateral equilibrium configurations and to get a full description of the symmetries of the bifurcating branches (cf. Theorems 5–7). As in the triangular case, the stability of this bifurcating branches can only be established numerically because one must linearize about the unknown bifurcating branch.

Notation: We let $\mathbb{R}^n$ denote the n dimensional space of column vectors with elements denoted by $\vec{\mathbf{x}}$, $\vec{\mathbf{y}}$,. . . The inner product of $\vec{\mathbf{x}}, \vec{\mathbf{y}} \in \mathbb{R}^n$ is denoted either by $\langle \vec{\mathbf{x}}, \vec{\mathbf{y}} \rangle$ or $\vec{\mathbf{x}}^t \vec{\mathbf{y}}$, where the superscript "t" denotes transpose. We denote the set of $n \times m$ matrices by $\mathbb{R}^{n\times m}$. For $L \in \mathbb{R}^{n\times m}$, we let $\ker(L) = \{\vec{\mathbf{x}} \in \mathbb{R}^n \,:\, L\vec{\mathbf{x}} = \vec{\mathbf{0}}\}$ and $\mathrm{Range}(L) = \{L\vec{\mathbf{x}} \,:\, \vec{\mathbf{x}} \in \mathbb{R}^n\}$. For a function $\vec{\mathbf{F}} \,:\, \mathbb{R}^n \to \mathbb{R}^m$, we denote its Fréchet derivative by $\mathrm{D}\vec{\mathbf{F}}$ which is given by the $m \times n$ matrix of partial derivatives of the components of $\vec{\mathbf{F}}$. If the variables in $\vec{\mathbf{F}}$ are given by $(\vec{\mathbf{x}}, \vec{\mathbf{y}})$, then $\mathrm{D}_{\vec{\mathbf{x}}}\vec{\mathbf{F}}$ denotes the derivative of $\vec{\mathbf{F}}$ with respect to the vector of variables $\vec{\mathbf{x}}$, i.e., the matrix of the partial derivatives of the components of $\vec{\mathbf{F}}$ with respect to the variables corresponding to $\vec{\mathbf{x}}$.

2. Equivariant Bifurcation from a Simple Eigenvalue

In this section, we provide an overview on some of the basic results on bifurcation theory from a simple eigenvalue for mappings between finite dimensional spaces, where the maps possess certain symmetries. The literature on this subject is extensive but we refer to [6,15,17] for details on the material presented in this section and further developments like for instance, the infinite dimensional case.

Let $\vec{\mathbf{F}} : \mathcal{U} \times \mathbb{R} \to \mathbb{R}^n$ where $\mathcal{U}$ is an open subset of $\mathbb{R}^n$, be a C^2 function, and consider the problem of characterizing the solution set of:

$$\vec{\mathbf{F}}(\vec{\mathbf{x}}, A) = \vec{\mathbf{0}}, \quad (\vec{\mathbf{x}}, A) \in \mathcal{U} \times \mathbb{R}. \tag{2}$$

We assume that there exists a (known) smooth function $\vec{\mathbf{g}}(\cdot)$ such that:

$$\vec{\mathbf{F}}(\vec{\mathbf{g}}(A), A) = \vec{\mathbf{0}}, \quad \forall\ A.$$

The set $\mathcal{T} = \{(\vec{\mathbf{g}}(A), A) : A \in \mathbb{R}\}$ is called the *trivial branch* of solutions of (2). We say that $(\vec{\mathbf{x}}_0, A_0) \in \mathcal{T}$ is a *bifurcation point* off the trivial branch $\mathcal{T}$, if every neighborhood of $(\vec{\mathbf{x}}_0, A_0)$ contains solutions of (2) not in $\mathcal{T}$. If we let

$$L(A) = \mathrm{D}_{\vec{\mathbf{x}}}\vec{\mathbf{F}}(\vec{\mathbf{g}}(A), A),$$

then by the Implicit Function Theorem, a necessary for $(\vec{\mathbf{x}}_0, A_0)$ to be a bifurcation point is that $L(A_0)$ must be singular, a condition well known to be not sufficient.

In many applications of bifurcation theory and for the problems considered in this paper, the mapping $\vec{\mathbf{F}}$ possesses symmetries due to the geometry of the underlying physical problem. The use of these symmetries in the analysis is useful for example to deal with problems in which $\dim\ker(L(A_0)) > 1$. Thus, we assume that for a proper subgroup $\mathcal{G}$ of $\mathbb{R}^{n\times n}$, characterizing the symmetries in the problem, the mapping $\vec{\mathbf{F}}$ satisfies:

$$\vec{\mathbf{F}}(P\vec{\mathbf{x}}, A) = P\vec{\mathbf{F}}(\vec{\mathbf{x}}, A), \quad \forall\, P \in \mathcal{G}. \tag{3}$$

Let $\vec{\mathbf{v}} \in \ker(L(A_0))$ and define the *isotropy subgroup* of $\mathcal{G}$ at $\vec{\mathbf{v}}$ by

$$\mathcal{H} = \{P \in \mathcal{G} : P\vec{\mathbf{v}} = \vec{\mathbf{v}}\}, \tag{4}$$

and the *$\mathcal{H}$–fixed point set* by

$$\mathbb{R}^n_{\mathcal{H}} = \{\vec{\mathbf{x}} \in \mathbb{R}^n : P\vec{\mathbf{x}} = \vec{\mathbf{x}},\ \forall P \in \mathcal{H}\}. \tag{5}$$

Clearly $\vec{\mathbf{v}} \in \mathbb{R}^n_{\mathcal{H}}$.

Let $\mathbb{P}_{\mathcal{H}} : \mathbb{R}^n \to \mathbb{R}^n$ be a linear map that projects onto $\mathbb{R}^n_{\mathcal{H}}$ that is $\mathrm{Range}(\mathbb{P}_{\mathcal{H}}) = \mathbb{R}^n_{\mathcal{H}}$ and $\mathbb{P}_{\mathcal{H}}(\mathbb{R}^n_{\mathcal{H}}) = \mathbb{R}^n_{\mathcal{H}}$. With $\mathcal{U}_{\mathcal{H}} = \mathbb{P}_{\mathcal{H}}(\mathcal{U}) = \mathcal{U} \cap \mathbb{R}^n_{\mathcal{H}}$, we define $\vec{\mathbf{F}}_{\mathcal{H}} : \mathcal{U}_{\mathcal{H}} \times \mathbb{R} \to \mathbb{R}^n_{\mathcal{H}}$ by:

$$\vec{\mathbf{F}}_{\mathcal{H}}(\vec{\mathbf{u}}, A) = \mathbb{P}_{\mathcal{H}}\vec{\mathbf{F}}(\vec{\mathbf{u}}, A), \quad (\vec{\mathbf{u}}, A) \in \mathcal{U}_{\mathcal{H}} \times \mathbb{R}. \tag{6}$$

An easy calculation now gives that

$$\mathrm{D}_{\vec{\mathbf{u}}}\vec{\mathbf{F}}_{\mathcal{H}}(\vec{\mathbf{u}}, A) = \mathbb{P}_{\mathcal{H}}\vec{\mathbf{F}}_{\vec{\mathbf{x}}}(\vec{\mathbf{u}}, A)\mathbb{P}_{\mathcal{H}}.$$

We assume that $\vec{\mathbf{g}}(A) \in \mathbb{R}^n_{\mathcal{H}}$ for all A, so that

$$\vec{\mathbf{F}}_{\mathcal{H}}(\vec{\mathbf{g}}(A), A) = \vec{\mathbf{0}}, \quad \forall\ A.$$

It follows now that $L_{\mathcal{H}}(A) : \mathbb{R}^n_{\mathcal{H}} \to \mathbb{R}^n_{\mathcal{H}}$ is given by:

$$L_{\mathcal{H}}(A) = \mathrm{D}_{\vec{\mathbf{u}}}\vec{\mathbf{F}}_{\mathcal{H}}(\vec{\mathbf{g}}(A), A) = \mathbb{P}_{\mathcal{H}}L(A)\mathbb{P}_{\mathcal{H}}.$$

Clearly $\vec{\mathbf{v}} \in \ker(L_{\mathcal{H}}(A_0))$. The *$\mathcal{H}$-reduced problem* is now given by:

$$\vec{\mathbf{F}}_{\mathcal{H}}(\vec{\mathbf{u}}, A) = \vec{\mathbf{0}}, \quad (\vec{\mathbf{u}}, A) \in \mathcal{U}_{\mathcal{H}} \times \mathbb{R}. \tag{7}$$

An important property relating (2) and (7) is that $(\vec{\mathbf{x}}, A) \in \mathcal{U}_{\mathcal{H}} \times \mathbb{R}$ is a solution of (2) if and only if $(\vec{\mathbf{x}}, A)$ is a solution of (7). The following result provides the required sufficient conditions for $(\vec{\mathbf{x}}_0, A_0)$ to be a bifurcation point of the $\mathcal{H}$-reduced problem.

Theorem 1 (Equivariant Bifurcation Theorem [19])**.** *Assume that for $A = A_0$ there exists $\vec{\mathbf{v}} \in \ker(L(A_0))$ that defines a proper isotropy subgroup $\mathcal{H}$ such that:*

$$\ker(L_{\mathcal{H}}(A_0)) = \operatorname{span}\{\vec{\mathbf{v}}\}, \quad L'_{\mathcal{H}}(A_0)\vec{\mathbf{v}} \notin \operatorname{Range}(L_{\mathcal{H}}(A_0)).$$

Then there exists a branch $\mathcal{C}_{\mathcal{H}}$ of nontrivial solutions of $\vec{\mathbf{F}}_{\mathcal{H}}(\vec{\mathbf{u}}, A) = \vec{\mathbf{0}}$ bifurcating from the trivial branch $\mathcal{T}$ at the point where $A = A_0$ and such that either:

1. *$\mathcal{C}_{\mathcal{H}}$ is unbounded in $\mathbb{R}^{n+1}$;*
2. *the closure of $\mathcal{C}_{\mathcal{H}}$ intersects the boundary $\partial\mathcal{U}$ of $\mathcal{U}$;*
3. *$\mathcal{C}_{\mathcal{H}}$ intersects $\mathcal{T}$ at a point $(\vec{\mathbf{x}}_*, A_*)$ where $A_* \neq A_0$.*

The proof of this theorem is basically an application of a result from Krasnoselski [18] that uses the homotopy invariance of the topological degree. The three alternatives in the statement of the theorem are usually referred to as the Crandall and Rabinowitz alternatives. The local version of this result (cf. [6]) that is, without the Crandall and Rabinowitz alternatives, can be obtained via the Lyapunov–Schmidt reduction method. A useful consequence of this reduction is an approximate formula for the bifurcating branch in a neighborhood of the bifurcation point. Let $\ker(L_{\mathcal{H}}(A_0)^t) = \operatorname{span}\{\vec{\mathbf{v}}^*\}$, where $\langle \vec{\mathbf{v}}^*, \vec{\mathbf{v}} \rangle = 1$, so that $\operatorname{Range}(L_{\mathcal{H}}(A_0)) = \left\{\vec{\mathbf{y}} \in \mathbb{R}^n_{\mathcal{H}} \, : \, \langle \vec{\mathbf{v}}^*, \vec{\mathbf{y}} \rangle = 0\right\}$. Now if we define

$$A^0 = \langle \vec{\mathbf{v}}^*, (\mathrm{D}_{\vec{\mathbf{u}}\vec{\mathbf{u}}}\vec{\mathbf{F}}^0_{\mathcal{H}}\vec{\mathbf{v}})\vec{\mathbf{v}} \rangle, \quad B^0 = \langle \vec{\mathbf{v}}^*, L'_{\mathcal{H}}(A_0)\vec{\mathbf{v}} \rangle. \tag{8}$$

(here the zero superscripts mean evaluated at $(\vec{\mathbf{x}}_0, A_0)$), then the bifurcating branch have the following asymptotic expansion (cf. [16]):

$$(\vec{\mathbf{x}}, A) = \left(\vec{\mathbf{g}}(A_0 + \varepsilon) + \varepsilon m \vec{\mathbf{v}} + O(\varepsilon^2), A_0 + \varepsilon\right), \tag{9}$$

where

$$m = -\frac{2B^0}{A^0}, \quad A^0 \neq 0. \tag{10}$$

3. The Three Particle Case

In this section, we consider the case in which the molecular array consists of three particles. The intermolecular energy is given by a smooth function $\phi \, : \, (0, \infty) \to \mathbb{R}$ called the *potential*. If (a, b, c) are the distances between the particles in the array, the total energy of the system is given by:

$$E(a, b, c) = \phi(a) + \phi(b) + \phi(c), \quad a, b, c > 0. \tag{11}$$

Also, the square of the area of the triangular array is given by Heron's formula:

$$g(a, b, c) \equiv s(s - a)(s - b)(s - c),$$

where $s = (a + b + c)/2$.

For any given number $A > 0$, we consider the following constrained minimization problem:

$$\left\{ \begin{array}{c} \min\limits_{a,b,c>0} E(a, b, c) \\ \text{subject to } g(a, b, c) = A^2. \end{array} \right. \tag{12}$$

Thus, we are looking for minimizers of the energy functional E subject to the constraint that the area of the array is A. The first-order necessary conditions for a solution of this problem are given by:

$$\left\{ \begin{array}{rcl} g(a,b,c) - A^2 & = & 0, \\ \vec{\nabla} E(a,b,c) + \lambda \vec{\nabla} g(a,b,c) & = & \vec{\mathbf{0}}, \end{array} \right. \tag{13}$$

where $\lambda \in \mathbb{R}$ is the Lagrange multiplier corresponding to the restriction $g(a,b,c) = A^2$. For any given value of $A > 0$, this is a nonlinear system of equations for the unknowns (λ, a, b, c) in terms of A. In general this system can have multiple solutions depending on the characteristics of the potential ϕ and the value of A.

3.1. Existence and Stability of Trivial States

An easy calculation shows that:

$$\vec{\nabla} E = \begin{bmatrix} \phi'(a) \\ \phi'(b) \\ \phi'(c) \end{bmatrix}, \quad \vec{\nabla} g = \frac{1}{4} \begin{bmatrix} a(b^2 + c^2 - a^2) \\ b(a^2 + c^2 - b^2) \\ c(a^2 + b^2 - c^2) \end{bmatrix}. \tag{14}$$

Thus, the system (13) is equivalent to:

$$\left\{ \begin{array}{rcl} \frac{1}{8}(a^2b^2 + a^2c^2 + b^2c^2) - \frac{1}{16}(a^4 + b^4 + c^4) - A^2 & = & 0, \\ \phi'(a) + \frac{\lambda}{4} a(b^2 + c^2 - a^2) & = & 0, \\ \phi'(b) + \frac{\lambda}{4} b(a^2 + c^2 - b^2) & = & 0, \\ \phi'(c) + \frac{\lambda}{4} c(a^2 + b^2 - c^2) & = & 0. \end{array} \right. \tag{15}$$

This system always has a solution with $a = b = c$. In fact, upon setting $a = b = c$ in (15), this system reduces to:

$$\frac{3}{16} a^4 = A^2, \quad \phi'(a) = -\frac{\lambda a^3}{4}. \tag{16}$$

Thus, we have the following result:

Lemma 1. *For any value of $A > 0$, the system (15) has a solution of the form $(\lambda_A, a_A, a_A, a_A, A)$ where:*

$$a_A = \frac{2\sqrt{A}}{\sqrt[4]{3}}, \quad \lambda_A = -\frac{4\phi'(a_A)}{a_A^3}. \tag{17}$$

We now characterize for which values of A, the solution provided in Lemma 16 is actually a minimizer, i.e., a solution of (12). To do this we need to examine the matrix $\left[\nabla^2 E + \lambda \nabla^2 g\right](\vec{\mathbf{v}}_A)$ where $\vec{\mathbf{v}}_A = (\lambda_A, a_A, a_A, a_A)$, over the subspace:

$$\mathcal{M} = \left\{ (x,y,z) \, : \, \vec{\nabla} g(\vec{\mathbf{v}}_A) \cdot (x,y,z) = 0 \right\}. \tag{18}$$

A straightforward calculation gives that:

$$\nabla^2 E = \begin{bmatrix} \phi''(a) & 0 & 0 \\ 0 & \phi''(b) & 0 \\ 0 & 0 & \phi''(c) \end{bmatrix}, \tag{19}$$

$$\nabla^2 g = \frac{1}{4} \begin{bmatrix} b^2 + c^2 - 3a^2 & 2ab & 2ac \\ 2ab & a^2 + c^2 - 3b^2 & 2bc \\ 2ac & 2bc & a^2 + b^2 - 3c^2 \end{bmatrix}. \tag{20}$$

It follows now that

$$\left[\nabla^2 E + \lambda \nabla^2 g\right](\vec{\mathbf{v}}_A) = \begin{bmatrix} \phi''(a_A) - \frac{\lambda_A a_A^2}{4} & \frac{\lambda_A a_A^2}{2} & \frac{\lambda_A a_A^2}{2} \\ \frac{\lambda_A a_A^2}{2} & \phi''(a_A) - \frac{\lambda_A a_A^2}{4} & \frac{\lambda_A a_A^2}{2} \\ \frac{\lambda_A a_A^2}{2} & \frac{\lambda_A a_A^2}{2} & \phi''(a_A) - \frac{\lambda_A a_A^2}{4} \end{bmatrix}, \tag{21}$$

and that

$$\mathcal{M} = \{(x, y, z) \,:\, x + y + z = 0\}.$$

Using (17) one can show now that the matrix (21) is positive definite over $\mathcal{M}$ if and only if:

$$\phi''(a_A) + \frac{3}{a_A}\phi'(a_A) > 0. \tag{22}$$

Thus, we have the following result:

Theorem 2. *Let $\phi : (0, \infty) \to \mathbb{R}$ be twice continuously differentiable function. Then the uniform array $(a, b, c) = (a_A, a_A, a_A)$ in Lemma 1 is a relative minimizer for the problem (12) for those values of A for which (22) holds.*

Example 1. *Consider the case of a potential that has the following form:*

$$\phi(r) = \frac{c_1}{r^{\delta_1}} - \frac{c_2}{r^{\delta_2}}, \tag{23}$$

where c_1, c_2 are positive constants and $\delta_1 > \delta_2 > 2$. (These constants determine the physical properties of the particle or molecule in question. The classical Lennard–Jones [13] potential is obtained upon setting $\delta_1 = 12$ and $\delta_2 = 6$.) For this function:

$$\phi'(r) = -\frac{c_1\delta_1}{r^{\delta_1+1}} + \frac{c_2\delta_2}{r^{\delta_2+1}}, \quad \phi''(r) = \frac{c_1\delta_1(\delta_1+1)}{r^{\delta_1+2}} - \frac{c_2\delta_2(\delta_2+1)}{r^{\delta_2+2}},$$

so that:

$$\phi''(r) + \frac{3}{r}\phi'(r) = \frac{c_1\delta_1(\delta_1-2)}{r^{\delta_1+2}} - \frac{c_2\delta_2(\delta_2-2)}{r^{\delta_2+2}}.$$

Since a_A is directly proportional to $\sqrt{A}$ (see (17)), we have that for (23), the stability condition (22) holds if and only if $A < A_0$, where A_0 is determined from the condition:

$$\frac{c_1\delta_1(\delta_1-2)}{a_A^{\delta_1+2}} - \frac{c_2\delta_2(\delta_2-2)}{a_A^{\delta_2+2}} = 0,$$

from which it follows that:

$$A_0 = \frac{\sqrt{3}}{4}\left[\frac{c_1\delta_1(\delta_1-2)}{c_2\delta_2(\delta_2-2)}\right]^{\frac{2}{\delta_1-\delta_2}}. \tag{24}$$

Thus, (17) is a (local) solution of (12) if and only if $A < A_0$. We will show that for $A > A_0$ there exist solutions that break the symmetry $a = b = c$.

Example 2. *A Buckingham potential has the form ([14,21]):*

$$\phi(r) = \alpha e^{-\beta r} - \frac{\gamma}{r^\eta}, \tag{25}$$

where $\alpha, \beta, \gamma, \eta$ are positive constants. Thus

$$\phi'(r) = -\alpha\beta \mathrm{e}^{-\beta r} + \frac{\gamma\eta}{r^{\eta+1}}, \quad \phi''(r) = \alpha\beta^2 \mathrm{e}^{-\beta r} - \frac{\gamma\eta(\eta+1)}{r^{\eta+2}},$$

from which it follows that:

$$\phi''(r) + \frac{3}{r}\phi'(r) = \alpha\beta\left[\beta - \frac{3}{r}\right]\mathrm{e}^{-\beta r} - \frac{\gamma\eta(\eta-2)}{r^{\eta+2}}.$$

After rearrangement, the stability condition (22) is equivalent to:

$$F(a_A) > G(a_A), \tag{26}$$

where

$$F(r) = \alpha\beta(\beta r - 3)\mathrm{e}^{-\beta r}, \quad G(r) = \frac{\gamma\eta(\eta-2)}{r^{\eta+1}}.$$

These functions generically look as in Figure 1 where for G we assumed that $\eta > 2$. Now clearly $F(r) < G(r)$ for r sufficiently large. Thus generically we expect the set of values of A for which (26) is satisfied to be of the form (A_0, A_1). Since F has a maximum at $r_m = \frac{4}{\beta}$, a sufficient condition for this is that $F(r_m) > G(r_m)$, or after rearrangement that the coefficients and exponents in (25) satisfy:

$$\alpha\beta \mathrm{e}^{-4} > \gamma\eta(\eta-2)\left(\frac{\beta}{4}\right)^{\eta+1}. \tag{27}$$

To check this condition against the results in [21], we let $D, R, \xi > 0$ with $\xi > \eta$, and define

$$\alpha = \frac{D\eta \mathrm{e}^{\xi}}{\xi - \eta}, \quad \beta = \frac{\xi}{R}, \quad \gamma = \frac{D\xi R^{\eta}}{\xi - \eta}. \tag{28}$$

It follows that (25) is now given in terms of D, R, ξ by:

$$\phi(r) = D\left[\frac{\eta}{\xi - \eta}\mathrm{e}^{\xi(1-\frac{r}{R})} - \frac{\xi}{\xi - \eta}\left(\frac{R}{r}\right)^{\eta}\right].$$

It is easy to check now that provided $\xi > \eta + 1$, then ϕ has negative minimum value at $r = R$. The results in ([21], Table 1, Page 202) show that the best fit of a normalized Buckingham potential to a normalized Lennard–Jones (12-6) potential ($\delta_1 = 12$ and $\delta_2 = 6$ in (23)) is achieved for $\xi = 14.3863$ and $\eta = 5.6518$. For these values one can check that (28) satisfy the inequality (27) independent of the values of D and R.

Example 3. *Consider a potential of the form*

$$\phi(r) = \frac{1}{2}kr^2 + \frac{1}{4}\beta r^4, \tag{29}$$

with $k > 0$ and $\beta \in \mathbb{R}$. This potential corresponds to a Hook-type spring when $\beta = 0$, a hard spring if $\beta > 0$, and a soft spring if $\beta < 0$. (More general versions of (29) have been used in the study of the control of multi-agent systems, e.g., [22,23].) For this potential

$$\phi''(r) + \frac{3}{r}\phi'(r) = 4k + 6\beta r^2.$$

Please note that the stability condition (22) holds when $\beta \geq 0$ independent of the value of A! That is, the symmetric state (17) is a minimizer for all values of A. In the case $\beta = 0$ is easy to show that this state is a global minimizer.

On the other hand, if $\beta < 0$, the stability condition holds if and only if $A < A_0$ where

$$A_0 = -\frac{k}{2\sqrt{3}\,\beta}.$$

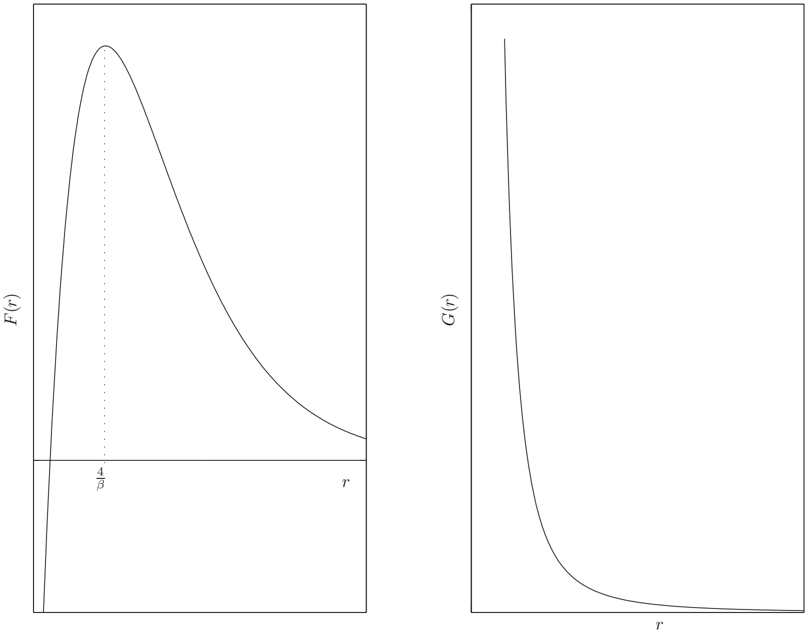

Figure 1. Generic graphs of the functions F and G appearing in the stability condition (26) for a Buckingham potential.

3.2. Existence and Stability of Nontrivial Solutions

We say that solutions of (13) are *trivial* if $a = b = c$ and call the set

$$\mathcal{T} = \{(\lambda_A, a_A, a_A, a_A, A) \,:\, \lambda_A, a_A \text{ given by (17)},\ A > 0\}\,, \tag{30}$$

the *trivial branch* parametrized by A. In this section, we show that there exist nontrivial solutions of (13) that bifurcate from the trivial branch.

If we let $\vec{\mathbf{x}} = (\lambda, a, b, c)$ and $\vec{\mathbf{G}} : \mathbb{R} \times (0, \infty)^4 \to \mathbb{R}^4$ be the left-hand side of (15), then this system is equivalent to $\vec{\mathbf{G}}(\vec{\mathbf{x}}, A) = \vec{\mathbf{0}}$. An easy calculation gives that

$$\mathrm{D}_{\vec{\mathbf{x}}}\vec{\mathbf{G}}(\vec{\mathbf{x}}, A) = \begin{bmatrix} 0 & (\vec{\nabla} g)^t \\ \vec{\nabla} g & \nabla^2 E + \lambda \nabla^2 g \end{bmatrix}. \tag{31}$$

If we evaluate now at the trivial branch (17), we get that

$$\mathrm{D}_{\vec{\mathbf{x}}}\vec{\mathbf{G}}(\vec{\mathbf{v}}_A, A) = \begin{bmatrix} 0 & \gamma & \gamma & \gamma \\ \gamma & \alpha & \beta & \beta \\ \gamma & \beta & \alpha & \beta \\ \gamma & \beta & \beta & \alpha \end{bmatrix},$$

where $\vec{\mathbf{v}}_A = (\lambda_A, a_A, a_A, a_A)$ and

$$\alpha = \phi''(a_A) - \frac{\lambda_A a_A^2}{4}, \quad \beta = \frac{\lambda_A a_A^2}{2}, \quad \gamma = \frac{a_A^3}{4}.$$

The eigenvalues of this matrix are $\alpha - \beta$, which is a double eigenvalue with geometric multiplicity two, and the simple eigenvalues

$$\frac{1}{2}\left[\alpha + 2\beta \pm \sqrt{(\alpha+2\beta)^2 + 12\gamma^2}\right],$$

which are always nonzero. A pair of linearly independent eigenvectors corresponding to $\alpha - \beta$ is $\left\{(0,-1,1,0)^t, (0,-1,0,1)^t\right\}$. Since

$$\alpha - \beta = \phi''(a_A) - \frac{3}{4}\lambda_A a_A^2 = \phi''(a_A) + \frac{3}{a_A}\phi'(a_A),$$

the double eigenvalue $\alpha - \beta$ becomes zero exactly at the value A_0 where the stability condition (22) fails by becoming zero. Thus according to standard theory of bifurcation theory, we can have either none, two or four branches of solutions of (15) bifurcating at the point where $A = A_0$. We now show that there are exactly four branches bifurcating from such a point: the trivial branch and three branches corresponding to isosceles triangles.

To avoid the complications of dealing with the two-dimensional kernel of (31) when evaluated at the trivial branch at $A = A_0$, we make use of the symmetries possessed by the mapping $\vec{\mathbf{G}}$. In particular, if we denote by $\mathcal{G}$ the subgroup of $\mathbb{R}^{4\times 4}$ of permutations that permute just the a, b, c components of any $\vec{\mathbf{x}} = (\lambda, a, b, c) \in \mathbb{R}^4$, then

$$\vec{\mathbf{G}}(P\vec{\mathbf{x}}, A) = P\vec{\mathbf{G}}(\vec{\mathbf{x}}, A), \quad \forall P \in \mathcal{G}. \tag{32}$$

Please note that every permutation in $\mathcal{G}$ changes the eigenvectors $\left\{(0,-1,1,0)^t, (0,-1,0,1)^t\right\}$ of $\alpha - \beta$. However, the eigenvector

$$\vec{\mathbf{v}} \equiv (0,-2,1,1)^t = (0,-1,1,0)^t + (0,-1,0,1)^t,$$

is unchanged by the proper subgroup of permutations $\mathcal{H}$ of $\mathcal{G}$ that permutes just the b, c components of any $\vec{\mathbf{x}} = (\lambda, a, b, c) \in \mathbb{R}^4$. Thus, $\mathcal{H}$ is the isotropy subgroup of $\mathcal{G}$ at $\vec{\mathbf{v}}$. The $\mathcal{H}$ fixed point set is given by:

$$\mathbb{R}^4_{\mathcal{H}} = \left\{(\lambda, a, b, b)^t \,:\, \lambda, a, b \in \mathbb{R}\right\}.$$

The projection $\mathbb{P}_{\mathcal{H}} : \mathbb{R}^4 \to \mathbb{R}^4_{\mathcal{H}}$ has matrix representation:

$$\mathbb{P}_{\mathcal{H}} = \begin{bmatrix} 1 & 0 & 0 & 0 \\ 0 & 1 & 0 & 0 \\ 0 & 0 & \frac{1}{2} & \frac{1}{2} \\ 0 & 0 & \frac{1}{2} & \frac{1}{2} \end{bmatrix},$$

and the $\mathcal{H}$ reduced problem is now:

$$\vec{\mathbf{G}}_{\mathcal{H}}(\vec{\mathbf{u}}, A) \equiv \mathbb{P}_{\mathcal{H}}\vec{\mathbf{G}}(\vec{\mathbf{u}}, A) = \vec{\mathbf{0}}, \quad (\vec{\mathbf{u}}, A) \in \mathbb{R}^4_{\mathcal{H}} \times (0, \infty).$$

Since $\mathcal{T} \subset \mathbb{R}^4_{\mathcal{H}} \times (0, \infty)$, it follows that $\mathcal{T}$ is a branch of solutions for the $\mathcal{H}$ reduced problem. Also, since

$$\mathrm{D}_{\vec{\mathbf{u}}}\vec{\mathbf{G}}_{\mathcal{H}}(\vec{\mathbf{u}}, A) = \mathbb{P}_{\mathcal{H}}\mathrm{D}_{\vec{\mathbf{x}}}\vec{\mathbf{G}}(\vec{\mathbf{u}}, A)\mathbb{P}_{\mathcal{H}}.$$

we have that $L_{\mathcal{H}}(A) : \mathbb{R}^4_{\mathcal{H}} \to \mathbb{R}^4_{\mathcal{H}}$ is given by:

$$L_{\mathcal{H}}(A) = \mathrm{D}_{\vec{\mathbf{u}}}\vec{\mathbf{G}}_{\mathcal{H}}(\vec{\mathbf{v}}_A, A) = \mathbb{P}_{\mathcal{H}}\mathrm{D}_{\vec{\mathbf{x}}}\vec{\mathbf{G}}(\vec{\mathbf{v}}_A, A)\mathbb{P}_{\mathcal{H}}.$$

Let

$$\mu(A) = \alpha - \beta = \phi''(a_A) + \frac{3}{a_A}\phi'(a_A). \tag{33}$$

We now establish a result for the existence of bifurcating branches for the reduced problem.

Theorem 3. *Let $\mu(A_0) = 0$ and assume that*

$$\frac{\mathrm{d}\mu}{\mathrm{d}A}(A_0) \neq 0. \tag{34}$$

Consider the system (13) *and its trivial branch of solutions* (30)*. Then from the point $(\lambda_0, a_0, a_0, a_0) \in \mathcal{T}$ bifurcate three branches of nontrivial solutions of* (13) *each corresponding to isosceles triangles.*

Proof. With the definitions and notation as above, a lengthy but otherwise elementary calculation shows that for any $A > 0$, $\mu(A)$ is a simple eigenvalue of $L_{\mathcal{H}}(A)$ restricted to $\mathbb{R}^4_{\mathcal{H}}$ with corresponding eigenvector $\vec{\mathbf{v}} = (0, -2, 1, 1)^t$. Thus

$$L_{\mathcal{H}}(A)\vec{\mathbf{v}} = \mu(A)\vec{\mathbf{v}}, \quad \forall\, A > 0.$$

In particular $\ker(L_{\mathcal{H}}(A_0)) = \operatorname{span}\{\vec{\mathbf{v}}\}$. If we differentiate with respect to A in the equation above and set $A = A_0$, we get that

$$L'_{\mathcal{H}}(A_0)\vec{\mathbf{v}} = \mu'(A_0)\vec{\mathbf{v}}.$$

Since $L_{\mathcal{H}}(A_0)$ is symmetric, we have that $\operatorname{Range}(L_{\mathcal{H}}(A_0)) = \{\vec{\mathbf{y}} \in \mathbb{R}^n_{\mathcal{H}} : \langle\vec{\mathbf{v}}, \vec{\mathbf{y}}\rangle = 0\}$. Thus, the hypotheses in Theorem 1 are satisfied if and only if $\mu'(A_0) \neq 0$. Thus, we get a branch of solutions of the reduced problem, equivalently (15), bifurcating from the trivial branch at the point where $A = A_0$. Since this branch belongs to $\mathbb{R}^4_{\mathcal{H}} \times \mathbb{R}$, we can use (32) to get that there exist two additional branches of solutions, one belonging to $\{(\lambda, b, a, b, A)^t : \lambda, a, b, A \in \mathbb{R}\}$ and the other in $\{(\lambda, b, b, a, A)^t : \lambda, a, b, A \in \mathbb{R}\}$. □

4. Four Particles in a Tetrahedron

We now consider the case of four particles arranged in a tetrahedron T. Let a, b, c, A, B, C be the distances between the particles where a, b, c denote the lengths of the edges joining a vertex of T, A the length of the edge opposite to a, B the length of the edge opposite to b, and C the length of the edge opposite to c. The six-tuple $\vec{\mathbf{a}} = (a, b, c, A, B, C)^t$ generates a tetrahedron ([20]) if and only if

$$g(\vec{\mathbf{a}}) > 0, \quad A < B + C, \quad B < A + C, \quad C < A + B, \tag{35}$$

where $g(\vec{\mathbf{a}})$ is given by the Cayley–Menger determinant:

$$g(\vec{\mathbf{a}}) = \begin{vmatrix} 0 & a^2 & b^2 & c^2 & 1 \\ a^2 & 0 & C^2 & B^2 & 1 \\ b^2 & C^2 & 0 & A^2 & 1 \\ c^2 & B^2 & A^2 & 0 & 1 \\ 1 & 1 & 1 & 1 & 0 \end{vmatrix}. \tag{36}$$

If we let $\mathbb{R}_+$ denote the set of positive real numbers, then we define

$$\mathcal{S} = \left\{ \vec{\mathbf{a}} = (a, b, c, A, B, C)^t \in \mathbb{R}^6_+ \;:\; (35) \text{ holds} \right\}.$$

Please note that $\mathcal{S}$ is open in $\mathbb{R}^6$. Moreover, any *regular* tetrahedron in which $a = b = c = A = B = C > 0$, is contained in $\mathcal{S}$.

If $\vec{\mathbf{a}} = (a,b,c,A,B,C)^t$ generates a tetrahedron, then so does $P\vec{\mathbf{a}}$ where $P = RQ$ and

1. R permutes (a,b,c) and (A,B,C) with the same permutation of three elements;
2. Q is any permutation of (a,b,c,A,B,C) in which the base of the tetrahedron is changed to another face. For example, (c,A,B,C,a,b) corresponds to reorienting the tetrahedron so that the base is given by (C,a,b).

Since there are six permutations of the type R and four of the type Q, we get that there are 24 permutations of the form $P = RQ$. These 24 permutations form a subgroup $\mathcal{R}$ of the group of permutations of six letters. Also, it is easy to show that

$$g(P\vec{\mathbf{a}}) = g(\vec{\mathbf{a}}), \quad \forall\, P \in \mathcal{R}. \tag{37}$$

As the Cayley–Menger determinant is directly proportional to the square of the volume of the tetrahedron (cf. (39)), this identity simply states that the volume of the tetrahedron remains the same after rotations of the base and independent of which face we use as the base.

The total energy of the system of four particles is given now by:

$$E(\vec{\mathbf{a}}) = \phi(a) + \phi(b) + \phi(c) + \phi(A) + \phi(B) + \phi(C), \tag{38}$$

where the intermolecular potential ϕ is as before. For any $V > 0$ we consider the constrained minimization problem:

$$\left\{ \begin{array}{c} \min\limits_{\mathcal{S}} \ E(\vec{\mathbf{a}}) \\ \text{subject to } g(\vec{\mathbf{a}}) = 288V^2. \end{array} \right. \tag{39}$$

The constraint here specifies that the tetrahedron determined by $\vec{\mathbf{a}}$ has volume V (cf. [20]). The first-order necessary conditions for a solution of this problem are given by (Since the inequality constraints in the definition of the set $\mathcal{S}$ are strict (non-active), the multipliers corresponding to these constraints are zero.): confirm.

$$\left\{ \begin{array}{rcl} g(\vec{\mathbf{a}}) - 288V^2 & = & 0, \\ \vec{\nabla} E(\vec{\mathbf{a}}) + \lambda \vec{\nabla} g(\vec{\mathbf{a}}) & = & \vec{\mathbf{0}}, \end{array} \right. \tag{40}$$

which is now a nonlinear system for the seven unknowns $(\lambda, \vec{\mathbf{a}})$ in terms of the parameter V.

4.1. Existence and Stability of Trivial States

Expanding the determinant in (36) and computing its partial derivatives, we get that

$$\begin{array}{rcl} \vec{\nabla} g(\vec{\mathbf{a}}) & = & 4\big[a(A^2(b^2+c^2+B^2+C^2-2a^2-A^2)+(b^2-c^2)(B^2-C^2)), \\ & & b(B^2(a^2+c^2+A^2+C^2-2b^2-B^2)+(a^2-c^2)(A^2-C^2)), \\ & & c(C^2(a^2+b^2+A^2+B^2-2c^2-C^2)+(a^2-b^2)(A^2-B^2)), \\ & & A(a^2(b^2+c^2+B^2+C^2-2A^2-a^2)-(b^2-C^2)(c^2-B^2)), \\ & & B(b^2(a^2+c^2+A^2+C^2-2B^2-b^2)-(a^2-C^2)(c^2-A^2)), \\ & & C(c^2(a^2+b^2+A^2+B^2-2C^2-c^2)-(a^2-B^2)(b^2-A^2))\big]. \end{array}$$

Since $\vec{\nabla} E(\vec{\mathbf{a}}) = (\phi'(a), \phi'(b), \phi'(c), \phi'(A), \phi'(B), \phi'(C))^t$, the system (40) when evaluated at the regular tetrahedron $\vec{\mathbf{a}} = (a,a,a,a,a,a)$, reduces to

$$4a^6 = 288V^2, \quad \phi'(a) + 4\lambda a^5 = 0.$$

Thus, we have the following result.

Lemma 2. *For any $V > 0$ the system (40) has the solution $(\lambda_V, \vec{\mathbf{a}}_V, V)$ where $\vec{\mathbf{a}}_V = (a_V, a_V, a_V, a_V, a_V, a_V)$ and*

$$a_V^3 = 6\sqrt{2}\,V, \quad \lambda_V = -\frac{\phi'(a_V)}{4a_V^5}. \tag{41}$$

We now examine the stability of the trivial state (41). A lengthy but otherwise elementary calculation shows that

$$H_V \equiv [\nabla^2 E + \lambda_V \nabla^2 g](\vec{\mathbf{a}}_V) = \begin{bmatrix} \alpha & \beta & \beta & 0 & \beta & \beta \\ \beta & \alpha & \beta & \beta & 0 & \beta \\ \beta & \beta & \alpha & \beta & \beta & 0 \\ 0 & \beta & \beta & \alpha & \beta & \beta \\ \beta & 0 & \beta & \beta & \alpha & \beta \\ \beta & \beta & 0 & \beta & \beta & \alpha \end{bmatrix}, \tag{42}$$

where

$$\alpha = \phi''(a_V) + \frac{3}{a_V}\phi'(a_V), \quad \beta = -\frac{2}{a_V}\phi'(a_V).$$

Since $\vec{\nabla} g(\vec{\mathbf{a}}_V) = 4a_V^5(1,1,1,1,1,1)^t$, we need examine the structure of H_V on the subspace of $\mathbb{R}^6$ given by

$$\mathcal{M} = \left\{ \vec{\mathbf{y}} \in \mathbb{R}^6 \,:\, y_1 + y_2 + y_3 + y_4 + y_5 + y_6 = 0 \right\}.$$

We have now the following result:

Theorem 4. *Let $\phi : (0, \infty) \to \mathbb{R}$ be twice continuously differentiable function. Then the matrix (42) is positive definite over $\mathcal{M}$ if and only if $\alpha > 0$ and $\alpha - 2\beta > 0$, which in turn are equivalent to*

$$\phi''(a_V) + \frac{3}{a_V}\phi'(a_V) > 0, \quad \phi''(a_V) + \frac{7}{a_V}\phi'(a_V) > 0. \tag{43}$$

Thus, the regular tetrahedron $\vec{\mathbf{a}}_V$ is a relative minimizer for the problem (39) for those values of V for which conditions (43) hold.

Proof. It is easy to check that $\mathcal{M} = \text{range}(M)$ where

$$M = \begin{bmatrix} 1 & 0 & 0 & 0 & 0 \\ 0 & 1 & 0 & 0 & 0 \\ 0 & 0 & 1 & 0 & 0 \\ -1 & -1 & -1 & -1 & -1 \\ 0 & 0 & 0 & 1 & 0 \\ 0 & 0 & 0 & 0 & 1 \end{bmatrix}.$$

The matrix corresponding to the quadratic form of H_V restricted to $\mathcal{M}$ is now given by $U_V = M^t H_V M$. The eigenvalues of U_V are:

$$\alpha \text{ (double)}, \quad \alpha - 2\beta, \quad \frac{1}{2}\left[7\alpha - 6\beta \pm \sqrt{16\alpha^2 + 9(\alpha - 2\beta)^2}\right].$$

Since the product of the last two of these eigenvalues is $6\alpha(\alpha - 2\beta)$, and $7\alpha - 6\beta = 3(\alpha - 2\beta) + 4\alpha$, we can conclude now that they are all positive if and only if $\alpha > 0$ and $\alpha - 2\beta > 0$. Thus, H_V restricted to $\mathcal{M}$ is positive definite provided these two conditions hold, which in turn implies that $\vec{\mathbf{a}}_V$ is a relative minimizer for problem (39). That $\alpha > 0$ and $\alpha - 2\beta > 0$ are equivalent to (43) follows from the definitions of α and β. □

Example 4. *For the Lennard–Jones potential* (23) *we have that:*

$$\begin{aligned}\phi''(r)+\frac{3}{r}\phi'(r) &= \frac{c_1\delta_1(\delta_1-2)}{r^{\delta_1+2}}-\frac{c_2\delta_2(\delta_2-2)}{r^{\delta_2+2}},\\ \phi''(r)+\frac{7}{r}\phi'(r) &= \frac{c_1\delta_1(\delta_1-6)}{r^{\delta_1+2}}-\frac{c_2\delta_2(\delta_2-6)}{r^{\delta_2+2}}.\end{aligned}$$

For simplicity, we assume $\delta_1 > 6$. We now have two cases:

1. *Assume that $\delta_2 \in (2, 6]$. Then the second condition in* (43) *is automatically satisfied and the first condition holds if and only if $V < V_0$, where V_0 is determined from the condition (cf.* (41)*):*

$$\frac{c_1\delta_1(\delta_1-2)}{r_0^{\delta_1+2}}-\frac{c_2\delta_2(\delta_2-2)}{r_0^{\delta_2+2}}=0,\quad r_0=a_{V_0},$$

from which it follows that:

$$V_0=\frac{\sqrt{2}}{12}\left[\frac{c_1\delta_1(\delta_1-2)}{c_2\delta_2(\delta_2-2)}\right]^{\frac{3}{\delta_1-\delta_2}}.$$

Thus, in this case the regular tetrahedron $\vec{\mathbf{a}}_V$ is a (local) solution of (39) *if and only if $V < V_0$.*

2. *If $\delta_2 > 6$, then the second condition in* (43) *holds if and only if $V < V_1$, where V_1 is determined from the condition:*

$$\frac{c_1\delta_1(\delta_1-6)}{r_1^{\delta_1+2}}-\frac{c_2\delta_2(\delta_2-6)}{r_1^{\delta_2+2}}=0,\quad r_1=a_{V_1},$$

from which it follows that:

$$V_1=\frac{\sqrt{2}}{12}\left[\frac{c_1\delta_1(\delta_1-6)}{c_2\delta_2(\delta_2-6)}\right]^{\frac{3}{\delta_1-\delta_2}}.$$

Since $\delta_1 > \delta_2 > 6$, it follows that $V_1 < V_0$. Thus, in this case the regular tetrahedron $\vec{\mathbf{a}}_V$ is a (local) solution of (39) *if and only if $V < V_1$.*

Example 5. *For the Buckingham* (25), *we have that*

$$\begin{aligned}\phi''(r)+\frac{3}{r}\phi'(r) &= \alpha\beta\left[\beta-\frac{3}{r}\right]\mathrm{e}^{-\beta r}-\frac{\gamma\eta(\eta-2)}{r^{\eta+2}},\\ \phi''(r)+\frac{7}{r}\phi'(r) &= \alpha\beta\left[\beta-\frac{7}{r}\right]\mathrm{e}^{-\beta r}-\frac{\gamma\eta(\eta-6)}{r^{\eta+2}}.\end{aligned}$$

Please note that the first condition in (43) *holds for an interval (V_0, V_1) of volume values under the conditions* (27) *in Example* 2*. The analysis now becomes rather complicated and we just describe it qualitatively. If $\eta > 6$, then the second condition in* (43) *would hold as well for values of V in an interval of the form (V_2, V_3) provided some condition similar to* (27) *holds. Depending as to whether or not the intersection $(V_0, V_1) \cap (V_2, V_3)$ is non-empty, we might get stable regular tetrahedrons. On the other hand, if $\eta \in (2, 6]$, then the second condition in* (43) *would hold as well for values of V in an interval of the form (V_4, ∞) and again the existence of trivial states will depend on whether the corresponding intersection is non-empty.*

Example 6. *For the potential* (29)

$$\phi''(r)+\frac{3}{r}\,\phi'(r)=4k+6\beta r^2,\quad \phi''(r)+\frac{7}{r}\,\phi'(r)=8k+10\beta r^2.$$

Please note that the stability conditions (43) *holds when $\beta \geq 0$ independent of the value of V! That is, the regular tetrahedron $\vec{\mathbf{a}}_V$ is a relative minimizer for the problem* (39) *for all values of V. In the case $\beta = 0$, since the functional* (38) *is convex, this state is a global minimizer.*

On the other hand, if $\beta < 0$, the first condition in (43) holds if $V < V_1$ and the second condition if $V < V_2$ where

$$V_1^2 = -\frac{k^3}{243\,\beta^3}, \quad V_2^2 = -\frac{8k^3}{1125\,\beta^3}.$$

Since $V_1 < V_2$ we get that conditions (43) hold both for $V < V_1$. For $V > V_1$ either one or both conditions fail.

4.2. Existence and Stability of Nontrivial States

Let $\vec{\mathbf{G}} : \mathbb{R} \times \mathcal{S} \times (0, \infty) \to \mathbb{R}^7$ be given by the left-hand side of (40):

$$\vec{\mathbf{G}}(\vec{\mathbf{x}}, V) = \begin{bmatrix} g(\vec{\mathbf{a}}) - 288V^2 \\ \vec{\nabla}E(\vec{\mathbf{a}}) + \lambda\vec{\nabla}g(\vec{\mathbf{a}}) \end{bmatrix},$$

where $\vec{\mathbf{x}} = (\lambda, \vec{\mathbf{a}})$. We have now that

$$\mathrm{D}_{\vec{\mathbf{x}}}\vec{\mathbf{G}}(\vec{\mathbf{x}}, V) = \begin{bmatrix} 0 & (\vec{\nabla}g(\vec{\mathbf{a}}))^t \\ \vec{\nabla}g(\vec{\mathbf{a}}) & \nabla^2 E(\vec{\mathbf{a}}) + \lambda\nabla^2 g(\vec{\mathbf{a}}) \end{bmatrix}. \tag{44}$$

It follows from (37) that

$$\begin{aligned} \vec{\nabla}g(P\vec{\mathbf{a}}) &= P\vec{\nabla}g(\vec{\mathbf{a}}), && \text{(45a)} \\ \nabla^2 g(P\vec{\mathbf{a}}) &= P\nabla^2 g(\vec{\mathbf{a}})P^t, \quad P \in \mathcal{R}, && \text{(45b)} \end{aligned}$$

with similar relations for the total energy E. It follows now from (45a) that

$$\vec{\mathbf{G}}(Q\vec{\mathbf{x}}, V) = Q\vec{\mathbf{G}}(\vec{\mathbf{x}}, V), \quad Q \in \mathcal{G}, \tag{46}$$

where

$$\mathcal{G} = \left\{ Q = \begin{bmatrix} 1 & \vec{\mathbf{0}}^t \\ \vec{\mathbf{0}} & P \end{bmatrix} \,:\, P \in \mathcal{R} \right\}.$$

Thus, the system (40) remains the same, up to reordering of the equations, when $\vec{\mathbf{x}} = (\lambda, \vec{\mathbf{a}})$ is replaced by $Q\vec{\mathbf{x}}$.

We now begin the analysis of the existence of solutions of the system (40) bifurcating from the trivial branch:

$$\mathcal{T} = \{(\lambda_V, \vec{\mathbf{a}}_V, V) \,:\, \lambda_V,\, \vec{\mathbf{a}}_V \text{ given by (41)},\ V > 0\}.$$

If we evaluate (44) at the trivial state $(\lambda_V, \vec{\mathbf{a}}_V, V)$, then this matrix reduces to:

$$\mathrm{D}_{\vec{\mathbf{x}}}\vec{\mathbf{G}}(\lambda_V, \vec{\mathbf{a}}_V, V) = \begin{bmatrix} 0 & (\vec{\nabla}g(\vec{\mathbf{a}}_V))^t \\ \vec{\nabla}g(\vec{\mathbf{a}}_V) & H_V \end{bmatrix}, \tag{47}$$

where $\vec{\nabla}g(\vec{\mathbf{a}}_V) = 4a_V^5(1,1,1,1,1,1)^t$ and H_V is given by (42). The matrix (47) has two eigenvalues which are nonzero for every value of $V > 0$, with the remaining eigenvalues given by:

1. $\mu_1(V) = \phi''(a_V) + \frac{3}{a_V}\phi'(a_V)$ with algebraic and geometric multiplicity three, and corresponding eigenvectors:
$$(0,-1,0,0,1,0,0)^t, \quad (0,0,-1,0,0,1,0)^t, \quad (0,0,0,-1,0,0,1)^t. \tag{48}$$
2. $\mu_2(V) = \phi''(a_V) + \frac{7}{a_V}\phi'(a_V)$ with algebraic and geometric multiplicity two, and corresponding eigenvectors:
$$(0,-1,1,0,-1,1,0)^t, \quad (0,-1,0,1,-1,0,1)^t. \tag{49}$$

Remark 1. *Please note that the expressions for these eigenvalues are the ones that appear in Theorem 4 characterizing the stability of the trivial state $(\lambda_V, \vec{\mathbf{a}}_V, V)$. Thus, the trivial state can change stability exactly when one of these two eigenvalues becomes zero.*

To deal with these kernels with dimension greater than one, we proceed as in the previous section by considering a suitable reduced problem in each case. These reductions are determined by the symmetries present in this problem which are embodied in (46).

4.2.1. The Eigenvalue $\mu_1(V)$

Let us take the eigenvector $\vec{\mathbf{g}} = (0,0,0,-1,0,0,1)^t$ of the eigenvalue $\mu_1(V)$ above. (The analysis for the other two eigenvectors is similar.) By inspection it is easy to get that the isotropy subgroup $\mathcal{H}$ of $\mathcal{G}$ at $\vec{\mathbf{g}}$ is given by:

$$\begin{aligned}\mathcal{H} \quad = \quad & \left\{ \begin{pmatrix} \lambda & a & b & c & A & B & C \\ \lambda & a & b & c & A & B & C \end{pmatrix}, \begin{pmatrix} \lambda & a & b & c & A & B & C \\ \lambda & b & a & c & B & A & C \end{pmatrix}, \right. \\ & \left. \begin{pmatrix} \lambda & a & b & c & A & B & C \\ \lambda & B & A & c & b & a & C \end{pmatrix}, \begin{pmatrix} \lambda & a & b & c & A & B & C \\ \lambda & A & B & c & a & b & C \end{pmatrix} \right\}.\end{aligned}$$

The $\mathcal{H}$-*fixed point set* is now given by:

$$\mathbb{R}^7_{\mathcal{H}} = \left\{ (\lambda, a, a, c, a, a, C)^t \ : \ \lambda, a, c, C \in \mathbb{R} \right\}. \tag{50}$$

The projection $\mathbb{P}_{\mathcal{H}} : \mathbb{R}^7 \to \mathbb{R}^7_{\mathcal{H}}$ has matrix representation:

$$\mathbb{P}_{\mathcal{H}} = \begin{bmatrix} 1 & 0 & 0 & 0 & 0 & 0 & 0 \\ 0 & \frac{1}{4} & \frac{1}{4} & 0 & \frac{1}{4} & \frac{1}{4} & 0 \\ 0 & \frac{1}{4} & \frac{1}{4} & 0 & \frac{1}{4} & \frac{1}{4} & 0 \\ 0 & 0 & 0 & 1 & 0 & 0 & 0 \\ 0 & \frac{1}{4} & \frac{1}{4} & 0 & \frac{1}{4} & \frac{1}{4} & 0 \\ 0 & \frac{1}{4} & \frac{1}{4} & 0 & \frac{1}{4} & \frac{1}{4} & 0 \\ 0 & 0 & 0 & 0 & 0 & 0 & 1 \end{bmatrix},$$

and the $\mathcal{H}$ reduced problem is now:

$$\vec{\mathbf{G}}_{\mathcal{H}}(\vec{\mathbf{u}}, V) \equiv \mathbb{P}_{\mathcal{H}} \vec{\mathbf{G}}(\vec{\mathbf{u}}, V) = \vec{\mathbf{0}}, \quad (\vec{\mathbf{u}}, V) \in \mathbb{R}^7_{\mathcal{H}} \times (0, \infty).$$

Since $\mathcal{T} \subset \mathbb{R}^7_{\mathcal{H}} \times (0, \infty)$, it follows that $\mathcal{T}$ is a branch of solutions for the $\mathcal{H}$ reduced problem. Also, since

$$\mathrm{D}_{\vec{\mathbf{u}}} \vec{\mathbf{G}}_{\mathcal{H}}(\vec{\mathbf{u}}, V) = \mathbb{P}_{\mathcal{H}} \mathrm{D}_{\vec{\mathbf{x}}} \vec{\mathbf{G}}(\vec{\mathbf{u}}, V) \mathbb{P}_{\mathcal{H}}.$$

we have that $L_{\mathcal{H}}(V) \ : \ \mathbb{R}^7_{\mathcal{H}} \to \mathbb{R}^7_{\mathcal{H}}$ is given by:

$$L_{\mathcal{H}}(V) = \mathrm{D}_{\vec{\mathbf{u}}} \vec{\mathbf{G}}_{\mathcal{H}}(\lambda_V, \vec{\mathbf{a}}_V, V) = \mathbb{P}_{\mathcal{H}} \mathrm{D}_{\vec{\mathbf{x}}} \vec{\mathbf{G}}(\lambda_V, \vec{\mathbf{a}}_V, V) \mathbb{P}_{\mathcal{H}}.$$

It easy to check now that $\mu_1(V)$ is a simple eigenvalue of $L_{\mathcal{H}}(V)$ restricted to $\mathbb{R}^7_{\mathcal{H}}$ with corresponding eigenvector $\vec{\mathbf{g}}$ that is

$$L_{\mathcal{H}}(V) \vec{\mathbf{g}} = \mu_1(V) \vec{\mathbf{g}}, \quad \forall \, V > 0.$$

We now have the result for the existence of bifurcating branches for the reduced problem. We omit the proof as it is similar to that of Theorem 3.

Theorem 5. *Let $\mu_1(V_1) = 0$ and assume that $\frac{\mathrm{d}\mu_1}{\mathrm{d}V}(V_1) \neq 0$. Then the system (40) has a branch of nontrivial solutions in $\mathbb{R}^7_{\mathcal{H}} \times (0, \infty)$ bifurcating from the trivial branch $\mathcal{T}$ at the point where $V = V_1$, where $\mathbb{R}^7_{\mathcal{H}}$ is given by (50).*

Remark 2. *It follows from (46) that there are two additional branches of nontrivial solutions of the system (40) of the forms:*

$$\{(\lambda, a, c, a, a, C, a) \,:\, \lambda \in \mathbb{R},\, a, c, C > 0\},$$
$$\{(\lambda, c, a, a, C, a, a) \,:\, \lambda \in \mathbb{R},\, a, c, C > 0\}.$$

We now consider the case of the eigenvector $\vec{\mathbf{g}} = (0, -1, -1, -1, 1, 1, 1)^T$ of $\mu_1(V)$. This eigenvector is obtained by adding the three eigenvectors in (48). By inspection, the isotropy subgroup $\mathcal{H}$ of $\mathcal{G}$ at $\vec{\mathbf{g}}$ is given by those permutations in $\mathcal{G}$ that permute the symbols (a, b, c) and (A, B, C) in $(\lambda, a, b, c, A, B, C)$ with the same permutation. (Thus, $\mathcal{H}$ has six elements.) The $\mathcal{H}$–fixed point set is now given by:

$$\mathbb{R}^7_{\mathcal{H}} = \{(\lambda, a, a, a, A, A, A)^t \,:\, \lambda, a, A \in \mathbb{R}\}. \tag{51}$$

The projection $\mathbb{P}_{\mathcal{H}} : \mathbb{R}^7 \to \mathbb{R}^7_{\mathcal{H}}$ has matrix representation:

$$\mathbb{P}_{\mathcal{H}} = \begin{bmatrix} 1 & 0 & 0 & 0 & 0 & 0 & 0 \\ 0 & \frac{1}{3} & \frac{1}{3} & \frac{1}{3} & 0 & 0 & 0 \\ 0 & \frac{1}{3} & \frac{1}{3} & \frac{1}{3} & 0 & 0 & 0 \\ 0 & \frac{1}{3} & \frac{1}{3} & \frac{1}{3} & 0 & 0 & 0 \\ 0 & 0 & 0 & 0 & \frac{1}{3} & \frac{1}{3} & \frac{1}{3} \\ 0 & 0 & 0 & 0 & \frac{1}{3} & \frac{1}{3} & \frac{1}{3} \\ 0 & 0 & 0 & 0 & \frac{1}{3} & \frac{1}{3} & \frac{1}{3} \end{bmatrix},$$

It follows now that for the $\mathcal{H}$ reduced problem, $\mu_1(V)$ is a simple eigenvalue with corresponding eigenvector $\vec{\mathbf{g}}$. The proof of the following result is as that of Theorem 3.

Theorem 6. *Let $\mu_1(V_1) = 0$ and assume that $\frac{\mathrm{d}\mu_1}{\mathrm{d}V}(V_1) \neq 0$. Then the system (40) has a branch of nontrivial solutions in $\mathbb{R}^7_{\mathcal{H}} \times (0, \infty)$ bifurcating from the trivial branch $\mathcal{T}$ at the point where $V = V_1$, where $\mathbb{R}^7_{\mathcal{H}}$ is given by (51).*

Remark 3. *By applying all the transformations in $\mathcal{G}$, it follows from (46) that there are three additional branches of solutions of the system (40) of the forms:*

$$\{(\lambda, A, A, a, a, a, A) \,:\, \lambda \in \mathbb{R},\, a, A > 0\},$$
$$\{(\lambda, a, A, A, A, a, a) \,:\, \lambda \in \mathbb{R},\, a, A > 0\},$$
$$\{(\lambda, A, a, A, a, A, a) \,:\, \lambda \in \mathbb{R},\, a, A > 0\}.$$

Thus, combining both theorems, we get that there are seven branches of nontrivial solutions bifurcating from the trivial branch $\{(\lambda_V, \vec{\mathbf{a}}_V, V) \,:\, V > 0\}$ at the value of $V = V_1$ where $\mu_1(V_1) = 0$ and $\mu_1'(V_1) \neq 0$.

4.2.2. The Eigenvalue $\mu_2(V)$

We now consider the case of the eigenvector $\vec{\mathbf{g}} = (0, -2, 1, 1, -2, 1, 1)^T$ of $\mu_2(V)$. This eigenvector is obtained by adding the eigenvectors in (49). By inspection, the isotropy subgroup $\mathcal{H}$ of $\mathcal{G}$ at $\vec{\mathbf{g}}$ is given by

$$\begin{aligned}\mathcal{H} \quad = \quad & \left\{ \begin{pmatrix} \lambda & a & b & c & A & B & C \\ \lambda & a & b & c & A & B & C \end{pmatrix}, \begin{pmatrix} \lambda & a & b & c & A & B & C \\ \lambda & a & c & b & A & C & B \end{pmatrix}, \right. \\ & \begin{pmatrix} \lambda & a & b & c & A & B & C \\ \lambda & A & C & b & a & c & B \end{pmatrix}, \begin{pmatrix} \lambda & a & b & c & A & B & C \\ \lambda & A & b & C & a & B & c \end{pmatrix}, \\ & \left. \begin{pmatrix} \lambda & a & b & c & A & B & C \\ \lambda & A & B & c & a & b & C \end{pmatrix}, \begin{pmatrix} \lambda & a & b & c & A & B & C \\ \lambda & A & c & B & a & C & b \end{pmatrix} \right\},\end{aligned}$$

with $\mathcal{H}$–fixed point set given by:

$$\mathbb{R}^7_{\mathcal{H}} = \{(\lambda, a, b, b, a, b, b) \,:\, \lambda, a, b \in \mathbb{R}\}\,. \tag{52}$$

The projection $\mathbb{P}_{\mathcal{H}} : \mathbb{R}^7 \to \mathbb{R}^7_{\mathcal{H}}$ has matrix representation:

$$\mathbb{P}_{\mathcal{H}} = \begin{bmatrix} 1 & 0 & 0 & 0 & 0 & 0 & 0 \\ 0 & \frac{1}{2} & 0 & 0 & \frac{1}{2} & 0 & 0 \\ 0 & 0 & \frac{1}{4} & \frac{1}{4} & 0 & \frac{1}{4} & \frac{1}{4} \\ 0 & 0 & \frac{1}{4} & \frac{1}{4} & 0 & \frac{1}{4} & \frac{1}{4} \\ 0 & \frac{1}{2} & 0 & 0 & \frac{1}{2} & 0 & 0 \\ 0 & 0 & \frac{1}{4} & \frac{1}{4} & 0 & \frac{1}{4} & \frac{1}{4} \\ 0 & 0 & \frac{1}{4} & \frac{1}{4} & 0 & \frac{1}{4} & \frac{1}{4} \end{bmatrix},$$

It follows now that for the $\mathcal{H}$-reduced problem, $\mu_2(V)$ is a simple eigenvalue with corresponding eigenvector $\vec{\mathbf{g}}$. The proof of the following result is as that of Theorem 3.

Theorem 7. *Let $\mu_2(V_2) = 0$ and assume that $\frac{\mathrm{d}\mu_2}{\mathrm{d}V}(V_2) \neq 0$. Then the system* (40) *has a branch of nontrivial solutions in $\mathbb{R}^7_{\mathcal{H}} \times (0, \infty)$ bifurcating from the trivial branch $\mathcal{T}$ at the point where $V = V_2$, where $\mathbb{R}^7_{\mathcal{H}}$ is given by* (52)*.*

Remark 4. *By applying all the transformations in $\mathcal{G}$, it follows from* (46) *that there are two additional branches of solutions of the system* (40) *of the forms:*

$$\begin{aligned}&\{(\lambda, b, a, b, b, a, b) \,:\, \lambda \in \mathbb{R},\, a, b > 0\}\,,\\ &\{(\lambda, b, b, a, b, b, a) \,:\, \lambda \in \mathbb{R},\, a, b > 0\}\,.\end{aligned}$$

5. Numerical Examples

In this section, we present some numerical examples illustrating the results of the previous sections. For simplicity we limit ourselves to the three particle problem. The examples show that the structure of the bifurcation diagrams is quite rich and complex. To construct the pictures in this section, we use the results of Theorem 3, in particular the symmetries given by (32), together with various numerical techniques to get full or detailed descriptions of the corresponding bifurcation diagram.

To compute approximations of the bifurcating solutions predicted by Theorem 3, one employs a predictor-corrector continuation method (cf. [24,25]). The bifurcation points off the trivial branch can be determined, by Theorem 3, from the solutions of the equation $\mu(A) = 0$ (cf. (17), (33)). Secondary bifurcation points off nontrivial branches can be detected by monitoring the sign of a certain determinant. Once a sign change in this determinant is detected, the bifurcation point can be computed by a bisection or secant type iteration. After detection and computation of a bifurcation point, then one can use formulas (8)–(10) to get an approximate point on the solution curve from which the continuation of the bifurcating branch can proceed.

Any trivial or nontrivial computed solution $(\vec{\mathbf{x}}^*, A^*)$ will be called *stable*, if the matrix $(\nabla^2 E + \lambda\nabla^2 g)(\vec{\mathbf{x}}^*, A^*)$ (cf. (31)) is positive definite when restricted to the tangent space at $\vec{\mathbf{x}}^*$ of the constraint of fixed area. Otherwise the point $(\vec{\mathbf{x}}^*, A^*)$ will be called *unstable*. We recall that the tangent space at $\vec{\mathbf{x}}^*$ of the constraint of fixed area is given by

$$\mathcal{M} = \left\{(x,y,z) \,:\, \vec{\nabla} g(\vec{\mathbf{x}}^*) \cdot (x,y,z) = 0\right\}.$$

Please note that since this space depends on the point $\vec{\mathbf{x}}^*$, then except for the trivial branch where the solution is known explicitly, the stability of a solution can only be determined numerically.

In our first example we consider the Lennard–Jones potential (23) with $c_1 = 1$, $c_2 = 2$, $\delta_1 = 12$, and $\delta_2 = 6$. (We obtained similar results for other values of c_1, c_2 like those for argon in which $c_1/c_2 = 3.4^6$ Å^6.) From equation (24) we get that the bifurcation point off the trivial branch is given approximately by $A_0 = 0.5877$. For the case of Theorem 3 in which $a = b$, we show in Figure 2 a close-up of the bifurcating branch near this bifurcation point, for the projection onto the A–a plane. In this figure and the others, the color red indicates unstable solutions while the stable ones are marked in green. Please note that the bifurcation is of the trans-critical type. It is interesting to note that for an interval of values of the parameter A to the left of A_0 in the figure (approximately $(0.5855, 0.5877)$), there are multiple states (trivial and nontrivial) which are stable, the trivial one with an energy less than the nontrivial state in this case. In Figure 3 we look at the same branches of solutions, again the projection onto the A–a plane, but for a larger interval of values of A. We now discover that there are two secondary bifurcation points (In Figure 3 there are bifurcations only corresponding to the values of $A_0 = 0.5877$, $A_1 = 0.6251$ and $A_2 = 0.6670$. The apparent crossing of a branch of scalene triangles and the trivial branch is just an artifact of the projection onto the A–a plane.) at approximately $A_1 = 0.6251$ and $A_2 = 0.6670$, and once again we have multiple stable states (with different symmetries) existing for an interval of values of the parameter A. The branches of solutions bifurcating at these values of A correspond to stable scalene triangles. Once a branch of solutions is computed, we can use the symmetries (32) to generate other branches of solutions. In Figure 4 we show all the solutions obtained via this process, projected to the abc space (no A dependence). Figure 5 show the same set of solution but with the branch or axis of trivial solutions coming out of the page. The figures clearly show the variety of solutions (stable and unstable) for the problem (12) as well as the rather complexity of the corresponding solution set.

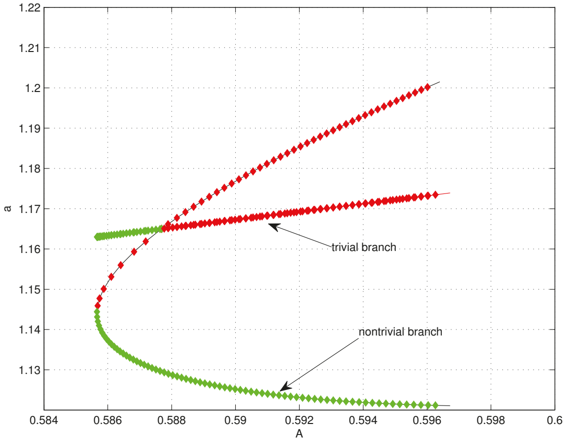

Figure 2. Bifurcation diagram for the a component vs. A for the system (13) in the case $a = b$ and a Lennard–Jones potential. The points in green represent local minima of (12) while those in red are either maxima or none.

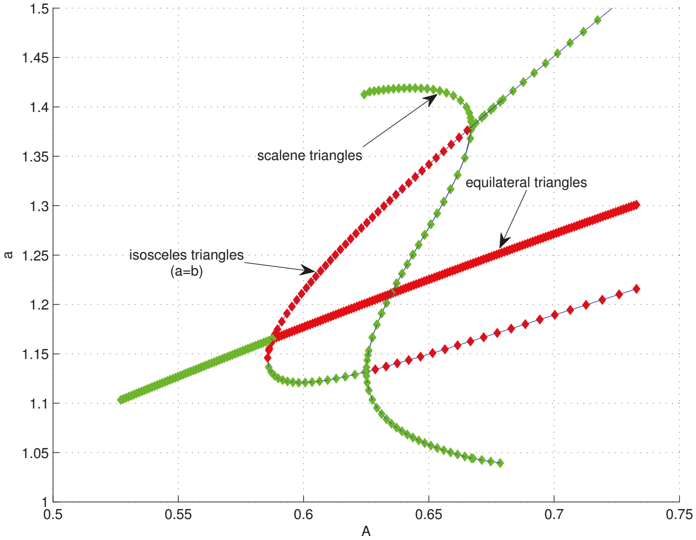

Figure 3. Bifurcation diagram for the system (13) in the case of a Lennard–Jones potential for a larger interval of values of A. There are secondary bifurcations into stable scalene triangles.

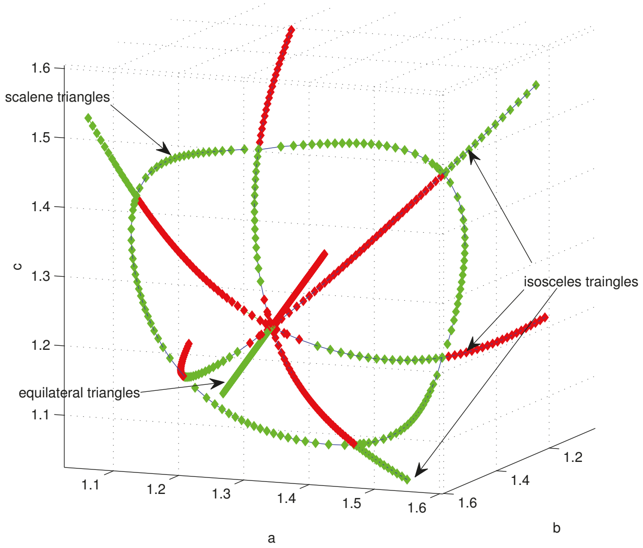

Figure 4. Solution set for the system (13) in the case of a Lennard–Jones potential without the A dependence.

For our next numerical example, we consider the Buckingham potential (25) with parameter values $\alpha = \beta = \gamma = 1$ and $\eta = 4$, which satisfy (27). In this case, we have two bifurcation points off the trivial branch (which correspond to solutions of $\mu(A) = 0$) at approximately $A_0 = 5.3154$ and $A_1 = 74.2253$. The trivial branch is stable for $A \in (A_0, A_1)$ and unstable otherwise. Both bifurcations are into isosceles triangles, and both are of trans-critical type but with different stability patterns. In Figure 6 we show the solution set for the case $a = b$. The plot shows the dependence of the a and c components on the area parameter A. In Figure 7 we show the projection of this set onto the c vs.

A plane where one can appreciate somewhat better the stability patterns at each bifurcation point, and that there is a turning point for $A \approx 46$ on the branch bifurcating from A_0. Please note that once again we have multiple stable states existing for an interval of values of the parameter A. No secondary bifurcations were detected in this case.

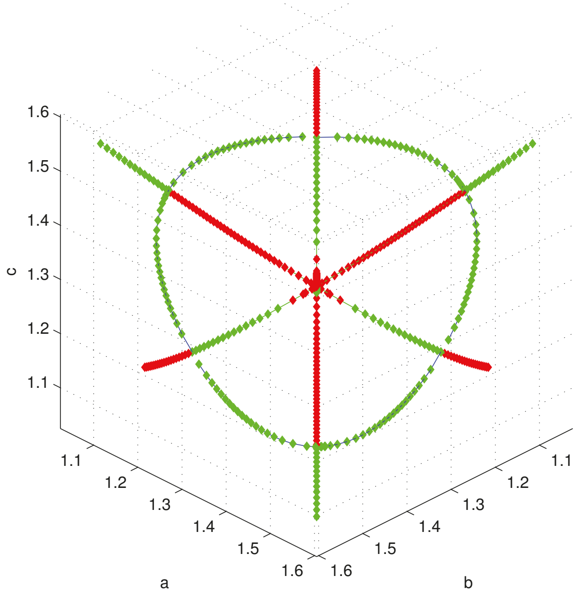

Figure 5. Solution set for the system (13) in the case of a Lennard–Jones potential without the A dependence with the branch of trivial solutions coming out of the page.

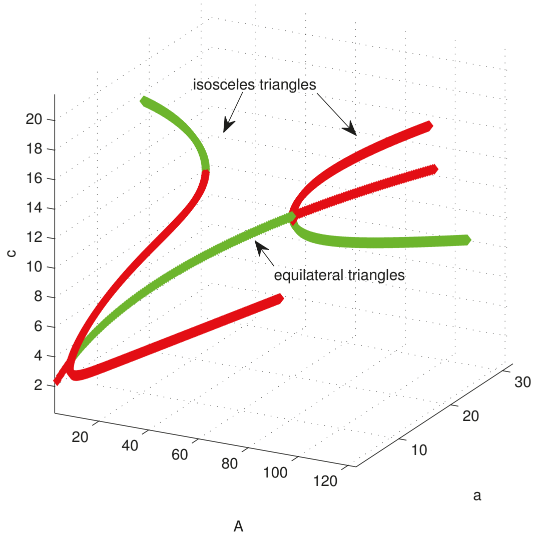

Figure 6. Dependence of the a and c components on the parameter A for the system (13) in the case $a = b$ and for a Buckingham potential.

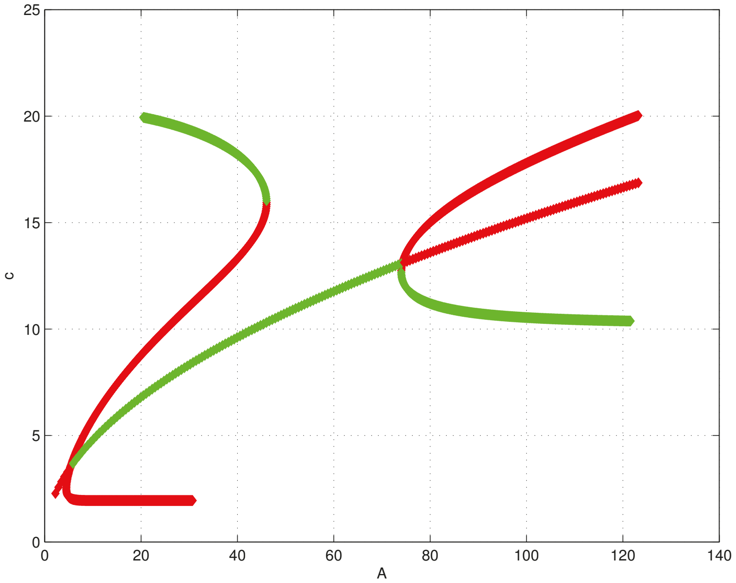

Figure 7. Projection onto the c vs. A plane of the set in Figure 6.

6. Final Comments

The variety or type of solutions obtained from Theorems 3, 5–7, could be predicted generically from an analysis of the symmetries present in our problem as given by (32) and (46). However, such an analysis does not guaranty the existence of solutions with the predicted symmetries. It is the application of the Equivariant Bifurcation Theorem 1 that actually yields the result that such solutions exist. The generic analysis however is a preliminary step in identifying the spaces in which Theorem 1 can be applied. We should also point out that the results on the bifurcating branches in Theorems 3, 5–7 are global in the sense that the so-called Crandall and Rabinowitz alternatives in Theorem 1 hold. That is, any bifurcating branch is either unbounded, or it intersects the boundary of the domain of definition of the operator in the equilibrium conditions, or it intersects the trivial branch at another eigenvalue.

The results of this paper might be useful in the analysis of the more general and complex problem of arrays with many particles. As the total area or volume of such an array is increased, thus reducing its density, one might expect that locally situations similar to the ones discussed in this paper might be taking place in different parts of the array. It is interesting to note here that the existence of multiple stable configurations detected in the numerical examples of Section 5, opens the possibility for the existence of multiple equilibrium (local) states in a large molecular array, reminiscent of the bubble formation phenomena mentioned in the introduction. Thus, as further analysis either via molecular dynamics simulations or theoretically would be the questions as to whether the local results in this paper are related or can predict the initiation of cavitation bubbles of different sizes in actual fluid or gases.

Author Contributions: Conceptualization, P.N.M., M.L.S.; methodology, P.N.M., M.L.S.; validation, M.L.S.; simulation, M.L.S.; formal analysis and investigation, P.N.M., M.L.S.; writing original draft preparation, writing and editing, P.N.M.; funding acquisition, P.N.M., M.L.S.

Funding: This research was funded by the National Science Foundation of USA under the Partnership for Research and Education in Materials Program of the University of Puerto Rico at Humacao (Grant No. NSF–DMR–1523463).

Acknowledgments: The author would like to thank the academic editor and the three anonymous referees for their constructive comments that have improved the presentation of this manuscript.

Conflicts of Interest: The authors declare no conflict of interest.

References

1. Lim, T.-C. Mathematical relationships for development of a molecular potential function converter. *Commun. Math. Comput. Chem.* **2003**, *49*, 155–169.
2. Tersoff, J. Modeling solid-state chemistry: Interatomic potentials for multicomponent systems. *Phys. Rev. B* **1989**, *39*, 5566–5568. [CrossRef]
3. Shang, Y. Lower Bounds for Gaussian Estrada Index of Graphs. *Symmetry* **2018**, *10*, 325. [CrossRef]
4. Collevecchio, A.; Konig, W.; Morters, P.; Sidorova, N. Phase transitions for dilute particle systems with Lennard-Jones potential. *Commun. Math. Phys.* **2010**, *299*, 603–630. [CrossRef]
5. Discher, D.E.; Boal, D.H.; Boey, S.K. Phase transitions and anisotropic responses of planar triangular nets under large deformation. *Phys. Rev. E* **1997**, *55*, 4762. [CrossRef]
6. Golubitsky, M. The Bénard problem, symmetry and the lattice of isotropy subgroups. In *Bifurcation Theory, Mechanics and Physics*; Bruter, C.P., Aragnol, A., Lichnorowicz, A., Eds.; Reidel: Dordrecht, The Netherlands, 1983; pp. 225–256.
7. Bazhirov, T.T.; Norman, G.E.; Stegailov, V.V. Cavitation in liquid metals under negative pressures. Molecular dynamics modeling and simulation. *J. Phys. Condens. Matter* **2008**, *20*, 114113. [CrossRef]
8. Blander, M.; Katz, J. Bubble Nucleation in Liquids. *AlChE J.* **1975**, *21*, 833–848. [CrossRef]
9. Fond, C. Cavitation Criterion for Rubber Materials: A Review of Void-Growth Models. *J. Polym. Sci. Part B Polym. Phys.* **2001**, *39*, 2081–2096. [CrossRef]
10. Horgan, C.O.; Polignone, D.A. Cavitation in nonlinearly elastic solids: A review. *Appl. Mech. Rev.* **1995**, *48*, 471–485. [CrossRef]
11. Chakraborty, D.; Chandra, A. An analysis of voids and necks in supercritical water. *J. Mol. Liquids* **2011**, *163*, 1–6. [CrossRef]
12. David, E.E.; David, C.W. Voronoi polyhedra as a tool for studying solvation structure. *J. Chem. Phys.* **1982**, *76*, 4611. [CrossRef]
13. Lennard-Jones, J.E. On the Determination of Molecular Fields. *Proc. R. Soc. Lond. A* **1924**, *106*, 463–477.
14. Buckingham, R.A. The classical equation of state of gaseous helium, neon and argon. *Proc. R. Soc. Lond. Ser. A Math. Phys. Sci.* **1938**, *168*, 264–283.
15. Ambrosetti, A. *A Premier on Nonlinear Analysis*; Cambridge University Press: Cambridge, UK, 1993.
16. Golubitsky, M.; Stewart, I.; Schaeffer, D. Singularities and Groups in Bifurcation Theory: Volume II. In *Applied Mathematical Sciences (Book 69)*; Springer: New York, NY, USA, 2000.
17. Kielhöfer, H. *Bifurcation Theory: An Introduction with Applications to Pdes*; Springer: New York, NY, USA, 2004.
18. Krasnoselski, M.A. *Topological Methods in the Theory of Nonlinear Integral Equations*; Pergamon: Oxford, UK, 1965.
19. Healey, T.H. Global bifurcation and continuation in the presence of symmetry with an application to solid mechanics. *SIAM J. Math Anal.* **1988**, *19*, 824–840. [CrossRef]
20. Wirth, K.; Dreiding, A.S. Edge lengths determining tetrahedrons. *Elem. Math.* **2009**, *64*, 160–170. [CrossRef]
21. Lim, T.-C. Alignment of Buckingham parameters to generalized Lennard-Jones potential functions. *Z. Naturforsch.* **2009**, *64*, 200–204. [CrossRef]
22. Shang, Y. Average consensus in multi-agent systems with uncertain topologies and multiple time-varying delays. *Linear Algebra Appl.* **2014**, *459*, 411–429. [CrossRef]
23. Shang, Y. Couple-group consensus of continuous-time multi-agent systems under Markovian switching topologies. *J. Frankl. Inst.* **2015**, *352*, 4826–4844, [CrossRef]
24. Keller, H.B. *Lectures on Numerical Methods in Bifurcation Problems*; Tata Institute of Fundamental Research, Springer: New York, NY, USA, 1986.
25. Allgower, E.L.; Georg, K. Introduction to numerical continuation methods. In *Classics in Applied Mathematics (Book 45)*; Society for Industrial and Applied Mathematics: Philadelphia, PA, USA, 2003.

symmetry

MDPI

Article

Noether-Like Operators and First Integrals for Generalized Systems of Lane- Emden Equations

M. Umar Farooq

Department of Basic Sciences and Humanities, College of E&ME, National University of Sciences and Technology, H-12, Islamabad 44000, Pakistan; m_ufarooq@yahoo.com

Received: 18 December 2018; Accepted: 15 January 2019; Published: 1 February 2019

Abstract: Coupled systems of Lane–Emden equations are of considerable interest as they model several physical phenomena, for instance population evolution, pattern formation, and chemical reactions. Assuming a complex variational structure, we classify the generalized system of Lane–Emden type equations in relation to Noether-like operators and associated first integrals. Various forms of functions appearing in the considered system are taken, and it is observed that the Noether-like operators form an Abelian algebra for the corresponding Euler–Lagrange-type systems. Interestingly, we find that in many cases, the Noether-like operators satisfy the classical Noether symmetry condition and become the Noether symmetries. Moreover, we observe that the classical Noetherian integrals and the first integrals we determine using the complex Lagrangian approach turn out to be the same for the underlying system of Lane–Emden equations.

Keywords: generalized Lane–Emden systems; Noether-like operator; conservation laws

1. Introduction

The famous Noether theorem [1] establishes an important connection between the conservation laws and symmetry properties of a system describable by a Lagrangian. From a mathematical point of view, it is the case that the essential physical explanation of a Euler–Lagrange system is hidden in its Lagrangian. The Lagrangian function, on the one hand, describes the time behavior of a mechanical system through the Euler–Lagrange equation, and on the other hand, it connects symmetries with first integrals of motion if they arise through Noether's theorem. The availability of a Noether symmetry is essential from two aspects: first, to determine conservation laws and, second, to reduce the underlying equation. A significant number of studies on Noether symmetries and first integrals have been reported in recent years. It is well known that if an equation possesses enough conserved quantities, it can be easily reduced to an integrable form.

In recent papers, the authors of [2,3] introduced the complex symmetry approach, which has been established as an appealing and elegant technique to study integrability properties of systems of ordinary differential equations (ODEs). Following the idea of [3–5], several studies have been done to view integrability properties of systems of partial differential equations (PDEs) and ODEs. For instance, the use of the complex variable technique to discuss linearization of systems of two second-order ODEs and PDEs has been presented in [6]. The procedure of converting a system of two second-order ODEs admitting Lie algebra of dimension d ($d \leq 4$) into linearizable form with the help of complex Lie point symmetries of the base equation was given in [7]. Using semi-invariants, Mahomed et al. [8] studied systems of two linear hyperbolic PDEs when they arise from a complex scalar ODE. They found that the semi-invariants under linear transformations correspond to complex semi-invariants of the $(1+1)$ linear hyperbolic equation in the complex domain. They also succeeded in linking these hyperbolic equations by introducing a complex variable structure on the manifold to the geometry of underlying differential equations. Qadir and Mahomed [9] employed the complex variable technique to study three- and four-dimensional systems of ODEs and PDEs that are transformable to a single complex ODEs. They showed that the acquired systems of ODEs are entirely different from the class that is obtained from single splitting of systems of two ODEs. Naz and Mahomed [10,11] presented a detailed analysis of the computation of Lie and Noether point symmetries of the k^{th}-order system of n ODEs by working in the complex domain. They also discussed the transonic gas flow, Maxwellian distribution, Klein–Gordon equation, dissipative wave, and Maxwellian tails by introducing complex variables. Wafo Soh and Mahomed [12] showed that by utilizing hypercomplexification, one can linearize Ermakov systems. Transforming systems of some Riccati-type equations to a single base equation, they constructed invariants of Able-type systems.

In the current study, we use the formulation of the Noether-like theorem presented in [3–5] and classify systems of Lane–Emden equations with respect to Noether-like operators they admit and related first integrals. On applying the complex symmetry approach, we see that additional insights are obtainable by utilizing the fact that a complex Lagrangian encodes information of two real Lagrangians, and it is derivable from a variational principle. As a consequence of the present study, many important symmetry properties can easily be analyzed using complex Lagrangians, and these help us to determine the invariant quantities of physically-coupled systems represented by ODEs.

The celebrated Lane–Emden (LE) equation given below is the simplest second-order ODE, which appears frequently in modeling one-dimensional problems in physics, astrophysics, and engineering, and it is still a subject of extensive analysis. A review by Wang [13], even though very selective in its list of references, covered almost all possible generalizations and qualitative properties of the LE equation.

Consider the well-known second-order LE equation:

$$y'' + \frac{n}{t}y' + f(y) = 0, \tag{1}$$

where n is a real number and $f(y)$ an arbitrary continuous function of y. The LE equation (1) has many physical applications. For instance, for fixed values of n and $f(y)$, it specifically models the thermal behavior of a spherical cloud of gas, stellar structure, an isothermal gaseous sphere, and the theory of thermionic currents [14–16]. In the literature, various techniques have been proposed concerning the solutions of Equation (1); see for example [17–20]. Several authors have proven existence and uniqueness results for the LE systems [21–24] (see also the references in these papers) and other related systems. Some other works that involve Noether symmetries and exact solutions of LE-type equations can be found in [25]. Moreover, the Noether symmetries of Equation (1) and exact solutions by taking various forms of $f(y)$ were investigated in [26].

Before going to the main discussion, it is important to recall studies in view of the Noether symmetry classification of coupled systems of LE equations. Recently, the authors of [27] took a system of LE equations given by a natural extension of (1), classified it with respect to Noether symmetries, and constructed first integrals of:

$$f'' + \frac{n}{x}f' + F_1(g) = 0, \qquad g'' + \frac{n}{x}g' + F_2(f) = 0, \tag{2}$$

where n is a real number constant and $F_1(g)$ and $F_2(f)$ are arbitrary functions. From a Noether symmetry, Muatjetjeja and Khalique [28], extended their own work and studied the classification of another system of LE equations given by:

$$f'' + \frac{n}{x}f' + h(x)g^q = 0, \qquad g'' + \frac{n}{x}g' + h(x)f^p = 0, \tag{3}$$

with respect to Noether symmetries and their first integrals. In this paper, we shall make a kind of comparison of how the complex Lagrangian formulation and the classical Noether symmetry approach generate the same first integrals for the following general class of the LE system:

$$f'' + \frac{n_1}{x}f' - \frac{n_2}{x}g' + F_1(f,g) = 0, \qquad g'' + \frac{n_2}{x}f' + \frac{n_1}{x}g' + F_2(f,g) = 0. \tag{4}$$

The famous LE system (4) has been used in modeling various physical problems such as pattern recognition, chemical reactions, and population evolution, to name a few. This system attracted the attention of many authors and has been an area of extensive research during the last couple of years (see [21–24,29,30] and the references therein).

We shall consider various forms of F_1 and F_2 to construct conserved quantities of the ensuing systems and show that reduction via quadrature can be obtained only in a few cases. We point out that the Noether-like operators we find for systems of Euler–Lagrange LE equations also satisfy the classical Noether symmetry condition for one of the known equivalent Lagrangians, emerge as Noether symmetries, and hence yield Noetherian first integrals for the subsequent systems. Thus, the Noetherian first integrals and the first integrals we obtain employing a complex Lagrangian approach turn out to be the same with respect to the Lagrangians for the underlying systems of ODEs. We shall see that many interesting insights can be obtained for systems of ODEs through the complex symmetry approach.

The layout of the paper is the following: in the next section, we briefly recall some basic definitions of Noether-like operators and the Noether-like theorem. Section 3 deals with the classification of Noether-like operators and associated first integrals for the system (4). In the last section, we present our concluding remarks.

2. Preliminaries on Noether-Like Operators and First Integrals

Before we consider the generalized system of LE equations in relation to their Noether-like operators and corresponding first integrals, it is instructive to have relevant definitions of these operators and the Noether-like theorem that will be used in our discussion. Moreover, to make the comparison, we also recall expressions for classical Noether symmetries and Noether's theorem. The contents of this section are taken from [3,4] (for more details, the reader is urged to see the references therein).

Consider the following system of nonlinear second-order ODEs:

$$f_i'' = w_i(x, f_1, f_1', f_2, f_2'), \qquad i = 1, 2. \tag{5}$$

Equation (5) represents a general class of a system of second-order ODEs and models various physical problems. However, here, we merely deal with those systems in (5) that are equivalent to a single scalar complex ODE, i.e., there exist transformations $f = f_1 + if_2$, $w = w_1 + iw_2$ that reduce the system (5) to a complex ODE, $f'' = w(x, f, f')$, which retain a variational structure. It is generally conceded that the construction of a Lagrangian for systems of nonlinear ODEs has been proven to be a complicated problem. However, we see here how one can study symmetry properties of Euler–Lagrange-type LE equations straightforwardly with the help of a complex Lagrangian, which encodes two real Lagrangians and enables us to cast the system (5) in a variational form.

Here, our aim is to determine the Noether-like operators and related first integrals of a coupled system of two LE equations. We start by assuming that the system (5) admits a complex Lagrangian $L(x, f, f')$, i.e. $L = L_1 + iL_2$. Therefore, we have two Lagrangians L_1 and L_2, which when utilized result in the following Euler–Lagrange-type system corresponding to (5):

$$\begin{aligned} &\frac{\partial L_1}{\partial f_1} + \frac{\partial L_2}{\partial f_2} - \frac{d}{dx}(\frac{\partial L_1}{\partial f_1'} + \frac{\partial L_2}{\partial f_2'}) = 0, \\ &\frac{\partial L_2}{\partial f_1} - \frac{\partial L_1}{\partial f_2} - \frac{d}{dx}(\frac{\partial L_2}{\partial f_1'} - \frac{\partial L_1}{\partial f_2'}) = 0. \end{aligned} \tag{6}$$

The operators $\mathbf{X}_1 = \varsigma_1(x, f_1, f_2)\frac{\partial}{\partial x} + \chi_1(x, f_1, f_2)\frac{\partial}{\partial f_1} + \chi_2(x, f_1, f_2)\frac{\partial}{\partial f_2}$ and $\mathbf{X}_2 = \varsigma_2(x, f_1, f_2)\frac{\partial}{\partial x} + \chi_2(x, f_1, f_2)\frac{\partial}{\partial f_1} - \chi_1(x, f_1, f_2)\frac{\partial}{\partial f_2}$ are known as Noether-like operators of (5) for the Lagrangians L_1 and L_2 if the following conditions hold:

$$\begin{aligned} \mathbf{X}_1^{(1)}L_1 - \mathbf{X}_2^{(1)}L_2 + (D_x\varsigma_1)L_1 - (D_x\varsigma_2)L_2 = D_xA_1, \\ \mathbf{X}_1^{(1)}L_2 - \mathbf{X}_2^{(1)}L_1 + (D_x\varsigma_1)L_2 + (D_x\varsigma_2)L_1 = D_xA_2, \end{aligned} \tag{7}$$

for appropriate functions A_1 and A_2. Here, $D_x = \frac{d}{dx}$.

Noether-like theorem:

If $\mathbf{X}_1$ and $\mathbf{X}_2$ are two Noether-like operators with respect to real Lagrangians L_1 and L_2, then (5) possesses the following two first integrals:

$$\begin{aligned} I_1 = \varsigma_1 L_1 - \varsigma_2 L_2 + \frac{\partial L_1}{\partial f_1'}(\chi_1 - f_1'\varsigma_1 - f_2'\varsigma_2) - \frac{\partial L_2}{\partial f_1'}(\chi_2 - f_1'\varsigma_2 - f_2'\varsigma_1) - A_1, \\ I_2 = \varsigma_1 L_2 + \varsigma_2 L_1 + \frac{\partial L_2}{\partial f_1'}(\chi_1 - f_1'\varsigma_1 - f_2'\varsigma_2) + \frac{\partial L_1}{\partial f_1'}(\chi_2 - f_1'\varsigma_2 - f_2'\varsigma_1) - A_2. \end{aligned} \tag{8}$$

Classical Noether symmetry condition:

A vector field $X = \varsigma(x, f_1, f_2)\frac{\partial}{\partial x} + \chi(x, f_1, f_2)\frac{\partial}{\partial f_1} + \eta(x, f_1, f_2)\frac{\partial}{\partial f_2}$ with its prolongation $X^{[1]} = X + (\dot{\chi} - \dot{f}_1\dot{\varsigma})\frac{\partial}{\partial \dot{f}_1} + (\dot{\eta} - \dot{f}_2\dot{\varsigma})\frac{\partial}{\partial \dot{f}_2}$ where '·' $= \frac{d}{dx}$ is known as a Noether point symmetry corresponding to the function $L(x, f_1, f_2, f_1', f_2')$ of (5) if the following equation holds:

$$X^{[1]}(L) + D_x(\varsigma)L = D_x(A) \tag{9}$$

Noether's theorem:

For $\mathbf{X}$ to be a Noether symmetry generator for the Lagrangian $L(x, f_1, f_2, f_1', f_2')$, the following equation:

$$I = A - \left[\varsigma L + (\chi - \varsigma\dot{f}_1)\frac{\partial L}{\partial \dot{f}_1} + (\eta - \varsigma\dot{f}_2)\frac{\partial L}{\partial \dot{f}_2}\right], \tag{10}$$

provides the Noetherian first integral of (5) related to $\mathbf{X}$.

3. Noether-Like Operators and First Integrals for Different forms of F_1 and F_2 in (4)

Major computational difficulties occur when trying to classify the general nonlinear LE equation with respect to Noether symmetry operators and corresponding first integrals. We see here how the Noether-like operators play an important role in deriving conserved quantities for dynamical systems and their reduction via quadrature.

Consider the following nonlinear system, which is a generalized coupled LE-type system:

$$\begin{aligned} f_1'' + \frac{n_1 f_1' - n_2 f_2'}{x} + F_1(f_1, f_2) = 0, \\ f_2'' + \frac{n_1 f_2' + n_2 f_1'}{x} + F_2(f_1, f_2) = 0, \end{aligned} \tag{11}$$

for which we have analyzed eight cases separately. Here, n_1, n_2 are constants and F_1, F_2 are arbitrary functions of f_1 and f_2, respectively. We take different forms of F_1 and F_2 in (11) and determine Noether-like operators and conserved quantities for the subsequent systems. Therefore, for this, we proceed as: one can readily verify that the pair of Lagrangians for the system (11) when invoking (6) is given by:

$$
\begin{aligned}
L_1 &= \frac{1}{2}x^{n_1}[cos\theta(f_1'^2 - f_2'^2) - 2sin\theta f_1' f_2'] - x^{n_1}[cos\theta \int (F_1 df_1 - F_2 df_2) - sin\theta \int (F_2 df_1 + F_1 df_2)],\\
L_2 &= \frac{1}{2}x^{n_1}[2cos\theta(f_1' f_2') + sin\theta(f_1'^2 - f_2'^2)] - x^{n_1}[cos\theta \int (F_2 df_1 + F_1 df_2) + sin\theta \int (F_1 df_1 - F_2 df_2)],
\end{aligned}
\tag{12}
$$

where $\theta = n_2 \ln x$.

Case 1. $F_1(f_1, f_2)$ and $F_2(f_1, f_2)$ are linear in f_1 and f_2, respectively.

In this case, we have a system of two linear ODEs. Using appropriate transformations, one can reduce the system of linear equations to a system of free particle equations, viz. $f_1'' = 0$, $f_2'' = 0$, which possesses nine Noether-like operators associated with the coupled Lagrangians (11), and they give ten first integrals. This case is well known and can be found in detail in [4].

Case 2. For $n_1, n_2 = 0$ and $F_1(f_1, f_2)$, $F_2(f_1, f_2)$ arbitrary and non-linear, as given in Case 1.

Equations (7) and (12), after some straightforward calculations, show that $\varsigma_1 = 1$, $\varsigma_2 = 0$, $\chi_1 = \chi_2 = 0$, and A_1, A_2 are constants. Therefore, we have a single Noether-like operator $\mathbf{X} = \frac{\partial}{\partial x}$. Using the pair of Lagrangians (12) and Noether-like operator $\mathbf{X}$ in (8), we obtain the following two first integrals:

$$
\begin{aligned}
I_1 &= \frac{1}{2}(f'^2 - g'^2) + \int [F_1 df - F_2 dg],\\
I_2 &= f'g' + \int [F_1 dg + F_2 df].
\end{aligned}
\tag{13}
$$

Interestingly, the Noether-like operator $\mathbf{X}$ is also a Noether symmetry for each of the Lagrangians (12), and (10) generates the same first integrals as given in (13) for System (11).

Case 3. If:

$$
\begin{aligned}
F_1(f_1, f_2) &= \frac{\alpha}{2}\log(f_1^2 + f_2^2) + \gamma f_1 + \delta,\ \alpha \neq 0,\\
F_2(f_1, f_2) &= \alpha \arctan(\frac{f_2}{f_1}) + \gamma f_2,\ \alpha \neq 0
\end{aligned}
\tag{14}
$$

and $n_1,\ n_2 = 0$ and $\delta = 0$, we obtain $\varsigma_1 = x,\ \varsigma = 0$, $\chi_1 = \chi_2 = 0$ with A_1, A_2 as constants. This falls into Case 2.

Case 4. For:

$$
\begin{aligned}
F_1(f_1, f_2) &= \frac{\alpha}{2}[f_1 \log(f_1^2 + f_2^2) - f_2 \arctan(f_2/f_1)] + \gamma f_1 + \delta, \alpha \neq 0,\\
F_2(f_1, f_2) &= \frac{\alpha}{2}[f_1 \arctan(f_2/f_1) + f_2 \log(f_1^2 + f_2^2)] + \gamma f_2 + \delta, \alpha \neq 0.
\end{aligned}
\tag{15}
$$

If $n_1,\ n_2 = 0$, we obtain $\varsigma_1 = x,\ \varsigma_2 = 0$, $\chi_1 = \chi_2 = 0$, and $A_1 = A_2 = k$, k being a constant. This also bring us back to Case 2.

Case 5. If $F = \alpha u^r$, $\alpha \neq 0$, $r \neq 0$, 1.

Here, we discuss the following three cases:

Case 5.1. For $n_1 = \frac{r+3}{r-1}$ and $n_2 = 0$, the Noether-like symmetry conditions (7) result in $\varsigma_1 = x$, $\varsigma_2 = 0$, $\chi_1 = \frac{2}{1-r}f_1$, $\chi_2 = \frac{2}{1-r}f_2$, with $A_1,\ A_2$ as constants. Therefore, we get two Noether-like operators:

$$
\mathbf{X}_1 = x\frac{\partial}{\partial x} + \frac{2}{1-r}\Big(f_1\frac{\partial}{\partial f_1} + f_2\frac{\partial}{\partial f_2}\Big),\quad \mathbf{X}_2 = \frac{2}{1-r}\Big(f_2\frac{\partial}{\partial f_1} - f_1\frac{\partial}{\partial f_2}\Big).
\tag{16}
$$

Utilizing (16) with (12), Equation (8) gives rise to two first integrals:

$$\begin{aligned} I_1 &= \frac{1}{2}x^{n_1+1}(f_1'^2 - f_2'^2) - \frac{\alpha}{r+1}x^{n_1+1}(f_1^2+f_2^2)^{\frac{r+1}{2}} cos\theta + \frac{2}{1-r}x^{n_1}(f_1f_1' - f_2f_2') - x^{n_1+1}(f_1'^2 - f_2'^2), \\ I_2 &= x^{n_1+1}f_1'f_2' - \frac{\alpha}{r+1}x^{n_1+1}(f_1^2+f_2^2)^{\frac{r+1}{2}} sin\theta + \frac{2}{1-r}x^{n_1}(f_1f_2' + f_1'f_2) - 2x^{n_1+1}f_1'f_2', \end{aligned} \tag{17}$$

for (11). Here, $\theta = (r+1)\arctan(f_2/f_1)$. Utilization of transformations $f_1 = w_1 x^{\frac{\nu+1}{1-r}}$ and $f_2 = w_2 x^{\frac{\nu+1}{1-r}}$ converts the above system (17) into an integrable form as:

$$\int \frac{dw}{\pm\sqrt{4(1-r)^{-2}w^2 - 2\alpha(1+r)^{-1}f^{r+1} - C_1}} = lnxC_2, \tag{18}$$

where C_1 and C_2 are constants. Here, we can see that the Lie algebra of Noether-like operators is Abelian, i.e., $[\mathbf{X}_1, \mathbf{X}_2] = 0$.

Case 5.2. If we set $n_1 = 2$, $n_2 = 0$, and $r = 5$, Equations (6) and (12) yield the famous Emden–Fowler system [3] given by:

$$\begin{aligned} f_1'' + \frac{2}{x}f_1' + \alpha(f_1^5 - 10f_1^3f_2^2 + 5f_1f_2^4) = 0, \\ f_2'' + \frac{2}{x}f_2' + \alpha(f_2^5 - 10f_1^2f_2^3 + 5f_1^4f_2) = 0, \end{aligned} \tag{19}$$

while the associated Lagrangians are:

$$\begin{aligned} L_1 &= \frac{1}{2}x^2(f_1'^2 - f_2'^2) - \frac{\alpha}{6}x^2[f_1^6 - 15f_1^4f_2^2 + 15f_1^2f_2^4 - f_2^6], \\ L_1 &= x^2f_1'f_2' - \frac{\alpha}{3}x^2[3f_1^5f_2 - 10f_1^3f_2^3 + 3f_1f_2^5]. \end{aligned} \tag{20}$$

It is easy to see that the Emden–Fowler system (19) admits the following two Noether-like operators:

$$\mathbf{X}_1 = 2x\frac{\partial}{\partial x} - f_1\frac{\partial}{\partial f_1} - f_2\frac{\partial}{\partial f_2}, \quad \mathbf{X}_2 = f\frac{\partial}{\partial f_2} - f_2\frac{\partial}{\partial f_1}. \tag{21}$$

Utilizing these operators in Equations (8) and (20), we obtain the following constant quantities:

$$\begin{aligned} I_1 &= x^3(f_1'^2 - f_2'^2) + x^2(f_1f_1' - f_2f_2') + \frac{1}{3}x^3(f_1^6 + 15f_1^2f_2^4 - 15f_1^4f_2^2 - f_2^6), \\ I_2 &= x^3f_1'f_2' + \frac{1}{2}x^2(f_1f_2' + f_1'f_2) + x^3(f_1f_2^5 - \frac{10}{3}f_1^3f_2^3 + f_1^5f_2), \end{aligned} \tag{22}$$

for (19). Upon checking, we see that for L_1 and L_2, the above system (19) admits $\mathbf{X}_1$ as a Noether symmetry. Therefore, from the classical Noether theorem, we can deduce the first integrals I_1 and I_2 (Noetherian integrals) for (19).

Case 5.3. If $n_1 = \frac{r+3}{r+1}$ with $r \neq -1$, we have $\varsigma_1 = x^{\frac{r-1}{r+1}}$, $\varsigma_2 = 0$, $\chi_1 = -\frac{2}{r+1}x^{\frac{-2}{r+1}}f_1$, $\chi_2 = -\frac{2}{r+1}x^{\frac{-2}{r+1}}f_2$, and $A_1 = \frac{2}{2(r+1)^2}(f_1^2 - f_2^2) + q$, $A_2 = \frac{4}{(r+1)^2}f_1f_2$, where q is constant. By invocation of the Noether-like theorem, the Noether-like operators given in (24) provide:

$$\begin{aligned} I_1 &= \frac{1}{2}x^2(f_1'^2 - f_2'^2) + \frac{\alpha}{r+1}x^2(f_1^2+f_2^2)^{\frac{r+1}{2}} cos\theta + \frac{2}{r+1}x(f_1f_1' - f_2f_2') + \frac{2}{(1+r)^2}(f_1^2 - f_2^2), \\ I_2 &= x^2f_1'f_2' + \frac{\alpha}{r+1}x^2(f_1^2+f_2^2)^{\frac{r+1}{2}} sin\theta + \frac{2}{r+1}x(f_1f_2' + f_1'f_2) + \frac{4}{(r+1)^2}f_1f_2, \end{aligned} \tag{23}$$

where $\theta = (r+1)\arctan(f_2/f_1)$. In this case, Noether-like operators are of the form:

$$\mathbf{X}_1 = x^{\frac{r-1}{r+1}}\frac{\partial}{\partial x} - \frac{2}{r+1}x^{-\frac{2}{r+1}}\left(f_1\frac{\partial}{\partial f_1} + f_2\frac{\partial}{\partial f_2}\right), \quad \mathbf{X}_2 = -\frac{2}{r+1}x^{-\frac{2}{r+1}}\left(f_2\frac{\partial}{\partial f_1} - f_1\frac{\partial}{\partial f_2}\right). \tag{24}$$

Applying the transformations $f_1 = w_1 x^{\frac{-\nu-1}{r+1}}$ and $f_2 = w_2 x^{\frac{-\nu-1}{r+1}}$, System (23) can be converted into the variable separable form:

$$\int \frac{dw}{\pm\sqrt{-2\alpha(r+1)^{-1}w^{r+1} + C_1}} = \frac{r+1}{2}x^{\frac{2}{r+1}} + C_2, \tag{25}$$

where C_1 and C_2 are arbitrary constants.

Case 6. If F_1 and F_2 are nonlinear and are of the form $F_1(f_1, f_2) = \alpha(f_1^2 - f_2^2) + \beta f_1 + \gamma$, $F_2(f_1, f_2) = 2\alpha f_1 f_2 + \beta f_2$, $\alpha,\ \beta,\ \gamma$ are constants, and $\alpha \neq 0$.
Here, the following subcases arise:

Case 6.1. If $n_1 = 5$ and $n_2 = 0$, $\beta = 0$ and $\gamma = 0$, we obtain from (7) that $\varsigma_1 = x$, $\varsigma_2 = 0$, $\chi_1 = -2f_1$, $\chi_2 = -2f_2$, and $A_1,\ A_2$ are constants. This case falls into Case 5.1.
Case 6.2. If $n_1 = 5$, $n_2 = 0$, $\beta^2 = 4\alpha\gamma$, Equations (7) and (12) yield $\varsigma_1 = x$, $\varsigma_2 = 0$, $\chi_1 = -(2f_1 + \frac{\beta}{\alpha})$, $\chi_2 = -2f_2$, $A_1 = \frac{\beta\gamma}{6\alpha}x^6$, and $A_2 = 0$. Therefore, Noether-like operators are of the form:

$$\mathbf{X}_1 = x\frac{\partial}{\partial x} - (2f_1 + \frac{\beta}{\alpha})\frac{\partial}{\partial f_1} - 2f_2\frac{\partial}{\partial f_2}, \quad \mathbf{X}_2 = (2f_1 + \frac{\beta}{\alpha})\frac{\partial}{\partial f_2} - 2f_2\frac{\partial}{\partial f_1}. \tag{26}$$

Invocation of the Noether-like theorem (8) along with Lagrangians and Noether-like operators $\mathbf{X}_1$ and $\mathbf{X}_2$ results in two first integrals:

$$\begin{aligned} I_1 &= \frac{1}{2}x^6(f_1'^2 - f_2'^2) + \frac{1}{3}\alpha x^6(f_1^3 - 3f_1f_2^2) + \frac{1}{2}\beta x^6(f_1^2 - f_2^2) + \gamma x^6 f + 2x^5(f_1f_1' - f_2f_2') + \frac{\beta}{\alpha}x^5 f_1' \\ &+ \frac{\beta\gamma}{6\alpha}x^6 \\ I_2 &= x^6 f_1'f_2' + \frac{1}{3}\alpha x^6(3f_1^2f_2 - f_2^3) + \beta x^6 f_1f_2 + \gamma x^6 f_2 + 2x^5(f_1f_2' + f_1'f_2) + \frac{\beta}{\alpha}x^5 f_2', \end{aligned} \tag{27}$$

for (11). Using the transformations $w_1 = x^{1+\nu}f_1 + \frac{\beta}{2\alpha}x^{\nu+1}$ and $w_1 = x^{\nu+1}f_2$, one can map the system (27) to a separable form:

$$C = 2w^2 - \frac{1}{2}x^2w'^2 - \frac{\alpha}{3}w^3, \tag{28}$$

where $w(x) = w_1 + iw_2$.

It can be verified that the Noether-like operator $\mathbf{X}_1$ in (26) is also a Noether symmetry for the Lagrangians L_1 and L_2 in Equation (12). The classical Noether's theorem generates the same Noetherian first integrals I_1 and I_2 given in Equation (27) with Lagrangians L_2 and L_1, respectively, for the resulting system of LE equations. Furthermore, we observe that $[\mathbf{X}_1, \mathbf{X}_2] = 0$, so these operators form an Abelian algebra.

Case 6.3. For $n_1 = \frac{5}{3}$, $n_2 = 0$, $\beta = 0$, and $\gamma = 0$, Equation (7) taking L_1 and L_2 from (12) with simple calculations gives $\varsigma_1 = x^{\frac{1}{3}}$, $\chi_1 = -\frac{2}{3}x^{\frac{-2}{3}}f_1$, $\chi_2 = -\frac{2}{3}x^{\frac{-2}{3}}f_2$, and $A_1 = \frac{2}{9}(f_1^2 - f_2^2) + k$, $A_2 = \frac{4}{9}(f_1f_2)$, and k is a constant. This case falls into Case 5.2.

Case 7. For $F_1(f_1, f_2) = \alpha e^{\beta f_1} cos(\beta f_2) + \gamma f_1 + \delta$, $F_2(f_1, f_2) = \alpha e^{\beta f_1} sin(\beta f_2) + \gamma f_2$, where $\alpha,\ \beta,\ \delta$ are constants and $\alpha \neq 0,\ \beta \neq 0$. Therefore, (11) takes the form:

$$\begin{aligned} f_1'' + \frac{n_1f_1' - n_2f_2'}{x} + \alpha exp(\beta f_1)cos(\beta f_2) + \gamma f_1 + \delta = 0, \\ f_2'' + \frac{n_1f_2' + n_2f_1'}{x} + \alpha exp(\beta f_1)sin(\beta f_2) + \gamma f_2 = 0, \end{aligned} \tag{29}$$

For $n_1 = 1,\ n_2 = 0,\ \gamma = 0,\ \delta = 0$, and $\beta = 1$, we obtain $\varsigma_1 = x,\ \varsigma_2 = 0, \chi_1 = -2,\ \chi_2 = 0$, and $A_1,\ A_2 = q$, where q is a constant. Therefore, the system (29) possesses the Noether-like operators:

$$\mathbf{X}_1 = x\frac{\partial}{\partial x} - \frac{2\partial}{\partial f_1}, \quad \mathbf{X}_2 = \frac{\partial}{\partial f_2}. \tag{30}$$

with the corresponding pair of Lagrangians:

$$\begin{aligned} L_1 &= \frac{1}{2}x(f_1'^2 - f_2'^2) - \alpha x e^{f_1} cos f_2, \\ L_2 &= x f_1' f_2' - \alpha x e^{f_1} sin f_2. \end{aligned} \tag{31}$$

Utilizing the Noether-like operators and Lagrangians given above, Equation (8) implies the first integrals:

$$\begin{aligned} I_1 &= \frac{1}{2}x^2(f_1'^2 - f_2'^2) + \alpha x^2 e^{f_1} cos f_2 + 2x f_1' \\ I_2 &= x^2 f_1' f_2' + \alpha x^2 e^{f_1} sin f_2 + 2x f_2'. \end{aligned} \tag{32}$$

It is important to mention here that the system (29) admits Noether-like operator $\mathbf{X}_1$ as a Noether symmetry [3], as it satisfies the classical Noether symmetry condition with Lagrangians L_1 and L_2 given in (31). Therefore, application of the classical Noether theorem remarkably generates two Noetherian first integrals, namely I_1 and I_2 given in (32). Here, again, the Lie bracket gives $[\mathbf{X}_1, \mathbf{X}_2] = 0$, which shows that the algebra of these operators is Abelian.

Case 8. Here, n_1, n_2 are nonzero, and $F_1(f_1, f_2),\ F_2(f_1, f_2)$ are arbitrary, but not of the form contained in the cases given above.

From Equation (7), after simple manipulations, we find that $\varsigma_1 = \varsigma_2 = 0, \chi_1 = \chi_2 = 0$, and A_1, A_2 are constants. We deduce that no Noether-like operators exist in this case.

4. Conclusions

In this paper, we have applied the complex Noether approach and attempted to classify a two-dimensional coupled system of LE equations that appears in physics and applied mathematics with respect to Noether-like-operators and corresponding first integrals by taking the functions F_1 and F_2 in their more general forms in Equation (11). In this study, we have observed that for some of the systems of LE equations, every pair of Noether-like operators forms an Abelian Lie algebra. We have also highlighted that for certain pairs of Lagrangians, the Noether-like operators become Noether symmetries of the Euler–Lagrange systems of LE equations and give rise to the same Noetherian first integrals as we determined from our complex approach. Therefore, the study of invariant quantities of many dynamical systems can be made with the help of complex Lagrangian formalism, which seems to be more simple and elegant.

Funding: This research received no external funding.

Acknowledgments: M.U. Farooq is thankful to Fazal M. Mahomed for his important comments on this paper. The author also expresses his gratitude to the referees for some useful suggestions.

Conflicts of Interest: The author declares no conflict of interest.

References

1. E Noether, I.V. Koönigliche Gesellschaft der Wissenschaften zu Göttingen. *Math. Phys.* **1918**, *2*, 235–269.
2. Ali, S.; Mahomed, F.M.; Qadir, A. Complex Lie symmetries for scalar second-order ordinary differential equations. *Nonlinear Anal. Real World Appl.* **2009**, *10*, 3335–3344 . [CrossRef]
3. Ali, S.; Mahomed, F.M.; Qadir, A. Complex Lie symmetries for variational problems. *J. Nonlinear. Math. Phys.* **2008**, *15*, 25–35. [CrossRef]

4. Farooq, M.U.; Ali, S.; Mahomed, F.M. Two dimensional systems that arise from the Noether classification of Lagrangian on the line. *Appl. Math. Comput.* **2011**, *217*, 6959–6973. [CrossRef]
5. Farooq, M.U.; Ali, S.; Qadir, A. Invariants of two-dimensional systems via complex Lagrangians with applications. *Commun. Nonlinear Sci. Num. Simul.* **2011**, *16*, 1804–1810. [CrossRef]
6. Ali, S.; Mahomed, F.M.; Qadir, A. Linearizability criteria for systems of two second-order differential equations by complex methods. *Nonlinear Dyn.* **2011**, *66*, 77–88. [CrossRef]
7. Ali, S.; Safdar, M.; Qadir, A. Linearization from complex Lie point Transformations. *J. Appl. Math.* **2014**, *2014*, 793247. [CrossRef]
8. Mahomed, F.M.; Qadir, A.; Ramnarain, A. Laplace-Type Semi-Invariants for a System of Two Linear Hyperbolic Equations by Complex Methods. *Math. Prob. Eng.* **2011**, *2011*, 202973. [CrossRef]
9. Qadir, A.; Mahomed, F.M. Higher dimensional systems of differential equations obtainable by iterative use of complex methods. *Int. J. Mod. Phys.* **2015**, *38*, 1560077. [CrossRef]
10. Naz, R.; Mahomed, F.M. Lie and Noether symmetries of systems of complex ordinary differential equations and their split systems. *Pramana J. Phys.* **2014**, 83, 920. [CrossRef]
11. Naz, R.; Mahomed, F.M. A complex Noether approach for variational partial differential equations. *Commun. Nonlinear Sci. Numer. Simul.* **2015**, *27*, 120–135. [CrossRef]
12. Soh, C.W.; Mahomed, F.M. Hypercomplex analysis and integration of systems of ordinary differential equations. *Math. Meth. Appl. Sci.* **2016**. [CrossRef]
13. Wong, J.S. On the generalized Emden–Fowler equation. *SIAM Rev.* **1975**, *17*, 339–360. [CrossRef]
14. Chandrasekhar, S. *An Introduction to the Study of Stellar Structure*; Dover: New York, NY, USA, 1957.
15. Davis, H.T. *Introduction to Nonlinear Differential and Integral Equations*; Dover: New York, NY, USA, 1962.
16. Richardson, O.W. *The Emission of Electricity from Hot Bodies*, 2nd ed.; Longmans, Green & Co.: London, UK, 1921.
17. Dehghan, M.; Shakeri, F. Approximate solution of a differential equation arising in astrophysics using the variational iteration method. *New Astron.* **2008**, *13*, 53–59. [CrossRef]
18. Ramos, J.I. Series approach to the Lane–Emden equation and comparison with the homotopy perturbation method. *Chaos Solitons Fractals* **2008**, *38*, 400–408. [CrossRef]
19. Marzban, H.R.; Tabrizidooz, H.R.; Razzaghi, M. Hybrid functions for nonlinear initial-value problems with applications to Lane–Emden type equations. *Phys. Lett. A* **2008**, *372*, 5883–5886. [CrossRef]
20. Ertrk, V.S. Differential transformation method for solving differential equations of Lane–Emden type. *Math. Comput. Appl.***2007**, *12*, 135–139. [CrossRef]
21. Serrin, J.; Zou, H. Non-existence of positive solutions of Lane–Emden systems. *Differ. Int. Equ.* **1996**, *9*, 635653.
22. Serrin, J.; Zou, H. Existence of positive solutions of the Lane–Emden system. *Atti del Seminario Matematico e Fisico Dell Universit'a di Modena* **1998**, *46*, 369–380.
23. Qi, Y.W. The existence of ground states to a weakly coupled elliptic system. *Nonlinear Anal. Theory Methods Appl.* **2002**, *48*, 905–925. [CrossRef]
24. Dalmasso, R. Existence and uniqueness of solutions for a semilinear elliptic system. *Int. J. Math. Math. Sci.* **2005**, *10*, 1507–1523. [CrossRef]
25. Muatjetjeja, B.; Khalique, C.M. Exact solutions of the generalized Lane–Emden equations of the first and second kind. *Pramana J. Phys.* **2011**, *77*, 545–554. [CrossRef]
26. Khalique, C.M.; Mahomed, F.M.; Muatjetjeja, B. Lagrangian formulation of a generalized Lane–Emden equation and double reduction. *J. Nonlinear Math. Phys.* **2008**, *15*, 152–161. [CrossRef]
27. Muatjetjeja, B.; Khalique, C.M. Lagrangian approach to a generalized coupled Lane–Emden system: Symmetries and first integrals. *Commun. Nonlinear Sci. Numer. Simul.* **2010**, *15*, 1166–1171. [CrossRef]
28. Muatjetjeja, B.; Khalique, C.M. First integrals for a generalized coupled Lane–Emden system. *Nonlinear Anal. Real World Appl.* **2011**, *12*, 1202–1212. [CrossRef]
29. Dai, Q.; Tisdell, C.C. Non-degeneracy of positive solutions to homogeneous second order differential systems and its applications. *Acta Math. Sci.* **2009**, *29*, 437–448.
30. Zou, H. A prior estimates for a semilinear elliptic system without variational structure and their application. *Math. Ann.* 2002, 323, 713–735. [CrossRef]

symmetry

MDPI

Article

Algorithm for Neutrosophic Soft Sets in Stochastic Multi-Criteria Group Decision Making Based on Prospect Theory

Yuanxiang Dong [1,*], Chenjing Hou [1], Yuchen Pan [2] and Ke Gong [3]

[1] School of Management Science and Engineering, Shanxi University of Finance and Economics, Taiyuan 030006, China
[2] Business School, Southwest University of Political Science & Law, Chongqing 401120, China
[3] School of Economics and Management, Chongqing Jiaotong University, Chongqing 400074, China
* Correspondence: dongyx@sxufe.edu.cn; Tel.: +86-1336-836-0537

Received: 24 July 2019; Accepted: 27 August 2019; Published: 29 August 2019

Abstract: To address issues involving inconsistencies, this paper proposes a stochastic multi-criteria group decision making algorithm based on neutrosophic soft sets, which includes a pair of asymmetric functions: Truth-membership and false-membership, and an indeterminacy-membership function. For integrating an inherent stochastic, the algorithm expresses the weights of decision makers and parameter subjective weights by neutrosophic numbers instead of determinate values. Additionally, the algorithm is guided by the prospect theory, which incorporates psychological expectations of decision makers into decision making. To construct the prospect decision matrix, this research establishes a conflict degree measure of neutrosophic numbers and improves it to accommodate the stochastic multi-criteria group decision making. Moreover, we introduce the weighted average aggregation rule and weighted geometric aggregation rule of neutrosophic soft sets. Later, this study presents an algorithm for neutrosophic soft sets in the stochastic multi-criteria group decision making based on the prospect theory. Finally, we perform an illustrative example and a comparative analysis to prove the effectiveness and feasibility of the proposed algorithm.

Keywords: neutrosophic soft sets; inconsistent information; prospect theory; stochastic multi-criteria group decision making

1. Introduction

Many complex issues in engineering, economics, environmental science and medical science involve uncertainties. In order to address these issues, the theory of possibility, fuzzy set [1], rough set [2], and interval mathematic [3] have been developed successively. However, the above theories have their inherent defects, which are mainly reflected in the inadequacy of parameterization tools [4]. In 1999, Molodtsov [4] initiated the soft set theory for modeling uncertainties from the parameterized point of view.

After Molodtsov, the research interests in the soft set theory have been growing rapidly, such as the algebraic structure [5,6], topology [7,8], normal parameter reduction [9], medical diagnosis [10], game theory [4], and decision making under uncertainties [11,12]. In addition, the study of hybrid models that are developed by combining the soft set theory with other mathematical tools, such as rough sets [13], fuzzy sets [14], and intuitionistic fuzzy sets [15], has also been an important research topic.

Under uncertain environments, a mass of inconsistent information appears due to diversities of source platforms and the differences in the acquisition time. To address issues involving inconsistencies, Smarandache [16] initiated neutrosophic sets from the perspective of philosophy. Subsequently, Maji [17] integrated neutrosophic sets into soft sets to propose neutrosophic soft sets, which retain the characteristics of neutrosophic sets and have adequate parameterization tools. Neutrosophic soft sets are characteristic by three independent functions, including a pair of asymmetric functions: Truth-membership and false-membership, and an indeterminacy-membership function. Among them, the truth-membership and false-membership represent the degree of belongingness and non-belongingness of an element with respect to parameters. The indeterminacy-membership shows the neutrality degree of an element related to parameters.

In recent years, the theory extensions of neutrosophic soft sets have made a rapid progress. Sahin and Küçük [18] constructed generalised neutrosophic soft sets. Deli and Broumi [19] refined the concept and operations of Maji's neutrosophic soft sets. In addition, they also studied the neutrosophic soft matrix and their operators. Considering that the approximate range is usually used to describe complex situations when there is no sufficient information, Deli [20] expanded the values of the truth-membership, indeterminacy-membership, and false-membership to the form of interval values to construct interval-valued neutrosiphic soft sets. Karaaslan [21] introduced the possibility of neutrosophic soft sets by assigning probability to the three function values and defined related properties and operations. In addition, the concepts of single-valued neutrosophic refined soft sets [22], generalized neutrosophic soft expert sets [23], and neutrosophic soft rough sets [24] were presented successively.

Meanwhile, neutrosophic soft sets are also employed in the fields of clustering, prediction and decision making under uncertainties, among which decision making under uncertainties is the most widely applied. Deli [20] proposed a decision making method of interval-valued neutrosophic soft sets by level soft sets, and illustrated it by an example. Peng and Liu [25] constructed three decision making algorithms of neutrosophic soft sets by evaluation based on the distance from average solution (EDAS), similarity measure, and level soft sets, respectively. Abu Qamar and Hassan [26] presented the similarity, distance, and fuzzy degree measures of Q-neutrosophic soft sets, and put forward the corresponding decision rule. Karaaslan [21] constructed a decision making method for the possibility of neutrosophic soft sets based on the and-product.

However, the existing studies mainly focus on decision making methods under a single decision maker, few scholars have studied group decision making problems by neutrosphic soft sets. At the same time, we also noticed that the existing methods have the following defects. On one hand, the above methods are mainly based on the expected utility theory, which assumes that decision makers are completelyrational. Actually, in decision making processes, decision makers do not make decisions in a complete rational manner, mainly showing that psychological expectations will greatly affect the actual decision making behavior. On the other hand, the parameter subjective weights are directly given determinate values [25], which do not fully reflect the hesitancies of decision makers' judgments under uncertain environments.

To make up for the gaps of existing researches, this study constructs an algorithm for the stochastic multi-criteria group decision making based on neutrosophic soft sets. Stochastic means that the weights of decision makers and parameters are uncertain or completely unknown under uncertainties. In this paper, neutrosophic numbers rather than determinate values are adopted to express the stochastic of the weights of decision makers and parameters. This method employs the prospect theory [27] rather than the expected utility theory to integrate the hesitancies of alternatives by decision makers' judgements. The prospect theory, a new theory of bounded rationality, is proposed from the point of view of cognitive psychology. In addition, it integrates the influence of psychological expectations on actual decision making behaviors into the decision making model. Therefore, the prospect theory is more in line with actual decision making behaviors under uncertainties [28]. Then, to establish the prospect decision matrix, we put forward the conflict degree measure of neutrosophic numbers and modify it to adapt group decision making. Moreover, on the purpose of aggregating in group decision making processes, this study proposes the weighted average aggregation rule and weighted geometric aggregation rule of neutrosophic soft sets.

To promote our discussion, some fundamental concepts of neutrosophic sets, soft sets, neutrosophic soft sets, and prospect theory are reviewed in Section 2. In Section 3, we establish the measures of determinacy degree and conflict degree, and construct the weighted average aggregation rule and weighted geometric aggregation rule of a neutrosophic soft set. In Section 4, this paper presents an algorithm for neutrosophic soft sets in the stochastic multi-criteria group decision making based on the prospect theory. In Section 5, to demonstrate the feasibility and effectiveness of the proposed algorithm, we perform an illustrative example and a comparative analysis.

2. Preliminaries

In this section, we briefly recall some basic concepts of neutrosophic sets, soft sets, neutrosophic soft sets, and prospect theory. More detailed conceptual basics can be found in references [4,16,17,27] (pp. 1–2).

2.1. Neutrosophic Soft Sets

Definition 1 [16] (p. 1). *Let U be the initial universal set, a neutrosophic set $A = \left\{ < u : T_{A(u)}, I_{A(u)}, F_{A(u)} >, u \in U \right\}$ consists of the truth-membership $T_{A(u)}$, the indeterminacy-membership $I_{A(u)}$, and false-membership $F_{A(u)}$ of element $u \in U$ to set A, where $T, I, F : U \to]^{-}0, 1^{+}[$. $]^{-}0, 1^{+}[$* is a non-standard interval, and the left and right borders of it are imprecise. Between them, $(^{-}0) = \{0 - x : x \in R^{*}, x \text{ is infinitesimal}\}$, *and* $(1^{+}) = \{1 + x : x \in R^{*}, x \text{ is infinitesimal}\}$.

For convenience, we employ $u =< T, I, F >$ to represent the element u in the neutrosophic set A, and it can be called a neutrosophic number.

Considering that neutrosophic sets are proposed from the philosophical point of view, it is difficult to apply to practical problems, such as management and engineering problems. Then, Haibin et al. [29] developed single valued neutrosophic sets.

Definition 2 [29]. *Let U be the universal set, a single valued neutrosophic set A over U can be defined as $A = \left\{ < u : T_{A(u)}, I_{A(u)}, F_{A(u)} >, u \in U \right\}$, where $T, I, F : U \to [0, 1]$. Similarly, the values of $T_{A(u)}$, $I_{A(u)}$* and *$F_{A(u)}$* stand for the truth-membership, indeterminacy-membership, and false-membership of *u to A*, respectively.

Definition 3 [30]. *Let $u =< T, I, F >$ be a neutrosophic number, then the score function, accuracy function and certainty function are defined as follows, respectively.*

$$s(u) = \frac{2 + T - I - F}{3}, \tag{1}$$

$$a(u) = T - F, \tag{2}$$

$$c(u) = T, \tag{3}$$

The score function is an important index for evaluating neutrosophic numbers. For a neutrosophic number $R =< T_r, I_r, F_r >$, the truth-membership T_r is positively correlated with the score function, and the indeterminacy-membership I_r and false-membership F_r are negatively correlated with the score function. In terms of the accuracy function, the greater the difference between the truth-membership T_r and false-membership F_r is, the more affirmative the statement is. Additionally, in regard to the certainty function, it positively depends on the truth-membership T_r.

On the basis of Definition 3, the comparison method between two neutrosophic numbers is represented as follows.

Definition 4 [30]. *Let $u_1 =< T_1, I_1, F_1 >, u_2 =< T_2, I_2, F_2 >$ be two neutrosophic numbers, the comparison relationships between u_1 and u_2* are as follows:

1. *If $s(u_1) > s(u_2)$, u_1 is superior to u_2 and it can be denoted by $u_1 \succ u_2$;*
2. *If $s(u_1) = s(u_2)$, $a(u_1) > a(u_2)$, u_1 is superior to u_2 and is denoted by $u_1 \succ u_2$;*
3. *If $s(u_1) = s(u_2)$, $a(u_1) = a(u_2)$ and $c(u_1) > c(u_2)$, u_1 is superior to u_2 and is denoted by $u_1 \succ u_2$;*
4. *If $s(u_1) = s(u_2)$, $a(u_1) = a(u_2)$ and $c(u_1) = c(u_2)$, u_1 is equal to u_2, denoted by $u_1 \succ u_2$.*

Example 1. *For two neutrosophic numbers $u_1 =< 0.8, 0.2, 0.4 >$ and $u_2 =< 0.7, 0.4, 0.1 >$, we can obtain that $s(u_1) = 2.2/3$, $s(u_2) = 2.2/3$, $a(u_1) = 1.2/3$, $a(u_2) = 1.8/3$, $c(u_1) = 2.4/3$ and $c(u_2) = 2.1/3$ based on Definition 3. Considering Definition 4, we can infer that u_2 is superior to u_1, as denoted by $u_2 \succ u_1$.*

Definition 5 [31]. *Let $u_1 =< T_1, I_1, F_1 >, u_2 =< T_2, I_2, F_2 >$ be two neutrosophic numbers, then the normalized Hamming distance between u_1 and u_2* is defined as follows:

$$D^{\triangle}(u_1, u_2) = \frac{(|T_1 - T_2| + |I_1 - I_2| + |F_1 - F_2|)}{3}. \tag{4}$$

Definition 6 [4] (p. 1). *Let U be the set of initial universe, E be the parameter set, and $P(U)$ be the power set of U. Then a pair (F, E)is called a soft set over U where F is a mapping given by $F : E \to P(U)$.*

Remark 1 [32]. *On account of the single valued neutrosophic set is an instance of the neutrosophic set, it is natural to infer that a single valued neutrosophic soft set is an instance of the neutrosophic soft set. However, Maji only considers neutrosophic soft sets, which take value from the standard subset of $[0, 1]$ rather than $]^{-}0, 1^{+}[$, so the definition of the single valued neutrosophic soft set is exactly the same as the concept of the neutrosophic soft set defined by Maji.*

Definition 7 [17] (p. 1). *Let U be the initial universal set, E be a set of parameters, and $P(U)$ be the set of all neutrosophic subsets of U. The collection (F, E) is regarded as a neutrosophic soft set over U, where F refers to the mapping $F : E \to P(U)$.*

Example 2. *Assume $U = \{u_1, u_2, u_3\}$ is a set of three cars under consideration, and $E = \{e_1 = \text{cheap}, e_2 = \text{equipment}, e_3 = \text{fuel consumption}\}$ be the set of parameters for describing the three. In this case, we can define a function $F : E \to P(U)$ as a neutrosophic soft set (F, E), and it is represented as follows:*

$$(F, E) = \left\{ \begin{array}{l} F(e_1) = \{< u_1, 0.8, 0.4, 0.3 >, < u_2, 0.5, 0.7, 0.3 >, < u_3, 0.2, 0.5, 0.8 >\} \\ F(e_2) = \{< u_1, 0.5, 0.7, 0, 4 >, < u_2, 0.7, 0.3, 0.2 >, < u_3, 0.5, 0.8, 0.5 >\} \\ F(e_3) = \{< u_1, 0.4, 0.6, 0.3 >, < u_2, 0.9, 0.3, 0.1 >, < u_3, 0.4, 0.7, 0.5 >\} \end{array} \right\}.$$

2.2. Prospect Theory

The prospect theory [27] (p. 2), proposed by Tversky and Kahneman, is a mainstream theory of behavioral science, and it studies human judgments or decision making behaviors under uncertain environments. The prospect theory mainly considers the value function and decision weight function. It implies three characteristics: Reference dependence, diminishing sensitivity and lose aversion. Reference dependence refers to the change of people's perception depending on the change of the relative value. Diminishing sensitivity means that utility decreases as income increases. Additionally, loss aversion signifies that people value losses more than gains.

The prospect theory states that decision makers choose the optimal alternative based on the prospect value, which is determined by the value function and decision weight function. The prospect value can be obtained as follows:

$$V = \sum v(x-r)\omega(p_t). \tag{5}$$

$v(x-r)$ is the value function as defined follows:

$$v(x-r) = \begin{cases} (x-r)^{\alpha}, & x \geq r \\ -\lambda(x-r)^{\beta}, & x < r \end{cases}, \tag{6}$$

where x is the evaluation value of an object, r is the reference point, then $(x-r)$ represents losses or gains. $x \geq r$ means gains, and the value function is concave; $x < r$ means losses, and the value function is convex. So α, β stand for the concave degree and convexity degree of the value function, respectively. λ is the risk aversion coefficient, and $\lambda > 1$ indicates that decision makers value risk more. By experimental verification, Tversky and Kahneman took the value of parameters as follows: $\alpha = \beta = 0.88,\ \lambda = 2.25$.

$\omega(P_t)$ is the decision weight function as defined follows:

$$\omega(p_t) = \frac{{p_t}^{\gamma}}{(({p_t}^{\gamma}) + ((1-p_t)^{\gamma}))^{\frac{1}{\gamma}}}, \tag{7}$$

where p_t is the objective possibility, and Tversky and Kahneman took the value of parameter γ as 0.61.

3. The Measures of Determinacy Degree and Conflict Degree and Neutrosophic Soft Set Aggregation Rules

In this section, we initiate the determinacy degree measure and conflict degree measure of neutrosophic numbers, and then develop two kinds of aggregation rules of a neutrosophic soft set.

3.1. The Measures of Determinacy Degree and Conflict Degree

This paper employs the Hamming distance of information theory, which is a well-known measure designed to provide insights into the similarity of information [33,34] and has been widely employed in distance measures [26,35], to measure the determinacy degree and conflict degree. Before this, we present the concept of a minimum conflict neutrosophic number and maximum conflict neutrosophic number.

Definition 8. *Let Minc* $=< 1, 0, 0 >$ *be the minimum conflict neutrosophic number, which means that the belongingness degree of an object is 1, and the non-belongingness degree and the neutrality degree of an object be zero, respectively. That is, the conflict degree of information is the smallest.*

Additionally, let Maxc $=< 0.5, 1, 0.5 >$ *be the maximum conflict neutrosophic number. That is, the neutrosophic number, whose neutrality degree is one, and the belongingness degree and non-belongingness degree is 0.5. In order words, the conflict degree of information is the greatest.*

Definition 9. *Let* $u =< T, I, F >$ *be a neutrosophic number, the determinacy degree of u based on Equation (4) can be defined as follows:*

$$d^{\Delta}(u) = \frac{(|T-1| + I + F)}{3}, \tag{8}$$

which measures the normalized Hamming distance between u and the minimum conflict neutrosophic number.

Similarly, the conflict degree of u is determined by the normalized Hamming distance between u and the maximum conflict neutrosophic number, and defined as follows:

$$c^{\Delta}(u) = \frac{(|T-0.5| + |I-1| + |F-0.5|)}{3} \tag{9}$$

Example 3. *Considering Example 1, the determinacy degree and conflict degree of u_1 can be computed as follows: $d^{\Delta}(u_1) = 0.8/3, c^{\Delta}(u_1) = 1.2/3$.*

3.2. Aggregation Rules of a Neutrosophic Soft Set

In this subsection, we define two kinds of aggregation rules of a neutrosophic soft set, namely the weighted average aggregation rule and weighted geometric aggregation rule.

Definition 10. *Weighted average aggregation rule. Let U be the initial universal set, E be the set of parameters, (F, E) be a neutrosophic soft set over U, as represented by $F(e_j)(x_i) =< F_T(e_j)(x_i), F_I(e_j)(x_i), F_F(e_j)(x_i) >$ $(i = 1, 2, \ldots, m; j = 1, 2, \ldots, n)$. Then, the weighted average aggregation rule of (F, E) can be denoted by $(F, E)^{\Gamma} = \left\{F^{\Gamma}(x_1), F^{\Gamma}(x_2), \ldots, F^{\Gamma}(x_m)\right\}$, and defined as*

$$F^{\Gamma}(x_i) = \prod_{j=1}^{n} F(e_j)(x_i)\omega_j =< 1 - \prod_{j=1}^{n} (1 - F_T(e_j)(x_i))^{\omega_j}, \prod_{j=1}^{n} (F_I(e_j)(x_i))^{\omega_j}, \prod_{j=1}^{n} (F_F(e_j)(x_i))^{\omega_j} > \quad (10)$$

where the vector $\omega = \{\omega_1, \omega_2, \ldots, \omega_n\}$ stands for the weights of parameters, and $\sum\limits_{j=1}^{n} \omega_j = 1$.

Based on Definition 10, the weighted geometric aggregation rule of a neutrosophic soft set is constructed.

Definition 11. *Weighted geometric aggregation rule. Considering the neutrosophic soft set (F, E) in Definition 10, we define the weighted geometric aggregation rule as $(F, E)^{\Theta} = \{F^{\Theta}(x_1), F^{\Theta}(x_2), \ldots, F^{\Theta}(x_m)\}$, and*

$$F^{\Theta}(x_i) = \prod_{j=1}^{n} (F(e_j)(x_i))^{\omega_j} =< \prod_{j=1}^{n} (F_T(e_j)(x_i))^{\omega_j}, 1 - \prod_{j=1}^{n} (1 - (F_I(e_j)(x_i)))^{\omega_j}, 1 - \prod_{j=1}^{n} (1 - (F_F(e_j)(x_i)))^{\omega_j} > \quad (11)$$

where the vector $\omega = \{\omega_1, \omega_2, \ldots, \omega_n\}$stands for the weights of parameters, and $\sum\limits_{j=1}^{n} \omega_j = 1$.

Example 4. *Consider Example 2. Assume that the weight vector of parameters is $\omega = \{0.4, 0.2, 0.3\}$, then we can obtain the results of the weighted average aggregation and weighted geometric aggregation as follows, respectively.*

$(F, E)^{\Gamma} = \{< u_1, 0.6077, 0.5537, 0.3584 >, < u_2, 0.7015, 0.4749, 0.2244 >, < u_3, 0.3169, 0.6512, 0.6467 >\}$.
$(F, E)^{\Theta} = \{< u_1, 0.6049, 0.9905, 0.9987 >, < u_2, 0.6837, 0.9973, 0.9998 >, < u_3, 0.3474, 0.9798, 0.9885 >\}$

4. Algorithm for Neutrosophic Soft Sets in Stochastic Multi-Criteria Group Decision Making Based on Prospect Theory

4.1. Problem Description

In this section, we give a concise description of a stochastic multi-criteria group decision making problem under neutrosophic soft sets. Let $U = \{x_1, x_2, \ldots, x_m\}$ be a set of m alternatives, $E = \{e_1, e_2, \ldots, e_n\}$ be a set of n parameters and $DM = \left\{Z_1, Z_2, \ldots Z_p\right\}$ be a set of p decision makers. Assume that $\omega^{(t)} =< \omega_T^{(t)}, \omega_I^{(t)}, \omega_F^{(t)} > (t = 1, 2, \ldots, p)$ is the neutrosophic weight of decision maker Z_t, $\delta_j^{(t)} =< \delta_{Tj}^{(t)}, \delta_{Ij}^{(t)}, \delta_{Fj}^{(t)} >$ is the neutrosophic subjective weight assigned for parameter e_j by decision maker Z_t, and the evaluation value of alternative x_i related to parameter e_j by decision maker Z_t is expressed as $F^{(t)}(e_j)(x_i) =< F_T^{(t)}(e_j)(x_i), F_I^{(t)}(e_j)(x_i), F_F^{(t)}(e_j)(x_i) >$. Given p neutrosophic soft sets $(F^{(t)}, E)$ $(t = 1, 2, \ldots, p)$ of alternatives evaluated by decision makers, and the tabular representation of $(F^{(t)}, E)$ $(t = 1, 2, \ldots, p)$ is shown in Table 1.

4.2. Determining the Determinacy Degree of Decision Makers

In stochastic multi-criteria group decision making problems, the weights of decision makers are stochastic and indeterminate. Therefore, how to obtain the weights as determinate values has become an important research topic. In this paper, we express the weights of decision makers as a neutrosophic number, and then compute the determinacy degree of decision makers to replace traditional weights.

Considering Definition 9, let $\omega_t =< \omega_t^T, \omega_t^I, \omega_t^F > (t = 1, 2, \ldots, p)$ be the neutrosophic weight of decision maker Z_t, then the determinacy degree of Z_t can be computed as follows by Equation (8):

$$d^{\Delta}(t) = \frac{1 - \frac{1}{3}(|\omega_t^T - 1| + \omega_t^I + \omega_t^F)}{\sum\limits_{t=1}^{p} 1 - \frac{1}{3}\left(|\omega_t^T - 1| + \omega_t^I + \omega_t^F\right)} (t = 1, 2, \ldots, p), \tag{12}$$

Table 1. Tabular representation of neutrosophic soft sets $(F^{(t)}, E)$ of alternatives.

		$(\mathbf{F}^{(1)}, \mathbf{E})$		
	e_1	e_2	$\ldots$	e_n
x_1	$F^{(1)}(e_1)(x_1)$	$F^{(1)}(e_2)(x_1)$	$\ldots$	$F^{(1)}(e_n)(x_1)$
x_2	$F^{(1)}(e_1)(x_2)$	$F^{(1)}(e_2)(x_2)$	$\ldots$	$F^{(1)}(e_n)(x_2)$
	$\vdots$	$\vdots$	$\ddots$	$\vdots$
x_m	$F^{(1)}(e_1)(x_m)$	$F^{(1)}(e_2)(x_m)$	$\ldots$	$F^{(1)}(e_n)(x_m)$
		$(\mathbf{F}^{(2)}, \mathbf{E})$		
	e_1	e_2	$\ldots$	e_n
x_1	$F^{(2)}(e_1)(x_1)$	$F^{(2)}(e_2)(x_1)$	$\ldots$	$F^{(2)}(e_n)(x_1)$
x_2	$F^{(2)}(e_1)(x_2)$	$F^{(2)}(e_2)(x_2)$	$\ldots$	$F^{(2)}(e_n)(x_2)$
$\vdots$	$\vdots$	$\vdots$	$\ddots$	$\vdots$
x_m	$F^{(2)}(e_1)(x_m)$	$F^{(2)}(e_2)(x_m)$	$\ldots$	$F^{(2)}(e_n)(x_m)$
$\vdots$	$\vdots$	$\vdots$	$\vdots$	$\vdots$
		$(\mathbf{F}^{(p)}, \mathbf{E})$		
	e_1	e_2	$\ldots$	e_n
x_1	$F^{(p)}(e_1)(x_1)$	$F^{(p)}(e_2)(x_1)$	$\ldots$	$F^{(p)}(e_n)(x_1)$
x_2	$F^{(p)}(e_1)(x_2)$	$F^{(p)}(e_2)(x_2)$	$\ldots$	$F^{(p)}(e_n)(x_2)$
$\vdots$	$\vdots$	$\vdots$	$\ddots$	$\vdots$
x_m	$F^{(p)}(e_1)(x_m)$	$F^{(p)}(e_2)(x_m)$	$\ldots$	$F^{(p)}(e_n)(x_m)$

4.3. Calculating the Comprehensive Weights of Parameters

In this paper, the parameter weights are determined by combining subjective weights with objective weights. Among them, subjective weights are obtained by aggregating neutrosophic subjective weights provided by decision makers, which is more accurate than the way directly given by determinate values [25] (p. 2). The objective weights are calculated by the information entropy method [35]. Then, the principle of minimum information entropy [36] is employed to obtain comprehensive weights of parameters by integrating subjective weights and objective weights. The system framework is presented in Figure 1.

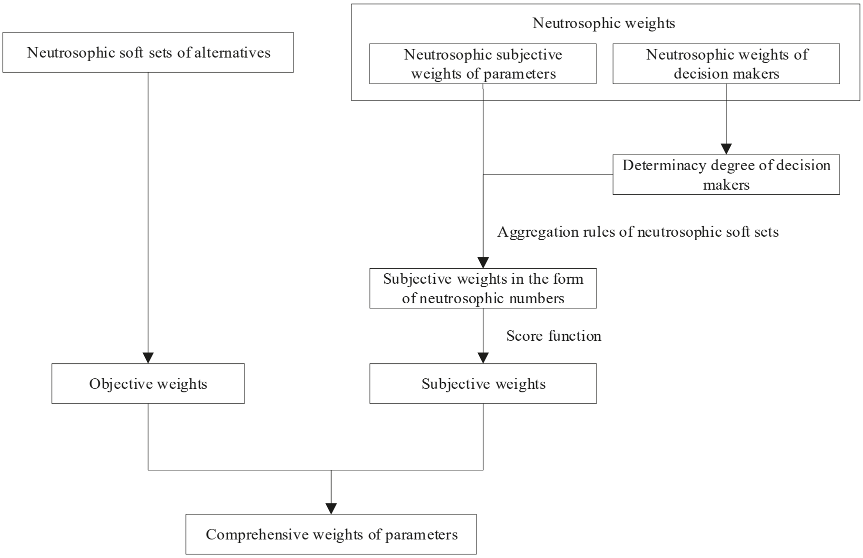
Neutrosophic weights
Neutrosophic soft sets of alternatives
Neutrosophic subjective weights of parameters
Neutrosophic weights of decision makers
Determinacy degree of decision makers
Aggregation rules of neutrosophic soft sets
Subjective weights in the form of neutrosophic numbers
Score function
Objective weights
Subjective weights
Comprehensive weights of parameters

Figure 1. The system framework of the computing comprehensive weights of parameters.

4.3.1. Computing the Subjective Weights

Under the stochastic environment, the judgements of decision makers are full of hesitancies. Considering this situation, instead of giving determinate values, this paper firstly aggregates neutrosophic subjective weights of parameters to obtain subjective weights in the form of neutrosophic numbers. Based on this, subjective weights are computed by the score function as Equation (1).

Assume parameter set $E = \left\{e_1, e_2, \ldots, e_j\right\}$ is the initial universal set, the set of decision makers $Z = \{z_1, z_2, \ldots, z_t\}$ is the parameter set, and $P(Z)$ is the set of all neutrosophic subsets of E. The neutrosophic soft set (F, Z) over E can be integrated by the weighted geometric aggregation rule as $(F, Z)^{\Theta} = \left\{F^{\Theta}(e_1), F^{\Theta}(e_2), \ldots, F^{\Theta}(e_m)\right\}$, and

$$F^{\Theta}(e_j) = \prod_{t=1}^{p} \delta_j^{(t)\,\psi_t} =< \prod_{t=1}^{p} \delta_{Tj}^{(t)\,\psi_t}, 1 - \prod_{t=1}^{p} (1 - \delta_{Ij}^{(t)})^{\psi_t}, 1 - \prod_{t=1}^{p} (1 - \delta_{Fj}^{(t)})^{\psi_t} >, \tag{13}$$

where $\delta_j^{(t)} =< \delta_{jT}^{(t)}, \delta_{Ij}^{(t)}, \delta_{Fj}^{(t)} > (j = 1, 2, \ldots, n)$ is the neutrosophic subjective weight assigned for parameter e_j by Z_t, and ψ_t is the determinacy degree of Z_t.

Then, the subjective weights can be computed by the score function as shown below:

$$SW_j = \frac{2 + \prod_{t=1}^{p} \delta_{Tj}^{(t)\,\psi_t} - (1 - \prod_{t=1}^{p} (1 - \delta_{Ij}^{(t)})^{\psi_t}) - (1 - \prod_{t=1}^{p} (1 - \delta_{Fj}^{(t)})^{\psi_t})}{3}. \tag{14}$$

4.3.2. Obtaining the Objective Weights: Information Entropy Method

Considering that the computation of objective weights is not the focus of this paper, we obtain objective weights by the information entropy method. The information entropy is used to measure the uncertainty of events. The greater the information entropy is, the greater the uncertainty degree. That is, the smaller the amount of information it carries, the smaller the weight is. Note that the uncertainty of neutrosophic numbers consists of two factors, one is the truth-membership and false-membership, and the other is the indeterminacy-membership.

Based on the information entropy method, we can obtain that the information entropy of parameter e_j given by decision maker Z_t is defined as:

$$E_j^t = 1 - \frac{1}{m}\sum\nolimits_{i=1}^{m}\left(F_T^{(t)}\left(e_j\right)(x_i) + F_F^{(t)}\left(e_j\right)(x_i)\right)|F_I^{(t)}\left(e_j\right)(x_i) - F_I^{(t)c}\left(e_j\right)(x_i)|(j = 1,2,\ldots,n). \tag{15}$$

Then, the comprehensive information entropy of parameter e_j is defined as follows:

$$E_j = \sum_{t=1}^{p} \varphi_t E_j^t (j = 1,2,\ldots,n) \tag{16}$$

where φ_t is the determinacy degree of decision maker Z_t computed by Equation (8).

So, the objective weights are obtained as:

$$OW_j = \frac{1 - E_j}{\sum\limits_{j=1}^{n} 1 - E_j}(j = 1,2,\ldots,n). \tag{17}$$

4.3.3. Calculating the Comprehensive Weights

Based on the principle of the minimum information entropy, the comprehensive weight of parameter ϖ_j can be calculated as follows:

$$\varpi_j = \frac{\sqrt{OW_j \cdot SW_j}}{\sum\limits_{j=1}^{n} \sqrt{OW_j \cdot SW_j}}, \tag{18}$$

where SW_j and OW_j represent the subjective weight and objective weight of parameter e_j, respectively.

4.4. Computing the Comprehensive Prospect Values

The comprehensive prospect values of alternatives are determined by the prospect decision matrix and the comprehensive weights of parameters. Next, we expound how to generate the prospect decision matrix and obtain comprehensive values of alternatives, respectively.

4.4.1. Constructing the Prospect Decision Matrix

The core of constructing the prospect decision matrix is to compute the value function and decision weight function. In terms of the value function, we need to analyze the distance between the reference point and the actual value. This paper regards the maximum conflict neutrosophic number as the reference point, then the distance can be treated as the conflict degree of the actual value. Additionally, actual values refer to the alternative evaluation values with respect to the parameters. As for the decision weight function, the objective possibility is seen as the determinacy degree of the decision makers. The system framework of constructing the prospect decision matrix is shown in Figure 2.

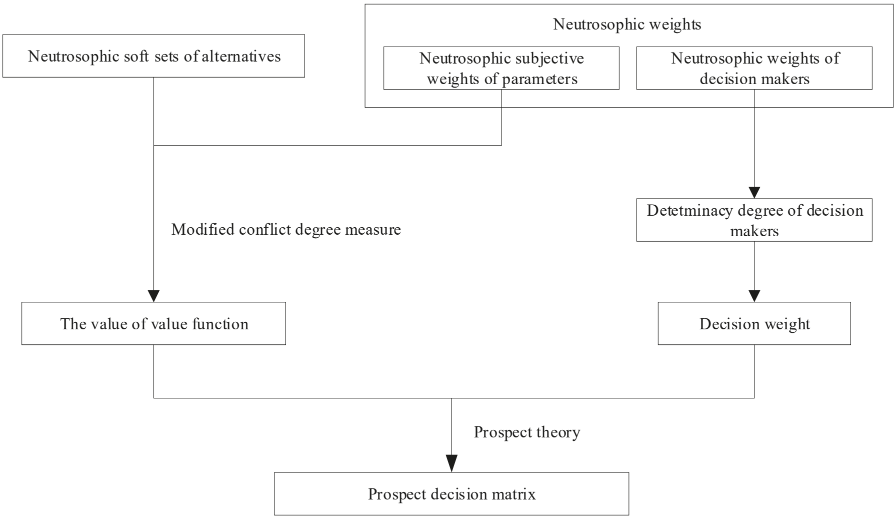
Neutrosophic soft sets of alternatives
Neutrosophic weights
Neutrosophic subjective weights of parameters
Neutrosophic weights of decision makers
Modified conflict degree measure
Detetminacy degree of decision makers
The value of value function
Decision weight
Prospect theory
Prospect decision matrix

Figure 2. The system framework of constructing the prospect decision matrix.

We assume that the neutrosophic soft sets of alternatives and neutrosophic subjective weights of parameters are both provided by decision makers. So, the conflict degree of the alternative evaluation values with respect to the parameters should take the neutrosophic subjective weights of parameters into account. Based on the conflict degree measure given by Definition 9, we develop a modified conflict degree measure by introducing the neutrosophic subjective weights of parameters.

Assume $F(e_j)(x_i) =< F_T(e_j)(x_i), F_I(e_j)(x_i), F_F(e_j)(x_i) >$ is a neutrosophic number, which represents the value of alternative x_i related to parameter e_j, and $\alpha_j =< \alpha_{jT}, \alpha_{jI}, \alpha_{jF} >$ is the neutrosophic subjective weight of parameter e_j. Considering the sum of α_{jT}, α_{jI} and α_{jF} may not be one, this paper normalizes them to be more consistent with the reality. Therefore, the measure of the modified conflict degree of $F(e_j)(x_i)$ is defined as follows:

$$mc^{\Delta}(F(e_j)(x_i)) = \frac{\alpha_{jT} \cdot \left|F_T(e_j)(x_i) - 0.5\right|}{\alpha_{jT} + \alpha_{jI} + \alpha_{jF}} + \frac{\alpha_{jI} \cdot \left|F_I(e_j)(x_i) - 1\right|}{\alpha_{jT} + \alpha_{jI} + \alpha_{jF}} + \frac{\alpha_{jF} \cdot \left|F_F(e_j)(x_i) - 0.5\right|}{\alpha_{jT} + \alpha_{jI} + \alpha_{jF}}. \tag{19}$$

Subsequently, calculate the prospect value of each alternative with respect to the parameters as follows:

$$V_{ij} = \sum_{t=1}^{p} w(z_t) v(F^{(t)}(e_j)(x_i) - x_0), \tag{20}$$

where

$$v(F^{(t)}(e_j)(x_i) - x_0) = \begin{cases} (mc^{\Delta}(F^{(t)}(e_j)(x_i), x_0))^{0.88}, & F^{(t)}(e_j)(x_i) \geq x_0 \\ -2.25(mc^{\Delta}(F^{(t)}(e_j)(x_i), x_0))^{0.88}, & F^{(t)}(e_j)(x_i) < x_0 \end{cases}, \tag{21}$$

$$\omega(Z_t) = \frac{(\psi_t)^{0.61}}{((\psi_t)^{0.61} + (1 - \psi_t)^{0.61})^{\frac{1}{0.61}}}. \tag{22}$$

Then, we can obtain the prospect decision matrix.

4.4.2. Computing the Comprehensive Prospect Values

Based on comprehensive weights of parameters and the prospect decision matrix, we can compute the comprehensive prospect values for alternatives as follows:

$$V_i = \sum_{j=1}^{n} \varpi_j V_{ij}. \tag{23}$$

The system framework of computing the comprehensive prospect values is shown in Figure 3.

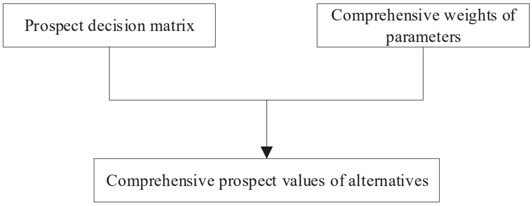
Prospect decision matrix
Comprehensive weights of parameters
Comprehensive prospect values of alternatives

Figure 3. The system framework of computing the comprehensive prospect values of alternatives.

4.5. Algorithm for Neutrosophic Soft Sets in Stochastic Multi-Criteria Group Decision Making Based on Prospect Theory

In this section, a novel algorithm for neutrosophic soft sets in stochastic multi-criteria group decision making based on the prospect theory is proposed. The detailed operation steps of Algorithm 1 are presented below.

Algorithm 1: Neutrosophic soft sets in stochastic multi-criteria group decision making based on the prospect theory

Step 1: Input a neutrosophic set, which represents neutrosophic weights of decision makers and two neutrosophic soft sets, including alternatives description as shown in Table 1 and neutrosophic subjective weights of parameters evaluated by decision makers.
Step 2: Normalize the neutrosophic soft sets of alternatives as follows:

$$(\overset{\triangle}{F}^{(t)}, E) = \begin{cases} (F_T^{(t)}(e_j)(x_i), F_I^{(t)}(e_j)(x_i), F_F^{(t)}(e_j)(x_i)), & e_j \text{ is a benefit parameter} \\ (F_F^{(t)}(e_j)(x_i), 1 - F_I^{(t)}(e_j)(x_i), F_T^{(t)}(e_j)(x_i)), & e_j \text{ is a cos t parameter} \end{cases} \tag{24}$$

Step 3: Compute the determinacy degree vector $\psi_{\mathrm{t}} = (\psi_1, \psi_2, \ldots, \psi_p)$ of decision makers by Equation (8);
Step 4: Construct the prospect decision matrix based on Equation (20).
Step 5: Obtain the comprehensive weight vector $\varpi_j = (\varpi_1, \varpi_2, \ldots, \varpi_n)$ by Equation (18);
Step 6: Calculate the comprehensive prospect value V_i for each alternative through Equation (23).
Step 7: Make a decision by ranking alternatives based on comprehensive prospect values.

5. An Application of the Proposed Algorithm

In order to verify the feasibility of the proposed algorithm, we discuss the investment decision of a finance institution. Meanwhile, the existing five methods [17,25,37] (pp. 1–2) are employed for a comparative analysis to prove the feasibility and superiority of the proposed algorithm.

5.1. Example Analysis

Credit scoring can help financial institutions reduce financial risks and non-performing loans. Generally, financial institutions assess the credit score of borrowers based on basic information, such as age, profession, education, income, capital gains, residence and borrowing frequency. Recently, a financial institution wants to invest an amount of money in borrowers. The institution initially selects five borrowers as candidates. In addition, the institution makes a decision by analyzing the following four parameters: Highly educated, higher borrowing frequency, higher income and higher capital gains. Subsequently, the institution assembles a team composed of three decision makers to make the investment decision. Suppose that $U = \{u_1, u_2, u_3, u_4, u_5\}$ is the set of candidates, $E = \{e_1, e_2, e_3, e_4\}$ is the parameter set, and $DM = \{Z_1, Z_2, Z_3\}$ is the set of decision makers. Let the neutrosophic soft sets $(F^{(t)}, E)$ $(t = 1, 2, 3)$ be the alternative evaluation values with respect to the parameters given by decision makers as follows.

$$(F^{(1)},E) = \left\{ \begin{array}{l} F^{(1)}(e_1) = \left\{< \frac{u_1}{0.60,0.35,0.80} >, < \frac{u_2}{0.70,0.50,0.60} >, < \frac{u_3}{0.80,0.40,0.70} >, < \frac{u_4}{0.65,0.50,0.50} >, < \frac{u_5}{0.75,0.30,0.60} >\right\} \\ F^{(1)}(e_2) = \left\{< \frac{u_1}{0.50,0.80,0.20} >, < \frac{u_2}{0.60,0.30,0.70} >, < \frac{u_3}{0.70,0.35,0.80} >, < \frac{u_4}{0.80,0.30,0.70} >, < \frac{u_5}{0.80,0.20,0.55} >\right\} \\ {F^{(1)}}_1(e_3) = \left\{< \frac{u_1}{0.60,0.50,0.80} >, < \frac{u_2}{0.70,0.50,0.20} >, < \frac{u_3}{0.80,0.60,0.30} >, < \frac{u_4}{0.70,0.40,0.70} >, < \frac{u_5}{0.85,0.30,0.60} >\right\} \\ F^{(1)}(e_4) = \left\{< \frac{u_1}{0.50,0.80,0.60} >, < \frac{u_2}{0.40,0.70,0.30} >, < \frac{u_3}{0.60,0.40,0.70} >, < \frac{u_4}{0.60,0.35,0.80} >, < \frac{u_5}{0.70,0.30,0.40} >\right\} \end{array} \right\}$$

$$(F^{(2)},E) = \left\{ \begin{array}{l} F^{(2)}(e_1) = \left\{< \frac{u_1}{0.60,0.35,0.80} >, < \frac{u_2}{0.70,0.50,0.60} >, < \frac{u_3}{0.80,0.40,0.70} >, < \frac{u_4}{0.65,0.50,0.50} >, < \frac{u_5}{0.75,0.30,0.60} >\right\} \\ F^{(2)}(e_2) = \left\{< \frac{u_1}{0.50,0.80,0.20} >, < \frac{u_2}{0.60,0.30,0.70} >, < \frac{u_3}{0.70,0.35,0.80} >, < \frac{u_4}{0.80,0.30,0.70} >, < \frac{u_5}{0.80,0.20,0.55} >\right\} \\ F^{(2)}(e_3) = \left\{< \frac{u_1}{0.60,0.50,0.80} >, < \frac{u_2}{0.70,0.50,0.20} >, < \frac{u_3}{0.80,0.60,0.30} >, < \frac{u_4}{0.70,0.40,0.70} >, < \frac{u_5}{0.85,0.30,0.60} >\right\} \\ F^{(2)}(e_4) = \left\{< \frac{u_1}{0.50,0.80,0.60} >, < \frac{u_2}{0.40,0.70,0.30} >, < \frac{u_3}{0.60,0.40,0.70} >, < \frac{u_4}{0.60,0.35,0.80} >, < \frac{u_5}{0.70,0.30,0.40} >\right\} \end{array} \right\}$$

$$(F^{(3)},E) = \left\{ \begin{array}{l} F^{(3)}(e_1) = \left\{< \frac{u_1}{0.60,0.35,0.80} >, < \frac{u_2}{0.70,0.50,0.60} >, < \frac{u_3}{0.80,0.40,0.70} >, < \frac{u_4}{0.65,0.50,0.50} >, < \frac{u_5}{0.75,0.30,0.60} >\right\} \\ F^{(3)}(e_2) = \left\{< \frac{u_1}{0.50,0.80,0.20} >, < \frac{u_2}{0.60,0.30,0.70} >, < \frac{u_3}{0.70,0.35,0.80} >, < \frac{u_4}{0.80,0.30,0.70} >, < \frac{u_5}{0.80,0.20,0.55} >\right\} \\ F^{(3)}(e_3) = \left\{< \frac{u_1}{0.60,0.50,0.80} >, < \frac{u_2}{0.70,0.50,0.20} >, < \frac{u_3}{0.80,0.60,0.30} >, < \frac{u_4}{0.70,0.40,0.70} >, < \frac{u_5}{0.85,0.30,0.60} >\right\} \\ F^{(3)}(e_4) = \left\{< \frac{u_1}{0.50,0.80,0.60} >, < \frac{u_2}{0.40,0.70,0.30} >, < \frac{u_3}{0.60,0.40,0.70} >, < \frac{u_4}{0.60,0.35,0.80} >, < \frac{u_5}{0.70,0.30,0.40} >\right\} \end{array} \right\}$$

The neutrisophic set D represents the neutrosophic weights of decision makers, and the neutrisophic soft set (F, Z) stands for neutrosophic subjective weights of parameters. They are valued as follows:

$$D = \{< Z_1, 0.3, 0.5, 0.7 >, < Z_2, 0.1, 0.4, 0.6 >, < Z_3, 0.6, 0.5, 0.2 >\}$$

$$(F,Z) = \left\{ \begin{array}{l} F(Z_1) = \left\{< \frac{e_1}{0.40,0.60,0.50} >, < \frac{e_2}{0.35,0.70,0.60} >, < \frac{e_3}{0.40,0.60,0.55} >, < \frac{e_4}{0.40,0.60,0.75} >\right\} \\ F(Z_2) = \left\{< \frac{e_1}{0.70,0.45,0.30} >, < \frac{e_2}{0.50,0.80,0.60} >, < \frac{e_3}{0.70,0.55,0.40} >, < \frac{e_4}{0.70,0.40,0.65} >\right\} \\ F(Z_3) = \left\{< \frac{e_1}{0.65,0.70,0.40} >, < \frac{e_2}{0.60,0.35,0.75} >, < \frac{e_3}{0.40,0.65,0.70} >, < \frac{e_4}{0.35,0.60,0.50} >\right\} \end{array} \right\}$$

Step 1: Input the neutrosophic soft sets $(F^{(t)}, E)(t = 1, 2, 3)$, (F, Z) and the neutrosophic set D.

Step2: There is no need to normalize the neutrosophic soft sets $(F^{(t)}, E)(t = 1, 2, 3)$ of alternatives, because the parameters adopted in this study are benefit parameters.

Step 3: Compute the determinacy degree vector of decision makers based on Equation (8) as follows:

$$\psi_t = \{0.3478, 0.4130, 0.2391\}$$

Step 4: Construct the prospect decision matrix based on Equation (20).

$$V_{\mathrm{ij}} = \begin{pmatrix} 0.3878 & 0.2846 & 0.3574 & 0.2274 \\ 0.3035 & 0.3751 & 0.3571 & 0.2712 \\ 0.4536 & 0.3834 & 0.3226 & 0.3180 \\ 0.3345 & 0.3294 & 0.3120 & 0.3776 \\ 0.3482 & 0.4482 & 0.4055 & 0.3481 \end{pmatrix}.$$

Step 5: Determine the comprehensive weight vector $\varpi_j = (\varpi_1, \varpi_2, \ldots, \varpi_n)$ for the parameters as Equation (18), and the neutrosophic subjective weights are aggregated by the weighted geometric aggregation rule as Equation (11).

$$\varpi_j = (0.2991, 0.2260, 0.2898, 0.1851)$$

Step 6: Obtain the comprehensive prospect value V_i by Equation (23).

$$V_1 = 0.3269, V_2 = 0.3292, V_3 = 0.3746, V_4 = 0.3348, V_5 = 0.3874.$$

Step 7: Make a decision by ranking the comprehensive prospect value of the five candidates.

$$x_5 \succ x_3 \succ x_4 \succ x_2 \succ x_1$$

Therefore, we can see that the optimal candidate is x_5. x_3, x_4 are suboptimal, and x_2, x_1 are the worst.

Furthermore, we also utilize the weighted average aggregation rule to compute the subjective weights of parameters. In addition, the computational procedure is shown as follows.

Step 1–4: Be consistent with the above steps 1–4.

Step 5: Determine the comprehensive weight vector $\varpi_j = (\varpi_1, \varpi_2, \ldots, \varpi_n)$ for the parameters as Equation (18), and the neutrosophic subjective weights are aggregated by the weighted average aggregation rule.

$$\varpi_j = (0.2903, 0.2127, 0.2523, 0.2447).$$

Step 6: Obtain the comprehensive prospect value V_i by Equation (23).

$$V_1 = 0.3254, V_2 = 0.3295, V_3 = 0.3744, V_4 = 0.3348, V_5 = 0.3876.$$

Step 7: Make a decision by ranking the five candidates.

$$x_5 \succ x_3 \succ x_4 \succ x_2 \succ x_1.$$

So the best optimal is still x_5, the following are x_3, x_4, and the worst are x_2, x_1.

Obviously, we can see that the ranking orders obtained by two aggregation rules of the neutrosophic soft set are the same.

5.2. Comparative Analysis

A comparative analysis with existing methods is performed to justify the feasibility and superiority of the proposed method. The existing methods include the method proposed by Maji [17] (p. 1), the three methods carried out by Peng and Liu [25] (p. 2) and the aggregated neutrosophic set method [37] (p. 11).

In the decision making method outlined by Maji [17] (p. 1), the final ranking is obtained based on the comparison matrix through briefly comparing with three membership function values. The three neutrosophic soft decision making methods [25] (p. 2) include the non-linear weighted comprehensive method to determine parameter comprehensive weights by combining objective weights and subjective weights. Objective weights are computed by the grey system method, and subjective weights are directly given determinate values. Then, three neutrosophic soft decision making methods are constructed based on EDAS, similarity measure, and the level soft set to rank alternatives in practical problems. Among the three, EDAS and the similarity measure methods obtain the final ranking based on the accurate calculation of alternative evaluation values. In addition, the level soft set method makes a decision by roughly comparing the threshold value with alternative evaluation values. In terms of the aggregated neutrosophic set method [37] (p. 11), alternatives are aggregated using the arithmetic average and sorted by TOPSIS.

Note that there are two crucial issues. On one hand, the above methods all make decisions under a single decision maker. In order to successfully apply them to group decision making, this paper employs the weighted average algorithm to the score of alternatives to all decision makers, based on the decision maker determinacy degree of this study. On the other hand, the method in [17] (p. 1) and [37] (p. 11) does not take parameter weights into consideration. Although the EDAS, similarity measure and level soft set methods [25] (p. 2) comprehensively consider objective weights and subjective weights, the subjective weights are directly given determinate values, which cannot reflect the hesitancies of decision makers under uncertainties. Considering this, the comparative analysis applies the subjective weights obtained from this study to the three methods in [25] (p. 2).

The final ranking of the stochastic multi-criteria group decision making problem mentioned in Section 5.1 are presented in Table 2, by utilizing the proposed method and the methods in [17,25,37] (pp. 1–2, 11). By comparison, the results of the proposed method are consistent with those of most comparison methods, which prove the effectiveness of the proposed method.

Table 2. A comparative study with some existing methods.

Method	The Final Ranking	The Optimal Alternative
The proposed method		
Weighted geometric neutrosophic rule	$x_5 > x_3 > x_4 > x_2 > x_1$	x_5
Weighted average neutrosophic rule	$x_5 > x_3 > x_4 > x_2 > x_1$	x_5
The determinacy degree of decision makers $\psi_t = \{0.3913, 0.2826, 0.3261\}$		
Maji [17]	$x_5 > x_4 > x_3 > x_2 > x_1$	x_5
EDAS [25]	$x_5 > x_3 > x_4 > x_2 > x_1$	x_5
Similarity [25]	$x_5 > x_3 > x_4 > x_2 > x_1$	x_5
Level soft set [25]	$x_5 > x_4 > x_3 > x_2 > x_1$	x_5
TOPSIS [37]	$x_5 > x_3 > x_4 > x_2 > x_1$	x_5

From Table 2, we can find that the final rankings of the proposed algorithm are different from Maji's method and the level soft set method. The difference can be attributed to two reasons. One is that both methods are approximate comparisons of the alternative evaluation values, and the original evaluation values are not used to the greatest extent. The other is that the threshold value difference of the level soft set method can directly lead to different final rankings. However, decision makers can hardly decide which threshold value to use.

Through comparison, the final rankings of the other three methods are consistent with the proposed method. Among them, EDAS also adopts the aggregation method just as the proposed method. Different from EDAS, the proposed method considers the psychological expectation of decision makers in the borrower selection issue. Thus, in complex group decision making problems, the proposed method can produce more reasonable results than existing methods.

From the above analysis, the main superiorities of the proposed method can be summarized into three aspects. Firstly, this study originally employs neutrosophic soft sets for handling stochastic multi-criteria group decision making problems, which cannot be solved in existing methods. Secondly, the proposed method expresses the weights of subjective weights of parameters by neutrosophic numbers, which can fully reflect the hesitancies of decision makers. Meanwhile, this study presents the weights of decision makers by neutrosophic numbers, which can better incorporate stochastic into the decision making process. Thirdly, the proposed method considers the psychological expectations of decision makers in the borrower selection process. Therefore, it is able to analyze the decision making behavior more objectively.

6. Conclusions

Under uncertain environments, a mass of inconsistent information appears. Neutrosophic soft sets are powerful tools to address these issues involving inconsistent information. Considering this, we develop a generalized stochastic multi-criteria group decision making framework under neutrosophic soft sets, by innovatively integrating the prospect theory and neutrosophic soft sets into our framework. This paper describes the reference point, the psychological expectations of decision makers, in the form of neutrosophic sets. Then, in addition, this study demonstrates how to compute the alternative prospect values as the reference for decision making.

We conduct experiments to test the feasibility and validity of our decision making framework. The main contributions of this paper are fourfold. Firstly, we construct a new algorithm for the stochastic multi-criteria group decision making based on neutrosophic soft sets, which can analyze inconsistent information in decision making effectively. Secondly, the weights of decision makers and parameter subjective weights are both expressed in the form of neutrosophic numbers. Compared with the way directly given determinate values in existing methods [25] (p. 2), the proposed method can embody the stochastic into decision making processes. Thirdly, the research successfully combines the prospect theory with neutrosophic softs sets to construct the stochastic multi-criteria group decision making algorithm. Compared with the existing literatures based on the expected utility theory [16,17,25,26] (pp. 1-2), this research considers the influence of psychological expectations on decision results. Finally, we explore the conflict degree measure of neutrosophic numbers and two aggregation rules of neutrosophic soft sets, and further define the measure of the modified conflict degree to accommodate the multi-criteria group decision making.

The proposed method is not only suitable for credit scoring, but also for decision-making problems in other fields, especially for decisions with inconsistent information. As a suggestion for future researches, we shall integrate more advanced decision theories into neutrosophic soft sets and address stochastic multi-criteria group decision making issues.

Author Contributions: Funding acquisition, Y.D.; Methodology, Y.D. and C.H.; Validation, Y.D. and C.H.; Writing—original draft, Y.D. and C.H.; Writing—review and editing, C.H., Y.P., and K.G.

Funding: This research was funded by the National Natural Science Foundation of China (Grant Nos. 71701116 and 71871034); Humanities and Social Science Fund of Ministry of Education of China (Grant No. 15YJC630016); Science and Technology Innovation Program in Higher Education Institutions of Shanxi Province ("Research on multi-level dynamic credit evaluation under conflict data") and Education Innovation Program for Postgraduate of Shanxi Province ("Research on Multi-level Dynamic Credit Evaluation of Personal Consumption Credit under Internet Conflict Data").

Acknowledgments: The authors gratefully acknowledge the editor of the Journal and anonymous reviewers for the detailed and valuable comments.

Conflicts of Interest: The authors declare no conflict of interest.

References

1. Zadeh, L.A. Fuzzy sets. *Inf. Control* **1965**, *8*, 338–353. [CrossRef]
2. Pawlak, Z. Rough sets. *Int. J. Comput. Inf. Sci.* **1982**, *11*, 341–356. [CrossRef]
3. Gorzałczany, M.B. A method of inference in approximate reasoning based on interval-valued fuzzy sets. *Fuzzy Sets Syst.* **1987**, *21*, 1–17. [CrossRef]
4. Molodtsov, D. Soft set theory-first results. *Comput. Math. Appl.* **1999**, *37*, 19–31. [CrossRef]
5. Aktaş, H.; Çağman, N. Soft sets and soft groups. *Inf. Sci.* **2007**, *177*, 2726–2735. [CrossRef]
6. Acar, U.; Koyuncu, F.; Tanay, B. Soft sets and soft rings. *Comput. Math. Appl.* **2010**, *59*, 3458–3463. [CrossRef]
7. Min, W.K. A note on soft topological spaces. *Comput. Math. Appl.* **2011**, *62*, 3524–3528. [CrossRef]
8. Çağman, N.; Karataş, S.; Enginoglu, S. Soft topology. *Comput. Math. Appl.* **2011**, *62*, 351–358. [CrossRef]
9. Danjuma, S.; Ismail, M.A.; Herawan, T. An alternative approach to normal parameter reduction algorithm for soft set theory. *IEEE Access* **2017**, *5*, 4732–4746. [CrossRef]

10. Yuksel, S.; Dizman, T.; Yildizdan, G.; Sert, U. Application of soft sets to diagnose the prostate cancer risk. *J. Inequalities Appl.* **2013**, *2013*, 229. [CrossRef]
11. Kamacı, H.; Atagün, A.O.; Sönmezoğlu, A. Row-products of soft matrices with applications in multiple-disjoint decision making. *Appl. Soft Comput.* **2018**, *62*, 892–914. [CrossRef]
12. Fatimah, F.; Rosadi, D.; Hakim, R.B.F.; Alcantud, J.C.R. N-soft sets and their decision making algorithms. *Soft Comput.* **2018**, *22*, 3829–3842. [CrossRef]
13. Feng, F.; Li, C.; Davvaz, B.; Ali, M.I. Soft sets combined with fuzzy sets and rough sets: A tentative approach. *Soft Comput.* **2010**, *14*, 899–911. [CrossRef]
14. Maji, P.K.; Biswas, R.; Roy, A.R. Fuzzy Soft Sets. *J. Fuzzy Math.* **2001**, *9*, 589–602.
15. Jiang, Y.; Tang, Y.; Chen, Q. An adjustable approach to intuitionistic fuzzy soft sets based decision making. *Appl. Math. Model.* **2011**, *35*, 824–836. [CrossRef]
16. Smarandache, F. *A Unifying Field in Logics. Neutrosophy: Neutrosophic Probability, Set and Logic*; American Research Press: Rehoboth, DE, USA, 1999.
17. Maji, P.K. Neutrosophic soft set. *Comput. Math. Appl.* **2013**, *45*, 555–562. [CrossRef]
18. Sahin, R.; Küçük, A. Generalised Neutrosophic Soft Set and its Integration to Decision Making Problem. *Appl. Math. Inf. Sci.* **2014**, *8*, 2751. [CrossRef]
19. Deli, I.; Broumi, S. Neutrosophic soft matrices and NSM-decision making. *J. Intell. Fuzzy Syst.* **2015**, *28*, 2233–2241. [CrossRef]
20. Deli, I. Interval-valued neutrosophic soft sets and its decision making. *Int. J. Mach. Learn. Cybern.* **2017**, *8*, 665–676. [CrossRef]
21. Karaaslan, F. Possibility neutrosophic soft sets and PNS-decision making method. *Appl. Soft Comput.* **2017**, *54*, 403–414. [CrossRef]
22. Karaaslan, F. Correlation coefficients of single-valued neutrosophic refined soft sets and their applications in clustering analysis. *Neural Comput. Appl.* **2017**, *28*, 2781–2793. [CrossRef]
23. Uluçay, V.; Şahin, M.; Hassan, N. Generalized neutrosophic soft expert set for multiple-criteria decision-making. *Symmetry* **2018**, *10*, 437. [CrossRef]
24. Al-Quran, A.; Hassan, N.; Marei, E. A Novel Approach to Neutrosophic Soft Rough Set under Uncertainty. *Symmetry* **2019**, *11*, 384. [CrossRef]
25. Peng, X.; Liu, C. Algorithms for neutrosophic soft decision making based on EDAS, new similarity measure and level soft set. *J. Intell. Fuzzy Syst.* **2017**, *32*, 955–968. [CrossRef]
26. Abu Qamar, M.; Hassan, N. Entropy, measures of distance and similarity of Q-neutrosophic soft sets and some applications. *Entropy* **2018**, *20*, 672. [CrossRef]
27. Kahneman, D.; Tversky, A. Prospect theory: An analysis of decisions under risk. *Econometrica* **1979**, *47*, 263–291. [CrossRef]
28. Peng, X.; Yang, Y. Algorithms for interval-valued fuzzy soft sets in stochastic multi-criteria decision making based on regret theory and prospect theory with combined weight. *Appl. Soft Comput.* **2017**, *54*, 415–430. [CrossRef]
29. Haibin, W.; Smarandache, F.; Zhang, Y.; Sunderraman, R. Single Valued Neutrosophic Sets. *Multispace Multistruct.* **2010**, *4*, 410–413.
30. Liu, C.; Luo, Y.S. Correlated aggregation operators for simplified neutrosophic set and their application in multi-attribute group decision making. *J. Intell. Fuzzy Syst.* **2016**, *30*, 1755–1761. [CrossRef]
31. Ye, J.; Du, S. Some distances, similarity and entropy measures for interval-valued neutrosophic sets and their relationship. *Int. J. Mach. Learn. Cybern.* **2019**, *10*, 347–355. [CrossRef]
32. Sahin, R.; Küçük, A. On similarity and entropy of neutrosophic soft sets. *J. Intell. Fuzzy Syst.* **2014**, *27*, 2417–2430.
33. Alfaro-García, V.G.; Merigó, J.M.; Gil-Lafuente, A.M.; Kacprzyk, J. Logarithmic aggregation operators and distance measures. *Int. J. Intell. Syst.* **2018**, *33*, 1488–1506. [CrossRef]
34. Choi, S.H.; Jung, S.H. Similarity Analysis of Actual Fake Fingerprints and Generated Fake Fingerprints by DCGAN. *Int. J. Fuzzy Log. Intell. Syst.* **2019**, *19*, 40–47. [CrossRef]
35. Biswas, P.; Pramanik, S.; Giri, B.C. Entropy based grey relational analysis method for multi-attribute decision making under single valued neutrosophic assessments. *Neutrosophic Sets Syst.* **2014**, *2*, 102–110.
36. Wu, K.; Jin, J. Attribute recognition method of regional ecological security evaluation based on combined weight on principle of relative entropy. *Sci. Geogr. Sin.* **2008**, *28*, 754–758.

37. Jiang, W.; Zhang, Z.; Deng, X. Multi-Attribute Decision Making Method Based on Aggregated Neutrosophic Set. *Symmetry* **2019**, *11*, 267. [CrossRef]

symmetry

MDPI

Article

On a Reduced Cost Higher Order Traub-Steffensen-Like Method for Nonlinear Systems

Janak Raj Sharma [1], Deepak Kumar [1,*] and Lorentz Jäntschi [2,*]

[1] Department of Mathematics, Sant Longowal Institute of Engineering and Technology, Longowal, Sangrur 148106, India

[2] Department of Physics and Chemistry, Technical University of Cluj-Napoca, Cluj-Napoca 400114, Romania

[*] Correspondence: deepak.babbi@gmail.com (D.K.); lorentz.jantschi@gmail.com (L.L.)

Received: 30 May 2019; Accepted: 4 July 2019; Published: 8 July 2019

Abstract: We propose a derivative-free iterative method with fifth order of convergence for solving systems of nonlinear equations. The scheme is composed of three steps, of which the first two steps are that of third order Traub-Steffensen-type method and the last is derivative-free modification of Chebyshev's method. Computational efficiency is examined and comparison between the efficiencies of presented technique with existing techniques is performed. It is proved that, in general, the new method is more efficient. Numerical problems, including those resulting from practical problems viz. integral equations and boundary value problems, are considered to compare the performance of the proposed method with existing methods. Calculation of computational order of convergence shows that the order of convergence of the new method is preserved in all the numerical examples, which is not so in the case of some of the existing higher order methods. Moreover, the numerical results, including the CPU-time consumed in the execution of program, confirm the accurate and efficient behavior of the new technique.

Keywords: nonlinear equations; systems; derivative-free methods; fast algorithms; computational efficiency

1. Introduction

We are concerned with the problem of solving a system of nonlinear equations

$$F(x) = 0. \tag{1}$$

This problem can precisely be stated as to find a solution vector $\alpha = (\alpha_1, \alpha_2, ..., \alpha_m)^T$ such that $F(\alpha) = 0$, where $\mathrm{F}(x) : D \subset \mathbb{R}^m \longrightarrow \mathbb{R}^m$ is the given nonlinear vector function $F(x) = (f_1(x), f_2(x), ..., f_m(x))^T$ and $x = (x_1, x_2, ..., x_m)^T$. The vector α can be computed as a fixed point of some function $\mathrm{M} : D \subset \mathbb{R}^m \to \mathbb{R}^m$ by means of fixed point iteration

$$\begin{aligned} x^{(0)} &\in D, \\ x^{(k+1)} &= \mathrm{M}(x^{(k)}),\ k \geq 0. \end{aligned} \tag{2}$$

Many applied problems in Science and Engineering are reduced to solve numerically the system $F(x) = 0$ of nonlinear equations (see, for example [1–6]). A plethora of iterative methods are developed in literature for solving such equations. A classical method is cubically convergent Chebyshev's method (see [7])

$$\begin{aligned} &x^{(0)} \in D, \\ &x^{(k+1)} = x^{(k)} - \Big(I + \frac{1}{2}L_F(x^{(k)})\Big)F'(x^{(k)})^{-1}F(x^{(k)}),\ k \geq 0, \end{aligned} \tag{3}$$

where $L_F(x^{(k)}) = F'(x^{(k)})^{-1}F''(x^{(k)})F'(x^{(k)})^{-1}F(x^k)$. This one-point iterative scheme depends explicitly on the first two derivatives of F. In [7], Ezquerro and Hernández present modification in Chebyshev's method that avoids the computation of second derivative F'' while maintaining third-order of convergence. It has the following form:

$$\begin{aligned} &x^{(0)} \in D, \\ &y^{(k)} = x^{(k)} - a\,F'(x^{(k)})^{-1}F(x^{(k)}), \\ &x^{(k+1)} = x^{(k)} - \frac{1}{a^2}F'(x^{(k)})^{-1}\big((a^2+a-1)F(x^{(k)}) + F(y^{(k)})\big),\ k \geq 0. \end{aligned} \tag{4}$$

There is an interest in constructing derivative free iterative processes obtained by considering an approximation of the first derivative of F from a divided difference of first order. One class of such methods is called the class of Secant-type methods which is obtained by replacing F' with the divided difference operator $[x^{(k-1)}, x^{(k)}; F]$. Using this operator a family of derivative free methods is given in [8]. The authors call this family the Chebyshev-Secant-type method and it is defined as

$$\begin{aligned} &x^{(-1)},\ x^{(0)} \in D, \\ &y^{(k)} = x^{(k)} - a\,[x^{(k-1)}, x^{(k)}; F]^{-1}F(x^{(k)}), \\ &x^{(k+1)} = x^{(k)} - [x^{(k-1)}, x^{(k)}; F]^{-1}\big(b\,F(x^{(k)}) + c\,F(y^{(k)})\big),\ k \geq 0, \end{aligned} \tag{5}$$

where a, b and c are non-negative parameters.

Another class of derivative free methods is the class of Steffensen-type processes that replaces F' with operator $[w(x^{(k)}), x^{(k)}; F]$, wherein $w : \mathbb{R}^m \to \mathbb{R}^m$. The work presented in [9] analyzes Steffensen-type iterative method which is given as

$$\begin{aligned} &x^{(0)} \in D, \\ &y^{(k)} = x^{(k)} - a\,[w(x^{(k)}), x^{(k)}; F]^{-1}F(x^{(k)}), \\ &x^{(k+1)} = x^{(k)} - [w(x^{(k)}), x^{(k)}; F]^{-1}\big(b\,F(x^{(k)}) + c\,F(y^{(k)})\big),\ k \geq 0. \end{aligned} \tag{6}$$

For $a = b = c = 1$ and $w(x^{(k)}) = x^{(k)} + \beta F(x^{(k)})$, β is an arbitrary non-zero constant, this method possesses third order convergence. In this case $y^{(k)}$ is Traub-Steffensen iteration [6]. For $\beta = 1$, $y^{(k)}$ belongs to Steffensen iteration [10]. Both of these iterations are quadratically convergent.

The two-step third order Traub-Steffensen-type method, i.e., the case of (6) for $a = b = c = 1$, can be written as

$$\begin{aligned} &x^{(0)} \in D,\ w(x^{(k)}) = x^{(k)} + \beta F(x^{(k)}), \\ &y^{(k)} = \mathrm{M}_{2,1}(x^{(k)}), \\ &x^{(k+1)} = \mathrm{M}_{3,1}(x^{(k)}, y^{(k)}) = y^{(k)} - [w(x^{(k)}), x^{(k)}; F]^{-1}F(y^{(k)}),\ k \geq 0, \end{aligned} \tag{7}$$

where $\mathrm{M}_{2,1}(x^{(k)}) = x^{(k)} - [w(x^{(k)}), x^{(k)}; F]^{-1}F(x^{(k)})$ is the quadratically convergent Traub-Steffensen scheme. Here and in the sequel, the symbol $\mathrm{M}_{p,i}$ is used for denoting an i-th iteration function of convergence order p. It can be observed that the third order scheme (7) is computationally more efficient than quadratically convergent Traub-Steffensen scheme. The reason is that the convergence order is increased from two to three at the cost of only one function evaluation without adding extra inverse operator. We discuss computational efficiency in later sections.

Researchers have always been trying to develop the iterative method with increasing efficiency since different methods converge to the solution with different convergence speed. This can be done either by increasing the convergence order or by decreasing the computational cost or both. In [11], Ren et al. have derived a fourth order derivative-free method that uses three F, three divided differences and two matrix inversions per iteration. Zheng et al. [12] have constructed two families of fourth order derivative-free methods for scalar nonlinear equations, that are extendable to solve systems of nonlinear equations. First family requires to evaluate three F, three divided differences and two matrix inversions, whereas the second family needs three F, three divided differences and three matrix inversions. Grau et al. presented a fourth order derivative-free method in [13] utilizing four F, two divided differences and two matrix inversions. Sharma and Arora [14] presented a fourth order derivative-free method that uses the evaluations of three F, three divided differences and one matrix inversion per each step.

In search of more fast techniques, researchers have also introduced sixth and seventh order derivative-free methods in [13,15–18]. The sixth order method in [13] proposed by Grau et al. requires five F, two divided differences and two matrix inverses. Sharma and Arora [17] also developed a method of at least sixth order which requires evaluation of five functions, two divided difference and one matrix inversion per iteration. The seventh order method proposed by Sharma and Arora [15] utilizes four F, five divided differences and two matrix inversions per iteration. The seventh order methods presented by Wang and Zhang [16] use four F, five divided differences and three matrix inversions. Ahmad et al. [18] proposed eighth order derivative free method without memory which uses six functions evaluations, three divided difference and one matrix inversion.

The main goal in this study is to develop a derivative-free method of high computational efficiency, that means a method with high convergence speed and low computational cost. Consequently, we present a Traub-Steffensen-type method of fifth order of convergence which requires the evaluations four F, two divided differences and only one matrix inversion per step. The scheme of the present contribution is simple and consists of three steps. Of the three steps, the first two are that of cubically convergent Traub-Steffensen-type scheme (7) whereas the third is derivative-free modification of Chebyshev's scheme (3). We show that the proposed method is more efficient than existing methods of similar nature.

The content of the rest of the paper is summarized as follows. Basic definitions relevant to the present work are stated in Section 2. In Section 3, the scheme of fifth order method is introduced and its convergence behavior is studied. In Section 4, the computational efficiency of the new method is examined and also compared with the existing derivative-free methods. In Section 5, the basins of attractors are presented to check the stability and convergence of the new method. Numerical tests are performed in Section 6 to verify the theoretical results as proved in Sections 3 and 4. Section 7 contains the concluding remarks.

2. Preliminary Results

2.1. Computational Order of Convergence

Let α be a solution of the function $F(x) = 0$ and $x^{(k-2)}$, $x^{(k-1)}$, $x^{(k)}$ and $x^{(k+1)}$ be the four consecutive iterations close to α. Then, the computational order of convergence (say, p_c) can be calculated using the formula (see [19])

$$p_c = \frac{\log(\|x^{(k+1)} - x^{(k)}\|/\|x^{(k)} - x^{(k-1)}\|)}{\log(\|x^{(k)} - x^{(k-1)}\|/\|x^{(k-1)} - x^{(k-2)}\|)}. \tag{8}$$

2.2. Divided Difference

Divided difference operator for multivariable function F (see [4,5,20]) is a mapping $[\cdot,\cdot\,;F] : D \times D \subset \mathbb{R}^m \times \mathbb{R}^m \rightarrow L(\mathbb{R}^m)$ which is defined as

$$[x,y;F](x-y) = F(x) - F(y), \forall\,(x,y)\;\in \mathbb{R}^m. \tag{9}$$

If F is differentiable, we can also define first order divided difference as (see [4,20])

$$[x+h,x\,;F] = \int_0^1 F'(x+th)\,dt,\,\forall\,(x,h)\;\in \mathbb{R}^m. \tag{10}$$

This also implies that

$$[x,x\,;F] = F'(x). \tag{11}$$

It can be seen that the divided difference operator $[x,y\,;F]$ is an $m \times m$ matrix and the definitions (9) and (10) are equivalent (for details see [20]). For computational purpose the following definition (see [5]), is used

$$[x,y\,;F]_{ij} = \frac{f_i(x_1,.....,x_j,y_{j+1},.....,y_m) - f_i(x_1,.....,x_{j-1},y_j,.....,y_m)}{x_j - y_j},\;\; 1 \le i,j \le m. \tag{12}$$

2.3. Computational Efficiency

Computational efficiency of an iterative method for solving $F(x) = 0$ is calculated by the efficiency index $E = p^{1/C}$, (for detail see [21,22]), where p is the order of convergence and C is the total cost of computation. The cost of computation C is measured in terms of the total number of function evaluations per iteration and the number of operations (that means products and quotients) per iteration.

3. The Method and Analysis of Convergence

Let us begin with the following three-step scheme

$$\begin{aligned} y^{(k)} &= \mathrm{M}_{2,1}(x^{(k)}),\\ z^{(k)} &= y^{(k)} - [w^{(k)},x^{(k)}\,;F]^{-1}F(y^{(k)}),\\ x^{(k+1)} &= z^{(k)} - \Big(I + \frac{1}{2}L_F(y^{(k)})\Big)F'(y^{(k)})^{-1}F(z^{(k)}), \end{aligned} \tag{13}$$

where $w^{(k)} = x^{(k)} + \beta F(x^{(k)})$, I is $m \times m$ identity matrix and $L_F(y^{(k)}) = F'(y^{(k)})^{-1}F''(y^{(k)})F'(y^{(k)})^{-1}F(y^k)$.

Note that this is a scheme whose first two steps are that of third order Traub-Steffensen-type method (7) whereas third step is based on Chebyshev's method (3). The scheme requires first and second derivatives of F at $y^{(k)}$. To make this a derivative-free method, we describe an approach as follows:

Consider the Taylor expansion of $F(z^{(k)})$ about $y^{(k)}$,

$$F(z^{(k)}) \approx F(y^{(k)}) + F'(y^{(k)})(z^{(k)} - y^{(k)}) + \frac{1}{2}F''(y^{(k)})(z^{(k)} - y^{(k)})^2. \tag{14}$$

Then, it follows that

$$\frac{1}{2}F''(y^{(k)})(z^{(k)} - y^{(k)})^2 \approx F(z^{(k)}) - F(y^{(k)}) - F'(y^{(k)})(z^{(k)} - y^{(k)}). \tag{15}$$

Using the fact that

$$F(z^{(k)}) - F(y^{(k)}) = [z^{(k)}, y^{(k)}; F](z^{(k)} - y^{(k)}),$$

(see, for example [4,5]), we can write (15) as

$$F''(y^{(k)})(z^{(k)} - y^{(k)}) \approx 2\big([z^{(k)}, y^{(k)}; F] - F'(y^{(k)})\big). \tag{16}$$

Then, using the second step of (13) in the above equation, it follows that

$$F''(y^{(k)})[w^{(k)}, x^{(k)}; F]^{-1}F(y^{(k)}) \approx -2\big([z^{(k)}, y^{(k)}; F] - F'(y^{(k)})\big). \tag{17}$$

Let us assume $F'(y^{(k)}) \approx [w^{(k)}, x^{(k)}; F]$, then (17) implies

$$F''(y^{(k)})[w^{(k)}, x^{(k)}; F]^{-1}F(y^{(k)}) \approx -2\big([z^{(k)}, y^{(k)}; F] - [w^{(k)}, x^{(k)}; F]\big). \tag{18}$$

In addition, we have that

$$\begin{aligned} L_F(y^{(k)}) &= F'(y^{(k)})^{-1}F''(y^{(k)})F'(y^{(k)})^{-1}F(y^k) \\ &\approx [w^{(k)}, x^{(k)}; F]^{-1}F''(y^{(k)})[w^{(k)}, x^{(k)}; F]^{-1}F(y^k). \end{aligned} \tag{19}$$

Using (18) in (19), we obtain that

$$\begin{aligned} L_F(y^{(k)}) &\approx [w^{(k)}, x^{(k)}; F]^{-1}F''(y^{(k)})[w^{(k)}, x^{(k)}; F]^{-1}F(y^k) \\ &\approx -2\big([w^{(k)}, x^{(k)}; F]^{-1}[z^{(k)}, y^{(k)}; F] - I\big). \end{aligned} \tag{20}$$

Now, we can write the third-step of (13) in modified form as

$$x^{(k+1)} = z^{(k)} - \big(2I - [w^{(k)}, x^{(k)}; F]^{-1}[z^{(k)}, y^{(k)}; F]\big)[w^{(k)}, x^{(k)}; F]^{-1}F(z^{(k)}). \tag{21}$$

Thus, we define the following new method:

$$\begin{aligned} y^{(k)} &= \mathrm{M}_{2,1}(x^{(k)}), \\ z^{(k)} &= \mathrm{M}_{3,1}(x^{(k)}, y^{(k)}), \\ x^{(k+1)} &= z^{(k)} - H(x^{(k)})[w^{(k)}, x^{(k)}; F]^{-1}F(z^{(k)}), \end{aligned} \tag{22}$$

wherein $H(x^{(k)}) = 2I - [w^{(k)}, x^{(k)}; F]^{-1}[z^{(k)}, y^{(k)}; F]$.

Since the scheme (22) is composed of Traub-Steffensen like steps, we call it the Traub-Steffensen-like method.

In order to explore the convergence properties of Traub-Steffensen-like method, we recall some important results from the theory of iteration functions. First, we state the following well-known result (see [3,23]):

Lemma 1. *Assume that $M : D \subset \mathbb{R}^m \to \mathbb{R}^m$ has a fixed point $\alpha \in int(D)$ and $M(x)$ is Fréchet differentiable on α. If*

$$\rho(M'(\alpha)) = \sigma < 1, \tag{23}$$

then α is a point of attraction for the iteration $x^{(k+1)} = M(x^{(k)})$, where ρ is a spectral radius of $M'(\alpha)$.

Next, we state a result which has been proven in [24] by Madhu et al. and that shows α is a point of attraction for a general iteration function of the form $M(x) = P(x) - Q(x)R(x)$.

Lemma 2. *Let $F : D \subset \mathbb{R}^m \to \mathbb{R}^m$ be sufficiently Fréchet differentiable at each point of an open convex set D of $\alpha \in D$, which is a solution of the nonlinear system $F(x) = 0$. Suppose that P, Q, $R : D \subset \mathbb{R}^m \to \mathbb{R}^m$ are sufficiently Fréchet differentiable functions (depending on F) at each point in the set D with the properties $P(\alpha) = \alpha$, $Q(\alpha) \neq 0$, $R(\alpha) = 0$. Then, there exists a ball*

$$S = \bar{S}(\alpha, \epsilon) = \{\|\alpha - x\| \leq \epsilon\} \subset D, \, \epsilon > 0,$$

on which the mapping

$$M : S \to \mathbb{R}^m, \, M(x) = P(x) - Q(x)R(x), \forall \, x \in S$$

is well defined. Moreover, $M(x)$ is Fréchet differentiable at α, thus

$$M'(\alpha) = P'(\alpha) - Q(\alpha)R'(\alpha).$$

Let us also recall the definition (10) of divided difference operator. Then, expanding $F'(x+th)$ in (10) by Taylor series at the point x and thereafter integrating, we have that

$$[x+h, x\,; F] = \int_0^1 F'(x+th)\, dt = F'(x) + \frac{1}{2}F''(x)h + \frac{1}{6}F'''(x)h^2 + \frac{1}{24}F^{(iv)}(x)h^3 + O(h^4), \tag{24}$$

where $h^i = (h, h, \overset{i}{\cdots}, h), h \in \mathbb{R}^m$. Let $e^{(k)} = x^{(k)} - \alpha$. Assuming that $\Gamma = F'(\alpha)^{-1}$ exists, then expanding $F(x^{(k)})$ and its first three derivatives in a neighborhood of α by Taylor's series, we have that

$$F(x^{(k)}) = F'(\alpha)\big(e^{(k)} + A_2(e^{(k)})^2 + A_3(e^{(k)})^3 + A_4(e^{(k)})^4 + A_5(e^{(k)})^5 + O((e^{(k)})^6)\big), \tag{25}$$

$$F'(x^{(k)}) = F'(\alpha)\big(I + 2A_2e^{(k)} + 3A_3(e^{(k)})^2 + 4A_4(e^{(k)})^3 + 5A_5(e^{(k)})^4 + O((e^{(k)})^5)\big), \tag{26}$$

$$F''(x^{(k)}) = F'(\alpha)\big(2A_2 + 6A_3e^{(k)} + 12A_4(e^{(k)})^2 + 20A_5(e^{(k)})^3 + O((e^{(k)})^4)\big) \tag{27}$$

and

$$F'''(x^{(k)}) = F'(\alpha)\big(6A_3 + 24A_4e^{(k)} + 60A_5(e^{(k)})^2 + O((e^{(k)})^3)\big), \tag{28}$$

where $A_i = \frac{1}{i!}\Gamma F^{(i)}(\alpha) \in L_i(\mathbb{R}^m, \mathbb{R}^m)$ and $(e^{(k)})^i = (e^{(k)}, e^{(k)}, \overset{i-times}{\cdots\cdots}, e^{(k)})$, $e^{(k)} \in \mathbb{R}^m$.

We are in a situation to analyze the behavior of Traub-Steffensen-like method. Thus, the following theorem is proved:

Theorem 1. *Let $F : D \subset \mathbb{R}^m \to \mathbb{R}^m$ be sufficiently Fréchet differentiable at each point of an open convex set D of $\alpha \in \mathbb{R}^m$, which is a solution of $F(x) = 0$. Assume that $x \in S = \bar{S}(\alpha, \epsilon)$ and $F'(x)$ is continuous and nonsingular at α, and $x^{(0)}$ close to α. Then, α is a point of attraction of the sequence $\{x^{(k)}\}$ generated by the Traub-Steffensen-like method (22). Furthermore, the sequence so developed converges locally to α with order at least 5.*

Proof. First we show that α is a point of attraction of Traub-Steffensen-like iteration. In this case, we have that

$$P(x) = z(x), \;\; Q(x) = H(x)[w, x\,; F]^{-1}, \;\; R(x) = F(z(x)).$$

Now, since $F(\alpha) = 0$, $\;\; [\alpha, \alpha\,; F] = F'(\alpha) \neq O$, we have

$$y(\alpha) = \alpha - [\alpha, \alpha\,; F]^{-1}F(\alpha) = \alpha - F'(\alpha)^{-1}F(\alpha) = \alpha,$$

$$z(\alpha) = \alpha - [\alpha, \alpha\,; F]^{-1}F(\alpha) - [\alpha, \alpha\,; F]^{-1}F(\alpha) = \alpha - F'(\alpha)^{-1}F(\alpha) - F'(\alpha)^{-1}F(\alpha) = \alpha,$$

$$H(\alpha) = 2I - [\alpha, \alpha\,; F]^{-1}[\alpha, \alpha\,; F] = I,$$

$$P(\alpha) = z(\alpha), \, P'(\alpha) = z'(\alpha),$$

$$Q(\alpha) = H(\alpha)[\alpha, \alpha\,; F]^{-1} = I\,[\alpha, \alpha\,; F]^{-1} = [\alpha, \alpha\,; F]^{-1} = F'(\alpha)^{-1} \neq O,$$
$$R(\alpha) = F(z(\alpha)) = F(\alpha) = 0,$$
$$R'(\alpha) = F'(z(\alpha))z'(\alpha) = F'(\alpha)z'(\alpha),$$
$$M'(\alpha) = P'(\alpha) - Q(\alpha)R'(\alpha) = z'(\alpha) - F'(\alpha)^{-1}F'(\alpha)z'(\alpha) = O,$$

so that $\rho(M'(\alpha)) = 0 < 1$ and by Lemma 1, α is a point of attraction of (22).

Let $e_w^{(k)} = w^{(k)} - \alpha = x^{(k)} + \beta F(x^{(k)}) - \alpha = e^{(k)} + \beta F(x^{(k)})$. Then using (25), it follows that

$$e_w^{(k)} = (I + \beta F'(\alpha))e^{(k)} + \beta F'(\alpha)\big((A_2(e^{(k)})^2 + A_3(e^{(k)})^3) + O((e^{(k)})^4\big). \tag{29}$$

Setting $x + h = w^{(k)}$, $x = x^{(k)}$, $h = e_w^{(k)} - e^{(k)}$ in Equation (24) and then using (26)–(29), we can write

$$\begin{aligned}[w^{(k)}, x^{(k)}\,; F] = F'(\alpha)\big(I + X_1A_2e^{(k)} + (\lambda A_2^2 + X_2A_3)(e^{(k)})^2 + X_1(2\lambda A_2A_3 \\ + X_3A_4)(e^{(k)})^3 + O((e^{(k)})^4)\big),\end{aligned} \tag{30}$$

where $\lambda = \beta F'(\alpha)$, $X_1 = \lambda + 2$, $X_2 = \lambda^2 + 3\lambda + 3$ and $X_3 = \lambda^2 + 2\lambda + 2$.

Expansion of the inverse of preceding divided difference operator is given as

$$\begin{aligned}[w^{(k)}, x^{(k)}\,; F]^{-1} = \big(I - X_1A_2(e^{(k)}) + ((1 + X_2)A_2^2 - X_2A_3)(e^{(k)})^2 - X_1((2 + X_3)A_2^3 \\ - 2(1 + X_3)A_2A_3 + X_3A_4)(e^{(k)})^3 + O((e^{(k)})^3)\big)\Gamma.\end{aligned} \tag{31}$$

By using (25) and (31) in the first step of method (22), we get

$$e_y^{(k)} = y^{(k)} - \alpha = (-1 + X_1)A_2(e^{(k)})^2 - (X_3A_2^2 + (1 - X_2)A_3)(e^{(k)})^3 + O((e^{(k)})^4). \tag{32}$$

Taylor expansion of $F(y^k)$ about α yields,

$$F(y^{(k)}) = F'(\alpha)\big(e_y^{(k)} + A_2(e_y^{(k)})^2 + O((e_y^{(k)})^3)\big). \tag{33}$$

From the second step of (22), on using (31) and (33), it follows that

$$\begin{aligned}e_z^{(k)} &= z^{(k)} - \alpha \\ &= X_1A_2(e^{(k)})e_y^{(k)} - A_2(e_y^{(k)})^2 - ((1 + X_2)A_2^2 - X_2A_3)(e^{(k)})^2e_y^{(k)} + O((e^{(k)})^5).\end{aligned} \tag{34}$$

By Taylor expansion of $F(z^k)$ about α,

$$F(z^{(k)}) = F'(\alpha)\big(e_z^{(k)} + A_2(e_z^{(k)})^2 + O((e_z^{(k)})^3)\big). \tag{35}$$

Equation (24), for $x + h = z^{(k)}$, $x = y^{(k)}$ and $h = e_z^{(k)} - e_y^{(k)}$, yields

$$\begin{aligned}[z^{(k)}, y^{(k)}\,; F] &= F'(\alpha)\big(I + A_2(e_z^{(k)} + e_y^{(k)}) + O((e^{(k)})^3)\big) \\ &= F'(\alpha)\big(I + (\lambda + 1)A_2^2(e^{(k)})^2 + O((e^{(k)})^3)\big).\end{aligned} \tag{36}$$

From (31) and (36), we have

$$\begin{aligned}H(x^{(k)}) &= 2I - [w^{(k)}, x^{(k)}\,; F]^{-1}[z^{(k)}, y^{(k)}\,; F] \\ &= I + X_1A_2e^{(k)} + \big(X_2A_3 - (X_1 + X_2)A_2^2\big)(e^{(k)})^2 + O((e^{(k)})^3).\end{aligned} \tag{37}$$

Equations (31) and (37) yield

$$H(x^{(k)})[w^{(k)}, x^{(k)}; F]^{-1} = \big(I - (\lambda^2 + 5\lambda + 5)A_2^2(e^{(k)})^2 + O((e^{(k)})^3)\big)\Gamma. \tag{38}$$

Applying Equations (34), (35) and (38) in the last step of method (22) and then simplifying, we get the error equation

$$e^{(k+1)} = (\lambda + 1)(\lambda + 2)(\lambda^2 + 5\lambda + 5)A_2^4(e^{(k)})^5 + O((e^{(k)})^6). \tag{39}$$

This completes the proof of Theorem 1. □

Thus, the Traub-Steffensen-like method (22) defines a one-parameter (β) family of derivative-free fifth order methods. Now onwards we denote it by $\mathrm{M}_{5,1}$. In terms of computational cost $\mathrm{M}_{5,1}$ utilizes four functions, two divided difference and one matrix inversion per each step. In the next section we will compare the computational efficiency of the new method with the existing derivative-free methods.

4. Computational Efficiency

In order to find the computational efficiency we will use the definition given in Section 2.3. The various evaluations and arithmetic operations that contribute towards the cost of computation are described as follows. For the computation of F in any iterative function we evaluate m scalar functions f_i, $(1 \leq i \leq m)$ and when computing a divided difference $[x, y; F]$ (see, Section 2.2) we evaluate $m(m-1)$ scalar functions, wherein $F(x)$ and $F(y)$ are evaluated separately. Furthermore, one has to add m^2 divisions from any divided difference. For the computation of inverse linear operator, a linear system can be solved that requires $m(m-1)(2m-1)/6$ products and $m(m-1)/2$ divisions in the LU decomposition process, and $m(m-1)$ products and m divisions in the resolution of two triangular linear systems. Moreover, we add m products for the multiplication of a vector by a scalar and m^2 products for multiplying a matrix by a vector or of a matrix by a scalar.

The comparison of computational efficiency of the present method $\mathrm{M}_{5,1}$ is drawn with second order method $\mathrm{M}_{2,1}$; third order method $\mathrm{M}_{3,1}$; fourth order methods by Ren et al. [11], Grau et al. [13] and Sharma-Arora [14]; fifth order method by Kumar et al. [25]; sixth order method by Grau et al. [13]; seventh order methods by Sharma-Arora [15] and Wang-Zhang [16]. These methods are expressed as follows:

Fourth order method by Ren et al. ($\mathrm{M}_{4,1}$):

$$\begin{aligned} y^{(k)} &= x^{(k)} - [u^{(k)}, x^{(k)}; F]^{-1}F(x^{(k)}), \\ x^{(k+1)} &= y^{(k)} - \big([y^{(k)}, x^{(k)}; F] + [y^{(k)}, u^{(k)}; F] - [u^{(k)}, x^{(k)}; F]\big)^{-1}F(y^{(k)}), \end{aligned}$$

where $u^{(k)} = x^{(k)} + F(x^{(k)})$.

Fourth order method by Grau et al. ($\mathrm{M}_{4,2}$):

$$\begin{aligned} y^{(k)} &= x^{(k)} - [u^{(k)}, v^{(k)}; F]^{-1}F(x^{(k)}) \\ x^{(k+1)} &= y^{(k)} - \big(2[y^{(k)}, x^{(k)}; F] - [u^{(k)}, v^{(k)}; F]\big)^{-1}F(y^{(k)}), \end{aligned}$$

where $u = x + F(x)$ and $v = x - F(x)$.

Sharma-Arora fourth order method ($\mathrm{M}_{4,3}$):

$$\begin{aligned} y^{(k)} &= x^{(k)} - [w^{(k)}, x^{(k)}; F]^{-1}F(x^{(k)}) \\ x^{(k+1)} &= y^{(k)} - \big(3I - [w^{(k)}, x^{(k)}; F]^{-1}([y^{(k)}, x^{(k)}; F] + [y^{(k)}, w^{(k)}; F])\big) \\ &\qquad \times [w^{(k)}, x^{(k)}; F]^{-1}F(y^{(k)}), \end{aligned}$$

where $w^{(k)} = x^{(k)} + \beta F(x^{(k)})$, β is a non-zero constant.

Fifth order method by Kumar et al. ($\mathrm{M}_{5,2}$):

$$\begin{aligned} y^{(k)} &= x^{(k)} - [w^{(k)}, x^{(k)}; F]^{-1} F(x^{(k)}) \\ z^{(k)} &= y^{(k)} - [w^{(k)}, x^{(k)}; F]^{-1} F(y^{(k)}) \\ x^{(k+1)} &= z^{(k)} - [x^{(k)}, y^{(k)}; F]^{-1} [w^{(k)}, x^{(k)}; F] [w^{(k)}, y^{(k)}; F]^{-1} F(z^{(k)}), \end{aligned}$$

where $w^{(k)} = x^{(k)} + F(x^{(k)})$.

Sixth order method by Grau et al. ($\mathrm{M}_{6,1}$):

$$\begin{aligned} y^{(k)} &= x^{(k)} - [u^{(k)}, v^{(k)}; F]^{-1} F(x^{(k)}) \\ z^{(k)} &= y^{(k)} - \big(2[y^{(k)}, x^{(k)}; F] - [u^{(k)}, v^{(k)}; F]\big)^{-1} F(y^{(k)}) \\ x^{(k+1)} &= z^{(k)} - \big(2[y^{(k)}, x^{(k)}; F] - [u^{(k)}, v^{(k)}; F]\big)^{-1} F(z^{(k)}). \end{aligned}$$

Wang-Zhang seventh order method ($\mathrm{M}_{7,1}$):

$$\begin{aligned} y^{(k)} &= x^{(k)} - [u^{(k)}, x^{(k)}; F]^{-1} F(x^{(k)}), \\ z^{(k)} &= y^{(k)} - \big([y^{(k)}, x^{(k)}; F] + [y^{(k)}, u^{(k)}; F] - [u^{(k)}, x^{(k)}; F]\big)^{-1} F(y^{(k)}) \\ x^{(k+1)} &= z^{(k)} - \big([z^{(k)}, x^{(k)}; F] + [z^{(k)}, y^{(k)}; F] - [y^{(k)}, x^{(k)}; F]\big)^{-1} F(z^{(k)}), \end{aligned}$$

where $u^{(k)} = x^{(k)} + F(x^{(k)})$.

Sharma-Arora seventh order method ($\mathrm{M}_{7,2}$):

$$\begin{aligned} y^{(k)} &= x^{(k)} - [w^{(k)}, x^{(k)}; F]^{-1} F(x^{(k)}) \\ z^{(k)} &= y^{(k)} - \big(3I - [w^{(k)}, x^{(k)}; F]^{-1}([y^{(k)}, x^{(k)}; F] + [y^{(k)}, w^{(k)}; F])\big) \\ &\qquad \times [w^{(k)}, x^{(k)}; F]^{-1} F(y^{(k)}) \\ x^{(k+1)} &= z^{(k)} - [z^{(k)}, y^{(k)}; F]^{-1}\big([w^{(k)}, x^{(k)}; F] + [y^{(k)}, x^{(k)}; F] - [z^{(k)}, x^{(k)}; F]\big) \\ &\qquad \times [w^{(k)}, x^{(k)}; F]^{-1} F(z^{(k)}). \end{aligned}$$

Let us denote efficiency indices of the methods $\mathrm{M}_{p,i}$ by $\mathrm{E}_{p,i}$ and their computational costs by $\mathrm{C}_{p,i}$. Then, using the definition of the Section 2.3 taking into account the above considerations of evaluations and operations, we have that

$$\mathrm{C}_{2,1} = \frac{1}{3}m^3 + 3m^2 + \frac{2}{3}m \quad \text{and} \quad \mathrm{E}_{2,1} = 2^{1/C_{2,1}}. \tag{40}$$

$$\mathrm{C}_{3,1} = \frac{1}{3}m^3 + 4m^2 + \frac{5}{3}m \quad \text{and} \quad \mathrm{E}_{3,1} = 3^{1/C_{3,1}}. \tag{41}$$

$$\mathrm{C}_{4,1} = \frac{2}{3}m^3 + 8m^2 - \frac{2}{3}m \quad \text{and} \quad \mathrm{E}_{4,1} = 4^{1/C_{4,1}}. \tag{42}$$

$$\mathrm{C}_{4,2} = \frac{2}{3}m^3 + 7m^2 + \frac{4}{3}m \quad \text{and} \quad \mathrm{E}_{4,2} = 4^{1/C_{4,2}}. \tag{43}$$

$$\mathrm{C}_{4,3} = \frac{1}{3}m^3 + 10m^2 + \frac{2}{3}m \quad \text{and} \quad \mathrm{E}_{4,3} = 4^{1/C_{4,3}}. \tag{44}$$

$$\mathrm{C}_{5,1} = \frac{1}{3}m^3 + 9m^2 + \frac{8}{3}m \quad \text{and} \quad \mathrm{E}_{5,1} = 5^{1/C_{5,1}}. \tag{45}$$

$$\mathrm{C}_{5,2} = m^3 + 11m^2 \quad \text{and} \quad \mathrm{E}_{5,2} = 5^{1/C_{5,2}}. \tag{46}$$

$$\mathrm{C}_{6,1} = \frac{2}{3}m^3 + 8m^2 + \frac{7}{3}m \quad \text{and} \quad \mathrm{E}_{6,1} = 6^{1/C_{6,1}}. \tag{47}$$

$$C_{7,1} = m^3 + 13m^2 - 2m \quad \text{and} \quad E_{7,1} = 7^{1/C_{7,1}}. \tag{48}$$

$$C_{7,2} = \frac{2}{3}m^3 + 17m^2 - \frac{2}{3}m \quad \text{and} \quad E_{7,2} = 7^{1/C_{7,2}}. \tag{49}$$

To compare the efficiency of considered iterative methods, say $M_{p,i}$ against $M_{q,j}$, we consider the ratio

$$R_{p,i;q,j} = \frac{\log E_{p,i}}{\log E_{q,j}} = \frac{C_{q,j}\log(p)}{C_{p,i}\log(q)}. \tag{50}$$

It is clear that when $R_{p,i;q,j} > 1$, the iterative method $M_{p,i}$ is more efficient than $M_{q,j}$.

$M_{3,1}$ *versus* $M_{2,1}$ *case*:

For this case the ratio (50) is given by

$$R_{3,1;2,1} = \frac{\left(\frac{1}{3}m^3 + 3m^2 + \frac{2}{3}m\right)\log(3)}{\left(\frac{1}{3}m^3 + 4m^2 + \frac{5}{3}m\right)\log(2)}.$$

It can be easily shown that $R_{3,1;2,1} > 1$ for $m \geq 2$. This implies that $E_{3,1} > E_{2,1}$ for $m \geq 2$. Thus, $M_{3,1}$ is more efficient than $M_{2,1}$ as we have stated in the introduction section.

$M_{5,1}$ *versus* $M_{2,1}$ *case*:

The ratio (50) is given by

$$R_{5,1;2,1} = \frac{\left(\frac{1}{3}m^3 + 3m^2 + \frac{2}{3}m\right)\log(5)}{\left(\frac{1}{3}m^3 + 9m^2 + \frac{8}{3}m\right)\log(2)}.$$

It is easy to prove that $R_{5,1;2,1} > 1$ for $m \geq 6$. Thus, we conclude that $E_{5,1} > E_{2,1}$ for $m \geq 6$.

$M_{5,1}$ *versus* $M_{3,1}$ *case*:

The ratio (50) is given by

$$R_{5,1;3,1} = \frac{\left(\frac{1}{3}m^3 + 4m^2 + \frac{5}{3}m\right)\log(5)}{\left(\frac{1}{3}m^3 + 9m^2 + \frac{8}{3}m\right)\log(3)}.$$

It can be checked that $R_{5,1;3,1} > 1$ for $m \geq 21$. Thus, we have that $E_{5,1} > E_{3,1}$ for $m \geq 21$.

$M_{5,1}$ *versus* $M_{4,1}$ *case*:

In this case the ratio

$$R_{5,1;4,1} = \frac{\left(\frac{2}{3}m^3 + 8m^2 - \frac{2}{3}m\right)\log(5)}{\left(\frac{1}{3}m^3 + 9m^2 + \frac{8}{3}m\right)\log(4)} > 1,$$

for $m \geq 3$, which implies that $E_{5,1} > E_{4,1}$ for $m \geq 3$.

$M_{5,1}$ *versus* $M_{4,2}$ *case*:

Here the ratio

$$R_{5,1;4,2} = \frac{\left(\frac{2}{3}m^3 + 7m^2 + \frac{4}{3}m\right)\log(5)}{\left(\frac{1}{3}m^3 + 9m^2 + \frac{8}{3}m\right)\log(4)} > 1,$$

for $m \geq 3$ which implies that $E_{5,1} > E_{4,2}$ for $m \geq 3$.

$M_{5,1}$ *versus* $M_{4,3}$ *case*:

Here the ratio

$$R_{5,1;4,3} = \frac{\left(\frac{1}{3}m^3 + 10m^2 + \frac{2}{3}m\right)\log(5)}{\left(\frac{1}{3}m^3 + 9m^2 + \frac{8}{3}m\right)\log(4)} > 1,$$

for $m \geq 2$ which implies that $\mathrm{E}_{5,1} > \mathrm{E}_{4,3}$ for $m \geq 2$.

$\mathrm{M}_{5,1}$ *versus* $\mathrm{M}_{5,2}$ *case*:

In this case the ratio

$$\mathrm{R}_{5,1;5,2} = \frac{m^3 + 11m^2}{\frac{1}{3}m^3 + 9m^2 + \frac{8}{3}m} > 1,$$

for $m \geq 2$ which means $\mathrm{E}_{5,1} > \mathrm{E}_{5,2}$ for $m \geq 2$.

$\mathrm{M}_{5,1}$ *versus* $\mathrm{M}_{6,1}$ *case*:

Here the ratio

$$\mathrm{R}_{5,1;6,1} = \frac{\left(\frac{2}{3}m^3 + 8m^2 + \frac{7}{3}m\right)\log(5)}{\left(\frac{1}{3}m^3 + 9m^2 + \frac{8}{3}m\right)\log(6)} > 1,$$

for $m \geq 8$ which means $\mathrm{E}_{5,1} > \mathrm{E}_{6,1}$ for $m \geq 8$.

$\mathrm{M}_{5,1}$ *versus* $\mathrm{M}_{7,1}$ *case*:

Here also the ratio

$$\mathrm{R}_{5,1;7,1} = \frac{\left(m^3 + 13m^2 - 2m\right)\log(5)}{\left(\frac{1}{3}m^3 + 9m^2 + \frac{8}{3}m\right)\log(7)} > 1,$$

for $m \geq 2$ which means $\mathrm{E}_{5,1} > \mathrm{E}_{7,1}$ for $m \geq 2$.

$\mathrm{M}_{5,1}$ *versus* $\mathrm{M}_{7,2}$ *case*:

Here also the ratio

$$\mathrm{R}_{5,1;7,2} = \frac{\left(\frac{2}{3}m^3 + 17m^2 - \frac{2}{3}m\right)\log(5)}{\left(\frac{1}{3}m^3 + 9m^2 + \frac{8}{3}m\right)\log(7)} > 1,$$

for $m \geq 2$ which means $\mathrm{E}_{5,1} > \mathrm{E}_{7,2}$ for $m \geq 2$.

The above results are summarized in the following theorem:

Theorem 2. *We have that*

(a) $E_{5,1} > E_{2,1}$ *for* $m \geq 6$.
(b) $E_{5,1} > E_{3,1}$ *for* $m \geq 21$.
(c) $\{E_{5,1} > E_{4,1}\ \ E_{5,1} > E_{4,2}\}$ *for* $m \geq 3$.
(d) $\{E_{3,1} > E_{2,1},\ E_{5,1} > E_{4,3},\ E_{5,1} > E_{5,2},\ E_{5,1} > E_{7,1},\ E_{5,1} > E_{7,2}\}$ *for* $m \geq 2$.
(e) $E_{5,1} > E_{6,1}$ *for* $m \geq 8$.

5. Complex Dynamics of Methods

Our aim is to analyze the complex dynamics of the new method based on graphical tool 'basins of attraction' of the zeros of polynomial $P(z)$ in complex plane. Visual display of the basins gives important information about the stability and convergence of iterative methods. This idea was introduced initially by Vrscay and Gilbert [26]. In recent times, many authors have used this concept in their work, see, for example [27,28] and references therein. We consider the method (22) to analyze the basins of attraction.

To start with we take the initial point z_0 in a rectangular region $R \in \mathbb{C}$ that contains all the zeros of a polynomial $P(z)$. The iterative method, when starting from point z_0 in a rectangle, either converges to the zero $P(z)$ or eventually diverges. Stopping condition for convergence is considered as 10^{-3} to a maximum of 25 iterations. If the required tolerance is not achieved in 25 iterations, we conclude that the iterative scheme starting at point z_0 does not converge to any root. The strategy adopted is as follows: A color is allocated to each initial point z_0 in the basin of attraction of a zero. If the iteration initiating at z_0 converges, then it represents the attraction basin with that assigned color to it, otherwise in the failing (divergence) situation in 25 iterations the iteration represents the black color.

We analyze the basins of attraction of the new method (for the choices $\beta = 10^{-2}$, 10^{-4}, 10^{-8}) on following three polynomials:

Example 1. *In the first case, consider the polynomial* $P_1(z) = z^2 - 1$ *which has zeros* $\{\pm 1\}$*. A grid of* 400×400 *points in a rectangle* $D \in \mathbb{C}$ *of size* $[-2, 2] \times [-2, 2]$ *is used for drawing the graphics. We assign the color red to each initial point in the basin of attraction of zero '1' and the color green to the points in the basin of attraction of zero '−1'. The graphics are shown in Figure 1 corresponding to* $\beta = 10^{-2}$, 10^{-4}, 10^{-8}*. Observing the behavior of the basins of the new method, we conclude that the convergence domain becoming wider as parameter* β *assumes smaller values since black zones (divergent points) are getting smaller in size.*

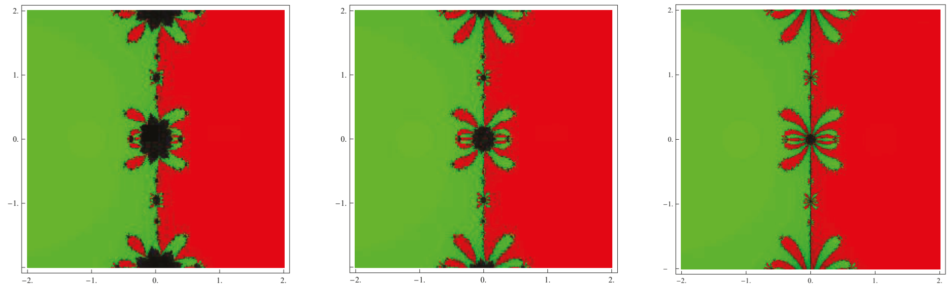

$\beta = 10^{-2}$ $\beta = 10^{-4}$ $\beta = 10^{-8}$

Figure 1. Basins of attraction for polynomial $P_1(z)$.

Example 2. *Let us consider the next polynomial as* $P_2(z) = z^3 - z$ *having zeros* $\{0, \pm 1\}$*. To draw the dynamical view, we select a rectangle* $D = [-2, 2] \times [-2, 2] \in \mathbb{C}$ *containing* 400×400 *grid points. Then, allocate the colors green, blue and red to each point in the basin of attraction of* 0, 1 *and* -1*, respectively. Basins for this example are exhibited in Figure 2 corresponding to parameter choices* $\beta = 10^{-2}$, 10^{-4}, 10^{-8} *in the proposed methods. In addition, observe that the basins are becoming larger and larger with the smaller values of* β*.*

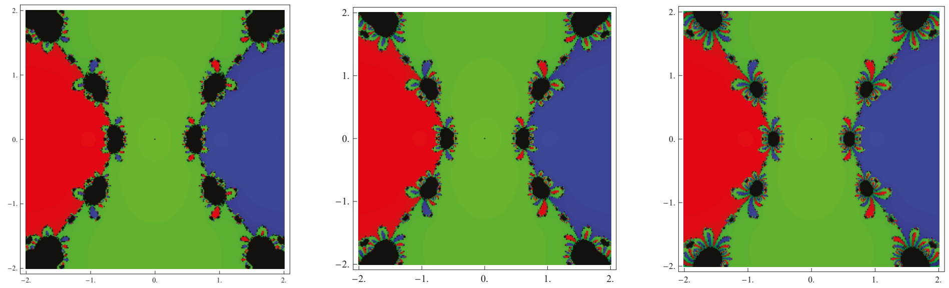

$\beta = 10^{-2}$ $\beta = 10^{-4}$ $\beta = 10^{-8}$

Figure 2. Basins of attraction for polynomial $P_2(z)$.

Example 3. *Lastly, we consider the polynomial as* $P_3(z) = z^5 + 2z - 1$ *having zeros* $\{-0.945068 \pm 0.854518i, 0.701874 \pm 0.879697i, 0.486389\}$*. To draw the dynamical view, we select a rectangle* $D = [-2, 2] \times [-2, 2] \in \mathbb{C}$ *containing* 400×400 *grid points. Then, allocate the colors green, blue, red, yellow and pink to each point in the basin of attraction of* $0.701874 + 0.879697i$, $-0.945068 - 0.854518i$, $0.701874 - 0.879697i$, 0.486389 *and* $-0.945068 + 0.854518i$*, respectively. Basins for this example are exhibited in Figure 3 corresponding to parameter choices* $\beta = 10^{-2}$, 10^{-4}, 10^{-8} *in the proposed methods. We observe that the basins are getting larger with the smaller values of* β*.*

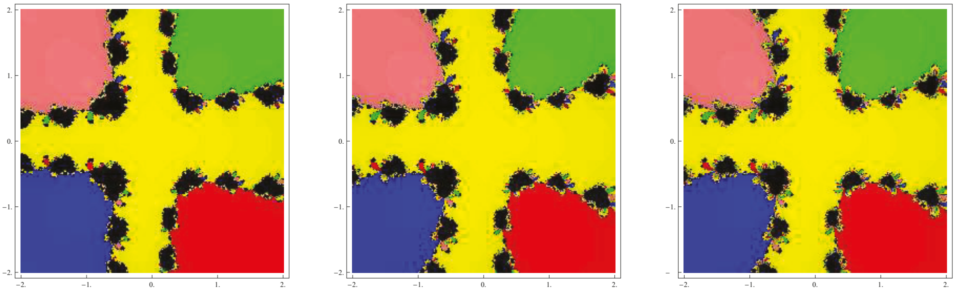

$\beta = 10^{-2}$ $\beta = 10^{-4}$ $\beta = 10^{-8}$

Figure 3. Basins of attraction for polynomial $P_3(z)$.

6. Numerical Tests

In this section, some numerical tests on different problems are performed to demonstrate the convergence behavior and computational efficiency of the method $M_{5,1}$. A comparison between the performance of $M_{5,1}$ with the existing methods $M_{2,1}$, $M_{3,1}$, $M_{4,j}$ $(j = 1, 2, 3)$, $M_{5,2}$, $M_{6,1}$, $M_{7,1}$ and $M_{7,2}$ is also drawn. The programs are performed in the processor with specifications Intel (R) Core (TM) i5-4210U CPU @ 1.70 GHz 2.40 GHz (64-bit Operating System) Microsoft Windows 10 Professional and are complied by *Mathematica* 10.0 using multiple-precision arithmetic. We record the number of iterations (k) required to converge to the solution such that the stopping condition

$$||x^{(k+1)} - x^{(k)}|| + ||F(x^{(k)})|| < 10^{-300}$$

is satisfied. In order to verify the theoretical order of convergence, the computational order of convergence (p_c) is obtained by using the Formula (8). In the comparison of performance of considered methods, we also include the real CPU time elapsed during the execution of program computed by the *Mathematica* command "TimeUsed[ ]".

The methods $M_{2,1}$, $M_{3,1}$, $M_{4,3}$, $M_{5,1}$ and $M_{7,2}$ are tested by using the value 0.01 for the parameter β. In numerical experiments we consider the following five problems:

Example 4. *Let us consider the system of two equations (selected from [29]):*

$$\begin{cases} x^2 + \sin x - e^y = 0, \\ 3x - \cos x - y = 0. \end{cases}$$

The initial guess assumed is $x^{(0)} = \{-1, -2\}^T$ *for obtaining the solution*

$$\alpha = \{-0.907430217073695 69\ldots, -3.3380632251862363\ldots\}^T.$$

Example 5. *Now considering the mixed Hammerstein integral equation (see [4]):*

$$x(s) = 1 + \frac{1}{5}\int_0^1 G(s,t)x(t)^3 dt,$$

wherein $x \in C[0,1]$; $s, t \in [0,1]$ *and the kernel G is*

$$G(s,t) = \begin{cases} (1-s)t, & t \le s, \\ s(1-t), & s \le t. \end{cases}$$

The above equation is transformed to a finite-dimensional problem by using the Gauss-Legendre quadrature formula

$$\int_0^1 f(t)dt \approx \sum_{j=1}^{m} \varpi_j f(t_j),$$

where the weights ϖ_j and abscissas t_j are obtained for $m = 8$ by Gauss-Legendre quadrature formula. Then, setting $x(t_i) = x_i$, $i = 1, 2, ..., 8$, we obtain the following system of nonlinear equations

$$5\, x_i - 5 - \sum_{j=1}^{8} a_{ij} x_j^3 = 0,$$

where

$$a_{ij} = \begin{cases} \varpi_j t_j (1 - t_i) & \text{if } j \le i, \\ \varpi_j t_i (1 - t_j) & \text{if } i < j, \end{cases} \qquad i = 1, 2, ...8.$$

wherein the abscissas t_j and the weights ϖ_j are known and produced in Table 1 for $m = 8$. The initial approximation assumed is

$$x^{(0)} = \{-1, -1, -1, -1, -1, -1, -1, -1\}^T$$

and the solution of this problem is:

$$\alpha = \{1.002096245031..., 1.009900316187..., 1.019726960993..., 1.026435743030..., \\ 1.026435743030..., 1.019726960993..., 1.009900316187..., 1.002096245031...\}^T.$$

Table 1. Weights and abscissas of Gauss-Legendre quadrature formula for $m = 8$.

j	t_j	ϖ_j
1	0.019855071751231884158219 57...	0.05061426814518812957626567...
2	0.10166676129318663020422303...	0.11119051722668723527217800...
3	0.23723379504183550709113047...	0.15685332293894364366898110...
4	0.40828267875217509753026193...	0.18134189168918099148257522...
5	0.59171732124782490246973807...	0.18134189168918099148257522...
6	0.76276620495816449290886952...	0.15685332293894364366898110...
7	0.89833323870681336979577696...	0.11119051722668723527217800...
8	0.98014492824876811584178043...	0.05061426814518812957626567...

Example 6. *Consider the system of 20 equations (see [29]):*

$$\tan^{-1}(x_i) + 1 - 2 \sum_{j=1, j \ne i}^{20} x_j^2 = 0, \quad 1 \le i \le 20,$$

This problem has the following two solutions:

$$\alpha_1 = \{0.1757683176158\ldots, 0.1757683176158\ldots, \cdot\cdot\cdot\cdot\cdot, 0.1757683176158\ldots\}^T.$$

and

$$\alpha_2 = \{-0.14968543422\ldots, -0.14968543422, \ldots, \cdot\cdot\cdot\cdot\cdot, -0.14968543422\ldots\}^T.$$

We intend to find the first solution and so choose the initial value: $x^{(0)} = \{0.5, 0.5, 0.5, \cdot\cdot\cdot\cdot\cdot, 0.5\}^T$.

Example 7. *Consider the boundary value problem:*

$$y'' + y^3 = 0, \quad y(0) = 0, \quad y(1) = 1.$$

Assuming the following partitioning of the interval $[0, 1]$*:*
$u_0 = 0 < u_1 < u_2 < \cdots < u_{n-1} < u_n = 1, \quad u_{j+1} = u_j + h, \quad h = 1/n.$

Setting $y_0 = y(u_0) = 0, y_1 = y(u_1), \cdots, y_{n-1} = y(u_{n-1}), y_n = y(u_n) = 1$. *If we discretize the problem by using the finite difference approximation for second derivative*

$$y''_m = \frac{y_{m-1} - 2y_m + y_{m+1}}{h^2}, \quad m = 1, 2, 3, \ldots, n-1,$$

we obtain a system of $n - 1$ *equations in* $n - 1$ *variables:*

$$y_{m-1} - 2y_m + y_{m+1} + h^2 y_m^3 = 0, \quad m = 1, 2, 3, \ldots, n-1.$$

In particular, let us solve this problem for $n = 51$*, that is for* $m = 50$ *by choosing* $y^{(0)} = \{-1, -1, -1, \cdots, -1\}^T$ *as the initial value. The solution vector* α *of this problem is*

$$\begin{aligned}
\{&0.02071138910\ldots, 0.04142277479\ldots, 0.06213413315\ldots, 0.08284539929\ldots, 0.10355644682\ldots,\\
&0.12426706739\ldots, 0.14497695018\ldots, 0.16568566142\ldots, 0.18639262397\ldots, 0.20709709683\ldots,\\
&0.22779815476\ldots, 0.24849466794\ldots, 0.26918528167\ldots, 0.28986839623\ldots, 0.31054214677\ldots,\\
&0.33120438344\ldots, 0.35185265167\ldots, 0.37248417270\ldots, 0.39309582441\ldots, 0.41368412246\ldots,\\
&0.43424520189\ldots, 0.45477479913\ldots, 0.47526823468\ldots, 0.49572039629\ldots, 0.51612572294\ldots,\\
&0.53647818972\ldots, 0.55677129350\ldots, 0.57699803975\ldots, 0.59715093054\ldots, 0.61722195374\ldots,\\
&0.63720257375\ldots, 0.65708372374\ldots, 0.67685579959\ldots, 0.69650865572\ldots, 0.71603160287\ldots,\\
&0.73541340802\ldots, 0.75464229671\ldots, 0.77370595761\ldots, 0.79259154985\ldots, 0.81128571300\ldots,\\
&0.82977457984\ldots, 0.84804379222\ldots, 0.86607851992\ldots, 0.88386348269\ldots, 0.90138297559\ldots,\\
&0.91862089765\ldots, 0.93556078378\ldots, 0.95218584022\ldots, 0.96847898326\ldots, 0.98442288125\ldots\}^T.
\end{aligned}$$

Example 8. *Consider the following Burger's equation (see [30]):*

$$\frac{\partial^2 f}{\partial u^2} + f\frac{\partial f}{\partial u} - \frac{\partial f}{\partial t} + g(u, t) = 0, \ (u, t) \in [0, 1]^2,$$

where $g(u, t) = -10e^{-2t}[e^t(2 - u + u^2) + 10u(1 - 3u + 2u^2)]$ *and function* $f = f(u, t)$ *satisfies the boundary conditions*

$$f(0, t) = f(1, t) = 0, \ f(u, 0) = 10u(u - 1) \text{ and } f(u, 1) = 10u(u - 1)/e.$$

Assuming the following partitioning of the domain $[0, 1]^2$*:*

$$\begin{aligned}
0 = &u_0 < u_1 < u_2 < \ldots\ldots\ldots < u_{n-1} < u_n = 1, \ u_{k+1} = u_k + h,\\
0 = &t_0 < t_1 < t_2 < \ldots\ldots\ldots < t_{n-1} < t_n = 1, \ t_{l+1} = t_l + h, \ h = 1/n.
\end{aligned}$$

Let us define $f_{k,l} = f(u_k, t_l)$ *and* $g_{k,l} = g(u_k, t_l)$ *for* $k, l = 0, 1, 2, \ldots\ldots. n$. *Then the boundary conditions would be* $f_{0,l} = f(u_0, t_l) = 0$, $f_{n,l} = f(u_n, t_l) = 0$, $f_{k,0} = f(u_k, t_0) = 10u_k(u_k - 1)$ *and* $f_{k,n} = f(u_k, t_n) = 10u_k(u_k - 1)/e$. *If we discretize Burger's equation by using the numerical formulas for the partial derivatives*

$$\left(\frac{\partial f}{\partial u}\right)_{i,j} = \frac{f_{i+1,j} - f_{i-1,j}}{2h}, \quad \left(\frac{\partial f}{\partial t}\right)_{i,j} = \frac{f_{i,j+1} - f_{i,j-1}}{2h},$$

$$\left(\frac{\partial^2 f}{\partial u^2}\right)_{i,j} = \frac{f_{i+1,j} - 2f_{i,j} + f_{i-1,j}}{h^2}, \ \ i,j = 1,2,......n-1,$$

then we obtain the following system of $(n-1)^2$ *nonlinear equations in* $(n-1)^2$ *variables:*

$$f_{i-1,j}(2 - hf_{i,j}) + h(f_{i,j-1} - f_{i,j+1}) - f_{i,j}(4 - hf_{i+1,j}) + 2f_{i+1,j} + 2h^2 g_{i,j} = 0, \tag{51}$$

where $i,j = 1,2......n-1$. *In particular, we solve this nonlinear system for* $n = 11$ *so that* $m = 100$ *by selecting* $f_{i,j} = 1$ *for* $i,j = 1,2......10$ *as the initial value. The solution of this system of nonlinear equations is given in Table 2.*

Table 2. The solution of system (51) with the unknowns $f_{i,j}$ for $i,j = 1,2,......10$.

$f_{i,1}$	$f_{i,2}$	$f_{i,3}$	$f_{i,4}$	$f_{i,5}$	$f_{i,6}$	$f_{i,7}$	$f_{i,8}$	$f_{i,9}$	$f_{i,10}$
−0.7546...	−0.6892...	−0.6290...	−0.5750...	−0.5236...	−0.4817...	−0.4306...	−0.4214...	−0.2583...	−0.3068...
−1.3583...	−1.2405...	−1.1322...	−1.0351...	−0.9422...	−0.8675...	−0.7741...	−0.7598...	−0.4358...	−0.5505...
−1.8111...	−1.6541...	−1.5096...	−1.3803...	−1.2559...	−1.1573...	−1.0309...	−1.0110...	−0.6951...	−0.7356...
−2.1130...	−1.9298...	−1.7611...	−1.6106...	−1.4649...	−1.3511...	−1.2014...	−1.1768...	−0.8755...	−0.8606...
−2.2639...	−2.0678...	−1.8869...	−1.7258...	−1.5690...	−1.4485...	−1.2860...	−1.2582...	−0.9783...	−0.9244...
−2.2639...	−2.0678...	−1.8868...	−1.7261...	−1.5686...	−1.4494...	−1.2850...	−1.2558...	−1.0040...	−0.9268...
−2.1129...	−1.9300...	−1.7609...	−1.6112...	−1.4637...	−1.3534...	−1.1987...	−1.1700...	−0.9534...	−0.8672...
−1.8111...	−1.6544...	−1.5093...	−1.3812...	−1.2544...	−1.1604...	−1.0272...	−1.0010...	−0.8270...	−0.7454...
−1.3583...	−1.2408...	−1.1320...	−1.0359...	−0.9407...	−0.8704...	−0.7706...	−0.7492...	−0.6255...	−0.5609...
−0.7546...	−0.6893...	−0.6289...	−0.5755...	−0.5227...	−0.4834...	−0.4285...	−0.4152...	−0.3496...	−0.3128...

In Tables 3–7 we present the numerical results produced for the methods $M_{2,1}$, $M_{3,1}$, $M_{4,j}$ $(j = 1,2,3)$, $M_{5,1}$, $M_{5,2}$, $M_{6,1}$, $M_{7,1}$ and $M_{7,2}$. Displayed in each table are the errors $||x^{(k+1)} - x^{(k)}||$ of first three consecutive approximations to corresponding solution of Examples 4–8, number of iterations (k) needed to converge to the required solution, computational order of convergence p_c, computational cost $C_{p,i}$, computational efficiency $E_{p,i}$ and elapsed CPU-time (e-time) measured in seconds. In each table the meaning of $A(-h)$ is $A \times 10^{-h}$. Numerical values of computational cost and efficiency are obtained according to the corresponding expressions given by (40)–(49). The e-time is calculated by taking the average of 50 performances of the program, where we use $||x^{(k+1)} - x^{(k)}|| + ||F(x^{(k)})|| < 10^{-300}$ as the stopping condition in a single performance of the program.

Table 3. Comparison of performance of methods for Example 4.

Methods	$\|\|x^{(2)} - x^{(1)}\|\|$	$\|\|x^{(3)} - x^{(2)}\|\|$	$\|\|x^{(4)} - x^{(3)}\|\|$	k	p_c	$C_{p,i}$	$E_{p,i}$	**e-Time**
$M_{2,1}(\beta = 0.01)$	9.94(−2)	4.45(−3)	7.14(−6)	9	2.000	16	1.04427	0.2887
$M_{3,1}(\beta = 0.01)$	2.93(−2)	8.14(−6)	1.42(−16)	6	3.000	22	1.05120	0.2630
$M_{4,1}$	3.73(−4)	1.71(−16)	6.94(−66)	5	4.000	36	1.03926	0.3234
$M_{4,2}$	6.17(−2)	7.75(−7)	5.63(−27)	5	4.000	36	1.03926	0.3165
$M_{4,3}(\beta = 0.01)$	5.35(−3)	2.42(−10)	7.56(−40)	5	4.000	44	1.03201	0.3362
$M_{5,1}(\beta = 0.01)$	1.76(−3)	4.72(−15)	4.11(−73)	4	5.000	44	1.03726	0.3297
$M_{5,2}$	1.89(−3)	2.96(−15)	2.04(−74)	4	5.000	52	1.03143	0.3972
$M_{6,1}$	2.97(−2)	8.66(−12)	1.81(−69)	4	6.000	42	1.04358	0.3120
$M_{7,1}$	2.23(−7)	4.55(−52)	0.000	3	7.000	56	1.03536	0.3468
$M_{7,2}(\beta = 0.01)$	7.93(−5)	4.14(−31)	3.40(−215)	3	7.000	72	1.02740	0.4125

Table 4. Comparison of performance of methods for Example 5.

Methods	$\|\|x^{(2)}-x^{(1)}\|\|$	$\|\|x^{(3)}-x^{(2)}\|\|$	$\|\|x^{(4)}-x^{(3)}\|\|$	k	p_c	$\mathrm{C}_{p,i}$	$\mathrm{E}_{p,i}$	**e-Time**
$\mathrm{M}_{2,1}(\beta = 0.01)$	0.202	$1.44(-3)$	$7.18(-8)$	9	2.000	368	1.001885	0.3437
$\mathrm{M}_{3,1}(\beta = 0.01)$	$1.73(-3)$	$1.24(-11)$	$4.56(-36)$	5	3.000	440	1.002500	0.2252
$\mathrm{M}_{4,1}$	0.276	$6.19(-6)$	$1.36(-24)$	5	4.000	848	1.001636	0.3532
$\mathrm{M}_{4,2}$	$9.94(-2)$	$4.12(-8)$	$1.23(-33)$	5	4.000	800	1.001734	0.3562
$\mathrm{M}_{4,3}(\beta = 0.01)$	$1.86(-2)$	$4.72(-11)$	$2.06(-45)$	5	4.000	816	1.001700	0.2749
$\mathrm{M}_{5,1}(\beta = 0.01)$	$1.20(-5)$	$3.49(-30)$	$7.35(-153)$	4	5.000	768	1.002098	0.2312
$\mathrm{M}_{5,2}$	$4.50(-2)$	$1.98(-11)$	$3.74(-58)$	5	5.000	1216	1.001324	0.4234
$\mathrm{M}_{6,1}$	$1.39(-2)$	$3.84(-17)$	$1.86(-104)$	4	6.000	872	1.002057	0.3063
$\mathrm{M}_{7,1}$	$1.12(-2)$	$7.70(-21)$	$6.01(-148)$	4	7.000	1328	1.001467	0.3862
$\mathrm{M}_{7,2}(\beta = 0.01)$	$8.66(-5)$	$4.24(-36)$	$3.01(-255)$	4	7.000	1424	1.001367	0.3625

Table 5. Comparison of performance of methods for Example 6.

Methods	$\|\|x^{(2)}-x^{(1)}\|\|$	$\|\|x^{(3)}-x^{(2)}\|\|$	$\|\|x^{(4)}-x^{(3)}\|\|$	k	p_c	$\mathrm{C}_{p,i}$	$\mathrm{E}_{p,i}$	**e-Time**
$\mathrm{M}_{2,1}(\beta = 0.01)$	0.336	$5.87(-2)$	$2.05(-3)$	10	2.000	3880	1.0001787	4.2530
$\mathrm{M}_{3,1}(\beta = 0.01)$	0.209	$4.29(-3)$	$6.08(-8)$	7	3.000	4300	1.0002555	3.3061
* $\mathrm{M}_{4,1}$	0.370	$2.50(-2)$	1.37	18	4.000	8520	1.0001627	15.469
$\mathrm{M}_{4,2}$	$8.97(-2)$	$1.02(-5)$	$2.23(-21)$	5	4.000	8160	1.0001699	3.4542
$\mathrm{M}_{4,3}(\beta = 0.01)$	0.133	$2.18(-4)$	$2.85(-15)$	6	4.000	6680	1.0002076	3.8634
$\mathrm{M}_{5,1}(\beta = 0.01)$	$8.15(-2)$	$3.67(-6)$	$1.08(-27)$	5	5.000	6320	1.0002547	3.3176
$\mathrm{M}_{5,2}$	0.434	$7.70(-2)$	$1.33(-2)$	7	5.000	12,400	1.0001298	7.2054
$\mathrm{M}_{6,1}$	$3.16(-2)$	$1.38(-10)$	$1.12(-60)$	4	6.000	8580	1.0002089	3.3585
* $\mathrm{M}_{7,1}$	1.572	$3.42(-4)$	$7.60(-25)$	5	7.000	13,160	1.0001478	5.7346
$\mathrm{M}_{7,2}(\beta = 0.01)$	$1.96(-2)$	$6.66(-13)$	$3.92(-86)$	4	7.000	12,120	1.0001606	4.3594

* The methods $\mathrm{M}_{4,1}$ and $\mathrm{M}_{7,1}$ converge to the solution α_2.

Table 6. Comparison of performance of methods for Example 7.

Methods	$\|\|x^{(2)}-x^{(1)}\|\|$	$\|\|x^{(3)}-x^{(2)}\|\|$	$\|\|x^{(4)}-x^{(3)}\|\|$	k	p_c	$\mathrm{C}_{p,i}$	$\mathrm{E}_{p,i}$	**e-Time**
$\mathrm{M}_{2,1}(\beta = 0.01)$	3.828	0.681	$1.23(-2)$	9	2.000	49,200	1.00001409	0.8928
$\mathrm{M}_{3,1}(\beta = 0.01)$	0.433	$9.62(-5)$	$1.74(-15)$	6	3.000	51,750	1.00002123	0.7183
$\mathrm{M}_{4,1}$	0.840	$9.07(-5)$	$9.18(-21)$	5	4.000	103,300	1.00001342	1.0475
$\mathrm{M}_{4,2}$	0.848	$9.54(-5)$	$1.13(-20)$	5	4.000	100,900	1.00001374	1.1896
$\mathrm{M}_{4,3}(\beta = 0.01)$	1.548	$3.85(-3)$	$5.75(-14)$	6	4.000	66,700	1.00002078	0.8284
$\mathrm{M}_{5,1}(\beta = 0.01)$	$4.06(-2)$	$1.22(-12)$	$2.82(-65)$	4	5.000	64,300	1.00002503	0.6102
$\mathrm{M}_{5,2}$	$8.16(-2)$	$3.64(-11)$	$7.86(-58)$	5	5.000	152,500	1.00001055	1.6563
$\mathrm{M}_{6,1}$	0.159	$1.20(-11)$	$2.24(-72)$	6	6.000	103,450	1.00001732	1.0313
$\mathrm{M}_{7,1}$	$9.92(-2)$	$1.26(-15)$	$7.09(-113)$	4	7.000	157,400	1.00001236	1.3457
$\mathrm{M}_{7,2}(\beta = 0.01)$	0.212	$6.80(-13)$	$3.00(-93)$	4	7.000	125,800	1.00001547	1.0938

Table 7. Comparison of performance of methods for Example 8.

Methods	$\|\|x^{(2)}-x^{(1)}\|\|$	$\|\|x^{(3)}-x^{(2)}\|\|$	$\|\|x^{(4)}-x^{(3)}\|\|$	k	p_c	$C_{p,i}$	$E_{p,i}$	**e-Time**
$M_{2,1}(\beta=0.01)$	1.980	1.78(−2)	2.66(−6)	9	2.000	363,400	1.000001907	7.6572
$M_{3,1}(\beta=0.01)$	0.951	1.31(−4)	4.43(−16)	6	3.000	373,500	1.000002941	5.9846
$M_{4,1}$	0.158	8.95(−8)	2.27(−25)	6	2.997	746,600	1.000001471	10.503
$M_{4,2}$	0.418	8.99(−6)	2.28(−19)	6	3.000	736,800	1.000001491	10.249
$M_{4,3}(\beta=0.01)$	0.453	5.14(−6)	9.22(−21)	6	3.001	433,400	1.000002535	6.5627
$M_{5,1}(\beta=0.01)$	0.137	3.08(−12)	3.28(−65)	4	5.001	423,600	1.000003815	4.8255
$M_{5,2}$	3.12(−2)	5.16(−13)	3.86(−55)	5	3.999	1,110,000	1.000001450	10.876
$M_{6,1}$	8.38(−2)	6.04(−11)	9.18(−46)	5	4.001	746,900	1.000001856	9.2656
$M_{7,1}$	1.75(−4)	1.74(−34)	4.89(−213)	4	5.999	1,129,800	1.000001586	10.235
$M_{7,2}(\beta=0.01)$	3.83(−3)	5.44(−25)	1.65(−155)	4	5.996	836,600	1.000002142	8.4533

From the numerical results displayed in Tables 3–7, it can be observed that like that of the existing methods the proposed new method shows consistent convergence behavior. Seventh order methods produce approximations with large accuracy due to their higher order of convergence, but they are less efficient. In Example 6, $M_{4,1}$ and $M_{7,1}$ do not converge to the required solution α_1. Instead, they converge to solution α_2 which is far off from initial approximation chosen. Calculation of computational order of convergence shows that the order of convergence of the new method is preserved in all the numerical examples. However, this is not true for some existing methods, e.g., $M_{4,j}$ $(j=1,2,3)$, $M_{5,2}$, $M_{6,1}$, $M_{7,1}$ and $M_{7,2}$, in Example 8. Values of the efficiency index shown in the penultimate column of each table also verify the theoretical results stated in Theorem 2. The efficiency results are also in complete agreement with the CPU time utilized in the execution of the program since the method with large efficiency uses less computing time than the method with small efficiency. Moreover, the proposed method utilizes less CPU time than existing higher order methods which points to the dominance of the method. In fact, the new method is especially more efficient for large systems of nonlinear equations.

7. Conclusions

In the foregoing study, we have developed a fifth order iterative method for approximating solution of systems of nonlinear equations. The methodology is based on third order Traub-Steffensen method and further developed by using derivative free modification of classical Chebyshev's method. The iterative scheme is totally derivative-free and so particularly suitable to those problems where derivatives are lengthy to compute. To prove the local fifth order of convergence for the new method, a development of first-order divided difference operator and direct computation by Taylor's expansion are used.

We have examined the computational efficiency of the new method. A comparison of efficiencies with that of the existing most efficient methods is also performed. It is proved that, in general, the new algorithm is more efficient. Numerical experiments are performed and the performance is compared with existing derivative-free methods. From numerical results it has been observed that the proposed method has equal or better convergence compared to existing methods. Theoretical results related to convergence order and computational efficiency have also been verified in the considered numerical problems. Similar numerical tests, performed for a variety of other different problems, have confirmed the above drawn conclusions to a good extent.

Author Contributions: Methodology, J.R.S.; writing, review and editing, J.R.S.; investigation, D.K.; data curation, D.K.; conceptualization, L.J; formal analysis, L.J.

Funding: This research received no external funding.

Conflicts of Interest: The authors declare no conflict of interest.

References

1. Argyros, I.K. Quadratic equations and applications to Chandrasekhar's and related equations. *Bull. Aust. Math. Soc.* **1985**, *32*, 275–292. [CrossRef]
2. Kelley, C.T. *Iterative Methods for Linear and Nonlinear Equations*; SIAM: Philadelphia, PA, USA, 1995.
3. Ostrowski, A.M. *Solution of Equations and Systems of Equations*; Academic Press: New York, NY, USA, 1960.
4. Ortega, J.M.; Rheinboldt, W.C. *Iterative Solution of Nonlinear Equations in Several Variables*; Academic Press: New York, NY, USA, 1970.
5. Potra, F.-A.; Pták, V. *Nondiscrete Induction and Iterarive Processes*; Pitman Publishing: Boston, MA, USA, 1984.
6. Traub, J.F. *Iterative Methods for the Solution of Equations*; Prentice-Hall: Englewood Cliffs, NJ, USA, 1964.
7. Ezquerro, J.A.; Hernández, M.A. An optimization of Chebyshev's method. *J. Complex.* **2009**, *25*, 343–361. [CrossRef]
8. Argyros, I.K.; Ezquerro, J.A.; Gutiérrez, J.M.; Hernández, M.A.; Hilout, S. On the semilocal convergence of efficient Chebyshev-Secant-type methods. *J. Comput. Appl. Math.* **2011**, *235*, 3195–3206. [CrossRef]
9. Argyros, I.K.; Ren, H. Efficient Steffensen-type algorithms for solving nonlinear equations. *Int. J. Comput. Math.* **2013**, *90*, 691–704. [CrossRef]
10. Steffensen, J.F. Remarks on iteration. *Skand. Aktuar Tidskr.* **1933**, *16*, 64–72. [CrossRef]
11. Ren, H.; Wu, Q.; Bi, W. A class of two-step Steffensen type methods with fourth-order convergence. *Appl. Math. Comput.* **2009**, *209*, 206–210. [CrossRef]
12. Zheng, Q.; Zhao, P.; Huang, F. A family of fourth-order Steffensen-type methods with the applications on solving nonlinear ODEs. *Appl. Math. Comput.* **2011**, *217*, 8196–8203. [CrossRef]
13. Grau-Sánchez, M.; Noguera, M.; Amat, S. On the approximation of derivatives using divided difference operators preserving the local convergence order of iterative methods. *J. Comput. Appl. Math.* **2013**, *237*, 363–372. [CrossRef]
14. Sharma, J.R.; Arora, H. An efficient derivative free iterative method for solving systems of nonlinear equations. *Appl. Anal. Discrete Math.* **2013**, *7*, 390–403. [CrossRef]
15. Sharma, J.R.; Arora, H. A novel derivative free algorithm with seventh order convergence for solving systems of nonlinear equations. *Numer. Algorithms* **2014**, *67*, 917–933. [CrossRef]
16. Wang, X.; Zhang, T. A family of Steffensen type methods with seventh-order convergence. *Numer. Algorithms* **2013**, *62*, 429–444. [CrossRef]
17. Sharma, J.R.; Arora, H. Efficient higher order derivative-free multipoint methods with and without memory for systems of nonlinear equations. *Int. J. Comput. Math.* **2018**, *95*, 920–938. [CrossRef]
18. Ahmad, F.; Soleymani, F.; Haghani, F.K.; Serra-Capizzano, S. Higher order derivative-free iterative methods with and without memory for systems of nonlinear equations. *Appl. Math. Comput.* **2017**, *314*, 199–211. [CrossRef]
19. Cordero, A.; Torregrosa, J.R. Variants of Newton's method for functions of several variables. *Appl. Math. Comput.* **2006**, *183*, 199–208. [CrossRef]
20. Genocchi, A. Relation entre la différence et la dérivée d'un même ordre quelconque. *Arch. Math. Phys. I* **1869**, *49*, 342–345.
21. Cordero, A.; Hueso, J.L.; Martínez, E.; Torregrosa, J.R. A modified Newton-Jarratt's composition. *Numer. Algorithms* **2010**, *55*, 87–99. [CrossRef]
22. Lotfi, T.; Bakhtiari, P.; Cordero, A.; Mahdiani, K.; Torregrosa, J.R. Some new efficient multipoint iterative methods for solving nonlinear systems of equations. *Int. J. Comput. Math.* **2015**, *92*, 1921–1934. [CrossRef]
23. Krasnoselsky, M.A.; Vainikko, G.M.; Zabreiko, P.P.; Rutitskii, J.B.; Stetsenko, V. J. *Approximate Solution of Operator Equations*; Nauka: Moscow, Russia, 1969. (In Russian)
24. Madhu, K.; Babajee, D.K.R.; Jayaraman, J. An improvement to double-step Newton method and its multi-step version for solving system of nonlinear equations and its applications. *Numer. Algorithms* **2017**, *74*, 593–607. [CrossRef]
25. Kumar, M.; Singh, A.K.; Srivastava, A. A new fifth order derivative free Newton-type method for solving nonlinear equations. *Appl. Math. Inf. Sci.* **2015**, *9*, 1507–1513.
26. Vrscay, E.R.; Gilbert, W.J. Extraneous fixed points, basin boundaries and chaotic dynamics for Schröder and König rational iteration functions. *Numer. Math.* **1988**, *52*, 1–16. [CrossRef]

27. Varona, J.L. Graphic and numerical comparison between iterative methods. *Math. Intell.* **2002**, *24*, 37–46. [CrossRef]
28. Scott, M.; Neta, B.; Chun, C. Basin attractors for various methods. *Appl. Math. Comput.* **2011**, *218*, 2584–2599. [CrossRef]
29. Xiao, X.Y.; Yin, H.W. Increasing the order of convergence for iterative methods to solve nonlinear systems. *Calcolo* **2016**, *53*, 285–300. [CrossRef]
30. Sauer, T. *Numerical Analysis*, 2nd ed.; Pearson Education, Inc.: Boston, MA, USA, 2012.

symmetry

MDPI

Article

On a Class of Optimal Fourth Order Multiple Root Solvers without Using Derivatives

Janak Raj Sharma [1,*], Sunil Kumar [1] and Lorentz Jäntschi [2,3,*]

[1] Department of Mathematics, Sant Longowal Institute of Engineering and Technology, Longowal, Sangrur 148106, India; sfageria1988@gmail.com
[2] Department of Physics and Chemistry, Technical University of Cluj-Napoca, 400114 Cluj-Napoca, Romania
[3] Institute of Doctoral Studies, Babeş-Bolyai University, 400084 Cluj-Napoca, Romania
* Correspondence: jrshira@yahoo.co.in (J.R.S.); lorentz.jantschi@gmail.com (L.J.)

Received: 23 October 2019; Accepted: 20 November 2019; Published: 26 November 2019

Abstract: Many optimal order multiple root techniques involving derivatives have been proposed in literature. On the contrary, optimal order multiple root techniques without derivatives are almost nonexistent. With this as a motivational factor, here we develop a family of optimal fourth-order derivative-free iterative schemes for computing multiple roots. The procedure is based on two steps of which the first is Traub–Steffensen iteration and second is Traub–Steffensen-like iteration. Theoretical results proved for particular cases of the family are symmetric to each other. This feature leads us to prove the general result that shows the fourth-order convergence. Efficacy is demonstrated on different test problems that verifies the efficient convergent nature of the new methods. Moreover, the comparison of performance has proven the presented derivative-free techniques as good competitors to the existing optimal fourth-order methods that use derivatives.

Keywords: iterative function; multiple root; composite method; derivative-free method; optimal convergence

MSC: 65H05; 41A25; 49M15

1. Introduction

We consider derivative-free methods for finding the multiple root (say, α) with multiplicity m of a nonlinear equation $f(t) = 0$, i.e., $f^{(j)}(\alpha) = 0,\ j = 0,\ 1,\ 2,\ \ldots, m-1$ and $f^{(m)}(\alpha) \neq 0$.

Several higher order methods, with or without the use of modified Newton's method [1]

$$t_{k+1} = t_k - m\frac{f(t_k)}{f'(t_k)}, \tag{1}$$

have been derived and analyzed in literature (see, for example, [2–15] and references cited therein). In such methods, one requires determining the derivatives of either first order or both first and second order. Contrary to this, higher-order derivative-free methods to compute multiple roots are yet to be investigated. These methods are important in the problems where derivative f' is complicated to process or is costly to evaluate. The basic derivative-free method is the Traub–Steffensen method [16], which uses the approximation

$$f'(t_k) \simeq \frac{f(t_k + \beta f(t_k)) - f(t_k)}{\beta f(t_k)}, \quad \beta \in \mathbb{R} - \{0\},$$

or

$$f'(t_k) \simeq f[s_k, t_k],$$

for the derivative f' in the classical Newton method in Equation (1). Here, $s_k = t_k + \beta f(t_k)$ and $f[s,t] = \frac{f(s)-f(t)}{s-t}$ is a divided difference of first order. In this way, the modified Newton method in Equation (1) transforms to the modified Traub–Steffensen derivative free method

$$t_{k+1} = t_k - m\frac{f(t_k)}{f[s_k, t_k]}. \tag{2}$$

The modified Traub–Steffensen method in Equation (2) is a noticeable improvement over the Newton method, because it preserves the convergence of order two without using any derivative.

In this work, we aim to design derivative-free multiple root methods of high efficient quality, i.e., the methods of higher convergence order that use the computations as small as we please. Proceeding in this way, we introduce a class of derivative-free fourth-order methods that require three new pieces of information of the function f per iteration, and hence possess optimal fourth-order convergence in the terminology of Kung–Traub conjecture [17]. This conjecture states that multi-point iterative functions without memory based on n function evaluations may attain the convergence order 2^{n-1}, which is maximum. The methods achieving this convergence order are usually called optimal methods. The new iterative scheme uses the modified Traub–Steffensen iteration in Equation (2) in the first step and Traub–Steffensen-like iteration in the second step. The methods are examined numerically on many practical problems of different kind. The comparison of performance with existing techniques requiring derivative evaluations verifies the efficient character of the new methods in terms of accuracy and executed CPU time.

The rest of the paper is summarized as follows. In Section 2, the scheme of fourth-order method is proposed and its convergence order is studied for particular cases. The main result for the general case is studied in Section 3. Numerical tests to demonstrate applicability and efficiency of the methods are presented in Section 4. In this section, a comparison of performance with already established methods is also shown. In Section 5, a conclusion of the main points is drawn.

2. Formulation of Method

To compute a multiple root with multiplicity $m \geq 1$, consider the following two-step iterative scheme:

$$\begin{aligned} z_k &= t_k - m\frac{f(t_k)}{f[s_k, t_k]}, \\ t_{k+1} &= z_k - H(x_k, y_k)\frac{f(t_k)}{f[s_k, t_k]}, \end{aligned} \tag{3}$$

where $x_k = \sqrt[m]{\frac{f(z_k)}{f(t_k)}}$, $y_k = \sqrt[m]{\frac{f(z_k)}{f(s_k)}}$ and $H : \mathbb{C}^2 \to \mathbb{C}$ is analytic in a neighborhood of $(0,0)$. Notice that this is a two-step scheme with first step as the Traub–Steffensen iteration in Equation (2) and the next step as the Traub–Steffensen-like iteration. The second step is weighted by the factor $H(x, y)$, thus we can call it weight factor or more appropriately weight function.

In the sequel, we study the convergence results of proposed iterative scheme in Equation (3). For clarity, the results are obtained separately for different cases based on the multiplicity m. Firstly, for the case $m = 1$, the following theorem is proved:

Theorem 1. *Assume that $f : \mathbb{C} \to \mathbb{C}$ is an analytic function in a domain containing a multiple zero (say, α) with multiplicity $m = 1$. Suppose that the initial point t_0 is close enough to α, then the convergence order of Equation (3) is at least 4, provided that $H_{00} = 0$, $H_{10} = 1$, $H_{01} = 0$, $H_{20} = 2$, $H_{11} = 11$ and $H_{02} = 0$, where $H_{ij} = \frac{\partial^{i+j}}{\partial x^i \partial y^j} H(x_k, y_k)|_{(x_k=0, y_k=0)}$, for $0 \leq i, j \leq 2$.*

Proof. Assume that the error at kth stage is $e_k = t_k - \alpha$. Using the Taylor's expansion of $f(t_k)$ about α and keeping into mind that $f(\alpha) = 0$ and $f'(\alpha) \neq 0$, we have

$$f(t_k) = f'(\alpha)e_k\big(1 + A_1e_k + A_2e_k^2 + A_3e_k^3 + A_4e_k^4 + \cdots\big), \tag{4}$$

where $A_n = \frac{1}{(1+n)!}\frac{f^{(1+n)}(\alpha)}{f'(\alpha)}$ for $n \in \mathbb{N}$.

Similarly we have the Taylor's expansion of $f(s_k)$ about α

$$f(s_k) = f'(\alpha)e_{s_k}\big(1 + A_1e_{s_k} + A_2e_{s_k}^2 + A_3e_{s_k}^3 + A_4e_{s_k}^4 + \cdots\big), \tag{5}$$

where $e_{s_k} = s_k - \alpha = e_k + \beta f'(\alpha)e_k\big(1 + A_1e_k + A_2e_k^2 + A_3e_k^3 + A_4e_k^4 + \cdots\big)$.

Then, the first step of Equation (3) yields

$$\begin{aligned} e_{z_k} &= z_k - \alpha \\ &= (1+\beta f'(\alpha))A_1e_k^2 - \big((2+2\beta f'(\alpha)+(\beta f'(\alpha))^2)A_1^2 - (2+3\beta f'(\alpha)+(\beta f'(\alpha))^2)A_2\big)e_k^3 + \big((4+5\beta f'(\alpha) \\ &\quad + 3(\beta f'(\alpha))^2 + (\beta f'(\alpha))^3)A_1^3 - (7+10\beta f'(\alpha)+7(\beta f'(\alpha))^2+2(\beta f'(\alpha))^3)A_1A_2 + (3+6\beta f'(\alpha) \\ &\quad + 4(\beta f'(\alpha))^2+(\beta f'(\alpha))^3)A_3\big)e_k^4 + O(e_k^5). \end{aligned} \tag{6}$$

Expanding $f(z_k)$ about α, it follows that

$$f(z_k) = f'(\alpha)e_{z_k}\big(1 + A_1e_{z_k} + A_2e_{z_k}^2 + A_3e_{z_k}^3 + \cdots\big). \tag{7}$$

Using Equations (4), (5) and (7) in x_k and y_k, after some simple calculations, we have

$$\begin{aligned} x_k = {} & (1+\beta f'(\alpha))A_1e_k - \big((3+3\beta f'(\alpha)+(\beta f'(\alpha))^2)A_1^2 - (2+3\beta f'(\alpha)+(\beta f'(\alpha))^2)A_2\big)e_k^2 + \big((8+10\beta f'(\alpha) \\ & + 5(\beta f'(\alpha))^2 + (\beta f'(\alpha))^3)A_1^3 - 2(5+7\beta f'(\alpha)+4(\beta f'(\alpha))^2+(\beta f'(\alpha))^3)A_1A_2 + (3+6\beta f'(\alpha) \\ & + 4(\beta f'(\alpha))^2+(\beta f'(\alpha))^3)A_3\big)e_k^3 + O(e_k^4) \end{aligned} \tag{8}$$

and

$$\begin{aligned} y_k = {} & A_1e_k - \big((3+2\beta f'(\alpha))A_1^2 - (2+\beta f'(\alpha))A_2\big)e_k^2 + \big((8+8\beta f'(\alpha)+3(\beta f'(\alpha))^2)A_1^3 \\ & - (10+11\beta f'(\alpha)+4(\beta f'(\alpha))^2)A_1A_2 + (3+3\beta f'(\alpha)+(\beta f'(\alpha))^2)A_3\big)e_k^3 + O(e_k^4). \end{aligned} \tag{9}$$

Developing $H(x_k, y_k)$ by Taylor series in the neighborhood of origin $(0,0)$,

$$H(x_k, y_k) \approx H_{00} + x_kH_{10} + y_kH_{01} + \frac{1}{2}x_k^2H_{20} + x_ky_kH_{11} + \frac{1}{2}y_k^2H_{02}. \tag{10}$$

Inserting Equations (4)–(10) into the second step of Equation (3), and then some simple calculations yield

$$\begin{aligned} e_{k+1} = {} & -H_{00}\,e_k + \big(H_{00} - H_{01} + \beta f'(\alpha)H_{00} - (-1+H_{10})(1+\beta f'(\alpha))\big)A_1e_k^2 - \frac{1}{2}\big((4+H_{02}-8H_{10}+2H_{11} \\ & + H_{20} + 4\beta f'(\alpha) - 10\beta f'(\alpha)H_{10} + 2\beta f'(\alpha)H_{11} + 2\beta f'(\alpha)H_{20} + 2(\beta f'(\alpha))^2 - 4(\beta f'(\alpha))^2H_{10} \\ & + (\beta f'(\alpha))^2H_{20} - 2H_{01}(4+3\beta f'(\alpha)) + 2H_{00}(2+2\beta f'(\alpha)+(\beta f'(\alpha))^2))A_1^2 - 2(2+\beta f'(\alpha))(H_{00} \\ & - H_{01} + \beta f'(\alpha)H_{00} - (-1+H_{10})(1+\beta f'(\alpha)))A_2\big)e_k^3 + \delta e_k^4 + O(e_k^5), \end{aligned} \tag{11}$$

where $\delta = \delta(\beta, A_1, A_2, A_3, H_{00}, H_{10}, H_{01}, H_{20}, H_{11}, H_{02})$. Here, expression of δ is not being produced explicitly since it is very lengthy.

It is clear from Equation (11) that we would obtain at least fourth-order convergence if we set coefficients of e_k, e_k^2 and e_k^3 simultaneously equal to zero. Then, solving the resulting equations, one gets

$$H_{00} = 0, \;\; H_{10} = 1, \;\; H_{01} = 0, \;\; H_{20} = 2, \;\; H_{11} = 1, \;\; H_{02} = 0. \tag{12}$$

As a result, the error equation is given by

$$e_{k+1} = (1 + \beta f'(\alpha))A_1\big((5 + 5\beta f'(\alpha) + (\beta f'(\alpha))^2)A_1^2 - (1 + \beta f'(\alpha))A_2\big)e_k^4 + O(e_k^5). \tag{13}$$

Thus, the theorem is proved. □

Next, we show the conditions for $m = 2$ by the following theorem:

Theorem 2. *Using the hypotheses of Theorem 1, the order of convergence of the scheme in Equation* (3) *for the case* $m = 2$ *is at least* 4*, if* $H_{00} = 0$, $H_{10} = 1$, $H_{01} = 1$, *and* $H_{20} = 8 - H_{02} - 2H_{11}$, *wherein* $\{|H_{11}|, |H_{02}|\} < \infty$.

Proof. Assume that the error at kth stage is $e_k = t_k - \alpha$. Using the Taylor's expansion of $f(t_k)$ about α and keeping in mind that $f(\alpha) = 0$, $f'(\alpha) = 0$, and $f^{(2)}(\alpha) \neq 0$, we have

$$f(t_k) = \frac{f^{(2)}(\alpha)}{2!}e_k^2\big(1 + B_1e_k + B_2e_k^2 + B_3e_k^3 + B_4e_k^4 + \cdots\big), \tag{14}$$

where $B_n = \frac{2!}{(2+n)!}\frac{f^{(2+n)}(\alpha)}{f^{(2)}(\alpha)}$ for $n \in \mathbb{N}$.

Similarly, we have the Taylor's expansion of $f(s_k)$ about α

$$f(s_k) = \frac{f^{(2)}(\alpha)}{2!}e_{s_k}^2\big(1 + B_1e_{s_k} + B_2e_{s_k}^2 + B_3e_{s_k}^3 + B_4e_{s_k}^4 + \cdots\big), \tag{15}$$

where $e_{s_k} = s_k - \alpha = e_k + \frac{\beta f^{(2)}(\alpha)}{2!}e_k^2\big(1 + B_1e_k + B_2e_k^2 + B_3e_k^3 + B_4e_k^4 + \cdots\big)$.

Then, the first step of Equation (3) yields

$$\begin{aligned} e_{z_k} &= z_k - \alpha \\ &= \frac{1}{2}\Big(\frac{\beta f^{(2)}(\alpha)}{2} + B_1\Big)e_k^2 - \frac{1}{16}\big((\beta f^{(2)}(\alpha))^2 - 8\beta f^{(2)}(\alpha)B_1 + 12B_1^2 - 16B_2\big)e_k^3 + \frac{1}{64}\big((\beta f^{(2)}(\alpha))^3 \\ &\quad - 20\beta f^{(2)}(\alpha)B_1^2 + 72B_1^3 + 64\beta f^{(2)}(\alpha)B_2 - 10B_1\big((\beta f^{(2)}(\alpha))^2 + 16B_2\big) + 96B_3\big)e_k^4 + O(e_k^5). \end{aligned} \tag{16}$$

Expanding $f(z_k)$ about α, it follows that

$$f(z_k) = \frac{f^{(2)}(\alpha)}{2!}e_{z_k}^2\big(1 + B_1e_{z_k} + B_2e_{z_k}^2 + B_3e_{z_k}^3 + B_4e_{z_k}^4 + \cdots\big). \tag{17}$$

Using Equations (14), (15) and (17) in x_k and y_k, after some simple calculations, we have

$$\begin{aligned} x_k = \frac{1}{2}\Big(\frac{\beta f^{(2)}(\alpha)}{2} + B_1\Big)e_k &- \frac{1}{16}\big((\beta f^{(2)}(\alpha))^2 - 6\beta f^{(2)}(\alpha)B_1 + 16(B_1^2 - B_2)\big)e_k^2 + \frac{1}{64}\big((\beta f^{(2)}(\alpha))^3 \\ &- 22\beta f^{(2)}(\alpha)B_1^2 + 4\big(29B_1^3 + 14\beta f^{(2)}(\alpha)B_2\big) - 2B_1\big(3(\beta f^{(2)}(\alpha))^2 + 104B_2\big) + 96B_3\big)e_k^3 + O(e_k^4) \end{aligned} \tag{18}$$

and

$$\begin{aligned} y_k = \frac{1}{2}\Big(\frac{\beta f^{(2)}(\alpha)}{2} + B_1\Big)e_k &- \frac{1}{16}\big(3(\beta f^{(2)}(\alpha))^2 - 2\beta f^{(2)}(\alpha)B_1 + 16(B_1^2 - B_2)\big)e_k^2 + \frac{1}{64}\big(7(\beta f^{(2)}(\alpha))^3 \\ &+ 24\beta f^{(2)}(\alpha)B_2 - 14\beta f^{(2)}(\alpha)B_1^2 + 116B_1^3 - 2B_1\big(11(\beta f^{(2)}(\alpha))^2 + 104B_2\big) + 96B_3\big)e_k^3 + O(e_k^4). \end{aligned} \tag{19}$$

Developing by Taylor series the weight function $H(x_k, y_k)$ in the neighborhood of origin $(0, 0)$,

$$H(x_k, y_k) \approx H_{00} + x_k H_{10} + y_k H_{01} + \frac{1}{2} x_k^2 H_{20} + x_k y_k H_{11} + \frac{1}{2} y_k^2 H_{02}. \tag{20}$$

Inserting Equations (14)–(20) intothe second step of Equation (3), and then some simple calculations yield

$$\begin{aligned} e_{k+1} = & -\frac{H_{00}}{2}\, e_k + \frac{1}{4}(2 + H_{00} - H_{01} - H_{10})\Big(\frac{\beta f^{(2)}(\alpha)}{2} + B_1\Big)e_k^2 - \frac{1}{64}\Big((\beta f^{(2)}(\alpha))^2(4 + 2H_{00} - 8H_{01} + H_{02} \\ & - 4H_{10} + 2H_{11} + H_{20}) + 4\beta f^{(2)}(\alpha)(-8 - 4H_{00} - H_{01} + H_{02} + H_{10} + 2H_{11} + H_{20})B_1 + 4(12 + 6H_{00} \\ & - 10H_{01} + H_{02} - 10H_{10} + 2H_{11} + H_{20})B_1^2 - 32(2 + H_{00} - H_{01} - H_{10})B_2\Big)e_k^3 + \phi\, e_k^4 + O(e_k^5), \end{aligned} \tag{21}$$

where $\phi = \phi(\beta, B_1, B_2, B_3, H_{00}, H_{10}, H_{01}, H_{20}, H_{11}, H_{02})$. Here, expression of ϕ is not being produced explicitly since it is very lengthy.

It is clear from Equation (21) that we would obtain at least fourth-order convergence if we set coefficients of e_k, e_k^2 and e_k^3 simultaneously equal to zero. Then, solving the resulting equations, one gets

$$H_{00} = 0, \;\; H_{10} = 1, \;\; H_{01} = 1, \;\; H_{20} = 8 - H_{02} - 2H_{11}. \tag{22}$$

As a result, the error equation is given by

$$e_{k+1} = \frac{1}{32}\Big(\frac{\beta f^{(2)}(\alpha)}{2} + B_1\Big)\big((2\beta f^{(2)}(\alpha)(3 + H_{02} + H_{11})B_1 + 22B_1^2 + ((\beta f^{(2)}(\alpha))^2(H_{02} + H_{11}) - 8B_2)\big)e_k^4 + O(e_k^5).$$

Thus, the theorem is proved. □

Below, we state the theorems (without proof) for the cases $m = 3$, 4, 5 as the proof is similar to the above proved theorems.

Theorem 3. *Using the hypotheses of Theorem 1, the order of convergence of scheme in Equation* (3) *for the case* $m = 3$ *is at least* 4*, if* $H_{00} = 0$*,* $H_{10} = 3 - H_{01}$*, and* $H_{20} = 12 - H_{02} - 2H_{11}$*, where* $\{|H_{01}|, |H_{02}|, |H_{11}|\} < \infty$*. Moreover, the scheme satisfies error equation*

$$e_{k+1} = \frac{1}{54}(\beta f^{(3)}(\alpha)(-3 + H_{01})C_1 + 12C_1^3 - 6C_1C_2)e_k^4 + O(e_k^5),$$

where $C_n = \frac{3!}{(3+n)!}\frac{f^{(3+n)}(\alpha)}{f^{(3)}(\alpha)}$ *for* $n \in \mathbb{N}$.

Theorem 4. *Using the hypotheses of Theorem 1, the order of convergence of scheme in Equation* (3) *for the case* $m = 4$ *is at least* 4*, if* $H_{00} = 0$*,* $H_{10} = 4 - H_{01}$*, and* $H_{20} = 16 - H_{02} - 2H_{11}$*, where* $\{|H_{01}|, |H_{02}|, |H_{11}|\} < \infty$*. Moreover, the scheme satisfies error equation*

$$e_{k+1} = \frac{1}{128}(13D_1^3 - 8D_1D_2)e_k^4 + O(e_k^5),$$

where $D_n = \frac{4!}{(4+n)!}\frac{f^{(4+n)}(\alpha)}{f^{(4)}(\alpha)}$ *for* $n \in \mathbb{N}$.

Theorem 5. *Using the hypotheses of Theorem 1, the order of convergence of scheme in Equation (3) for the case $m = 5$ is at least 4, if $H_{00} = 0$, $H_{10} = 5 - H_{01}$, and $H_{20} = 20 - H_{02} - 2H_{11}$, where $\{|H_{01}|, |H_{02}|, |H_{11}|\} < \infty$. Moreover, the scheme satisfies error equation*

$$e_{k+1} = \frac{1}{125}\left(7E_1^3 - 5E_1E_2\right)e_k^4 + O(e_k^5),$$

where $E_n = \frac{5!}{(5+n)!}\frac{f^{(5+n)}(\alpha)}{f^{(5)}(\alpha)}$ for $n \in \mathbb{N}$.

Remark 1. *We can observe from the above results that the number of conditions on H_{ij} is 6, 4, 3, 3, 3 corresponding to cases $m = 1, 2, 3, 4, 5$ to attain the fourth-order convergence of the method in Equation (3). The cases $m = 3, 4, 5$ satisfy the common conditions, $H_{00} = 0$, $H_{10} = m - H_{01}$, and $H_{20} = 4m - H_{02} - 2H_{11}$. Nevertheless, their error equations differ from each other as the parameter β does not appear in the equations for $m = 4, 5$. It has been seen that when $m \geq 4$ the conditions on H_{ij} are always three in number and the error equation in each such case does not contain β term. This type of symmetry in the results helps us to prove the general result, which is presented in next section.*

3. Main Result

For the multiplicity $m \geq 4$, we prove the order of convergence of the scheme in Equation (3) by the following theorem:

Theorem 6. *Assume that the function $f : \mathbb{C} \to \mathbb{C}$ is an analytic in a domain containing zero α having multiplicity $m \geq 4$. Further, suppose that the initial estimation t_0 is close enough to α. Then, the convergence of the iteration scheme in Equation (3) is of order four, provided that $H_{00} = 0$, $H_{10} = m - H_{01}$, and $H_{20} = 4m - H_{02} - 2H_{11}$, wherein $\{|H_{01}|, |H_{11}|, |H_{02}|\} < \infty$. Moreover, the error in the scheme is given by*

$$e_{k+1} = \frac{1}{2m^3}\left((9+m)K_1^3 - 2mK_1K_2\right)e_k^4 + O(e_k^5).$$

Proof. Taking into account that $f^{(j)}(\alpha) = 0$, $j = 0, 1, 2, \ldots, m-1$ and $f^m(\alpha) \neq 0$, then, developing $f(t_k)$ about α in the Taylor's series,

$$f(t_k) = \frac{f^m(\alpha)}{m!}e_k^m\left(1 + K_1e_k + K_2e_k^2 + K_3e_k^3 + K_4e_k^4 + \cdots\right), \tag{23}$$

where $K_n = \frac{m!}{(m+n)!}\frac{f^{(m+n)}(\alpha)}{f^{(m)}(\alpha)}$ for $n \in \mathbb{N}$.

In addition, from the expansion of $f(s_k)$ about α, it follows that

$$f(s_k) = \frac{f^m(\alpha)}{m!}e_{s_k}^m\left(1 + K_1e_{s_k} + K_2e_{s_k}^2 + K_3e_{s_k}^3 + K_4e_{s_k}^4 + \cdots\right), \tag{24}$$

where $e_{s_k} = s_k - \alpha = e_k + \frac{\beta f^m(\alpha)}{m!}e_k^m\left(1 + K_1e_k + K_2e_k^2 + K_3e_k^3 + K_4e_k^4 + \cdots\right)$. From the first step of Equation (3),

$$\begin{aligned} e_{z_k} &= z_k - \alpha \\ &= \frac{K_1}{m}e_k^2 + \frac{1}{m^2}\left(2mK_2 - (1+m)K_1^2\right)e_k^3 + \frac{1}{m^3}\left((1+m)^2K_1^3 - m(4+3m)K_1K_2 + 3m^2K_3\right)e_k^4 + O(e_k^5). \end{aligned} \tag{25}$$

Expansion of $f(z_k)$ around α yields

$$f(z_k) = \frac{f^m(\alpha)}{m!}e_{z_k}^2\left(1 + K_1e_{z_k} + K_2e_{z_k}^2 + K_3e_{z_k}^3 + K_4e_{z_k}^4 + \cdots\right). \tag{26}$$

Using Equations (23), (24) and (26) in the expressions of x_k and y_k, we have that

$$x_k = \frac{K_1}{m}e_k + \frac{1}{m^2}(2mK_2 - (2+m)K_1^2)e_k^2 + \frac{1}{2m^3}((7+7m+2m^2)K_1^3 - 2m(7+3m)K_1K_2 + 6m^2K_3)e_k^3 + O(e_k^4) \quad (27)$$

and

$$y_k = \frac{K_1}{m}e_k + \frac{1}{m^2}(mK_2 - (2+m)K_1^2)e_k^2 + \frac{1}{2m^3}((6+7m+2m^2)K_1^3 - 2m(6+3m)K_1K_2 + 6m^2K_3)e_k^3 + O(e_k^4). \quad (28)$$

Developing $H(x_k, y_k)$ in Taylor's series in the neighborhood of origin $(0,0)$,

$$H(x_k, y_k) \approx H_{00} + x_kH_{10} + y_kH_{01} + \frac{1}{2}x_k^2H_{20} + x_ky_kH_{11} + \frac{1}{2}y_k^2H_{02}. \quad (29)$$

Inserting Equations (23)–(29) into the second step of Equation (3), it follows that

$$\begin{aligned} e_{k+1} = &-\frac{H_{00}}{m}e_k + \frac{1}{m^2}(H_{00} - H_{01} - H_{10} + m)K_1e_k^2 - \frac{1}{2m^3}((H_{02} - 6H_{10} + 2H_{11} + H_{20} + 2m - 2mH_{10} + 2m^2 \\ &+ 2(1+m)H_{00} - 2(3+m)H_{01})K_1^2 - 4m(H_{00} - H_{01} - H_{10} + m)K_2)e_k^3 + \frac{1}{2m^4}((5H_{02} - 13H_{10} + 10H_{11} \\ &+ 5H_{20} + 2m + 2mH_{02} - 11mH_{10} + 4mH_{11} + 2mH_{20} + 4m^2 - 2m^2H_{10} + 2m^3 + 2(1+m)^2H_{00} \\ &- (13 + 11m + 2m^2)H_{01})K_1^3 - 2m(2H_{02} - 11H_{10} + 4H_{11} + 2H_{20} + 4m - 3mH_{10} + 3m^2 + (4+3m)H_{00} \\ &- (11+3m)H_{01})K_1K_2 + 6m^2(H_{00} - H_{01} - H_{10} + m)K_3)e_k^4 + O(e_k^5). \end{aligned} \quad (30)$$

It is clear that we can obtain at least fourth-order convergence if the coefficients of e_k, e_k^2, and e_k^3 vanish. On solving the resulting equations, we get

$$H_{00} = 0, \;\; H_{10} = m - H_{01}, \;\; H_{20} = 4m - \;H_{02} - 2\,H_{11}. \quad (31)$$

Then, error of Equation (30) is given by

$$e_{k+1} = \frac{1}{2m^3}((9+m)K_1^3 - 2mK_1K_2)e_k^4 + O(e_k^5). \quad (32)$$

Thus, the theorem is proved. □

Remark 2. *The proposed scheme in Equation* (3) *reaches fourth-order convergence provided that the conditions of Theorems 1–3 and 6 are satisfied. This convergence rate is achieved by using only three function evaluations, viz.* $f(t_n)$, $f(s_n)$, *and* $f(z_n)$, *per iteration. Therefore, the scheme in Equation* (3) *is optimal by the Kung–Traub hypothesis [17].*

Remark 3. *It is important to note that parameter* β, *which is used in* s_k, *appears only in the error equations of the cases* $m = 1, 2, 3$ *but not for* $m \geq 4$. *For* $m \geq 4$, *we have observed that this parameter appears in the coefficients of* e_k^5 *and higher order. However, we do not need such terms to show the required fourth-order convergence.*

Some Special Cases

We can generate many iterative schemes as the special cases of the family in Equation (3) based on the forms of function $H(x, y)$ that satisfy the conditions of Theorems 1, 2 and 6. However, we restrict ourselves to the choices of low-degree polynomials or simple rational functions. These choices should be such that the resulting methods may converge to the root with order four for $m \geq 1$. Accordingly, the following simple forms are considered:

(1) Let us choose the function

$$H(x_k, y_k) = x_k + m\,x_k^2 + (m-1)y_k + m\,x_k\,y_k,$$

which satisfies the conditions of Theorems 1, 2 and 6. Then, the corresponding fourth-order iterative scheme is given by

$$t_{k+1} = z_k - \big(x_k + m\,x_k^2 + (m-1)y_k + m\,x_k\,y_k\big)\frac{f(t_k)}{f[s_k, t_k]}. \tag{33}$$

(2) Next, consider the rational function

$$H(x_k, y_k) = -\frac{x_k + m\,x_k^2 - (m-1)y_k(m\,y_k - 1)}{m\,y_k - 1},$$

satisfying the conditions of Theorems 1, 2 and 6. Then, corresponding fourth-order iterative scheme is given by

$$t_{k+1} = z_k + \frac{x_k + m\,x_k^2 - (m-1)y_k(m\,y_k - 1)}{m\,y_k - 1}\,\frac{f(t_k)}{f[s_k, t_k]}. \tag{34}$$

(3) Consider another rational function satisfying the conditions of Theorems 1, 2 and 6, which is given by

$$H(x_k, y_k) = \frac{x_k - y_k + m\,y_k + 2m\,x_k\,y_k - m^2\,x_k\,y_k}{1 - m\,x_k + x_k^2}.$$

The corresponding fourth-order iterative scheme is given by

$$t_{k+1} = z_k - \frac{x_k - y_k + m\,y_k + 2m\,x_k\,y_k - m^2\,x_k\,y_k}{1 - m\,x_k + x_k^2}\,\frac{f(t_k)}{f[s_k, t_k]}. \tag{35}$$

For each of the above cases, $z_k = t_k - m\frac{f(t_k)}{f[s_k,t_k]}$. For future reference, the proposed methods in Equations (33)–(35) are denoted by NM1, NM2, and NM3, respectively.

4. Numerical Results

To validate the theoretical results proven in previous sections, the special cases NM1, NM2, and NM3 of new family were tested numerically by implementing them on some nonlinear equations. Moreover, their comparison was also performed with some existing optimal fourth-order methods that use derivatives in the formulas. We considered, for example, the methods by Li et al. [7,8], Sharma and Sharma [9], Zhou et al. [10], Soleymani et al. [12], and Kansal et al. [14]. The methods are expressed as follows:

Li–Liao–Cheng method (LLC):

$$z_k = t_k - \frac{2m}{m+2}\,\frac{f(t_k)}{f'(t_k)},$$
$$t_{k+1} = t_k - \frac{m(m-2)\left(\frac{m}{m+2}\right)^{-m} f'(z_k) - m^2 f'(t_k)}{f'(t_k) - \left(\frac{m}{m+2}\right)^{-m} f'(z_k)}\,\frac{f(t_k)}{2f'(t_k)}.$$

Li–Cheng–Neta method (LCN):

$$\begin{aligned} z_k &= t_k - \frac{2m}{m+2}\frac{f(t_k)}{f'(t_k)}, \\ t_{k+1} &= t_k - \alpha_1 \frac{f(t_k)}{f'(z_k)} - \frac{f(t_k)}{\alpha_2 f'(t_k) + \alpha_3 f'(z_k)}, \end{aligned}$$

where

$$\begin{aligned} \alpha_1 &= -\frac{1}{2}\frac{\left(\frac{m}{m+2}\right)^m m(m^4+4m^3-16m-16)}{m^3-4m+8}, \\ \alpha_2 &= -\frac{(m^3-4m+8)^2}{m(m^4+4m^3-4m^2-16m+16)(m^2+2m-4)}, \\ \alpha_3 &= \frac{m^2(m^3-4m+8)}{\left(\frac{m}{m+2}\right)^m (m^4+4m^3-4m^2-16m+16)(m^2+2m-4)}. \end{aligned}$$

Sharma–Sharma method (SS):

$$\begin{aligned} z_k &= t_k - \frac{2m}{m+2}\frac{f(t_k)}{f'(t_k)}, \\ t_{k+1} &= t_k - \frac{m}{8}\Big[(m^3-4m+8) - (m+2)^2\Big(\frac{m}{m+2}\Big)^m \frac{f'(t_k)}{f'(z_k)} \\ &\qquad \times \Big(2(m-1) - (m+2)\Big(\frac{m}{m+2}\Big)^m \frac{f'(t_k)}{f'(z_k)}\Big)\Big]\frac{f(t_k)}{f'(t_k)}. \end{aligned}$$

Zhou–Chen–Song method (ZCS):

$$\begin{aligned} z_k &= t_k - \frac{2m}{m+2}\frac{f(t_k)}{f'(t_k)}, \\ t_{k+1} &= t_k - \frac{m}{8}\Big[m^3\Big(\frac{m+2}{m}\Big)^{2m}\Big(\frac{f'(z_k)}{f'(t_k)}\Big)^2 - 2m^2(m+3)\Big(\frac{m+2}{m}\Big)^m \frac{f'(z_k)}{f'(t_k)} \\ &\qquad + (m^3+6m^2+8m+8)\Big]\frac{f(t_k)}{f'(t_k)}. \end{aligned}$$

Soleymani–Babajee–Lotfi method (SBL):

$$\begin{aligned} z_k &= t_k - \frac{2m}{m+2}\frac{f(t_k)}{f'(t_k)}, \\ t_{k+1} &= t_k - \frac{f'(z_k)f(t_k)}{q_1(f'(z_k))^2 + q_2 f'(z_k)f'(t_k) + q_3(f'(t_k))^2}, \end{aligned}$$

where

$$\begin{aligned} q_1 &= \frac{1}{16}m^{3-m}(2+m)^m, \\ q_2 &= \frac{8-m(2+m)(-2+m^2)}{8m}, \\ q_3 &= \frac{1}{16}(-2+m)m^{-1+m}(2+m)^{3-m}. \end{aligned}$$

Kansal–Kanwar–Bhatia method (KKB):

$$
\begin{aligned}
z_k &= t_k - \frac{2m}{m+2}\frac{f(t_k)}{f'(t_k)},\\
t_{k+1} &= t_k - \frac{m}{4} f(t_k)\left(1 + \frac{m^4 p^{-2m}\left(-\frac{f'(z_k)}{f'(t_k)} + p^{-1+m}\right)^2(-1+p^m)}{8(2p^m + m(-1+p^m))}\right)\\
&\qquad \times \left(\frac{4-2m+m^2(-1+p^{-m})}{f'(t_k)} - \frac{p^{-m}(2p^m+m(-1+p^m))^2}{f'(t_k)-f'(z_k)}\right),
\end{aligned}
$$

where $p = \frac{m}{m+2}$.

Computational work was compiled in the programming package of Mathematica software [18] in a PC with Intel(R) Pentium(R) CPU B960 @ 2.20 GHz, 2.20 GHz (32-bit Operating System) Microsoft Windows 7 Professional and 4 GB RAM. Performance of the new methods was tested by choosing value of the parameter $\beta = 0.01$. The tabulated results obtained by the methods for each problem include: (a) the number of iterations (k) required to obtain the solution using the stopping criterion $|t_{k+1} - t_k| + |f(t_k)| < 10^{-100}$; (b) the estimated error $|t_{k+1} - t_k|$ in the first three iterations; (c) the calculated convergence order (CCO); and (d) the elapsed time (CPU time in seconds) in execution of a program, which was measured by the command "TimeUsed[ ]". The calculated convergence order (CCO) to confirm the theoretical convergence order was calculated by the formula (see [19])

$$\mathrm{CCO} = \frac{\log|(t_{k+2}-\alpha)/(t_{k+1}-\alpha)|}{\log|(t_{k+1}-\alpha)/(t_k-\alpha)|}, \quad \text{for each } k = 1, 2, \ldots \tag{36}$$

The following numerical examples were chosen for experimentation:

Example 1. *Planck law of radiation to calculate the energy density in an isothermal black body [20] is stated as*

$$\phi(\lambda) = \frac{8\pi ch\lambda^{-5}}{e^{ch/\lambda kT} - 1}. \tag{37}$$

where λ is wavelength of the radiation, c is speed of light, T is absolute temperature of the black body, k is Boltzmann's constant, and h is Planck's constant. The problem is to determine the wavelength λ corresponding to maximum energy density $\phi(\lambda)$. Thus, Equation (37) leads to

$$\phi'(\lambda) = \left(\frac{8\pi ch\lambda^{-6}}{e^{ch/\lambda kT} - 1}\right)\left(\frac{(ch/\lambda kT)e^{ch/\lambda kT}}{e^{ch/\lambda kT} - 1} - 5\right) = A.B. \ (say)$$

Note that a maxima for ϕ will occur when $B = 0$, that is when

$$\frac{(ch/\lambda kT)e^{ch/\lambda kT}}{e^{ch/\lambda kT} - 1} = 5.$$

Setting $t = ch/\lambda kT$, the above equation assumes the form

$$1 - \frac{t}{5} = e^{-t}. \tag{38}$$

Define

$$f_1(t) = e^{-t} - 1 + \frac{t}{5}. \tag{39}$$

The root $t = 0$ is trivial and thus is not taken for discussion. Observe that for $t = 5$ the left-hand side of Equation (38) is zero and the right-hand side is $e^{-5} \approx 6.74 \times 10^{-3}$. Thus, we guess that another root might occur *somewhere near to $t = 5$. In fact, the expected root of Equation (39) is given by $\alpha \approx 4.96511423174427630369$ with $t_0 = 5.5$. Then, the wavelength of radiation (λ) corresponding to maximum energy density is*

$$\lambda \approx \frac{ch}{4.96511423174427630369(kT)}.$$

The results so obtained are shown in Table 1.

Example 2. *Consider the van der Waals equation (see [15])*

$$\Big(P + \frac{a_1 n^2}{V^2}\Big)(V - na_2) = nRT,$$

that explains the nature of a real gas by adding two parameters a_1 and a_2 in the ideal gas equation. To find the volume V in terms of rest of the parameters, one requires solving the equation

$$PV^3 - (na_2P + nRT)V^2 + a_1n^2V - a_1a_2n^2 = 0.$$

One can find values of n, P, and T, for a given a set of values of a_1 and a_2 of a particular gas, so that the equation has three roots. Using a particular set of values, we have the function

$$f_2(t) = t^3 - 5.22t^2 + 9.0825t - 5.2675,$$

that has three roots from which one is simple zero $\alpha = 1.72$ and other one is a multiple zero $\alpha = 1.75$ of multiplicity two. However, our desired zero is $\alpha = 1.75$. The methods are tested for initial guess $t_0 = 2.5$. Computed results are given in Table 2.

Example 3. *Next, we assume a standard nonlinear test function which is defined as*

$$f_3(t) = \Big[\tan^{-1}\Big(\frac{\sqrt{5}}{2}\Big) - \tan^{-1}(\sqrt{t^2-1}) + \sqrt{6}\Big(\tan^{-1}\Big(\sqrt{\frac{t^2-1}{6}}\Big) - \tan^{-1}\Big(\frac{1}{2}\sqrt{\frac{5}{6}}\Big)\Big) - \frac{11}{63}\Big]^3.$$

The function f_3 has multiple zero at $\alpha = 1.8411027704926161\ldots$ of multiplicity three. We select initial approximation $t_0 = 1.6$ to obtain zero of this function. Numerical results are exhibited in Table 3.

Example 4. *Lastly, we consider another standard test function, which is defined as*

$$f_4(t) = t(t^2+1)(2e^{t^2+1} + t^2 - 1)\cosh^2\Big(\frac{\pi t}{2}\Big).$$

The function f_4 has multiple zero at i of multiplicity four. We choose the initial approximation $x_0 = 1.2i$ for obtaining the zero of the function. Numerical results are displayed in Table 4.

Table 1. Numerical results for Example 1.

Method	k	$\lvert t_2 - t_1\rvert$	$\lvert t_3 - t_2\rvert$	$\lvert t_4 - t_3\rvert$	**CCO**	**CPU-Time**
LLC	4	1.51×10^{-5}	1.47×10^{-23}	1.30×10^{-95}	4.000	0.4993
LCN	4	1.55×10^{-5}	1.73×10^{-23}	2.65×10^{-95}	4.000	0.5302
SS	4	1.52×10^{-5}	1.51×10^{-23}	1.47×10^{-95}	4.000	0.6390
ZCS	4	1.57×10^{-5}	1.87×10^{-23}	3.75×10^{-95}	4.000	0.6404
SBL	4	1.50×10^{-5}	1.43×10^{-23}	1.19×10^{-95}	4.000	0.8112
KKB	fails	-	-	-	-	-
NM1	3	5.59×10^{-6}	1.35×10^{-25}	0	4.000	0.3344
NM2	3	5.27×10^{-6}	9.80×10^{-26}	0	4.000	0.3726
NM3	3	5.43×10^{-6}	1.16×10^{-25}	0	4.000	0.3475

Table 2. Numerical results for Example 2.

Method	k	$\lvert t_2 - t_1 \rvert$	$\lvert t_3 - t_2 \rvert$	$\lvert t_4 - t_3 \rvert$	CCO	CPU-Time
LLC	6	9.09×10^{-2}	8.03×10^{-3}	2.33×10^{-5}	4.000	0.0780
LCN	6	9.09×10^{-2}	8.03×10^{-3}	2.33×10^{-5}	4.000	0.0784
SS	6	9.26×10^{-2}	8.58×10^{-3}	3.11×10^{-5}	4.000	0.0945
ZCS	6	9.62×10^{-2}	9.84×10^{-3}	5.64×10^{-5}	4.000	0.0792
SBL	6	9.09×10^{-2}	8.03×10^{-3}	2.33×10^{-5}	4.000	0.0797
KKB	6	8.97×10^{-2}	7.62×10^{-3}	1.68×10^{-5}	4.000	0.0934
NM1	6	9.91×10^{-2}	1.08×10^{-2}	8.79×10^{-5}	4.000	0.0752
NM2	6	8.06×10^{-2}	5.08×10^{-3}	2.81×10^{-5}	4.000	0.0684
NM3	6	8.78×10^{-2}	7.02×10^{-3}	1.31×10^{-5}	4.000	0.0788

Table 3. Numerical results for Example 3.

Method	k	$\lvert t_2 - t_1 \rvert$	$\lvert t_3 - t_2 \rvert$	$\lvert t_4 - t_3 \rvert$	CCO	CPU-Time
LLC	4	1.11×10^{-4}	9.02×10^{-19}	3.91×10^{-75}	4.000	2.5743
LCN	4	1.11×10^{-4}	8.93×10^{-19}	3.72×10^{-75}	4.000	2.6364
SS	4	1.11×10^{-4}	8.71×10^{-19}	3.29×10^{-75}	4.000	2.8718
ZCS	4	1.11×10^{-4}	8.16×10^{-19}	2.38×10^{-75}	4.000	2.8863
SBL	4	1.11×10^{-4}	8.63×10^{-19}	3.15×10^{-75}	4.000	3.2605
KKB	4	1.11×10^{-4}	9.80×10^{-19}	5.87×10^{-75}	4.000	2.9011
NM1	4	2.31×10^{-5}	4.04×10^{-21}	3.78×10^{-84}	4.000	2.2935
NM2	4	2.07×10^{-5}	1.32×10^{-21}	2.18×10^{-86}	4.000	2.5287
NM3	4	2.11×10^{-5}	1.66×10^{-21}	6.36×10^{-86}	4.000	2.4964

Table 4. Numerical results for Example 4.

Method	k	$\lvert t_2 - t_1 \rvert$	$\lvert t_3 - t_2 \rvert$	$\lvert t_4 - t_3 \rvert$	CCO	CPU-Time
LLC	4	2.64×10^{-4}	2.13×10^{-15}	9.11×10^{-60}	4.000	1.7382
LCN	4	2.64×10^{-4}	2.14×10^{-15}	9.39×10^{-60}	4.000	2.4035
SS	4	2.64×10^{-4}	2.18×10^{-15}	1.01×10^{-59}	4.000	2.5431
ZCS	4	2.65×10^{-4}	2.24×10^{-15}	1.14×10^{-59}	4.000	2.6213
SBL	4	2.66×10^{-4}	2.28×10^{-15}	1.23×10^{-59}	4.000	3.2610
KKB	4	2.61×10^{-4}	2.00×10^{-15}	6.83×10^{-60}	4.000	2.6524
NM1	4	1.43×10^{-4}	1.29×10^{-16}	8.61×10^{-65}	4.000	0.5522
NM2	4	4.86×10^{-5}	5.98×10^{-20}	1.36×10^{-79}	4.000	0.6996
NM3	4	6.12×10^{-5}	6.69×10^{-19}	9.54×10^{-75}	4.000	0.6837

From the computed results shown in Tables 1–4, we can observe a good convergence behavior of the proposed methods similar to those of existing methods. The reason for good convergence is the increase in accuracy of the successive approximations per iteration, as is evident from numerical results. This also points to the stable nature of methods. It is also clear that the approximations to the solutions by the new methods have accuracies greater than or equal to those computed by existing methods. We display the value 0 of $|t_{k+1} - t_k|$ at the stage when stopping criterion $|t_{k+1} - t_k| + |f(t_k)| < 10^{-100}$ has been satisfied. From the calculation of computational order of convergence shown in the penultimate column in each table, we verify the theoretical fourth-order of convergence.

The efficient nature of presented methods can be observed by the fact that the amount of CPU time consumed by the methods is less than the time taken by existing methods (result confirmed by similar numerical experiments on many other different problems). The methods requiring repeated evaluations of the roots (such as the ones tackled in [21–24]), also may benefit greatly from the use of proposed methods (NM1–NM3, Equations (33)–(35)).

5. Conclusions

In this paper, we propose a family of fourth-order derivative-free numerical methods for obtaining multiple roots of nonlinear equations. Analysis of the convergence was carried out, which proved the order four under standard assumptions of the function whose zeros we are looking for. In addition, our designed scheme also satisfies the Kung–Traub hypothesis of optimal order of convergence. Some special cases are established. These are employed to solve nonlinear equations including those arising in practical problems. The new methods are compared with existing techniques of same order. Testing of the numerical results shows that the presented derivative-free methods are good competitors to the existing optimal fourth-order techniques that require derivative evaluations in the algorithm. We conclude the work with a remark that derivative-free methods are good alternatives to Newton-type schemes in the cases when derivatives are expensive to compute or difficult to obtain.

Author Contributions: Methodology, J.R.S.; writing, review and editing, J.R.S.; investigation, S.K.; data curation, S.K.; conceptualization, L.J.; formal analysis, L.J.

Funding: This research received no external funding.

Conflicts of Interest: The authors declare no conflict of interest.

References

1. Schröder, E. Über unendlich viele Algorithmen zur Auflösung der Gleichungen. *Math. Ann.* **1870**, *2*, 317–365. [CrossRef]
2. Hansen E.; Patrick, M. A family of root finding methods. *Numer. Math.* **1977**, *27*, 257–269. [CrossRef]
3. Victory, H.D.; Neta, B. A higher order method for multiple zeros of nonlinear functions. *Int. J. Comput. Math.* **1983**, *12*, 329–335. [CrossRef]
4. Dong, C. A family of multipoint iterative functions for finding multiple roots of equations. *Int. J. Comput. Math.* **1987**, *21*, 363–367. [CrossRef]
5. Osada, N. An optimal multiple root-finding method of order three. *J. Comput. Appl. Math.* **1994**, *51*, 131–133. [CrossRef]
6. Neta, B. New third order nonlinear solvers for multiple roots. *App. Math. Comput.* **2008**, *202*, 162–170. [CrossRef]
7. Li, S.; Liao, X.; Cheng, L. A new fourth-order iterative method for finding multiple roots of nonlinear equations. *Appl. Math. Comput.* **2009**, *215*, 1288–1292.
8. Li, S.G.; Cheng, L.Z.; Neta, B. Some fourth-order nonlinear solvers with closed formulae for multiple roots. *Comput Math. Appl.* **2010**, *59*, 126–135. [CrossRef]
9. Sharma, J.R.; Sharma, R. Modified Jarratt method for computing multiple roots. *Appl. Math. Comput.* **2010**, *217*, 878–881. [CrossRef]
10. Zhou, X.; Chen, X.; Song, Y. Constructing higher-order methods for obtaining the multiple roots of nonlinear equations. *J. Comput. Appl. Math.* **2011**, *235*, 4199–4206. [CrossRef]
11. Sharifi, M.; Babajee, D.K.R.; Soleymani, F. Finding the solution of nonlinear equations by a class of optimal methods. *Comput. Math. Appl.* **2012**, *63*, 764–774. [CrossRef]
12. Soleymani, F.; Babajee, D.K.R.; Lotfi, T. On a numerical technique for finding multiple zeros and its dynamics. *J. Egypt. Math. Soc.* **2013**, *21*, 346–353. [CrossRef]
13. Geum, Y.H.; Kim Y.I.; Neta, B. A class of two-point sixth-order multiple-zero finders of modified double-Newton type and their dynamics. *Appl. Math. Comput.* **2015**, *270*, 387–400. [CrossRef]
14. Kansal, M.; Kanwar, V.; Bhatia, S. On some optimal multiple root-finding methods and their dynamics. *Appl. Appl. Math.* **2015**, *10*, 349–367.
15. Behl, R.; Zafar, F.; Alshormani, A.S.; Junjua, M.U.D.; Yasmin, N. An optimal eighth-order scheme for multiple zeros of unvariate functions. *Int. J. Comput. Meth.* **2019**, *16*, 1843002. [CrossRef]
16. Traub, J.F. *Iterative Methods for the Solution of Equations*; Chelsea Publishing Company: New York, NY, USA, 1982.
17. Kung, H.T.; Traub, J.F. Optimal order of one-point and multipoint iteration. *J. Assoc. Comput. Mach.* **1974**, *21*, 643–651. [CrossRef]

18. Wolfram, S. *The Mathematica Book*, 5th ed.; Wolfram Media: Bengaluru, India, 2003.
19. Weerakoon, S.; Fernando, T.G.I. A variant of Newton's method with accelerated third-order convergence. *Appl. Math. Lett.* **2000**, *13*, 87–93. [CrossRef]
20. Bradie, B. *A Friendly Introduction to Numerical Analysis*; Pearson Education Inc.: New Delhi, India, 2006.
21. Jäntschi L.; Bolboacă S.D. Conformational study of C_{24} cyclic polyyne clusters. *Int. J. Quantum Chem.* **2018**, *118*, e25614. [CrossRef]
22. Azad H.; Anaya K.; Al-Dweik A. Y.; Mustafa M. T. Invariant solutions of the wave equation on static spherically symmetric spacetimes admitting G7 isometry algebra. *Symmetry* **2018**, *10*, 665. [CrossRef]
23. Matko, V.; Brezovec, B. Improved data center energy efficiency and availability with multilayer node event processing. *Energies* **2018**, *11*, 2478. [CrossRef]
24. Jäntschi L. The eigenproblem translated for alignment of molecules. *Symmetry* **2019**, *11*, 1027. [CrossRef]

symmetry

MDPI

Article

Facility Location Problem Approach for Distributed Drones

Jared Lynskey, Kyi Thar, Thant Zin Oo and Choong Seon Hong *

Department of Computer Science and Engineering, Kyung Hee University, Yongin-si, Gyeonggi-do 17104, Korea; jared@khu.ac.kr (J.L.); kyithar@khu.ac.kr (K.T.); tzoo@khu.ac.kr (T.Z.O.)

* Correspondence: cshong@khu.ac.kr

Received: 2 January 2019; Accepted: 15 January 2019; Published: 20 January 2019

Abstract: Currently, industry and academia are undergoing an evolution in developing the next generation of drone applications. Including the development of autonomous drones that can carry out tasks without the assistance of a human operator. In spite of this, there are still problems left unanswered related to the placement of drone take-off, landing and charging areas. Future policies by governments and aviation agencies are inevitably going to restrict the operational area where drones can take-off and land. Hence, there is a need to develop a system to manage landing and take-off areas for drones. Additionally, we proposed this approach due to the lack of justification for the initial location of drones in current research. Therefore, to provide a foundation for future research, we give a justified reason that allows predetermined location of drones with the use of drone ports. Furthermore, we propose an algorithm to optimally place these drone ports to minimize the average distance drones must travel based on a set of potential drone port locations and tasks generated in a given area. Our approach is derived from the Facility Location problem which produces an efficient near optimal solution to place drone ports that reduces the overall drone energy consumption. Secondly, we apply various traveling salesman algorithms to determine the shortest route the drone must travel to visit all the tasks.

Keywords: drone deployment; drone port; traveling salesman; facility location problem

1. Introduction

Recent reports from the Federal Aviation Agency state that there will be an increase from 2.75 to 4.47 million small drones operating in the United States by 2021. Since the end of May 2017, more than 772,000 owners have already registered with the Federal Aviation Administration (FAA) [1]. The main reason for the sudden increase in drone ownership is due to consumers purchasing drones for their high mobility and applications in the field of computer vision [2]. Thus, a shift in vision related jobs (building inspection, traffic monitoring and temporary cellular coverage extension) slowly being taken over by drones to perform these tasks. This is because drones can provide the required perspective for jobs such as bird's eye view. Additionally, by using machines to take pictures in hazardous areas, we can minimize the risk to human safety. However, there is still no proposal on the initial deployment of drones which do not include random placement. Furthermore, the cost of privately owning drones can be far too expensive for companies who may only require drones for a single task, in comparison to renting drones [3]. In the case of a rental system, companies and users are not required to purchase a drone allowing the cost to be fairly distributed amongst them. Although the cost to rent can reduce the overall cost when compared to owning a drone. Typically, users must visit a rental center to collect the drone. Otherwise, the drone must fly from the shop to the task, reducing the total energy available for completing tasks. Therefore, to overcome these foreseen issues, an unmanned drone rental service that utilizes drones placed at distributed drone ports is necessary. By providing a public service that allows the rental of distributed autonomous drones waiting at drone ports, this can reduce the total number of drones in the sky and the total cost of utilizing drones to complete tasks requested by the user. Thus, we propose an algorithm that can be applied to a shared drone service to reduce the excessive utilization to increase the efficiency by intelligently placing drone ports in respect to the demand and limitations of drones.

1.1. Motivation for Distributed Drone Ports

In this paper, we assume that drones will return to the drone port and charge after each cycle since there are already companies creating landing pads, including Skysense (San Francisco, CA, USA) [4]. We imagine that drones must land, take off and be stored at the base of the drone port to charge drones while they are not completing tasks in the air to remove the risk of users being injured by rotating blades and electrical components that charge the drone. Multiple charging pads can be distributed over an area to reduce the average distance drones must travel to recharge. By doing so, we believe the cost of operating a fleet of drones located at distributed drone ports will be less than the cost of operating a central drone port because miniature drones don't require a large drone and can be located from small areas such as building tops to open fields closer to tasks. Finally, the introduction of drone ports will give future research a foundation to justify their initial placement of drones.

1.2. Related Work

This section encompasses the work done by researchers who look at the problem of optimally placing drones in the sky. However, from our research, we noticed that none of their work justified the reason for the initial and final location of drones in their work. Thus, we proposed an idea to justify further work's reasoning of the initial and final location of drones. The authors in paper [5] propose a discrete and continuous environment to determine the location of drones based on the users. However, they fail to consider where these drones will begin and end their mission. Related work in the field of deploying drones to provide coverage has been growing in interest. In Ref. [6], authors proposed an optimal transport approach to minimize the energy consumption to gather data from moving clusters of IoT (Internet of Things) devices. Works related to a rental system outline the challenges of providing enough assets to satisfy the number of users in the area.

1.3. Challenges

One challenge faced with proposing a rental system is the finite number of combinations possible between the number of drone ports, the location of drone ports and the association between tasks and drones located at drone ports. Thus, we require an efficient mixed integer problem approach to solve our facility location framework. To complement our facility location framework, we apply a subfield of machine learning, clustering, to quickly identify the most efficient central points as drone ports.

Using the original facility location framework to solve the problem is a complex procedure that does not guarantee an optimal solution because it only considers the average distance between the drone ports and facilities. We also need to find the round-trip path to ensure that the drone can complete all the tasks in its cluster.

Drones come in a variety of classes as outlined in Table 1. However, previous research shows, among the available class of drones, the outlook looks the most promising for mini drones. This is due to the fact that mini drones are expected to reach a level of autonomous control within the next five years that meets FAA requirements. Despite the current legal roadblocks imposed by the FAA, there is likely still going to be an increasing demand for mini drones in civilian. Mostly due to their small size compared with larger drones, mini drones have a much greater intrinsic safety rating [7]. Furthermore, the reason for choosing mini drones to complete tasks is due to their high mobility and much lower cost compared with larger drones. Academics are already working to implement vision systems to allow drones to land [8].

Table 1. The various class of drones available.

Category Name	Mass [kg]	Range [km]	Flight Altitude [m]	Endurance [Hours]
Micro	<5	<10	250	1
Mini	<20/30/150	<10	150/250/300	<2
Close Range	25–150	10–30	3000	2–4
Medium Range	50–250	30–70	3000	3–6
High Alt. Long Endurance	>250	>70	>3000	>6

1.4. Facility Location Problem

The Facility Location problem consists of a set of potential drone port locations L. We use this set of potential drone locations to discretize our solution space. Secondly, there is also a set of task locations D that must be serviced, as seen in Figure 1. The objective is to pick a subset l of drone ports to open that minimizes the average distance between each customer and facility. The Uncapacitated Facility Location (UFLP) and Capacitated Facility Location (CFLP) constitute the basic discrete facility location formulation with an abundance of papers based on their extensions by relaxing one or more of the underlying assumptions. The current state-of-the-art algorithm for solving Facility Location problems is proposed by [9]. They provide a close approximation to the global optimum. We can apply the facility location problem formulation since a drone port is considered to be a facility with limited output and a task can be considered as a customer, with a required demand. However, because our problem is not related to delivery trucks, we must make some adjustments to the original problem to ensure that the drones can perform the task without running out of energy. For the situation where there is delay, a congested facility location problem can be applied to minimize the waiting times for customers [10]. Next, we apply the shortest path algorithm to confirm if a generated cluster of tasks can be served by the drone port facility. In Figure 1, we illustrate the decision-making process. The light shaded gray drone ports are the drone ports that were not constructed. Otherwise, the drone ports selected to optimally serve tasks based on information such the population density and task arrival rate. Each cell in Figure 1 represents the discrete space of potential drone port places.

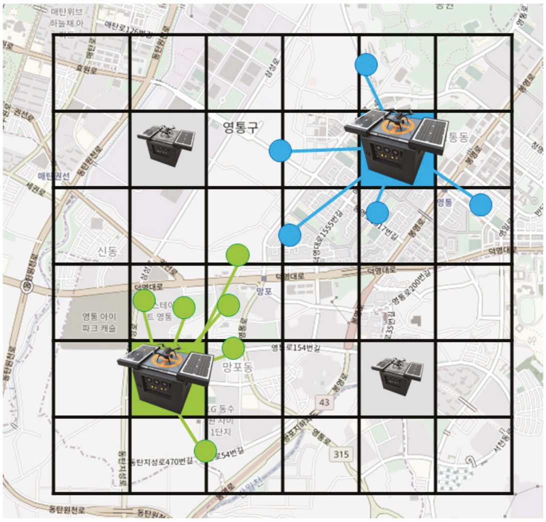

Figure 1. An example of selecting drone ports based on a set of potential 'facility' locations.

1.5. K-Means Clustering Algorithms

Papers that utilize drones to provide coverage to a cluster of users such as [11] attempt to maximize the ground users' battery life by deploying drones in areas where existing macro base stations can not provide sufficient coverage. Their numerical analysis showed promising results due to the fact that their algorithm was able to position drones so that over 60% of users fell within a drone's coverage. However, they did not benchmark their algorithm with other clustering methods, therefore making it difficult to truly understand if their approach was any better than other methods including exhaustive search. One interesting point was their data was based on real Beijing downtown trajectory data. The authors who proposed a k-means stochastic approach gave promising results with a level of complexity $O(\frac{1}{t})$ under general conditions [12] with mini batches improving the speed of convergence even more.

2. Materials and Methods

We envision that multiple drone ports will be managed by a central controller that is responsible for assigning autonomous grounded drones waiting at a drone port to tasks located within the drones operational coverage, removing the need for users to privately own a drone. A drone port is designed to be a small designated take-off, landing and charging area for autonomous drones. Our method to solve this is based on a facility location problem. Furthermore, our tasks only include those related to computers, which just requires the drone to visit the task location, take a photo, and then return to the base or move on to the next task. The tasks considered in this paper assumed that the drone is capable of completing the digital task at the requested location without the need to adjust its path to deliver a physical object, such as a delivery service. We apply k-means to reduce the complexity by implementing a clusters subject to our framework based on the facility problem. Once the model is matured, it allows us to determine the optimal location to install drone ports based on task demand. Then, for additional tasks, we can immediately assign tasks to their respective drone port, thus reducing the computational time to optimally associate drone port and tasks. Lastly, we distributed the drone ports over an area to increase the average number of tasks a drone can complete in one charge compared to a centralized drone port approach. In this section, we explain our system model and justify our approach to solve the issue of placing drones efficiently in an area. Finding the optimal solution for a Facility location problem is NP-Hard, it is not therefore advisable to use an exhaustive method to determine the optimal number of drones. Our algorithm utilizes clustering to reduce the initial search space of possible paths, thus improving the efficiency of our algorithm while giving a near optimal route for drones. We also perform heuristic analysis to find the point at which each drone can complete all of its tasks assigned to it during the cluster phase.

2.1. Central Controller

In our model, we consider a central controller that is responsible for a set of drone ports that each have one drone. By using a central controller, we can assume that information containing the drone state, drone port and task state is available. Therefore, giving a large advantage over a completely distributed systems since information is accessible in a single place and can be used to increase the co-operation between drones waiting at drone ports.

2.2. Drone Port

We propose the idea of a drone port that is connected via existing infrastructure to a central controller then controls the drone and dispatches it to a job. Our model will consider a drone's initial position (x, y) at a drone port as well as the energy consumption e to fly to and from the task, and the energy consumed while completing a task, and the distance flown before it can perform a task τ.

2.3. Objective

Drones are considered to be resourced constrained devices; therefore, it is important that our cost function puts an emphasis on maximizing the utility of a drone in one charge cycle, while ensuring that it can safely return back to the drone to charge. Thus, the objective function is to minimize the number of drone ports in a given area to serve as many tasks as possible. Then, we analyze the result by applying various traveling salesman algorithms to see which algorithm maximizes the number of tasks that can be completed subject to task delay and energy constraints.

2.4. Tasks

Tasks are generated by actual users or artificial intelligent agents that require data or images that can only be collected by drones due to the location or danger to human safety. Since we can assume that our tasks will be periodically requested, it is feasible to estimate an arrival rate based on factors around the area, such as population density. The tasks in terms of a facility location problem are known as the customers that must be served by some facility. In terms of drone demand, we can apply different degrees of energy requirements to complete a task. For example, a task may require v units of energy to perform a task, so, therefore, there must be v units of energy available in the drone's battery to complete the task.

In Figure 2, we illustrate that a drone can only land and take off at its own drone port, in the case of a single drone at a drone port.

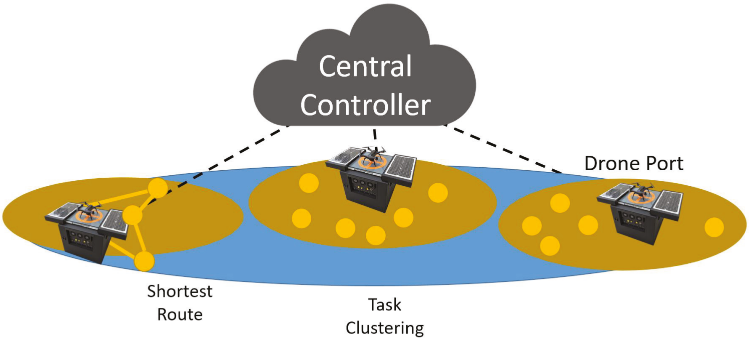

Figure 2. An example of a distributed drone port system.

2.5. Energy Consumption

We estimate the energy consumption to be the following:

$$e_{c+1} = e_c - \sum_{T \in d_i} t_p + \sum_{T \in d_i} ||v*||\gamma. \tag{1}$$

The energy consumption is calculated by the measuring the distance the drone must travel multiplied by its energy consumption rate and the total energy required by its respective tasks. The approximate energy function is vital because it calculates the energy remaining in a drone and allows us to determine if the path generated is feasible. The energy level after a cycle is denoted as e_{c+1}. This energy level is calculated from the current energy state minus the task energy t_p and distance traveled $||v*||$ multiplied with an energy consumption constant γ [13]. Equation (1) shows that the drone's energy in the next cycle is its current energy minus the power requirements of the task and the distance traveled to complete those tasks and return to its station.

2.6. Facility Location Problem

The objective of an capacitated facility location is to minimize the distance between the tasks and central drone port. We use this technique in combination with a shortest route algorithm to ensure that the coverage size and the number of drones is suitable to satisfy all the tasks generated near the drone port. In our initial formulation, introduce variable x_i, x_j containing the co-ordinates of potential drone ports and tasks, respectively, where $z_i = 1, \dots, n$ where $x_i = 1$ if drone port i is built, and $x_i = 0$, otherwise. We can treat the drone port acts as a facility because it contains the service subject to the energy constraint, known as the supply.

2.7. Capital Expenditure

In respect to capital expenditure, our objective is to minimize the total monetary cost of building new infrastructure. In the below cost function, our goal is to reduce the total distance between the drone port x_i and tasks x_j. Since we are limited by the budget F, it is impossible to build every potential drone port i:

$$\begin{array}{lll}
\text{minimize} & \sum\limits_{d_i} d_{ij}, & \\
\text{subject to} & \sum\limits_{i \in A} \quad c_i z_i \leq F, & i = 1, ..., n, \\
 & \quad x_j \in \{0,1\}, & j = 1, ..., m, \\
 & \quad d_{ij} = ||x_i - x_j||_2. &
\end{array} \tag{2}$$

2.8. Operational Expenditure

In respect to operational expenditure, our objective is to maximize the number of jobs denoted as y_{ij} the index of a job while satisfying constraints such as τ_j delay for every job. Furthermore, each drone must return back to its drone port. Lastly, the path generated must not exceed the drone's energy capacity denoted as the function $f(d_{ij})$

$$\begin{array}{lll}
\text{maximize} & \sum\limits_{i}\sum\limits_{j} y_{ij}, & \\
\text{subject to} & \sum\limits_{j} \quad y_{ij} f(d_{ij}) \leq B_i & i = 1, ..., n, \\
 & \quad x_0 = x_{fac}, & \\
 & \quad x_{final} = x_{fac}, & \\
 & \quad \tau_j \leq \hat{\tau}_j, & \\
 & \quad f(d_{ij}) = P * d_{ij} + \eta, & \\
 & \quad \tau_j = t_{complete} - t_{arrival}. &
\end{array} \tag{3}$$

2.9. Drone Port Placement Algorithm

Algorithm 1 is an overview of our proposed algorithm to efficiently place drones in a distributed area. We develop a heuristic approach by implementing a clustering and traveling salesman problem ensemble to determine the feasibility our algorithm's output data. We continue to increase the number of drone ports until each drone has enough energy to perform all of the tasks in its coverage.

Algorithm 1 Facility Location Problem for Drones

```
procedure DRONE PORT PLACEMENT AND SHORTEST ROUTE
    $i \leftarrow$ max number of droneports
    $T \leftarrow$ Task Locations array
    $P \leftarrow$ Set of drone ports array
    $P_{max} \leftarrow$ max number of droneports
    $p \leftarrow$ Initial number of droneports
    while $p \leq P_{max}$ do
        $clusters \leftarrow GenerateCluster(Tasks, p)$
        $shortestroute \leftarrow TSP(tasks, droneport)$
        $e \leftarrow f(d_i j)$
        if $e \geq \theta$ then
            Break
        else
            $p \leftarrow p + 1$
    return Drone Port location
    return Shortest Routes
```

2.10. Traveling Salesman Problem

After creating the clusters, we apply a shortest route algorithm to ensure that the drone can perform all of the tasks allocated to it while completing a round-trip back to its original drone port. It is denoted as the Traveling Salesman Problem (TSP) below.

3. Performance Evaluation

Our simulation was conducted on a PC with the operating system Ubuntu 16.04. We applied the algorithms in Table 2 written in Python 3.5 to conduct our simulations. The area size for our simulation is 1000 × 1000 units.

Table 2. Algorithms we compared.

Algorithm	Type	Author
2-opt	Shortest Path	[14]
Genetic Algorithm	Shortest Path	[15]
Exhaustive Search	Shortest Path	
Ant Colony	Shortest Path	[16]
k-means	Clustering	[17]

3.1. Coverage Size effect on the Combinatorial Search Space

In Figure 3, we analyzed the combination space size in log units if clustering was not applied. Increasing the potential coverage size and the number of potential drone ports exponentially increases the search space. The average complexity is given by $O(kn^T)$, where n is the number of combinations and T is the maximum number of iterations. In practice, the k-means algorithm is fast, but it tends to return a local minima. To avoid this, we used a bottom up approach to avoid falling in to any local minima [18]. This means we can effectively reduce the number of combinations greatly by applying k-means instead of using a naive approach such as a fixed coverage area. The constraints in our proposal ensure that no task appears outside a drone port's range due to improper clustering.

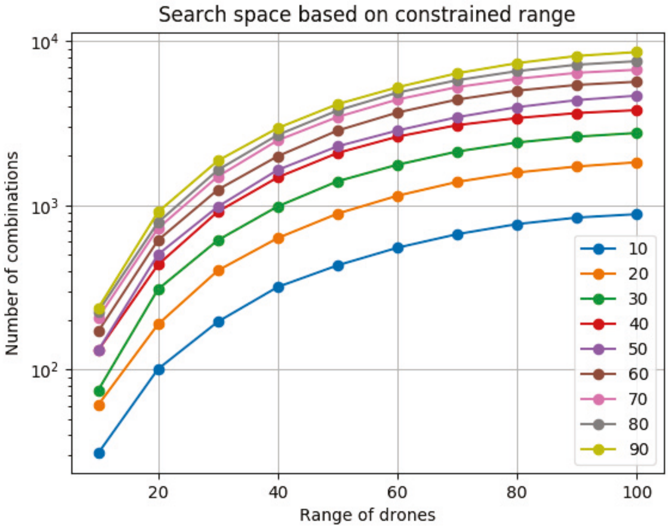

Figure 3. The worst case to determine the optimal solution for possible drone port coverage sizes.

3.2. Average Round Trip Distance

In Figure 4, we determined the coverage and round trip distance. The result comes from our problem formulation constraint, which is that the drone must visit all the tasks assigned within its cluster. Our k-means selects locations based on shortest average distance between the potential drone port point and task locations. The red line shows the optimal solution. It may provide the shortest path and least cost, but it is computationally expensive by almost 50% on average compared with the approximation algorithms. The issue with the genetic algorithm shown in Figure 4 is due to the random approach it takes to converge to the optimal solution. This may have been due to not allowing enough generations to fine the combination that gives the shortest path. Secondly, the 2-opt algorithm performs slight worse, due to being a single thread and with a limited number of iterations to find the optimal solution. Each time the number of drone ports increases, the number of combinations between drone ports and tasks is restricted—thus allowing the solver to find the optimal solution with multiple solution sub-spaces to solve producing a near-optimal solution. The genetic algorithm was able to find a near-optimal solution once the sub-spaces were small enough so its random choices had a larger impact on the distance traveled.

3.3. Infrastructure and Energy Cost

In Figure 5, we compared the cost of having drones fly further versus the cost of installing a drone port. For this experiment, we set the cost of a drone flying per unit distance γ to 0.5. In addition, the cost of a drone port to c 2. If our cost to install a drone port was a lot less than the operating cost of a drone, then there would likely be a lot more drone ports since more ports would be possible without increasing the budget. However, this cost does not consider the on-going costs of maintenance for the drones and drone ports. These values can be configured later to reflect actual prices of drone ports and electricity.

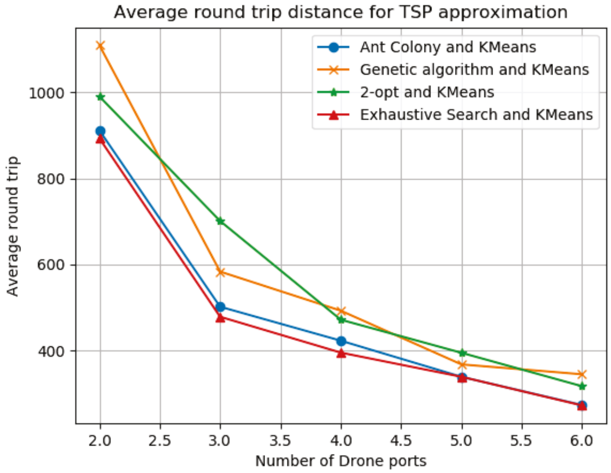

Figure 4. Average round trip for drones based on k-means clustering and Traveling Salesman Approximation.

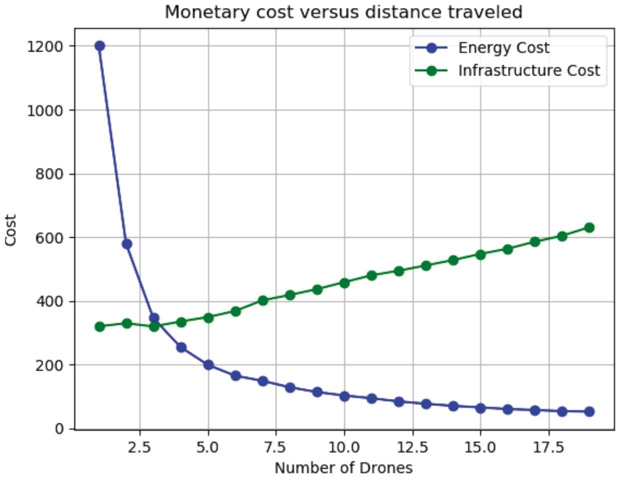

Figure 5. Infrastructure vs. monetary cost.

3.4. Discussion

Further studies that are concerned with the efficient placement of drone ports can now consider our model to further reduce their model's complexity and reduce the distance each drone requires to visit each task. The algorithm is also robust to environments with dynamic arrival rates since we are not randomly placing drone port areas. Instead, by using the k-means cluster, we can efficiently determine areas to install drone ports, centroids where there is a high density of tasks appearing. Although our research was able to show a reduction in the distance covered by drones, our model does not consider factors such as external costs such as maintaining a distributed system. We imagine this cost will be negligible since there is little to no moving parts associated with a drone port, and only the drone. Furthermore, the charging speed and properties of a drone port are still undecided. This system can also be further improved by including terrain data to minimize the difference in the drone port and flight altitude height to which the drone must fly. We did not cover the implications of security or privacy in this paper, but it is something to realize since our framework could be used to spy as noted in [19], therefore identifying rouge tasks is important. Several additional avenues for drone port include the following—firstly, considering information such as buildings or landmarks to include in the final decision-making to create a path that the drone can follow to complete the task; secondly, adding more capacity at drone ports to allow multiple drones to land and take off; thirdly, optimizing the coverage in a way that maximizes co-operation between drones such as a chain link deliver system; and, fourthly, creating boundaries for partitions between two central controllers would allow for a hybrid solution with each sub-space of an area having its own controller. Lastly, we also wish to work on improving the computational efficiency of our proposed algorithm.

4. Conclusions

We proposed a novel algorithm to manage distributed drone ports with a centralized controller to ensure maximum co-operation between drones and fair allocation of tasks. The main goal of this system is to efficiently assign grounded drones at drone ports with their respective tasks. Our combination of approximation algorithms ensures that the cluster of tasks belonging to each drone port are within the drone's coverage. Second, the drone can perform the maximum number before returning to the drone port to recharge. We show that utilizing the Ant algorithm for our cluster round trip for drones minimizes the distance traveled for each drone. By utilizing this approach, further tasks assigned to an area can be immediately be assigned without the need to recalculate the entire environment.

Author Contributions: Conceptualization, J.L.; Methodology, J.K., K.T., T.Z.O.; Software, J.L.; Validation, J.L., Y.Y. and Z.Z.; Formal Analysis, J.L., K.T., T.Z.O.; Investigation, J.K., K.T.; Resources, X.X.; Data Curation, J.K.; Writing—Original Draft Preparation, J.K., K.T.; Writing—Review and Editing, J.L.; Visualization, J.K.; Supervision, C.S.H.

Funding: This research was supported by the MSIT(Ministry of Science and ICT), Korea, under the Grand Information Technology Research Center support program (IITP-2018-2015-0-00742) supervised by the IITP(Institute for Information and communications Technology Promotion).

Conflicts of Interest: The authors declare no conflict of interest.

Abbreviations

Notation used in this article

Notation	Explanation
e_c	Set of drone ports
t_p	Set of drones
d_i	Drone i
$v*$	Vector
γ	Drone energy level
d_{ij}	Distance between task j and drone port i
c_i	Cost to build drone port
z_i	Decision variable to build drone port
x_j	Decision variable for drone i to complete task j
y_{ij}	Task completion state $\{0,1\}$
x_0	Drone initial position
x_0	Drone final position
τ_j	Calculated task completion delay
$\hat{\tau}_j$	Earliest deadline first constraint
$f(d_{ij})$	Power Function
$\tau_{complete}$	Drone energy function
$\tau_{arrival}$	Minimum drone energy
η	Task's drone energy consumption
η	Task's drone energy consumption

References

1. FAA. Unmanned Aircraft System. *FAA Aerosp. Forecast.* **2018**. Available online: https://www.faa.gov/data_research/aviation/aerospace_forecasts/media/Unmanned_Aircraft_Systems.pdf (accessed on 12 November 2018).
2. Kanellakis, C.; Nikolakopoulos, G. Survey on Computer Vision for UAVs: Current Developments and Trends. *J. Intell. Robot. Syst.* **2017**, *87*, 141–168. [CrossRef]
3. Purwanda, I.G.; Adiono, T.; Situmorang, S.; Dawani, F.; Samhany, H.A.; Fuada, S. Prototyping design of a low-cost bike sharing system for smart city application. In Proceedings of the 2017 International Conference on ICT For Smart Society (ICISS), Tangerang, Indonesia, 18–19 September 2017; pp. 1–6. [CrossRef]
4. Puiatti, A. Dronesense: Drone Charging Pad. 2014. Available online: https://www.skysense.co/ (accessed on 3 April 2018).
5. Sharafeddine, S.; Islambouli, R. On-Demand Deployment of Multiple Aerial Base Stations for Traffic Offloading and Network Recovery. *arXiv* **2018**, arXiv:1807.02009.
6. Chen, M.; Mozaffari, M.; Saad, W.; Yin, C.; Debbah, M.; Hong, C.S. Caching in the sky: Proactive deployment of cache-enabled unmanned aerial vehicles for optimized quality-of-experience. *IEEE J. Sel. Areas Commun.* **2017**, *35*, 1046–1061. [CrossRef]
7. Floreano, D.; Wood, R.J. Science, technology and the future of small autonomous drones. *Nature* **2015**, *521*, 460. [CrossRef] [PubMed]
8. Cesetti, A.; Frontoni, E.; Mancini, A.; Zingaretti, P.; Longhi, S. A Vision-Based Guidance System for UAV Navigation and Safe Landing Using Natural Landmarks. *J. Intell. Robot. Syst.* **2010**, *57*, 233–257. [CrossRef]
9. Ahmadian, S.; Swamy, C. Improved approximation guarantees for lower-bounded facility location. In Proceedings of the International Workshop on Approximation and Online Algorithms, Ljubljana, Slovenia, 13–14 September 2012; pp. 257–271.
10. Desrochers, M.; Marcotte, P.; Stan, M. The congested facility location problem. *Locat. Sci.* **1995**, *3*, 9–23. [CrossRef]
11. Iellamo, S.; Lehtomaki, J.J.; Khan, Z. Placement of 5G Drone Base Stations by Data Field Clustering. In Proceedings of the 2017 IEEE 85th Vehicular Technology Conference (VTC Spring), Sydney, Australia, 4–7 June 2017; pp. 1–5. [CrossRef]
12. Tang, C.; Monteleoni, C. Convergence rate of stochastic k-means. *arXiv* **2016**, arXiv:1610.04900.
13. Geng, Q.; Zhao, Z. A kind of route planning method for UAV based on improved PSO algorithm. In Proceedings of the 2013 25th Chinese Control and Decision Conference (CCDC), Guiyang, China, 25–27 May 2013; pp. 2328–2331. [CrossRef]
14. Croes, G.A. A method for solving traveling-salesman problems. *Oper. Res.* **1958**, *6*, 791–812. [CrossRef]
15. Mitchell, M. *An Introduction to Genetic Algorithms*; MIT Press: Cambridge, MA, USA, 1998.
16. Dorigo, M.; Birattari, M.; Blum, C.; Clerc, M.; Stützle, T.; Winfield, A. In *Ant Colony Optimization and Swarm Intelligence, Proceedings of the 6th International Conference, ANTS 2008, Brussels, Belgium, 22–24 September 2008*; Springer: Berlin/Heidelberg, Germany, 2008; Volume 5217.
17. Kanungo, T.; Mount, D.M.; Netanyahu, N.S.; Piatko, C.D.; Silverman, R.; Wu, A.Y. An efficient k-means clustering algorithm: Analysis and implementation. *IEEE Trans. Pattern Anal. Mach. Intell.* **2002**, *27*, 881–892. [CrossRef]
18. Arthur, D.; Vassilvitskii, S. k-means++: The advantages of careful seeding. In Proceedings of the Eighteenth Annual ACM-SIAM Symposium on Discrete Algorithms. Society for Industrial and Applied Mathematics, Philadelphia, PA, USA, 7–9 January 2007; pp. 1027–1035.
19. Gonzalez, G. Autonomous Vehicles, Drones Offer New Insurer Risks and Opportunities. Available online: https://www.businessinsurance.com/article/20171207/NEWS06/912317799/Autonomous-vehicles,-drones-offer-new-insurer-risks-and-opportunities(accessed on 12 June 2018).

symmetry

Article

Parametric Jensen-Shannon Statistical Complexity and Its Applications on Full-Scale Compartment Fire Data

Flavia-Corina Mitroi-Symeonidis [1,2], Ion Anghel [2] and Nicuşor Minculete [3,*]

[1] Academy of Economic Studies, Department of Applied Mathematics, Calea Dorobantilor 15-17, Sector 1, RO-010552 Bucharest, Romania; fcmitroi@yahoo.com

[2] Police Academy "Alexandru Ioan Cuza", Fire Officers Faculty, Str. Morarilor 3, Sector 2, RO-022451 Bucharest, Romania; ion.anghel@academiadepolitie.ro

[3] Faculty of Mathematics and Computer Science, Transilvania University of Braşov, Str. Iuliu Maniu50, 500091 Braşov, Romania

* Correspondence: minculete.nicusor@unitbv.ro

Received: 12 November 2019; Accepted: 19 December 2019; Published: 20 December 2019

Abstract: The order/disorder characteristics of a compartment fire are researched based on experimental data. From our analysis performed by new, pioneering methods, we claim that the parametric Jensen-Shannon complexity can be successfully used to detect unusual data, and that one can use it also as a means to perform relevant analysis of fire experiments. Thoroughly comparing the performance of different algorithms (known as permutation entropy and two-length permutation entropy) to extract the probability distribution is an essential step. We discuss some of the theoretical assumptions behind each step and stress that the role of the parameter is to fine-tune the results of the Jensen-Shannon statistical complexity. Note that the Jensen-Shannon statistical complexity is symmetric, while its parametric version displays a symmetric duality due to the a priori probabilities used.

Keywords: full-scale fire experiment; compartment fire; permutation entropy; two length permutation entropy; time series analysis; parametric Jensen-Shannon statistical complexity; symmetric duality

1. Introduction

We aim to perform a local entropic analysis of the evolution of the temperature during a full-scale fire experiment and seek a straightforward, general, and process-based model of the compartment fire. We propose a new statistical complexity and compare known algorithms dedicated to the extraction of the underlying probabilities, checking their suitability to point out the abnormal values and structure of the experimental time series. For recent research on the fire phenomena performed using entropic tools, see Takagi, Gotoda, Tokuda and Miyano [1] and Murayama, Kaku, Funatsu, and Gotoda [2].

The experimental data was collected during a full-scale fire experiment conducted at the Fire Officers Faculty in Bucharest. We briefly include here the description of the experimental setup (Materials and Methods). Details can be found in [3].

The experiment has been carried out using a container (single-room compartment) having the following dimensions: 12 m × 2.2 m × 2.6 m. A single ventilation opening was available, namely the front door of the container, which remained open during the experiment. Parts of the walls and the ceiling of the container were furnished with oriented strand boards (OSB). The fire source has been a wooden crib made of 36 pieces of wood strips 2.5 cm × 2.5 cm × 30 cm, on which has been poured 500 mL ethanol shortly before ignition. The fire bed was situated in a corner of the compartment, at 1.2 m below the ceiling. The measurement devices consisted of six built-in K-type thermocouples, which were fixed at key locations (see Figure 1) and connected to a data acquisition logger. Flames were observed to impinge on the ceiling and exit through the opening, and we also noted the ignition of crumpled newspaper and stages of fire development that are known as indicators of flashover.

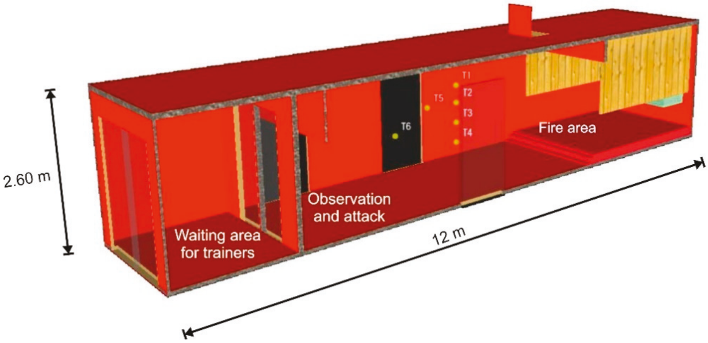

Figure 1. Arrangement of the flashover container.

In Section 2, we present the theoretical background and briefly summarize the approaches that are used to model fire.

Section 3 is dedicated to the results regarding the analysis of the collected raw data.

2. Theoretical Background and Remarks

2.1. Entropy and Statistical Complexity

The natural logarithm is used below, as elsewhere in this paper.

Shannon's entropy [4] is defined as $H(P) = -\sum_{i=1}^{n} p_i \log p_i$, where $P = \left(p_1, \ldots, p_n\right)$ is a finite probability distribution. It is nonnegative and its maximum value is $H(U) = \log n$, where $U = \left(\frac{1}{n}, \ldots, \frac{1}{n}\right)$. Throughout the paper, we use the convention $0 \cdot \log 0 = 0$.

The Kullback-Leibler divergence [5] is defined by

$$D(P||R) = \sum_{i=1}^{n} p_i(\log\ p_i - \log\ r_i) \tag{1}$$

where $P = \left(p_1, \ldots, p_n\right)$ and $R = (r_1, \ldots, r_n)$ are probability distributions. It is nonnegative and it vanishes for $P = R$.

If the value 0 appears in probability distributions $P = \left(p_1, \ldots, p_n\right)$ and $R = (r_1, \ldots, r_n)$, it must appear in the same positions for the sake of significance. Otherwise, one usually consider the conventions $0 \log \frac{0}{b} = 0$ for $b \geq 0$ and $a \log \frac{a}{0} = \infty$ for $a > 0$. We remark that these are strong limitations and such conditions rarely occur in practice.

To overcome this issue, the following divergence, well-defined, is used in the literature.

The Jensen-Shannon divergence (see [6,7]) is given by

$$JS(P||R) = \frac{1}{2}D\left(P||\frac{P+R}{2}\right) + \frac{1}{2}D\left(R||\frac{P+R}{2}\right) = H\left(\frac{P+R}{2}\right) - \frac{H(P)+H(R)}{2}. \tag{2}$$

The disequilibrium-based statistical complexity (LMC statistical complexity) introduced in 1995 by López-Ruiz, Mancini, and Calbet in [8] is defined as $C(P) = D(P)\frac{H(P)}{\log n}$, where $D(P)$, which is interpreted as disequilibrium, is the quadratic distance $D(P) = \sum_{i=1}^{n} \left(p_i - \frac{1}{n}\right)^2$.

Interpreted as entropic non-triviality (in Lamberti et al. [9] and Zunino et al. [10]), the Jensen-Shannon statistical complexity is defined by $C^{(JS)}(P) = Q_{(JS)}(P)\frac{H(P)}{\log n}$, where the disequilibrium $Q_{(JS)}(P)$ is $Q_{(JS)}(P) = k{\cdot}JS(P\|U)$. Here, $k = (\max_P JS(P\|U))^{-1}$ is the normalizing constant and $U = \left(\frac{1}{n}, \ldots, \frac{1}{n}\right)$. Therefore, we have $0 \le C^{(JS)}(P) \le 1$.

For the convenience of the interested reader, we include the following method to determine the normalizing constant (a result stated for computational purposes, without proof, in [9]).

Proposition 1. *Using the above notation, for the computation of the normalizing constant,* $k = (\max_P JS(P\|U))^{-1}$, *the maximum is attained for* P *such that there exists* i, $p_i = 1$.

It holds that $k = \left(\log 2 - \frac{1}{2}\log\frac{n+1}{n} - \frac{\log(n+1)}{2n}\right)^{-1}$.

Proof. We have the following calculations:

$$JS(P\|U) = H\left(\frac{P+U}{2}\right) - \frac{H(P)+H(U)}{2} = \frac{1}{2}\sum_{i=1}^{n} p_i \log p_i - \frac{1}{2}\log n - \sum_{i=1}^{n}\left(\frac{p_i}{2} + \frac{1}{2n}\right)\log\left(\frac{p_i}{2} + \frac{1}{2n}\right). \quad (3)$$

$$\frac{\partial JS(P\|U)}{\partial p_i} = \frac{1}{2}\log p_i + \frac{1}{2} - \frac{1}{2}\log\left(\frac{p_i}{2} + \frac{1}{2n}\right) - \frac{1}{2} = \frac{1}{2}\log p_i - \frac{1}{2}\log\left(\frac{p_i}{2} + \frac{1}{2n}\right). \quad (4)$$

$$\frac{\partial^2 JS(P\|U)}{\partial pi^2} = \frac{1}{2p_i} - \frac{1}{4\left(\frac{p_i}{2} + \frac{1}{2n}\right)} = \frac{1}{2p_i} - \frac{1}{2p_i + \frac{2}{n}} > 0,\ \frac{\partial^2 JS(P\|U)}{\partial p_i \partial p_j} = 0. \quad (5)$$

So, the Hessian of $JS(P\|U)$ is everywhere positive definite, whence $JS(P\|U)$ is (strictly) convex on the open convex set $\left\{(p_1, \ldots, p_n) : 0 < p_i < 1 \text{ for all } i,\ \sum_{i=1}^{n} p_i = 1\right\}$. Therefore, $JS(P\|U)$ cannot have a maximum inside (otherwise, it would be constant), and the points of maximum must lie on the boundary. See Theorem 3.10.10 in [11] (p. 171). Such points exist, because $JS(P\|U)$ is continuous on the compact set $\Delta = \left\{(p_1, \ldots, p_n) : 0 \le p_i \le 1 \text{ for all } i,\ \sum_{i=1}^{n} p_i = 1\right\}$. The function $JS(P\|U)$ is continuous and convex on the compact convex set Δ, so its maximum lies on the set of vertices of Δ (where $p_i = 1$ for one i). See Theorem 3.10.11 in [11] (p. 171). Since $JS(P\|U)$ does not depend on the order of the components of P, the maximum value is attained at all vertices, so it can be straightforwardly computed by setting $P = (1, 0, \ldots, 0)$. □

Remark 1. *Note that the maximal value of* $JS(P\|U)$ *is* $\log 2 - \frac{1}{2}\log\frac{n+1}{n} - \frac{\log(n+1)}{2n} \nearrow \log 2$, *as* $n \to \infty$. *Since* $JS(P\|U)$ *is bounded from above by* $\log 2$, *independently of* n, *the normalization of* $JS(P\|U)$ *in the definition of the Jensen-Shannon complexity does not seem to be relevant, and one could simply consider* $JS(P\|U)\frac{H(P)}{\log n}$.

Let $\lambda \in [0, 1]$. *The parametric Jensen-Shannon divergence (see for instance, [6]) is given by*

$$\begin{aligned} JS_\lambda(P\|R) &= (1-\lambda)D(P\|(1-\lambda)P + \lambda R) + \lambda D(R\|(1-\lambda)P + \lambda R) \\ &= H((1-\lambda)P + \lambda R) - ((1-\lambda)H(P) + \lambda H(R)). \end{aligned} \quad (6)$$

It is positive and it vanishes for $P = R$ *or* $\lambda = 0$ or 1. *See also Figure 2.*

The values $1-\lambda$ *and* λ *are interpreted as a priori probabilities. Note that* $JS_\lambda(P\|R) = JS_{1-\lambda}(R\|P)$ *and* JS_λ *is not symmetric, unless* $\lambda = 0.5$.

Mutatis mutandis, from Donald's identity (Lemma 2.12 in [12]), one has

$$JS_\lambda(P\|R) + D((1-\lambda)P + \lambda R\|Q) = (1-\lambda)D(P\|Q) + \lambda D(R\|Q) \quad (7)$$

for an arbitrarily fixed $\lambda \in [0,1]$. One needs only straightforward computation to check that it holds. Therefore,

$$JS_\lambda(P\|R) = \min\{(1-\lambda)D(P\|Q) + \lambda D(R\|Q) : Q = \\ \left(q_1, \ldots, q_n\right) \text{ is a finite probability distribution}\Big\}. \tag{8}$$

We introduce the parametric Jensen-Shannon statistical complexity as

$$C_\lambda^{(JS)}(P) \equiv JS_\lambda(P\|U)\frac{H(P)}{\log n}. \tag{9}$$

As in the case of the complexities $C(P), C^{(JS)}(P)$, the new ones, $C_\lambda^{(JS)}(P)$, would be zero (minimum complexity) for $P = U$ or if there exists i such that $p_i = 1$. These two cases describe very different states of the system, both of which are extreme circumstances being considered simple, namely the states with respectively maximum and minimum entropy.

We do not need to normalize $JS_\lambda(P\|U)$ in the definition of the parametric Jensen-Shannon complexity (possibly one can feel more comfortable with its normalized version in other frameworks), but we stress that one can easily prove, following the same recipe as above, that its maximum value is attained for P such that there exists i, $p_i = 1$.

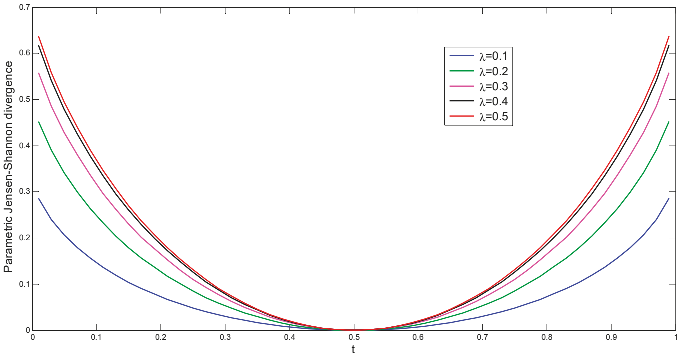

Figure 2. The parametric Jensen-Shannon divergence $JS_\lambda(P\|1-P)$, for $P = (t, 1-t)$, $t \in [0,1]$.

Proposition 2. *Let* $\lambda \in [0,1]$. *Using the above notation, it holds*

$$\max_P JS_\lambda(P\|U) = -\lambda\log\lambda - (1-\lambda)\log(1-\lambda) - (1-\lambda)\log\left(1 + \frac{\lambda}{(1-\lambda)n}\right) - \frac{\lambda}{n}\log\frac{(1-\lambda)n+\lambda}{\lambda}. \tag{10}$$

Moreover, $\max_P JS_\lambda(P\|U) \nearrow -\lambda\log\lambda - (1-\lambda)\log(1-\lambda) \leq \log 2$, *as* $n \to \infty$.

Proof. We omit the computation of $\max_P JS_\lambda(P\|U)$, which is straightforward.

To justify the monotonicity, it is enough to prove that $f(x) = \frac{\lambda}{x}\log\frac{(1g\lambda)x+\lambda}{\lambda}$ is decreasing:

$$f'(x) = -\frac{\lambda}{x^2}\left[\frac{\lambda}{(1-\lambda)x+\lambda} - 1 - \log\frac{\lambda}{(1-\lambda)x+\lambda}\right] < 0, \text{ for } \lambda \in (0,1) \text{ and } x > 0. \tag{11}$$

Furthermore, it is obvious that $(1-\lambda)\log\left(1 + \frac{\lambda}{(1-\lambda)n}\right) + \frac{\lambda}{n}\log\frac{(1-\lambda)n+\lambda}{\lambda} \to 0$.

The last inequality follows from Jensen's inequality, which is applied to the concave logarithmic function.

Therefore, $JS_\lambda(P\|U)$ is bounded from above by $\log 2$, independently of n. □

Remark 2. *We split this result into two inequalities (of independent interest), which can be proved by the same technique. Namely, it holds that*

$$\max_{P} D(P\|(1-\lambda)P+\lambda U) \nearrow -\log(1-\lambda) \tag{12}$$

and

$$\max_{P} D(U\|(1-\lambda)P+\lambda U) \nearrow -\log\lambda, \tag{13}$$

as $n\to\infty$.

Proposition 3. *Let* $\lambda,\mu\in[0,1]$. *Using the above notation, the following inequality holds:*

$$\min\left\{\frac{1-\lambda}{1-\mu},\frac{\lambda}{\mu}\right\}JS_{\mu}(P\|R)\le JS_{\lambda}(P\|R)\le \max\left\{\frac{1-\lambda}{1-\mu},\frac{\lambda}{\mu}\right\}JS_{\mu}(P\|R) \tag{14}$$

where $P=\left(p_1,\ldots,p_n\right)$ *and* $R=(r_1,\ldots,r_n)$ *are two finite probability distributions.*

Proof. The result is a particular case of Theorem 3.2 from [13]. We include here an alternative proof for the sake of completeness.

It is known that the entropy H is concave; Hence, $H((1-\lambda)P+\lambda R)\ge(1-\lambda)H(P)+\lambda H(R)$. We prove that

$$\min\left\{\frac{1-\lambda}{1-\mu},\frac{\lambda}{\mu}\right\}[H((1-\mu)P+\mu R)-(1-\mu)H(P)-\mu H(R)]\le \tag{15}$$

$$H((1-\lambda)P+\lambda R)-(1-\lambda)H(P)-\lambda H(R)\le \tag{16}$$

$$\max\left\{\frac{1-\lambda}{1-\mu},\frac{\lambda}{\mu}\right\}[H((1-\mu)P+\mu R)-(1-\mu)H(P)-\mu H(R)]. \tag{17}$$

We consider $0\le\frac{1-\lambda}{1-\mu}\le\frac{\lambda}{\mu}$, so $\lambda\ge\mu$, which implies, by the concavity of H, that

$$(1-\lambda)H(P)+\lambda H(R)+\min\left\{\frac{1-\lambda}{1-\mu},\frac{\lambda}{\mu}\right\}[H((1-\mu)P+\mu R)-(1-\mu)H(P)-\mu H(R)]= \tag{18}$$

$$(1-\lambda)H(P)+\lambda H(R)+\frac{1-\lambda}{1-\mu}[H((1-\mu)P+\mu R)-(1-\mu)H(P)-\mu H(R)]= \tag{19}$$

$$\frac{\lambda-\mu}{1-\mu}H(R)+\frac{1-\lambda}{1-\mu}H((1-\mu)P+\mu R)\le H\left(\frac{\lambda-\mu}{1-\mu}R+\frac{1-\lambda}{1-\mu}((1-\mu)P+\mu R)\right)=$$

$$H((1-\lambda)P+\lambda R), \tag{20}$$

because it holds $\frac{\lambda-\mu}{1-\mu}+\frac{1-\lambda}{1-\mu}=1$ and $\lambda-\mu\ge0$.

For the second inequality, we have

$$(1-\lambda)H(P)+\lambda H(R)+\max\left\{\frac{1-\lambda}{1-\mu},\frac{\lambda}{\mu}\right\}[H((1-\mu)P+\mu R)-(1-\mu)H(P)-\mu H(R)]= \tag{21}$$

$$(1-\lambda)H(P)+\lambda H(R)+\frac{\lambda}{\mu}[H((1-\mu)P+\mu R)-(1-\mu)H(P)-\mu H(R)]=$$

$$-\frac{\lambda-\mu}{\mu}H(P)+\frac{\lambda}{\mu}H((1-\mu)P+\mu R)\ge H((1-\lambda)P+\lambda R), \tag{22}$$

because it holds that $\frac{\lambda}{\mu}H((1-\mu)P+\mu R)\ge H((1-\lambda)P+\lambda R)+\frac{\lambda-\mu}{\mu}H(P)$, which is equivalent to

$$H((1-\mu)P+\mu R)\ge\frac{\mu}{\lambda}H((1-\lambda)P+\lambda R)+\frac{\lambda-\mu}{\lambda}H(P). \tag{23}$$

For $0 \le \frac{\lambda}{\mu} \le \frac{1-\lambda}{1-\mu}$, the proof is similar. □

Remark 3. *For* $\lambda \in [0,1]$, μ *∈(0,1), and* $R = U$ *in Equation (1), then the following inequality holds:*

$$\min\left\{\frac{1-\lambda}{1-\mu}, \frac{\lambda}{\mu}\right\} JS_{\mu}(P\|U) \le JS_{\lambda}(P\|U) \le \max\left\{\frac{1-\lambda}{1-\mu}, \frac{\lambda}{\mu}\right\} JS_{\mu}(P\|U). \tag{24}$$

For $\mu = \frac{1}{2}$ *in Equation (3), we obtain:*

$$2\min\{1-\lambda, \lambda\} JS(P\|U) \le JS_{\lambda}(P\|U) \le 2\max\{1-\lambda, \lambda\} JS(P\|U). \tag{25}$$

Multiplying by $\frac{H(P)}{\log n}$ *in Equation (4), we deduce the following inequality related to the parametric Jensen-Shannon statistical complexity:*

$$2k\min\{1-\lambda, \lambda\} C^{(JS)}(P) \le C_{\lambda}^{(JS)}(P) \le 2k\max\{1-\lambda, \lambda\} C^{(JS)}(P), \tag{26}$$

where $k = \log 2 - \frac{1}{2}\log\frac{n+1}{n} - \frac{\log(n+1)}{2n}$.

2.2. Extraction of the Underlying Probability Distribution

The permutation entropy (PE) [14] quantifies randomness and the complexity of a time series based on the appearance of ordinal patterns, that is on comparisons of neighboring values of a time series. For other details on the PE algorithm applied to the present experimental data, see [3].

Let $T = (t_1, \ldots, t_n)$ be a time series with distinct values.

Step 1. The increasing rearranging of the components of each j-tuple $\left(t_i, \ldots, t_{i+j-1}\right)$ as $\left(t_{i+r_1-1}, \ldots, t_{i+r_j-1}\right)$ yields a unique permutation of order j denoted by $\pi = \left(r_1, \ldots, r_j\right)$, which is an encoding pattern that describes the up-and-downs in the considered j-tuple.

Simple numerical examples may help clarify the concepts throughout this section.

Example 1. *For the five-tuple* (2.3, 1, 3.1, 6.1, 5.2), *the corresponding permutation (encoding) is* (2, 1, 3, 5, 4).

Step 2. The absolute frequency of this permutation (the number of j-tuples which are associated to this permutation) is

$$k_{\pi} \equiv \#\left\{i : i \le n-(j-1), \left(t_i, \ldots, t_{i+j-1}\right) \text{ is of type } \pi\right\}. \tag{27}$$

These values have the sum equal to the number of all the consecutive j-tuples; that is, $n-(j-1)$.

Step 3. The permutation entropy of order j is defined as $PE(j) \equiv -\sum_{\pi} p_{\pi} \log p_{\pi}$, where $p_{\pi} = \frac{k_{\pi}}{n-(j-1)}$ is the relative frequency.

In [14], the measured values of the time series are considered distinct. The authors neglect equalities and propose to break them by adding small random perturbations (random noise) to the original series.

Another known approach is to rank the equalities according to their order of emergence (to rank the equalities with their sequential/chronological order, see for instance [15,16]). We use this method throughout the paper to compute $PE(j)$ for $j = 3, 4, 5$.

Applying the PE algorithm for experimental fire data, $C_{\lambda}^{(JS)}(P)$ cannot be zero. The number of the encoding patterns that occur is >1, and these patterns are not equiprobable: some patterns may be rare or locally forbidden (that is, one encounters such patterns at some thermocouples, but not in all six time series), as discussed in [3].

We briefly describe now the encoding steps in the TLPE algorithm (Two-Length Permutation Entropy algorithm) given by Watt and Politi in [17]; other details are provided in [3].

Step 1 given the j-tuple $T = \left(t_1, \ldots, t_j\right)$, we start encoding the last $k \le j$ elements $\left(t_{j-k+1}, \ldots, t_j\right)$ according to the ordinal position of each element; that is, every t_s is replaced by a symbol which indicates the position occupied by t_s within the increasing rearranging of the considered k-tuple.

Next, we proceed by encoding each previous element t_m up to $m = 1$ according to the symbol provided by **Step 1** applied to the k-tuple $(t_m, \ldots, t_{m+k-1})$.

Example 2. *Encoding obtained by the chronological ordering of equal values* (4.1, 4.1, 4.1, 5, 2.1) → (1, 1, 2, 3, 1) *for* $k = 3$ *and* $j = 5$*.*

Step 2 and **Step 3**, they coincide with **Step 2** and **Step 3** in the PE algorithm above.

This algorithm leads, after computing the relative frequencies of the encoding sequences, to the two-length permutation entropy (TLPE (k, j)).

Given the pair (k, j) of values, the number of symbolic (encoding) sequences of length j is $k!k^{j-k}$, which is a number that can be much smaller than j!, so this algorithm is faster, it involves a simplified computation, and sometimes it makes the results more relevant for big values of j.

We deal with the equal values by using the same method as for PE; that is, we consider them ordered chronologically.

In the next section, we apply the above techniques and observe their capability to discern the changes of the parametric Jensen-Shannon statistical complexity of the experimental data.

3. Raw Data Analysis

The raw data set under consideration consists of measured temperatures during a compartment fire: six thermocouples T1, . . . , T6 measure the temperatures every second during the experiment. Hence, we get six time series consisting of 3046 entries (data points), and we aim to a better understanding of these results by modeling the time series using information theory, and to assess the performance of the discussed statistical complexities.

We plot the parametric Jensen-Shannon statistical complexity against the parameter (for $\lambda \in \{0, 0.2, \ldots, 1\}$). We notice the unusual plotting for the time series at T5, which is definitely not caused by the position of this thermocouple. The graph corresponding to the time series at T5 is far from the rest of the graphs for the other thermocouples; hence, smaller values were obtained for the statistical complexities, with no apparent experiment related or mathematical reason. See Figures 3–7.

We conclude that the PE and TLPE algorithms can be successfully used to detect unusual data collected in fire experiments: different embedding dimensions and different algorithms used to determine the underlying probabilities provide the same conclusion, the hierarchy among the statistical complexities established for the thermocouples T1–T5 is the same, and T5 is always at a bigger distance from the rest of them. The position of the thermocouple T5 does not justify this big difference (see Figure 1). This also agrees with the smaller values provided at T5 by the LMC statistical complexity in Figure 8.

It is not clear in [9] why only the disequilibrium provided by JS has been considered and why JS_λ has been avoided. Using experimental data, we have verified that the parametric Jensen-Shannon complexity can be used for the analysis of the time series related to the fire dynamics: except for the trivial cases $\lambda = 0$ or 1, the results are not altered by the non-symmetry of JS_λ for $\lambda \neq 0.5$ (however, the embedding dimension j has to be adequate to the amount of data), so one can draw similar conclusions as for $\lambda = 0.5$. See Figure 8 (the plots obtained by PE(3), PE(4), TLPE(3,5), and TLPE(2,5) look similar, so we do not include them here). We have limitations for the choice of the embedding dimension j, since the factorial increases fast, and one then requires a bigger amount of data n. So, as a guideline for choosing the embedding dimension, the value of the statistical complexities remains relevant for j such that $n \gg j!$. See also [18].

Moreover, the proposed parametric Jensen-Shannon statistical complexities complement and validate the information provided bythe usual LMC and Jensen-Shannon statistical complexities. See Figures 8 and 9 for a quick comparison to the descriptions provided by the Jensen-Shannon and

LMC statistical complexities. According to our findings, the parametric Jensen-Shannon statistical complexity is a valid tool for the analysis of the evolution of the temperature in compartment fire data. The slight differences that appear between the upper line (corresponding to $\lambda = 0.5$) in Figure 9 and the one in Figure 10 are because the Jensen-Shannon complexity [9] is defined using the normalized Jensen-Shannon divergence, while we introduced the parametric Jensen-Shannon divergence in the LMC style, that is without normalizing the disequilibrium.

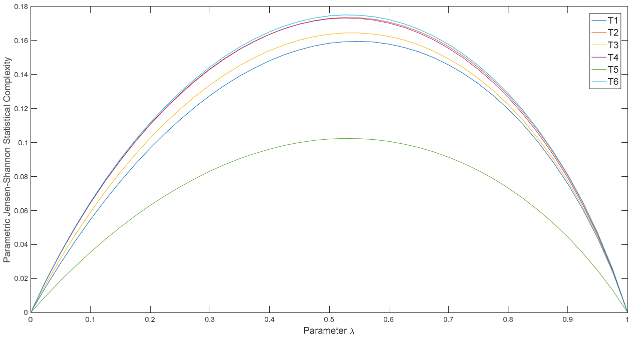

Figure 3. Plot obtained using the PE(5) algorithm. PE: permutation entropy.

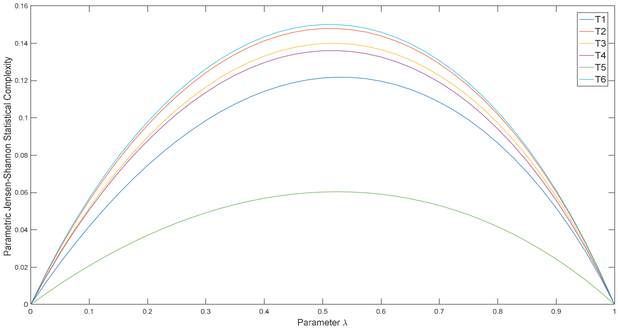

Figure 4. Plot obtained using the PE(4) algorithm.

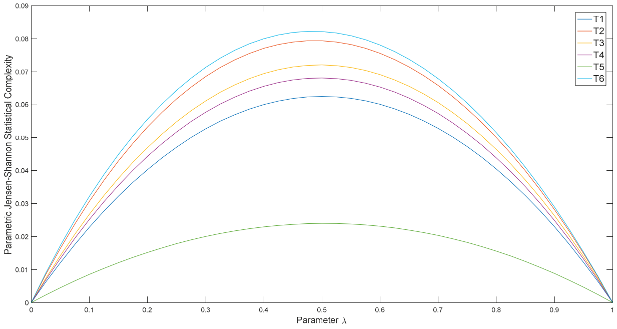

Figure 5. Plot obtained using the PE(3) algorithm.

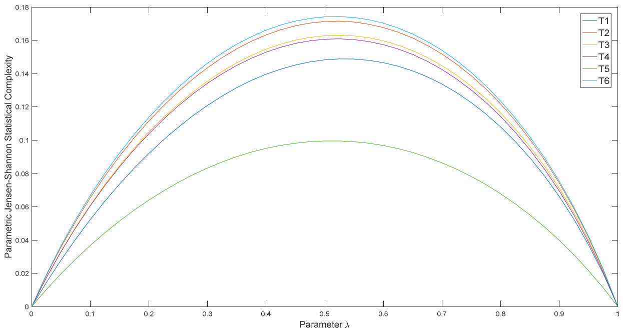

Figure 6. Plot obtained using the TLPE(3,5) algorithm.TLPE: Two-Length Permutation Entropy algorithm.

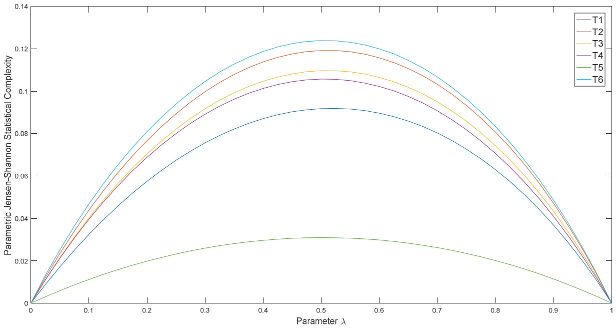

Figure 7. Plot obtained using the TLPE(2,5) algorithm.

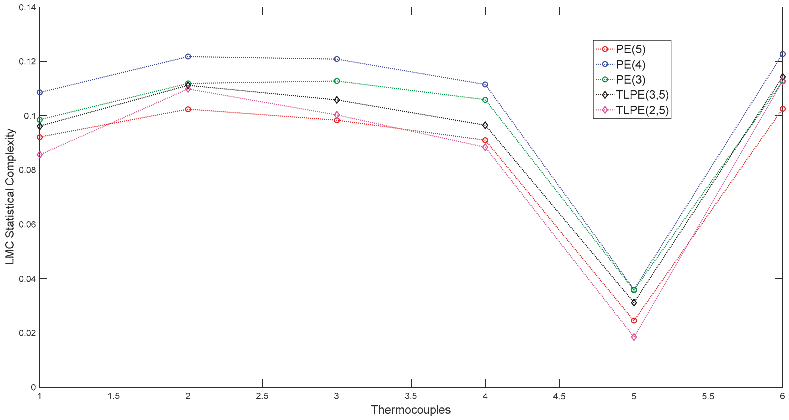

Figure 8. Statistical complexity.

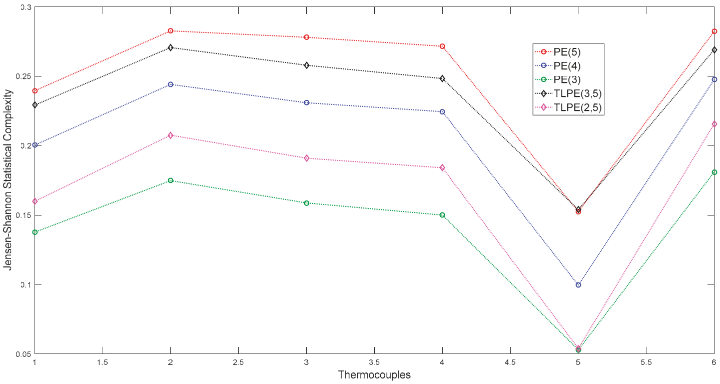

Figure 9. Jensen-Shannon statistical complexity ($\lambda = 1/2$).

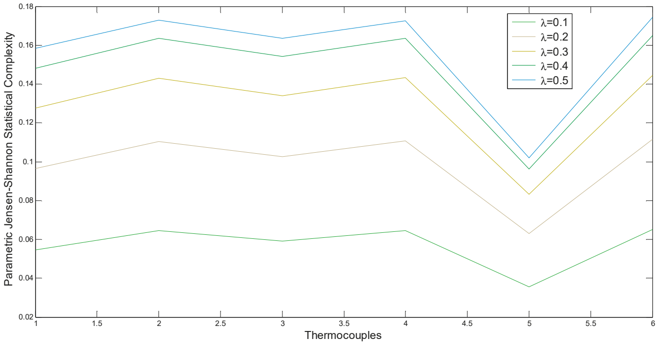

Figure 10. Obtained for the parametric Jensen-Shannon complexity using the PE(5)algorithm.

The most relevant aspect is that by applying the formula for the parametric Jensen-Shannon complexity, one gets similar plots, regardless of the embedding dimension and the encoding type algorithms used to determine the probability distribution, so the analysis is coherent and not misleading. Similarities with other in use complexity formulae would certainly improve the whole picture and bring us one step closer to the understanding of their ability to capture the behavior of various phenomena, in this particular case the fire dynamics. See Figures 8–10. We remark that these types of similarities might yield further mathematical results stating relationships among these mathematical notions: the (parametric) Jensen-Shannon and the LMC complexities.

4. Concluding Remarks on the Limitations of Our Study

The newly proposed complexities are used to analyze a full-scale experimental data set collected from a compartment fire.

For various algorithms and various embedding dimensions, more comparisons can be performed from this point onwards. We could not answer the questions about the merits and demerits of the known statistical complexities: such aspects are not yet clear in the literature, even in other frameworks where the permutation entropy has already been used by many researchers. Therefore, we discussed the relevance of the use of statistical complexities in the framework of fire data: small changes in the algorithms or choosing different embedding dimensions does not affect the interpretation of the results and the conclusions. This means that this new mathematical tool (the parametric Jensen-Shannon complexity) is informally staying “stable” in the framework of fire data. The accuracy of the interpretations can definitely be improved by the choice of the parameters, but the degree of its change cannot be estimated out of the data gathered in just one experiment: further research is required.

Other recent results on the analysis of this data set can be found in [19]. To understand this material the reader is referred to [20]. For the use of the permutation entropy in another framework see [21,22].

Our results might also indicate a turbulenceor a malfunction of the thermocouple T5 (an improperly calibrated scale); however, it is beyond the scope of the present paper to discuss it in detail.

Author Contributions: The work presented here was carried out in collaboration between all authors. All authors contributed equally and significantly in writing this article. All authors have contributed to the manuscript. All authors have read and agreed to the published version of the manuscript.

Funding: This work was supported by a grant of the Romanian Ministry of Research and Innovation, CCCDI-UEFISCDI, project number PN-III-P1-1.2-PCCDI-2017-0350/38PCCDI within PNCDI III.

Acknowledgments: The authors thank Eleutherius Symeonidis for the argumentation of the proof of Proposition 1.

Conflicts of Interest: The authors declare no conflict of interest.

References

1. Takagi, K.; Gotoda, H.; Tokuda, I.T.; Miyano, T. Dynamic behavior of temperature field in a buoyancy-driven turbulent fire. *Phys. Lett. A* **2018**, *382*, 3181–3186. [CrossRef]
2. Murayama, S.; Kaku, K.; Funatsu, M.; Gotoda, H. Characterization of dynamic behavior of combustion noise and detection of blowout in a laboratory-scale gas-turbine model combustor. *Proc. Combust. Inst.* **2019**, *37*, 5271–5278. [CrossRef]
3. Mitroi-Symeonidis, F.-C.; Anghel, I.; Lalu, O.; Popa, C. The permutation entropy and its applications on fire tests data. *arXiv* **2019**, arXiv:1908.04274.
4. Shannon, C.E. A mathematical theory of communication. *Bell Syst. Tech. J.* **1948**, *27*, 379–423. [CrossRef]
5. Kullback, S.; Leibler, L.A. On information and sufficiency. *Ann. Math. Stat.* **1951**, *22*, 79–86. [CrossRef]
6. Lin, J. Divergence measures based on the Shannon entropy. *IEEE-Trans. Inf. Theory* **1991**, *37*, 145–151. [CrossRef]
7. Rao, C.R.; Nayak, T.K. Cross entropy, dissimilarity measures, and characterizations of quadratic entropy. *IEEE Trans. Inform. Theory* **1985**, *31*, 589–593. [CrossRef]
8. López-Ruiz, R.; Mancini, H.L.; Calbet, X. A statistical measure of complexity. *Phys. Lett. A* **1995**, *209*, 321–326. [CrossRef]
9. Lamberti, P.W.; Martin, M.T.; Plastino, A.; Rosso, O.A. Intensive entropic non-triviality measure. *Phys. A Stat. Mech. Appl.* **2004**, *334*, 119–131. [CrossRef]
10. Zunino, L.; Soriano, M.C.; Rosso, O.A. Distinguishing chaotic and stochastic dynamics from time series by using a multiscale symbolic approach. *Phys. Rev. E* **2012**, *86*, 046210. [CrossRef]
11. Niculescu, C.P.; Persson, L.-E. *Convex Functions and their Applications. A Contemporary Approach*, 2nd ed.; CMS Books in Mathematics; Springer-Verlag: New York, NY, USA, 2018; Volume 23.
12. Donald, M.J. Further results on the relative entropy. *Math. Proc. Camb. Philos. Soc.* **1987**, *101*, 363–373. [CrossRef]
13. Mitroi-Symeonidis, F.-C. About the precision in Jensen-Steffensen inequality. *Ann. Univ. Craiova Ser. Mat. Inform.* **2010**, *37*, 73–84.
14. Bandt, C.; Pompe, B. Permutation entropy: A natural complexity measure for time series. *Phys. Rev. Lett.* **2002**, *88*, 174102. [CrossRef] [PubMed]
15. Cao, T.; Tung, W.W.; Gao, J.B.; Protopopescu, V.A.; Hively, L.M. Detecting dynamical changes in time series using the permutation entropy. *Phys. Rev. E* **2004**, *70*, 046217. [CrossRef]
16. Duan, S.; Wang, F.; Zhang, Y. Research on the biophoton emission of wheat kernels based on permutation entropy. *Optik* **2019**, *178*, 723–730. [CrossRef]
17. Watt, S.J.; Politi, A. Permutation entropy revisited. *Chaos Solitons Fractals* **2019**, *120*, 95–99. [CrossRef]
18. Riedl, M.; Müller, A.; Wessel, N. Practical considerations of permutation entropy. *Eur. Phys. J. Spec. Top.* **2013**, *222*, 249–262. [CrossRef]
19. Mitroi-Symeonidis, F.-C.; Anghel, I.; Furuichi, S. Encodings for the calculation of the permutation hypoentropy and their applications on full-scale compartment fire data. *Acta Tech. Napoc. Ser. Appl. Math. Mech. Eng.* **2019**, *62*, 607–616.

20. Furuichi, S.; Mitroi-Symeonidis, F.-C.; Symeonidis, E. On some properties of Tsallis hypoentropies and hypodivergences. *Entropy* **2014**, *16*, 5377–5399. [CrossRef]
21. Araujo, F.H.A.; Bejan, L.; Rosso, O.A.; Stosic, T. Permutation entropy and statistical complexity analysis of Brazilian agricultural commodities. *Entropy* **2019**, *21*, 1220. [CrossRef]
22. Song, Y.; Ju, Y.; Du, K.; Liu, W.; Song, J. Online road detection under a shadowy traffic image using a learning-based illumination-independent image. *Symmetry* **2018**, *10*, 707. [CrossRef]

symmetry

MDPI

Article

The Asymmetric Alpha-Power Skew-*t* Distribution

Roger Tovar-Falón [1,*], Heleno Bolfarine [2] and Guillermo Martínez-Flórez [1]

[1] Departamento de Matemáticas y Estadística, Facultad de Ciencias Básicas, Universidad de Córdoba, Montería 230027, Colombia; guillermomartinez@correo.unicordoba.edu.co

[2] Departamento de Estatística, IME, Universidade de São Paulo, São Paulo 1010, Brazil; hbolfar@ime.usp.br

* Correspondence: rjtovar@correo.unicordoba.edu.co

Received: 13 November 2019; Accepted: 25 December 2019; Published: 2 January 2020

Abstract: In this paper, we propose a new asymmetric and heavy-tail model that generalizes both the skew-*t* and power-*t* models. Properties of the model are studied in detail. The score functions and the elements of the observed information matrix are given. The process to estimate the parameters in model is discussed by using the maximum likelihood approach. Also, the observed information matrix is shown to be non-singular at the whole parametric space. Two applications to real data sets are reported to demonstrate the usefulness of this new model.

Keywords: alpha-power skew-*t* distribution; skew-*t* distribution; power-*t* distribution; asymmetry; Fisher information matrix; maximum likelihood estimation

1. Introduction

In recent years, there has been considerable interest in the statistical literature related to flexible families of distributions able of modeling data that present high degree of asymmetry, with kurtosis index greater or smaller than the captured by normal model. In this context, two proposals that have shown a promising behavior in this type of situations are the skew-normal (SN) distribution of Azzalini [1] and the power-normal (PN) distribution of Durrans [2]. The SN distribution has been widely studied by many authors, and its main drawback is that it presents singular Fisher information matrix, implying the inference is useless from the theory of large samples using the maximum likelihood (ML) approach. Although the PN model has a shorter asymmetry range than SN distribution, it presents non-singular information matrix and can easily be extended to censored scenarios, as it has a simple distribution function, see, for example, in Martínez-Flórez et al. [3].

The PN model is part of a wide family of distributions known as alpha-power, which has been widely studied by many authors. In addition to the normal distribution, the Birnbaum–Saunders (BS) distribution [4] has also been considered, see, for example, in Martínez-Flórez et al. [5], who propose an extension of the BS distribution based on the asymmetric alpha-power family of distributions to illustrate the applicability of the new proposal with a data set is related to the lifetimes in cycles $\times 10^{-3}$ $n = 101$ aluminum $6061 - T6$ pieces cut in parallel angle to the rotation direction of rolling at the rate of 18 cycles per second and maximum stress of 21.000 psi. More details of the PN distribution can be found in Gupta and Gupta [6] and Pewsey et al. [7].

An alternative propose for modeling asymmetric data that unifies the two previous approaches was introduced by Martínez-Flórez et al. [8]. The proposed model, which is called alpha-power skew-normal (APSN), has non-singular Fisher information matrix, and it can fit data with much more asymmetry than PN models it can handle. In addition, symmetry can be tested by using the likelihood ratio statistic, as the properties of large samples are satisfied for the ML estimator.

Another set of distributions with non-singular information matrices, useful for modeling asymmetric and heavy-tailed data, are based on generalizations of the Student-*t* distribution, see, for example, in [9–13]. Azzalini and Capitanio [9] for example, introduced a skew-*t* (ST) distribution as an extension of the SN model for modeling asymmetric and heavy-tailed data as follows; The random variable X is said to have the ST distribution with parameter λ and degrees of freedom ν, if X has the probability density function (PDF) given by

$$f_{ST}(x;\lambda,\nu) = 2f_T(x;\nu)\,\mathcal{F}_T\left(\lambda\sqrt{\frac{\nu+1}{x^2+\nu}}x;\nu+1\right), \quad x\in\mathbb{R} \tag{1}$$

where $\lambda\in\mathbb{R}$ is a parameter that controls the skewness of the distribution, and $f_T(\cdot;\nu)$ and $\mathcal{F}_T(\cdot;\nu)$ denote the PDF and the cumulative distribution function (CDF) of a standard Student-t distribution with ν degree of freedom, respectively. The ST distribution, like an extension of the SN model, inherits the problem of the singularity of the information matrix and before this inconvenience Zhao and Kim [14] proposed the power Student-t (PT) distribution, whose information matrix is non-singular and for a given degree of freedom, the kurtosis range surpasses the kurtosis range of the skew-t model at all times. The PT distribution is defined as follows. The random variable X is said to have the PT distribution with parameter α, and degrees of freedom ν, if X has PDF given by

$$f_{PT}(x;\alpha,\nu) = \alpha f_T(x;\nu)\left[\mathcal{F}_T(x;\nu)\right]^{\alpha-1}, \quad x\in\mathbb{R} \tag{2}$$

where $\alpha>0$ is a parameter that controls the form of the distribution, and, again, $f_T(\cdot;\nu)$ and $\mathcal{F}_T(\cdot;\nu)$ denote the PDF and the CDF of a standard Student-t distribution, respectively.

Based on the properties of the ST model, to fit data with high degree of asymmetry and the characteristic of the PN model to capture kurtosis larger than the normal model, in this paper, we introduce a new distribution for modeling asymmetric and heavy-tailed data. The proposed model possess non-singular information matrix, and it is able to fit data with far more asymmetry than ST and PT models can handle and with large sample properties satisfied for the ML estimator. The model introduced in this paper is named as alpha-power skew-t (APST) model and it extends both, ST and PT models. The APSN model by Martínez-Flórez et al. [8] is also a particular case when ν tends to infinite. Note that symmetry can be tested using the likelihood ratio statistics with its large sample chi-square distribution.

The rest of this paper is organized as follows. Section 2 introduces the APST model and some of its properties like moments are studied. In particular, skewness and kurtosis indices are computed showing that their ranges surpass those of the ST and PT models. Section 3 deals with the ML estimation for the location-scale situation and its observed information matrix is derived. The extension to censored data is also presented. Finally, two applications are shown in Section 4, revealing that the model proposed can present much improvement over competitors.

2. The Alpha-Power Skew-t Distribution

Definition 1. *The random variable X is said to have an alpha-power skew-t (APST) distribution, if X has PDF given by*

$$f_{APST}(x;\lambda,\alpha,\nu) = \alpha f_{ST}(x;\lambda,\nu)\left[\mathcal{F}_{ST}(x;\lambda,\nu)\right]^{\alpha-1}, \tag{3}$$

for $x\in\mathbb{R}$, $\lambda\in\mathbb{R}$, and $\alpha,\nu\in\mathbb{R}^+$. Functions $f_{ST}(\cdot)$ and $\mathcal{F}_{ST}(\cdot)$ denote the PDF and the CDF of the standard ST distribution. A random variable having $f_{APST}(x;\lambda,\alpha,\nu)$ distribution is denoted shortly by $X\sim \mathrm{APST}(\lambda,\alpha,\nu)$.

Figure 1 displays the form of the APST distribution for some selected values of the parameters λ and α for $\nu=6$. Note from the figure that the asymmetry and kurtosis of the APST distribution are affected by the parameters α and λ; therefore, the APST model is more flexible to model data that can be highly skewed, as well as heavier tails than ST and PT models.

The following result provides some special cases of the model (3), which occur for different values of λ, α, and ν.

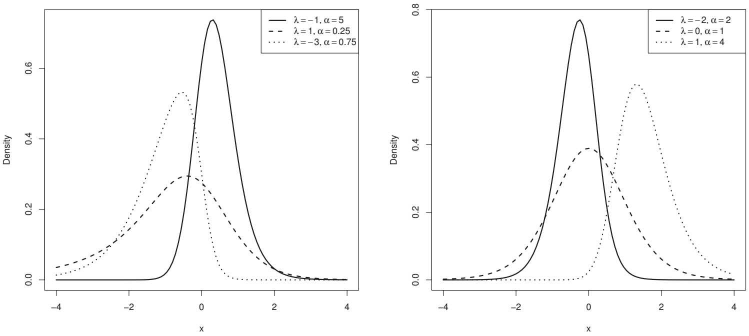

Figure 1. Probability density function of APST$(\lambda, \alpha, 10)$ for some values of λ and α.

Proposition 1. *Let* $X \sim \mathrm{APST}(\lambda, \alpha, \nu)$*,*

(i) *if* $\lambda = 0$*, then* $X \sim \mathrm{PT}(\alpha, \nu)$*,*
(ii) *if* $\alpha = 1$*, then* $X \sim \mathrm{ST}(\lambda, \nu)$*,*
(iii) *if* $\lambda = 0$ *and* $\alpha = 1$*, then* $X \sim \mathrm{T}(\nu)$*, where* $\mathrm{T}(\nu)$ *denotes the Student-t disribution with* ν *degree of freedom.*
(iv) *if* $\nu \to +\infty$*, then* $X \sim \mathrm{APSN}(\lambda, \alpha)$*,*
(v) *if* $\lambda = 0$ *and* $\nu \to +\infty$*, then* $X \sim \mathrm{PN}(\alpha)$*,*
(vi) *if* $\alpha = 1$ *and* $\nu \to +\infty$*, then* $X \sim \mathrm{SN}(\lambda)$*,*
(vii) *if* $\lambda = 0$*,* $\alpha = 1$ *and* $\nu \to +\infty$*, then* $X \sim \mathrm{N}(0, 1)$*,*

Proof. The proof of (i)–(vii) is immediate from the definition of APST distribution. □

2.1. Moments

The following proposition presents an expression to compute the k-th moment of a random variable APST(λ, α, ν).

Proposition 2. *Let* $X \sim \mathrm{APST}(\lambda, \alpha, \nu)$*, then*

$$\mathbb{E}\left[X^k\right] = \mathbb{E}\left[\left(\mathcal{F}_{ST}^{-1}(Y; \lambda, \nu)\right)^k\right] \tag{4}$$

where Y *follows a* Beta$(\alpha, 1)$ *distribution and* $\mathcal{F}_{ST}^{-1}(\cdot; \lambda, \nu)$ *is the inverse of the function* $\mathcal{F}_{ST}(\cdot; \lambda, \nu)$*.*

Proof. We have by definition that

$$\mathbb{E}\left[X^k\right] = \int_{\mathbb{R}} x^k \alpha f_{ST}(x) \left(\mathcal{F}_{ST}(x; \lambda, \nu)\right)^{\alpha - 1} dx$$

thus, letting $y = \mathcal{F}_{ST}(x; \lambda, \nu)$, then $x = \mathcal{F}_{ST}^{-1}(y; \lambda, \nu)$, it follows that

$$\mathbb{E}\left[X^k\right] = \int_0^1 \alpha \left(\mathcal{F}_{ST}^{-1}(y; \lambda, \nu)\right)^k y^{\alpha - 1} dy$$

which is the expected value of the function $\left(\mathcal{F}_{ST}^{-1}(Y; \lambda, \nu)\right)^k$, where Y follows a beta distribution with parameters α and 1. □

The indices of skewness ($\sqrt{\beta_1}$) and kurtosis (β_2) of APST distribution can be calculated by using the moments (4) as follows,

$$\sqrt{\beta_1} = \frac{\mu_3 - 3\mu_1\mu_2 + 2\mu_1^3}{(\mu_2 - \mu_1^2)^{3/2}} \quad \text{and} \quad \beta_2 = \frac{\mu_4 - 4\mu_1\mu_3 + 6\mu_2\mu_1^2 - 3\mu_1^4}{(\mu_2 - \mu_1^2)^2}$$

where $\mu_k = \mathbb{E}[X^k]$ for $k = 1, \ldots, 4$. Table 1 presents the ranges of possible values for the indices of asymmetry and kurtosis for ST(λ, ν), PT(α, ν), and APST(λ, α, ν) distributions, for values of λ between -40 and 40, values of α between 0.5 and 50, and for values of $\nu = 2, 3, 4, 5, 6, 7$. It can seen from Table 1 that the length of the admissible intervals for the skewness and the kurtosis parameters of the APST distribution are larger than the corresponding intervals of the ST and PT distributions. This is an indicator that the APST model is more flexible in terms of asymmetry and kurtosis than the ST and PT models.

Table 1. Skewness and kurtosis for the models ST(λ, ν), PT(α, ν), and APST(λ, α, ν), for $\lambda \in (-40, 40)$, $\alpha \in (0.5, 50)$ and $\nu = 2, \ldots 7$.

	Skew$-t$		**Power$-t$**		**Alpha$-$Power Skew$-t$**	
ν	**Skewness**	**Kurtosis**	**Skewness**	**Kurtosis**	**Skewness**	**Kurtosis**
2	$(-0.963, 0.963)$	$(3.170, 3.489)$	$(-0.119, 3.040)$	$(1.552, 10.436)$	$(-2.452, 14.314)$	$(1.395, 864.385)$
3	$(-0.950, 0.950)$	$(3.146, 3.357)$	$(-0.086, 1.362)$	$(1.325, 3.223)$	$(-2.130, 4.902)$	$(1.628, 114.098)$
4	$(-1.853, 1.853)$	$(5.099, 7.824)$	$(-0.530, 1.178)$	$(3.461, 5.299)$	$(-1.898, 3.215)$	$(3.153, 29.874)$
5	$(-0.947, 0.947)$	$(3.051, 3.327)$	$(-0.475, 0.271)$	$(1.176, 3.130)$	$(-1.968, 3.046)$	$(3.862, 19.925)$
6	$(-1.681, 1.681)$	$(4.554, 7.279)$	$(-0.533, 1.118)$	$(3.974, 5.173)$	$(-1.681, 2.145)$	$(3.892, 11.893)$
7	$(-0.944, 0.944)$	$(3.007, 3.367)$	$(-0.710, 0.243)$	$(1.264, 3.082)$	$(-1.535, 2.536)$	$(3.136, 15.924)$

2.2. Distribution Function

Proposition 3. *Let $X \sim$ APST(λ, α, ν), then the CDF of X, namely, $\mathcal{F}_{APST}(x; \lambda, \alpha, \nu)$ is*

$$\mathcal{F}_{APST}(x; \lambda, \alpha, \nu) = \left[\mathcal{F}_{ST}(x; \lambda, \nu)\right]^{\alpha}, \quad x \in \mathbb{R}. \tag{5}$$

Proof. The proof is immediate and it follows from results of Durrans [2]. □

The inversion method can be used to generate a random variable with APST distribution. Thus, taking $\lambda \in \mathbb{R}$, $\alpha, \nu \in \mathbb{R}^+$ and a random variable with uniform distribution, namely, $U \sim$ U$(0, 1)$, random variable X with APST(λ, α, ν) distribution is generated by taking

$$X = \mathcal{F}_{ST}^{-1}\left(U^{1/\alpha}; \lambda, \nu\right).$$

Remark 1. *We consider a truncated* APST(λ, α) *distribution to obtain a new and useful lifetime distribution. A random variable T has a truncated alpha-power skew-t distribution (at zero), denoted by TAPST(λ, α, ν), if its PDF is given by*

$$f(t) = \frac{\alpha f_{ST}(t, \lambda, \nu)\left[\mathcal{F}_{ST}(t, \lambda, \nu)\right]^{\alpha-1}}{1 - \left[\mathcal{F}_{ST}(0, \lambda, \nu)\right]^{\alpha}}; \quad t > 0 \tag{6}$$

The survival and hazard rate functions of a random variable T following a TAPST(λ, α, ν) *distribution are given by*

$$\mathcal{S}_T(t) = P(T > t) = \frac{1 - \left[\mathcal{F}_{ST}(0, \lambda, \nu)\right]^{\alpha} - \left[\mathcal{F}_{ST}(t, \lambda, \nu)\right]^{\alpha}}{1 - \left[\mathcal{F}_{ST}(0, \lambda, \nu)\right]^{\alpha}}; \quad t > 0 \tag{7}$$

and

$$h_T(t) = \frac{\alpha f_{ST}(t, \lambda, \nu)\left[f_{ST}(t, \lambda, \nu)\right]^{\alpha-1}}{1 - \left[\mathcal{F}_{ST}(0, \lambda, \nu)\right]^{\alpha} - \left[\mathcal{F}_{ST}(t, \lambda, \nu)\right]^{\alpha}}; \quad t > 0 \tag{8}$$

respectively.

2.3. Location and Scale Extension

We can also consider a generalization of a APST distribution by adding location and scale parameters. The following definition gives a generalization of the APST model.

Definition 2. *Let $X \sim \text{APST}(\lambda, \alpha, \nu)$. The APST density of location and scale is defined as the distribution of $Y = \mu + \sigma X$, for $\mu \in \mathbb{R}$ and $\sigma > 0$. The corresponding PDF is given by*

$$f_{APST}(y; \mu, \sigma, \lambda, \alpha, \nu) = \frac{\alpha}{\sigma} f_{ST}\left(\frac{y-\mu}{\sigma}; \lambda, \nu\right) \left[\mathcal{F}_{ST}\left(\frac{y-\mu}{\sigma}; \lambda, \nu\right)\right]^{\alpha-1}, \quad x \in \mathbb{R}, \tag{9}$$

for $\lambda \in \mathbb{R}$ and $\alpha, \nu \in \mathbb{R}^+$. A random variable following a APST distribution of location and scale is denoted by $Y \sim \text{APST}(\mu, \sigma, \lambda, \alpha, \nu)$.

The k-th moment of a random variable $Y \sim \text{APST}(\mu, \sigma, \lambda, \alpha, \nu)$ can be obtained from the formula

$$\mathbb{E}[Y^k] = \sum_{i=0}^{k} \binom{k}{i} \mu^i \sigma^{k-i} \mathbb{E}[X^{k-i}],$$

where $X \sim \text{APST}(\lambda, \alpha, \nu)$.

3. Statistical Inference for APST Distribution

This section concerns likelihood inference about the parameter vector $\boldsymbol{\theta} = (\mu, \sigma, \lambda, \alpha, \nu)^\top$ of the location-scale family defined in Equation (9). Let $\mathbf{Y} = (Y_1, \ldots, Y_n)^\top$ be a random sample of the distribution $\text{APST}(\mu, \sigma, \lambda, \alpha, \nu)$. The log-likelihood function for $\boldsymbol{\theta} = (\mu, \sigma, \lambda, \alpha, \nu)^\top$ can be written as follows,

$$\begin{aligned}\ell(\boldsymbol{\theta}; \mathbf{Y}) \propto{}& n \log \alpha - n \log \sigma - \frac{n}{2} \log \nu \\ &+ n \log \Gamma\left(\frac{\nu+1}{2}\right) - n \log \Gamma\left(\frac{\nu}{2}\right) - \frac{\nu+1}{2} \sum_{i=1}^{n} \log\left(1 + \frac{z_i^2}{\nu}\right) \\ &+ \sum_{i=1}^{n} \log \mathcal{F}_T\left(\lambda z_i \sqrt{\frac{\nu+1}{z_i^2+\nu}}; \nu+1\right) + (\alpha-1) \sum_{i=1}^{n} \log \mathcal{F}_{ST}(z_i; \lambda, \nu)\end{aligned} \tag{10}$$

where $z_i = (y_i - \mu)/\sigma$. Thus, by differentiating the log-likelihood function, we obtain the following score equations,

$$\begin{aligned}\frac{\partial \ell(\boldsymbol{\theta}; \mathbf{Y})}{\partial \mu} ={}& \frac{\nu+1}{\sigma\nu} \sum_{i=1}^{n} z_i \left(1 + \frac{z_i^2}{\nu}\right)^{-1} \\ &- \frac{\lambda}{\sigma} \sum_{i=1}^{n} w_i \left(1 + \frac{z_i^2}{\nu}\right)^{-1} \frac{f_T(\lambda z_i w_i; \nu+1)}{\mathcal{F}_T(\lambda z_i w_i; \nu+1)} - \frac{\alpha-1}{\sigma} \sum_{i=1}^{n} \frac{f_{ST}(z_i; \lambda, \nu)}{\mathcal{F}_{ST}(z_i; \lambda, \nu)} = 0\end{aligned} \tag{11}$$

$$\begin{aligned}\frac{\partial \ell(\boldsymbol{\theta}; \mathbf{Y})}{\partial \sigma} ={}& -\frac{n}{\sigma} + \frac{\nu+1}{\sigma\nu} \sum_{i=1}^{n} z_i^2 \left(1 + \frac{z_i^2}{\nu}\right)^{-1} - \frac{\lambda}{\sigma} \sum_{i=1}^{n} z_i w_i \left(1 + \frac{z_i^2}{\nu}\right)^{-1} \frac{f_T(\lambda z_i w_i; \nu+1)}{\mathcal{F}_T(\lambda z_i w_i; \nu+1)} \\ &- \frac{\alpha-1}{\sigma} \sum_{i=1}^{n} z_i \frac{f_{ST}(z_i; \lambda, \nu)}{\mathcal{F}_{ST}(z_i; \lambda, \nu)} = 0\end{aligned} \tag{12}$$

$$\frac{\partial \ell(\boldsymbol{\theta};\mathbf{Y})}{\partial \lambda} = \sum_{i=1}^{n} z_i w_i \frac{f_T\left(\lambda z_i w_i;\nu+1\right)}{\mathcal{F}_T\left(\lambda z_i w_i;\nu+1\right)} - \frac{\alpha-1}{\pi(1+\lambda^2)} \sum_{i=1}^{n} \frac{\left(1+(1+\lambda^2)z_i^2/\nu\right)^{-\frac{\nu}{2}}}{\mathcal{F}_{ST}(z_i;\lambda,\nu)} = 0, \tag{13}$$

$$\frac{\partial \ell(\boldsymbol{\theta};\mathbf{Y})}{\partial \alpha} = \frac{n}{\alpha} + \sum_{i=1}^{n} \log \mathcal{F}_{ST}(z_i;\lambda,\nu) = 0, \tag{14}$$

$$\begin{aligned}
\frac{\partial \ell(\boldsymbol{\theta};\mathbf{Y})}{\partial \nu} &= \frac{n\alpha}{2}\left(\psi\left(\frac{\nu+1}{2}\right) - \psi\left(\frac{\nu}{2}\right) - \frac{1}{\nu}\right) - \frac{1}{2}\sum_{i=1}^{n} \log\left(1+\frac{z_i^2}{\nu}\right) \\
&+ \frac{\nu+1}{2\nu^2}\sum_{i=1}^{n} z_i^2 \left(1+\frac{z_i^2}{\nu}\right)^{-1} \\
&+ \frac{\lambda}{2\nu(\nu+1)}\sum_{i=1}^{n} z_i^3 w_i \left(1+\frac{z_i^2}{\nu}\right)^{-1} \frac{f_T\left(\lambda z_i w_i;\nu+1\right)}{\mathcal{F}_T\left(\lambda z_i w_i;\nu+1\right)} \\
&- \frac{\lambda}{2\nu(\nu+1)}\sum_{i=1}^{n} z_i w_i \left(1+\frac{z_i^2}{\nu}\right)^{-1} \frac{f_T\left(\lambda z_i w_i;\nu+1\right)}{\mathcal{F}_T\left(\lambda z_i w_i;\nu+1\right)} \\
&- \frac{(\alpha-1)}{2\pi(\nu+1)}\frac{\lambda}{(1+\lambda^2)}\sum_{i=1}^{n} \frac{\left(1+(1+\lambda^2)z_i^2/\nu\right)^{-\frac{\nu}{2}}}{\mathcal{F}_{ST}(z_i;\lambda,\nu)} + \frac{\alpha-1}{2}\sum_{i=1}^{n} \frac{g(z_i;\nu)}{\mathcal{F}_{ST}\left(z_i;\lambda,\nu\right)} = 0
\end{aligned} \tag{15}$$

where $\psi(\cdot)$ is the digamma function, $w_i = \sqrt{\frac{\nu+1}{x_i^2+\nu}}$ for $i = 1,\ldots,n$, and $g(x;\nu)$ is the function defined by

$$\begin{aligned}
g(x;\nu) = \int_{-\infty}^{x} &\left\{\frac{(\nu+1)}{\nu^2}s^2\left(1+\frac{s^2}{\nu}\right)^{-1} - \log\left(1+\frac{s^2}{\nu}\right)\right\} f_{ST}(s;\lambda,\nu)ds \\
&- \frac{\lambda}{\pi\nu}\int_{-\infty}^{x} s\left(1+\frac{s^2}{\nu}\right)^{-1}\left\{1+(1+\lambda^2)\frac{s^2}{\nu}\right\}^{-\frac{\nu+2}{2}} ds
\end{aligned} \tag{16}$$

Equations (11)–(15) include nonlinear functions; therefore, it is not possible to obtain explicit forms of the maximum likelihood estimators (MLEs), and they must be calculated by using numerical methods. In this work, we used the *maxLik* function of R Development Core Team [15] which uses the Newton–Raphson optimization method. The elements of the observed information matrix are easily obtained after calculating the second derivative of the log-likelihood function and multiplying by -1, that is,

$$j_{\theta_i\theta_k} = -\frac{\partial \ell(\boldsymbol{\theta};\mathbf{Y})}{\partial\theta_i\partial\theta_k}, \quad i,k = 1,2,\ldots,5 \tag{17}$$

where $\boldsymbol{\theta} = (\mu,\sigma,\lambda,\alpha,\nu)^\top$. This elements are given in the Appendix A. To find the standard errors (EE) of the MLEs and calculate confidence intervals, the information matrix $\mathbf{I}$ (or Fisher information) must be calculated, which is defined as the expected value of the second derived from the log-likelihood function or less the expected value of the Hessian matrix; from this matrix, we calculate the EE as the diagonal elements of the inverse of this matrix. The elements of the $\mathbf{I}$ matrix are obtained as

$$\mathbf{I}(i,k) = -E\left(\frac{\partial \ell(\boldsymbol{\theta};\mathbf{Y})}{\partial\theta_i\partial\theta_k}\right), \quad i,k = 1,2,\ldots,5 \tag{18}$$

The role of the Fisher information in the asymptotic theory of maximum-likelihood estimation was emphasized by Ronald Fisher following some initial results by Francis Edgeworth, see Lehman and Casella [16] and Frieden [17] for more details. The Fisher-information matrix is used to calculate the covariance matrices associated with maximum-likelihood estimates, and it can also be used in the formulation of test statistics, such as the Wald test.

As the expected value under the APST distribution and the second-order derivatives are not direct, numerical methods must be used to obtain the explicit form of the information matrix $\mathbf{I}$.

Therefore, we use the observed information matrix to calculate the standard errors in the rest of the document.

When ν tends to infinite the ST distribution converges to the SN distribution and we recall that the information matrix of a random variable $X \sim \text{SN}(\mu, \sigma, \lambda)$ which is denoted by $\mathbf{I}_\lambda(\boldsymbol{\varphi})$, where $\boldsymbol{\varphi} = (\mu, \sigma, \lambda)^\top$, is singular for $\lambda = 0$. Therefore, it is convenient to use a centered parameterization of the ST distribution proposed by Arellano-Valle and Azzalini [18].

The centered parameterization of the SN distribution was proposed as an alternative to the problem of singularity of the information matrix of the SN when $\lambda = 0$. Arellano-Valle and Azzalini [19] proposed a second representation of the SN by defining a new random variable X as

$$X = \mu + \sigma \left(\frac{Z - \mathbb{E}[Z]}{\sqrt{\text{Var}[Z]}} \right),$$

where $\mu \in \mathbb{R}$ and $\sigma > 0$ are parameters of the random variable X and $Z \sim \text{SN}(\lambda)$. This representation is called centered parameterization, as $\mathbb{E}[X] = \mu$ and $\text{Var}[X] = \sigma^2$ and it is denoted by $\text{CSN}(\mu, \sigma, \gamma_1)$, where $-0.9953 < \gamma_1 < 0.9953$. Under the centered parameterization model, μ, σ, and $\gamma_1 = \sqrt{\beta_1}$ represent the mean, the standard deviation and the skewness index of X, respectively. If $Z \sim \text{SN}(\lambda)$ then $\mathbb{E}[Z] = b\delta$ and $\text{Var}[Z] = 1 - (b\delta)^2$, where $b = \sqrt{2/\pi}$ and $\delta = \lambda/\sqrt{1+\lambda^2}$; it has that the random variable X can be written as $X = \mu + \sigma Z$ which has $\text{SN}(\lambda_1, \lambda_2, \lambda)$ distribution, where

$$\lambda_1 = \mu - c\sigma\gamma_1^{1/3}, \quad \lambda_2 = \sigma\sqrt{1 + c^2\gamma_1^{2/3}}, \quad \lambda = \frac{c\gamma_1^{1/3}}{\sqrt{b^2 + c^2(b^2-1)\gamma_1^{2/3}}} \tag{19}$$

with $c = \{2/(4-\pi)\}^{1/3}$. Under this denomination, the information matrix can be written as $\mathbf{I}_{\gamma_1} = \mathbf{D}^\top \mathbf{I}_\lambda \mathbf{D}$, where $\mathbf{D}$ is a matrix that represents the derivative of the parameters of the standard representation (λ_1, λ_2 and λ) regarding to the new parameters (μ, σ and γ_1). It also follows that the information matrix converges to a diagonal matrix $\boldsymbol{\Sigma}_c^{-1} = \text{diag}(\sigma^2, \sigma^2/2, 6)$ when $\lambda \to 0$. This guarantees the existence and uniqueness of the MLEs of λ_1 and λ_2 for each fixed value of λ.

Following this same line of thought, we suppose that Y follows the model (1) with location parameter $\mu \in \mathbb{R}$ and scale parameter $\sigma > 0$, that is,

$$f_{ST}(y; \mu, \sigma, \lambda, \nu) = \frac{2}{\sigma} f_T\left(\frac{y-\mu}{\sigma}; \nu\right) \mathcal{F}_T\left(\lambda\sqrt{\frac{\nu+1}{Q_y+\nu}}\left(\frac{y-\mu}{\sigma}\right); \nu+1\right), \quad y \in \mathbb{R} \tag{20}$$

where $\lambda \in \mathbb{R}$ and $Q_y = ((y-\mu)/\sigma)^2$. This representation relates to the direct parameterization of the ST distribution with parameter vector $\boldsymbol{\rho} = (\mu, \sigma, \lambda, \nu)^\top$. It follows that $Z_T = (Y-\mu)/\sigma \sim \text{ST}(\lambda, \nu)$, and by the stochastic representation of the ST distribution is given by $Z_T = Z/\sqrt{V}$, where $Z \sim \text{SN}(\lambda)$ and $V \sim \chi^2_\nu/\nu$. This entails to compute the first four cumulants of Z_T denoted by $\mu_1(\delta, \nu)$, $\mu_2(\delta, \nu)$, $\mu_3(\delta, \nu)$ and $\mu_4(\delta, \nu)$, see [18]. The centered parameterization of the ST distribution of a random variable Y comes by defining

$$\mu_t = \mathbb{E}[Y] = \mu + \sigma\mu_1(\delta, \nu) = \mu + \sigma b_\nu \delta$$

$$\sigma_t^2 = \text{Var}[Y] = \sigma^2\mu_2(\delta, \nu) = \eta^2\left\{\frac{\nu}{\nu-2} - b_\nu^2\delta^2\right\},$$

$$\gamma_{1t} = \frac{\mu_3(\delta,\nu)}{\mu_2(\delta,\nu)^{3/2}} = \frac{b_\nu \delta}{\mu_2(\delta,\nu)^{3/2}} \left\{ \frac{\nu(3-\delta^2)}{\nu-3} - \frac{3\nu}{\nu-2} + 2b_\nu^2\delta^2 \right\}$$

$$\gamma_{2t} = \frac{\mu_4(\delta,\nu)}{\mu_2(\delta,\nu)^2} = \frac{1}{\mu_2(\delta,\nu)^2} \left\{ \frac{3\nu^2}{(\nu-2)(\nu-4)} - \frac{4b_\nu^2\delta^2\nu(3-\delta^2) + \frac{6b_\nu^2\delta^2\nu}{\nu-2} - 4b_\nu^4\delta^4}{\nu-3} \right\} - 3.$$

The new representation is defined as the centered skew-*t* distribution with parameter vector $\tilde{\boldsymbol{\rho}} = (\mu, \sigma^2, \gamma_1, \gamma_2)^\top$. According to Arellano-Valle and Azzalini [18], the information matrix of this representation can be written as

$$\mathbf{I}(\tilde{\boldsymbol{\rho}}) = \mathbf{B}^\top \mathbf{I}(\boldsymbol{\rho})\mathbf{B},$$

where $\mathbf{B}$ is a matrix representing the derivative of the parameter vector $\boldsymbol{\rho}$ with respect to the new vector $\tilde{\boldsymbol{\rho}}$. It can shown that $b_\nu \to b$ when $\nu \to \infty$, see [18]. Therefore, the parameters of the centered ST model converge to $\mu_t \to \mu$, $\sigma_t^2 \to \sigma^2$, and $\gamma_{1t} \to \gamma_1$ when $\nu \to \infty$, that is, the parameters of the CSN. As $Z_T \to \mathrm{SN}(\lambda)$ when $\nu \to \infty$, it follows that the random variable Y converges to a distribution with information matrix

$$\mathbf{I}(\mu, \sigma^2, \gamma_1, \alpha) = \begin{pmatrix} \mathbf{I}_{\boldsymbol{\theta}_1\boldsymbol{\theta}_1} & \mathbf{I}_{\boldsymbol{\theta}_1,\alpha} \\ \mathbf{I}_{\boldsymbol{\theta}_1,\alpha}^\top & I_{\alpha,\alpha} \end{pmatrix}, \tag{21}$$

where the elements of the diagonal correspond to the information of the parameter vector $\boldsymbol{\theta}_1 = (\mu, \sigma^2, \gamma_1)$ and α, and $\mathbf{I}_{\boldsymbol{\theta}_1,\alpha}$ is the joint information of $\boldsymbol{\theta}_1 = (\mu, \sigma^2, \gamma_1)^\top$ and α. Now, when $\lambda \to 0$ and $\alpha = 1$, it can be shown that $\mathbf{I}_{\boldsymbol{\theta}_1\boldsymbol{\theta}_1} \to \mathrm{diag}(\sigma^2, \sigma^2/2, 6)$, with determinant equal to $0.3333/\sigma^4$, and $\mathbf{I}_{\boldsymbol{\theta}_1,\alpha} = (0.9031/\sigma, -0.5956/\sigma, 0.7206)^\top$; therefore, the determinant $|\mathbf{I}(\mu, \sigma^2, \gamma_1, \alpha)| \neq 0$, and it concludes that the random variable Y converges to a distribution with information matrix non-singular when ν tends to infinite.

3.1. Extension to Censored Data

Based on the goodness of the APST distribution to fit asymmetric and heavy-tailed data, in this section we introduce the censored APST model which we will be denote by CAPST.

Definition 3. *Suppose that the random variable Y follows APST distribution, and consider a random sample $\mathbf{Y} = (Y_1, Y_2, \ldots, Y_n)$ where only the Y_i values greater than a constant k are recorded. In addition, for values $Y_i \leq k$ only the value of k is recorded. Therefore, for $i = 1, 2, \ldots, n$, the observed values Y_i^o can be written as*

$$Y_i^o = \begin{cases} k, & \textit{if } Y_i \leq k, \\ Y_i, & \textit{if } Y_i > k. \end{cases}$$

The resulting sample is said to be a censored APST, and we say that Y is a censored random variable APST. We will use the notation $Y \sim \mathrm{CAPST}(\boldsymbol{\theta})$, where $\boldsymbol{\theta} = (\mu, \sigma, \lambda, \alpha, \nu)^\top$.

From Definition 3 it follows that $P(Y_i^o = k) = P(Y_i \leq k) = \{\mathcal{F}_{ST}((k-\mu)/\sigma)\}^\alpha$ and for the observations $Y_i^o = Y_i$, the distribution of Y_i^o is the same of Y_i, i.e., $Y_i^o \sim \mathrm{APST}(\boldsymbol{\theta})$. For convenience, we choose to work with the case of left-censored data; however, the followings results can be extended to other types of censorship.

3.2. Properties of the CAPST Model

Let $Y \sim \mathrm{CAPST}(\mu, \sigma, \lambda, \alpha, \nu)$,

1. If $\alpha = 1$, then $Y \sim \mathrm{CST}(\mu, \sigma, \lambda, \nu)$, where CST indicates the censored skew-*t* model.
2. If $\lambda = 0$, then $Y \sim \mathrm{CPT}(\mu, \sigma, \alpha, \nu)$, where CPT indicates the censored power-*t* model.
3. If $\alpha = 1$ and $\lambda = 0$, then $Y \sim \mathrm{CT}(\mu, \sigma, \nu)$, that is, the censored Student-*t* model follows.
4. If $\nu \to +\infty$, then $Y \sim \mathrm{CAPSN}(\mu, \sigma, \lambda, \alpha)$, where CAPSN indicates the censored alpha-power skew-normal model.

5. If $\alpha = 1$ and $\nu \to +\infty$, then $Y \sim \text{CSN}(\mu, \sigma, \lambda)$, that is, the censored skew-normal model follows.
6. If $\lambda = 0$ and $\nu \to +\infty$, then $Y \sim \text{CPN}(\mu, \sigma, \alpha)$, that is, the censored power-normal model follows.
7. If $\alpha = 1$, $\lambda = 0$ and $\nu \to +\infty$, then $Y \sim \text{CN}(\mu, \sigma^2)$, that is, the censored normal model follows.

The estimates of the parameters of the model can be obtained via maximum likelihood method, where the log-likelihood function is given by

$$\begin{aligned}\ell(\boldsymbol{\theta}; \mathbf{Y}) \propto \alpha \sum_0 \log \mathcal{F}_{ST}\left(\frac{k-\mu}{\sigma}; \lambda, \nu\right) + n_1 \log \alpha - n_1 \log \sigma - \frac{n_1}{2} \log \nu \\ + n_1 \log \Gamma\left(\frac{\nu+1}{2}\right) - n_1 \log \Gamma\left(\frac{\nu}{2}\right) - \frac{\nu+1}{2} \sum_1 \log\left(1 + \frac{x_i^2}{\nu}\right) \\ + \sum_1 \log \mathcal{F}_T\left(\lambda x_i \sqrt{\frac{\nu+1}{x_i^2+\nu}}; \nu+1\right) + (\alpha - 1) \sum_1 \log \mathcal{F}_{ST}(x_i; \lambda, \nu)\end{aligned}$$

where $x_i = (y_i - \mu)/\sigma$; $\sum_1$ and $\sum_0$ are the sum over censored individuals and uncensored individuals, respectively; and n_1 is the number of uncensored individuals.

4. Real Data Applications

In this section, we illustrate the applicability of the proposed model in Section 2 by analyzing two data sets. We use the statistical software *R* [15], version 3.5.3 with the package *maxLike* for maximizing the corresponding likelihood functions. For comparing purposes of various models, the AIC Akaike [20], BIC Schwarz [21], and corrected AIC (CAIC) Bozdogan [22] information criteria were used.

4.1. Application 1: Volcano Heights Data

Consider the data set related to heights of 1520 volcanoes in the world which is available in website dx.doi.org/10.5479/si.GVP.VOTW4-2013 [23]. Table 2 presents the summary statistics for the data set. It can be noted that the asymmetry and kurtosis indices seem to indicate that the use of an asymmetric and heavy-tailed model is appropriate to analyze this data set. We analyzed these data by fitting the Student-*t*, ST, PT, and APST distributions.

Table 2. Volcano heights data: Statistical summary.

n	Mean	Variance	$\sqrt{b_1}$	b_2
1520	16.7760	15.6682	0.6461	4.3809

Table 3 shows the parameter estimates, together with their corresponding standard errors (SE). Note that the values of the standard errors of the μ and σ estimates for the APST model are smaller than the corresponding standard errors of the respective parameters for the Student-*t*, ST, and PT models. Table 3 also presents some model selection criteria, together with the values of the log-likelihood. The AIC, BIC, and CAIC criteria indicate that the APST model seems to provide better fit to the volcanoes heights data than the T, ST, and PT models, supporting the asymmetry assertion of the volcano's heights variable. Figure 2 shows the graphs *QQplot* of the fitted models. It can be clearly seen from the figure that the APST model fits the data better than the Student-*t*, ST, and PT models. In addition, we can use the likelihood ratio (LR) test statistic to conform our claim. To do this, we consider the following hypotheses,

$$H_0 : (\lambda, \alpha) = (0, 1) \ (\text{T}(\mu, \sigma, \nu)) \quad \text{v.s} \quad H_1 : (\lambda, \alpha) \neq (0, 1) \ (\text{APST}(\mu, \sigma, \lambda, \alpha, \nu)),$$

The value of the LR test statistic is $-2\log(\Lambda) = -2\big(\ell_T(\hat{\theta}) - \ell_{APST}(\hat{\theta})\big)$ =134.823 and comparing this quantity with χ^2_2 =5.9914, the null hypotheses is rejected. The APST model is also compared with the ST and PT models by considering the hypotheses

$$H_{01} : \alpha = 1 \ (\mathrm{ST}(\mu, \sigma, \lambda, \nu)) \quad \text{v.s} \quad H_{11} : \alpha \neq 1 \ (\mathrm{APST}(\mu, \sigma, \lambda, \alpha, \nu)),$$

and

$$H_{02} : \lambda = 0 \ (\mathrm{PT}(\mu, \sigma, \alpha, \nu)) \quad \text{v.s} \quad H_{12} : \lambda \neq 0 \ (\mathrm{APST}(\mu, \sigma, \lambda, \alpha, \nu)),$$

respectively. The respective values of the LR test statistic are given by $-2\log(\Lambda_1) = -2\big(\ell_{ST}(\hat{\theta}) - \ell_{APST}(\hat{\theta})\big)$ =26.620 and $-2\log(\Lambda_2) = -2\big(\ell_{PT}(\hat{\theta}) - \ell_{APST}(\hat{\theta})\big)$ =45.660 and comparing these quantities with χ^2_1 =3.8414, both null hypotheses are rejected. Finally, Figure 3left shows the histogram of the volcano heights variable, whereas Figure 3right presents the empirical CDF (solid line) together with the CDF of the fitted APST model (dotted line).

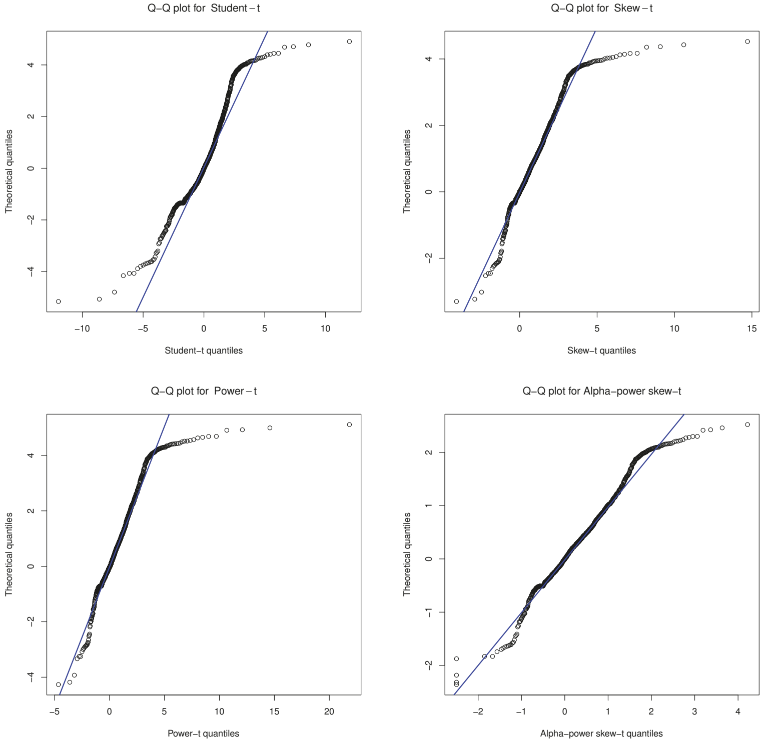

Figure 2. Volcano height data: QQplot for Student-*t*, ST, PT, and APST models.

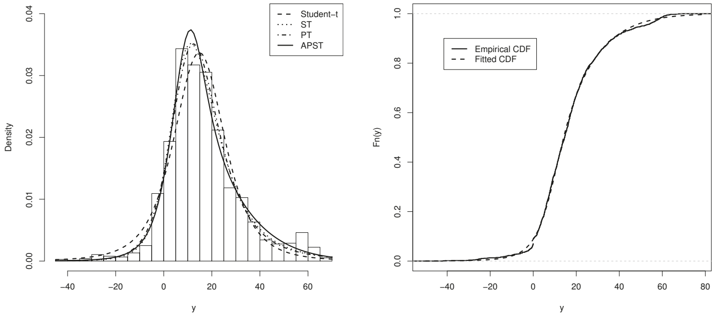

Figure 3. (**Left**) Graph of fitted densities to volcano height data. (**Right**) Empirical CDF and CDF of fitted APST model.

Table 3. Parameter estimates (SE) for the fitted models to the volcano height data.

	Distribution			
Estimates	**Student-*t***	**ST**	**PT**	**APST**
$\hat{\mu}$	14.7835(0.3615)	4.7469(0.6892)	8.4027(0.7923)	11.5509(0.1337)
$\hat{\sigma}$	11.0045(0.3975)	14.1532(0.7237)	11.8146(0.4707)	22.6885(0.0792)
$\hat{\lambda}$	–	1.5673(0.1838)	–	5.2347(0.2870)
$\hat{\alpha}$	–	–	1.7912(0.1147)	0.3205(0.0347)
$\hat{\nu}$	3.4156(0.3601)	3.4075(0.3454)	2.7473(0.2566)	12.8734(2.9729)
$\hat{\ell}$	−6273.35	−6219.25	−6228.77	−6205.94
AIC	12,552.70	12,446.49	12,465.53	12,421.87
BIC	12,568.68	12,467.79	12,486.53	12,448.50
CAIC	12,571.68	12,471.79	12,490.83	12,453.50

4.2. Application 2: Stellar Abundances Data

The second data set is related to measurements for 68 solar-type stars, which are available in the package *astrodatR* of the software *R* [24] under the name *Stellar abundances*. These data were previously analyzed Mattos et al. [25] by using the Scale Mixture of Skew Normal Censored Regression (SMSNCR) models. We take only the response variable: log *N(Be)*, which represents the log of the abundance of beryllium scaled to Sun's abundance (i.e., the Sun has $\log N(Be) = 0.0$)

In astronomical research, a previously identified sample of objects (stars, galaxies, quasars, X-ray sources, etc.) is observed at some new wavebands. According to Feigelson [24], due to limited sensitivities, some objects may be undetected, leading to upper limits in their derived luminosities. For this dataset we have 12 left-censored data points, i.e., 12 undetected beryllium measurement, that represents 19.35% of observations. Table 4 presents the ML estimates for the parameters of the censored Studen-*t* (CT), censored skew-*t* (CST), censored power-*t* (CPT), and censored alpha-power skew-*t* (CAPST) models, together with their corresponding standard errors. Table 4 also compares the fit of the four models using the model selection criteria (AIC, CAIC and BIC). Note that, again, the CAPST model with heavy tails have better fit than the CT, CST, and CPT models.

To identify atypical observations and/or model mispecification, we analyzed the transformation of the martingale residual, r_{MT_i}, proposed in Barros et al. [26]. These residuals are defined by

$$r_{MTi} = \text{sign}(r_{Mi})\sqrt{-2[r_{Mi} + \delta_i \log(\delta_i - r_{M_i})]}, \qquad i = 1, \ldots, n$$

where $r_{Mi} = \delta_i + \log S(y_i; \hat{\boldsymbol{\theta}})$ is the martingal residual proposed by Ortega et al. [27], where $\delta_i = 0, 1$ indicates whether the *i*-th observation is censored or not, respectively; $\text{sign}(r_{Mi})$ denotes the sign of

r_{Mi}; and $S(y_i;\hat{\boldsymbol{\theta}}) = P_{\hat{\boldsymbol{\theta}}}(Y_i > y_i)$ represents the survival function evaluated at y_i, where $\hat{\boldsymbol{\theta}}$ are the MLE for $\boldsymbol{\theta}$. The plots of r_{MT_i} with generated confidence envelopes are presented in Figure 4. From this figure, we can see clearly that the CST, CPT, and CAPST models fit better the data than the CT model, since, in that cases, there are not observations which lie outside the envelopes. The Figure 5 shows the graph of the densities of the different models fitted to the stellar abundances data. From the figure, the CAPST model seems to fit better the stellar abundances data than CT, CST and CPT models.

Table 4. Parameter estimates (SE) for the fitted models to the stellar abundances data.

	Distribution			
Estimates	**CT**	**CST**	**CPT**	**CAPST**
$\hat{\mu}$	1.0314(0.0010)	1.2306(0.0018)	1.2098(0.0052)	1.1761(0.0054)
$\hat{\sigma}$	0.1596(0.0012)	0.2712(0.0058)	0.0818(0.0008)	0.0905(0.0020)
$\hat{\lambda}$	–	−3.5655(3.7748)	–	0.6580(0.5031)
$\hat{\alpha}$	–	–	0.1705(0.0208)	0.1518(0.0251)
$\hat{\nu}$	0.9974(0.0884)	1.2501(0.1774)	6.0927(0.7501)	6.0999(0.7326)
$\hat{\ell}$	−29.50743	−18.87016	−17.67113	−14.80241
AIC	65.01487	45.74033	43.34227	39.60482
BIC	71.67339	54.61836	52.22030	50.70236
CAIC	59.38987	38.37525	35.97719	30.57256

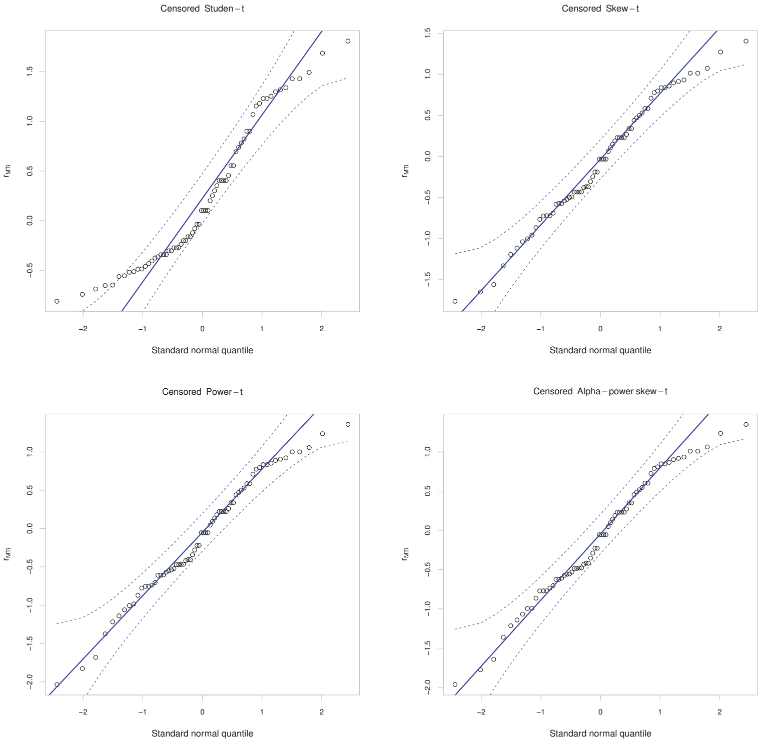

Figure 4. Stellar abundances data. Envelopes of transformed martingale residuals for CT, CST, CPT, and CAPST models.

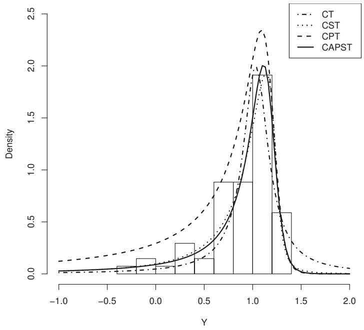

Figure 5. Graph of fitted densities to stellar abundances data.

5. Conclusions

In this work, a new asymmetric model has been introduced. It is based on the combination of skew-t [1] and power-t [2] models. The new model presents greater ranges of asymmetry and kurtosis, which is very useful for modeling skewed and heavy-tailed data. The problem of estimating the parameters in the model is dealt by using the maximum likelihood approach which is also used for developing large sample properties for the estimators. The elements of the observed information matrix are analytically obtained. The likelihood ratio statistics can be used for testing the APST null hypothesis since the Student-t, ST, and PT models are special cases of the model entertained. Two applications to volcano heights data and stellar abundances data indicate that the proposed model can be a useful alternative to the ST and PT models.

Author Contributions: Individual contributions to this article: conceptualization, R.T.-F., H.B., and G.M.-F.; methodology, R.T.-F., H.B., and G.M.-F.; software, R.T.-F., H.B., and G.M.-F.; validation, R.T.-F., H.B., and G.M.-F.; formal analysis, R.T.-F., H.B., and G.M.-F.; investigation, R.T.-F., H.B., and G.M.-F.; resources, R.T.-F., H.B., and G.M.-F.; writing-original draft preparation, R.T.-F., H.B., and G.M.-F.; writing-review and editing, R.T.-F., H.B., and G.M.-F. All authors have read and agreed to the published version of the manuscript.

Funding: This research received no external funding. The research of R. Tovar-Falón was supported by the Conselho Nacional de Desenvolvimento Científico e Tecnológico (CNPq/Brazil) under grant 140831/2014-2.

Acknowledgments: We thank the anonymous referees for helpful suggestions which improved the article.

Conflicts of Interest: The authors declare no conflict of interest.

Appendix A

In this section, expressions for the elements of the observed information matrix of the alpha-power skew-t model are provided. Initially we suppose that $Y \sim \text{APST}(\mu,\sigma,\lambda,\alpha,\nu)$, and for $i = 1,\ldots,n$ we define $z_i = (y_i - \mu)/\sigma$, $w_i = \sqrt{(\nu+1)/(z_i^2+\nu)}$, $r_1(z;\nu) = f_T(z;\nu)/\mathcal{F}_T(z;\nu)$, $r_2(z;\lambda,\nu) = f_{ST}(z;\lambda,\nu)/\mathcal{F}_{ST}(z;\lambda,\nu)$, and $r_3(z;\lambda,\nu) = \left(1+(1+\lambda^2)\frac{z^2}{\nu}\right)^{-\frac{\nu}{2}}/\mathcal{F}_{ST}(z;\lambda,\nu)$. Denoting the elements of the observed information matrix of the APST model by $j_{\mu\mu}, j_{\mu\sigma}, \ldots, j_{\alpha\alpha}$, and after some algebraic manipulations, we obtain

$$\begin{aligned}
j_{\mu\mu} = &-\frac{1}{\sigma^2}\frac{\nu+1}{\nu^2}\sum_{i=1}^{n} z_i^2\Big(1+\frac{z_i^2}{\nu}\Big)^{-2} + \frac{1}{\sigma^2}\frac{\nu+1}{\nu}\sum_{i=1}^{n}\Big(1+\frac{z_i^2}{\nu}\Big)^{-2} \\
&+ \frac{\lambda}{\sigma^2}\sum_{i=1}^{n} z_i w_i\Big(1+\frac{z_i^2}{\nu}\Big)^{-1} r_1(\lambda z_i w_i;\nu+1) \\
&+ \frac{2}{\sigma^2}\frac{\lambda}{\nu}\sum_{i=1}^{n} z_i w_i\Big(1+\frac{z_i^2}{\nu}\Big)^{-2} r_1(\lambda z_i w_i;\nu+1) \\
&+ \frac{\lambda^3}{\sigma^2}\frac{\nu+2}{\nu}\sum_{i=1}^{n} z_i w_i\Big(1+\frac{z_i^2}{\nu}\Big)^{-2}\Big(1+(1+\lambda^2)\frac{z_i^2}{\nu}\Big)^{-1} r_1(\lambda z_i w_i;\nu+1) \\
&+ \frac{\lambda^2}{\sigma^2}\frac{\nu+1}{\nu}\sum_{i=1}^{n}\Big(1+\frac{z_i^2}{\nu}\Big)^{-3}\big[r_1(\lambda z_i w_i;\nu+1)\big]^2
\end{aligned}$$

$$\begin{aligned}
j_{\mu\sigma} = &-\frac{\lambda}{\sigma^2}\frac{\alpha-1}{\pi}\sum_{i=1}^{n}\Big(1+\frac{z_i^2}{\nu}\Big)^{-1}\Big(1+(1+\lambda^2)\frac{z_i^2}{\nu}\Big)^{-1} r_3(z_i;\lambda,\nu) \\
&+ \frac{\alpha-1}{\sigma^2}\frac{\nu+1}{\nu}\sum_{i=1}^{n} z_i\Big(1+\frac{z_i^2}{\nu}\Big)^{-1} r_2(z_i;\lambda,\nu) + \frac{\alpha-1}{\sigma^2}\sum_{i=1}^{n}\big[r_2(z_i;\lambda,\nu)\big]^2 \\
&\frac{2}{\sigma^2}\frac{\nu+1}{\nu}\sum_{i=1}^{n} z_i\Big(1+\frac{z_i^2}{\nu}\Big)^{-2} \\
&+ \frac{\lambda^3}{\sigma^2}\frac{\nu+2}{\nu}\sum_{i=1}^{n} z_i^2 w_i\Big(1+\frac{z_i^2}{\nu}\Big)^{-2}\Big(1+(1+\lambda^2)\frac{z_i^2}{\nu}\Big)^{-1} r_1(\lambda z_i w_i;\nu+1) \\
&+ \frac{2}{\sigma^2}\frac{\lambda}{\nu}\sum_{i=1}^{n} z_i^2 w_i\Big(1+\frac{z_i^2}{\nu}\Big)^{-2} r_1(\lambda z_i w_i;\nu+1) \\
&- \frac{\lambda}{\sigma^2}\sum_{i=1}^{n} w_i\Big(1+\frac{z_i^2}{\nu}\Big)^{-2} r_1(\lambda z_i w_i;\nu+1) \\
&+ \frac{\lambda^2}{\sigma^2}\frac{\nu+1}{\nu}\sum_{i=1}^{n} z_i\Big(1+\frac{z_i^2}{\nu}\Big)^{-3}\big[r_1(\lambda z_i w_i;\nu+1)\big]^2 \\
&- \frac{\lambda}{\sigma^2}\frac{\alpha-1}{\pi}\sum_{i=1}^{n} z_i\Big(1+\frac{z_i^2}{\nu}\Big)^{-1}\Big(1+(1+\lambda^2)\frac{z_i^2}{\nu}\Big)^{-1} r_3(z_i;\lambda,\nu) \\
&- \frac{\alpha-1}{\sigma^2}\sum_{i=1}^{n} r_2(z_i;\lambda,\nu) + \frac{\alpha-1}{\sigma^2}\frac{\nu+1}{\nu}\sum_{i=1}^{n} z_i^2\Big(1+\frac{z_i^2}{\nu}\Big)^{-1} r_2(z_i;\lambda,\nu) \\
&+ \frac{\alpha-1}{\sigma^2}\sum_{i=1}^{n} z_i\big[r_2(z_i;\lambda,\nu)\big]^2
\end{aligned}$$

$$\begin{aligned}
j_{\mu\lambda} =& -\frac{\lambda^2}{\sigma}\frac{\nu+2}{\nu}\sum_{i=1}^{n} z_i^2 w_i \Big(1+\frac{z_i^2}{\nu}\Big)^{-1}\Big(1+\big(1+\lambda^2\big)\frac{z_i^2}{\nu}\Big)^{-1} r_1(\lambda z_i w_i;\nu+1)\\
&+\frac{1}{\sigma}\sum_{i=1}^{n} w_i\Big(1+\frac{z_i^2}{\nu}\Big)^{-1} r_1(\lambda z_i w_i;\nu+1)\\
&-\frac{\lambda}{\sigma}\frac{\nu+1}{\nu}\sum_{i=1}^{n} z_i\Big(1+\frac{z_i^2}{\nu}\Big)^{-2}\big[r_1(\lambda z_i w_i;\nu+1)\big]^2\\
&+\frac{\alpha-1}{\pi\sigma}\sum_{i=1}^{n} z_i^2\Big(1+\frac{z_i^2}{\nu}\Big)^{-1} r_3(z_i;\lambda,\nu)\\
&+\frac{\alpha-1}{\pi\sigma}\frac{1}{1+\lambda^2}\sum_{i=1}^{n} r_2(z_i;\lambda,\nu) r_3(z_i;\lambda,\nu)
\end{aligned}$$

$$j_{\mu\alpha} =\frac{1}{\sigma}\sum_{i=1}^{n} r_2(z_i;\lambda,\nu)$$

$$\begin{aligned}
j_{\mu\nu} =& -\frac{1}{\sigma\nu}\sum_{i=1}^{n} z_i\Big(1+\frac{z_i^2}{\nu}\Big)^{-1}+\frac{\nu+1}{\sigma\nu^2}\sum_{i=1}^{n} z_i\Big(1+\frac{z_i^2}{\nu}\Big)^{-2}\\
&+\frac{\lambda}{\sigma\nu^2}\sum_{i=1}^{n} z_i^2 w_i\Big(1+\frac{z_i^2}{\nu}\Big)^{-2} r_1(\lambda z_i w_i;\nu+1)\\
&+\frac{\lambda}{2\sigma}\frac{1}{\nu(\nu+1)}\sum_{i=1}^{n}(z_i^2-1) w_i\Big(1+\frac{z_i^2}{\nu}\Big)^{-2} r_1(\lambda z_i w_i;\nu+1)\\
&+\frac{\lambda^3}{2\sigma}\frac{\nu+2}{\nu^2(\nu+1)}\sum_{i=1}^{n} z_i^2(z_i^2-1) w_i\Big(1+\frac{z_i^2}{\nu}\Big)^{-2}\Big(1+\big(1+\lambda^2\big)\frac{z_i^2}{\nu}\Big)^{-1} r_1(\lambda z_i w_i;\nu+1)\\
&-\frac{\lambda^2}{2\sigma}\frac{1}{\nu^2}\sum_{i=1}^{n} z_i(z_i^2-1)\Big(1+\frac{z_i^2}{\nu}\Big)^{-3}\big[r_1(\lambda z_i w_i;\nu+1)\big]^2\\
&+\frac{\lambda}{2\pi\sigma}\frac{\alpha-1}{\nu+1}\sum_{i=1}^{n} z_i\Big(1+\big(1+\lambda^2\big)\frac{z_i^2}{\nu}\Big)^{-1} r_3(z_i;\lambda,\nu)\\
&+\frac{\alpha-1}{2\pi\sigma(\nu+1)}\frac{\lambda}{1+\lambda^2}\sum_{i=1}^{n} r_2(z_i;\lambda,\nu) r_3(z_i;\lambda,\nu)+\frac{\alpha-1}{2\sigma}\frac{\nu+1}{\nu^2}\sum_{i=1}^{n} z_i^2\Big(1+\frac{z_i^2}{\nu}\Big)^{-1} r_2(z_i;\lambda,\nu)\\
&-\frac{\alpha-1}{2\sigma}\sum_{i=1}^{n}\log\Big(1+\frac{z_i^2}{\nu}\Big) r_2(z_i;\lambda,\nu)-\frac{\alpha-1}{2\sigma}\sum_{i=1}^{n}\frac{g(z_i,\nu)}{\mathcal{F}_{ST}(z_i;\lambda,\nu)} r_2(z_i;\lambda,\nu)\\
&+\frac{\lambda}{2\pi\sigma}\frac{\alpha-1}{\nu}\sum_{i=1}^{n} z_i\Big(1+\frac{z_i^2}{\nu}\Big)^{-1}\Big(1+\big(1+\lambda^2\big)\frac{z_i^2}{\nu}\Big)^{-1} r_3(z_i;\lambda,\nu)
\end{aligned}$$

$$\begin{aligned}
j_{\sigma\sigma} =& -\frac{n}{\sigma^2} + \frac{1}{\sigma^2}\frac{\nu+1}{\nu}\sum_{i=1}^{n} z_i^2\Big(1+\frac{z_i^2}{\nu}\Big)^{-1} + \frac{2}{\sigma^2}\frac{\nu+1}{\nu}\sum_{i=1}^{n} z_i^2\Big(1+\frac{z_i^2}{\nu}\Big)^{-2} \\
&- \frac{2\lambda}{\sigma^2}\sum_{i=1}^{n} z_i w_i\Big(1+\frac{z_i^2}{\nu}\Big)^{-2} r_1(\lambda z_i w_i;\nu+1) \\
&- \frac{\lambda}{\sigma^2\nu}\sum_{i=1}^{n} z_i^3 w_i\Big(1+\frac{z_i^2}{\nu}\Big)^{-2} r_1(\lambda z_i w_i;\nu+1) \\
&+ \frac{\lambda^3}{\sigma^2}\frac{\nu+2}{\nu}\sum_{i=1}^{n} z_i^3 w_i\Big(1+\frac{z_i^2}{\nu}\Big)^{-2}\Big(1+\big(1+\lambda^2\big)\frac{z_i^2}{\nu}\Big)^{-1} r_1(\lambda z_i w_i;\nu+1) \\
&+ \frac{\lambda^2}{\sigma^2}\frac{\nu+1}{\nu}\sum_{i=1}^{n} z_i^2\Big(1+\frac{z_i^2}{\nu}\Big)^{-3} r_1(\lambda z_i w_i;\nu+1) \\
&- \frac{\lambda}{\sigma^2}\frac{\alpha-1}{\pi}\sum_{i=1}^{n} z_i^2\Big(1+\frac{z_i^2}{\nu}\Big)^{-1}\Big(1+\big(1+\lambda^2\big)\frac{z_i^2}{\nu}\Big)^{-1} r_3(z_i;\lambda,\nu) \\
&- \frac{2(\alpha-1)}{\sigma^2}\sum_{i=1}^{n} z_i r_2(z_i;\lambda,\nu) - \frac{\alpha-1}{\sigma^2}\frac{\nu+1}{\nu}\sum_{i=1}^{n} z_i^3\Big(1+\frac{z_i^2}{\nu}\Big)^{-1} r_2(z_i;\lambda,\nu) \\
&+ \frac{\alpha-1}{\sigma^2}\sum_{i=1}^{n} z_i^2 r_2(z_i;\lambda,\nu)
\end{aligned}$$

$$\begin{aligned}
j_{\sigma\lambda} =& \frac{1}{\sigma}\sum_{i=1}^{n} z_i w_i\Big(1+\frac{z_i^2}{\nu}\Big)^{-1} r_1(\lambda z_i w_i;\nu+1) \\
&+ \frac{\lambda^2}{\sigma}\frac{\nu+2}{\nu}\sum_{i=1}^{n} z_i^3 w_i\Big(1+\frac{z_i^2}{\nu}\Big)^{-1}\Big(1+\big(1+\lambda^2\big)\frac{z_i^2}{\nu}\Big)^{-1} r_1(\lambda z_i w_i;\nu+1) \\
&+ \frac{\lambda}{\sigma}\frac{\nu+1}{\nu}\sum_{i=1}^{n} z_i\Big(1+\frac{z_i^2}{\nu}\Big)^{-2}\big[r_1(\lambda z_i w_i;\nu+1)\big]^2 \\
&- \frac{\alpha-1}{\pi\sigma}\sum_{i=1}^{n} z_i^2\Big(1+\frac{z_i^2}{\nu}\Big)^{-1} r_3(z_i;\lambda,\nu) \\
&+ \frac{\alpha-1}{\pi\sigma}\frac{1}{1+\lambda^2}\sum_{i=1}^{n} r_2(z_i;\lambda,\nu) r_3(z_i;\lambda,\nu)
\end{aligned}$$

$$j_{\sigma\alpha} = \frac{1}{\sigma}\sum_{i=1}^{n} z_i r_2(z_i;\lambda,\nu)$$

$$\begin{aligned}
j_{\sigma\nu} = & -\frac{1}{\sigma\nu}\sum_{i=1}^{n} z_i^2\Big(1+\frac{z_i^2}{\nu}\Big)^{-1} + \frac{1}{\sigma}\frac{\nu+1}{\nu^2}\sum_{i=1}^{n} z_i^2\Big(1+\frac{z_i^2}{\nu}\Big)^{-2} \\
& + \frac{\lambda}{\sigma\nu^2}\sum_{i=1}^{n} z_i^3 w_i\Big(1+\frac{z_i^2}{\nu}\Big)^{-2} r_1(\lambda z_i w_i;\nu+1) \\
& + \frac{\lambda}{2\sigma}\frac{1}{\nu(\nu+1)}\sum_{i=1}^{n} z_i(z_i^2-1)w_i\Big(1+\frac{z_i^2}{\nu}\Big)^{-2} r_1(\lambda z_i w_i;\nu+1) \\
& - \frac{\lambda^3}{2\sigma}\frac{\nu+2}{\nu^2(\nu+1)}\sum_{i=1}^{n} z_i^3(z_i^2-1)w_i\Big(1+\frac{z_i^2}{\nu}\Big)^{-2}\Big(1+\big(1+\lambda^2\big)\frac{z_i^2}{\nu}\Big)^{-1} r_1(\lambda z_i w_i;\nu+1) \\
& - \frac{\lambda^2}{2\sigma\nu^2}\sum_{i=1}^{n} z_i^2(z_i^2-1)\Big(1+\frac{z_i^2}{\nu}\Big)^{-3}\big[r_1(\lambda z_i w_i;\nu+1)\big]^2 \\
& + \frac{\lambda}{2\pi\sigma}\frac{\alpha-1}{\nu(\nu+1)}\sum_{i=1}^{n} z_i^2(z_i^2-1)\Big(1+\frac{z_i^2}{\nu}\Big)^{-1}\Big(1+\big(1+\lambda^2\big)\frac{z_i^2}{\nu}\Big)^{-1} r_3(z_i;\lambda,\nu) \\
& + \frac{\alpha-1}{2\pi\sigma(\nu+1)}\frac{\lambda}{1+\lambda^2}\sum_{i=1}^{n} z_i r_2(z_i;\lambda,\nu) r_3(z_i;\lambda,\nu) \\
& + \frac{\alpha-1}{2\sigma}\frac{\nu+1}{\nu^2}\sum_{i=1}^{n} z_i^3\Big(1+\frac{z_i^2}{\nu}\Big)^{-1} r_1(\lambda z_i w_i;\nu+1) \\
& - \frac{\alpha-1}{2\sigma}\sum_{i=1}^{n} z_i \log\Big(1+\frac{z_i^2}{\nu}\Big) r_1(\lambda z_i w_i;\nu+1) \\
& - \frac{\alpha-1}{2\sigma}\sum_{i=1}^{n} z_i \frac{g(z_i,\nu)}{\mathcal{F}_{ST}(z_i,\lambda,\nu)} r_2(z_i;\lambda,\nu)
\end{aligned}$$

$$\begin{aligned}
j_{\lambda\lambda} = & \frac{\lambda(\nu+2)}{\nu}\sum_{i=1}^{n} z_i^3 w_i\Big(1+\big(1+\lambda^2\big)\frac{z_i^2}{\nu}\Big)^{-1} r_1(\lambda z_i w_i;\nu+1) \\
& + \frac{\nu+1}{\nu}\sum_{i=1}^{n} z_i\Big(1+\frac{z_i^2}{\nu}\Big)^{-1}\big[r_1(\lambda z_i w_i;\nu+1)\big]^2 \\
& - \frac{2(\alpha-1)}{\pi}\frac{\lambda}{(1+\lambda^2)^2}\sum_{i=1}^{n}\Big(1+\big(1+\lambda^2\big)\frac{z_i^2}{\nu}\Big)^{-1} r_3(z_i;\lambda,\nu) \\
& - \frac{\alpha-1}{\pi}\frac{\lambda}{1+\lambda^2}\frac{\nu+2}{\nu}\sum_{i=1}^{n} z_i^2\Big(1+\big(1+\lambda^2\big)\frac{z_i^2}{\nu}\Big)^{-1} r_3(z_i;\lambda,\nu) \\
& + \frac{\alpha-1}{\pi^2(1+\lambda^2)^2}\sum_{i=1}^{n}\big[r_3(z_i;\lambda,\nu)\big]^2
\end{aligned}$$

$$j_{\lambda\alpha} = \frac{1}{\pi(1+\lambda^2)} \sum_{i=1}^{n} r_3(z_i;\lambda,\nu)$$

$$\begin{aligned}
j_{\lambda\nu} =& -\frac{1}{2\nu(\nu+1)} \sum_{i=1}^{n} z_i(z_i^2-1)w_i\Big(1+\frac{z_i^2}{\nu}\Big)^{-1} r_1(\lambda z_i w_i;\nu+1) \\
&+ \frac{\lambda^2}{2\nu^2}\frac{\nu+2}{(\nu+1)^2} \sum_{i=1}^{n} z_i^3(z_i^2-1)w_i\Big(1+\frac{z_i^2}{\nu}\Big)^{-1}\Big(1+\big(1+\lambda^2\big)\frac{z_i^2}{\nu}\Big)^{-1} r_1(\lambda z_i w_i;\nu+1) \\
&+ \frac{\lambda}{2\nu^2} \sum_{i=1}^{n} z_i^2(z_i^2-1)\Big(1+\frac{z_i^2}{\nu}\Big)^{-2}\big[r_1(\lambda z_i w_i;\nu+1)\big]^2 \\
&+ \frac{\alpha-1}{2\pi(\nu+1)}\frac{1-\lambda^2}{(1+\lambda^2)^2} \sum_{i=1}^{n} r_3(z_i;\lambda,\nu) + \frac{\alpha-1}{2\pi(\nu+1)}\frac{\lambda}{(1+\lambda^2)^2} \sum_{i=1}^{n} \big[r_3(z_i;\lambda,\nu)\big]^2 \\
&- \frac{\alpha-1}{2\pi(\nu+1)}\frac{\lambda^2}{1+\lambda^2} \sum_{i=1}^{n} z_i^2\Big(1+\big(1+\lambda^2\big)\frac{z_i^2}{\nu}\Big)^{-1} r_3(z_i;\lambda,\nu) \\
&- \frac{\alpha-1}{2\pi(1+\lambda^2)} \sum_{i=1}^{n} \frac{g(z_i,\nu)}{\mathcal{F}_{ST}(z_i,\lambda,\nu)} r_3(z_i;\lambda,\nu) \\
&- \frac{\alpha-1}{2\pi} \sum_{i=1}^{n} \frac{g_1(z_i,\nu)}{\mathcal{F}_{ST}(z_i,\lambda,\nu)}
\end{aligned}$$

$$j_{\alpha\alpha} = \frac{n}{\alpha^2}$$

$$\begin{aligned}
j_{\alpha\nu} =& -\frac{n}{2}\psi\left(\frac{\nu+1}{2}\right) + \frac{n}{2}\psi\left(\frac{\nu}{2}\right) + \frac{n}{2\nu} \\
&+ \frac{1}{2\pi(\nu+1)}\frac{\lambda}{1+\lambda^2} \sum_{i=1}^{n} r_3(z_i;\lambda,\nu) - \frac{1}{2}\sum_{i=1} \frac{g(z_i,\nu)}{\mathcal{F}_{ST}(z_i,\lambda,\nu)}
\end{aligned}$$

$$
\begin{aligned}
j_{\nu\nu} = & -\frac{n\alpha}{2\nu^2} - \frac{n\alpha}{4}\psi_1\Big(\frac{\nu+1}{2}\Big) + \frac{n\alpha}{4}\psi_1\Big(\frac{\nu}{2}\Big) - \frac{\nu-1}{2\nu^3}\sum_{i=1}^{n} z_i^2\Big(1+\frac{z_i^2}{\nu}\Big)^{-1} \\
& + \frac{\nu+1}{2\nu^3}\sum_{i=1}^{n} z_i^2\Big(1+\frac{z_i^2}{\nu}\Big)^{-2} \\
& + \frac{\lambda}{4(\nu+1)^2}\frac{1}{\nu^2}\sum_{i=1}^{n} z_i(z_i^2-1)(z_i^2+4\nu+3)w_i\Big(1+\frac{z_i^2}{\nu}\Big)^{-2} r_1(\lambda z_i w_i;\nu+1) \\
& - \frac{\lambda}{4\nu(\nu+1)}\Big(\psi\Big(\frac{\nu+2}{2}\Big) - \psi\Big(\frac{\nu+1}{2}\Big) - \frac{1}{\nu+1}\Big) \\
& \quad \sum_{i=1}^{n} z_i(z_i^2-1)w_i\Big(1+\frac{z_i^2}{\nu}\Big)^{-1} r_1(\lambda z_i w_i;\nu+1) \\
& - \frac{\lambda^3}{4(\nu+1)}\frac{\nu+2}{\nu^3}\sum_{i=1}^{n} z_i^3(z_i^2-1)\Big(1+\frac{z_i^2}{\nu}\Big)^{-2}\Big(1+(1+\lambda^2)\frac{z_i^2}{\nu}\Big)^{-1} r_1(\lambda z_i w_i;\nu+1) \\
& + \frac{\lambda}{4\nu(\nu+1)}\sum_{i=1}^{n} z_i(z_i^2-1)\log\Big(1+\frac{\lambda^2 z_i^2}{\nu+z_i^2}\Big) r_1(\lambda z_i w_i;\nu+1) \\
& + \frac{\lambda^2}{4\nu^3(\nu+1)}\sum_{i=1}^{n} z_i^2(z_i^2-1)^2\Big(1+\frac{z_i^2}{\nu}\Big)^{-3}\big[r_1(\lambda z_i w_i;\nu+1)\big]^2 \\
& - \frac{\alpha-1}{2\pi(\nu+1)^2}\frac{\lambda}{1+\lambda^2}\sum_{i=1}^{n} r_3(z_i;\lambda,\nu) \\
& + \frac{\alpha-1}{4\pi(\nu+1)}\frac{\lambda}{\nu}\sum_{i=1}^{n} z_i^2\Big(1+(1+\lambda^2)\frac{z_i^2}{\nu}\Big)^{-1} r_3(z_i;\lambda,\nu) \\
& - \frac{\alpha-1}{4\pi(\nu+1)}\frac{\lambda}{1+\lambda^2}\sum_{i=1}^{n}\log\Big(1+(1+\lambda^2)\frac{z_i^2}{\nu}\Big) r_3(z_i;\lambda,\nu) \\
& + \frac{\alpha-1}{4\pi(\nu+1)}\frac{\lambda}{1+\lambda^2}\Big(\psi\Big(\frac{\nu+1}{2}\Big) - \psi\Big(\frac{\nu}{2}\Big) - \frac{1}{\nu}\Big)\sum_{i=1}^{n} r_3(z_i;\lambda,\nu) \\
& - \frac{\alpha-1}{2\pi(\nu+1)}\frac{\lambda}{1+\lambda^2}\sum_{i=1}^{n}\frac{g(z_i,\nu)}{\mathcal{F}_{ST}(z_i,\lambda,\nu)} r_3(z_i;\lambda,\nu) \\
& + \frac{\alpha-1}{4\pi^2(\nu+1)^2}\frac{\lambda^2}{(1+\lambda^2)^2}\sum_{i=1}^{n}\big[r_3(z_i;\lambda,\nu)\big]^2 \\
& + \frac{\alpha-1}{4}\sum_{i=1}^{n}\Big(\frac{g(z_i,\nu)}{\mathcal{F}_{ST}(z_i,\lambda,\nu)}\Big)^2 - \frac{\alpha-1}{2}\sum_{i=1}^{n}\frac{g_2(z_i,\nu)}{\mathcal{F}_{ST}(z_i,\lambda,\nu)}
\end{aligned}
$$

where $g(z;\nu)$ is given in Equation (16), and $g_1(z;\nu)$ and $g_2(z;\nu)$ are given in Equations (A1) and (A3), respectively.

$$
\begin{aligned}
g_1(x;\nu) = & \int_{-\infty}^{x} \left\{ \frac{(\nu+1)s^2}{\nu(s^2+\nu)} - \log\left(1+\frac{s^2}{\nu}\right) \right\} \left\{ 1+\frac{(1+\lambda^2)s^2}{\nu} \right\}^{-\frac{\nu+2}{2}} sds \\
& - \int_{-\infty}^{x} \frac{s}{s^2+\nu} \left\{ 1+\frac{(1+\lambda^2)s^2}{\nu} \right\}^{-\frac{\nu+2}{2}} ds \\
& + \int_{-\infty}^{x} \frac{\lambda^2(\nu+2)s^3}{(s^2+\nu)(\nu+(1+\lambda^2)s^2)} \left\{ 1+\frac{(1+\lambda^2)s^2}{\nu} \right\}^{-\frac{\nu+2}{2}} ds
\end{aligned}
\tag{A1}
$$

$$
\begin{aligned}
g_2(x;\nu) = & \int_{-\infty}^{x} \left\{ \frac{s^2(s^2\nu-2\nu-s^2)}{\nu^2(s^2+\nu)^2} + \frac{1}{2}\left[\frac{(\nu+1)s^2}{\nu(s^2+\nu)} - \log\left(1+\frac{s^2}{\nu}\right) \right]^2 \right\} f_{ST}(s;\lambda,\nu)ds \\
& + \frac{\lambda}{2\pi(\nu+1)} \int_{-\infty}^{x} \frac{s(s^2-1)}{(s^2+\nu)} \left\{ \frac{(\nu+1)s^2}{\nu(s^2+\nu)} - \log\left(1+\frac{s^2}{\nu}\right) \right\} \\
& \quad \times \left\{ 1+\frac{(1+\lambda^2)s^2}{\nu} \right\}^{-\frac{\nu+2}{2}} ds \\
& + \frac{\lambda}{\pi} \int_{-\infty}^{x} \frac{s}{(s+\nu)^2} \left\{ 1+\frac{(1+\lambda^2)s^2}{\nu} \right\}^{-\frac{\nu+2}{2}} ds
\end{aligned}
\tag{A2}
$$

$$
\begin{aligned}
& + \frac{\lambda}{2\pi}\left(\psi\left(\frac{\nu+1}{2}\right) - \psi\left(\frac{\nu}{2}\right) - \frac{1}{\nu} \right) \int_{-\infty}^{x} \frac{s}{s^2+\nu} \left\{ 1+\frac{(1+\lambda^2)s^2}{\nu} \right\}^{-\frac{\nu+2}{2}} ds \\
& - \frac{\lambda}{2\pi} \int_{-\infty}^{x} \frac{s}{s^2+\nu} \left\{ \frac{(\nu+2)(1+\lambda^2)s^2}{\nu(\nu+(1+\lambda^2)s^2)} - \log\left(1+\frac{(1+\lambda^2)s^2}{\nu}\right) \right\} \\
& \quad \times \left\{ 1+\frac{(1+\lambda^2)s^2}{\nu} \right\}^{-\frac{\nu+2}{2}} ds
\end{aligned}
\tag{A3}
$$

References

1. Azzalini, A. A class of distributions which includes the normal ones. *Scand. J. Stat.* **1985**, *12*, 171–178.
2. Durrans, S.R. Distributions of fractional order statistics in hydrology. *Water Resour. Res.* **1992**, *28*, 1649–1655. [CrossRef]
3. Martínez-Flórez, G.; Bolfarine, H.; Gómez, H.W. The alpha–power tobit model. *Commun. Stat. Theory Methods* **2013**, *42*, 633–643. [CrossRef]
4. Birnbaum, Z.W.; Saunders, S.C. A new family of life distributions. *J. Appl. Probab.* **1969**, *6*, 319–327. [CrossRef]
5. Martínez-Flórez, G.; Bolfarine, H.; Gómez, H.W. An alpha-power extension for the Birnbaum-Saunders distribution. *Statistics* **2014**, *48*, 896–912. [CrossRef]
6. Gupta, R.D.; Gupta, R.C. Analyzing skewed data by power-normal model. *Test* **2008**, *17*, 197–210. [CrossRef]
7. Pewsey, A.; Gómez, H. W.; Bolfarine, H. Likelihood–based inference for power distributions. *Test* **2012**, *21*, 775–789. [CrossRef]
8. Martínez-Flórez, G.; Bolfarine, H.; Gómez, H.W. Skew-normal alpha-power model. *Stat. J. Theor. Appl. Stat.* **2014**, *48*, 1414–1428. [CrossRef]
9. Azzalini, A.; Capitanio, A. Distributions generated by perturbation of symmetry with emphasis on a multivariate skew-*t* distribution. *J. R. Stat. Soc. Ser. B (Stat. Methodol.)* **2003**, *65*, 367–389. [CrossRef]
10. Branco, M.D.; Dey, D.K. General class of multivariate skew-elliptical distributions. *J. Multivar. Anal.* **2001**, *79*, 99–113. [CrossRef]
11. Durrans, S.R. Multivariate skew *t*-distribution. *Stat. J. Theor. Appl. Stat.* **2003**, *37*, 359–363.
12. Sahu, S.K.; Dey, D.K.; Branco, M.D. A new class of multivariate skew distributions with applications to Bayesian regression models. *Can. J. Stat.* **2003**, *31*, 129–150. [CrossRef]
13. Jones, M.C.; Faddy, M.J. A skew extension of the *t*-distribution, with Applications. *J. R. Stat. Soc. Ser. B (Stat. Methodol.)* **2003**, *65*, 159–174. [CrossRef]

14. Zhao, J.; Kim, H.M. Power *t* distributions. *Commun. Stat. Appl. Methods* **2016**, *23*, 321–334.
15. R Development Core Team. *R: A Language and Environment for Statistical Computing*; R Foundation for Statistical Computing: Vienna, Austria, 2018. Available online: http://www.R-project.org (accessed on 10 October 2019).
16. Lehman, E.L.; Casella, G. *Theory of Point Estimation*, 2nd ed.; Springer: New York, NY, USA, 1998.
17. Frieden, B.R. *Science from Fisher Information: A Unification*; Cambridge Univerisity Press: Cambridge, UK, 2004.
18. Arellano-Valle, R.B.; Azzalini, A. The centered parameterization and related quantities of the skew–*t* distribution. *J. Multivar. Anal.* **2013**, *113*, 73–90. [CrossRef]
19. Arellano-Valle, R.B.; Azzalini, A. The centered parametrization for the multivariate skew-normal distribution. *J. Multivar. Anal.* **2008**, *99*, 1362–1382. [CrossRef]
20. Akaike, H. A new look at statistical model identification. *IEEE Trans. Autom. Contr.* **1974**, *19*, 716–722. [CrossRef]
21. Schwarz, G. Estimating the dimension of a model. *Ann. Stat.* **1978**, *6*, 461–464. [CrossRef]
22. Bozdogan, H. Model selection and akaike's information criterion (AIC): The general theory and its analytical extensions. *Psychometrika* **2010**, *52*, 345–370. [CrossRef]
23. Siebert, L.; Simkin, T.; Kimberly, P. Global Volcanism Program. In *Volcanoes of the World*; v. 4.6.0.; Venzke, E., Ed.; Smithsonian Institution: Washington, DC, USA, 2013. Available online: https://doi.org/10.5479/si.GVP.VOTW4-2013 (accessed on 10 October 2019).
24. Feigelson, E.D. astrodatR: Astronomical Data. R Package v. 0.1. Available online: http://CRAN.R-project.org/package=astrodatR (accessed on 10 October 2019).
25. Mattos, T.; Garay, A.M.; Lachos, V.H. Likelihood-based inference for censored linear regression models with scale mixtures of skew-normal distributions. *J. Appl. Stat.* **2018**, *45*, 2019–2066. [CrossRef]
26. Barros, M.; Galea, M.; González, M.; Leiva, V. Influence diagnostics in the tobit censored response model. *Stat. Methods Appl.* **2010**, *19*, 379–397. [CrossRef]
27. Ortega, E.M.; Bolfarine, H.; Paula, G.A. Influence diagnostics in generalized log-gamma regression models. *Comput. Stat. Data Anal.* **2003**, *42*, 165–186. [CrossRef]

symmetry

MDPI

Article

A Test Detecting the Outliers for Continuous Distributions Based on the Cumulative Distribution Function of the Data Being Tested

Lorentz Jäntschi [1,2]

[1] Department of Physics and Chemistry, Technical University of Cluj-Napoca, 400641 Cluj, Romania; lorentz.jantschi@chem.utcluj.ro or lorentz.jantschi@gmail.com

[2] Chemical Doctoral School, Babeș-Bolyai University, 400084 Cluj-Napoca, Romania

Received: 12 June 2019; Accepted: 24 June 2019; Published: 25 June 2019

Abstract: One of the pillars of experimental science is sampling. Based on the analysis of samples, estimations for populations are made. There is an entire science based on sampling. Distribution of the population, of the sample, and the connection among those two (including sampling distribution) provides rich information for any estimation to be made. Distributions are split into two main groups: continuous and discrete. The present study applies to continuous distributions. One of the challenges of sampling is its accuracy, or, in other words, how representative the sample is of the population from which it was drawn. To answer this question, a series of statistics have been developed to measure the agreement between the theoretical (the population) and observed (the sample) distributions. Another challenge, connected to this, is the presence of outliers - regarded here as observations wrongly collected, that is, not belonging to the population subjected to study. To detect outliers, a series of tests have been proposed, but mainly for normal (Gauss) distributions—the most frequently encountered distribution. The present study proposes a statistic (and a test) intended to be used for any continuous distribution to detect outliers by constructing the confidence interval for the extreme value in the sample, at a certain (preselected) risk of being in error, and depending on the sample size. The proposed statistic is operational for known distributions (with a known probability density function) and is also dependent on the statistical parameters of the population—here it is discussed in connection with estimating those parameters by the maximum likelihood estimation method operating on a uniform U(0,1) continuous symmetrical distribution.

Keywords: test for outliers; order statistics; extreme values; confidence intervals; Monte-Carlo simulation

1. Introduction

Many statistical techniques are sensitive to the presence of outliers and all calculations, including the mean and standard deviation can be distorted by a single grossly inaccurate data point. Therefore, checking for outliers should be a routine part of any data analysis.

To date, several tests have been developed for the purpose of identifying outliers of certain distributions. Most of the studies are connected with the Normal (or Gauss) distribution [1]. The first paper that attracted attention on this matter is [2] and this was followed by studies that identified the derivation of the distribution of the extreme values in samples taken from Normal distributions [3]. Then, a series of tests were developed by Thompson in 1935 [4], these were subjected to evaluation [5], and revised [6,7].

For other distributions such as the Gamma distribution, procedures for detecting outliers were proposed [8], revised [9], and unfortunately proved to be inefficient [10].

The first attempt to generalize the criterion for detecting outliers for any distribution can be found in [11], but further research on this subject is scarce apart from a notable recent attempt by Bardet and Dimby [12].

The Grubbs test is a frequently used test for detecting the outliers of a Normal distribution [7]. For a sample (x), the Grubbs' test statistic takes the largest absolute deviation from the sample mean ($\overline{x}$) in units of the sample standard deviation (s) in order to calculate the risk of being in error (α_G) when stating that the most departed values from the mean (min(x), max(x) or both) are not outliers (see Table 1). The associated probabilities of the observed (p_G) are obtained from the Student t distribution [13].

Table 1. The Grubbs statistic.

Sample statistic (G)	Associated probability ($p_G = 1\text{-}\alpha_G$)	Equation
$G_{“min”} = \frac{\overline{x}-\min(x)}{s}$	$\alpha_G = n{\cdot}\text{CDF}_{“\text{Student t}”}\left(-\sqrt{\frac{n(n-2)}{\left(\frac{n-1}{G}\right)^2-n}}, n-2\right)$	(1)
$G_{“max”} = \frac{\max(x)-\overline{x}}{s}$		
$G_{“all”} = \max(G_{“min”}, G_{“max”})$	$\alpha_G = 2n{\cdot}\text{CDF}_{“\text{Student t}”}\left(-\sqrt{\frac{n(n-2)}{\left(\frac{n-1}{G}\right)^2-n}}, n-2\right)$	(2)

One should note that the Grubbs test statistic produces a symmetrical confidence interval (see Equations (1) and (2)). The Grubbs statistic as given in Table 1, is intended to be used with the parameters of the population (μ and σ), which are determined using the central moments (CM) method ($\hat{\mu} = \overline{x} = \sum x/\text{n}$; $\hat{\sigma} = \text{s} = \left(\sum (x-\overline{x})^2\right)^{1/2}/\text{n}$).

Here, a method is proposed for constructing the confidence intervals for the extreme values of any continuous distribution for which the cumulative distribution function is also obtainable. The method involves the direct application of a simple test for detecting the outliers. The proposed method is based on deriving the statistic for the extreme values for the uniform distribution. Also, the proposed method provides a symmetrical confidence interval in the probability space.

2. Materials and Methods

The Grubbs test (Table 1) is based on the fact that if outliers exist, then these are "localized" as the maximum value and/or the minimum value in the dataset. Thus, the Grubbs test is essentially a sort of order statistic [14].

Some introductory elements are required for describing the proposed procedure. When a sample of data is tested under the null hypothesis that it follows a certain distribution, it is intrinsically assumed that the distribution is known. The usual assumption is that we possess its probability density function (PDF, for a continuous distribution) or its probability distribution function (PDF for a discrete distribution). The discussion below relates to continuous distributions, although the treatment of discrete distributions are similar to certain degree. Nevertheless, a major distinction between continuous and discrete distributions in the treatment of data is made here; that is, a continuous distribution is "dense", e.g., between any two distinct observations it is possible to observe another while in the case of a discrete distribution, this is generally not true.

Even when the PDF is known (possibly intrinsically), its (statistical) parameters may not necessarily be known, and this raises the complex problem of estimating the parameters of the (population) distribution from the sample; however, this issue is outside the scope of this paper. In general, the estimation of the parameters of the distribution of the data is biased by the presence of the outliers in the data, and thus, identifying the outliers along with the estimation of the parameters of the distribution is a difficult task because two statistical hypotheses are operating. Assuming that the parameters ("parameters") of the distribution (of the PDF) are obtained using the maximum likelihood estimation method (MLE, Equation (3); see [15]), there is some suggestion that the uncertainty accompanying this estimation is transmitted to the process of detecting the outliers.

$$\prod \text{PDF}(\text{X};\ “\text{parameters}”) \rightarrow \text{max.} \ \Rightarrow \sum \ln\left(\text{PDF}(\text{X};\ “\text{parameters}”)\right) \rightarrow \text{min.} \tag{3}$$

It should be noted that Equation (3) is a simplified version of the MLE method, since the real use of it requires and involves partial derivatives of the parameters; see Source code (MathCad language) for the MLE estimations in the Supplementary Materials available online.

Either way (whether the uncertainty accompanying this estimation is transmitted to the process of detecting the outliers or not), once an estimate for the parameters of the distribution is available, a test (most desirably, a test based on a statistic) for detecting the presence of an outlier must provide the probability of observing that (assumed) "outlier" as a randomly drawn value from the distribution. What to do next with the probability is another statistical "trick": to observe a value with a probability less than an imposed "level" (usually 5%) is defined as an unlikely event, and therefore, the suspicion regarding the presence of the outlier is justified. With regard to the statistical "trick" mentioned above, the opinion of the author of this manuscript is that one "observation" is not enough. Actually, there should be a series of observations, that come from a series of statistics, each providing a probability. Then, the unlikeliness of the event can be safely ascertained by using Fisher's "combining probability from independent tests" method (FCS, Equation (4); see [16–18]:

$$-\sum_{i=1}^{\tau} \ln(\mathrm{p_i}) \sim \chi^2(\tau) \rightarrow \alpha_{\mathrm{FCS}} = 1 - \mathrm{CDF}_{\chi^2}\left(-\sum_{i=1}^{\tau} \ln(\mathrm{p_i}); \tau\right) \tag{4}$$

where $\mathrm{p}_1, \ldots, \mathrm{p}_\tau$ are probabilities from τ independent tests, $\mathrm{CDF}\chi^2$ is the χ^2 cumulative distribution function (see also up until Equation (6) below), and $\mathrm{p_{FCS}}$ is the combined probability from independent tests.

Taking the general case, for $(x_1, \ldots, x_n)$ as n independent draws (or observations) from a (assumed known) continuous distribution defined by its probability density function, PDF $(\mathrm{x}; (\pi_\mathrm{j})_{1\leq \mathrm{j}\leq \mathrm{m}})$ where $(\pi_\mathrm{j})_{1\leq \mathrm{j}\leq \mathrm{m}}$ are the (assumed unknown) m statistical parameters of the distribution, by way of integration for a (assumed known) domain (D) of the distribution, we may have access to the associated cumulative density function (CDF) $\mathrm{CDF}(\mathrm{x}; (\pi_\mathrm{j})_{1\leq \mathrm{j}\leq \mathrm{m}}; \mathrm{PDF})$, simply expressed as (Equation (5)):

$$\mathrm{CDF}(\mathrm{x};\ (\pi_{\mathrm{j})1\leq \mathrm{j}\leq \mathrm{m}}) = \int_{\inf(D)}^{x} \mathrm{PDF}(\mathrm{x};\ (\pi_\mathrm{j})_{1\leq \mathrm{j}\leq \mathrm{m}}) \tag{5}$$

where inf(D) was used instead of min(D) to include unbounded domains (e.g., when inf(D) = -∞; "inf" stands for infimum, "min" stands for minimum). Please note that having the PDF and CDF does not necessarily imply that we have an explicit formula (or expression) for any of them. However, with access to numerical integration methods [19], it is enough to have the possibility of evaluating them at any point (x).

Unlike $\mathrm{PDF}(\mathrm{x}; (\pi_\mathrm{j})_{1\leq \mathrm{j}\leq \mathrm{m}})$, $\mathrm{CDF}(\mathrm{x}; (\pi_\mathrm{j})_{1\leq \mathrm{j}\leq \mathrm{m}})$ is a bijective function and therefore, it is always invertible (even if we do not have an explicit formula; let "InvCDF" be its inverse, Equation (6)):

$$\text{if p} = \mathrm{CDF}(\mathrm{x}; (\pi_\mathrm{j})_{1\leq \mathrm{j}\leq \mathrm{m}}), \text{ then x} = \mathrm{InvCDF}(\mathrm{p}; (\pi_\mathrm{j})_{1\leq \mathrm{j}\leq \mathrm{m}}), \text{ and vice-versa} \tag{6}$$

$\mathrm{CDF}(\mathrm{x}; (\pi_\mathrm{j})_{1\leq \mathrm{j}\leq \mathrm{m}};$ "PDF") is a strong tool that greatly simplifies the problem at hand: the problems of analyzing any distribution function (PDF) are translated such that only one needs to be analyzed (the continuous uniform distribution). That is, a series of observed data $(\mathrm{x_i})_{1\leq \mathrm{i}\leq \mathrm{n}}$ is expressed through their associated probabilities $\mathrm{p_i} = \mathrm{CDF}(\mathrm{x_i}; (\pi_\mathrm{j})_{1\leq \mathrm{j}\leq \mathrm{m}})$ (for $1\leq \mathrm{i}\leq \mathrm{n}$) and the analysis can be conducted on the $(\mathrm{p_i})_{1\leq \mathrm{i}\leq \mathrm{n}}$ series instead.

Since the analysis of the $(\mathrm{p_i})_{1\leq \mathrm{i}\leq \mathrm{n}}$ series of probabilities is a native case of order statistics, the discussion now turns to order statistics. The first studies in this area were by the fathers of modern statistics, Karl Pearson [20] and Ronald A. Fisher [3] while the first order statistic applicable to any distribution (not only the normal distribution) was first studied by Cramér and Von Mises (see [21,22]).

An order statistic operating on probabilities ($(p_i)_{1\le i\le n}$) will sort the values (let $(q_i)_{1\le i\le n}$ be the series of sorted $(p_i)_{1\le i\le n}$ values, Equation (7)) and will assess its departure from the continuous uniform distribution (where it is assumed that SORT is a procedure that sorts ascending the values).

$$(q_i)_{1\le i\le n} \leftarrow \mathrm{SORT}((p_i)_{1\le i\le n}) \tag{7}$$

Since the assessment of the departure from the continuous uniform distribution cannot be made directly, the use of a series of order statistics was proposed by several authors including: Cramér and Von Mises [21,22], Kolmogorov-Smirnov [23–25], Anderson-Darling [26,27], Kuiper V [28], Watson U^2 [29], and the H1 Statistic [18]; see Equation (8). They remain in use today.

For instance, the Kolmogorov-Smirnov (KS) method (see Equation (8); the Kolmogorov-Smirnov statistic) calculates the $\mathrm{KS}_{\mathrm{Statistic}}$ and later tests the value (from a sample) against the threshold of a chosen significance level (usually 5%).

In order to have certain thresholds for a series of significance levels, these statistics can be derived from Monte-Carlo (“MC”) simulations [30], and deployed for a large number of samples in order to reflect, as best as possible, the state of the population.

$$\begin{aligned}
KS_{Statistic} &= \sqrt{\mathrm{n}}\cdot\max_{1\le i\le n}\left(q_i - \tfrac{i-1}{n}, \tfrac{i}{n} - q_i\right)\\
KV_{Statistic} &= \sqrt{\mathrm{n}}\cdot\left(\max_{1\le i\le n}\left(q_i - \tfrac{i-1}{n}\right) + \max_{1\le i\le n}\left(\tfrac{i}{n} - q_i\right)\right)\\
AD_{Statistic} &= -n - \tfrac{1}{n}\cdot\sum_{i=1}^{n}(2i-1)\cdot\ln(q_i\cdot(1-q_{n-i}))\\
CM_{Statistic} &= \tfrac{1}{12n} + \sum_{i=1}^{n}\left(\tfrac{2\cdot i-1}{2\cdot n} - q_i\right)^2\\
WU_{Statistic} &= \mathrm{CM}_{\mathrm{Statistic}} + \left(\tfrac{1}{2} - \tfrac{1}{n}\sum_{i=1}^{n} q_i\right)^2\\
H1_{Statistic} &= -\sum_{i=1}^{n} q_i\cdot\ln(q_i) - \sum_{i=1}^{n}(1-q_i)\cdot\ln(1-q_i)
\end{aligned} \tag{8}$$

3. Proposed Outlier Detection Statistic

A statistic was developed to be applicable to any distribution. For a series of probabilities ($(p_i)_{1\le i\le n}$) or (sorted probabilities, $(q_i)_{1\le i\le n}$) associated with a series of (repeated drawing) observations ($(x_i)_{1\le i\le n}$), the $(r_i)_{1\le i\le n}$ differences are calculated as Equation (9):

$$r_i = |p_i - 0.5|, \text{ for } 1 \le i \le n \tag{9}$$

The statistic called “g1” (see below) was generated based on the formula given in Equation (9) (given as Equation (10)).

$$g1 = \max_{1\le i\le n} r_i \tag{10}$$

It should be noted that Equations (9) and (10) provide the same result regardless of whether the calculation is made on a sorted series of probabilities ($(q_i)_{1\le i\le n}$) or not (then it is made on $(p_i)_{1\le i\le n}$).

Regarding the name of this new proposed statistic (“g1”), when Equations (1) and (2) ($G_{\text{“min”}}$, $G_{\text{“max”}}$, $G_{\text{“all”}}$) and Equation (9) are compared, for a standard normal distribution N(x; μ=0,σ=1) the equation defining $G_{\text{“all”}}$ becomes much more like Equation (9), with the difference being that in Equation (2) the sample mean ($\bar{x}$) is used as an estimate for the mean of the population (μ) and the sample standard deviation (s) is used as an estimate for the standard deviation of the population (σ) while Equation (9) basically expresses the same in terms of associated probabilities ($p_i = P(X \le x_i) = \mathrm{CDF}_{\text{“Normal”}}(x_i; \mu,\sigma)$, $0.5 = P(X \le \mu) = \mathrm{CDF}_{\text{“Normal”}}(\mu; \mu,\sigma)$).

Therefore, the proposed statistic very much resembles the Grubbs test for normality (and hence its name). One difference is that in the Grubbs test sample statistics are used to calculate the sample $G_{\text{“all”}}$ value ($\bar{x}$ and s), thereby reducing the degrees of freedom associated with the value (from n to n-2) while for the g1 value (and statistic) the degrees of freedom remain unchanged (n). The major difference is actually the one that makes the proposed statistic generalizable to any distribution—the mean used in the Grubbs test is replaced by the median—the beauty of this change is that for symmetrical distributions (including a Normal distribution) these two coincide.

A further connection with other statistics must also be noted. If any sample is resampled by extracting only the smallest and the largest of its values, then the Kolmogorov-Smirnov statistic for those subsamples almost perfectly resembles (by setting n = 2 in Equations (8)–(1)) the proposed "g1" statistic.

Since CDF is a bijective function (see Equation (6)), the proposed generalization of the Grubbs test for detecting the outliers for Normal distribution into the "g1" statistic for detecting the outliers for any distribution is a natural extension of it. The "g1" test associated with the "g1" statistic will be able to operate in the probability space ($(p_i)_{1\leq i\leq n}$ or $(q_i)_{1\leq i\leq n}$) instead of the observed space ($(x_i)_{1\leq i\leq n}$), the calculation formula (Equations (9) and (10)) is slightly different (to those given in Equations (1) and (2)), and the probability associated with the departure will no longer be extracted from the Student t distribution (as in Equations (1) and (2)). The change from mean (μ for $G_{\text{"all"}}$) to median (0.5 in Equation (9)) is a safe extension for any distribution type, since Equation (9) measures (or accounts for) the extreme departures from the equiprobable point—having an observation y ($y \leftarrow X$) with $y \leq \text{InvCDF}_{\text{"Any distribution"}}(0.5; \text{"parameters"})$ and an observation z ($z \leftarrow X$) with $z \geq \text{InvCDF}_{\text{"Any distribution"}}(0.5; \text{"parameters"})$ is equiprobable.

One way to associate a probability with the "g1" statistic is to do a Monte-Carlo (MC) simulation.

4. Simulation Study

A MC study was conducted. Two different strategies were developed in order to deal efficiently with a very large amount of data, and specifically, to solve the order statistics problem (that is, first sampling from the uniform distribution, and later using Equations (7)–(10). One of those alternatives has been described in [14] and the other is described below. Table 2 shows the details of the conducted MC study.

Table 2. Details of the MC simulation on "g1" outlier detection statistic.

Parameter	Meaning	Setting
n	sample size of the observed	from 2 to 12
m	sample size of the MC simulation	10^8
p	control points for the probability	999
resa	internal resamples (repetitions)	10
repe	external repetitions	7

For each sample size of the observed *n* in each run *m* samples (see Table 2) were generated from the standard uniform continuous distribution (e.g., from the [0, 1] interval). The outlier detection statistic "g1" was calculated (Equations (9) and (10)). From a large pool of sampled and resampled data ($m\cdot resa\cdot repe = 7\cdot 10^9$ in Table 2, repetitions were joined *(n, p, g1)* as pairs from the *p·n* control points, that is, where the probability was from 0.001 to 0.999 with a step of 0.001 for each n (from 2 to 12). The external repetitions (resa = 7 in Table 2) were joined together by taking the median (since the median is a sufficiency statistic [31] for any order statistic such as in the extraction of (*n*, *p*, *g1*) pairs from the *p·n* control points). The MC simulation was conducted with the configuration set as defined in Table 2. The obtained data were recorded in separate files by sample size and analyzed as such.

The objective associated (with any statistic) is to obtain the cumulative distribution function (CDF, Equation (5)), and thus by evaluating the CDF for the value of the statistic obtained from the sample (Equations (9) and (10)) to obtain a probability for the sampling. Please note that only in the lucky cases are we able to do this; Generally only the critical values (values corresponding to certain risks of being in error) or approximation formulas are available (see for instance [21,24,26,28,29]). Here, the analytical CDF formula was obtained for the "g1" outlier detection statistic.

5. The Analytical Formula of CDF for g1

The "g1" statistic have a very simple calculation formula (see Equation (9)) and, as expected, its CDF formula is also very simple (see Equation (11)). Thus, for a calculated sample statistic g1 (x ← g1 in Equation (11)), the significance level (α ← 1-p) is immediate (Equation (11), where P represents the probability that the random variable X takes on a value less than or equal to x).

$$p = \text{CDF}_{\text{"}g1\text{"}}(x;n) = \text{P}(\text{X} \le \text{x}) = (2{\cdot}x)^n,\ \alpha = 1-p = 1-(2{\cdot}x)^n \tag{11}$$

6. Simulation Results for the Distribution of the "g1" Statistic

The results of the simulation for n varying from 2 to 10 were sufficient to provide a clear indication of the analytical formula for the CDF of "g1". Descriptive statistics including Standard Error (SE, the standard error formula is given as Equation (12)) between the expected probability (from MC simulation) and the calculated probability (from Equation (11), $\hat{p}_i \leftarrow (2{\cdot}x_i)^n$) and the highest positive and highest negative departures are given in Table 3.

$$SE = \sqrt{\frac{1}{999}\sum_{i=1}^{999}(p_i - \hat{p}_i)^2},\ p_i = \frac{i}{1000} \tag{12}$$

Table 3. Descriptive statistics for the agreement in the calculation of the "g1" statistic (Equation (10) vs. Equation (11)).

n	SE	min$(p_i{-}\hat{p}_i)$		max$(p_i{-}\hat{p}_i)$	
2	**2.9×10^{-6}**	-7.9×10^{-6}	at p = 0.694	5.7×10^{-6}	at p = 0.427
3	5.6×10^{-6}	-1.2×10^{-5}	at p = 0.787	1.6×10^{-6}	at p = 0.118
4	2.2×10^{-6}	-5.6×10^{-6}	at p = 0.234	3.7×10^{-6}	at p = 0.613
5	6.0×10^{-6}	-1.2×10^{-5}	at p = 0.546	2.3×10^{-6}	at p = 0.080
6	3.5×10^{-6}	-5.8×10^{-6}	at p = 0.797	9.2×10^{-6}	at p = 0.196
7	5.0×10^{-6}	-9.6×10^{-6}	at p = 0.777	3.8×10^{-6}	at p = 0.035
8	4.2×10^{-6}	-8.4×10^{-6}	at p = 0.675	3.9×10^{-6}	at p = 0.948
9	3.3×10^{-6}	-9.1×10^{-6}	at p = 0.269	7.9×10^{-6}	at p = 0.689
10	2.8×10^{-6}	-6.4×10^{-6}	at p = 0.443	6.6×10^{-6}	at p = 0.652

As can be observed in Table 3 the standard error (SE) slowly decreases beginning with n = 7, being two orders of magnitude smaller (actually it is about 200 times smaller) than the step from the MC experiment. Since the standard error alone is not proof that Equation (11) is the true CDF formula for providing the probability for the g1 statistic, the smallest and the highest difference between the observed and the expected probabilities are also given in Table 3. They substantiate that Equation (11) is indeed the right estimate for the CDF of g1. For convenience, Figure 1 shows the value of the error in each observation point (999 points corresponding to p = 0.001 up to p = 0.999 for each n from 2 to 12).

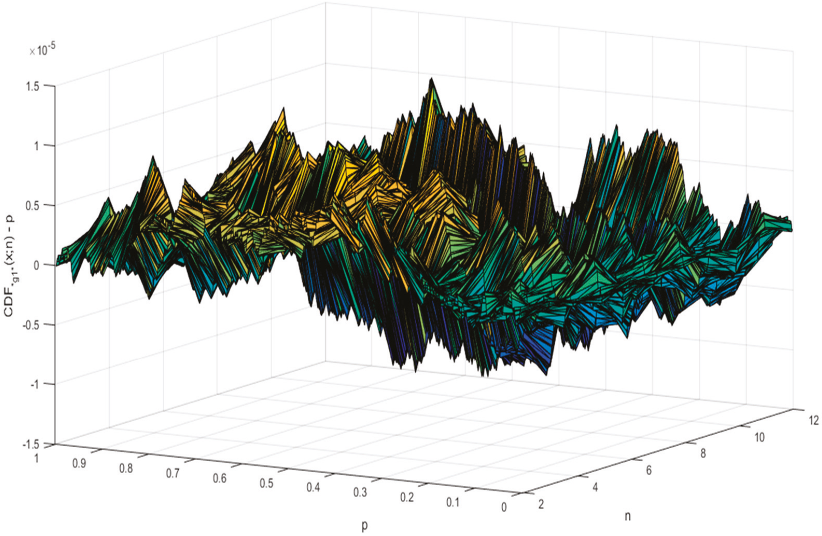

Figure 1. Departures between expected and observed probabilities for g1 statistic (Equation (10) vs. Equation (11)).

Regarding the estimation error (of the "g1" statistic) depicted in Figure 1, the "g1" statistic is rarely bigger than 10^{-5}, never bigger than $1.5\cdot\times 10^{-5}$ and tends to become smaller with the increase in sample size (n). Using Equation (11), Figure 2 depicts the shape of the $\text{CDF}_{\text{"g1"}}$(x;n).

With regard to the "g1" statistic (depicted in Figure 2), the domain for a variable distributed by the "g1" statistic (see Equation (11)) has values between 0 and 0.5 with the mode at p = 0 (a vertical asymptote at p = 0), a median of $n^{-1}\cdot 2^{-1/n}$ (and having a left asymmetry decreasing with the increasing of n and converging (for n → ∞) to symmetry) and mean of 1/2(n+1).

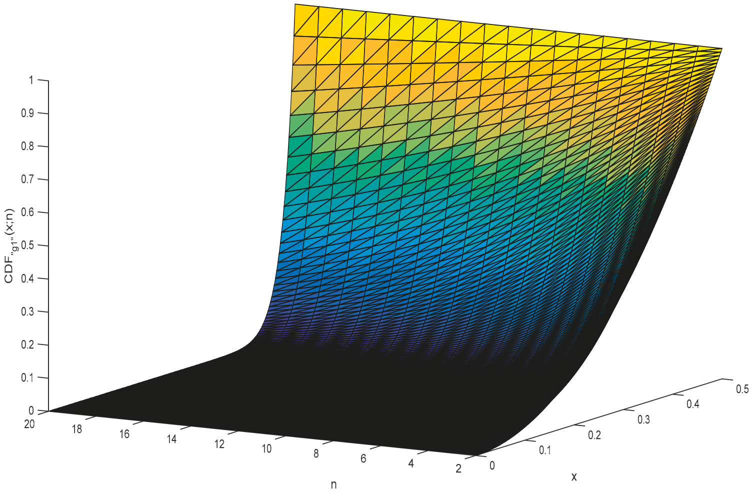

Figure 2. $\text{CDF}_{\text{"g1"}}$(x;n) for n = 2 to n = 20.

The expression of CDF$_{“g1”}$ is easily inverted (see Equation (13)).

$$\text{CDF}_{“g1”}(x;\ n)\ =\ (2x)^n\ \rightarrow\ \text{InvCDF}_{“g1”}(p;\ n)\ =\ \sqrt[n]{p}/2 \tag{13}$$

7. from “g1” Statistic to “g1” Confidence Intervals for the Extreme Values

Equation (13) can be used to calculate the critical values of the “g1” statistic for any values of α ($\alpha \leftarrow$ 1-p) and n. The critical values of the “g1” statistic acts as the boundaries of the confidence intervals.

By setting the risk of being in error α (usually at 5%), then p = 1-α and Equation (13) can be used to calculate the statistic associated with it (InvCDF$_{“g1”}$(1-α;n) = $\sqrt[n]{1-\alpha}/2$). By placing this value into Equations (9) and (10), the (extreme) probabilities can be extracted (Equation (14)).

$$\max_{1\le i\le n}\left|p_i - 0.5\right| = \sqrt[n]{1-\alpha}/2.\ \rightarrow\ \text{p}_{\text{extreme}}(\alpha)\ =\ 0.5\ \pm\ \sqrt[n]{1-\alpha}/2 \tag{14}$$

One should note that the confidence interval defined by Equation (14) is symmetric.

In order to arrive at the confidence intervals for the extreme values in the sampled data (Equation (15)) it is necessary to use the inverse of the CDF (again), and for the distribution of the sampled data.

$$\text{x}_{\text{extreme}}(\alpha) = \text{InvCDF}_{“\text{Distribution}”}(0.5 \pm \sqrt[n]{1-\alpha}/2; “\text{parameters}”) \tag{15}$$

To illustrate the calculation of the confidence intervals for the extreme values in the sampled data, a series of 206 data was chosen from [32]. The data were tested against the assumption that it follows a generalized Gauss-Laplace distribution (Equation (16), a symmetrical distribution), and later if there were some observations suspected to be outliers. The steps of this analysis and the obtained results are given in Table 4.

$$\text{PDF}_{“\text{GL}”}(x;\mu,\sigma,k) = c_1\sigma^{-1}e^{-|c_0 z|^k},\ c_0 = \left(\frac{\Gamma(3/k)}{\Gamma(1/k)}\right)^{1/2},\ c_1 = \frac{kc_0}{2\Gamma(1/k)},\ z = \frac{x-\mu}{\sigma} \tag{16}$$

The greatest departure from the median (0.5) for the 206 PCB dataset (Table 4) was 9.603 (CDF$_{“GL”}$(9.603; μ = 6.47938, σ = 0.82828, k = 1.79106) = 0.9998). Due to the force of this deviation from the median, 9.603 was suspected as being an outlier and was removed (it should be noted that in a broader context, an outlier can be also seen as an atypical observation, correctly collected from the population observation, as part of the data generation process and thus it may be maintained in the sample but probably with a less weight). The same procedure (as in Table 4) can be applied to the remaining data (205 observations). Then, InvCDF$_{“g1”}$(1-0.05; 205) = 0.499875, p$_{\text{min}}$(n=205) = 0.0001251; and p$_{\text{max}}$(n=205) = 0.9998749. The MLE estimates for the parameters of the Gauss-Laplace distribution remain unchanged (μ = 6.47938, σ = 0.82828, k = 1.79106) and the removed observation (9.603) is still not an outlier (x$_{\text{max}}$ = InvCDF$_{“GL”}$(0.9998749; μ = 6.47938, σ = 0.82828, k = 1.79106) = 9.7166 > 9.603).

Table 4. Distribution analysis for a series of 206 measurements for the octanol water partition coefficient (K$_{\text{ow}}$) of polychlorinated biphenyls expressed in logarithmic scale (log$_{10}$(K$_{\text{ow}}$))

Step	Results
Dataset (given for convenience)	4.151; 4.401; 4.421; 4.601; 4.941; 5.021; 5.023; 5.150; 5.180; 5.295; 5.301; 5.311; 5.311; 5.335; 5.343; 5.404; 5.421; 5.447; 5.452; 5.452; 5.481; 5.504; 5.517; 5.537; 5.537; 5.551; 5.561; 5.572; 5.577; 5.577; 5.627; 5.637; 5.637; 5.667; 5.667; 5.671; 5.677; 5.677; 5.691; 5.717; 5.743; 5.751; 5.757; 5.761; 5.767; 5.767; 5.787; 5.811; 5.817; 5.827; 5.867; 5.897; 5.897; 5.904; 5.943; 5.957; 5.957; 5.987; 6.041; 6.047; 6.047; 6.047; 6.057; 6.077; 6.091; 6.111; 6.117; 6.117; 6.137; 6.137; 6.137; 6.137; 6.137; 6.142; 6.167; 6.177; 6.177; 6.177; 6.204; 6.207; 6.221; 6.227; 6.227; 6.231; 6.237; 6.257; 6.267; 6.267; 6.267; 6.291; 6.304; 6.327; 6.357; 6.357; 6.367; 6.367; 6.371; 6.427; 6.457; 6.467; 6.487; 6.497; 6.511; 6.517; 6.517; 6.523; 6.532; 6.547; 6.583; 6.587; 6.587; 6.587; 6.607; 6.611; 6.647; 6.647; 6.647; 6.647; 6.647; 6.657; 6.657; 6.671; 6.671; 6.677; 6.677; 6.677; 6.697; 6.704; 6.717; 6.717; 6.737; 6.737; 6.737; 6.747; 6.767; 6.767; 6.767; 6.797; 6.827; 6.857; 6.867; 6.897; 6.897; 6.937; 6.937; 6.957; 6.961; 6.997; 7.027; 7.027; 7.027; 7.057; 7.071; 7.087; 7.087; 7.117; 7.117; 7.117; 7.121; 7.123; 7.147; 7.151; 7.177; 7.177; 7.187; 7.187; 7.207; 7.207; 7.207; 7.211; 7.247; 7.247; 7.277; 7.277; 7.277; 7.281; 7.304; 7.307; 7.307; 7.321; 7.337; 7.367; 7.391; 7.427; 7.441; 7.467; 7.516; 7.527; 7.527; 7.557; 7.567; 7.592; 7.627; 7.627; 7.657; 7.657; 7.717; 7.747; 7.751; 7.933; 8.007; 8.164; 8.423; 8.683; 9.143; 9.603
For n = 206 calculate the probability that the extreme values contain an outlier by using Equation (13)	At α = 5% risk being in error InvCDF$_{“g1”}$(1-0.05; 206) = 0.498755

Table 4. *Cont.*

Step	Results
Calculate the critical probabilities for the extreme values by using Equations (9) and (10)	g1 = 0.498755 → $\|0.5 - p_{min/max}\|$ = 0.498755 → 1 - $2p_{min/max}$ = ± 0.99751 → p_{min} = 0.0001245; p_{max} = 0.9998755

Estimate the parameters of the distribution fitting the dataset (distribution: Gauss-Laplace; μ - location parameter; σ - scale parameter; k - shape parameter)	Initial estimates (from a hybrid CM & MLE method): μ = 6.4806; σ = 0.83076; k = 1.4645;
	MLE estimates (by applying eq.3): μ = 6.47938; σ = 0.82828; k = 1.79106;

Calculate the lower and the upper bound for the extreme values by using InvCDF of the distribution fitting the data (Equation (15))	$\text{InvCDF}_{\text{“GL”}}$(0.0001245; μ = 6.47938, σ = 0.82828, k = 1.79106) = 3.2409 $\text{InvCDF}_{\text{“GL”}}$(0.9998755; μ = 6.47938, σ = 0.82828, k = 1.79106) = 9.7178
Make the conclusion regarding the outliers	Since the smallest value in the dataset is 4.151 (> 3.24) and the largest value is 9.603 (< 9.71), at 5% risk being in error there are no outliers in the dataset on the assumption that data follows the Gauss-Laplace distribution

8. Proposed Procedure for Detecting the Outliers

The procedure for detecting the outliers should start with measuring the agreement between the observed and estimated (Figure 3).

Figure 3 contains a statistical "trick", namely, when there are no outliers the statistics measuring the gap between the observation and the model (order statistics, Equation (6)) are in agreement (their associated probabilities are not too far from each other). When outliers exist, the order statistics are also sensitive to their presence. Since this is a separate subject, for further discussion please see the series of papers beginning with [32–34].

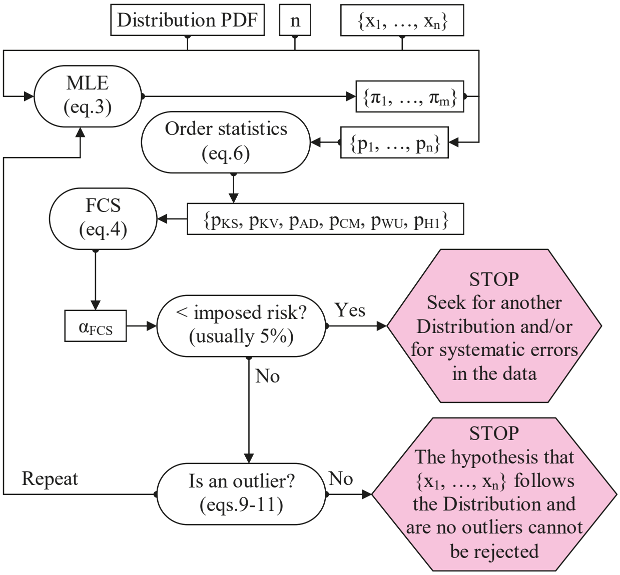
Distribution PDF
n
{x1, …, xn}
MLE (eq.3)
{π1, …, πm}
Order statistics (eq.6)
{p1, …, pn}
FCS (eq.4)
{pKS, pKV, pAD, pCM, pWU, pH1}
αFCS
< imposed risk? (usually 5%)
Yes
STOP Seek for another Distribution and/or for systematic errors in the data
No
Repeat
Is an outlier? (eqs.9-11)
No
STOP The hypothesis that {x1, …, xn} follows the Distribution and are no outliers cannot be rejected

Figure 3. The procedure for detecting outliers.

9. Second Simulation Assessing "Grubbs" and "g1" Outlier Detection Alternatives

Another MC study was designed to test the claim that the proposed method provides consistent results. This second MC simulation is much simpler than the one used to derive the data for constructing the outlier statistics (Figure 4).

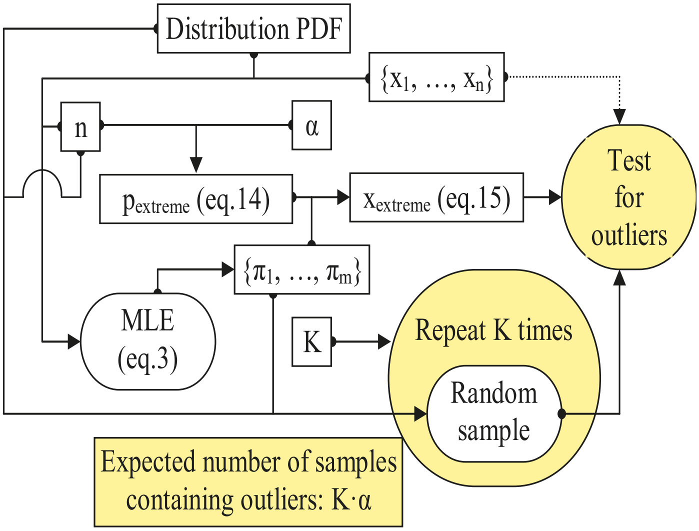

Figure 4. The procedure for testing the outlier statistics.

The data used here as a proof of the facts are from [7] and all cases involve a Normal distribution (Distribution = Normal in Equation (15); PDF and CDF for Normal distribution in Equation (18); a symmetrical distribution) with α = 5% risk being in error. The parameters of the Normal distribution (μ and σ) are determined for each case, as well as the sample size (Equation (17)).

$$x_{\text{extreme}}(\alpha) = \text{InvCDF}_{\text{``Normal''}}(0.5 \pm 0.5 \cdot \sqrt[n]{1-\alpha}; \mu, \sigma) \quad (17)$$

$$\text{PDF}_{\text{``Normal''}}(x; \mu, \sigma) = \frac{e^{-\frac{(x-\mu)^2}{\sigma^2}}}{\sigma\sqrt{2\pi}}, \ \text{CDF}_{\text{``Normal''}}(x; \mu, \sigma) = \int_{-\infty}^{x} \text{PDF}_{\text{``Normal''}}(t; \mu, \sigma)dt \quad (18)$$

For comparison, the same strategy for calculating the confidence intervals of the extreme values for the Normal distribution with the Grubbs test statistic (Equation (2)) was used to provide an alternate result (Equation (19)).

$$x_{\text{crit}}(\alpha) = \overline{x} \pm G_{\text{crit}}(\alpha) \cdot s, G_{\text{crit}}(\alpha) = \frac{\text{n}-1}{\sqrt{n}}\sqrt{\frac{t_G^2(\alpha)}{\text{n}-2+t_G^2(\alpha)}}, \ t_G = \text{InvCDF}_{\text{``Student t''}}(\frac{\alpha}{2n}, \text{n}-2) \quad (19)$$

The steps followed in this analysis are given in the Table 5.

Table 5. Comparison of the steps of the analysis and simulation for extreme values confidence intervals (proposed method vs. Grubbs test)

Step	Action (step 0 is setting the dataset; $\alpha \leftarrow 0.05$)
1	Estimate (with MLE, Equation (3)) parameters (μ, σ) of the Normal distribution; calculate the associated CDFs (Equation (18))
2	Calculate the order statistics, their associated risks being in error, FCS and p_{FCS} (Equations (6) and (4))
3	For n and α calculate the confidence intervals for the extreme values by using (a) Equation (6) and (17) and (b) Equation (19)
4	Run the MC experiment (Figure 4) for K = 10000 (and then the expected number of outliers is 500) samples and count the samples containing outliers for the existing method (Grubbs, Equation (19); with μ and σ from CM method) and for the proposed method (g1, Equations (13)–(15) and (17); with μ and σ from the MLE method)

Results of the analysis using the steps given in Table 5 for the first dataset are given in Table 6.

Table 6. Outlier analysis results for {568, 570, 570, 570, 572, 572, 572, 578, 584, 596} dataset.

<table>
<tr><th>Step</th><th colspan="8">Results (for α = 5%)</th></tr>
<tr><td>1</td><td colspan="8">$\mu = 575.2$; $\sigma = 8.256$ (MLE) → CPs = {0.1916, 0.2644, 0.2644, 0.2644, 0.3492, 0.3492, 0.3492, 0.6328, 0.8568, 0.9941}</td></tr>
<tr><td rowspan="3">2</td><td><b>Statistic</b></td><td><b>AD</b></td><td><b>KS</b></td><td><b>CM</b></td><td><b>KV</b></td><td><b>WU</b></td><td><b>H1</b></td><td><b>FCS</b></td></tr>
<tr><td>Value</td><td>1.137</td><td>1.110</td><td>0.206</td><td>1.715</td><td>0.182</td><td>5.266</td><td>12.293</td></tr>
<tr><td>$\alpha_{\text{Statistic}}$</td><td>0.288</td><td>0.132</td><td>0.259</td><td>0.028</td><td>0.049</td><td>0.343</td><td>0.056</td></tr>
<tr><td>3</td><td colspan="8">$x_{\text{crit}}(5\%) = 575.2 \pm 2.29 \cdot 8.7025$; $p_{\text{extreme}}(5\%) = 0.5 \pm \text{InvCDF}_{\text{"g1"}}(1\text{-}0.05; 10)$; $x_{\text{extreme}}(5\%) = \{552.086, 598.314\}$</td></tr>
<tr><td rowspan="3">4</td><td colspan="2"><b>Number of samples containing outliers</b></td><td colspan="3"><b>Existing method (Grubbs)</b></td><td colspan="3"><b>Proposed method (g1)</b></td></tr>
<tr><td colspan="2">First run</td><td colspan="3">1977 (19.77%)</td><td colspan="3">510 (5.1%)</td></tr>
<tr><td colspan="2">Second run</td><td colspan="3">2009 (20.09%)</td><td colspan="3">526 (5.26%)</td></tr>
</table>

In regard to the results given in Table 6:

At step 1, CPs are the cumulative probabilities ({$p_1, \ldots, p_{10}$} in Figure 3) associated with the series of the observations from the sample ({$x_1, \ldots, x_{10}$} in Figure 3).

At step 2, the data passes the normality test (α_{FCS} = 7% > 5% = α, see Figure 3).

Step 3 was made for n = 10 (see Figure 4). (a) The proposed method does not detect outliers in the sample (552.086 < 568, 596 < 598.314); (b) Grubbs test detect 596 as being an outlier (596 > 595.13).

At step 4 (see Figure 4), since {510, 526} are comparable with 500 and {1977, 2009} are much greater than 500, the results lead to the conclusion that the existing method produces type I errors by leading to false positive detection of outliers in the samples while the proposed method does not.

10. Going Further with the Outlier Analysis

What if "596" is removed from the sample? The following table provides mirror-like results for this scenario (Table 7).

Table 7. Outlier analysis results for {568, 570, 570, 570, 572, 572, 572, 578, 584} dataset.

<table>
<tr><th>Step</th><th colspan="8">Results (for α = 5%)</th></tr>
<tr><td>1</td><td colspan="8">$\mu = 572.889$; $\sigma = 4.725$ (MLE) → CPs = {0.1504, 0.2705, 0.2705, 0.2705, 0.4254, 0.4254, 0.4254, 0.8603, 0.9907}</td></tr>
<tr><td rowspan="3">2</td><td><b>Statistic</b></td><td><b>AD</b></td><td><b>KS</b></td><td><b>CM</b></td><td><b>KV</b></td><td><b>WU</b></td><td><b>H1</b></td><td><b>FCS</b></td></tr>
<tr><td>Value</td><td>0.935</td><td>1.057</td><td>0.174</td><td>1.535</td><td>0.155</td><td>4.678</td><td>9.715</td></tr>
<tr><td>$\alpha_{\text{Statistic}}$</td><td>0.389</td><td>0.167</td><td>0.327</td><td>0.082</td><td>0.088</td><td>0.394</td><td>0.137</td></tr>
<tr><td>3</td><td colspan="8">$x_{\text{crit}}(5\%) = 572.89 \pm 2.215 \cdot 5.011$; $p_{\text{extreme}}(5\%) = 0.5 \pm \text{InvCDF}_{\text{"g1"}}(1\text{-}0.05; 9)$; $x_{\text{extreme}}(5\%) = \{559.822, 585.956\}$</td></tr>
<tr><td rowspan="3">4</td><td colspan="2"><b>Number of samples containing outliers</b></td><td colspan="3"><b>Existing method (Grubbs)</b></td><td colspan="3"><b>Proposed method (g1)</b></td></tr>
<tr><td colspan="2">First run</td><td colspan="3">2341 (23.41%)</td><td colspan="3">563 (5.63%)</td></tr>
<tr><td colspan="2">Second run</td><td colspan="3">2333 (23.33%)</td><td colspan="3">543 (5.43%)</td></tr>
</table>

As can be observed in Table 7, the data is not in good agreement with normality (α_{FCS} in Table 6 is 7%, while in Table 7 it is 16%) and there is no change in the accuracy of the classification ({563, 543} comparable with 500, {2341, 2333} is much greater than 500; the existing method produces type I errors by leading to false positive detection of outliers in the samples, while the proposed method does not). When comparing the results given in Table 6 with the results given in Table 7 it should be noted that both tests (Grubbs and the newly proposed g1) produce somewhat confusing results (see Table 8 for side-by-side outcomes).

Table 8. Side-by-side comparison of the analysis of the samples.

Sample	**{568, 570, 570, 570, 572, 572, 572, 578, 584, 596}**	**{568, 570, 570, 570, 572, 572, 572, 578, 584}**
At 5% risk being in error can the hypothesis that the sample was drawn from a normal distribution be rejected?	No (α_{FCS} = 7%)	No (α_{FCS} = 15.8%)
Grubbs confidence interval for 'no outliers' at 5% risk being in error	(555.27, 595.13) 596 is detected as being outlier	(561.79, 583.99) 584 is detected as being outlier
g1 confidence interval for 'no outliers' at 5% risk being in error	(552.08, 598.32) no outliers	(559.82, 585.96) no outliers

Table 8 highlights the fact that based on the {568, 570, 570, 570, 572, 572, 572, 578, 584} sample, the g1 test may be interpreted as identifying 596 as being an outlier. This is not quite true because the g1 test was not intended to be used in this way. That is, 596 is outside of the dataset, so at the time of constructing the confidence intervals for the extreme values, the information regarding its observation was missing.

Another trial was done, this time with **601** replacing **596** in the initial dataset (Table 9).

Table 9. Outlier analysis results for the {568, 570, 570, 570, 572, 572, 572, 578, 584, **601**} dataset.

Step	**Results (for α = 5%)**							
1	From the CM method: μ = 575.7; σ = 10.067; from MLE method: μ = 575.7; σ = 9.550							
2	**Statistic**	**AD**	**KS**	**CM**	**KV**	**WU**	**H1**	**FCS**
	Value	1.267	1.109	0.225	1.774	0.198	5.411	13.652
	$\alpha_{\text{Statistic}}$	0.241	0.132	0.226	0.018	0.035	0.254	0.034
3	Grubbs confidence interval for 'no outliers' at 5% risk being in error: (552.647,598.753); **601** is an outlier g1 confidence interval for 'no outliers' at 5% risk being in error: (548.963, 602.437); no outliers							

In a further trial, **604** replaced **596** in the initial dataset (Table 10).

Table 10. Outlier analysis results for the {568, 570, 570, 570, 572, 572, 572, 578, 584, 604} dataset.

Step	**Results (for α = 5%)**							
1	From the CM method: μ = 576.0; σ = 10.914; from MLE method: μ = 576.0; σ = 10.354							
2	**Statistic**	**AD**	**KS**	**CM**	**KV**	**WU**	**H1**	**FCS**
	Value	1.348	1.108	0.238	1.803	0.209	5.481	14.468
	$\alpha_{\text{Statistic}}$	0.216	0.133	0.206	0.015	0.028	0.215	0.025
3	Grubbs confidence interval for 'no outliers' at 5% risk being in error: (551.00, 601.00); 604 is an outlier g1 confidence interval for 'no outliers' at 5% risk being in error: (547.01, 604.99); no outliers							

The conclusion is simple (see the results in the Tables 6, 7, 9 and 10): A test will hardly ever detect an outlier for a small sample; it is more likely to reject the hypothesis of the sample drawn from the distribution itself!

The same trick was used on a bigger sample and the results are shown in Table 11 (the dataset is from Table 4).

Table 11. Outlier analysis results for Table 4 dataset under the assumption of normal distribution.

<table>
<tr><th>Step</th><th colspan="8">Results (for α = 5%)</th></tr>
<tr><td>1</td><td colspan="8">Table 5 Dataset; Normal distribution → CM: μ = 6.481; σ = 0.831; MLE: μ = 6.481; σ = 0.829</td></tr>
<tr><td rowspan="3">2</td><td><b>Statistic</b></td><td><b>AD</b></td><td><b>KS</b></td><td><b>CM</b></td><td><b>KV</b></td><td><b>WU</b></td><td><b>H1</b></td><td><b>FCS</b></td></tr>
<tr><td>Value</td><td>0.439</td><td>0.484</td><td>0.049</td><td>0.952</td><td>0.047</td><td>104.2</td><td>1.276</td></tr>
<tr><td>$\alpha_{\text{Statistic}}$</td><td>0.812</td><td>0.965</td><td>0.886</td><td>0.852</td><td>0.743</td><td>0.641</td><td>0.973</td></tr>
<tr><td>3</td><td colspan="8">Grubbs confidence interval for ’no outliers’ at 5% risk being in error: (3.492, 9.470); 9.603 is an outlier
g1 confidence interval for ’no outliers’ at 5% risk being in error: (3.444, 9.517); 9.603 is an outlier</td></tr>
<tr><td rowspan="3">4</td><td colspan="3"><b>Number of samples containing outliers</b></td><td colspan="3"><b>Existing method (Grubbs)</b></td><td colspan="2"><b>Proposed method (g1)</b></td></tr>
<tr><td colspan="3">First run</td><td colspan="3">637 (6.37%)</td><td colspan="2">511 (5.11%)</td></tr>
<tr><td colspan="3">Second run</td><td colspan="3">630 (6.3%)</td><td colspan="2">481 (4.81%)</td></tr>
</table>

On one hand, as the results in Table 11 prove, the proposed method correctly identifies the confidence interval for the extreme values, while the existing method does not.

On the other hand, the results in Table 11 also show that the likelihood of identifying the outliers increases with the sample size, making it perfectly possible to identify outliers with the proposed method, although this is not the case in small samples. It is possible to detect the outliers in small samples as well, but not when the parameters of the distribution are derived from the sample data—only when the parameters of the distribution are known a priori or determined from other samples (the results given in Tables 6–10 are proof of this).

11. Further Discussion

The obtained expression for CDF of “g1” (Equation (11)) reveals the domain of a random variable distributed by the “g1” statistic ([0, 0.5]), which is consistent with the definition of “g1” (Equations (9) and (10)).

Independently of the shape of the theoretical distribution being tested (the generic case is defined by Equation (5)), as defined by Equations (9) and (10), the newly proposed statistic “g1” defines a symmetric confidence interval for the extreme values in samples in the probability space (Equation (14)). Later, this symmetric confidence interval may be changed back into an asymmetrical one when it is expressed in the domain of the theoretical distribution being tested (Equation (15)). It should be recognized that “g1” uses a symmetrization strategy to obtain the confidence interval for the extreme values in samples.

It might seem that the literature on robust statistics was ignored in this work, however, this is not entirely true. In fact, a whole pool of robust statistics was used extensively in the study (see Equation (8)), introduced as a tool in Table 5 and involved in the later calculations (Tables 6, 7 and 9, Tables 10 and 11). Also, it should be noted that the substitution of the mean by the median is not a new idea; it is well known in the field of robust statistics (for example, Watson U^2 [29], the $\text{WU}_{\text{Statistic}}$ in Equation (8), uses it).

A short literature survey provides several of examples of current real applications that require the proposed method. Thus, in signal processing, non-stationary, non-Gaussian, spiky signals are usually regarded as outliers and thus discarded (see [35–38] as typical cases). In this context, it should be noted that Mood’s median test is preferred to the Kruskal-Wallis test when outliers are present [39]. The identification of outliers is also recognized as an issue in the validation of protein structures, and the current methods are revised in [40]. Other examples can be found in [41].

In the wider context, an alternate window-based strategy has been proposed in which outliers are detected in each window by the Tukey method and labeled so that they can be excluded from the realization of the process points to be used for model identification [42]. A contingency-based strategy proposes maximization of true positive (TP) values and minimization of false negative (FN) and false positive (FP) values [43]. Finally, another distribution testing procedure has been proposed in [44].

12. Conclusions

A new method for detecting outliers was proposed in this paper. The method is applicable to any continuous distribution at any risk being in error. It was proved that the method correctly detects the outliers. For a normal distribution at 5% risk being in error, it was also shown that the proposed method outperforms the classical Grubbs test for detecting the outliers.

Supplementary Materials: Details of the software used for deriving the results given in the figures and tables, algorithms and source codes are given as supplementary material available online at http://www.mdpi.com/2073-8994/11/6/835/s1.

Funding: This research received no external funding.

Acknowledgments: Thanks to my colleague S.D. Bolboacă and for our fruitful discussions during the development stage of the study, which helped and motivated the author to complete the study.

Conflicts of Interest: The author declares no conflict of interest.

References

1. Gauss, C.F. *Theoria Motus Corporum Coelestium*; (Translated in 1857 as "Theory of Motion of the Heavenly Bodies Moving about the Sun in Conic Sections" by C. H. Davis. Little, Brown: Boston. Reprinted in 1963 by Dover: New York); Perthes et Besser: Hamburg, Germany, 1809; pp. 249–259.
2. Tippett, L.H.C. The extreme individuals and the range of samples taken from a normal population. *Biometrika* **1925**, *17*, 151–164. [CrossRef]
3. Fisher, R.A.; Tippett, L.H.C. Limiting forms of the frequency distribution of the largest and smallest member of a sample. *Proc. Camb. Philos. Soc.* **1928**, *24*, 180–190. [CrossRef]
4. Thompson, W.R. On a criterion for the rejection of observations and the distribution of the ratio of the deviation to the sample standard deviation. *Ann. Math. Stat.* **1935**, *6*, 214–219. [CrossRef]
5. Pearson, E.; Sekar, C.C. The efficiency of the statistical tools and a criterion for the rejection of outlying observations. *Biometrika* **1936**, *28*, 308–320. [CrossRef]
6. Grubbs, F.E. Sample criteria for testing outlying observations. *Ann. Math. Stat.* **1950**, *21*, 27–58. [CrossRef]
7. Grubbs, F.E. Procedures for detecting outlying observations in samples. *Technometrics* **1969**, *11*, 1–21. [CrossRef]
8. Nooghabi, M.; Nooghabi, H.; Nasiri, P. Detecting outliers in gamma distribution. *Commun. Stat. Theory Methods* **2010**, *39*, 698–706. [CrossRef]
9. Kumar, N.; Lalitha, S. Testing for upper outliers in gamma sample. *Commun. Stat. Theory Methods* **2012**, *41*, 820–828. [CrossRef]
10. Lucini, M.; Frery, A. Comments on "Detecting Outliers in Gamma Distribution" by M. Jabbari Nooghabi et al. (2010). *Commun. Stat. Theory Methods* **2017**, *46*, 5223–5227. [CrossRef]
11. Hartley, H. The range in random samples. *Biometrika* **1942**, *32*, 334–348. [CrossRef]
12. Bardet, J.-M.; Dimby, S.-F. A new non-parametric detector of univariate outliers for distributions with unbounded support. *Extremes* **2017**, *20*, 751–775. [CrossRef]
13. Gosset, W. The probable error of a mean. *Biometrika* **1908**, *6*, 1–25.
14. Jäntschi, L.; Bolboacă, S.-D. Computation of probability associated with Anderson-Darling statistic. *Mathematics* **2018**, *6*, 88. [CrossRef]
15. Fisher, R. On an Absolute Criterion for Fitting Frequency Curves. *Messenger Math.* **1912**, *41*, 155–160.
16. Fisher, R. Questions and answers #14. *Am. Stat.* **1948**, *2*, 30–31.
17. Bolboacă, S.D.; Jäntschi, L.; Sestraș, A.F.; Sestraș, R.E.; Pamfil, D.C. Supplementary material of 'Pearson-Fisher chi-square statistic revisited'. *Information* **2011**, *2*, 528–545. [CrossRef]
18. Jäntschi, L.; Bolboacă, S.D. Performances of Shannon's Entropy Statistic in Assessment of Distribution of Data. *Ovidius Univ. Ann. Chem.* **2017**, *28*, 30–42. [CrossRef]
19. Davis, P.; Rabinowitz, P. *Methods of Numerical Integration*; Academic Press: New York, NY, USA, 1975; pp. 51–198.
20. Pearson, K. Note on Francis Gallon's problem. *Biometrika* **1902**, *1*, 390–399.
21. Cramér, H. On the composition of elementary errors. *Scand. Actuar. J.* **1928**, *1*, 13–74. [CrossRef]
22. Von Mises, R.E. *Wahrscheinlichkeit, Statistik und Wahrheit*; Julius Springer: Berlin, Germany, 1928; pp. 100–138.

23. Kolmogorov, A. Sulla determinazione empirica di una legge di distribuzione. *Giornale dell'Istituto Italiano degli Attuari* **1933**, *4*, 83–91.
24. Kolmogorov, A. Confidence Limits for an Unknown Distribution Function. *Ann. Math. Stat.* **1941**, *12*, 461–463. [CrossRef]
25. Smirnov, N. Table for estimating the goodness of fit of empirical distributions. *Ann. Math. Stat.* **1948**, *19*, 279–281. [CrossRef]
26. Anderson, T.W.; Darling, D.A. Asymptotic theory of certain "goodness-of-fit" criteria based on stochastic processes. *Ann. Math. Stat.* **1952**, *23*, 193–212. [CrossRef]
27. Anderson, T.W.; Darling, D.A. A Test of Goodness-of-Fit. *J. Am. Stat. Assoc.* **1954**, *49*, 765–769. [CrossRef]
28. Kuiper, N.H. Tests concerning random points on a circle. *Proc. Koninklijke Nederlandse Akademie van Wetenschappen Series A* **1960**, *63*, 38–47. [CrossRef]
29. Watson, G.S. Goodness-Of-Fit Tests on a Circle. *Biometrika* **1961**, *48*, 109–114. [CrossRef]
30. Metropolis, N.; Ulam, S. The Monte Carlo Method. *J. Am. Stat. Assoc.* **1949**, *44*, 335–341. [CrossRef] [PubMed]
31. Fisher, R.A. On the mathematical foundations of theoretical statistics. *Philos. Trans. R. Soc. A* **1922**, *222*, 309–368. [CrossRef]
32. Jäntschi, L. Distribution fitting 1. Parameters estimation under assumption of agreement between observation and model. *Bull. UASVM Hortic.* **2009**, *66*, 684–690.
33. Jäntschi, L.; Bolboacă, S.D. Distribution fitting 2. Pearson-Fisher, Kolmogorov-Smirnov, Anderson-Darling, Wilks-Shapiro, Kramer-von-Misses and Jarque-Bera statistics. *Bull. UASVM Hortic.* **2009**, *66*, 691–697.
34. Bolboacă, S.D.; Jäntschi, L. Distribution fitting 3. Analysis under normality assumption. *Bull. UASVM Hortic.* **2009**, *66*, 698–705.
35. Liu, K.; Chen, Y.Q.; Domański, P.D.; Zhang, X. A novel method for control performance assessment with fractional order signal processing and its application to semiconductor manufacturing. *Algorithms* **2018**, *11*, 90. [CrossRef]
36. Paiva, J.S.; Ribeiro, R.S.R.; Cunha, J.P.S.; Rosa, C.C.; Jorge, P.A.S. Single particle differentiation through 2D optical fiber trapping and back-scattered signal statistical analysis: An exploratory approach. *Sensors* **2018**, *18*, 710. [CrossRef] [PubMed]
37. Teunissen, P.J.G.; Imparato, D.; Tiberius, C.C.J.M. Does RAIM with correct exclusion produce unbiased positions? *Sensors* **2017**, *17*, 1508. [CrossRef] [PubMed]
38. Pan, Z.; Liu, L.; Qiu, X.; Lei, B. Fast vessel detection in Gaofen-3 SAR images with ultrafine strip-map mode. *Sensors* **2017**, *17*, 1578. [CrossRef] [PubMed]
39. Vergura, S.; Carpentieri, M. Statistics to detect low-intensity anomalies in PV systems. *Energies* **2018**, *11*, 30. [CrossRef]
40. Chen, L.; He, J.; Sazzed, S.; Walker, R. An investigation of atomic structures derived from X-ray crystallography and cryo-electron microscopy using distal blocks of side-chains. *Molecules* **2018**, *23*, 610. [CrossRef] [PubMed]
41. Bolboacă, S.D.; Jäntschi, L. The effect of leverage and influential on structure-activity relationships. *Comb. Chem. High Throughput Screen.* **2013**, *16*, 288–297. [CrossRef] [PubMed]
42. Faes, L.; Porta, A.; Nollo, G.; Javorka, M. Information decomposition in multivariate systems: Definitions, implementation and application to cardiovascular networks. *Entropy* **2017**, *19*, 5. [CrossRef]
43. Li, G.; Wang, J.; Liang, J.; Yue, C. Application of sliding nest window control chart in data stream anomaly detection. *Symmetry* **2018**, *10*, 113. [CrossRef]
44. Paolella, M.S. Stable-GARCH models for financial returns: Fast estimation and tests for stability. *Econometrics* **2016**, *4*, 25. [CrossRef]

MDPI
St. Alban-Anlage 66
4052 Basel
Switzerland
Tel. +41 61 683 77 34
Fax +41 61 302 89 18
www.mdpi.com

Symmetry Editorial Office
E-mail: symmetry@mdpi.com
www.mdpi.com/journal/symmetry

MDPI
St. Alban-Anlage 66
4052 Basel
Switzerland

Tel: +41 61 683 77 34
Fax: +41 61 302 89 18

www.mdpi.com

ISBN 978-3-03943-792-4